

**NASA TECHNICAL
MEMORANDUM**

NASA TM X-62,464

NASA TM X-62,464

(NASA-TM-X-62464) ELEVENTH ANNUAL
CONFERENCE ON MANUAL CONTROL (NASA) 719 p
HC \$17.25 CSCL 051

N75-33675
THRU
N75-33719
Unclas
41164

G3/54

**ELEVENTH ANNUAL CONFERENCE
ON MANUAL CONTROL**

**Ames Research Center
Moffett Field, Calif. 94035**

May 1975



1. Report No. NASA TM X-62,464		2. Government Accession No.		3. Recipient's Catalog No.	
4. Title and Subtitle ELEVENTH ANNUAL CONFERENCE ON MANUAL CONTROL				5. Report Date	
				6. Performing Organization Code	
7. Author(s)				8. Performing Organization Report No. A-6211	
9. Performing Organization Name and Address Ames Research Center, NASA Moffett Field, Calif. 94035				10. Work Unit No. 504-09-33	
				11. Contract or Grant No.	
12. Sponsoring Agency Name and Address National Aeronautics and Space Administration Washington, D. C. 20546				13. Type of Report and Period Covered Technical Memorandum	
				14. Sponsoring Agency Code	
15. Supplementary Notes Proceedings of a meeting held at Ames Research Center, Moffett Field, California, May 21-23, 1975					
16. Abstract <p>This volume contains a compilation of written versions of papers presented at the Eleventh Annual Conference on Manual Control in a meeting held at NASA-Ames Research Center, May 21-23, 1975. Five main topics were discussed during this three-day conference. These were covered in sessions on Concurrent Tasks, Physiological Systems, Controls and Displays, Performance/Workload Evaluation, and System Identification. Forty-nine papers are included with presentations on results of analytical studies to develop and evaluate human operator models for a range of control task, vehicle dynamics and display situations; results of tests of physiological control systems and applications to medical problems; and on results of simulator and flight tests to determine display, control and dynamics effects on operator performance and workload for aircraft, automobile and remote control systems.</p>					
17. Key Words (Suggested by Author(s)) Manual control, Physiological control, Man-machine systems, Displays, Vehicle handling qualities, Operator performance, Flight management systems, Simulation			18. Distribution Statement Unlimited STAR Category - 54		
19. Security Classif. (of this report) Unclassified		20. Security Classif. (of this page) Unclassified		21. No. of Pages 722	22. Price* \$17.25

FOREWORD

This volume contains the proceedings of the Eleventh Annual Conference on Manual Control held at NASA-Ames Research Center from May 21 to 23, 1975. The program agenda and format are generally adhered to in this report which contains complete manuscripts of most of the papers presented at the meeting.

This was the eleventh in a series of conferences dating back to December 1964. These earlier meetings and their proceedings are listed below:

First Annual NASA-University Conference on Manual Control, The University of Michigan, December 1964. (Proceedings not printed.)

Second Annual NASA-University Conference on Manual Control, MIT, February 28 to March 2, 1966, NASA SP-128.

Third Annual NASA-University Conference on Manual Control, University of Southern California, March 1-3, 1967, NASA SP-144.

Fourth Annual NASA-University Conference on Manual Control, The University of Michigan, March 21-23, 1968, NASA SP-192.

Fifth Annual NASA-University Conference on Manual Control, MIT, March 27-29, 1969, NASA SP-215.

Sixth Annual Conference on Manual Control, Wright-Patterson AFB, April 7-9, 1970.

Seventh Annual Conference on Manual Control, University of Southern California, June 2-4, 1971, NASA SP-281.

Eighth Annual Conference on Manual Control, University of Michigan, Ann Arbor, Michigan, May 17-19, 1972.

Ninth Annual Conference on Manual Control, Massachusetts Institute of Technology, May 23-25, 1973.

Tenth Annual Conference on Manual Control, Wright-Patterson AFB, April 9-11, 1974.

PENDING PAGE BLANK NOT FILMED

GENERAL CHAIRMAN:
Melvin Sadoff
Biotechnology Division
NASA Ames Research Center

CO-CHAIRMAN:
Thomas E. Wempe
Man-Machine Integration Branch
NASA Ames Research Center

CONTENTS

Session I. CONCURRENT TASKS

Chairman: Duane McRuer

	Page
1. Multivariable Manual Control With Simultaneous Visual and Auditory Presentation of Information, <i>by Hartmut Uhlemann and Georg Geiser</i>	3
2. Experiments in Pilot Decision-Making During Simulated Low Visibility Approaches, <i>by Renwick E. Curry, John K. Lauber, and Charles E. Billings</i>	19
3. Tracking Performance Under Time Sharing Conditions With a Digit Processing Task: A Feedback Control Theory Analysis, <i>by Daniel Gopher and Christopher D. Wickens</i>	33
4. Time Estimation as a Secondary Task to Measure Workload, <i>by Sandra G. Hart</i>	64
5. Failure Detection by Pilots During Automatic Landing: Models and Experiments, <i>by Eli G. Gai and R. E. Curry</i>	78
6. Human Factors Research Problems in Electronic Voice Warning System Design, <i>by C. A. Simpson and D. H. Williams</i>	94
7. A Decision and Control Multi-Axis Pilot Model Based on an Urgency for Action Concept, <i>by J. J. Pollard and R. A. Hannen</i>	107
8. Discrete Time Modelization of Human Pilot Behavior, <i>by Daniel Cavalli and Dominique Soulatges</i>	119
9. Human Interaction With an Intelligent Computer in Multi-Task Situations, <i>by William B. Rouse</i>	130
10. A Model for Simultaneous Monitoring and Control, <i>by R. E. Curry, David L. Kleinman, and William C. Hoffman</i> ...	144
11. Detection of System Failures in Multi-Axes Tasks, <i>by Arye R. Ephrath</i>	151
12. Driver Decision-Making Research in a Laboratory Simulation, <i>by R. Wade Allen, Stephen H. Schwartz, and Henry R. Jex</i> ..	170

SESSION II. PHYSIOLOGICAL SYSTEMS

Chairman: William H. Levieon

13. Recognition of Stimulus Displays - An Electrophysiological Analysis, by Victor S. Johnston.....	173
14. A Two-Dimensional Tracker to Test and Evaluate Patients Afflicted With Nervous System Disorders, by Hugh P. Bergeron and James D. Holt.....	179 SUMMARY ONLY
15. Frequency Modulated Cutaneous Orientation Feedback From Artificial Arms, by Moshe Solomonow, Amos Freedy, and John Lyman.....	180
16. Role of Stretch Reflex in Voluntary Movements, by Gerald L. Gottlieb and Gyan C. Agarwal.....	192
17. Head-Eye Tracking in Two-Dimensional Pursuit Tasks, by D. K. Shirachi and J. H. Black, Jr.....	204
18. Effects of Low Frequency Vibration of a Limb, by Gyan C. Agarwal and Gerald L. Gottlieb.....	217

SESSION III. CONTROLS AND DISPLAYS

Chairman: Gary Beasley

19. Manual Control Display for a Four-Dimensional Landing Approach, by James T. Silverthorn and Robert L. Swaim...	245
20. Simulator Evaluation of a Perspective Clipped-Pole Display and a Thrust-Vector Controller For VTOL Zero-Zero Landings, by M. R. Murphy and R. K. Greif.....	268
21. Information and Display Requirements for an Independent Landing Monitor, by J. S. Karmarker, J. A. Sorensen, and A. V. Phatak.....	283 SUMMARY ONLY
22. Lagged Low Order Control Systems With Powered Controls, by E. C. Poulton.....	284
23. Results of a Flight Investigation of Control-Display Interactions for VTOL Decelerating Descending Instrument Approaches Using the X-22A Aircraft, by J. V. Lebacqz and E. W. Aiken.....	297

24.	A Simulator Study on Information Requirements for Precision Hovering, <i>by James L. Lemons and Theodore A. Dukes.....</i>	325
25.	Motion-Base Simulator Tests of Low Frequency Aircraft Motion on the Passenger Ride Environment, <i>by Hugh P. Bergeron and James D. Holt.....</i>	337
26.	A Model-Based Analysis of a Display for Helicopter Landing Approach, <i>by Ronald A. Hess and L. William Wheat</i>	338
27.	Simulation of Man-Machine Interaction on Shuttle Payload Manipulator, <i>by R. O. Hookway and R. S. Jackson.....</i>	356
28.	Unique Wide Field of View Visual Simulation, <i>by John Niemela.....</i>	377
29.	Test Procedures and Performance Measures Sensitive to Automobile Steering Dynamics, <i>by Richard Klein, Duane McRuer, and David Weir.....</i>	383
30.	An Interactive Driving Simulation for Driver Control and Decision-Making Research, <i>by R. Wade Allen, Jeffrey R. Hogge, and Stephen H. Schwartz.....</i>	396
31.	Effects of Automobile Steering Characteristics on Driver Vehicle System Dynamics in Regulation Tasks, <i>by Duane McRuer and Richard Klein.....</i>	408
32.	A Kinesthetic-Tactual Display for Stall Deterrence, <i>by Richard D. Gilson, Ronald W. Ventola, and Robert E. Fenton.....</i>	440

SESSION IV. PERFORMANCE/WORKLOAD EVALUATION

Chairman: Charles E. Billings

33.	Verbal Workload in Distributed Air Traffic Management, <i>by J. G. Kreifeldt, B. Pardo, T. Wempe, and E. Huff.....</i>	455
34.	Effects of Automobile Steering Characteristics on Driver/Vehicle System Performance in Discrete Maneuvers, <i>by Richard H. Klein and Duane T. McRuer.....</i>	472
35.	The Effects of Stability Augmentation on the Gust Response of a STOL Aircraft During a Curved Manual Approach, <i>by Milton B. Porter, Jr. and Robert L. Swaim..</i>	486

36.	Subjective Evaluation With FAA Criteria - A Multi-dimensional Scaling Approach, <i>by J. G. Kreifeldt, L. Parkin, T. E. Wempe, and E. F. Huff</i>	504
37.	Slushy Weightings for the Optimal Pilot Model, <i>by James D. Dillow, Douglas G. Picha, and Ronald O. Anderson</i>	526
38.	A Theoretical Study of the Pilot as a System Monitor, <i>by P. H. Wewerinke</i>	541
39.	Human Performance Evaluation in Dual-Axis Critical Task Tracking, <i>by Malcolm L. Ritchie and N. S. Nataraj</i>	548
40.	Continuous Performance Measurement in Flight Systems, <i>by Edward M. Connelly, Nicholas A. Sloan, and Robert M. Zeskind</i>	561

SESSION V: SYSTEM IDENTIFICATION

Chairman: Remwick E. Curry

41.	Problems, Questions and Results in the Use of the BBN-Model, <i>by Dieter Dey</i>	577
42.	Performance Evaluation of Tracking Based on a Low Pass Filter Model, <i>by Daniel W. Repperger</i>	599
43.	A Study of Pilot Behavior During Controlling the Lateral Directional Motion of Airplanes in Turbulent Air, <i>by Goro Beppu</i>	625
44.	A Multiloop Approach to Modeling Motion Sensor Responses, <i>by Andrew M. Junker, Daniel W. Repperger and John A. Neff</i>	645
45.	Effects of Control-Stick Parameters on Tracking Performance in a Vibration Environment, <i>by William H. Levison</i> .	656
46.	Evaluation of Optimal Control Type Models for the Human Gunner in an Anti-Aircraft Artillery (AAA) System, <i>by Anil V. Phatak and Kenneth M. Kessler</i>	675
47.	Comparison of Human Driver Dynamics in Simulators With Complex and Simple Visual Displays and in an Automobile on the Road, <i>by Duane T. MoRuer and Richard H. Klein</i>	684
48.	Manual and Automatic Control of Surface Effect Ships, <i>by Warren F. Clement, John J. Shanahan, and R. Wade Allen</i> ..	692

49. The Effects of Bedrest on Crew Performance During Simulated Shuttle Reentry, by Henry R. Jex, Richard A. Peters, Richard J. DiMarco, and R. Wade Allen.....

711 SUMMARY
(NAC)

SESSION I
CONCURRENT TASKS

Chairman: DUANE T. McRUER

* N75 33676

MULTIVARIABLE MANUAL CONTROL WITH SIMULTANEOUS VISUAL
AND AUDITORY PRESENTATION OF INFORMATION*

By Hartmut Uhlemann and Georg Geiser

Fraunhofer-Gesellschaft, Institut für Informationsverarbeitung
in Technik und Biologie, Karlsruhe, Federal Republic of Germany

SUMMARY

Multivariable manual compensatory tracking experiments were carried out in order to determine typical strategies of the human operator and conditions for improvement of his performance if one of the visual displays of the tracking errors is supplemented by an auditory feedback.

Experiments with one, two and four zero-order systems show that the operator's performance is only improved through use of combined presentation of one tracking error if

- at least two systems are to be controlled,
- the visual displays are separate,
- the visual display which is auditorally supported represents only one system.

Because the tracking error of the system which is only visually displayed is found to decrease, but not in general that of the auditorally supported system, it was concluded that the auditory feedback unloads the visual system of the operator who can then concentrate on the remaining exclusively visual displays.

This conclusion was confirmed by further two-axis experiments with variable lateral angular distance between the two visual displays, the right one of which being auditorally supported. Due to the changing strategies of the operator the auditory aid has little influence if the two visual displays are close together ($\sim 20^\circ$), whereas the tracking error of the solely visual display decreases if the angular distance between the two visual displays is enlarged. In the case of tracking signals with low cut-off frequencies (e.g. 0.04 rad/s) the tracking error of the auditory supported system also decreases slightly, but for higher cut-off frequencies (e.g. 0.64 rad/s) there exists an angular range where the auditorally supported display leads to a tracking error which is higher than that which occurs without support.

*This research was supported by the German Federal Ministry of Defense.

INTRODUCTION

The human operator of a technical process often has to accomplish several tasks at the same time with a high degree of precision. The information needed is presented to him mostly by visual displays; the cockpit of an aircraft or the control room of a nuclear power station are impressive examples of the great number of parallel displays which are often required.

In multivariable manual control tasks several displays must be read sequentially by the human operator, and corresponding reactions must be carried out. In critical situations the visual channel may be overloaded. Therefore the question is whether the human operator's performance may be improved if the visual channel is unburdened by means of combining visual and auditory presentation of information.

In the past, several studies dealt with this question; however, the earlier studies gave more qualitative than quantitative results. In recent years a few detailed investigations have been published, some of which are discussed below.

Vinje and Pitkin (Ref. 1) posed the question of whether for single axis tracking tasks the human control characteristics change with a combined visual and auditory presentation of the control error as compared with either a visual or auditory presentation alone. The control task was one-degree-of-freedom compensatory tracking. The input was Mc Ruer's "sum-of-sine-waves" function with variable bandwidth. Different system dynamics were used. For auditory control the tracking error was converted to the frequency of a specific auditory signal and presented using a one-ear and a two-ear display. On the visual display, which was deliberately adjusted in order to correspond with the auditory display, a dot moved along one of two separate vertical paths. The magnitude of the tracking error was indicated by the vertical position of the dot, and the sign of the error determined on which path the dot moved. The authors report that for the task considered humans can perform equally well with auditory or visual displays, providing the auditory and visual presentations contain equivalent information on tracking error. Furthermore the operator's performance with one- or two-ear displays is equal and the combined visual and auditory presentation improves the operator's performance slightly.

This slight improvement was examined by the authors in a further study (Ref. 2) where they used four different visual displays and the two-ear auditory display of the preceding study. By means of the critical tracking task according to Jex et al. (Ref. 3) the critical tracking parameter as an indicator of the operator's effective time delay was measured for each of the five different displays separately and also for the four combinations of auditory and visual displays. In every

case the value of the critical tracking parameter increased a statistically significant amount when one of the visual displays was used in combination with the auditory display. It was concluded that the operator's inherent processing delays were reduced when operating with a combined display.

A further study was conducted by Vinje (Ref. 4) using a difficult six-degree-of-freedom hover control task of a simulated V/STOL aircraft in turbulence. A single-degree-of-freedom auditory display substituted or supported one visual display. The results showed different performances of the subjects, but in general the tracking error was least when a combined display was used. Furthermore the subjects could control an auditorally displayed function and another visually displayed function better than if the two functions were both presented visually on separate displays. They also commented that the workload was reduced when the auditory displays were used.

The decrease of workload and the improvement of performance just mentioned may be explained by the assumption that the auditorally supported or replaced display has to be looked at rarely or not at all. Thus the subjects spend more time on the other displays while still receiving the auditory information.

Large and significant differences between visual and combined display of tracking information are shown by the study of Mirchandani (Ref. 5) under different experimental conditions. The subjects had to control a dual-axis compensatory tracking task with the primary task of controlling a second-order plant, and the secondary task of controlling a first order plant. The tracking error of the primary task was presented by the displacement of a vertical line on an oscilloscope, the display for the secondary task was a separate oscilloscope with a horizontal line. In a number of the experiments the visual display of the secondary task was supplemented by an auditory display which indicated the tracking error by the pitch and the volume of a tone. Mirchandani reports that the tracking error decreases significantly if the secondary task is supplemented by an auditory display. The tracking error of the primary task also decreases to some extent in this case.

From these studies it may be concluded that different results have been obtained concerning the effect of the combined presentation of control error. Because of different experimental conditions general design rules for applications can hardly be derived. Therefore further experiments have been carried out, some of which are discussed below. These experiments were undertaken not to evaluate the operator's describing function under the condition of combined presentation of information but to develop practice-oriented rules for the use of combined presentation of tracking error.

THE EXPERIMENTS

The two experiments which are reported in this paper were undertaken to answer especially the following questions:

- How does the number of simultaneous tracking tasks influence the effect of the combined presentation of one control error?
- What are the strategies of the operator as a function of the angular distance between two visual displays, one of which being auditorally supported?

In the first experiment the tracking performance for one-, two- and four-degree-of-freedom tracking tasks was investigated. The tracking error was displayed visually; one of the visual displays could be supported auditorally.

The second experiment was carried out with a two-degree-of-freedom tracking task with two separate visual displays, one of which was auditorally supported. The tracking error was measured as a function of the lateral angular distance between the two separate visual displays.

Both experiments were carried out with the same experimental setup, with which up to four independent systems can be used. All experiments were compensatory tracking tasks with zero-order systems. Fig. 1 shows a schematic diagram of the experimental setup where for simplicity only two of the four possible systems are presented. The experimental runs were controlled by a process computer which also generated the input-signals of the systems by use of a program. These input-signals were sample functions of white noise which passed through a second-order linear filter with adjustable cut-off frequency.

The visual displays of the tracking error were shown on different oscilloscopes. For the one- and two-degree-of-freedom tracking tasks a vertical line moved horizontally on a cathode ray tube (Tektronix 5103N); the four-degree-of-freedom tracking task was visually displayed by two points, each of which could move in two dimensions on the same CRT. The test series with variable lateral angular distance between the two visual displays of a two-degree-of-freedom tracking task were carried out with two oscilloscopes (Tektronix RM 503). The controls of the system were one or two joy-sticks with movement directions compatible with the corresponding visual display.

The auditory display which could be used alone or as a supplement to a visual display consisted of a voltage-amplitude converter transforming the error-voltage to the volume of a tone of 800 cps. In this way the volume of the tone was zero if the control error was zero, and according to the sign of the error the tone was heard in the right or left earphone. In previous experiments this kind of auditory display turned out to be the best of a number of alternatives.

The input-signals and the control error were stored digitally on magnetic tape. The dependent variable of the trials was the rms tracking error, normalized by relating it to the rms value of the corresponding input-signal. Each session consisted of five trials of approximately 100 s duration. After each trial the bandwidth of the input-signal was increased by a factor of 2.

The subjects were colleagues of our institute who have participated for several years in such experiments and may therefore be regarded as trained operators.

EXPERIMENTS WITH ONE-, TWO- AND FOUR-DEGREE-OF-FREEDOM TRACKING TASKS

In our experiments the rms tracking error with auditory presentation alone was always much greater (approximately twice the amount) as with visual or with combined presentation. Therefore the results with auditory presentation alone are not discussed in the following.

In Fig. 2 the rms tracking error of the one-degree-of-freedom tracking task with visual and combined presentation is plotted for different values of the bandwidth of the input-signal. Each point is the mean of 26 trials. These results do not confirm the conclusion of Vinje and Pitkin (Ref. 1) that for single-axis tracking tasks the combined auditory and visual presentation of the tracking error improves operator performance. The results change if there are two axes to be controlled (Fig. 3). Both tracking errors were displayed visually on one oscilloscope by two vertical lines with a lateral angular distance of 40° as seen by the subjects. The error of the first system was displayed by the position of the right line, and control was effected by means of a compatible joy-stick with the right hand. This display was partly auditorally supplemented. For the second system the left line and another joy-stick for the left hand was present. This system was visually displayed only. Compared with the trials with one axis the bandwidth of the input-signals was reduced.

The points of Fig. 3 are the mean of 10 trials. The upper part shows the rms tracking error of the first system with visual (circles) and combined (triangles) presentation. The latter improves operator performance slightly for low bandwidths of the input-signal. The results of the second system are plotted in the lower part of Fig. 3. Here for all bandwidths of the input-signal the tracking error decreases if the first system is auditorally supported. The amount of the improvement must be seen in relation to the absolute value of the tracking error without auditory aid. In general the combined presentation of one system's tracking error improves the error of the other system which is not auditorally supported. This does not coincide with the results of Mirchandani (Ref. 5) obtained with an asymmetrical dual-axis tracking task.

Our results confirm the hypothesis already mentioned that the combined presentation unloads the operator by reducing his visual scanning activity. Because the fixation rate of the auditorally supplemented visual display can be diminished the operator gains time for fixation of the other visual display. Consequently, the control error of the not supported system decreases.

For further investigation of this hypothesis four-degree-of-freedom tracking tasks were carried out. Here the display was an oscilloscope with two points (angular distance 50°) moving in two dimensions, and the controls were two compatible joy-sticks. The axes were numbered 1 to 4 and attached to the directions of the moving points of the display and to the joy-sticks according to Fig. 4. The results (means of 12 trials) are shown in Figs. 5a and 5b. Compared with the two-degree-of-freedom tracking task the rms tracking error of the four-dimensional task has not increased. There are two reasons for this:

- Between these two experiments the subjects participated in further manual control experiments which are not reported here. Through these their training level was further improved.
- Furthermore it has been shown by Levison and Elkind (Ref. 6) that the manual control of two systems is hardly more difficult than of one system if the two systems are symmetrical, if the control error is displayed by one point, and if the control is one compatible joy-stick.

The upper part of Fig. 5a shows the rms tracking error of the first system which was displayed in part visually (circles) and in part as a combined system (triangles). Here, in accordance with the other authors, a slight improvement for the combined display system can be seen, whereas no effect is indicated for the third system which is displayed (visually only) by the same point and controlled with the same joy-stick (Fig. 5a, lower part). Contrary to the experiment with two dimensions the auditory support does not influence left hand controlled system 2 and 4 which are only visually displayed (Fig. 5b). This is explained by the fact that the operator's fixation activity is not reduced if the auditorally supplemented visual display is an integrated display for another system. For the control of the four dimensions the operator has to scan the two points equally whether there is an auditory support for one dimension or not.

The results of these experiments confirm the hypothesis which was inferred from the literature: The combined presentation improves the operator performance only if there is more than one system to be controlled and if these systems have separate, not integrated displays.

TWO-AXIS EXPERIMENT WITH VARIABLE LATERAL ANGULAR DISTANCE
BETWEEN TWO SEPARATE DISPLAYS

A further experiment was undertaken in order to evaluate the influence of the lateral angular distance between two separate displays. Only two systems were to be controlled, and the control error was displayed visually on two oscilloscopes by a vertical line. Again the right visual display was partly auditorally supplemented. The lateral visual angle between the two visual displays was variable, beginning at 20° .

Fig. 6 shows the rms tracking error as a function of the lateral visual angle for three values of the bandwidth of the input-signal. The results were gained from 8 subjects who carried out three sessions on different days. Because the exclusively visual presentation of the two dimensions results in symmetrical curves they are summarized in one curve (circles). In this case the rms tracking error increases for all three cut-off frequencies with growing lateral angular distance between the two visual displays.

Because of symmetry the subjects shared their fixation activity equally on both visual displays. As the distance between them is increased the time lost by fixation changes between the two visual displays also increases, therefore decreasing the control performance. If a combined display is used the curves of the auditorally supported system (triangles) and of the merely visual presentation (squares) diverge. Up to 20° the fixation activity is partitioned equally between the two visual displays. If the values of the bandwidth of the input-signals are large and if the angle between the two visual displays is greater than 30° , the subjects' strategies tend to concentrate their fixations on that visual display which is not auditorally supplemented. The other system with combined display is more and more controlled by means of the auditory display. Therefore the control error of the system with visual display only decreases, and that of the system with combined display increases. Beyond a certain angle the tracking error of the combined display system is only read from the auditory part of the display. In that case a further increase of the angle has no influence whereas with visual presentation alone the control error continues to increase with increasing angle. Consequently, there is an angular distance beyond which for combined presentation the control errors of both systems are lower than those corresponding to visual presentation only.

This effect is not distinct for input-signals with low cut-off frequencies. There is sufficient time to change the fixations between the two visual displays. Therefore the auditory support leads only to a slight improvement in operator performance.

CONCLUSIONS

Together with the previous studies from the literature the experiments described above lead to some rules for the practical use of combined displays for manual control:

1. If the operator has to control several systems, visual displays are to be recommended. These displays are to be positioned closely together; in general, integrated displays are highly suitable.
2. If it is not possible to arrange the displays closely together, the auditory support of a peripherally located visual display has the following effects:
 - If the input-signal varies slowly the control error of both systems decreases.
 - For higher cut-off frequencies of the input-signal there is an angular range from approximately 20° to 70° where control error of the peripheral display increases, whereas the performance with the visually displayed systems in the centre increases markedly.
 - Beyond an angle of 70° the auditory support is to be unconditionally recommended.
3. In any case the visual displays are indispensable.
4. The auditory support should be attached to the least important control system.
5. The auditory supplemented visual display must not be integrated with other visual displays.

REFERENCES

1. Vinje, E.W.; E.T. Pitkin: "Human Operator Dynamics for Aural Compensatory Tracking", IEEE Trans. Syst. Man Cybern., vol. SMC-2, pp. 504-512, Sept. 1972.
2. Pitkin, E.T.; E.W.Vinje: "Comparison of Human Operator Critical Tracking Task Performance with Aural and Visual Displays", IEEE Trans. Syst. Man Cybern., vol SMC-3, pp. 184-187, March 1973.
3. Jex, H.R.; J.D. McDonnell; A.V. Phatak: "A Critical Tracking Task for Manual Control Research", IEEE Trans. Human Factors Electron., vol. HFE-7, pp. 138-143, Dec. 1966.
4. Vinje, E.W.: "Flight Simulator Evaluation of Audio Displays for IFR Hover Control", 8th Annual Conference on Manual Control, University of Michigan, Ann Arbor, Mich., 1972.
5. Mirchandani, P.B.: "An Auditory Display in a Dual-Axis Tracking Task", IEEE Trans. Syst. Man Cybern., vol. SMC-2, pp.375-380, July 1972.
6. Levison, W.H.; J.I. Elkind: "Studies of Multi-Variable Manual Control Systems: Two Axis Compensatory Systems with Compatible Integrated Display and Control", NASA CR-554, 1966.

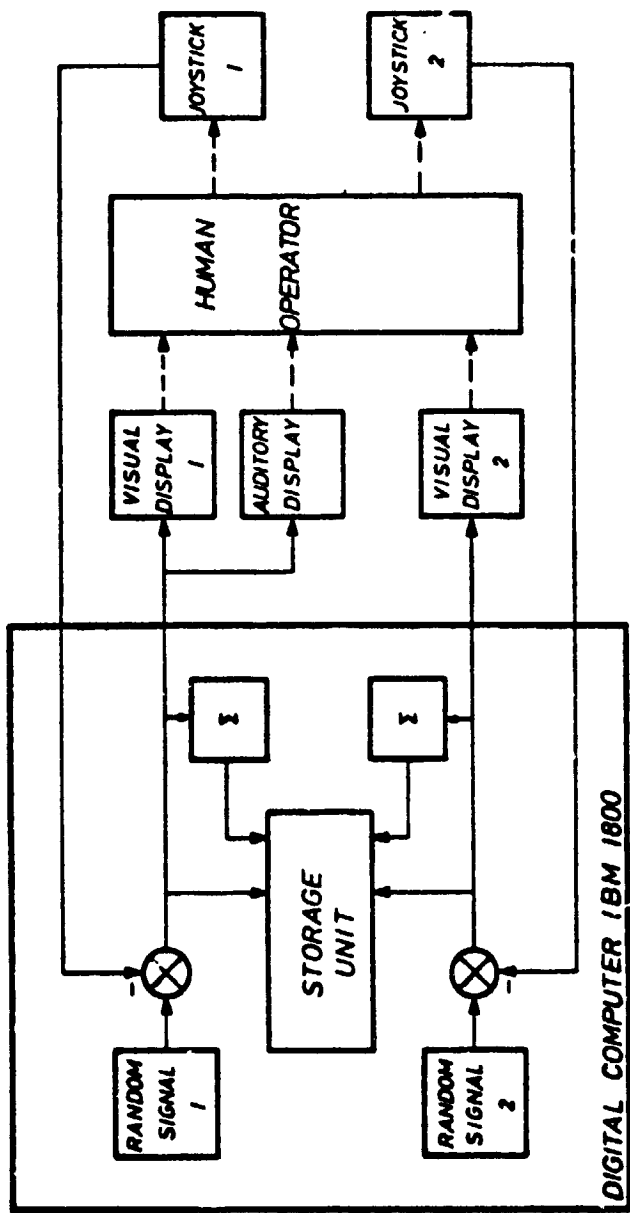
KEY TO LETTER DESIGNATION OF THE CURVES AND DISPLAYS

c → combined visual and auditory presentation

v → visual presentation only

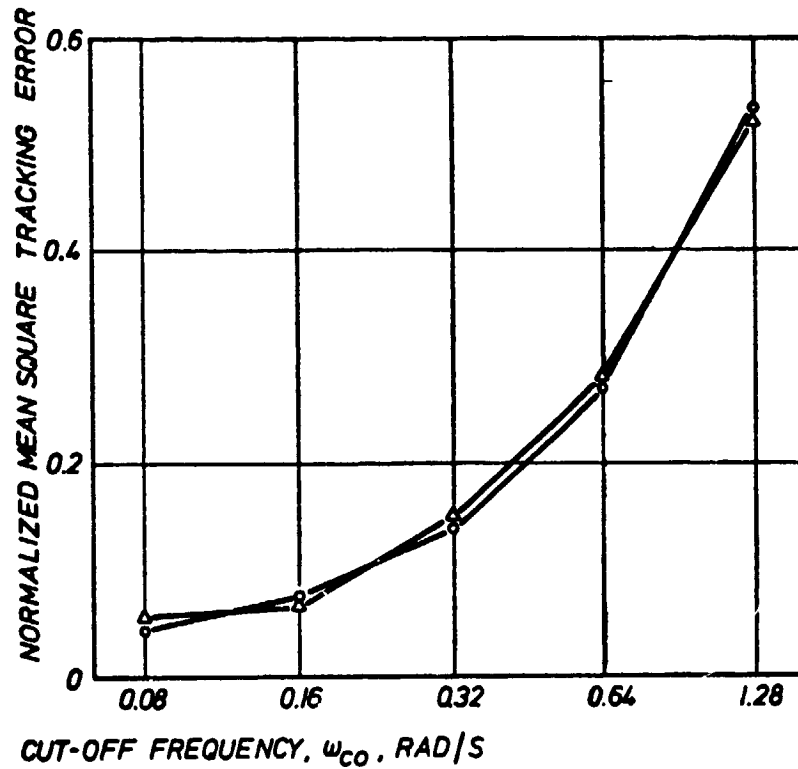
e.g.:

c ⊙ vv → four-degree-of-freedom tracking task with combined presentation of the first dimension and visual presentation of the others; plot of the results of the second dimension.



SCHEMATIC DIAGRAM OF THE TWO-DIMENSIONAL COMPENSATORY TRACKING EXPERIMENT WITH VISUAL AND COMBINED VISUAL AND AUDITORY DISPLAYS

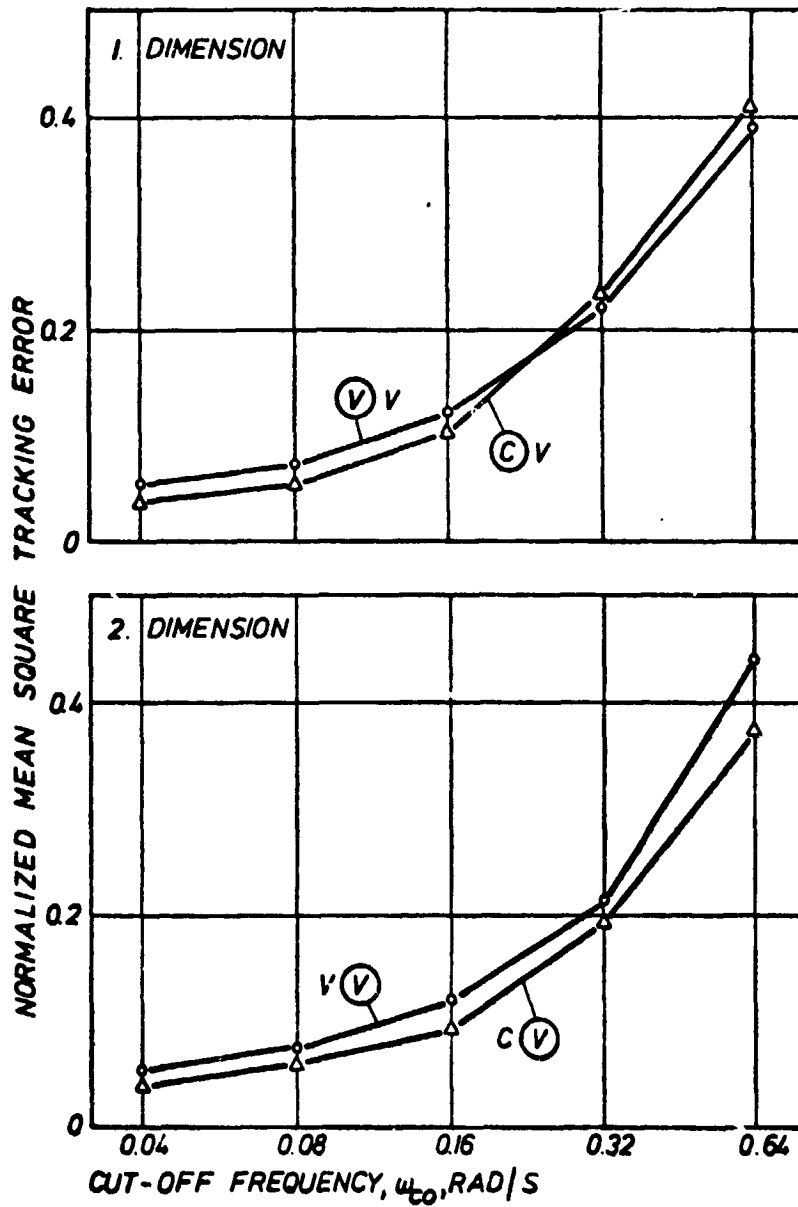
FIG. 1



EFFECT OF VISUAL AND COMBINED DISPLAYS ON NORMALIZED TRACKING ERROR, ONE DIMENSION

- - VISUAL PRESENTATION
- △ - COMBINED VISUAL AND AUDITORY PRESENTATION

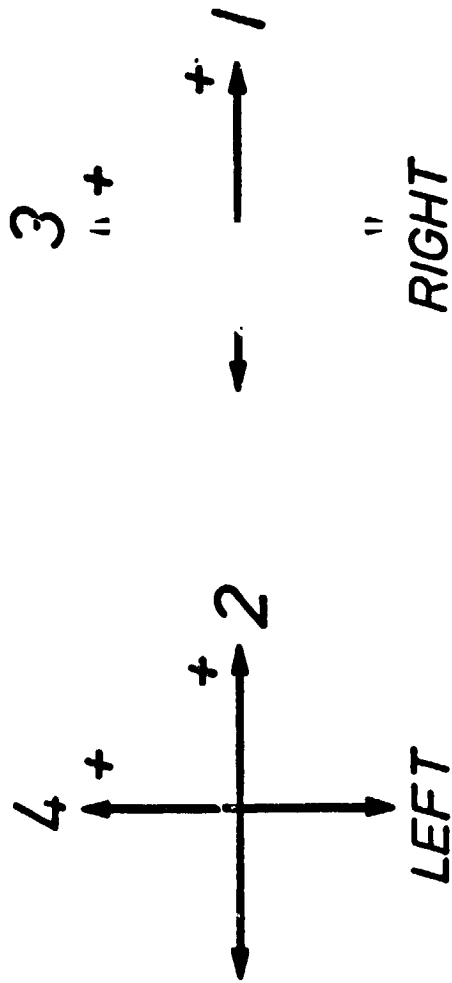
FIG. 2



EFFECT OF VISUAL AND COMBINED DISPLAYS ON NORMALIZED TRACKING ERROR, TWO DIMENSIONS

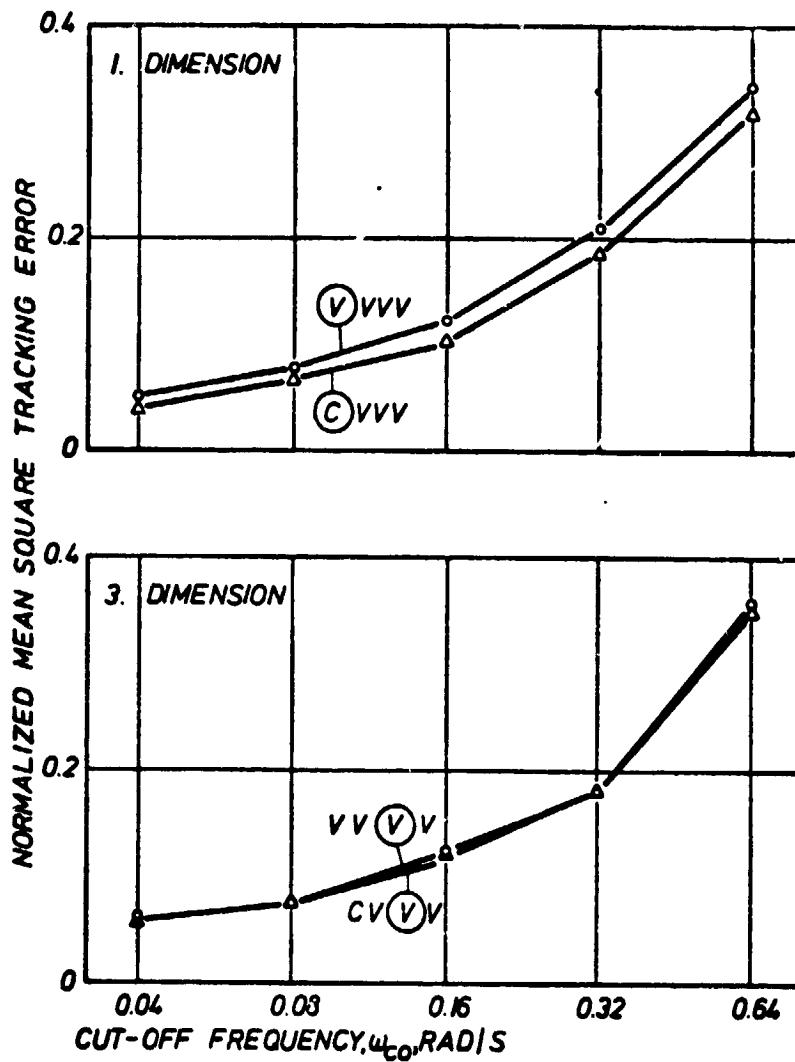
- - VISUAL ONLY
- △ - COMBINED (1. DIMENSION)

FIG. 3



CRT-DISPLAY USED FOR THE FOUR-DIMENSIONAL TRACKING
EXPERIMENT AND COMPATIBLE DIRECTIONS OF THE TWO JOYSTICKS

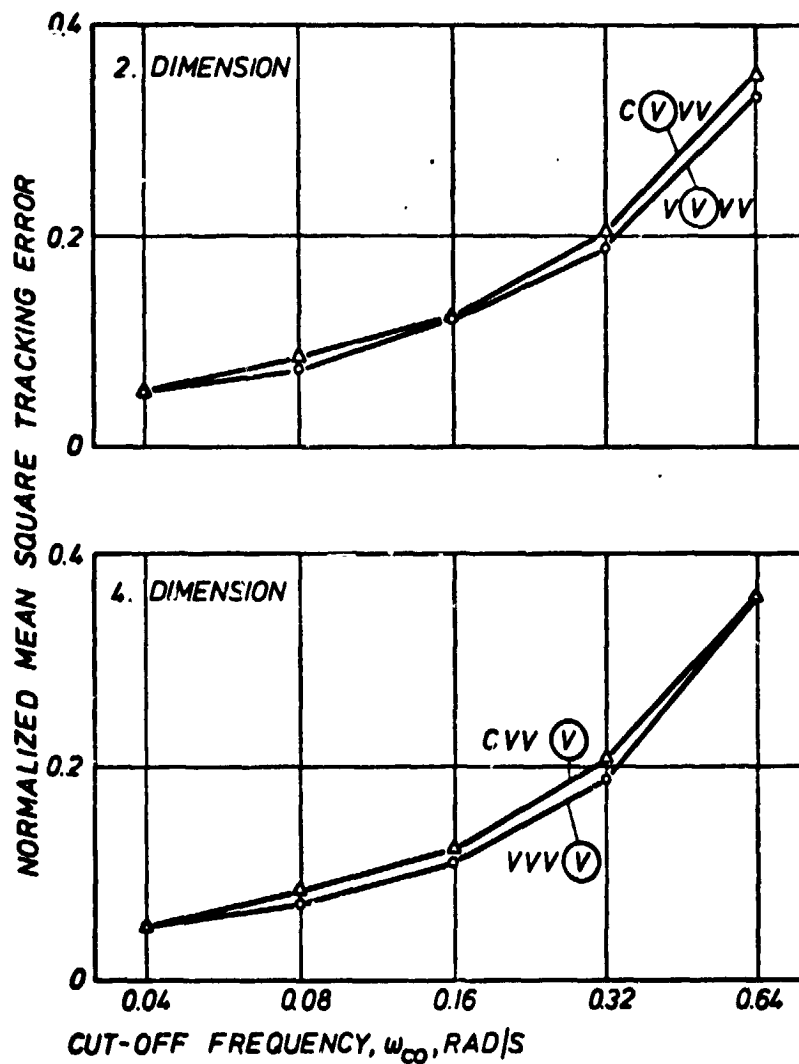
FIG. 4



EFFECT OF VISUAL AND COMBINED DISPLAYS ON NORMALIZED TRACKING ERROR, FOUR DIMENSIONS

- - VISUAL ONLY
- Δ - COMBINED (1. DIMENSION)

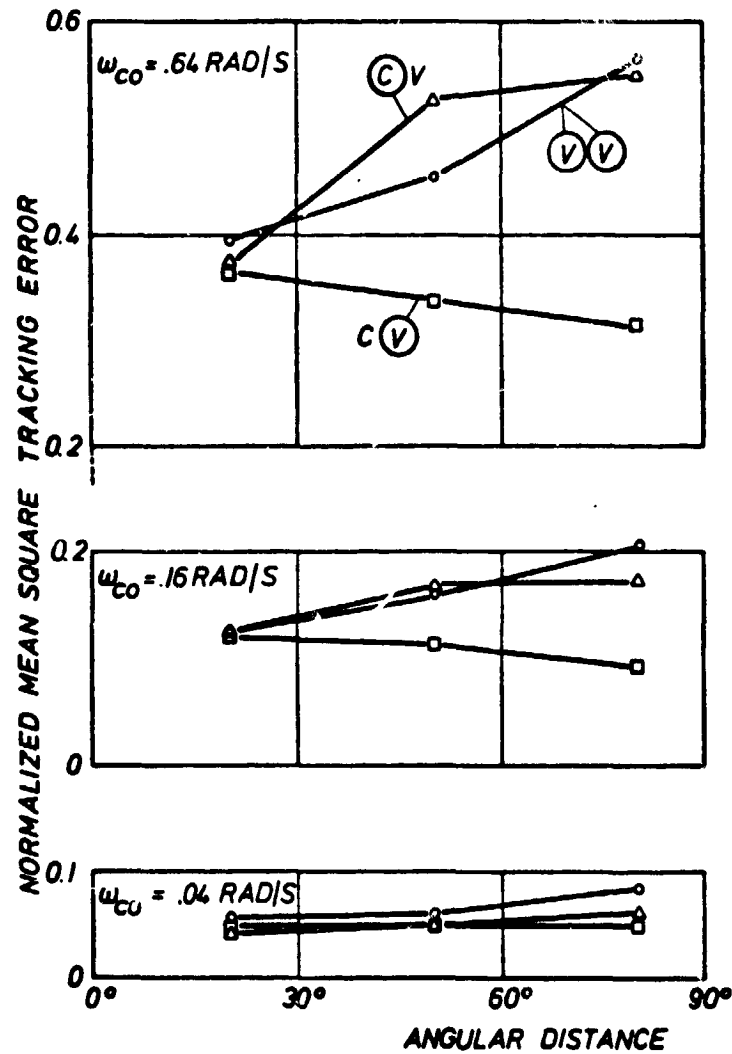
FIG. 5A



EFFECT OF VISUAL AND COMBINED DISPLAYS ON NORMALIZED TRACKING ERROR, FOUR DIMENSIONS

- - VISUAL ONLY
- △ - COMBINED (1. DIMENSION)

FIG. 5B



TRACKING ERROR VERSUS ANGULAR DISTANCE BETWEEN TWO SEPARATE DISPLAYS FOR DIFFERENT CUT-OFF FREQUENCIES OF THE INPUT SIGNAL, TWO DIMENSIONS

- - VISUAL ONLY, MEAN VALUE, 1. AND 2. DIM.
- △ - COMBINED (1. DIM.), RESULTS 1. DIM.
- - COMBINED (1. DIM.), RESULTS 2. DIM.

FIG. 6

1 N75 83677

EXPERIMENTS IN PILOT DECISION-MAKING DURING SIMULATED LOW VISTBILITY APPROACHES

Renwick E. Curry
Man Vehicle Laboratory
Department of Aeronautics & Astronautics
Massachusetts Institute of Technology
Cambridge, MA 02139

John K. Lauber & Charles E. Billings
Man-Machine Integration Branch
Ames Research Center
NASA
Moffett Field, CA 94035

INTRODUCTION

Despite a vast accumulation of operational experience with the conduct of low visibility instrument approaches, little is understood about the decision-making behavior of pilots who fly these approaches. Likewise, there is little information regarding the man, system, and task-related factors which influence this decision-making behavior. Such information is essential for the rational design of new systems, or for the redesign of existing systems in order to correct known deficiencies.

A major problem which has inhibited the study of pilot decision-making behavior in the laboratory has been the unavailability of tasks which incorporate the essential cognitive features of the real task, and which include those motivational or stress-inducing features known to influence decision-making performance. This paper describes a task which was designed to simulate the cognitive features of low visibility instrument approaches, and to produce controlled amounts of subjective stress in pilots serving as subjects in experiments using the task.

Pilot behavior during low visibility instrument approaches can be analyzed into at least two major categories: one is the continuous closed-loop manual tracking behavior necessary to control the aircraft, and the other is the cognitive, decision-making behavior required to make the decision to continue the approach and landing, or to execute a missed approach. It is the second category of behavior with which we are concerned here.

The difficulty of a decision-making task is, in part, determined by the uncertainty of the data used to make a decision. For example, the decision to "go around" is a relatively easy one if, at the missed approach point, there is nothing to be seen outside the aircraft, or if the approach lights and runway have been clearly visible for the last two miles of the approach. It is when the approach lights or runway are barely visible, and then only intermittently, that the decision-making task becomes more difficult.

A second class of variables which are known to influence the outcome of decision-making tasks is best illustrated by the various kinds of psychological stressors acting upon the pilot. Of particular interest here are the pressures perceived by the pilot to complete the approach, to make an on-time arrival, to save fuel, and even to save "face".

We have assumed that it is necessary to use a simulation task which incorporates both kinds of variables, informational and psychological, to successfully study pilot decision-making behavior in the laboratory. The task below was designed to meet those requirements. This paper describes our preliminary experiments in the measurement of decisions and the inducement of stress in simulated low visibility approaches.

METHOD

A schematic of the apparatus as seen by the pilot-subject is shown in Fig. 1. The buttons available to the subject are RVR (to request an RVR reading), turn rate buttons (left, 0, or right), and GA, the go around button to initiate a missed approach.

In the central portion of the CRT is a plan view of the approach. In the lower part of the screen are three dots corresponding to the position of the approaching aircraft (present position, position one second ago, and position 5 seconds ago). In the center of the screen are two pairs of dots corresponding to the middle marker location, equivalent to the 200 foot decision height for a Category I approach. Farther up the screen are the runway outline, threshold, and three pairs of approach lights or lead-in lights. Above that are scores posted for the results of any one trial: on this approach the subject would receive 100 points for a safe landing and -40 points for a missed approach. On the left of the screen is an RVR scale with two indices corresponding to 0 RVR and that for the legal minimum (2400 feet). On the right side of the screen is an altimeter which has a dynamic range of 0 to 220 feet. The pointer indicating altitude is pegged at the upper right until the aircraft nears the middle marker; as the aircraft passes through the middle marker, the indicated altitude passes through 200 feet.

A random wind disturbance from the side (correlation time of 50 seconds) is introduced to provide a moderately easy control task for the pilot. Control is maintained by pushing one of the three turn-rate buttons. The aircraft has the capability of being in either the 0 turn rate (constant heading) or a standard turn rate to the right or left. The pilot's task in these approaches is to "fly" the aircraft through the gate, over the approach lights, and on to the runway. (The aircraft's position shown in Figure 1 is close to the initial condition point.) Only lateral position is important, for if the pilot crosses the extended threshold line, but is not over the runway a crash is recorded. If at any time before the aircraft crosses the extended threshold line, the pilot hits the go-around button, a standard rate left turn is initiated until the heading reaches 60° from "North" at which time the computer program assumes that a missed approach was made.

The runway and approach lights may appear either to the right or left of the middle marker center line, and may be closer or farther away than the nominal position to represent electronic guidance errors. This is the appropriate aircraft-centered view, and simulates the case when one is flying the ILS with needles exactly centered, but finds the runway to the left or right when break-out occurs, and the case when one is either high or low of the indicated altitude.

The slant range "visibility" is included in the program, even though the intensity in the CRT has only two values (on, off). There are 5 "characters" drawn by the PDF-12 graphics system under visibility control: the three pairs of lead-in lights, and the right and left halves of the runway/threshold lights. Should the center of any of these five characters be within a square (centered at the aircraft position) whose half-width is the slant range visibility, then this character will be turned "on" and will be visible. The approach lights are turned off as one gets close to each pair, to simulate their passing

underneath the nose of the airplane; this also prevents the subject from obtaining unrealistic lateral guidance information.

A computer program was written to generate files of approach trajectories and currently has a catalogue of nine approach trajectories. Five of these trajectories have constant (but different) slant range visibilities leading to the following effect: when the middle marker is passed, nothing is in view; soon the first approach light appears, followed by the second and then the third; as the first approach light is neared, it disappears (passes underneath), and then the runway/threshold lights suddenly appear and a safe landing can be accomplished. The decreasing slant range visibility in this group of five trajectories is such that one must proceed farther and farther beyond the middle marker (or below decision height) before the first approach light is sighted. The fifth of these five trajectories is zero-zero visibility, so the approach lights and runway/threshold lights never appear. The other four trajectories correspond to:

- (1) a high visibility approach (runway and approach lights are visible as shown in Figure 1 at all times)
- (2) an extremely optimistic RVR reading, but very low slant range visibility
- (3) passing through a fog bank after initial acquisition of the approach lights: the approach lights and runway lights "drop out", only to reappear after three to four seconds
- (4) fog bank as in (3), but the approach and runway lights do not reappear.

PROCEDURE

In the first set of experiments, we had the following objectives:

- (1) structure the experimental setting to make the pilot as aversive as possible by a crash in the simulator as he would be in real life
- (2) to alter the decision strategies by manipulating the relative values of a landing and a missed approach.

The first objective was desirable to make the decisions as meaningful as possible. After "sacrificing" several pilots, we finally arrived at the following procedure.

As the subject is led into the experimental chamber, he is shown a poster-sized list on the wall of people who have previously been subjects in the experiment. Each subject is listed by name, organization, and score (the total number of points accumulated over the 50 data trials). The first subject on the list was a fictitious one (in this case) and in place of his point score was the word CRASHED in bright red letters. The experimenter writes in the subject's name and organization (e.g. Joe Jones, TWA) and leaves the score column blank. The subject is told at that time that should he crash during the data trials, even if on the first data trial, his services are no longer required. That is, in terms of the experiment, he is "dead".

It was obvious to the subject at this point that he was committed to follow through the experiment, and the idea that he might crash and have the event recorded for all to see had a very noticeable effect on almost all the subjects.

Each of the pilots was allowed a total of 25 practice approaches, the first 10 of which were high visibility approaches so that he could become familiar with the dynamics of the simulation, the wind and turbulence levels, and the layout of the approach lights, runway, etc. After a brief rest period, the pilots participated in the 50 data trials -- it was during these trials that a crash would mean immediate dismissal.

The 50 data trials were composed of six "wild card" approaches, e.g. the approach lights dropping out and then reappearing, or approach lights dropping out and not coming back. The remaining 44 trials were the ones examined for pilot decision-making behavior and consisted of eleven replications of four meteorological visibility levels of 0, 20, 30 and 40 display units, where a visibility of 50 corresponded to having the first approach light come into view as decision height was reached.

These 44 approaches were assigned go-around scores of 100 points for the highest visibility down through -80 points for the lowest visibility and were not assigned randomly, but in a manner which we thought would make the decision most difficult. In general, a negative score corresponded to a low visibility approach and a high positive score to the high visibility approaches.

The data recorded during each approach consisted of a "frame" composed of the current x,y position, the displayed RVR, the state of the turn-rate control and the state of the go-around button. These frames were recorded whenever a control action was executed, an RVR request made, and when the go-around button was pressed. From these data, we can infer the number of times the RVR was requested, the control activity, and the altitude and cross track error at the time of go-around should one be requested.

QUESTIONNAIRE

Thirteen pilot-subjects participated in the test and completed a questionnaire, but as the simulation was changed after the first three pilots, they were not included in the data regarding the simulation itself. Of the remaining 10 subjects, 8 are airline pilots and 2 are IFR rated NASA employees.

The questionnaire consisted of 3 major parts: recent experience in low visibility approaches and missed approaches; fidelity of the decision simulation; and stress ratings for actual low visibility approaches and the simulation.

Recent Experience

Of the 10 pilots completing the questionnaire, 7 had made a total of 37 Category I approaches within the last 12 months (six of these 37 approaches were military approaches). Only 2 missed approaches were made by these 7 pilots. When asked what were the most common causes for executing a missed approach (based on their experience), the 3 most frequently mentioned items were

runway alignment/crosswinds	7 times
visibility	5 times
other traffic	3 times

Simulation Fidelity

The subjects were asked to comment via the questionnaire about the simulator fidelity only with respect to the decision of whether or not to continue an approach. This was done both on a semantic differential scale (Totally Unlike - Completely Identical) and by soliciting comments on the similarities and dissimilarities of the simulation to an actual low visibility approach. The ratings of the subjects are shown in Table I where it is seen that the mean fidelity rating is 5.2 with a standard deviation of 1.87, indicating the usual dispersion in intersubject ratings.

Comments on the similarities of the simulation to a low visibility approach detailed the assimilation of information through different sources (RVR, altitude, and runway alignment). When commenting on the dissimilarities, 3 pilots mentioned the lack of danger ("one will not die if you miss", "... lacks the element of danger"). Two of the pilots mentioned that in a real approach more reliance would be placed on decision height, i.e., that it is a cut and dried decision (a go, no-go situation). Another commented that he felt the reward structure was not correct because in actual flight the rewards for going below minima may be the loss of job, etc, whereas reward here is a higher point count.

There were other comments made about dissimilarities of the simulator and the actual approach: three pilots mentioned that the visual cues were different, and one pilot mentioned the fixed turn rate characteristics of the simulator. Those were offered even though the question specifically asked about the similarities of decision making; either the questions were misunderstood or these factors really do influence the decision. In either case, we felt that these latter two factors are of secondary importance in the light of the other dissimilarities mentioned by the pilots.

Stress Ratings

The pilots were asked to rate the stress of the experimental task and an actual low visibility approach on a semantic differential scale (Not at all stressful - Extremely stressful); the results are shown in the other columns of Table I. We have added columns showing the difference in stress rating, and the simulator stress (rating) as a fraction of the actual stress (rating). Of these 10 subjects, three felt that the simulator was at least as stressful as an actual low visibility approach. At the other extreme, is subject number six who reported that the simulator "lacks the element of danger".

RESULTS

One pilot misunderstood the instructions because he initiated a missed approach after safely crossing the threshold many times during the 50 data trials and therefore received less than full point score. His data were not analyzed.

Learning

A statistical test was used to ascertain whether or not a learning effect was present for the subject group by performing an analysis of variance on the

pull-up altitude for those 11 approaches made under zero/zero visibility conditions. This analysis of variance included the approach number as a covariate and, if significant, would suggest a linear trend in pull-up altitude with trial number. The results of this analysis of variance indicated that the covariate of approach (trial) number did not contribute a statistically significant linear component to the pull-up altitude. Thus the linear trend was ignored in the remainder of the analyses.

Classification of Approaches into Land/Go-Around

The 44 approaches for each of the 9 pilots were examined for classification into the classes of land/go-around using a stepwise discriminant analysis program (BMD 07M). The variables included for the selection in the stepwise discrimination were the following:

$(V/V_{MAX})^n$	n = 1,2,3	Actual visibility on the approach ($0 \leq V/V_{MAX} \leq 1$)
$(S/S_{MAX})^n$	n = 1,2,3	Score increment for selecting a go-around ($-0.80 \leq S/S_{MAX} \leq 1.0$)
$(V/V_{MAX})(S/S_{MAX})$		Interaction between visibility and score
LOC		Visible localizer deviation at go-around

The linear, quadratic, and cubic component of visibility and go-around score are self explanatory and the interaction term was included to test for its significance. The localizer deviation was also included and taken to be the maximum visible localizer deviation. It was set to 0 on the 0/0 approaches since it would not be available to the pilot, and was also set to zero on the approaches which were successfully completed.

The significant variables selected by the stepwise discriminant program are shown in Table II for each subject; these coefficients have been normalized so that the coefficient of V/V_{MAX} is unity. In this table, an increase in the discriminant function will put the approach into the "land" class. The resulting classification using this discriminant function is also shown in the table and it gives very good results on these data (although one must be cognizant that the classification is performed on the data from which the discriminant function was determined.)

The major points to be ascertained from the table are first, the go-around score was almost useless as a basis for discriminating among approaches with the exception of Subject number 6. (This particular discriminant function must be treated with care since it incorporates almost all the variables and includes a sign of V/V_{MAX} which is opposite from all the other discriminant functions.) The second point of interest is the nearly equal coefficient on the quadratic component of visibility, indicating the decrease in effectiveness of actual visibility in classifying an approach into "land". Thus the

contribution of visibility to the discriminant function varies from 0 (for V/V_{MAX} of 0) to 0.4 (for $V/V_{MAX} = 1.0$) for most subjects.

The coefficient for the localizer deviation can be used to determine the sensitivity of the cross-track error in classifying approaches into "land" or "go-around". This result is shown in the right hand column of Table II and is the localizer error (in degrees) which has the same effect on the discriminant function as a full-range change in slant range visibility. This gives the importance of localizer error relative to visibility in determining the classification.

A DYNAMIC DECISION MODEL

In this section, we briefly describe a decision-theoretic approach to the modelling of pilot decisions during the simulation of low visibility approaches. A straightforward application of the Subjective Expected Utility (SEU) theory is complicated by the dynamic character of the decisions since the theory relates to static decision alternatives, rather than the everchanging situations experienced by pilots. Nonetheless, we have developed an extension (based on SEU models) which appears to be plausible, and it is one which we think will be a valuable tool in further investigations.

The dynamic decision model is based on the assumption of the existence of a decision function which can be written

$$D(V,S,L,h) = \bar{U}_{LAND} - \bar{U}_{GA} \quad (1)$$

where D is the decision function, an explicit function of visibility (V), go-around score/incentive (S), the cross-track or localizer deviation (L), and the current altitude (h). This decision function is the comparison of the SEU for \bar{U}_{LAND} and the SEU for making a missed approach or a go-around \bar{U}_{GA} . Under the assumption that the utilities for landing, crashing, and going around are independent of the probabilities, Subjective Expected Utilities take the form

$$\bar{U}_{LAND} = P_{LAND}(V,L,h)U(LAND) + P_{CRASH}(V,L,h)U(CRASH) \quad (2)$$

$$\bar{U}_{GA} = 1 \cdot U(GO AROUND) = U(S) \quad (3)$$

where P_{LAND} and P_{CRASH} are the subjective probabilities for landing and crashing and $U(\cdot)$ is the corresponding utility. These expressions show the dependence on the approach variables V , L , h and the incentive for going around S .

A schematic plot of the decision function and how it might change with altitude is shown in Figure 2. We have displayed possible variations of \bar{U}_{LAND} during an approach and its comparison with \bar{U}_{GA} which remains constant throughout the approach. If at any time the SEU of landing becomes less than that of going around, the decision is made to initiate a missed approach.

A missed approach, denoted by the solid line of Figure 2, is a sketch of how the SEU of landing might behave during an approach for which the approach lights are never sighted. The SEU of landing decreases with altitude because the subjective probability of landing is decreasing (and that of crashing is increasing) until, at point A, a missed approach is initiated. The SEU of an

approach shown by the dotted line starts out higher than the previous approach (perhaps because of a larger reported RVR) and it, too, decreases until point B when the approach lights are sighted. This causes an immediate jump in the probability of landing (hence the step change in SEU of landing) and from this point gradually increases until point C when the landing is successfully accomplished. If, on the other hand, the aircraft starts deviating from the localizer (say) at point D, and the pilot has difficulty in stabilizing the approach, then the subjective probability for landing will decrease causing a decrease in the SEU for landing until point E where a missed approach is initiated because of misalignment with the runway.

The point of greatest interest, of course, is at the instant of deciding to initiate a missed approach. At this instant the SEU of landing and go-around are equal, i.e.

$$U_{\text{LAND}}(V, L, h^*) = U_{\text{GA}}(S) \quad (4)$$

where h^* is the altitude at which the go-around decision was made and is written

$$h^* = g(V, L, S) \quad (5)$$

To test for the possible existence of such a relation, we performed a stepwise regression (using BMD 02R) on the go-around score (S/S_{MAX}), score/visibility interaction ($S/S_{\text{MAX}}(V/V_{\text{MAX}})$), and the localizer deviation (L). The main effects of meteorological visibility were not included because the majority of the go-around decisions were made under 0/0 visibility conditions. Table III shows the regression coefficients selected by the stepwise regression program; those coefficients which have a non-zero value as indicated by Student's t test are indicated with an asterisk. Note that the data for subjects 2,3,4 are not included because the stepwise regression program did not find a significant regression on the variables indicated. The multiple regression coefficient is highest for those cases for which few go-around decisions were made during approaches when any visibility existed (recall that 11 of the approaches shown were made under 0/0 conditions). While the coefficients indicate the type of behavior one would expect, e.g. an increased decision altitude due to increased go-around scores, these data must be considered preliminary because of the experimental design (see the discussion section).

These results are quite encouraging and indicate that the subjectively expected utility model proposed here may lead to a valuable viewpoint from which to examine pilot decision making during low visibility approach.

SUMMARY

Stress

One of the major goals outlined for this preliminary set of experiments was to investigate methods of applying psychological stress analogous to the stress of an actual low visibility approach. It was found that the stress rating in the simulation, as reported on semantic differential scales, was an average of 0.8 times the stress rating of an actual low visibility approach. The success in applying the stress was not uniform, however, for several

subjects reported they "would not die" if they crashed in the simulation. Other subjects remarked that descending below the decision height of 200 feet would result in censure by regulatory or company authorities; this seemed as important to them as the prospect of an (unlikely) crash. Thus it may be meaningful to include another penalty in the simulation; if the subjects are "caught" descending below minimums, they will be penalized (say) by a score equivalent to two or three landings.

Go-Around Incentives

The range of go-around scores did not induce as much behavioral change as was expected, and the results of the experiment indicate that considerably more score differential will be required to induce pilots to initiate a missed approach. For example, when offered 100 points for the no-risk go-around or 100 points for a successful landing, most pilots initiated the approach and almost all continued until touchdown, even though a riskless go-around was available. This suggests that the utility of landing is strongly affected by the accomplishment of this feat, or that the level of risk taking in a go-around is too low and this alternative does not present enough of a challenge to the pilots.

Behavioral Models

One model of behavior which may apply here is the Theory of Achievement Motivation (Atkinson, 1964). This model is of a form similar to the SEU model described above except that the utilities depend on the subjective probabilities: for example, the utility of succeeding at an easy task is low, while succeeding on a difficult (high risk) task is high. Conversely, the utility of failing on an easy task is low (one loses face), whereas there is no disutility (loss of face) on failing to succeed on a risky task. Risk taking behavior is said to be determined by two personality traits; need for achievement and test anxiety. The Theory of Achievement Motivation predicts that those individuals with a high need for achievement and a low test anxiety will take an intermediate level of risk, whereas individuals with a low need for achievement and high test anxiety will take extreme levels of risk: a low level of risk to insure success, or a high level of risk in which success is not really expected. Atkinson draws analogies to aspirations in employment as well as more quantitative behavioral tests such as the "ring toss" experiment. We have conducted some informal experiments at MIT using a ball-toss paradigm involving two levels of difficulty; the results of this undergraduate student project will be reported elsewhere.

A preliminary attempt was made to apply the Theory of Achievement Motivation to the experimental results described above. An obvious measure of test anxiety is the stress ratio recorded by the subjects (stress in the simulation/ stress in actual low visibility approach). Measures of success and need for achievement are ambiguous, however, since point score and number of landings may be considered as measures of both.

Nonetheless, if one considers (a) the final score as a measure of success; (b) the stress fraction as the measure of test anxiety; and (c) the number of landings as the measure of the need for achievement (e.g. sticking with an

approach through approach light dropout, etc.), then classification of the pilots on this basis (b) and (c), indicates the following: the pilots with the lower success level (lower score) exhibited a low need for achievement and high test anxiety (as the theory predicts), but the pilots with a higher success level (higher score) exhibited not only a high need for achievement but a higher stress level (rather than the theoretically predicted low stress). Although there are not enough subjects to validate this conjecture statistically, it may well be that the Theory of Achievement Motivation is not applicable in those cases where the result of the failure is catastrophic, and that modification to the theory may be required for situations such as are considered here.

In summary, both a dynamic version of Subjective Expected Utility Models and (a modified) Theory of Achievement Motivation may be useful in describing decision behavior of pilots in a simulated low visibility approach.

REFERENCES

Atkinson, J.W. An Introduction to Motivation, Princeton, N.J.:Van Nostrand, 1964.

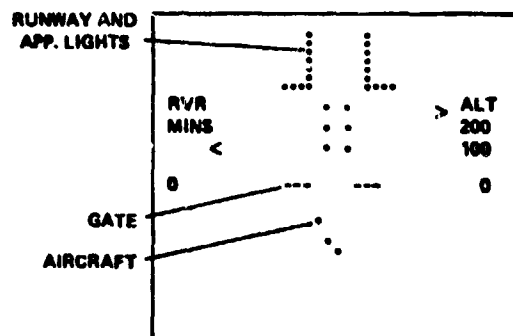


Figure 1 Subject's display panel

Subject/ Organiza- tion	Simulator Fidelity Rating	Stress Rating -Actual Approach	Stess Rating Simulator	$S_{SIM} - S_{ACT}$	$\frac{S_{SIM}}{S_{ACT}}$
1/A	7	3	2	-1	.67
2/B	7	4	6	2	1.50
3/C	3	7	3	-4	.43
4/B	3	8	5	-3	.62
5/B	7	8	6*	-2	.75
6/A	4	7	2	-5	.28
7/A	7	6	6	0	1.00
8/C	6.5	5.5	5.5	0	1.00
9/D	2.8	7	4	-3	.57
10/D	5	8	6.5	-1.5	.81
Mean	5.23	6.35	4.60	-1.75	.763
S.D.	1.87	1.73	1.73	2.01	.344

* Indicated a change to 2 later in the trials

TABLE I Semantic differential ratings of simulator fidelity and stress

SUB	$\frac{V}{V_{MAX}}$	$\left(\frac{V}{V_{MAX}}\right)^2$	$\left(\frac{S}{S_{MAX}}\right)$	$\left(\frac{S}{S_{MAX}}\right)^2$	$\left(\frac{S}{S_{MAX}}\right)^3$	$\left(\frac{S}{S_{MAX}}\right)\left(\frac{V}{V_{MAX}}\right)$	LOC	CLASSIFICATION G R O U P L L G L G	LOCALIZER DEVIATION EQUIVALENT TO FULL VISIBILITY CHANGE
1	1.0	-0.155				-0.352	-0.0185	23 0 1 20	45.6°
2	1.0	-0.650					-0.00432	31 0 0 13	81.0°
3	1.0	-0.507	-0.065			-0.180	-0.0109	33 0 0 11	45.0°
4	1.0	-0.673					-0.0045	29 0 1 14	72.6°
5	1.0	-0.746					-0.00695	30 0 1 13	36.1°
6	-1.0	1.34	0.650	0.14	-0.417	-0.793	-0.0066	23 0 0 21	51.2°
7	1.0	-0.619					-0.00848	29 0 0 15	44.3°
8	1.0	-0.695	-0.101				-0.00679	27 0 1 16	44.9°
9	1.0	-0.635					-0.0088	30 0 1 13	41.5°

Table II Coefficients of Discriminant Function (Normalized such that $|V/V_{MAX}| = 1.0$)

SUB	CONST	$\frac{S}{S_{MAX}}$	$\left(\frac{S}{S_{MAX}}\right)^2$	$\left(\frac{S}{S_{MAX}}\right)^3$	$\left(\frac{S}{S_{MAX}} \frac{V}{V_{MAX}}\right)$
1	98.6	124*	45*	-106*	9.1
5	17.3	-143.3*	-136.7*		318*
6	44.9	30.6	66.5*	19.7	-62.8
7	101.0	245*	41.3*	-185*	
8	71.3	111.6*	10.1	-93.6*	-140*
9	-17.4	-78.5		79.1*	-44.4*

	LOCALIZER	MULTIPLE ρ	σ_e (ft)	N
1	1.41*	0.77	16.1	21
5	-0.070	0.92	10.5	14
6		0.69	26.5	21
7	-3.83*	0.97	5.0	15
8	-0.32	0.91	10.5	17
9	1.02	0.94	6.2	14

TABLE III Regression coefficients for altitude of go-around decision

N75 22678

TRACKING PERFORMANCE UNDER TIME SHARING CONDITIONS

WITH A DIGIT PROCESSING TASK: A FEEDBACK CONTROL THEORY ANALYSIS¹

By Daniel Gopher and Christopher D. Wickens

University of Illinois at Urbana-Champaign

ABSTRACT

A one dimensional compensatory tracking task and a digit processing reaction time task were combined in a three-phase experiment designed to investigate tracking performance in time-sharing. The two tasks were compared when performed singly and in combination both with equal sub-task priorities, and with different combinations of unequal task priorities. Adaptive techniques, elaborate feedback devices, and on-line standardization procedures were used to adjust task difficulty to the ability of each individual subject and manipulate time sharing demands. Feedback control analysis techniques were employed in the description of tracking performance. The experimental results show that when the dynamics of a system are constrained, in such a manner that man-machine system stability is no longer a major concern of the operator, he tends to adopt a first order control describing function, even with tracking systems of higher order. This particular linear strategy may reflect the low level of practice, or limited system knowledge of the current subjects. It is accompanied by a second non-linear strategy which appears as a component of high frequency remnant power, and seems to be adaptive, in the sense that it reduces tracking error. When attention is divided between tracking and a concurrent task, tracking gain appears to decrease by a magnitude that is proportional to the amount of attention diverted to the concurrent task. Attention diversion to a concurrent task leads to an increase in remnant level, or non-linear power. This decrease in linearity is reflected both in the output magnitude spectra of the subjects, and in the linear fit of the amplitude ratio functions. Processing time does not appear to be affected in any consistent manner by performance requirements on the tracking task, although it is affected by the change of demands on the concurrent performance task.

¹ Contractual support for this project was provided by the Life Sciences Program, Air Force Office of Scientific Research, Contract Number F44620-70-C-0105. Dr. Charles E. Hutchinson was the scientific monitor of the contract.

INTRODUCTION

In real world situations, a manual control task is only rarely performed in isolation from other tasks that may be imposed upon the operator. Furthermore, in these situations, the priorities and demands of the concurrent performed tasks are frequently shifting, contingent upon the dynamically changing operational environment. The present study investigated tracking behavior in dual-task situations and utilized feedback control analysis, coupled with new experimental procedures to manipulate time sharing priorities, in order to specify the nature of time-sharing decrements in tracking performance.

While feedback control analysis has proven to be of great value to the human factors engineer, allowing the specification and prediction of stability and performance characteristics of manually controlled vehicles, it has also proven to be of interest to psychologists. This is because many of the parameters that are measured in the transfer function, or describing function of the human operator, appear to have very real psychological meaning; that is, these parameters correspond to processes, such as reaction time, and information transmission rate that are important aspects of human information-processing behavior. Given this correspondence between the describing function parameters on the one hand, and behavioral phenomena on the other, along with the increasing ease of measuring the describing function parameters, as new algorithms are developed, it is of interest to the psychologist to observe the changes in these parameters that take place when various experimental conditions, such as stress, practice, or time sharing are manipulated. In this manner, indications of the fundamental changes in human information processing that underlie such manipulations, can be revealed. Furthermore, a knowledge of the specific processing changes underlying performance in multi-task environments, may have important implications for the design of systems, particularly if these changes lead to an overall deterioration in system performance.

Although a large volume of research has been conducted concerning feedback-control analysis of human tracking behavior (1), and an equally voluminous amount has utilized the tracking paradigm in some aspects of divided attention research (2), relatively few studies have systematically examined the effects of divided attention on the specific performance parameters of tracking that are revealed by a feedback control analysis. Furthermore, no study has coupled such an analysis with a careful experimental control and manipulation of the allocation of attention between tracking and a subsidiary task.

Those studies that have examined the effects of divided attention on tracking unanimously reveal that tracking performance, as assessed by such global measures as mean-squared error, or time-on-target, deteriorates under time sharing (divided attention) conditions. However, beyond this, there seems to be little consistency concerning the specific parameter changes underlying this increase in tracking error. Since increases in error may theoretically be produced by increases in time-delay or remnant,

decreases in tracking gain, or a change in the form of the transfer function, any of these parameter changes could plausibly underlie the divided attention increase in tracking error.

In the psychological research on attention, the effect upon information processing that is most commonly attributed to the division of attention, is an increase in processing time, or time-delay. Thus it seems reasonable that divided attention in tracking should produce an increase in the measured parameter assumed to correspond to processing time: effective time delay, or τ_e . An experiment by Cliff (3) obtained this effect when tracking was performed concurrently with an auditory shadowing task, while a variety of research performed with the Critical Tracking Task (4), has obtained consistent decreases in the stability parameter λ (corresponding to an inverse measure of the subject's effective time-delay) under divided attention conditions (5, 6).

In fact, McRuer (7) has found that this measure correlates quite highly with the subjectively rated difficulty (the Cooper-Harper rating) of a concurrently performed task and has therefore argued that tracking time-delay (as assessed by the Critical Task) is an accurate predictor of "reserve processing capacity" -- the amount of attention or capacity "left over" to devote to the critical task, after an amount of attention has been channeled to the primary task to maintain some fixed performance criterion.

Despite these findings, however, the occurrence of processing delays in tracking under time-sharing has not been universally observed. For example, Watson (8) found only very slight increases in processing time (as assessed by open-loop operator phase lag) when subjects were required to perform auditory and visual secondary tasks, and Levison, Elkind, and Ward (9) similarly obtained little increase in phase lag with time sharing, as additional tracking tasks were required to be performed by their subjects. Wickens (10) found no increase in the measured parameter τ_e , under time-sharing, although he obtained a clear performance decrement in mean-squared error when the secondary tasks (signal detection, and application of a constant force) were required.

A more robust effect of time sharing on tracking appears to be an increase in remnant, or output power uncorrelated with input, which has been obtained, in one form or another, in many of the dual-task tracking studies (8, 9, 10, 11). Although remnant may arise from a number of potential sources, some of which may in fact be adaptive or beneficial to tracking performance (i.e., discrete, or "bang-bang" control responses), Levison et al. (9) have argued that the remnant increase resulting from their time-sharing conditions is a non-adaptive, perceptual-motor "noise," added to the tracking signal and is the major contributor to the decrement in performance.

Four studies have also identified clear and consistent decreases in the open-loop gain parameter, under time-sharing. Wickens (10) and Baty (11) both found a large, significant decrease in crossover frequency, as secondary tasks were introduced, while data from Levison et al., (9) and

Cliff (3) indicate that the overall open-loop amplitude ratio function is reduced when additional tasks (concurrent tracking, and auditory shadowing respectively) are imposed.

Finally, without the benefit of a formal feedback control analysis, Fuchs (12) observed, using an analog model matching algorithm, that subjects give relatively more weight to lower derivatives of the error signal under time-sharing. Fuch's finding may be interpreted as indicating that a change in the overall form of the transfer function (adjustment of lag or lead constants) results from divided attention, in addition to any shift in operating parameters that might take place.

The above studies provide varied, and sometimes conflicting findings. The current research is an attempt to identify more precisely what parameter changes do occur in tracking under time-sharing. Furthermore, it was hoped to identify which, if any parameters are sensitive, not only to the presence or absence of a second task, but to the amount of attention allocated to the tracking task. (Conversely, assuming a limited amount of attention, the amount of attention diverted to a second task.)

The design of the experiment is based on a method developed by Gopher and North (13, 14, 15) for the evaluation of operator attention capacity and task load in time-sharing conditions. The method originates in the traditional secondary task approach (16, 17). However, major modifications of this paradigm are proposed. In the present method, pairs of tasks are compared in single- and dual-task combinations. Adaptive techniques, on-line standardization procedures and elaborated feedback devices are utilized to adjust task difficulty to the performance ability of each individual subject and manipulate inter-task priorities in time-sharing. The method allows the examination of three separate questions: (1) The ability of subjects to perform a single focused attention task with gradual increase of difficulty. (2) The general ability of subjects to cope with time-sharing requirements in dual-task configurations. (3) The ability of subjects to mobilize and readjust the allocation of attention with a change in task priorities. In the present experiment a one-dimensional compensatory tracking task was combined with a digit processing reaction time task.

Identification of parameters which would quantitatively reflect attention allocation as related to the above three aspects would not only provide valuable information concerning the nature of attention in information processing, but also might suggest predictive methods of monitoring momentary fluctuations of operator attention via on-line measurement of performance output. This could provide a valuable feedback loop, to alert the operator if attention (as measured by the parameter in question) falls below a specified value.

METHOD

Subjects

Twenty-four naive subjects participated in the experiment. All were males, students, with no previous experience in flight or laboratory tracking tasks. The average age of the subjects was 22 years ranging from 18 to 28.

Apparatus

Figure 1 presents the general experimental layout of the study. The equipment included a Raytheon 704 digital computer which generated inputs to a cathode-ray tube (CRT) display and processed signals from a decimal keyboard and a manual tracking controller. The computer provided digital signals to a symbol generator that converted them to analog inputs to draw displays on a Hewlett-Packard, 4 (10.03 cm) x 3-(7.56 cm) inch, Model 1300A CRT for the digit processing and tracking tasks. A light-touch 4 x 3 matrix keyboard produced digital signals for direct input to the computer. The controller used in the tracking task was a spring-centered, linear dual-axis hand control, that required a 23 oz. breakout force and 30 oz. pressure to maintain a full deflection. Only lateral control motion was involved, and the range of possible lateral deflection was ± 35 degrees (controller gain in the present experiment was $10^\circ/1$ cm. for unit gain). An auditory warning device generated two distinct tones to provide performance feedback for the individual tasks. The display and control devices were located in a sound-attenuating performance booth with controlled ventilation and lighting.

Peripheral devices used to input subject information and experimental conditions and to print out information on subject performance included a magnetic tape drive, a card reader, a Gould 4800 electrostatic line printer, and an on-line ASR-33 teletype.

The computer program included three modes of operation. In mode 1, identification information for each subject and the selection of the experimental phases were input via the teletype and card reader. Mode 2 included the generation of the displays and processing of subject performance. Mode 3 generated plots and tables on the line printer. At the termination of this sequence, the program returned to mode 1 for further instructions. Three real-time cycles in mode 2 included one of 20 msec. to refresh the display; one of 60 msec. to process inputs from the keyboard and manual controller and to calculate information used in the refresh cycle, and a one-second cycle to keep track of elapsed time in each phase, to terminate the session or make an appropriate change in conditions during a phase, and to record performance information calculated during the 60 msec. cycle.

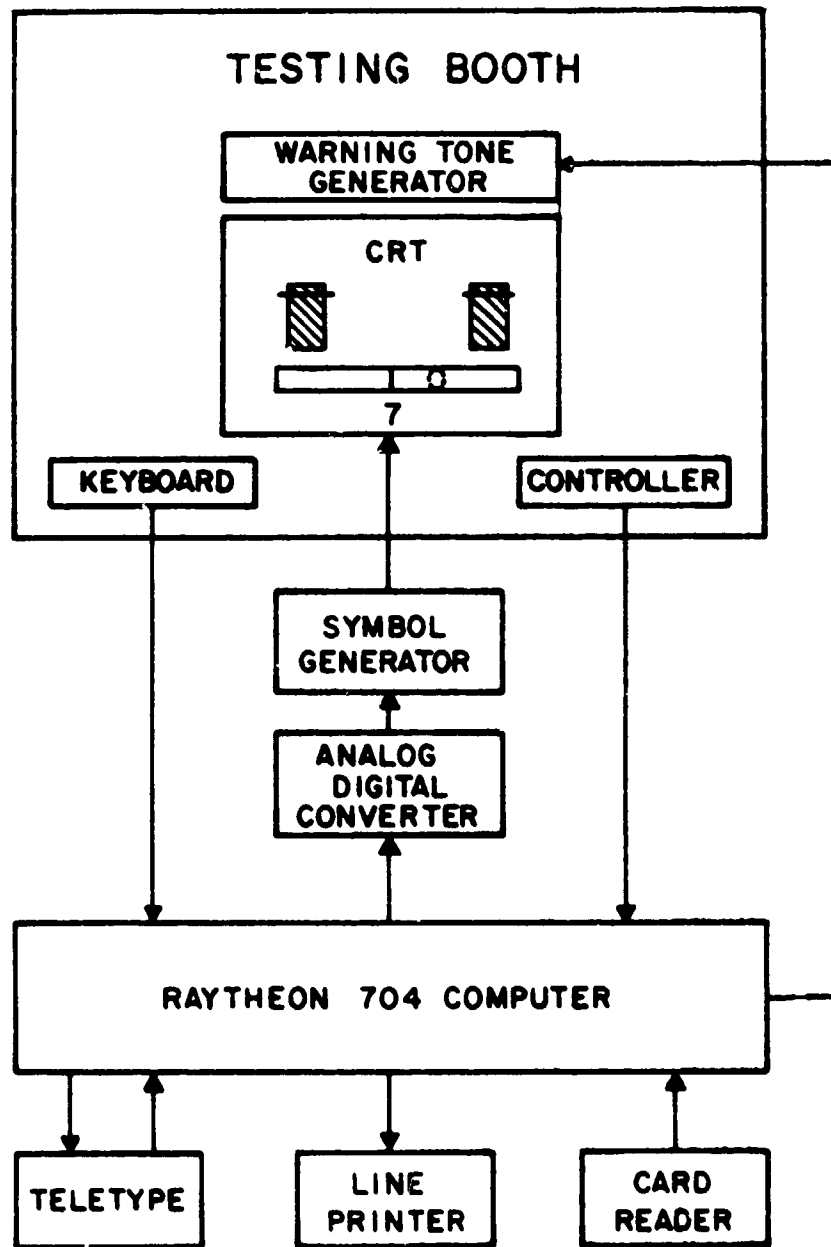


Figure 1. Equipment interfaces in the experiment.

Procedure

Phase 1 tracking. The subject performed a one-dimensional compensatory tracking task for a four-minute period during which system dynamics were adaptively manipulated to increase and decrease task difficulty. This was accomplished by adjusting the relative portions of first and second-order determinants according to the error output of the subject. This adaptive variable was originally suggested by Ince and Williges (18) and has been applied to adaptive training by Gopher, Williges, Williges, and Damos (19) and to adjustment of task difficulty by Gopher and North (14).

The subject was asked to keep a moving circle in the center of a horizontal bar by left-right movements of the controller. A random-noise band-limited disturbance with a cutoff frequency of two rad./sec. was added in parallel with the stick inputs (disturbance frequency was controlled by a fifth-order digital filter which created a -6 dB/decade slope within the bandwidth and -20 dB/decade slope above the cutoff frequency).

Figure 2 presents a block diagram of the tracking system. The figure shows the first and the second integrators and their respective gains and the values α and $1-\alpha$ which determined the relative portions of first and second integrations. Each integrator was followed by a limiter which constrained its maximum output such that the tracking symbol could not go off the screen and could not exceed a certain velocity. The system was thus inherently stable. This was necessary to protect the continuity of the experiment and constrain the task to the general ability of the naive subjects. Within the limits the system revealed the characteristics of a linear first order, second order or mixed system. Error tolerance was .10 of scale absolute error. The step size of the adaptive variable α was .0005 per 60 msec. cycle. After four minutes of adaptive adjustment α was fixed at the value reached by the subject, and he was given an additional two minute period of tracking during which RMS errors were recorded over 10 sec. intervals. Data points for the control feedback analysis were recorded before the operator and after the controller to model the subject.

Phase 1 digit processing. Random single digits between zero and nine were presented on the CRT display and were cancelled by the subject by pressing the corresponding digit on the keyboard. When a digit was correctly cancelled, a new digit immediately appeared as generated by the computer (delay was 60 msec.). Average latency was computed for successive blocks of five trials. The subject was stopped as soon as the difference between two successive five trial blocks was less than five percent, but not before the subject performed a minimum of 20 trials. Average and standard deviation were computed for the final ten trials of this task. Values for both tracking and digit tasks were stored in the computer for use in Phase 2.

Phase 2. In Phase 2 (five minutes) the subject was instructed to perform both tasks simultaneously to the best of his ability with equal task priorities. The acceleration percentage of the control stick and the generation rate of new digits (in the case of no response) were those that

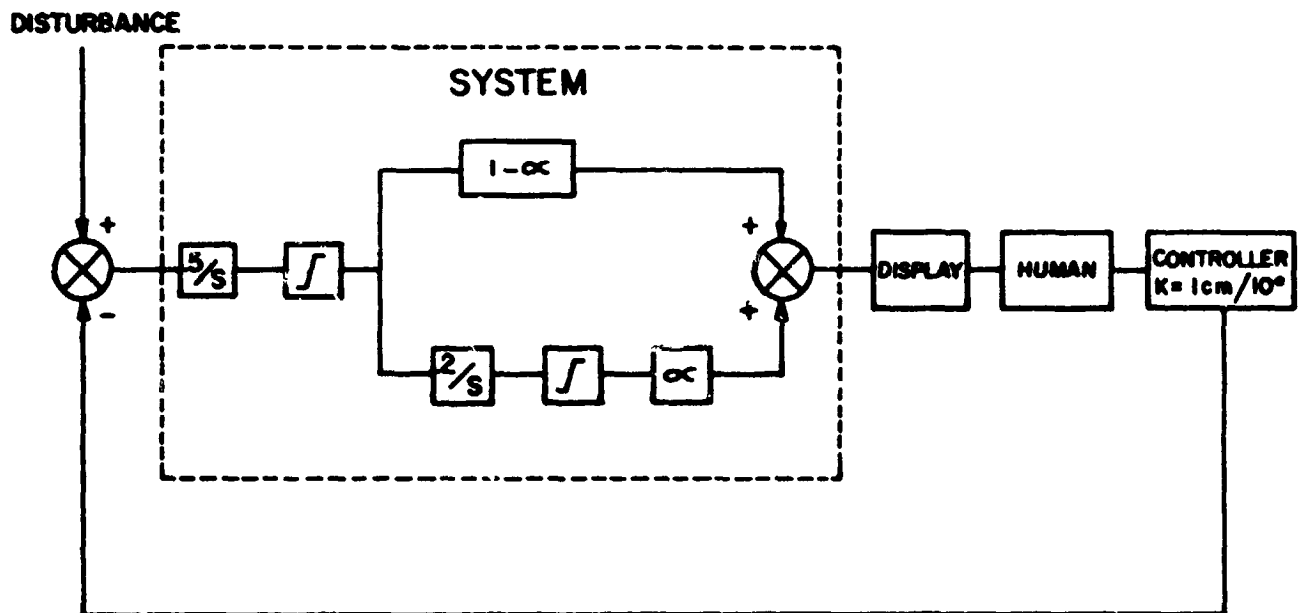


Figure 2. One-dimensional, adaptive, compensatory tracking system.

were obtained by each subject in the single task performance. In addition to the tracking display and the digits, this phase included a visual feedback indicator for each task which appeared as a bar graph varying in height contingent upon performance. This performance bar could move vertically from a zero point toward the top of the display. The desired level of performance was indicated by a short horizontal line positioned about half the distance from the zero point to the top of the display. This line represented the average of the single-task performance recorded in Phase 1 for each subject.

Thus, if this average is regarded as an estimate of subject's maximum ability, Phase 2 imposed a double-load on the subjects. The distance on the display from the zero point (no bar graph showing) to the desired performance line was 2.5 standard score units, computed by subtracting the momentary tracking error score, or digit latency response in Phase 2, from the average score of Phase 1 and dividing this difference by the standard deviation about the subject's own mean in Phase 1. The performance bar for the tracking represented integrated error over ten second periods, while blocks of five trials were averaged for the digit task performance bar. Figure 3 depicts the general form of the display in this phase.

In addition to the visual feedback, an auditory warning was used to indicate an error score or a latency score 1.65 standard units below Phase 1 performance. Separate, highly discriminable tones were used to signify degraded performance on each task. Performance measures were stored by the computer for tabular and graphical output and used in Phase 3.

Phase 3. Phase 3 was identical to Phase 2 in task structure. However, the desired level of performance and standard deviation used in manipulating the performance bars and auditory warning now reflected the performance in Phase 2 instead of Phase 1. An additional manipulation in Phase 3 included the presentation of different desired performance levels by changing the height of the desired performance line on the display. The investigation of the effect of these changes was conducted in five sub-phases. Increased requirements, indicated by a higher desired line, actually required the subject to perform at .53 standard units better than his average performance in Phase 2 (20 percent increase in performance), while decreased requirements, indicated by a lowered desired line, required a performance .53 standard units below his average (20 percent decrease in performance). The five experimental conditions in this phase included increased demand on one task with the other remaining at the Phase 2 average level (two conditions, labeled 3B and 3C), and increased demand on one task with decreased demand on the other (two conditions, labeled 3D and 3E). The fifth condition (3A) represented the equal performance demand situation, and was identical to the display in Phase 2. The order of presentation of conditions 3B, 3C, 3D, and 3E was counterbalanced among subjects.

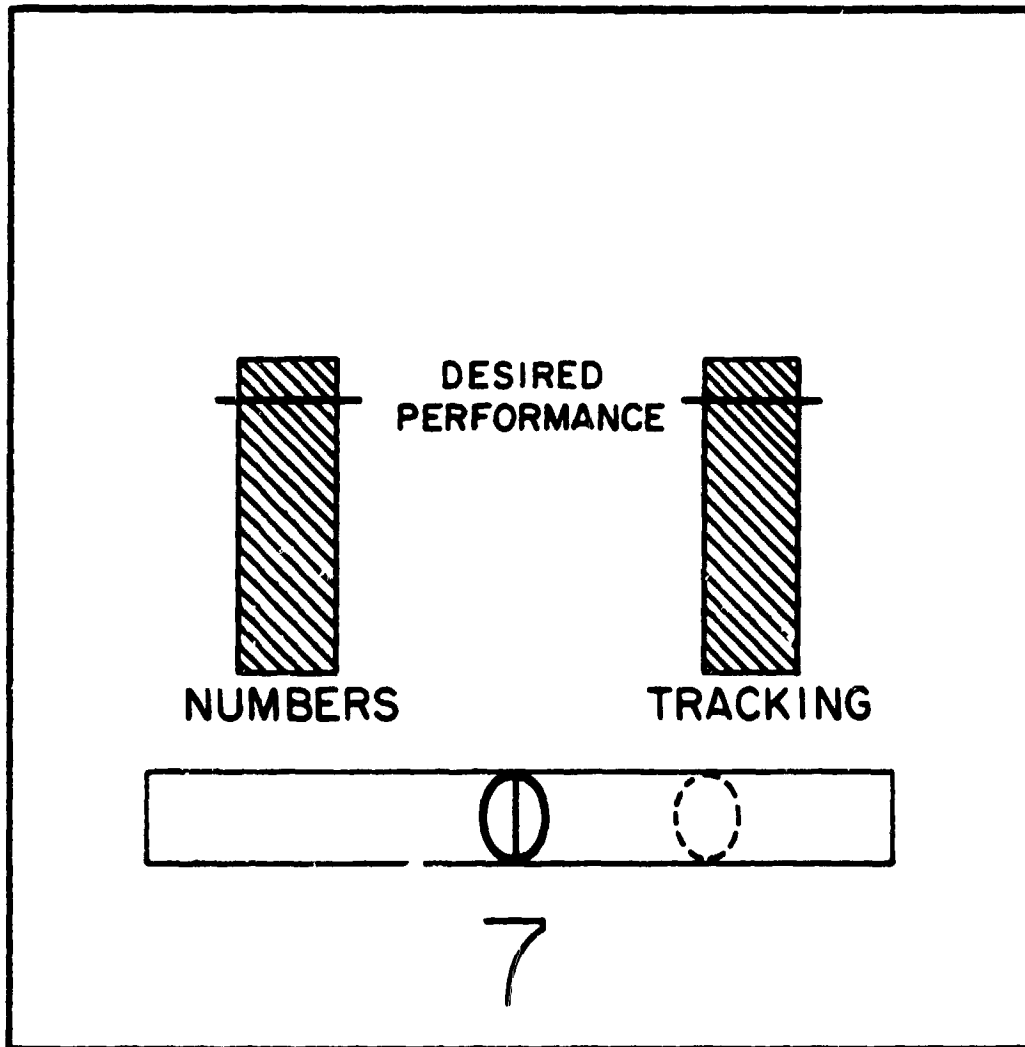


Figure 3. Subject's display in Phase 2 (equal task priorities).

RESULTS

Single Task Performance

Table 1 presents the averages and standard deviations of the main performance measures on the two tasks in the single-task condition.

Table 1
Measures of Single-Task Performance

	Average	SD
Tracking - Percentage Acceleration	80.75	13.57
- RMSE (last 2 min.)	.158	.036
Digit Processing - Response Latency (sec.)	.902	.142

Both the acceleration percentage measures of tracking performance and the latency of correct responses in the digit processing task indicate a relatively wide range of individual differences in the performance of these tasks. A low and statistically nonreliable correlation was found between subjects' performance scores on the two tasks ($r = .096$, $p > .05$). This result implies that the two tasks represent different ability dimensions, although both are composed of visual processing, motor response and reaction-time pressure. Major differences between the two are that the tracking is externally paced and continuous while the digit task is self paced and discrete. Based on preliminary testing, it was determined that the four minute adaptive training would be sufficient to adapt subject to a stabilized level of performance on the present tracking task. It was expected that this method would equalize subjects with regard to tracking errors during the last two minutes of this phase, and as a result the correlation between percent acceleration and RMS Error would be negligible. This correlation was indeed low and non-reliable ($r = .17$, $p > .05$) confirming the success of the adaptive manipulation.

Time-Sharing Performance

Digit processing. Three major component scores have been developed to evaluate digit processing performance in time-sharing. The first is the average response time (ART), which represents the average latency for all the responses made by the subject. The second is the response interval (RI), computed by dividing the total time of the session by the total number of responses. This score is different from the average response time because some of the digits were totally missed. The last score is the

correct response interval (CRI) computed by dividing the total time of the session by the number of correct responses only. The differences between RI and CRI provide estimates of speed accuracy tradeoffs. The differences between RI and ART allow a distinction between the average time of a single stimulus-response cycle (ART) and the frequency or rate of these cycles (RI). Table 2 presents the averages of the three measures in the various time-sharing conditions. The horizontal axis of the matrix represents the tracking task demands. The vertical axis represents the digit processing

Table 2
Performance Measures of Digit Processing in Time-Sharing

		Tracking Demands		
		.3	.5	.7
Digit Processing Demands	.3			<u>3E</u> ART 1.12 RI 1.24 CRI 1.36
	.5		<u>3A</u> ART 1.11 RI 1.24 CRI 1.43	<u>3C</u> ART 1.10 RI 1.23 CRI 1.42
	.7	<u>3D</u> ART .994 RI 1.11 CRI 1.26	<u>3B</u> ART 1.01 RI 1.10 CRI 1.24	

ART - Average response time
 RI - Response interval
 CRI - Correct response interval

Phase 2 (Equal Priorities, First Presentation)
 ART 1.11
 RI 1.39
 CRI 1.72

demands. The cells within the matrix are the various time-sharing conditions. Table 2 results show the expected improvement of the average measures as the demands on the digit task are increased. There is a slight deviation from this trend in condition 3A which can probably be accounted by practice effects, because this condition always preceded the other four conditions. (The order of presentation of the latter was counterbalanced across subjects.) This interpretation is further supported if the results of Phase 2 and 3A are compared (t_{3A-2A} , $RI = 7.57$,

$p < .001$; CRI = 8.32, $p < .001$, df 23; no reliable difference in ART). The general improvement of digit processing performance with increased demand was highly reliable in analysis of variance (ART, $F = 20.55$, $p < .001$; RI, $F = 16.08$, $p < .001$; CRI, $F = 12.72$, $p < .001$; df for all comparisons 2/46). Note that the major change occurred when demand was increased from .5 to .7. These results are typical for high ability subjects (as these subjects were in general) and are related to the experimental instruction to keep the level of performance at the desired performance line or above (North and Gopher (15)).

Tracking performance. Prior to the detailed description of tracking performance as manifested in the feedback control analysis, it might be instructive to present an overview of the manipulation as reflected in the general Root Mean Square (RMS) error scores. Table 3 presents the average RMS error scores in the various time-sharing conditions and in single-task performance.

Table 3

Tracking RMS Error Scores (Percent of Scale) in Time-Sharing Performance

		Tracking Demands		
		.3	.5	.7
Digit Processing Demands	.3			<u>3E</u> .375
	.5		<u>3A</u> .477	<u>3C</u> .385
	.7	<u>3D</u> .491	<u>3B</u> .481	

Single-Task Performance = .158
Phase 2 (Dual-Task Equal Priorities) = .502

Table 3 results demonstrate the success of the experimental manipulation. First, there is a large increase in the average RMS scores from single to dual task performance. Secondly, within the dual-task conditions the scores reveal the expected monotonic decrease of RMS errors as the demands on tracking increase. This effect was highly reliable in an analysis of variance ($F = 17.42$, $p < .001$, df 2/46). Note again that the difference between the .5 and .7 levels is much larger than the difference between .5 and .3 demands. Holding constant the tracking demands and increasing the demand on digit processing (3E-3C, 3A-3B), produced an increase in the

average RMS score, although this increase failed to reach the common levels of statistical reliability.

Feedback Control Analysis

Symbols and Abbreviations

$e(t)$	Error signal (displayed input) in time domain
$o(t)$	Operator stick output in time domain
HFM	Average high frequency output magnitude (3.3-10 rad./sec.)
LFM	Average low frequency output magnitude (.24-3.3 rad./sec.)
RMSE	Root Mean Square Error (percent of scale)
S	LaPlace operator
ϕ_e	Fourier transform of error signal
ϕ_e^*	Inverse Fourier transform of error signal
ϕ_o	Fourier transform of output signal
ϕ_o^*	Inverse Fourier transform of output signal
τ_e	Effective time-delay
ω_c	0 dB crossover frequency
K_a^c	Controlled element percentage acceleration, (α)

On each tracking trial, the displayed error signal $e(t)$, and the subject's output signal $o(t)$ were sampled at a frequency of 13 Hz for a period of 123 seconds, or a total of 2048 samples. Employing the Fast Fourier Transform of these signals, the quantities ϕ_e , ϕ_e^* , ϕ_o , and ϕ_o^* were then obtained. From these quantities, Bode plots of the phase and amplitude ratio characteristics were constructed for each subject in each time-sharing condition (20). Since subject output, rather than system output was measured, the Bode plots represented the open-loop dynamics of the subject alone, rather than those of the man-machine system, reflecting our concern with human, rather than man-machine system behavior. Because the particular system dynamics employed, containing limiters that guaranteed system stability, were unlike those normally used in engineering oriented tracking research, no prior assumptions were made concerning the form of the operator describing functions, and no attempts were made to fit the tracking data to any specific quasi-linear model. The main objective of the analysis was to determine the changes in parameters that assessed tracking time-delay, gain, and remnant or noise, under various time-sharing loads, rather than to determine the agreement of these parameters

with the predictions of any particular model. Furthermore, because data points were not calculated for the low frequency region -- a region that was not of great interest in our research -- no effort was made to determine a complete describing function modeling the subject's tracking behavior.

Gain parameters. Linear regression lines were fit to the 29 amplitude-ratio points of the original Bode plots, for each subject in each condition. Figure 4 shows an example of the amplitude ratio and phase lag plots of the outputs of two subjects in Phase 3E (dual task performance: tracking .7, digits .3). Note that the two subjects have very different portions of first and second order elements in system dynamics (.600 and .986). The linear fit for the amplitude ratio functions of the two subjects is quite satisfactory especially in the crossover region.

The two Bode plots are typical to the behavior of all subjects in all conditions, including single-task performance. The linear correlations of the regression lines were uniformly high (average $r = -.81$) and the goodness of fit of the lines increased with increased demands on the tracking task. The slopes of the amplitude ratio functions were found to average slightly over -20 dB/decade and it was therefore assumed that subjects were responding approximately as a first order (k/S) system. Given this assumption, two general gain parameters were extracted: the intercept of the regression line (technically the subject's log amplitude ratio at 1 radian/sec.), and the 0 dB crossover frequency of the subject alone. These are both parameters that would be assumed to covary positively with subject gain. In addition, because the system gain varied from subject to subject according to the percentage acceleration, it was felt that the combined gain of the man-machine system may represent a parameter that is less sensitive to variation in system dynamics. Thus the man-machine crossover frequency (ω_c) was adapted as another measure of system gain. ω_c was computed by combining the known amplitude ratio function of the system (within the constraints), with the empirically derived function of the subject, and determining the resulting frequency at which $\log(AR) = 0$, ω_c . Table 4 presents the amplitude ratio parameters in the various experimental conditions, ordered according to decreasing priority on the tracking task.

Table 4

Amplitude Ratio Parameters of Tracking Performance

	Intercept (dB at 1 rad.)		Operator ω_c (rad.)		Operator + System ω_c (rad.)		Linear Fit (Median Correlation)
	\bar{X}	SD	\bar{X}	SD	\bar{X}	SD	
Single Task	17.15	1.78	4.59	.73	3.91	.34	.88
Phase 3E	15.50	3.85	4.04	1.02	3.66	.21	.87
Phase 3C	14.66	3.00	4.13	.80	3.76	.39	.79
Phase 3A	13.47	3.18	3.74	.55	3.57	.30	.79
Phase 2	12.71	3.35	3.69	.68	3.49	.19	.78
Phase 3B	13.23	2.98	3.80	.87	3.64	.43	.76
Phase 3D	13.43	3.79	3.69	.55	3.51	.19	.78

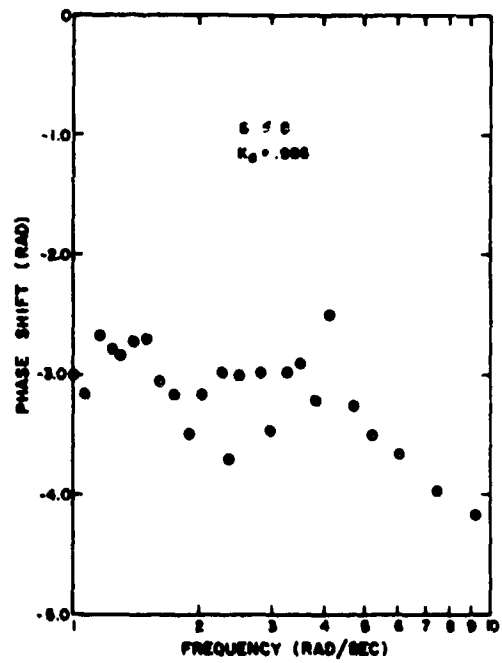
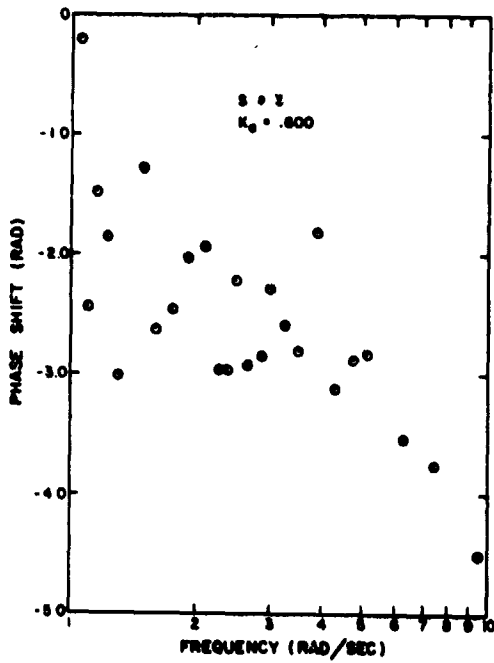
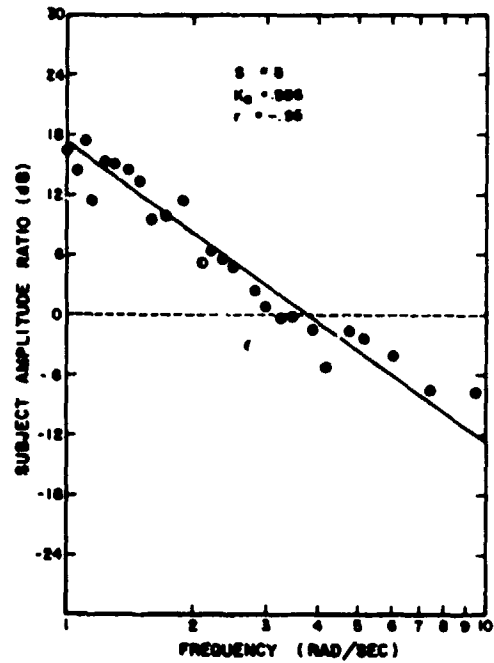
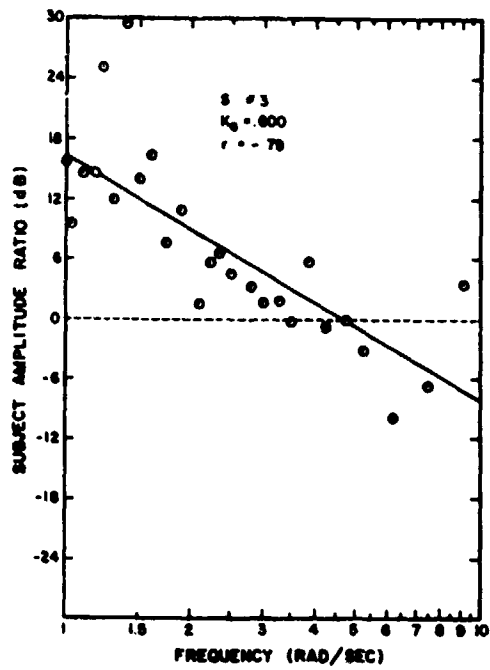


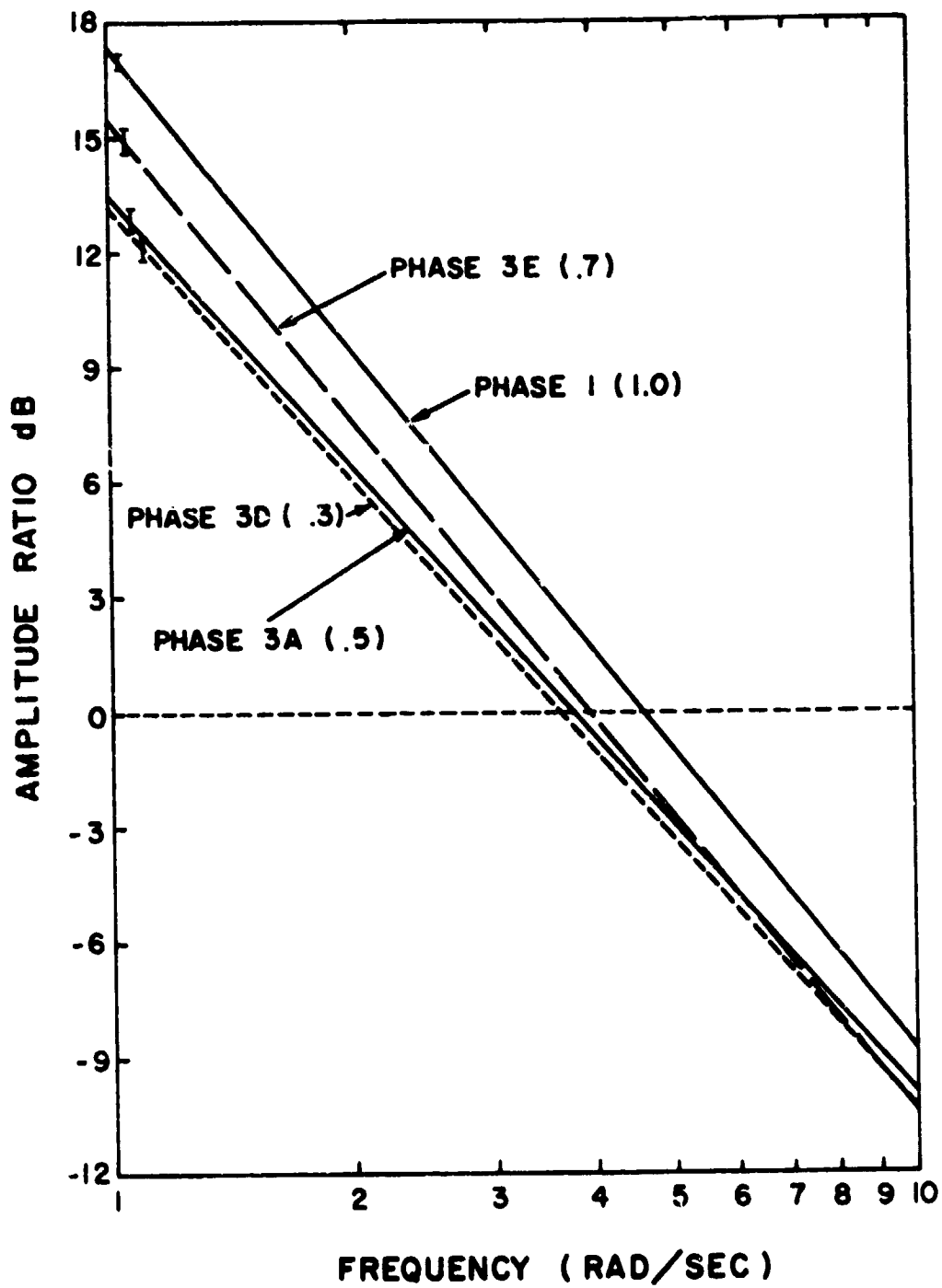
Figure 4. Time-sharing, amplitude ratio and phase lag data, of two subjects controlling systems with different percentage acceleration (K_a).

As Table 4 shows, there is a monotonic decrease of all the gain parameters as the demand on the tracking task decreases. The largest decrease occurs in the transition from single to dual-task performance. These results correspond with the RMS analysis presented in Table 3. Note that the correction for system dynamic by computing the operator-system ω_c , reduced considerably the standard deviations of the average estimates. The analysis of variance of these differences proved the decrease of gain with decreased demand on the tracking task to be statistically reliable. (F ratios for the various measures are: Intercept, $F = 10.85$, $p < .001$; Operator ω_c , $F = 10.74$, $p < .001$; Operator-System ω_c , $F = 13.73$, $p < .001$; df for all analyses were 3/69). The differences between the conditions remained statistically reliable when single-task measures were removed and dual-task, time-sharing conditions were compared within themselves. In this second analysis the operator alone ω_c parameter reached only the 10 percent level of significant (primarily due to the large standard deviations), while the intercept and the combined operator machine ω_c reached .02 and .04 levels of significance respectively.

A further clarification of the amplitude ratio results can be gained if we examine the amplitude ratio functions averaged across subjects, as presented in Figure 5. Figure 5 presents the average functions for the major four experimental conditions. The large difference between single and dual-task conditions is very clear. Within the dual-task conditions the differences are larger in the low frequency as compared with the high frequency regions. Subjects appear to introduce larger gain compensation in the low frequency region. Figure 6 shows the effects of practice on time-sharing performance comparing Phase 2 (the first dual-task condition) and Phase 3A (the second replication of equal task priorities). The effects of increased practice are similar to those of increased demand; higher intercept, and higher crossover frequency.

Another trend that can be observed in Table 4 is the increased linear fit of the regression line extracted for the amplitude ratio function with increased demands on tracking. This trend was statistically tested by sign tests, which compared the regression coefficients of the subjects for each pair of experimental conditions, and proved to be statistically reliable ($p < .05$). The difference between Phases 3E and 3C was also reliable, i.e., when tracking demands remained at .7 level and the demands on digit processing were increased from .3 to .5 there was a decrease in subject's linearity ($p < .02$).

Time delay measures. While the amplitude ratio data for all subjects produced relatively linear, organized, and consistent sets of results, the Bode plots of the subject's phase data indicated much lower consistency and increased deviation from strict linear predictions. For example, linear correlations between phase lag and frequency (predictably high and negative for a pure time delay), were generally low, rarely reaching reliability. A part of this difficulty is probably attributable to the use of a random, as opposed to a deterministic process to generate the input signals. This factor, coupled with the limited amount of measurement data (2 minutes) used to generate each Bode plot, made it unlikely



I = S. E. Mean

Figure 5. Operator's amplitude ratio functions in four experimental conditions (average across subjects).

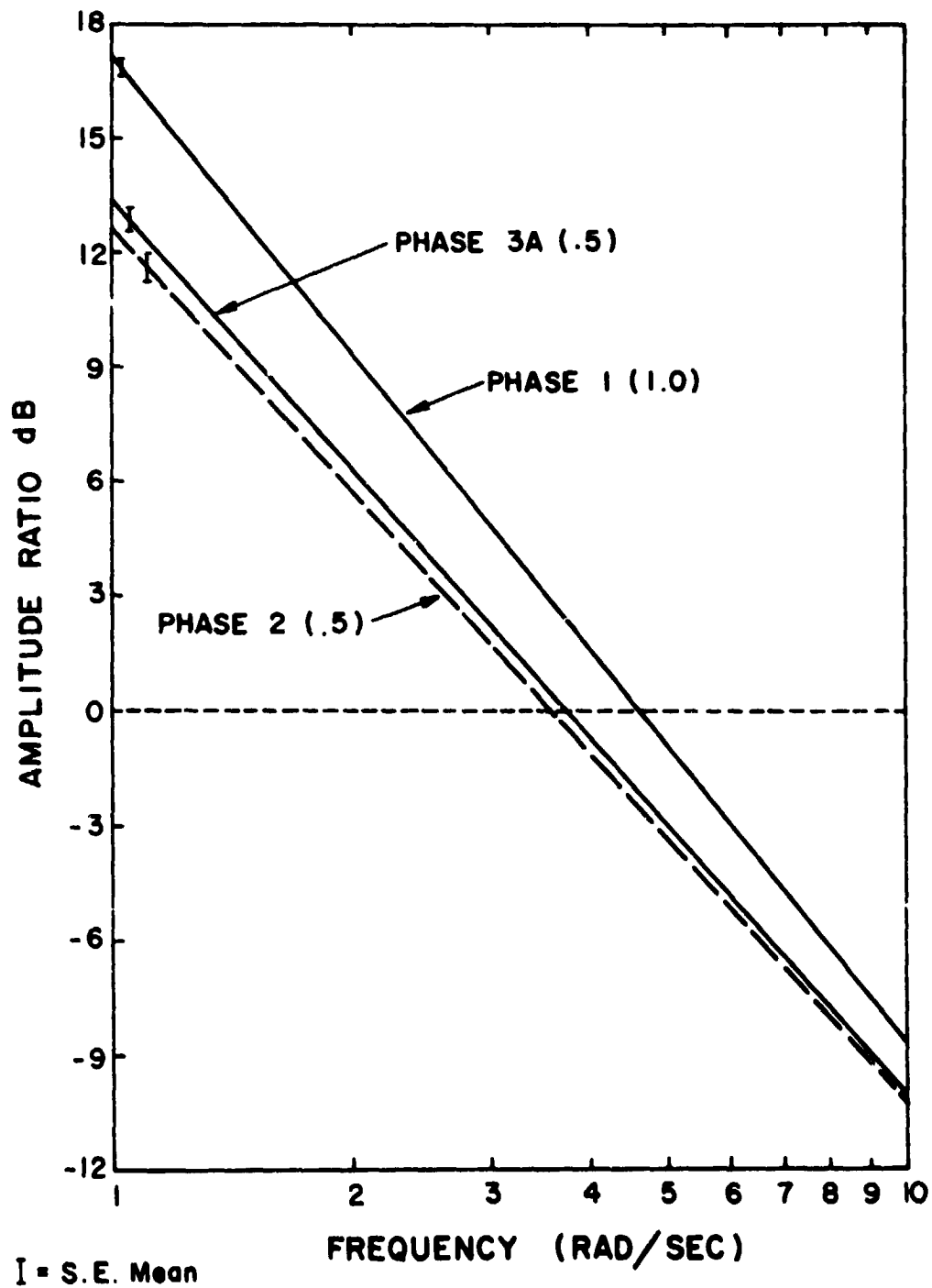


Figure 6. Practice effects as reflected in average amplitude ratio functions (2 + 3A).

that all measurement frequencies would be adequately represented in the input signal for a given trial, thereby producing noisy data. An additional contributing factor may be the subject performance included intermittencies and inconsistencies under time-sharing effecting primarily the phase data. (This possibility is enhanced as a result of the inherent stability of the controlled element.) Typical examples of phase lag data can be observed in the Bode plots of the two subjects in Figure 4.

Despite the reduced quality of the data, an effort was made to obtain general time-delay measures of subject's performance. One measure was the average, overall time lag of the response (including equalization factors and effective time-delay). This measure was computed by dividing the phase shift of each data point by the corresponding frequency and averaging across frequencies from 1.4 to 9.5 Rad./Sec. The second measure was the effective (pure) time-delay. To obtain this measure unconfounded with the phase lag contributed by the subject's equalization strategy (in this instance, normally approximating the behavior of a single integrator), the equalization factor was first inferred from the slope of the amplitude ratio data for each subject. This factor was then transformed to a constant phase equalization (normally around $\pi/2$ radians), and then subtracted at each measurement frequency from the total phase lag, to reveal the component of phase lag due to pure time-delay (i.e., that component unassociated with equalization elements). The effective time delay measure was then obtained by dividing the phase shift at each measurement frequency, by measurement frequency, and averaging across the 21 data points from 1.4 rad./sec. to 9.5 rad./sec.

Finally, it was desirable to define a measure of the consistency of subject behavior because linear fit measures were unsatisfactory in the analysis of phase data. It was determined to adapt the standard deviation of the effective time-delay measure across the 21 data points as an estimate of the subject's consistency.

Table 5 presents the values of the three time measures in the various experimental conditions. As the table shows both the overall time-delay and the effective time-delay do not exhibit much variation in the different experimental conditions, including single-task performance. The average effective time delay decreases as tracking demands in the dual-task situation were increased from .3 (3D) to .5 (3A) to .7 (3E) but these differences did not reach statistical reliability. The only reliable differences in the average time measures is the increase of the effective time-delay from 3E to 3C (holding high demands on the tracking constant and increasing digit processing demands; $t = 2.103$, $df = 23$, $p < .05$).

The consistency measures in Table 5, however, do manifest the effect of the manipulation with increased consistency as tracking demands increase. These results correspond with the results of the amplitude ratio analysis and were statistically reliable (sign tests for the pairs, 2A-3A-practice effects, 3E-3A, 3E-3D, 3C-3E, 3E-3D, all reached .01 levels of significance, and the single-task performance had reliably the lowest variability)

Table 5

Operator Time Delay Parameters in Tracking Performance
(average across frequencies)

Conditions	Overall Time Lag (sec.)		Effective Time-Delay τ_e (sec.)		τ_e Consistency, SD Within Subjects (sec.)
	\bar{X}	SD	\bar{X}	SD	\bar{X}
1	1.13	.07	.337	.118	.192
3E	1.07	.12	.281	.140	.203
3C	1.06	.12	.355	.156	.264
3A	1.04	.13	.346	.174	.326
2A	1.04	.13	.365	.169	.333
3B	1.06	.14	.365	.161	.351
3D	1.06	.16	.353	.207	.358

Magnitude spectra. The third aspect examined in the feedback control analysis was the subject's output magnitude spectrum, $\sqrt{\phi_o * \phi_o}$. For the purposes of the analysis, this spectrum was divided into two regions: the range from 0.24 rad./sec. to 3.3 rad./sec., encompassing the power within the input signal bandwidth, and the range from 3.3 rad./sec. to 10 rad./sec., representing only power beyond the cutoff frequency, and therefore the power generated only by the subject. This latter component then represents the high frequency portion of remnant power.

An estimate of the mean magnitude/rad./sec. in each of these regions was then obtained for each subject and condition, by averaging the magnitude values across measurement frequency. Separate measures were employed for later analysis of the mean low-frequency magnitude (LFM), and the mean high-frequency remnant magnitude (HFM).

Table 6 presents the output magnitude measures of the two regions for the different experimental conditions. There is a general increase of the output magnitude in the dual-task conditions as compared with the single-task condition. This increase is much more pronounced in the low frequency region. Within time-sharing conditions, if the three major conditions are compared (3E (.7) - 3A (.5) - 3D (.3)) an interesting reversal is revealed. While the low frequency magnitude is negatively related to increase in tracking demands, tracking demand and average magnitude are positively related in the high frequency region. The interpretation of this outcome, which is believed to be related to the general strategy of the subjects in the performance of the present tracking task, is postponed until the general discussion section.

Figure 7 presents an example of the magnitude spectra of subjects 3 and 8. Subject 8 results are presented for both single-task and time-sharing

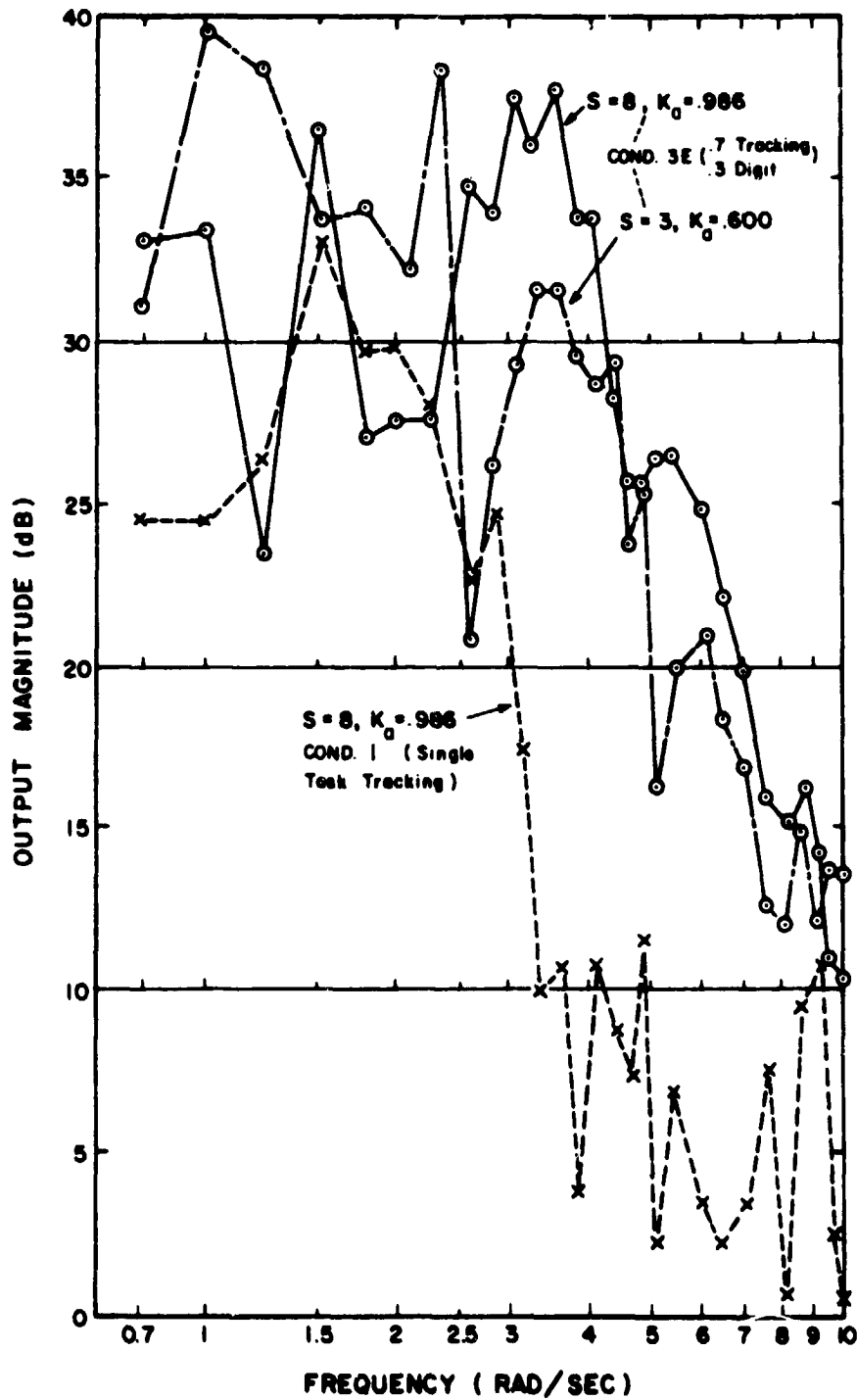


Figure 7. Output magnitude spectra of two subjects in single and dual task performance.

Table 6

Operator Average Output Magnitude in Low and High Frequency Regions

Conditions	Low Frequency Magnitude aB (.24 - 3.3 Rad./Sec.)		High Frequency Magnitude aB (3.3 - 10 Rad./Sec.)	
	\bar{X}	SD	\bar{X}	SD
Single-Task	31.34	7.98	11.89	4.94
3E	52.81	18.4	16.56	7.61
3C	57.53	15.23	14.94	5.31
3A	58.47	21.27	16.83	7.52
2A	55.32	21.10	13.85	6.11
3B	54.26	17.64	13.16	5.54
3D	59.91	18.82	14.07	5.44

performance. Note the difference in the output magnitude of subject 8 in single and dual-task conditions, and the difference between the two subjects (with different system dynamics). Subject 3 reveals higher response magnitudes in the low frequency region, while subject 8 is higher in the medium and high regions.

Correlation of feedback control parameters with RMS errors. Subjects' performance in the various time-sharing conditions revealed relatively large variability of performance effectiveness as defined by the overall RMS error scores. It may be informative to examine the relation between these scores and the feedback control parameters. These correlations are presented in Table 7 for the main feedback control parameters. The table indicates that

Table 7

Correlations of Feedback Control Parameters
with RMS Error Scores in Time-Sharing Performance

Conditions/ Parameter	Amplitude		Subject ω_c	Overall Time Lag	Effective Time-Delay	LFM	HFM
	Ratio	Intercept (1 rad./sec.)					
Phase 3E	-.276		-.443*	-.185	.039	.599**	.53 **
3C	-.68 **		-.36	-.18	.332	.700**	.406*
3A	-.529**		-.491*	.03	.499*	.66 **	.383
2A	-.33		-.244	-.166	-.02	.220	.198
3B	-.662**		-.62 **	-.168	.172	.483*	.329
3D	-.53 **		-.13	.056	.446*	.522**	.135

*p < .05

**p < .01

the best predictors of RMS errors are the low frequency magnitude scores (positive correlation) and the amplitude ratio intercept (negative correlation). The first can be regarded as an estimate of the subject low frequency remnant, while the second represents the low frequency gain. Note that high frequency magnitude is mostly uncorrelated with RMS error. Another interesting result is that there are two reliable correlations of effective time-delay with RMS error, both are in conditions that include high demands on the digit task while tracking is lower or equal.

The effect of the adaptive manipulation. The last group of results is concerned with the adaptive adjustment of control dynamics to the ability of each individual subject. With increased portions of second order integrations in the controlled element dynamics, subjects were expected to introduce increased lead to compensate for the increased lag of the system. In a pure second order system subjects were expected to act as a differentiator (20). However, it has already been shown in previous sections that the linear portion of subjects behavior can best be approximated by an integrator. This behavior is most salient in the Bode plots of subjects 3 and 8 (Figure 4) in both the amplitude ratio and phase lag data.

In both plots the contribution of τ is evident at high frequencies. However, the equalization factor of the two subjects appears to be in the opposite direction from that which would be predicted from the dynamics of the system being controlled. Subject #3, controlling a system that is a mixture of first and second order elements, shows a phase lag of approximately 2.3 rad./sec., while subject #8, controlling what is essentially a pure second order system manifests a greater phase lag, approximately 3.1 rad./sec. The data thus suggests that subjects did not adapt their equalization strategy to the dynamics of the system, but rather, compensated for the greater difficulty of the higher order system by some other strategy (it should be remembered that the stability of the system was protected by the limiters).

To identify the feedback control correlates of the adaptive manipulation the percentage acceleration measure was correlated with the feedback control measures in both single and dual-task conditions. The percentage acceleration score did not produce reliable correlations with RMS error scores in single or dual-task performance. The main feedback control measure which showed reliable and relatively high correlations with percentage acceleration throughout the experiment was the high frequency magnitude measure. In single-task performance this correlation was .515 ($p < .01$) and in Phase 2 $r = .658$, $p < .01$. This pattern of correlations repeated in other time-sharing conditions (3A, $r = .423$, $p < .05$; 3B, $r = .452$, $p < .05$; 3C, $r = .475$, $p < .05$; 3E, $r = .447$, $p < .05$). The correlations between percentage acceleration and low frequency magnitude were always lower and mostly nonreliable. These correlations suggest that subjects were compensating for increased percentage acceleration by a non-linear, high frequency strategy (such as "bang-bang" control) which was manifested in the HFM data.

DISCUSSION

The current results may be considered along two different dimensions; the main effects of the attention manipulations on tracking performance, and the between-subject correlation effects. The first dimension consists of those control theory parameters that show systematic shifts in their value as a function of increasing or decreasing demand on the tracking task. The second dimension included the correlational effects obtained between various experimental variables. These correlations provided confirmative or supportive evidence for the conclusions drawn from the main effects. In the following discussion, these two dimensions will be treated in parallel.

In the first place, clear evidence was provided that the overall measure of tracking performance (RMSE) was sensitive to the experimental manipulation of attention allocation. RMSE rose monotonically as less attention was required of (and presumably devoted to) the tracking task. Furthermore, for equal tracking demand conditions, RMSE rose as more attention was demanded by digit processing.

The feedback control analysis of subjects' tracking behavior revealed that this behavior can best be approximated by a k/S system, and that the goodness of fit of this approximation increased with increase of tracking priorities. This behavior clearly deviates from the strict predictions of McRuer's widely accepted crossover model (21) which requires the operator in a second order system (k/S^2) to respond as a kS or a differentiator, such that the joint transfer function of the man-machine system will become k/S . The deviation of the present experiment from these predictions can be accounted for by two major factors, the nature of the system, and the lack of experience of the naive subjects.

An important feature of the present tracking system was the inclusion of limiters that guaranteed the stability of the system. These limiters were necessary to avoid abrupt discontinuities of the experiment when the subject temporarily lost control over the situation, in particular under time-sharing conditions. Without the limiters, the tracking symbol could go off the screen for relatively long periods and return to the screen from an unexpected direction. In turn, such an event could upset the subjects, interfere with the continuity of the experiment and create difficulties in the measurement and interpretation of results (this is especially true for naive and unexperienced subjects). The limiters can therefore be perceived as created to satisfy "Psychological Reality." In the present context this requirement resulted in a controlled element which differs from similar systems employed in control theory research. Given the stability of the controlled elements, where the effects of large errors are tempered, the subjects adapted a response mode which has been shown to be appropriate to an unconstrained position system (21), i.e., their rate of response was proportional to the position of the tracking symbol on the screen.

This mode of response caused an increased mismatch between system dynamic and subject behavior with increased percentage acceleration, because within the constraint the present system revealed the characteristics of a linear system. To compensate for this mismatch subjects appear to employ a second, non-linear, high frequency response strategy, such as "bang-bang" control or similar behavior. This interpretation is supported by several experimental indications. First, a positive correlation was shown between the percentage acceleration scores and the high frequency output measures of subjects' performance, while no systematic correlations were found between the above two variables and RMS error scores. Hence, the high frequency output magnitude scores seem to include an effective response strategy which is related to the order of the system, or to the degree of mismatch between the linear response mode of the subjects and the actual system dynamics. Secondly, increased demands on the tracking task in time-sharing produced a monotonic increase of the high frequency magnitude average (Table 6), without changing the pattern of correlations with RMSE. The subjects, therefore, appear to use both linear and non-linear response modes to correct errors, compensate for system lags, and improve performance with increased demands.

The major objective of the component analysis of tracking behavior in time-sharing, was to determine what specific processing changes underlie changes in RMS errors, as revealed by the fine-grained analysis provided by feedback control theory. Table 4 suggests that a fundamental effect of attention demand occurred in the measures of tracking gain. The two parameters that would normally correspond with a measure of overall subject gain, the 1 rad./sec. amplitude-ratio value (intercept) and the subject crossover frequency, both are monotonically and reliably decreasing as less attention is devoted to tracking. That this effect is one that is responsible for the overall decrease in RMSE, is given some support by the fact that the correlations between RMSE and intercept, and between RMSE and crossover frequency are uniformly negative and in most cases relatively high and statistically reliable. Thus subjects with high gain values are found to be better trackers, while the gain value for all subjects tends to decrease, along with increased RMSE, with decreasing attention. This relation between gain and attention is similar to that obtained by Wickens (10) and Bary (11), who found gain (as measured by the man-machine ω_c) to decrease significantly from single to dual task conditions.

The current results suggest further that gain is a parameter that may be adjusted continuously, in accordance with relatively subtle cognitive priorities and demands, a lability which was previously demonstrated by Rupp (22). The view of tracking gain, as a parameter that directly reflects the amount of attention allocated to a task, and thus represents some sort of a measure of "effort," receives support from a number of converging sources. Kahneman (23) has argued that attention and effort may be conceptualized as closely related internal processes. Since mean-squared control velocity, and therefore physical effort or exertion increases monotonically with gain, and gain here is found to increase with attention, it may well be that physical effort (gain) and mental effort

(attention) are, in fact closely interrelated in the present manual control task.

A second parameter that appears to be affected by the attention demands of the second task is the measure of total low-frequency output magnitude (power below 3 rad./sec.), referred to as LFM. A comparison between the single-task condition level and the mean time-sharing levels of the LFM parameter revealed a significant increase when the secondary task was required. Furthermore, as tracking demand decreased within the time-sharing conditions, LFM appeared to increase still further. It should be noted that the components of LFM come from two sources: the error-correlated power, and the subject-injected remnant power. However, since the error-correlated component would decrease as gain decreased, and a large drop in gain was obtained, both from single to dual task performance, and as tracking demand decreased in dual task conditions, it is clear that an increase in the injected remnant component rather than the correlated power, was responsible for the increase in total LFM, as the time-sharing task was added and as demand for tracking decreased. The between-subject correlation data suggest that this remnant increase was "non-adaptive," in the sense that it contributed to an overall increase in RMSE, since the correlations between LFM and RMSE were uniformly high and positive across all conditions (average correlation = +.530).

Further evidence that remnant power reflects qualitatively the amount of attention devoted to tracking is provided by the results that the linear fit of the amplitude ratio function decreases systematically as tracking demand is decreased. This linear fit, reflecting the subject's degree of linearity, could be expected to decrease as more remnant power is contributed by the subject. The notion that remnant level (at low frequencies) is reflective of attention demands receives support in the experimental literature from the research of Levison, et al. (9), Wickens (10), and Baty (11). Specifically, Levison, et al. obtained similar results to the findings reported here, that remnant level reflects in a quantitative manner, the amount of attention allocated to a tracking task (in their case, manipulated by adding one, two, or three concurrent tracking tasks).

The above discussion of attention-related increases in remnant power referred only to power within the low frequency region (LFM). Although an increase was also observed in HFM from single to dual task performance, it should be noted that this was not statistically reliable, and furthermore may well have been attributable to the subject's adaptive non-linear control strategies described in previous sections.

The current results indicated an absence of an observed effect of attention demand on the measure of processing time delay, τ_e . This is surprising, in light of the general association in psychological research, of time-delay and attention (24), and the fact that some manual control studies have directly observed an increase in time-delay (or an equivalent measure) as a function of the presence of a secondary task (3, 5, 6, 7).

It may be argued, of course, that the current phase lag data were sufficiently noisy so as to preclude obtaining consistent, sensitive measures of time-delay, and this, of course, is a realistic possibility. However, four factors negate this argument. In the first place, the results are consistent with those obtained by Wickens (10) and Levison, et al. (9), who also found divided attention effects localized only in gain and remnant measures. In the second place, at least one experimental manipulation in the current experiment, the attention demanded by digit processing when tracking demand was held constant, did significantly affect the mean level of the measured τ_e parameter. Thirdly, in time-sharing conditions where digit processing priorities were equal or higher than those of the tracking task, significant correlations were found between τ_e and RMSE in the expected direction (subjects with higher RMSE scores tracked with greater τ_e). Finally, the consistency of the τ_e measures reliably increased with increase in the relative priorities of tracking. This suggests that the experimental measure of τ_e was in fact a behaviorally real one, which was relatively insensitive to experimental manipulation.

Together, the results of the analysis for the gain and time-delay parameters suggest that the voluntary adjustment and reallocation of attention is primarily accomplished by changes in the operator gain parameters. Time parameters, though contributing to the overall efficiency of performance, are not as readily adjusted in time-sharing performance. Instead, however, tracking processing delay is influenced indirectly by the attention demanded by the digit processing task. As the demand for the digit task increases, for a given level of tracking demand, the time to process the tracking signal increases. Thus there appears to be a clear asymmetry between the effects of manipulating demands on a given task and changing the demands of a concurrently performed task.

It is interesting to note that, with the exception of Cliff's study (3), those tracking studies that have obtained an increase in processing time under dual-task conditions have all employed the critical (or subcritical) task, requiring the subject to track an unstable system. This system is unique in that it constrains, or forces the subject to adopt a minimum time-delay in order to maximize single task performance. In tracking an inherently stable system on the other hand, as used by Levison, et al. (9), Wickens (10), and Baty (11), a subject can maximize performance (minimize RMSE) either by reducing τ_e , or at a given level of τ_e by increasing gain to a maximum value. In this two-degrees-of-freedom situation, if the subject chooses to maximize single-task performance by a gain increase, rather than a τ_e decrease, then τ_e may not necessarily be at a minimum single task value. In this case, it would not necessarily be expected to show increases when secondary tasks are added. Therefore, unlike the unstable critical task, the τ_e effect would not necessarily be obtained. In the present study, time-sharing requirements do not seem to effect the latency or the frequency of the operator responses, but the quality and consistency of these responses.

CONCLUSIONS

1. When the dynamics of a system are constrained, in such a manner that man-machine system stability is no longer a major concern of the operator, he tends to adopt a first order control describing function, even with tracking systems of higher order. This particular linear strategy may reflect the low level of practice, or limited system knowledge of the current subjects. It is accompanied by a second non-linear strategy which is reflected in a component of high frequency remnant power, and seems to be adaptive, in the sense that it reduces tracking error.
2. When attention is divided between tracking and a concurrent task, tracking gain appears to decrease by a magnitude that is proportional to the amount of attention diverted to the concurrent task.
3. Attention diversion to a concurrent task leads to an increase in remnant level, or non-linear power. This decrease in linearity is reflected both in the output magnitude spectra of the subjects, and in the linear fit of the amplitude ratio function.
4. Processing time does not appear to be affected in any consistent manner by performance requirements on the tracking task, although it is affected by the change of demands on the digit processing task.
5. One final point should be made concerning the present experiment and analysis, which is that our perspectives are those of psychologists, rather than engineers. Therefore, given that our interest is primarily in human tracking behavior, including the process of practice and training, and the effects of attention on the parameters describing that behavior, rather than in the total man-machine system, our analysis has focused specifically upon human parameters, instead of those of the man-machine system. This bias resulted in a particular system in which man-machine system stability was guaranteed. Thus, what is in many studies the primary reason for adopting a man-machine system approach, was in the current experiment eliminated. What we hope we have accomplished in this study is an integration of a concern for behavioral phenomena, with the techniques and perspectives of control engineering, and a demonstration of the value of such an integration for human factors research.

REFERENCES

1. Sheridan, T. B. and Ferrell, W. Man Machine Systems. Cambridge, Mass.: MIT Press, 1974.
2. Poulton, E. C. Tracking Skill and Manual Control. New York: Academic Press, 1974.
3. Cliff, R. C. The effects of attention sharing in a dynamic dual-task environment. Proceedings 7th Annual NASA-Univ. Conference on Manual Control, NASA SP-281, June 1971, pp 307-326.
4. Jex, H. R., McDonnell, J. D., and Phatac, A. C. A "critical" tracking task for manual control research. IEEE Transactions on Human Factors in Electronics, 1966, HFE-7, pp 138-144.
5. Jex, H. R. Two applications of the critical instability task to secondary workload research. IEEE Transactions on Human Factors in Electronics, 1967, HFE-8, pp 279-282.
6. Jex, H. R., Jewell, W. F., and Allen R. W. Development of the dual-task and cross-coupled critical tasks. Proceedings 8th Annual Conference on Manual Control, AFFDL-TR-72-92, May 1972, pp 529-552.
7. McRuer, D. The Development of Pilot-in-the-Loop Analysis. System Technology, Inc. Paper No. 129, 1972.
8. Watson, B. L. The Effect of Secondary Tasks on Pilot Describing Functions in a Compensatory Tracking Task. University of Toronto Institute for Aerospace Studies. UTIAS Technical Note No. 17, June 1972.
9. Levison, W. H., Elkind, J. I., and Ward, J. L. Studies of Multivariable Manual Control Systems: A Model for Task Interference. NASA CR-1746, May 1971.
10. Wickens, C. D. The Effect of Time-Sharing on the Performance of Information Processing Tasks: A Feedback Control Analysis. University of Michigan, Human Performance Center Tech. Report No. 51, August 1974.
11. Baty, D. L. Human transformation rates during one-to-four axis tracking. Proceedings 7th Annual Conference on Manual Control, 1971, NASA SP-281, pp 293-306.
12. Fuchs, A. The progression-regression hypothesis in perceptual-motor skill learning. Journal of Experimental Psychology. 1962, 63, pp 177-182.

13. Gopher, D. and North, R. A. The measurement of attention capacity through concurrent task performance with individual difficulty level and shifting priorities. Proceedings of the Eighteenth Annual Meeting of the Human Factors Society. Santa Monica, Calif.: Human Factors Society, October 1974.
14. Gopher, D. and North, R. A. The measurement of operator capacity by manipulation of dual task demands. University of Illinois at Urbana-Champaign: Aviation Research Laboratory, TR ARL-74-21/AFOSR-74-15, Savoy, Ill., 1974.
15. North, R. A. and Gopher, D. Measures of attention as predictors of flight performance. Human Factors, 1975, (in press).
16. Rolfe, J. M. The secondary task as a measure of mental load. In W. T. Singleton, R. S. Easterby, and D. E. Whitfield, (Eds.). Measurement of Man at Work. London: Taylor and Francis, 1971.
17. Knowles, W. B. Operator loading tasks. Human Factors, 1963, 5, pp 151-161.
18. Ince, F. and Williges, R. C. Detecting slow changes in system dynamics. Human Factors, 1974, 16, pp 277-284.
19. Gopher, D., Williges, B. H., Williges, R. C. and Damos, D. L. Varying the type and number of adaptive variables in continuous tracking. Journal of Motor Behavior. 1975 (in press).
20. Shirley, R. Application of a modified Fast Fourier Transform to calculate operator describing functions. Proceedings 5th Annual NASA-University Conference on Manual Control. Cambridge, Mass.: March 1969.
21. McDuer, D., Grapham, D., Krendel, E., and Reisener, W., Jr. Human pilot dynamics in compensatory systems -- theory models and experiments with controlled element and forcing function variations. AIFDL-TR-65-15, Wright Patterson AFB, 1965.
22. Rupp, G. On the Voluntary Control of the Crossover Model Parameters and its Relevance to Motor Skills. Unpublished Doctoral Dissertation. University of Michigan, 1974.
23. Kahneman, D. Attention and Effort. Englewood Cliffs, N.J.: Prentice-Hall, 1973.
24. Keele, S. W. Attention and Human Performance. Pacific Palisades, Calif.: Goodyear, 1973.

N75 33679

TIME ESTIMATION AS A SECONDARY TASK TO MEASURE WORKLOAD

Sandra G. Hart

University of California
Berkeley, California*

SUMMARY

Variation in the length of time productions and verbal estimates of duration was investigated to determine the influence of concurrent activity on time perception. The length of 10-, 20-, and 30-sec intervals produced while performing six different compensatory tracking tasks was significantly longer, 23% on the average, than those produced while performing no other task. Verbal estimates of session duration, taken at the end of each of 27 experimental sessions, reflected a parallel increase in subjective underestimation of the passage of time as the difficulty of the task performed increased. These data suggest that estimates of duration made while performing a manual control task provide stable and sensitive measures of the workload imposed by the primary task, with minimal interference.

INTRODUCTION

Inasmuch as variation in subjective temporal experience has been associated with the perceptual, cognitive, and motor load of concurrent activity (ref. 1) it is conceivable that variation in the estimates of duration made by pilots flying different simulations could be used to evaluate the workload imposed by different cockpit displays. It is often difficult to infer the relative merits of one cockpit display configuration over another from performance measures such as RMS errors. The fact that equivalent performances are observed in simulated flights using different display parameters does not necessarily imply that pilots find the cockpit displays to be equally useful or equally desirable. Pilots frequently report otherwise.

Many secondary tasks have been developed to evaluate the workload imposed by a task of interest. These tasks are often designed to increase the overall workload in order to measure the amount of residual capacity for work still available during performance of the main task. The assumption is that processing resources of the operator are limited and that his performance will deteriorate when several activities compete for the same resources (ref. 2). A secondary task may interfere with performance on the main task if it employs the same sensory-motor pathways as the main task or interferes functionally with it (ref. 1). An alternative type of secondary task is one that does not interfere functionally with the main task but does require some attention. As attention required by the primary task increases, performance on the secondary task deteriorates providing an indirect measure of primary task demands. The latter type of secondary task was considered optimal for judging the workload imposed by different simulation configurations.

*This research was conducted at NASA-Ames Research Center under NASA grant NCA-2-OR-050-503.

Time estimation has several advantages as a secondary measure of primary task workload. The duration and regularity of temporal estimates has been associated with the workload imposed by concurrent activity (refs. 1,3). Since cockpit displays are designed to reduce distraction, stress, and perceptual and motor load, it is possible that variation in the duration and regularity of time estimates made by pilots while flying different simulation configurations might provide a sensitive measure of how different displays affect pilot effort. Time estimation does not appear to interfere functionally with, nor use the same sensory-motor pathways as, piloting tasks. Michon (ref. 1) demonstrated that primary task performance was not affected adversely by concurrent timing tasks. To the contrary, it was performance on the secondary timing task that suffered when primary task demands increased. Temporal estimation is an activity that is normally performed in flight, and is therefore acceptable to pilots, and can be presented as an integral part of a manual control task so it is not perceived as an additional task. Time estimation tasks can be learned easily and are relatively stable across time with respect to learning effects, and can be implemented and scored easily.

If time estimation is to be used as a secondary task, some consideration should be devoted to the processes involved in human time perception. Although time perception is not based on any obvious external stimulus dimension, as visual and auditory perception are, humans are able to deal effectively with the concepts of simultaneity, succession, and duration. They are able to estimate the duration and sequence of past events and produce comparatively accurate intervals of time. Although chronometers provide objective standards to which subjective temporal experiences can be referenced, it should be emphasized that objective clock time is not directly equivalent to psychological or subjective time (ref. 4). External timekeeping mechanisms simply provide generally agreed upon names for different durations and make precise synchronization in the temporal domain possible.

There are many other physical phenomena that are also used for timekeeping (ref. 5). William James (ref. 6), and more recently Ornstein (ref. 4) and Frankenhaeuser (ref. 7) have suggested that the mental content of intervals produces the subjective experience of duration without reference to any physiological processes.

Many recurring physiological processes can also serve as subjective clocks against which the duration of stimuli or activities can be compared (ref. 8). These are biological clocks in the sense that repeating cycles of a biological process may be used to measure off intervals of commensurate frequency. However, it is not possible to designate any one of these processes as *the* organ for time perception (ref. 9). Attempts to show that such biological processes as alpha rhythm (ref. 10), heart rate (ref. 11), body temperature (ref. 12), or respiration (ref. 13) serve as the biological clock have failed. It is more likely that humans learn to equate the period and frequency of these and other recurring physiological and environmental processes to specific external time standards.

The current work is based on the above mentioned hypothesis that any experience that has been timed against some external standard can be used as a "subjective clock" for timekeeping. Humans learn from everyday experience how long different activities last and how regularly they recur. They are able to generate (from memory) examples of processes that take approximately a second, an hour, a day, and so on, and they are also able to equate the duration of activities that take about the same time. When asked to estimate the duration of an interval, an individual compares the current time sample to a set of remembered temporal equivalences or prototypes whose duration has been equated to standard units of time. Short intervals may be processed as single units in short term memory, whereas longer intervals may be evaluated by counting (in long term

memory) repeated segments that have more manageable lengths. When asked to produce a specific interval of time, individuals may either rehearse a sequence of "timing" events in memory or monitor repeated occurrences of a physiological (e.g., arterial pulse) or environmental process (e.g., diurnal variations) that represent subjective clock units of appropriate duration.

These temporal prototypes, or subjective clocks, are constantly compared with and adjusted to external clock time, as individuals are rewarded for conforming with the temporal conventions of their culture. However, subjective temporal units are not exact nor accurate with respect to the standard clock nor perfectly consistent, thus time estimates do show variations. Factors that affect the rate of biological rhythms serving as subjective clocks, such as stress, drugs, illness, and fatigue have also been shown to affect the duration of subjective estimates based on them (refs. 3, 8, 9, 10, 11, 12, 13). Increasing or decreasing the amount and complexity of information presented may also affect subjective temporal experience because a particular amount of mental processing and storage had been associated with longer or shorter presentation times in the past (ref. 4). Time estimates may vary because repeated events are sampled regularly or counted incorrectly. For example, if successive "ticks" of a subjective clock go unnoticed or uncounted, the objective time taken to produce an interval lengthens and the subjective impression underestimates the actual time elapsed. If the conscious rehearsal of remembered equivalences for units of time requires attention, timing may be disrupted by concurrent tasks that also require attention (refs. 1, 14, 15). Since timekeeping most likely involves multiple processes (ref. 16), an individual may have to cope with discrepant information produced by his various subjective clocks. He may decide to discount the output of one or more of the subjective clocks entirely and intellectually reassess subjective impressions of duration on the basis of other sources of information, resulting in random or systematic errors if the correction factor is inaccurate or applied incorrectly.

The integrated output of subjective clocks is the only aspect of the human timing mechanism available for experimental evaluation. The period and frequency of subjective clocks, their consistency, the regularity with which they are sampled, their appropriateness, and any intellectual reassessment applied to their output can only be inferred. The underlying processes from which estimates are derived are difficult to measure, but something can be said about the observable behavior. That is, reliable variations in temporal estimates can be related to specific environmental manipulations, and predictions can be made about the perception of time in analogous situations.

This study was designed to examine the effect of concurrent manual control activity on time estimation. It is assumed that time estimation is an attentive process (refs. 1, 14, 15) that involves mental rehearsal of some sequence of events that represents subjective equivalences for units of clock time. Distraction provided by a concurrent task limits the amount of attention that can be devoted to time estimation. As attention is diverted from time estimation, whether by distraction or reduction in alertness, the subjective impression of how much time has passed drops progressively behind the measurement of elapsed time provided by an external clock (ref. 14), because objective time is continuous whereas the experience of time may be subject to lapses. Thus, under distracting conditions, it is expected that the objective time taken to produce an interval will increase, and subjects will underestimate the passage of time in retrospect. If such a relationship is found, it would provide further evidence that variation in the perception of time could provide a sensitive measure of the workload imposed by manual control tasks using different display configurations.

METHOD

Subjects

Nine commercial airline pilots participated in this study as paid volunteers. The men were 32-40 yr of age and held the position of first officer.

Apparatus

This study was conducted in a dim sound-attenuated experimental chamber at NASA-Ames Research Center. Subjects were seated in a comfortable reclining chair with the cathode-ray tube (CRT) used to display the time estimation and tracking tasks located at a viewing distance of 92 cm. The presentation of experimental conditions and data acquisition were controlled by a PDP-12 computer. Lateral and vertical errors on the tracking tasks were sampled 20 times per sec, and time estimates were recorded to the nearest 0.05 sec. RMS error and temporal estimates were analyzed off-line by a Xerox Sigma-9 computer.

A two-axis, low-inertia, lightly damped Kraft sidearm controller was mounted on the right arm of the pilot's chair. A molded handgrip was mounted on the shaft of the controller, and a response button used for time estimation was located beneath the subject's thumb. An intercom system allowed communication between the experimenter and subject.

Time Estimation Task

The pilots were asked to estimate elapsed time by two methods, production by the means of a response button and verbal estimation of session length. The time production task required that subjects produce one of three standard intervals (10, 20, or 30 sec) 7 times during each of the 21 experimental sessions that involved time productions. Subjects were instructed to press the response button once to begin their productions when the message "EST ___ SEC" appeared on the CRT, and to press it again whenever they felt that the specified amount of time had elapsed. For three sessions, producing 10-, 20-, or 30-sec intervals was the only task. For 18 other sessions, 10-, 20-, or 30-sec intervals were produced while performing each of six compensatory tracking tasks.

Pilots were also asked to verbally estimate, in minutes and seconds, the length of each of the 27 experimental sessions immediately after each session ended. Session length varied from 1 to 6 min depending on the length of the standard interval to be produced during the session and the accuracy of productions.

Tracking Task

Six levels of a compensatory tracking task were developed to produce progressively greater degrees of distraction from the time estimation task. The tracking tasks consisted of a CRT display upon which was displayed a 1.26 cm stationary cross that pilots were told represented the nose of an aircraft, and a 12.7 cm moving horizontal and/or vertical line that pilots were told represented

the glide slope and localizer, respectively, in an actual piloting task. The maximum travel of the two moving lines subtended a visual angle of 0.14 rad (7.9 degrees of arc).

The pilot's task was to keep the vertical and/or horizontal lines centered on the reference cross using the sidarm controller to compensate for the random perturbations produced by one of two forcing functions. The display had an inside-out, fly-to arrangement so that the controlled elements (vertical and/or horizontal lines) moved in a direction opposite to stick displacement. That is, if the driven lines were to the left and below the reference cross, controller movement to the left and forward was the correct response.

The output of a random number generator provided a rectangular distribution of frequencies simulating white noise with a bandwidth of 62 rad/sec. This signal was passed through either of two second-order filters having a damping ratio of 0.707, with a natural frequency of 0.5 rad/sec (the "easy" task) or 1.5 rad/sec (the "hard" task). The forcing functions were chosen for their "easy" and "hard" characteristics on the basis of data from a preliminary study employing three subjects. The standard deviations were 2.10 cm for the easy vertical and horizontal forcing functions and 2.58 cm for the hard vertical and horizontal forcing functions (see fig. 1).

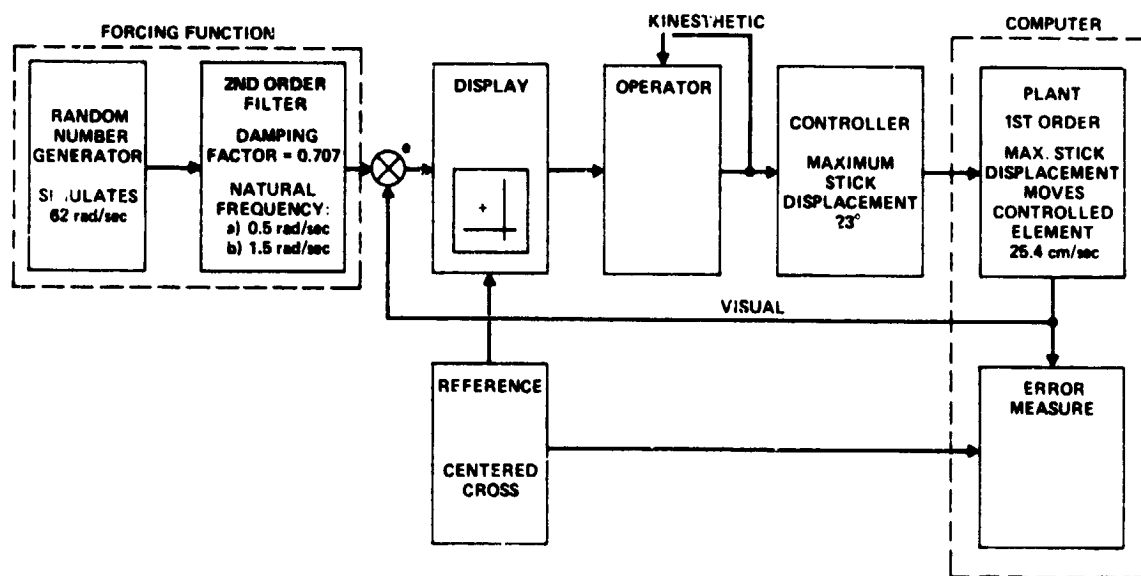


Figure 1.- Block diagram of experimental tracking tasks.

The first-order plant was programmed such that maximum displacement of the controller, 23° from neutral in any direction, produced a maximum controlled element velocity of 25.4 cm/sec. Maximum controller throw corresponded to a 3.8 cm movement of the subject's hand at the position of his middle finger (fig. 1).

Experimental Design

Pilots were instructed to perform each tracking and time estimation task as consistently and accurately as possible, although they were not given performance feedback for any of the tasks. They were asked to make verbal estimates and productions based on their subjective impression of elapsed time, without counting. Following instructions, subjects were familiarized with the equipment by a series of practice sessions that involved time production alone, tracking alone, or time production while tracking.

During the first three sessions, pilots were required to produce seven 10-sec intervals, then seven 20-sec intervals, and finally seven 30-sec intervals. Time production and verbal estimation of session length were the only tasks performed during these three sessions (fig. 2a).

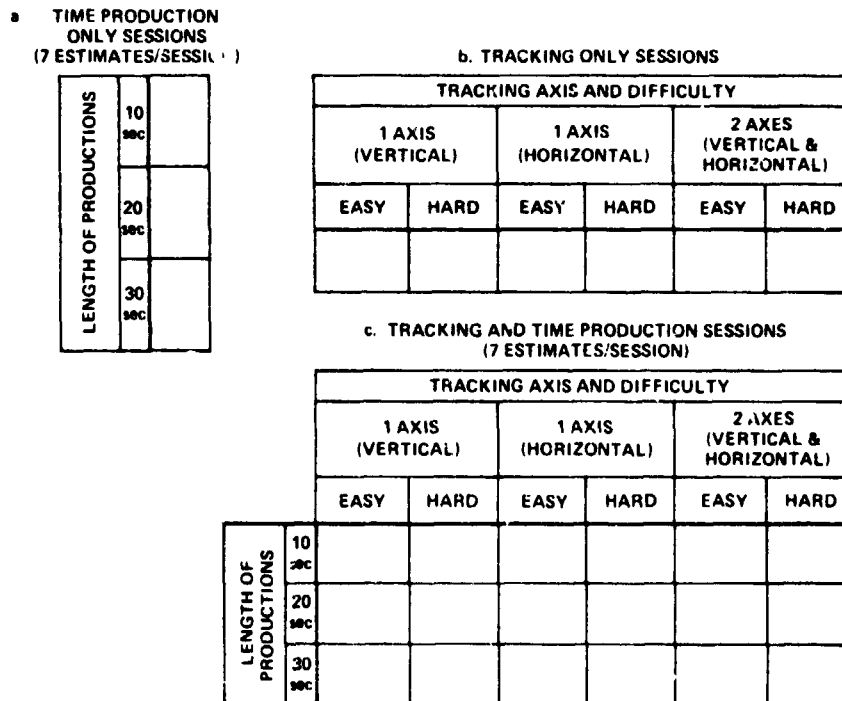


Figure 2. Experimental design (n=9).

Subjects experienced each of the six tracking tasks during the next six sessions. They were not required to produce intervals of 10, 20, or 30 sec during these six sessions, although they were asked to verbally estimate the duration of each session at its conclusion. Tracking only sessions were randomly varied in length from 2-4 min (fig. 2b).

During the last 18 sessions, subjects were asked to produce seven estimates of either 10, 20, or 30 sec while performing each of six tracking tasks (fig. 2c). Each pilot participated in all 27 experimental sessions. Although a preliminary study indicated no order effects for the time estimation tasks, such effects were found for successive levels of the tracking tasks. Therefore, experimental

sessions were presented in a quasi-random order so that no level of the time production or tracking tasks were repeated twice in a row. The last 18 sessions were presented in a different order to each subject.

An intertrial interval randomly varied ± 1.0 sec around a mean of 10 sec occurred after each of the seven productions made within a session. A 3-min rest interval followed each of the 27 experimental sessions. Subjects were asked to verbally estimate the duration of the immediately preceding session during this period. A 10-min rest period was given every 30 min during which subjects were allowed to leave the experimental chamber. The entire experiment lasted about 2.5 hr per subject, although the exact length depended on the length of time productions made by individual subjects.

RESULTS AND DISCUSSION

Tracking Task Results

Pilot performance on the tracking tasks used in this study indicated that the different conditions represented different degrees of difficulty. Tracking performance improved between tracking only and tracking with concurrent time production sessions, indicating that subjects had not reached asymptotic performance levels (table 1). The ratios of RMS error to RMS input for the six tracking tasks were significantly different ($F = 144.74$; $df = 5,40$; $p < 0.001$) as a function of the number of axes controlled simultaneously and the difficulty of the forcing function (fig. 3). There were no apparent differences between performance measures on the vertical and horizontal axes for either the easy or hard forcing functions, so they were combined for tabular and graphic presentation. There were also no significant differences in tracking performance due to session length ($F = 2.70$; $df = 2,16$; $p > 0.10$). Relative RMS error increased from 0.24 to 0.30 as subjects were required to control one axis at a time or both simultaneously, and from 0.22 to 0.31 as the difficulty of the task increased from the easy to the hard forcing function.

RMS error scores were significantly different for successive segments of each session ($F = 2.68$; $df = 6,48$; $p < 0.05$). This difference did not reflect any consistent improvement or decrement in performance, however, but indicated that RMS error scores did not provide a stable measure of moment-to-moment workload. Tracking performance measures were thus not very useful in providing an indication of task difficulty for relatively short periods of time.

The time estimation task did not appear to degrade performance on the tracking task. The relative RMS error was somewhat higher for sessions in which tracking was the only task than for sessions in which time intervals were produced while tracking (table 1). It is

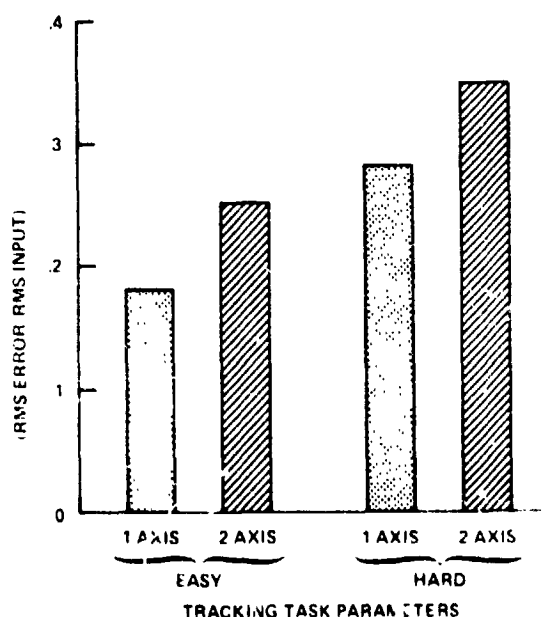


Figure 3. Mean relative RMS tracking error for sessions with concurrent time production ($n=9$)

TABLE 1.- RELATIVE RMS ERROR

[RMS Error/RMS Input]

		Tracking only				Tracking with concurrent time production			
Difficulty		Easy		Hard		Easy		Hard	
No. Axes		1	2	1	2	1	2	1	2
Subject number	1	0.07	0.16	0.22	0.29	0.10	0.16	0.18	0.27
	2	.27	.39	.34	.52	.23	.33	.31	.45
	3	.26	.42	.32	.46	.13	.19	.23	.27
	4	.23	.28	.34	.35	.19	.31	.27	.34
	5	.11	.24	.25	.33	.13	.15	.24	.30
	6	.18	.31	.37	.59	.19	.23	.23	.29
	7	.37	.40	.28	.42	.19	.36	.29	.45
	8	.30	.48	.52	.49	.15	.35	.39	.52
	9	.32	.58	.24	.32	.18	.36	.28	.28
Mean		.21	.36	.32	.42	.18	.25	.27	.35
St. Dev.		.09	.12	.09	.10	.06	.08	.06	.09

also possible that tracking performance improved during later sessions because subjects had not yet reached asymptotic performance levels and that the effect of concurrent timing tasks on tracking performance cannot be clearly determined from this study.

Time Production Results

It was observed that successive productions within each session were not significantly different from each other ($F = 1.54$; $df = 6,48$; $p > 0.10$), confirming McGrath and O'Hanlon's (ref. 17) conclusion that subjects make repeated estimates under similar circumstances with a high degree of consistency. This indicates that the duration of single productions, representing brief periods of time, might provide a more stable measure of moment-to-moment workload imposed by concurrent activity than RMS error measures, which are only meaningful over periods lasting several minutes.

A convenient way to depict variation in the subjective appreciation of duration as measured by the length of productions (i.e., the subject's effort to delineate operatively a given interval of time) and verbal estimates of duration is to form a ratio between the length of subjective estimates and the interval of clock time that they represent. Productions that last longer than the interval of clock time that they represent, and verbal estimates that are shorter than the amount of elapsed time measured by the clock, represent equivalent lengthening of subjective units of duration relative to clock units. For example, if an individual's subjective units of duration are half again as long as

objective clock units, he would take 18 sec to produce a 12-sec interval, and would verbally estimate that an interval that actually lasted 12 sec, lasted only 8 sec. The 18-sec production and 8-sec verbal estimate in this example reflect an equivalent ratio between subjective and objective units of time equal to 1.5.

Productions of 10, 20, and 30 sec were quite accurate with respect to the clock, on the average, during sessions in which time production was the only task (fig. 4). However, the characteristic length of productions made by different subjects represented different degrees of accuracy with respect to the clock (table 2). The ratio of subjective to objective duration for 10-, 20-, and 30-sec productions ranged from 0.81 (19% shorter than the standard) to 1.77 (77% longer than the standard) for individual subjects.

As attention was diverted from time estimation, the average length of productions increased 23%, on the average across all tracking conditions. The average ratio of subjective to objective time ranged from 1.02 (2% longer than the standard) to 1.82 (82% longer than the standard) during the most difficult tracking task for individual subjects. This increase in the length of subjective units of duration with increasing distraction was statistically significant for 10-, 20-, and 30-sec productions ($F = 8.61$; $df = 6, 48$; $p < 0.001$).

The relative length of subjective units of duration increased by 20% with a concurrent single axis easy tracking task, and by 25% with a concurrent two axis hard tracking task relative to the length of productions made while performing no other task (fig. 5). This increase in the length of productions with concurrent distraction was nearly twice as great for subjects whose baseline productions were equal to, or shorter than, the length of the interval specified (Subjects 2, 5, 6, and 7), than for subjects whose baseline productions were already considerably longer than the interval specified (Subjects 3, 4, 8, and 9). If an individual's subjective units of duration were already considerably longer than external clock units under conditions involving minimal distraction, it appeared

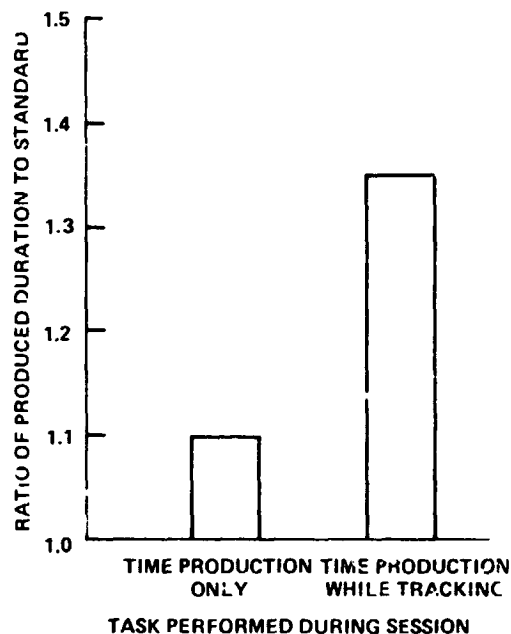


Figure 4.— Average increase in subjective duration as concurrent taskload increased from time production only, to time production while tracking; time production measure (n=9).

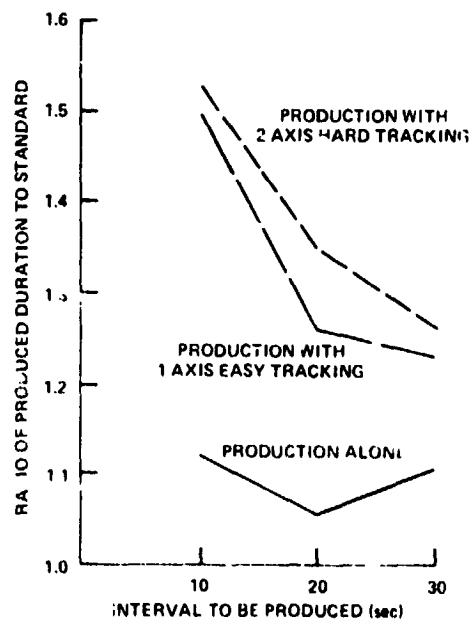


Figure 5.— Average increase in subjective duration as concurrent task difficulty increased; time production measure (n=9).

TABLE 2.-- TIME PRODUCTIONS
[Length of Estimates/Standard]

Activity during session		Time production only				Time production while performing 1 axis easy tracking				Time production while performing 2 axis hard tracking			
Length of production		10	20	30	Mean	10	20	30	Mean	10	20	30	Mean
Subject number	1	1.13	0.89	1.00	1.10	1.72	1.07	1.17	1.32	1.89	1.39	1.08	1.45
	2	.85	.84	.85	.85	1.28	1.13	1.14	1.18	1.34	1.23	1.29	1.29
	3	1.28	.98	1.02	1.09	1.20	1.28	1.35	1.28	1.53	1.33	1.72	1.53
	4	1.09	1.74	1.77	1.53	1.95	1.52	1.62	1.69	2.00	1.93	1.53	1.82
	5	1.02	1.00	1.03	1.02	1.21	1.11	.82	1.05	1.78	1.55	.90	1.41
	6	.79	.80	1.00	.86	1.46	1.14	.95	1.18	1.02	1.32	1.13	1.16
	7	.91	.73	.79	.81	1.07	1.17	1.06	1.10	1.25	.67	1.14	1.02
	8	1.57	1.33	1.30	1.40	1.34	1.60	1.20	1.38	1.46	1.15	1.33	1.31
	9	1.43	1.12	1.20	1.25	2.22	1.25	1.75	1.74	1.47	1.48	1.11	1.35
Mean		1.12	1.05	1.11	1.10	1.49	1.25	1.23	1.32	1.53	1.34	1.25	1.37
St. Dev.		.25	.30	.28	.24	.37	.18	.28	.23	.30	.32	.24	.21

TABLE 3.-- VERBAL ESTIMATES OF SESSION LENGTH
[Length of Interval/Length of Estimate]

Activity during session		Time production only				Tracking only		Time production while performing							
Length of production		10	20	30	Mean	1 axis easy	2 axis hard	1 axis easy tracking				2 axis hard tracking			
Subject number		10	20	30	Mean	-	-	10	20	30	Mean	10	20	30	Mean
Subject number	1	1.36	1.38	1.22	1.32	1.83	1.22	1.09	1.29	1.09	1.16	1.39	1.12	1.29	1.27
	2	1.14	.81	.94	.96	.94	1.64	1.10	1.58	.93	1.20	1.87	1.38	1.45	1.57
	3	1.20	1.22	1.10	1.17	1.01	.61	1.06	1.10	1.00	1.07	2.13	1.78	1.27	1.73
	4	1.04	.76	.76	.85	1.43	1.29	1.65	1.95	1.13	1.58	1.62	1.25	1.13	1.33
	5	1.26	1.05	.99	1.10	1.22	1.36	1.07	1.28	1.03	1.13	1.52	1.39	.89	1.27
	6	1.04	.72	1.14	1.03	1.04	.96	1.10	1.38	1.58	1.35	1.03	1.38	1.55	1.32
	7	.89	.74	.70	.78	1.30	1.34	1.01	1.23	1.11	1.12	1.57	1.02	1.51	1.37
	8	1.62	.76	1.03	1.13	1.80	1.75	1.41	1.67	1.86	1.65	1.49	1.33	1.49	1.44
	9	1.84	.80	1.32	1.32	1.34	.82	1.67	1.05	1.42	1.38	1.20	1.57	1.48	1.42
Mean		1.27	.94	1.02	1.07	1.32	1.22	1.24	1.39	1.24	1.29	1.54	1.36	1.34	1.41
St. Dev.		.28	.22	.19	.16	.30	.35	.25	.27	.30	.20	.31	.21	.21	.14

that he truncated the length of his productions under distracting conditions so that they rarely exceeded twice the length of the interval specified. This could be due to intellectual reassessment applied to the subjective impression of duration, or reflect an upper limit in the range of durations considered subjectively equivalent to 10, 20, or 30 sec under different conditions.

The length of 10-, 20-, and 30-sec productions relative to the length of the standard interval being estimated was approximately the same when time estimation was the only task. There was a significant difference in the relative length of 10-, 20-, and 30-sec productions across all experimental conditions, however, ($F = 7.48$; $df = 2,16$; $p < 0.01$), because 20- and 30-sec productions were relatively more accurate than 10-sec productions when there was concurrent distraction. Although the length of all productions increased as attention was diverted by tracking tasks, this effect was most pronounced for 10-sec productions (fig. 5). The length of 10-sec productions increased 35% on the average, relative to the length of productions made without distraction, whereas 20- and 30-sec productions lengthened only 23% and 12%, respectively. Since sessions involving 20- and 30-sec productions lasted longer than sessions involving 10-sec productions, it is possible that subjects might have had more time to become accustomed to the current tracking task parameters. Thus, performing the concurrent tracking task might have been relatively less distracting during longer sessions. If this was the case, it would have had the effect of increasing the amount of attention that could be focused on time estimation, thereby increasing the accuracy of estimation. Since the ratio of subjective to objective time was approximately the same for 10-, 20-, and 30-sec productions made without distraction, it does not appear to be characteristic of the intervals estimated per se.

It is also possible that longer sessions were more stressful, even though RMS error on the tracking tasks was not affected by session length. Hypothetically, stress would tend to reduce the length of subjective units of duration (ref. 3) thereby reducing the length of productions. It would be necessary to standardize session length, rather than the number of productions made per session as was done in the present study, to further investigate this phenomena.

Variability among the seven productions made during each session increased as the difficulty of the concurrent tracking task increased. This is consistent with Michon's (ref. 1) suggestion that irregularity of timing responses reflects the perceptual and motor load of concurrent tasks. For example, the squared deviations of individual 10-sec productions from the mean length of productions made during different sessions increased from 3 sec^2 (when time production was the only task) to 8 sec^2 (for productions made while tracking a single-axis easy task) to 10 sec^2 (for productions made while performing a two-axis hard task), averaged across subjects.

In conjunction with longer objective time taken to produce intervals under conditions of increasing distraction, increased variability between successive productions provides further support for the conclusion that time estimation requires attention for accuracy and consistency. The regularity with which attention could be directed to the timing task varied from session to session as a function of the amount of attention required by concurrent activity. Estimates were internally consistent and relatively accurate with respect to the clock under low distraction conditions. As attention was diverted from rehearsing or monitoring the events used for subjective timing, the regularity with which estimates were made decreased and subjects took longer to produce 10, 20, and 30 sec estimates during sessions in which they were also performing a tracking task. This increase in variability and length of productions occurred for all subjects.

Verbal Estimate Results

Subjects tended to verbally estimate session length in round numbers (e.g., 2 min and 15 sec), resulting in less precise measures of subjective duration than the length of time productions, which were measured exactly by a clock. Despite a relative lack of precision, verbal estimates of session length also reflected the degree to which attention had been diverted from timekeeping during the preceding session. The length of verbal estimates decreased significantly with respect to the actual length of sessions as the amount of distraction during the preceding session increased. This decrease in the length of verbal estimates relative to elapsed time indicates that subjective units of duration increased in length as distraction increased. This reflects the same increase in the length of subjective units of duration that was indicated by the length of productions made during the session.

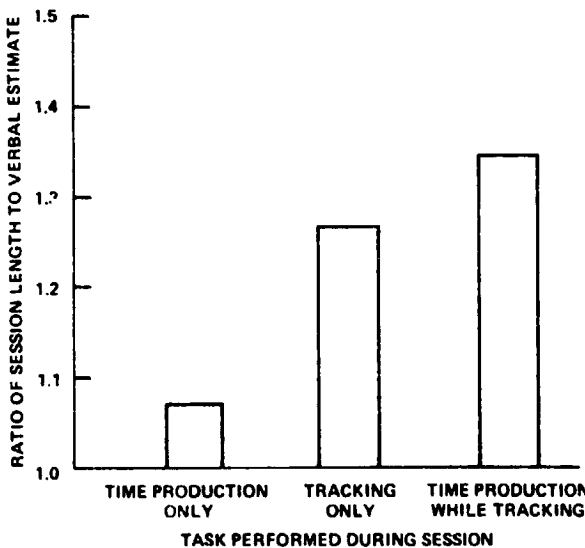


Figure 6.— Average increase in subjective duration as task load during preceding session increased from time production only, to tracking only, to time production and tracking; verbal estimate measure (n=9).

Three types of task loads were presented in the 27 experimental sessions. In three sessions, time production was the only task. In six other sessions, tracking was the only task. In 18 sessions, time production and tracking were both required. As the task load in the preceding session increased from time production alone to tracking alone, subjective units of duration measured by the length of verbal estimates relative to session length increased by 19%. As the task load increased from time production alone to time production while tracking, subjective units of duration measured by the length of verbal estimates relative to session length, increased 26%. On the average, subjective units of duration also increased as the difficulty of the tracking task performed during a session increased, but only for sessions in which time production and tracking were both required (table 3). There was a significant differ-

ence between: the length of verbal estimates made of sessions involving minimal distraction (time production alone) and those involving maximum distraction (time production while tracking) for sessions that involved 10-, 20-, or 30-sec productions ($F = 7.14$; $df = 6,48$; $p < 0.001$). There was no difference in the relative length of verbal estimates as a function of the length of productions made during the preceding session, however ($F = 3.77$; $df = 2,16$; $p > 0.10$).

Concluding Remarks

These data lend support to the hypothesis that concurrent tasks reliably distract subjects from time estimation. The duration of subjective time estimates appears to be a useful measure of the workload imposed by a manual control task, providing a more stable indication of task load from moment to moment than RMS error. As workload increases, humans seem progressively less able to attend to timing tasks, thereby increasing the length of their temporal productions relative to the objective standard and verbally underestimating the passage of time relative to measurements provided by a clock. It has been shown that time estimation, as employed here, does not appear to conflict with performance on a manual control task, rather that time estimation accuracy suffers when primary task demands increase. It is anticipated that the duration and variability of time estimates during complex control tasks, such as aircraft simulations, will reflect the perceptual and motor load imposed by a primary task. To the extent that different displays reduce perceptual load and usefully integrate information for pilots, reliable variations on a concurrent time estimation task are predicted.

REFERENCES

1. Michon, J. A.: Tapping regularity as a measure of perceptual motor load. *Ergonomics*, Vol. 9, pp. 401-412, 1966.
2. Norman, D. A.: On data-limited and resource limited processing. *Cognitive Psychology*, Vol. 7, pp. 44-64, 1975.
3. Curton, E. D.; and Lordahl, D.S.: Effects of attentional focus and arousal on time estimation. *J. Exp. Psycho.*, Vol. 103, No. 5, pp. 861-867, 1974.
4. Ornstein, R. E.: *On the experience of time*. Baltimore: Penguin Books, 1970.
5. Einstein, A., and Infeld, L.: *The evolution of physics: The growth of ideas from early concept to relativity and quanta*. New York: Simon and Schuster, p. 187, 1938.
6. James, W.: *Psychology*. Cleveland: Fine Edition Press, ch. 17, 1948.
7. Frankenhaeuser, M.: *Estimation of time, an experimental study*. Stockholm: Almqvist and Wiksell, 1959.
8. Holubar, J.: *The sense of time: An electroencephalographic study of its mechanisms in man*. Cambridge, Mass.: The M.I.T. Press, 1961.
9. Fischer, R.: Biological time. In Fraser, J. T. (ed.) *The voices of time*. New York: Braziller, 1966.
10. Werboff, J.: Time judgement as a function of electroencephalographic activity. *Exp. Neurol.*, Vol. 6, pp. 152-160, 1962.
11. Bell, C. R.; and Provins, K. A.: Relation between physiological measures to environmental heat and time judgements. *J. Exp. Psychol.*, Vol. 66, No. 6, pp. 572-579, 1963.
12. Fox, R. H.; Bradbury, P.A.; Hampton, I. F. G.; and Legg, C. F.: Time judgement and body temperature. *J. Exp. Psychol.*, Vol. 75, No. 1, pp. 88-96, 1967.

13. Cahoon, R. L.: Physiological arousal and time estimation. *Perceptual and Motor Skills*, Vol. 28, pp. 259-268, 1969.
14. Anliker, J.: Variation in alpha voltage of the electroencephalogram and time perception. *Science*, Vol. 140, No. 3573, pp. 1307-1309, 1963.
15. Massaro, D. W.; and Kahn, B. J.: Effects of central processing on auditory recognition. *J. Exp. Psychol.*, Vol. 97, No. 1, pp. 51-58, 1973.
16. Stroud, J. M.: The fine structure of psychological time. In Quastler, H. (ed.) *Information theory and psychology*, Glencoe, Ill.: Free Press, pp. 174-207, 1955.
17. McGrath, J. J.; and O'Hanlon, J. F.: Method for measuring the rate of subjective time. *Perceptual and Motor Skills*, Vol. 24, pp. 1235-1240, 1967.

N75 33680

FAILURE DETECTION BY PILOTS DURING AUTOMATIC LANDING: MODELS AND EXPERIMENTS *

Eli G. Gai
C.S. Draper Laboratories
Room DL7-173
75 Cambridge Parkway
Cambridge, MA 02142

R.E. Curry
Man Vehicle Laboratory
Room 37-219
M. I. T.
Cambridge, MA 02139

ABSTRACT

A model of the pilot as a monitor of instrument failures during automatic landing is proposed. The failure detection model of the pilot consists of two stages: a linear estimator (Kalman Filter) and a decision mechanism which is based on sequential analysis. The filter equations are derived from a simplified version of the linearized dynamics of the airplane and the control loop. The perceptual observation noise is modelled to include the effects of the partition of attention among the several instruments. The final result is a simple model consisting of a high pass filter to produce the observation residuals, and a decision function which is a pure integration of the residuals minus a bias term

The dynamics of a Boeing 707 were used to simulate the fully coupled final approach in a fixed base simulator which also included failures in the airspeed, glideslope, and localizer indicators. Subjects monitored the approaches and detected the failures; their performance was compared with the predictions of the model with good agreement between the experimental data and the model.

INTRODUCTION

The introduction of the "all weather" automatic landing system changes the role of the pilot during landing. Under normal conditions, the pilot is not in the control loop, but his main task is to monitor the proper operation of the automatic system. This, of course, shifts his role from manual controller to decision maker.

The problem of modelling the pilot as a controller has been addressed by several researchers, and satisfactory models exist using classical control theory (1) or optimal control theory (2). Models for the pilot as a failure detector have only recently been addressed (3), and some conjecture has been suggested (4).

In this paper, a model of a pilot as a monitor of system failures is proposed and applied to an automatic landing. The model consists of two stages: a linear estimator and a decision mechanism. The linear estimator is the Kalman Filter which is similar to that used in the optimal controller model; the outputs used here are the measurement residuals rather than the estimates. The decision mechanism is based on sequential analysis (5) modified for the special case of failure detection (6). Experiments were designed to validate the proposed model in which subjects monitored failures in simulated automatic ILS

*Sponsored by NASA Grant NGR 22-009-733, NASA Ames Research Center

approaches in a fixed-based jet transport cockpit. The results of these experiments are then compared to the prediction of the model.

PROBLEM STATEMENT AND SIMPLIFICATION

A functional block diagram of the failure detection model is shown in Figure 1. A basic assumption in the structure of the first stage (the estimation) is that the dynamical characteristics of the system that produces the input signals are known by the observer. Therefore, before the modelling of the failure detection system, we will discuss the model that the pilot has in mind (the internal model) for the airplane dynamics and control loops.

The true airplane dynamics, when angular accelerations are neglected, can be defined by nine first order nonlinear differential equations. Two decoupled autopilots are used to regulate the vertical error between the aircraft position and the glideslope beam, and the horizontal (angular) error between aircraft position and localizer beam. In addition, a third control loop controls the aircraft airspeed. This configuration was used in the simulation that automatically landed the Boeing 707 dynamics used in our experiments (7).

Since the pilot is outside the control loop his inputs consist only of the displayed variables on his instrument panel. If the control system is designed properly, these displays will show nominal values with variation due to outside perturbations. It seems reasonable to assume that the pilot will use the linearized version of the automatic system around the nominal values. In addition, we will assume that the longitudinal and lateral dynamics are decoupled in the pilot's model. The block diagrams of the three control loops are shown in Figure 2, and the basic configuration was taken from reference 8. Therefore the three closed loop transfer functions are given by

$$\frac{\delta u}{\delta u_n} = \frac{10(S+0.1)}{(S+8.8)(S+.98)(S+0.13)} \quad (1)$$

where: u - velocity
 γ - flight path angle
 θ - pitch
 ψ - heading

$$\frac{\delta \gamma}{\delta \theta_n} = \frac{31.3}{(S+0.5)(S+5.5)(S^2+5.45S+11.4)} \quad (2)$$

$$\frac{\delta \psi}{\delta \psi_n} = \frac{47}{(S^2+11S+58)(S^2+1.5S+0.81)} \quad (3)$$

The letter δ is used to identify the inputs as perturbations rather than commands, and the outputs are the responses to these perturbations. The subscript n is used because the input perturbations are modelled as zero mean white Gaussian processes. The source for these perturbations is usually the wind gusts, and therefore the inputs to the subsystem are correlated and are derived from the amplitude and direction of these gusts. Two of the above subsystems are of fourth order and one is of third order. Another integration of each subsystem output is needed to obtain the aircraft position. Therefore, we assume that the pilot uses only the dominant poles, namely the ones

with the longer time constants. The final model that is used in the pilot model is

$$\frac{\delta u}{\delta u_n} = 1/(S+1) \quad (4)$$

$$\frac{\delta \gamma}{\delta \theta_n} = 1/((S+0.5)(S+2.7)) \quad (5)$$

$$\frac{\delta \psi}{\delta \psi_n} = 1/(S^2+1.5S+0.81) \quad (6)$$

Note that the steady state gain and the steady state variance of the response to a stationary random input were kept the same as in the original systems.

Having three decoupled systems, we can define 8 state variables by transforming equations (4) to (6) to their state space format. Define

$$\begin{aligned} x_1 &= \int \delta u & x_2 &= \delta u & x_3 &= \int \delta \gamma & x_4 &= \delta \gamma \\ x_5 &= 0.585 \delta \alpha & x_6 &= \int \delta \psi & x_7 &= \delta \psi & x_8 &= g \delta \phi / V_0 \end{aligned} \quad (7)$$

The dynamics in matrix notation are:

$$\dot{\underline{X}} = \underline{F}\underline{X} + \underline{G}\underline{U} \quad (8)$$

where

$$\underline{F} = \begin{bmatrix} F_1 & 0 & 0 \\ 0 & F_2 & 0 \\ 0 & 0 & F_3 \end{bmatrix} \quad \underline{F}_1 = \begin{bmatrix} 0 & 1 \\ 0 & 1 \end{bmatrix} \quad \underline{F}_2 = \begin{bmatrix} 0 & 1 & 0 \\ 0 & 0 & 1 \\ 0 & -1.35 & -3.2 \end{bmatrix}$$

$$\underline{F}_3 = \begin{bmatrix} 0 & 1 & 0 \\ 0 & 0 & 1 \\ 0 & -0.81 & -1.5 \end{bmatrix} \quad \underline{U}^T = [\delta u_n, \delta \theta_n, \delta \psi_n] \quad \underline{G}^T = \begin{bmatrix} 0 & 1 & 0 & 0 & 0 & 0 & 0 & 0 \\ 0 & 0 & 0 & 0 & 1.35 & 0 & 0 & 0 \\ 0 & 0 & 0 & 0 & 0 & 0 & 0 & 0.81 \end{bmatrix}$$

The perturbations in the aircraft position in terms of the above state variables are given by (using the fact that γ_0 is small):

$$\begin{aligned} \delta x &= \cos \psi_0 x_1 - v_0 \sin \psi_0 x_6 \\ \delta y &= \sin \psi_0 x_1 - v_0 \cos \psi_0 x_6 \\ \delta z &= \gamma_0 x_1 + v_0 x_3 \end{aligned} \quad (9)$$

where the subscript 0 designates nominal values.

All the variables that are displayed to the pilot can now be represented as linear functions of the state variables

1. Glideslope Indicator: $y_1 = (-\cos \psi_0 / x_N^2 + \gamma_0 / x_N) x_1 + v_0 x_3 / x_N + v_0 \sin \psi_0 x_6 / x_N^2$
2. Localizer: $y_2 = [\cos \psi_0 / (1.23 - x_N)^2 + \sin \psi_0 / (1.23 - x_N)] x_1 + [v_0 \cos \psi_0 / (1.23 - x_N) - v_0 \sin \psi_0 / (1.23 - x_N)^2] x_6$
3. Airspeed indicator. $y_3 = x_2$

4. Altitude indicator: $y_4 = x_4 + x_5/0.585$ (pitch)
 $y_4 = v_0 x_8/g$ (roll angle)
5. Horizontal situation display: $y_6 = x_7$
6. Altimeter: $y_7 = \gamma_0 x_1 + v_0 x_3$
7. Vertical speed indicator: $y_8 = \gamma_0 x_2 + v_0 x_4$

x_N in the above equations is the nominal value in the x direction which is time varying.

THE FAILURE DETECTION MODEL

In the last section we suggested a simplified linear model which the pilot is assumed to use as a model for the instrument output dynamics. On the basis of these dynamics the failure detection model that was suggested by Gai (6) is used. As mentioned before, the model consists of two stages: a linear estimator and a decision mechanism. The linear estimator, the Kalman Filter, is shown in Figure 3. It should be noted that due to the time dependency of the measurements the Kalman gain $K(t)$ is time varying. The filter produces estimates for the state $\hat{x}(t)$ and the measurements $\hat{y}(t)$ as well as the measurement error (residual) $\varepsilon(t)$ which is defined as

$$\varepsilon(t) = y(i) - \hat{y}(t) \quad (10)$$

Any of these three quantities can be used as an input to the decision mechanism. The observation residual is preferred for the following reasons:

1. The state variables are non-unique variables that can be defined in many ways, while the observation residual is unique and well-defined for the subject.
2. The dimension of the state is in general larger than the dimension of the residual.
3. The residual is more sensitive than the observation to the effect of the failure (9).
4. The residual is a zero mean white process (10) in the unfailed mode so successive observations are independent for Gaussian processes.

In the instrument failure mode, we will assume that a deterministic mean is added to the measurement so that the residual is still white Gaussian with the same variance but with a non-zero mean.

Since the pilot is using 3 instruments the problem of sharing of attention has to be accounted for. This is done through the measurement noise in the observer model (11). If the pilot is observing more than one instrument, his observation noise for each observation is increased by a constant factor that is inversely proportional to the fraction of attention that he spends monitoring that specific instrument. Finally, it should be noted that although the state equations are decoupled, the Kalman Filter is a coupled 8 dimensional system because of the coupling through the measurements. The model of the estimation scheme is shown in Figure 4.

The decision mechanism is based on sequential analysis (5). The classical sequential analysis uses the likelihood ratio $\lambda(m)$ as a decision function after m observations. Two criteria levels, A and B, are chosen, and the decision rule is

$$\begin{array}{ll} \text{if } \lambda(m) \geq A & \text{choose "failure"} \\ \text{if } \lambda(m) \leq B & \text{choose "normal"} \\ \text{if } B < \lambda(m) < A & \text{take another observation} \end{array}$$

A and B are determined by the desired probability of false alarm $P(\text{FA})$ and the probability of miss $P(\text{MS})$ follows (5)

$$A = (1 - P(\text{MS})) / P(\text{FA}) \qquad B = P(\text{MS}) / (1 - P(\text{FA})) \qquad (11)$$

Since in our case, both distributions are white Gaussian with equal variances and means zero and θ_1 (failure), the decision function (for $\theta_1 > 0$) is (6)

$$\lambda(m) = \sum_{i=1}^m \{e_i - \theta_1/2\} \qquad (12)$$

the upper criterion level is $(\ln A) / \theta_1$ (13)

and the lower criterion level is $(\ln B) / \theta_1$ (14)

The classical theory cannot be applied directly to the failure detection problem because the basic assumption in the derivation was that the same mode exists during the entire period. A failure detection problem is characterized by a transition from the normal mode to the failure mode at some random time t_f . In order to overcome this difficulty, we followed Chein (12) by:

1. Resetting the decision function to zero whenever $\lambda(m)$ is negative.
2. Using only an upper criterion level A_1 which is modified to keep the same mean time between two false alarms as before including the resetting.

The value of A_1 is related to A and B in equation (11) by the equation

$$A_1 - \ln A_1 - 1 = -\{\ln A + (A - 1) \ln B / (1 - B)\}$$

The modified decision function is shown in Figure 5 and the block diagram of the basic decision mechanism is shown in Figure 6. For the case $\theta_1 < 0$, the decision function is

$$\lambda(m) = \sum_{i=1}^m (e_i + \theta_1/2) \qquad (15)$$

and only the lower criterion level is used. This criterion level is

$$-(\ln A) / \theta_1 \qquad (16)$$

The final block diagram of the decision mechanism is shown in Figure 7.

The operation of the proposed model is actually quite simple in principle. Its basic properties are:

1. A high pass filter as a first stage to obtain the residuals
2. Integration of the residual and comparison to a fixed threshold as a

decision mechanism (6).

3. Only three parameters control the performance of the model:
 - a. The parameter designating the mean of a "failed" process, θ_1
 - b. The signal to noise ratio of the observation noise in the Kalman Filter
 - c. The probabilities of the two types of error $P(FA)$ and $P(MS)$.

EXPERIMENTAL VALIDATION

Method

The Adage Model 30 Graphics Computer was used to simulate the non-linear dynamics of a Boeing 707 and the control loops (7). The output variables were fed into the instrument panel of a fixed based Boeing 707 simulator.

The simulation included the last five minutes of flight prior to touch down from 10 miles from threshold and at 2500 feet altitude; the approach and landing were fully automatic. The failures that were used were instrument failures, so that they affected only the output variables and were not fed back to the system. In order to limit the experimental requirements, we considered only failures in two instruments, the glideslope (GS) indicator and the airspeed (AS) indicator. Four levels of failures were included for each of the two instruments. All failures were deterministic step changes that were fed into the instrument through a single pole low pass filter with 0.1 second time constant. The magnitude of the failures for the AS indicator were

$$c_1 = 2\sigma_v \quad c_2 = 3\sigma_v \quad c_3 = 4\sigma_v \quad c_4 = 5\sigma_v \quad (17)$$

and for the GS indicator

$$c_1 = \sigma_{GS} \quad c_2 = 1.5\sigma_{GS} \quad c_3 = 2\sigma_{GS} \quad c_4 = 2.5\sigma_{GS} \quad (18)$$

where σ_v and σ_{GS} are the standard deviations of the perturbation from the nominal of the displayed variable on the AS and GS indicators respectively. The cutoff frequency of these perturbations were $\pi/6$ radians/sec. Two random number generators were used to choose the failure in each run; one determined the instrument and the other the size of the failure. In addition, a third random number generator was used to determine the time of failure, t_f .

There was a single failure in 90% of the runs. The high percentage of runs with failures was chosen to provide enough data in a reasonable experimental time. There was no feedback to the pilot concerning his performance because it was felt that such feedback would bias his decision, by driving him to try to compensate for previous errors, or to overrelax after several correct decisions.

Each subject participated in three experimental sessions each of which included 16 runs, or a total of 48 runs. When the pilot detected a failure, he pressed a button and the run was terminated. Otherwise, the run would go until touch down. After termination of each run the subject was asked to fill out a form in which he stated which instrument failed and how he detected the failure.

At the beginning of each session, a set of instructions was read to the subject. In particular, he was told that failure would either be in the AS or GS indicator, but that he could use other instruments for verification.

Results

The experimental results for two subjects are summarized in Table 1. The table shows the mean and standard deviation of the detection time for failures in the two instruments. The results are also shown in Figures 8 through 11. These figures include the mean detection times that were predicted by the model. These mean values were obtained by the use of a Monte Carlo simulation, with the same number of runs as in the experiment. The values for the three model parameters were:

$$\text{SNR} = 36 \quad P(\text{FA}) = P(\text{MS}) = 0.05 \quad \theta_1 = 0.25 \quad (19)$$

The level of $P(\text{FA})$ was determined on the basis of the actual false alarm rate that was found in the experimental data. For both subjects, the predicted results seem to fit the experimental data well. Of course, better fit could be obtained by change of the parameters in equation (19).

CONCLUSIONS

In this paper we proposed a model for the performance of a pilot as a failure detector of instrument failures during an automatic landing. The model consists of two stages: a linear estimator and a decision mechanism. The linear estimator is the Kalman Filter which is determined from a simplified model of displayed-variable dynamics that are used by the pilot. The filter also accounts for the pilot's time sharing between instruments through the observation noise. The decision mechanism is based on classical sequential analysis with some modification for the failure detection case.

An experiment designed to test the validity of the model is described. In this experiment, subjects had to detect failures in the glideslope and air-speed indicators during a simulated landing in a Boeing 707 fixed base simulator. The results show that the predicted detection times fit the experimental data well. It should be remembered, however, that only instrument failures in the form of a change in the mean were discussed. Additional work is needed to verify the model to include failures that involve dynamic changes as well.

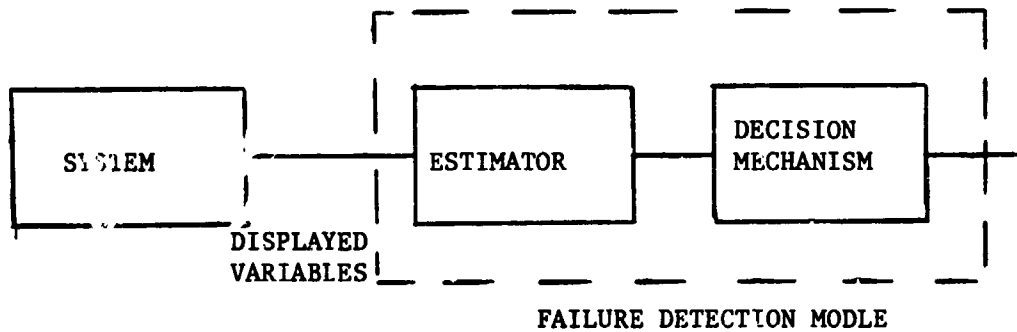


FIGURE 1 SCHEMATIC BLOCK DIAGRAM

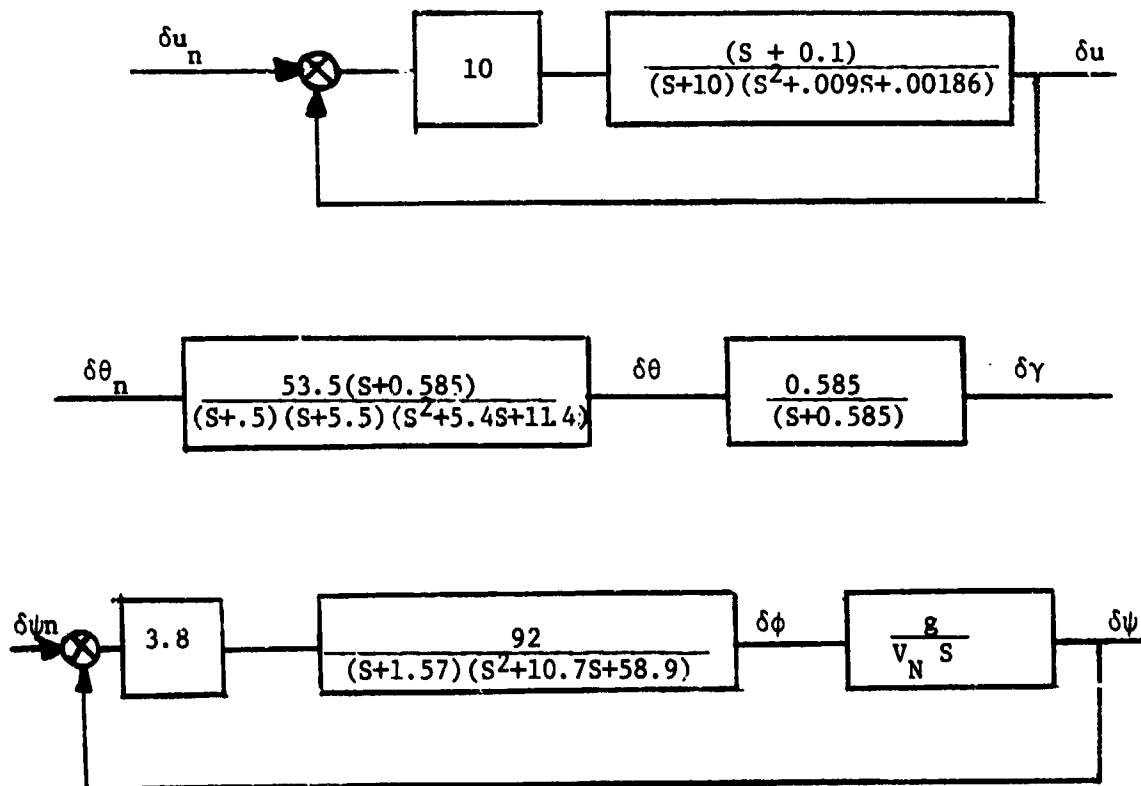


FIGURE 2 BLOCK DIAGRAM OF THE THREE CONTROL LOOPS

C-2

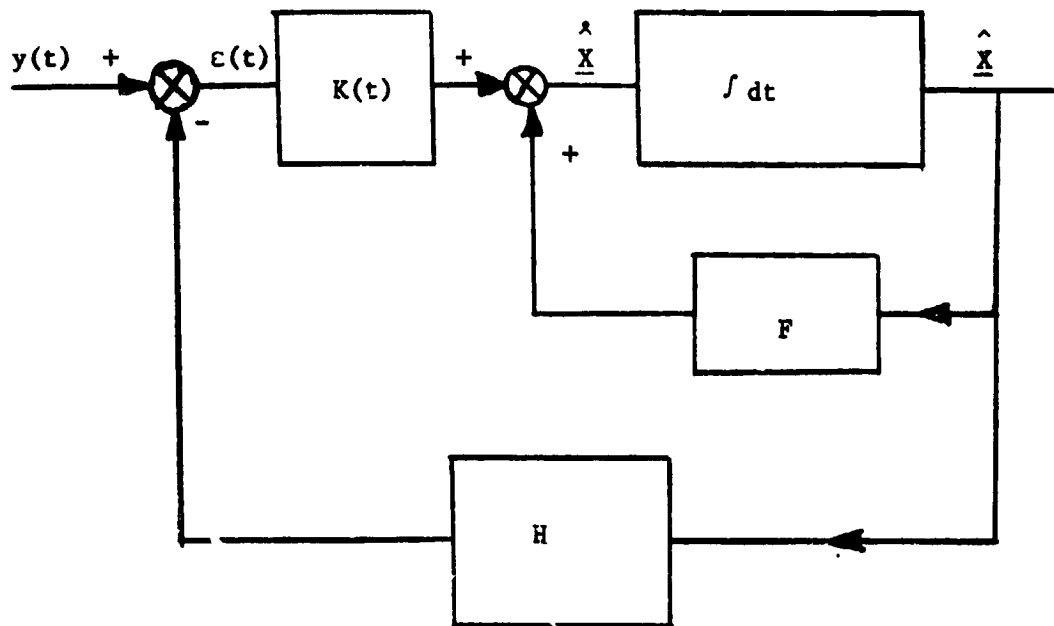


FIGURE 3 LINEAR ESTIMATOR (KALMAN FILTER)

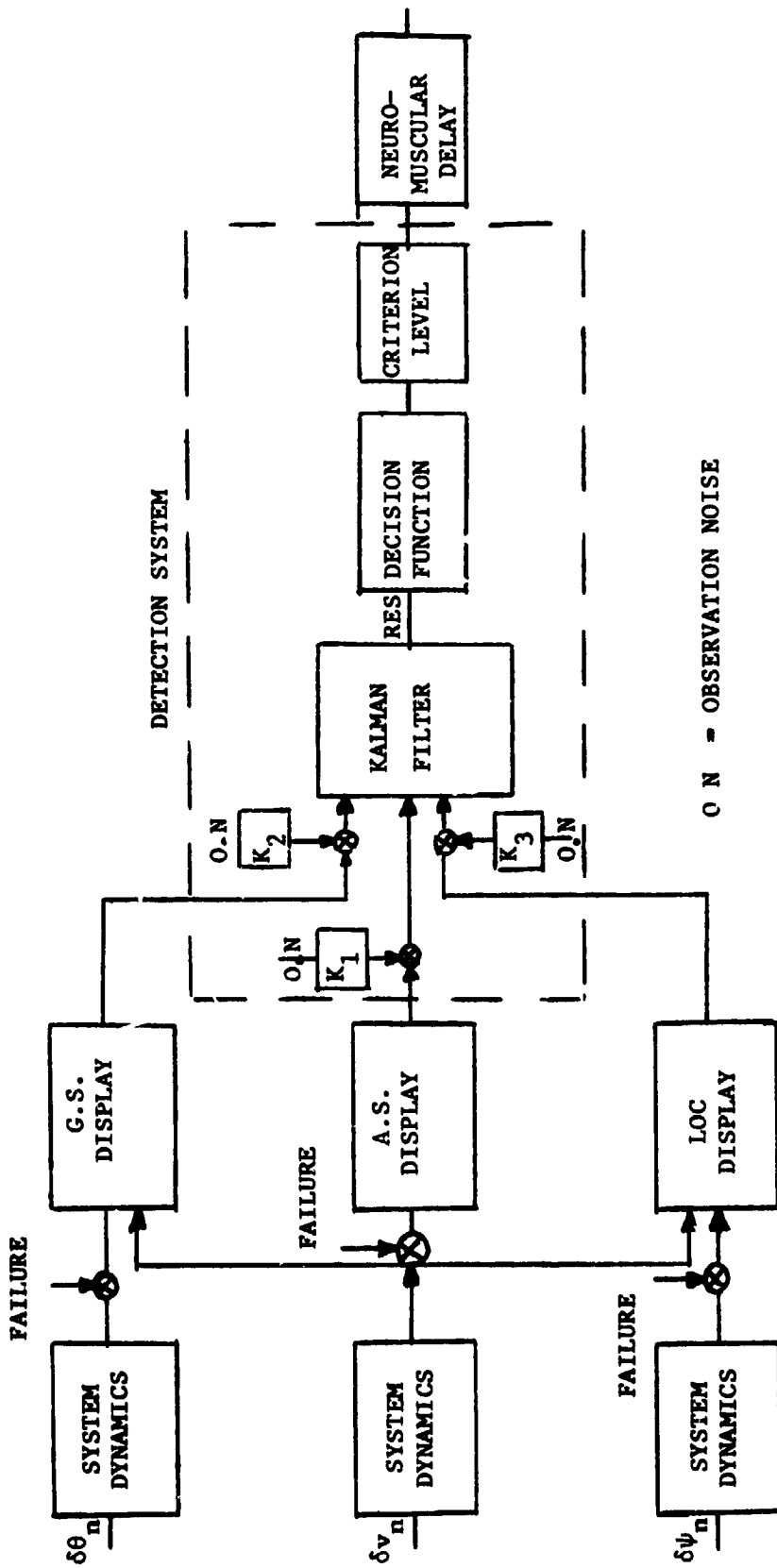


FIGURE 4. FUNCTIONAL DIAGRAM OF FAILURE DETECTION DURING AUTOMATIC LANDING

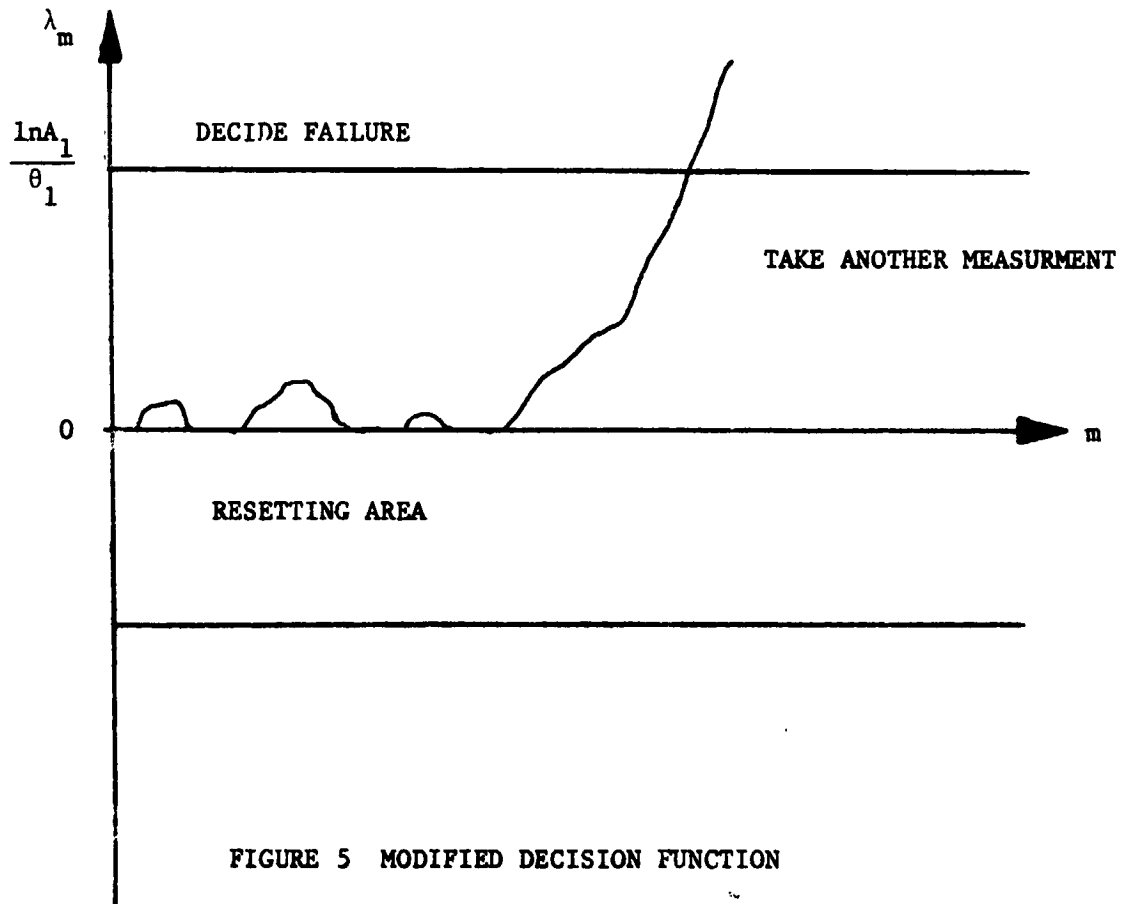


FIGURE 5 MODIFIED DECISION FUNCTION

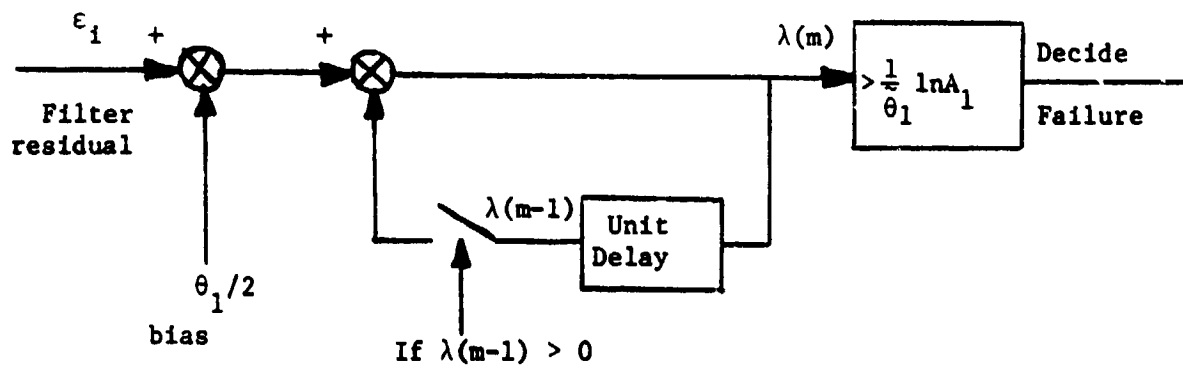


FIGURE 6 DECISION MECHANISM

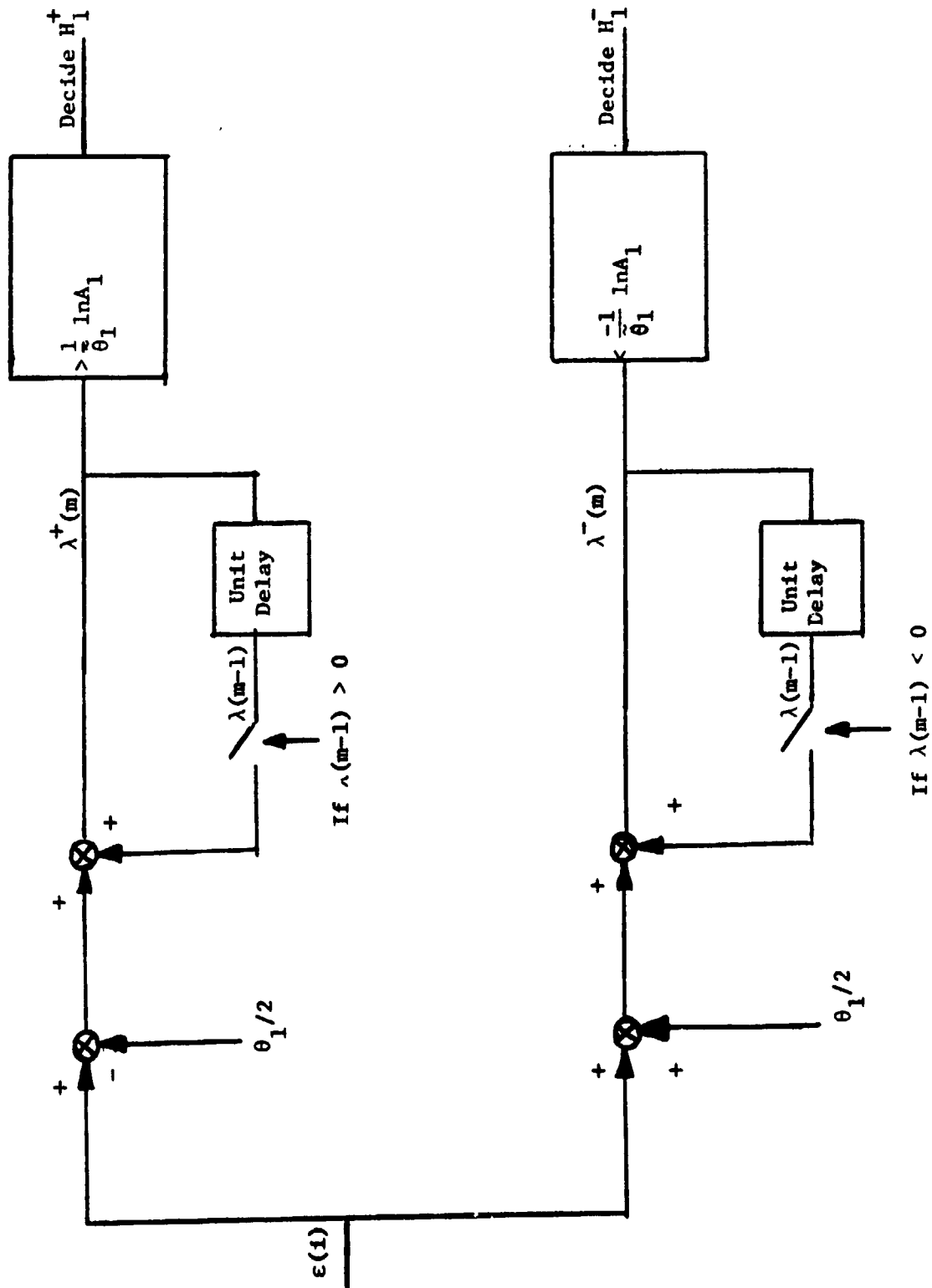


FIGURE 7. COMPLETE BLOCK DIAGRAM OF THE DECISION MECHANISM

FIGURE 8 DETECTION TIMES FOR GS FAILURES (FIRST SET, SUBJECT B.M)

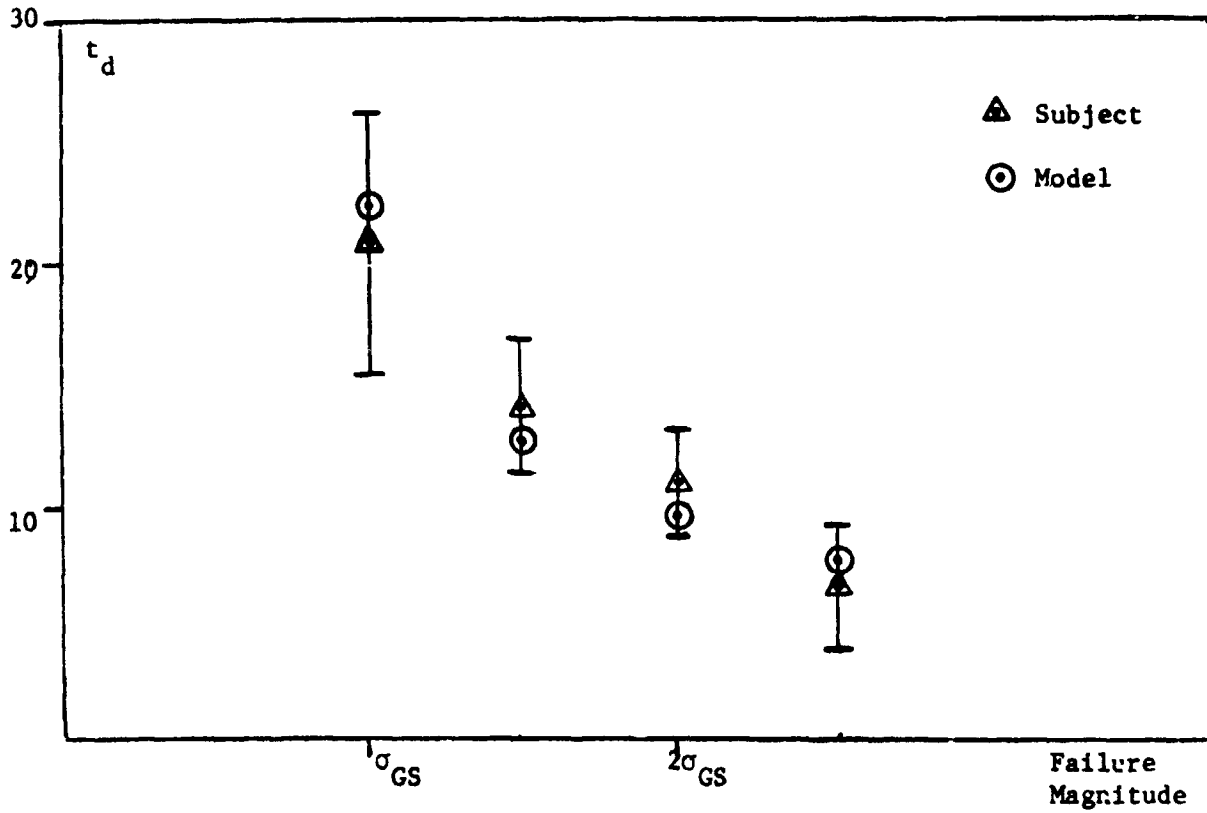
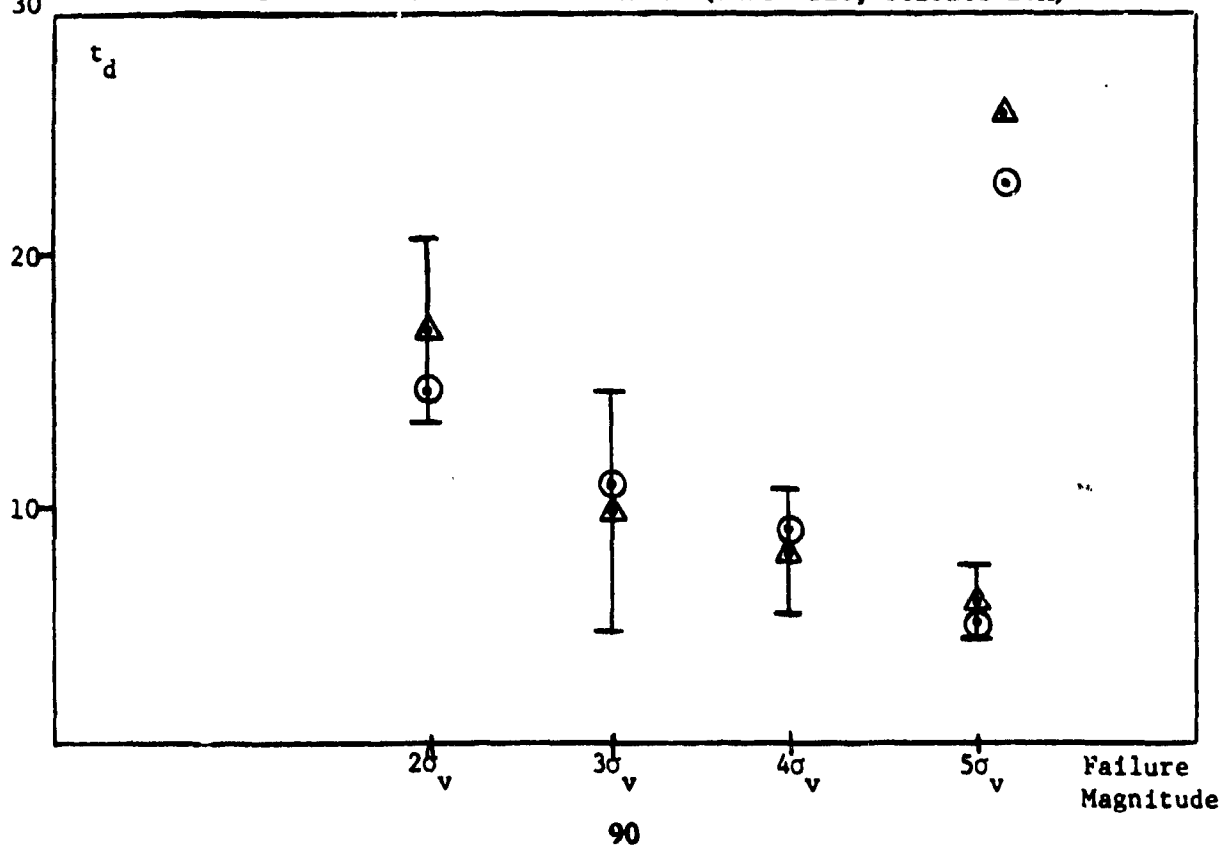


FIGURE 9 DETECTION TIMES FOR AS FAILURES (FIRST SET, SUBJECT B.M)



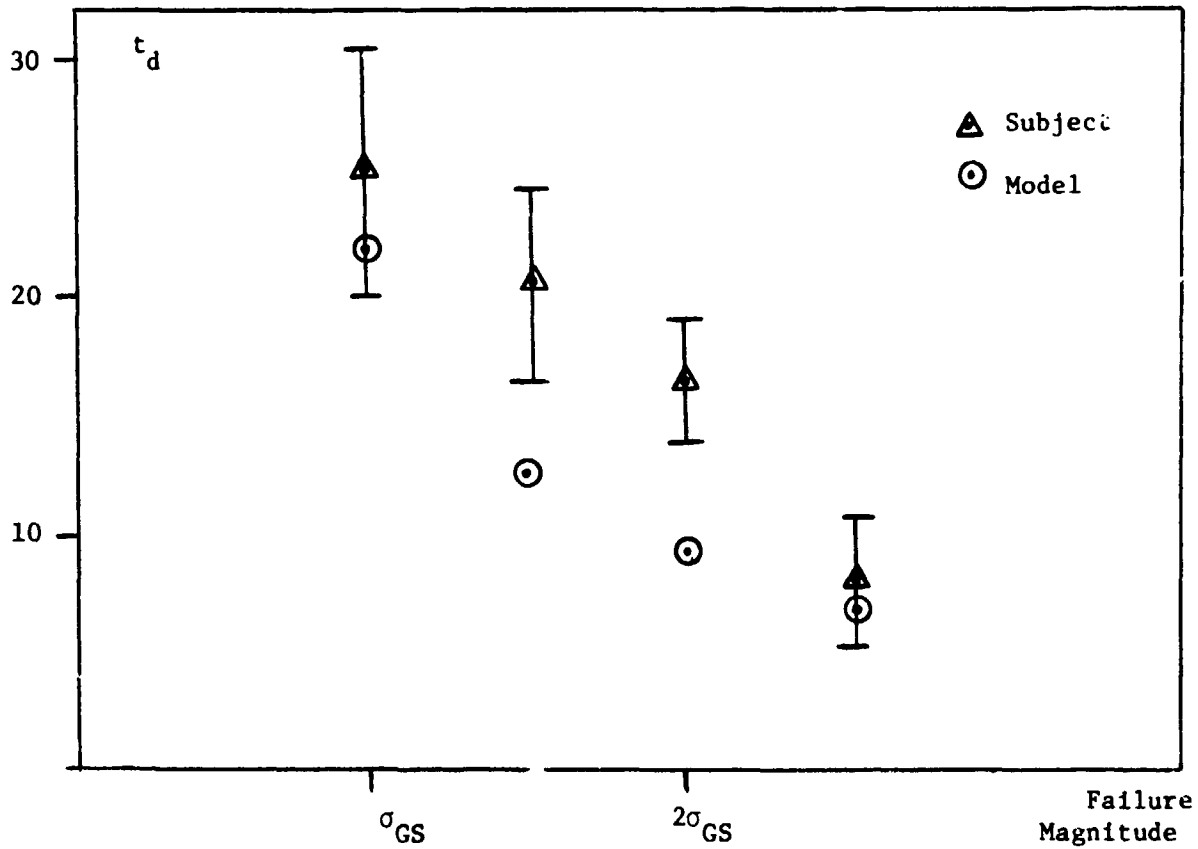


FIGURE 10 DETECTION TIMES FOR GS FAILURES (FIRST SET, SUBJECT C.C)

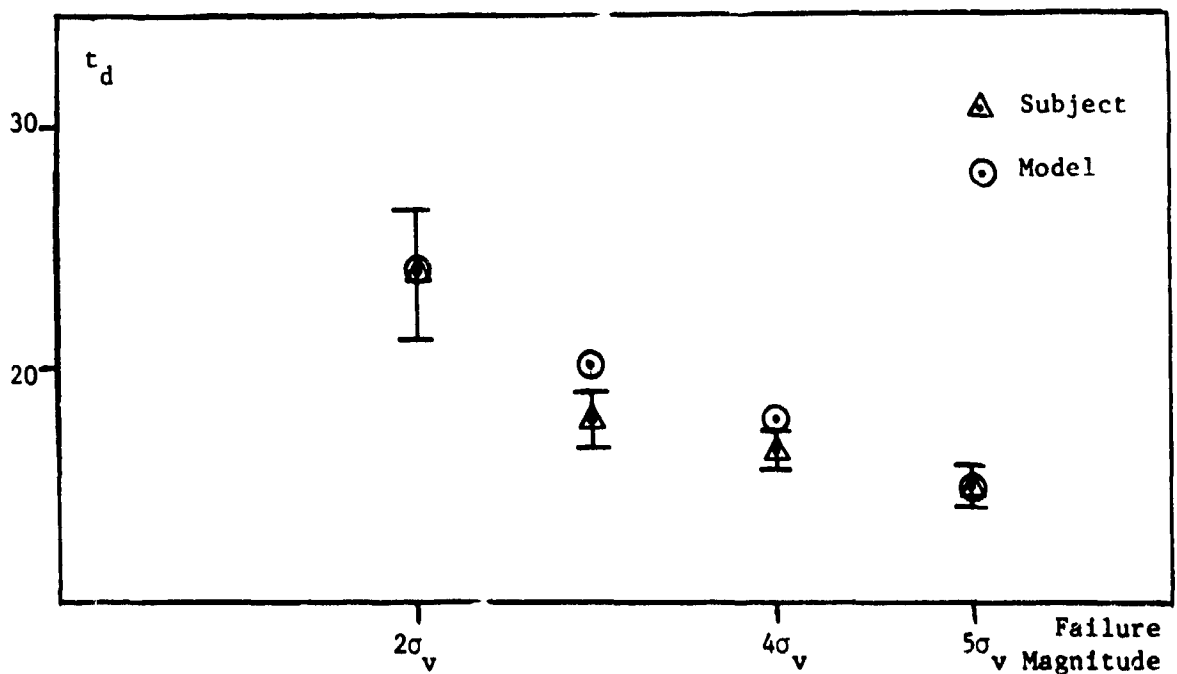


FIGURE 11 DETECTION TIMES FOR AS FAILURES (FIRST SET, SUBJECT C.C)

SUBJECT	INSTRUMENT	FAILURE MAGNITUDE	DETECTION TIMES (SECONDS)			
			C ₁	C ₂	C ₃	C ₄
B.M	AS	E(td)	20.8	13.8	10.8	6.3
		σ_{td}	5.9	2.7	2.1	2.7
	GS	E(td)	16.4	9.8	7.7	5.98
		σ_{td}	3.6	4.9	2.4	1.1
C.C	AS	E(td)	25.4	20.8	16.9	8.2
		σ_{td}	5.9	4.0	2.5	2.8
	GS	E(td)	14.0	6.9	6.3	5.0
		σ_{td}	2.8	1.0	0.9	0.9

TABLE I SUBJECTS PERFORMANCE IN EXPERIMENTAL SESSIONS

REFERENCES

1. McRuer, D.T., Jex, H.R., "A review of quasilinear pilot models", IEEE Transactions on HFE 8, 1967.
2. Kleinman, D.L., Baron, S., "Manned vehicle systems analysis by means of modern control theory", Bolt Beranek and Newman Report #1967, 1970.
3. Sheridan, T.B., Ferrel, W.R. Man Machine Systems MIT Press, 1974.
4. Phatak, A.V., Kleinman, D.L. "Current status of models for the human operator as a controller and decision maker in manned aerospace systems" Proceedings of the AGARD Conference, #114, October, 1972.
5. Wald, A. Sequential Analysis, J. Wiley, 1947.
6. Gai, E.G. "Psychophysical models for signal detection with time varying uncertainty", Ph.D. Thesis, Department of Aeronautics and Astronautics, Massachusetts Institute of Technology, January 1975.
7. Ephrath, A.R. "Pilot performance in zero visibility precision approach" Ph.D. Thesis, Department of Aeronautics and Astronautics, Massachusetts Institute of Technology, June, 1975.
8. Blacklock, J.H. Automatic Control of Aircraft and Missiles, J. Wiley, 1965.
9. Schweppe, F.C. Uncertain Dynamic Systems, Prentice Hall, 1973.
10. Kailath, T. "The innovation approach to detection and estimation theory" Proceedings of the IEEE, 58, 1970.
11. Levison, W.H. "A control theory model for human decision making" Proceedings of the Seventh Annual Conference on Manual Control, 1971.
12. Chien, T.T. "An adaptive technique for a redundant sensor navigation system", C.S. Draper Laboratory Report T-560, 1972.

N75 33681

HUMAN FACTORS RESEARCH PROBLEMS IN ELECTRONIC

VOICE WARNING SYSTEM DESIGN*

By C. A. Simpson and D. H. Williams

NASA Ames Research Center

SUMMARY

The speech messages issued by voice warning systems must be carefully designed in accordance with general principles of human decision-making processes, human speech comprehension, and the conditions in which the warnings can occur. The operator's effectiveness must not be degraded by messages that are either inappropriate or difficult to comprehend. Important experimental variables include message content, linguistic redundancy, signal/noise ratio, interference with concurrent tasks, and listener expectations generated by the pragmatic or real-world context in which the messages are presented.

INTRODUCTION

The human factors engineer has often been called in to patch some control or display system that was found to be unworkable as originally produced. This usually results in compromise designs, and requests by the human factors engineer to be placed in the design cycle earlier.

A new class of devices is being developed and produced, for which manufacturers may welcome some design guidance; these are *voice warning* devices. Such devices have seen limited use due to the expense and complexity of the required analog storage and playback system. Now digital techniques can store digitized speech (using approximately 3000 bits of memory per second of stored speech) or codes for synthesized speech segments (100 bits/sec) in read-only memory chips; digital synthesizers coupled with a small computer can create human-sounding speech rapidly and reliably. The job of human factors engineers and applied psycholinguists is to specify the content and format of these voice messages *before* they are programmed into the device.

This paper reviews past research that is relevant to the problem of synthesizer voice warning message design, discusses some issues relevant to the choice of a voice warning system, and lists some of the known human factors and linguistic design criteria. General areas in which further research is required are discussed using specific examples taken from requirements for cockpit voice warning systems.

*This research was performed while the authors held NRC resident research associateships at Ames Research Center.

VOICE WARNING RESEARCH TO DATE

A number of evaluation studies have been performed on human voice warning systems to study the overall effectiveness of voice warning systems in various military aircraft (refs. 1-4). Comparisons have been made among visual warnings, auditory nonspeech warnings, and voice warnings (refs. 1, 3, and 4) with the general findings that auditory warnings elicit corrective action faster than visual warnings (refs. 1, 3, and 4) and that, as flight task loading increases, pilots responded faster to voice warnings than to nonspeech auditory warnings; they did not scan the annunciator panel when given a voice warning whereas they did check the panel visually before responding to an auditory tone (ref. 3).

To our knowledge, little research has been done on the linguistic structure of voice warning messages, except for the phonetic confusability of messages (ref. 2). Research is now underway to define more general principles for the length, content, and structure of these messages, but until much more work has been done in this area, past empirical and theoretical work in psycholinguistics must be extrapolated to cover the design problem in question.

SOME ISSUES WITH CURRENT WARNING SYSTEMS

At the present time, both auditory and visual signals are used for warnings. Tactile warnings (such as stick shakers) are less generally used and are most useful when they can be associated with a particular control that is being grasped when the warning is possible. The visual channel in airline operations is currently heavily loaded much of the time - most heavily during landing operations. Similar visual loadings occur in other complex man-machine systems such as nuclear reactors.

The auditory channel can also be quite heavily loaded in aircraft because of radio communications and by intracockpit communications. However, if research shows that pilots have difficulty attending to voice warning messages superimposed on a background of competing verbal messages, then much of this background could be blocked electronically for a message of lifesaving priority.

Ambiguity becomes a problem if auditory warnings are restricted to tones, for it is known that, for simple tones, coding by frequency yields about five reliable discriminations (ref. 5). A two-dimensional coding of tones (such as frequency and intensity) can give eight discriminable tone warnings. Even when discriminable tone warnings are used, reliably associating a large number of them with the correct responses can be a problem.

Voice warning systems have been offered as a solution. Obviously, the number of possible warnings codable in human speech is essentially infinite, and the only practical limitation is the cost and weight involved in carrying extra IC chips for each additional message. However, in developing a voice warning system, great care must be taken to make it compatible with the total

man-machine system it serves. Voice warnings may not be appropriate in all situations. Research is needed to determine the best modality for various warnings. The set of warnings given verbally must then be designed to be unambiguous, accurate, easily perceived and interpreted, and satisfying other human factors criteria.

Obviously, it is impossible to specify in detail an all-purpose warning message set. Situations that trigger warnings must be defined, and if voice warnings are being considered, then the human factors and linguistics inputs are appropriate.

EXAMPLE OF VOICE WARNING

To illustrate the problems and factors that must be considered in the message design process, a specific example was chosen: the ground proximity warning system (GPWS) now being installed in commercial airliners. In all cases, the warning is: *WHOO, WHOO - Pull up! Pull up!* This warning will be given when the following flight situations occur (ref. 6):

1. Excessive descent rate below 2500 ft above ground
2. Excessive closure rate with rising terrain
3. Descent during takeoff up to 750 ft above ground
4. Not in landing configuration below 500 ft above ground
5. Excessively low on the glide slope

The case for voice warnings was strengthened after a recent crash despite the fact that a radio altimeter sounded 800-Hz tone warnings several times before impact with the ground (ref. 7). In this instance, it would seem that either (1) the crew did not hear the tone, or (2) they disbelieved it, or (3) it took them too long to decide what the tone meant, or (4) they misinterpreted the meaning of the tone. Problems (1) and (3) are common to all warning systems. They involve masking noise, habituation, and false alarm rates and require well-known human factors analysis techniques. Problems (3) and (4), which involve fast and accurate comprehension of incoming information, might be solved by giving the pilot a voice warning. Flashing lights may divert visual attention from flight tasks and pilots might have difficulty remembering the meanings of different tones, clackers, beeps and buzzers. A speech message uses an extremely familiar code and the pilot need not divert his visual attention.

HUMAN FACTORS DESIGN CRITERIA

A warning must always result in timely action. If one were absolutely sure of the correct action in all circumstances, and if there were no chance of a false alarm, then the obvious thing to do would be to take the man entirely out of the loop and install actuators to take the correct action when the problem was first sensed. An example is the stick-pushers used when some modern jets approach a stall. Actuators are arranged so that, unless the system is disabled or overpowered, the airplane will not let itself be stalled.

Since the consequences of a stall in these aircraft are so severe, and the prevention so easily accomplished, a stick-pusher was chosen. If a warning can be connected to some control or combination of controls that will always prevent accidents, and will malfunction at a rate less than the current rate of those accidents, then it should be installed. As will be shown later, the situation is not nearly so simple in many cases.

If a stick-pusher or its equivalent cannot be used to avoid accidents, there is then the problem of placing the man in the loop with maximum effectiveness. A possible design philosophy would be to tell the operator what to do, rather than what is wrong. This would hopefully allow almost instant correct responses, since no human processing time would be required to decide the action to be taken. When a deeper analysis is made, it becomes clear that this philosophy will be difficult to implement, and it may not have the desired effect.

First, it must be remembered that all the operators in the GPWS case are (necessarily) airline pilots. Before they initiate a violent maneuver or decisive action (such as pulling a fire bottle in their aircraft at the behest of an automatic system), they will almost certainly check all information available to them to verify that a critical situation exists. In the case of a GPWS, if a single warning such as "pull up" is given, the pilot must remember which kinds of situations are likely to trigger this warning, then begin checking for these situations. This will probably take at least as much time and probably more time than if the system had announced the condition that initiated the warning.

After the pilot is notified that some undesirable condition exists, it is necessary to ensure that he take the proper corrective action. For example, assume the GPWS alarm has been triggered by an excessive sink rate below 2500 ft AGL. This could be caused either by (1) insufficient airspeed (settling rapidly) or (2) a high-speed dive or spiral. If it was an insufficient airspeed problem, then adding power and pitching down, possibly adding takeoff flaps and cleaning up any spoilers, landing gear, etc., would be appropriate, all depending on any airframe damage or known malfunctions (i.e., one would probably not elect takeoff flaps if there was known hydraulic system damage). If the problem was a high-speed dive, then one would reduce power (or even use reversers if allowed), level the wings, and pitch up gently, depending on airspeed. It would be very difficult to specify actions to be taken in just this one example, with so many possible actions and so many decisions to be made. When all possible situations that would trigger a GPWS are considered, and all the possible courses of action are described and the decisions enumerated, an instruction set of staggering complexity results. Even if the hardware could be designed to give the pilot all relevant flight information and required corrective actions, it is difficult to make an *a priori* decision as to just how much of this information should be given to the pilot. Similar problems would be expected to emerge when warnings for other complex systems are considered.

Leaving the operator as much flexibility as possible in the decision process permits him to make the kinds of decisions humans are better at making

than computers, those requiring integration of unexpected information to find novel solutions for unique situations. On the other hand, in just those situations when the operator has forgotten a normally routine operation, perhaps due to high task loading as a result of fatigue or an emergency situation, etc., it might take him longer than usual to decide the proper action to take. To speed the operator's decision process, perhaps the voice warning should also tell him what actions the computer thinks are required. This would work well under normal operating conditions. But when some systems are malfunctioning, for example, the operator would have to make a unique decision based on all available information and the particular situation. In such situations, it is possible that he would ignore the recommendations of the voice warning system. Designing the system to announce the problem rather than issue a command would avoid this. Commands versus advisories must be submitted to experimental test. One cannot predict the particular set of tradeoffs in response time, accuracy of decision and control movements, and flexibility of the operator to respond to abnormal and often unique situations.

Future technological developments may provide a way to implement a requirement for a large set of warning messages. Speech synthesizers are now being developed which can create an unlimited message set when driven by a rather small computer. In some future system then, warning messages may be able to tell the operator what is wrong and indicate what he should do about each situation. In the sink rate example above, the computer could check air-speed and aircraft configuration and say either (1) "aircraft settling - add power, wheels up, spoilers retracted," or (2) "high-speed dive - power off, level wings, pitch up," or the appropriate emergency checklist items for the aircraft involved.

Note that this system would satisfy all the general requirements for a warning system - it is unambiguous; the pilot knows what is wrong, and is advised what to do in each different situation, thus ensuring that the warning is effective. Since the warning is auditory, his vision is not distracted from crucial instruments, thus making the warning compatible with continued visual monitoring of glide slope, attitude displays, etc. Of course, research must be conducted to determine whether voice warnings adversely affect performance on visual flight tasks.

For lower-cost situations or more immediate applications, we must consider what sort of warnings should be provided, given the current state of the art. The current GPWS system, for example, gives a single voice command - "pull up." It was argued above that "pull up" may not be the best warning in many cases. If we cannot give the ideal warnings, that is, an analysis of the situation and the emergency checklist items appropriate to that situation, then what is next best?

Since the GPWS is designed to know the mode it is in when it was triggered, that is, it can distinguish between "excessive sink rate" and "glide-slope deviation," then it should be able to provide separate outputs for each warning situation. Thus, we could generate a different warning, either tactical, tone, visual, or spoken, for each critical situation. It was argued above that speech might be the most suitable mode for such warnings, so the

question is: can speech messages be designed to tell a pilot what to do in each warning mode? It seems likely that the answer is no, not without sensors not presently fitted to aircraft. Discriminating between the low-speed settling case and the high-speed dive should be no problem, but the out-of-configuration, glide-slope deviation and sinking-after-takeoff warnings could be due to such a large variety of causes that no single action or set of actions can be specified which would always be appropriate.

The best form for warnings, then, would seem to be to tell the pilot what the GPWS thinks is wrong and let him decide, based on his knowledge, what to do. Thus, if he is at FL 390 in clear bright sunshine and hears "ground warning," (1) he looks out the window, (2) checks the radio altimeter, finds that it is reading 1000 ft and acting very erratic, and (3) pulls the circuit breaker to get rid of the warning.

The problem remains: how should the messages be worded to ensure fast and accurate comprehension? The speech message must be designed as carefully as the hardware.

LINGUISTIC DESIGN CRITERIA

The numerous variables found to affect the reception of human speech messages by a human listener can be grouped into five general categories:

Physical Environment:

- Signal/noise ratio
- Noise characteristics
- Masking by other signals

Characteristics of Transmission System:

- Frequency response
- Signal/system-noise ratio
- Spatial separation of competing messages

Pragmatic Context:

- Listener expectation from real-world situation
- Type and complexity of response

Psycholinguistic Factors:

- Phonetic confusability
- Number of syllables
- Natural frequency of usage
- Number of message repetitions
- Repetition rate
- Syntactic context
- Semantic context
- Complexity of syntactic structure
- Complexity of semantic structure

Listener Skills and Training:

- Practice with message set
- Familiarity with phraseology type
- Familiarity with real-world message context

- Familiarity with a specific acoustic distortion
- Familiarity with a particular accent

Aspects of the *physical environment* that affect speech recognition and comprehension are signal/environmental noise ratios and the masking of signals by other signals (refs. 8-15). The *characteristics of transmission systems* include the frequency response of the system, the audio level of the output, the signal/system-noise ratio, the number of repetitions of a message, the choice of output device, for example, speaker versus headphones and, in the case of competing verbal messages, monaural versus binaural versus dichotic presentation, differential filtering, spatial separation, differential voice qualities, and sequencing versus simultaneous presentation (refs. 8 and 16-18).

Effects of the *linguistic structure* of the material include the listener's expectations derived from phonological, syntactic, and semantic context; the number of possible responses; for isolated words, the number of syllables, the phonetic confusability of the possible responses, the frequency of occurrence of words in natural usage, grammatical form class; cognitive difficulty of processing specific syntactic and semantic sentence structures (refs. 8, 13, and 19-35). The *pragmatic context* in which messages are received and acted upon also affects the listener's comprehension of them. His expectations, given a particular real-world situation, can limit the alternatives he considers in processing a verbal message. This is one of the least studied areas of speech perception but some work has demonstrated the existence of such effects (refs. 36-38), and linguistic theory is currently providing quantities of theoretical discussions on the subject. Another pragmatic variable that affects speech comprehension is the type and complexity of the responses required of the listener (refs. 11 and 39). In a thought provoking article, Chapanis (ref. 40) cited the following example to illustrate how complex syntax or word order, together with a lack of consideration for the pragmatic context in which a message is to be used, can result in poor message comprehension:

NOTICE: This radio uses a long life pilot lamp that may stay on for a short ime if radio is turned off before radio warms up and starts to play.

The intent of the message is, according to Chapanis,

NOTICE: Don't worry if the pilot lamp should stay on for a little while after you turn the radio off.

To most readers, the second version is much easier to understand. Chapanis made two types of changes. First, he reduced the number of clauses or sentence-sized ideas from five to three. His other change concerns the pragmatic context in which the message is to be used. The message user will not be a radio repairman nor an electronics engineer. There is therefore no need to include in this message any of the technical reasons for the pilot lamp remaining on after the radio is turned off. In the new version, the radio user has all the information he needs and none of the unessential distracting ideas. Finally, we must consider the *listener's skills and training*. Fletcher

and Steinberg (ref. 8) found effects for listener familiarity with the distortion type of a particular transmission system. Familiarity with message sets of words and the interactions with S/N ratio and word frequency has been studied by Pollack, Rubenstein, and Decker (refs. 41-43). We know of no research other than that of Simpson now in progress on the effects of familiarity with a particular type of phraseology learned prior to and independently of the laboratory test experience. In addition to familiarity with message sets and formats, we can expect the listener's prior training for performing a particular real-world task (such as flying an aircraft) to affect his comprehension of flight-related messages.

The effects of the above variables are not always obvious since we tend to take for granted our ability to speak and understand speech. But we can expect them to play a role in an operator's comprehension of synthesized speech messages presented by a voice warning system. Their effect may be even greater than for human speech to the extent that the synthesized speech is less intelligible overall than human speech. The added context of a specific real-world situation in which warning messages will be presented will also have its effects. Most of the research on speech intelligibility, articulation values, and speech comprehension has been divorced from any particular pragmatic context such as the cockpit environment. The only exception we know is the body of research done on competing messages which used simulations of air traffic control (ATC) communications (refs. 9, 11, 16-18, and 39).

Message optimization will require analysis of the gain and penalties obtained from a number of factors. Within a specific real-world context, some of the psycholinguistic variables mentioned above may have little or no effect on message comprehension - others may be extremely important. Given listeners (say airline pilots) highly trained to perform a specific task (flying an aircraft) and therefore familiar with a specific body of terminology (ATC phraseology, routine checklist items, navigation terms, emergency checklist items), we need to assess the effects of such linguistic variables as length of utterance, number of syllables, syntactic and semantic context, voice pitch, intonation contours, rate of speech, message repetition, and rate of repetition on the speed and accuracy of the listeners' comprehension. These variables must be tested both in single task mode with the listener merely attending to the warning messages and also in flight simulation where the effects of task loading, unexpected events, time sharing of attention, and situational or pragmatic context can be introduced. We may find that synthesized warning messages that are always comprehensible to a practiced listener pilot sitting in a sound booth go entirely unnoticed or must be repeated several times when the same listener pilot is flying a simulated approach on the gauges and not expecting a warning message.

Using a GPWS as an example, we can examine the interactions between various linguistic and human factors variables in voice warning system design. For voice warning messages in the cockpit, we will need to study different wordings for the same information to see which wording produces the fastest and most accurate control responses by pilots. Suppose the system decided the aircraft was too close to the ground in cruise configuration. Such a condition could arise on an approach in which the pilot had neglected to lower the

flaps and landing gear. If we assume that a future system would be able to distinguish between this situation and a similar one in which the pilot in cruise configuration accidentally flies too close to the terrain, we would want it to issue a message telling the pilot the problem and perhaps also to get the gear and flaps down. One of the speech comprehension factors that may affect pilot response times to such a message is the redundancy in the encoding of the message. We can choose a wording that is extremely economical in terms of the number of words in the message: *Landing - Flaps - Gear*. If the pilot misses any of the words in this message, he also misses the information conveyed by those words and cannot get that information from any other words in the message. The pragmatic context in which the message occurs, namely, approach for landing, will help the pilot decide what the message might have said, but that process also takes time. Either the pilot will have to perform visual checks on various systems that could have failed and/or he will wait for the voice message to be repeated.

If the messages are worded using a normal sentence structure, they will be longer, but each part of the information in the message will be conveyed by more than one word. Then if the pilot does not hear one of the words in the message, he can reduce the number of possible choices, using the words he did understand. For the message about the gear and flaps, a more redundant wording would be: *You're on final approach. Put the flaps and landing gear down.*

Note that one needs to hear only either *put* or *down* to understand that something (flaps, spoilers, or gear) must be extended. If one hears either *landing* or *gear*, he will realize that the message is about the landing gear. Note also that the beginning of the message gets the pilot's attention so he will be listening when the critical part is said.

The effects of different sentence structures must be studied to see which structures are most quickly understood with the least amount of misinterpretation. The shortest version in terms of number of words and pronunciation time may not be the most effective.

Once we have determined what information to give the pilot and the best syntactic structure to use, the semantics of the message must still be considered. This is another aspect of sentence wording. Syntax deals with the order of the words in the sentence. Semantics deals with the meaning of the words in the sentence. It is important to realize that the meaning of a word is always partially determined by its syntactic and semantic relationships to the other words in the sentence. Word meanings are also partially determined by the real-world situation or pragmatic context in which they are said. All of these factors combine to determine which of several possible meanings a particular word or sentence has. If you hear the word *slip*, you may think of a piece of paper. If you hear it in the sentence "*You will need to slip the Cub into this short mountain strip,*" you are unlikely to think about pieces of paper. If you hear "*Be careful not to slip on the wet floor,*" you probably won't think about pieces of paper or airplanes in understanding the meaning of the word *slip*.

We saw above that the message "pull up" was not always appropriate for situations that trigger the GPWS. In this case, the pragmatics of the flight situation actually contradict the semantics of the message. If we choose the wording of a message so that it can have different meanings in different flight situations, we can both economize on the total number of messages and give the pilot the flexibility of responding appropriately to different situations. For example, "climb immediately" could be interpreted as increase thrust and angle of attack, or increase thrust and lower the nose, or increase thrust and hold pitch constant, depending on the context.

CONCLUDING REMARKS

These examples illustrate the kind of analysis and research which should be done to design effective voice warning systems. While the example was specifically for a GPWS, the same considerations would apply to a voice warning for other kinds of complex systems, in vehicles or fixed installations.

REFERENCES

1. Bate, A. J.: Cockpit Warning Systems Comparative Study. Aerospace Medical Research Laboratory, Air Force Systems Command, Wright-Patterson Air Force Base, Ohio, May 1969.
2. Brown, J. E.; Bertone, C. M.; and Obermayer, R. W.: Army Aircraft Voice-Warning System Study. Human Engineering Laboratories, Aberdeen Proving Ground, Maryland, Feb. 1968.
3. Kemmerling, P.; Geiselhart, R.; Thornburn, D. E.; and Cronburg, J. G.: A Comparison of Voice and Tone Warning Systems as a Function of Task Loading. Deputy for Engineering, Aeronautical Systems Division, Air Force Systems Command, Wright-Patterson Air Force Base, Ohio, Sept. 1969.
4. Lillebce, M. L.: Evaluation of Astropower, Inc. Auditory Information Display Installed in the VA-3B Airplane. Final Rept., Naval Air Test Center, U.S. Naval Air Station, Patuxent River, Maryland, June 1963.
5. Morgan, C. T.; Cook, J. S.; Chapanis, A.; and Lund, M. W.: Human Engineering Guide to Equipment Design. McGraw-Hill Book Co., New York, 1963.
6. Anon.: Sundstrand Challenged in GPWS Sweeps. Aviation Week and Space Technology. March 31, 1975, pp. 36-37.
7. Yodice, J. S.: Cleared for the Approach: Fatal Clearance. AOPA Pilot, April 1975, pp. 64-69.
8. Fletcher, H.; and Steinberg, J. C.: Articulation Testing Methods. Bell System Technical Journal, Vol. 8, 1929, pp. 806-854.

9. Broadbent, D. E.: Listening to One of Two Synchronous Messages. *Journal of Experimental Psychology*, Vol. 44, 1952, pp. 51-55.
10. Cherry, E. C.: Some Experiments on the Recognition of Speech, with One and Two Ears. *Journal of the Acoustical Society of America*, Vol. 25, 1953, pp. 975-979.
11. Poulton, E. C.: Simultaneous and Alternate Listening and Speaking. *Journal of the Acoustical Society of America*, Vol. 27, 1955, pp. 1204-1207.
12. Hirsh, I. J.; and Bowman, W. D.: Masking of Speech by Bands of Noise. *Journal of the Acoustical Society of America*, Vol. 25, 1953, pp. 1175-1180.
13. Miller, G. A.; and Nicely, P. E.: An Analysis of Perceptual Confusions Among Some English Consonants. *Journal of the Acoustical Society of America*, Vol. 27, 1955, pp. 338-352.
14. Pickett, J. M.: Perception of Vowels Heard in Noises of Various Spectra. *Journal of the Acoustical Society of America*, Vol. 29, 1957, pp. 613-620.
15. Fröhlich, G. H.: Pure Tone Hearing Losses in Pilots and Their Effects on Sentence Intelligibility in Quiet and Aircraft Noise. Paper presented at 1975 Annual Meeting, Aerospace Medical Association, San Francisco, April 1975.
16. Spieth, W.; Curtis, J. F.; and Webster, J. C.: Responding to One of Two Simultaneous Messages. *Journal of the Acoustical Society of America*, Vol. 26, 1954, pp. 391-396.
17. Webster, J. C.; and Thompson, P. O.: Responding to Both of Two Overlapping Messages. *Journal of the Acoustical Society of America*, Vol. 26, 1954, pp. 396-402.
18. Webster, J. C.; and Sharpe, L.: Improvements in Message Reception Resulting from "Sequencing" Competing Message. *Journal of the Acoustical Society of America*, Vol. 27, 1955, pp. 1194-1198.
19. Miller, G. A.; and Selfridge, J. A.: Verbal Context and the Recall of Meaningful Material. *American Journal of Psychology*, Vol. 63, 1950, pp. 176-184.
20. Miller, G. A.; Heise, G. A.; and Lichten, W.: The Intelligibility of Speech as a Function of the Context of the Test Materials. *Journal of Experimental Psychology*, Vol. 41, 1951, pp. 329-335.
21. Howes, D.: On the Relation Between the Intelligibility and Frequency of Occurrence of English Words. *Journal of the Acoustical Society of America*, Vol. 29, 1957, pp. 296-305.

22. Rosenzweig, M. R.; and Postman, L.: Intelligibility as a Function of Frequency of Usage. *Journal of Experimental Psychology*, Vol. 54, 1957, pp. 412-421.
23. Rubenstein, H.; and Pollack, I.: Word Predictability and Intelligibility. *Journal of Verbal Learning and Verbal Behavior*, Vol. 2, 1963, pp. 147-158.
24. Mehler, J.: Some Effects of Grammatical Transformations on the Recall of English Sentences. *Journal of Verbal Learning and Verbal Behavior*, Vol. 2, 1963, pp. 346-351.
25. Fillenbaum, S.; Jones, L. V.; and Rapoport, A.: The Predictability of Words and Their Grammatical Classes as a Function of Rate of Deletion from a Speech Transcript. *Journal of Verbal Learning and Verbal Behavior*, Vol. 2, 1963, pp. 186-194.
26. Savin, H. B.; and Perchonock, E.: Grammatical Structure and the Immediate Recall of English Sentences. *Journal of Verbal Learning and Verbal Behavior*, Vol. 4, 1965, pp. 348-353.
27. Martin, E.; and Roberts, K. H.: Grammatical Factors in Sentence Retention. *Journal of Verbal Learning and Verbal Behavior*, Vol. 5, 1966, pp. 211-218.
28. Slobin, D. I.: Recall of Full and Truncated Passive Sentences in Connected Discourse. *Journal of Verbal Learning and Verbal Behavior*, Vol. 7, 1968, pp. 876-891.
29. Slobin, D. I.: Grammatical Transformations and Sentence Comprehension in Childhood and Adulthood. *Journal of Verbal Learning and Verbal Behavior*, Vol. 5, 1966, pp. 219-227.
30. Huttenlocher, J.: Constructing Spatial Images: A Strategy in Reasoning. *Psychological Review*, Vol. 75, 1968, pp. 550-560.
31. Clark, H. H.: Linguistic Processes in Deductive Reasoning. *Psychological Review*, Vol. 76, 1969, pp. 387-404.
32. Cairns, H. S.; and Foss, D. J.: Falsification of the Hypothesis that Word Frequency is a Unified Variable in Sentence Processing. *Journal of Verbal Learning and Verbal Behavior*, Vol. 10, 1971, pp. 41-43.
33. Rohrman, N. S.; and Gore, S. A.: Using Ambiguous Words. *Papers in Linguistics*, Vol. 6, 1973, pp. 507-516.
34. Haviland, S. E.; and Clark, H. H.: What's New? Acquiring New Information as a Process in Comprehension. *Journal of Verbal Learning and Verbal Behavior*, Vol. 13, 1974, pp. 512-521.

35. Hofmann, M. A.; Sanders, M. G.; Harding, D. F.; and Frezell, T. L.: Communication During Terrain Flight. Paper presented at 1975 Annual Meeting of The Aerospace Medical Association, San Francisco, April 1975.
36. Wason, P. C.: The Processing of Positive and Negative Information. Quarterly Journal of Experimental Psychology, Vol. 11, 1959, pp. 92-107.
37. Wason, P. C.: The Contexts of Plausible Denial. Journal of Verbal Learning and Verbal Behavior, Vol. 4, 1965, pp. 7-11.
38. Bruce, D.J.: Effects of Context Upon the Intelligibility of Heard Speech. Cherry, C.(ed): Information Theory. Third London Symposium, 1956, pp.245-252.
39. Webster, J. C.; and Solomon, L. N.: Effects of Response Complexity Upon Listening to Competing Messages. Journal of the Acoustical Society of America, Vol. 27, 1955, pp. 1199-1203.
40. Chapanis, A.: Words, Words, Words. Human Factors, Vol. 7, 1965, pp. 1-17.
41. Pollack, I.; Rubenstein, H.; and Decker, L.: Intelligibility of Known and Unknown Message Sets. Journal of the Acoustical Society of America, Vol. 31, 1959, pp. 273-279.
42. Pollack, I.: Reaction Times to Unknown Word Sets in Noise. Language and Speech, Vol. 6, 1963, pp. 189-195.
43. Pollack, I.; and Rubenstein, H.: Response Times to Known Message Sets in Noise. Language and Speech, Vol. 6, 1963, pp. 57-62.

N75 33682

A DECISION AND CONTROL MULTI-AXIS PILOT MODEL

BASED ON AN URGENCY FOR ACTION CONCEPT

J. J. Pollard, Capt USAF
AF Flight Dynamics Laboratory

Dr. R. A. Hannen
Wright State University

SUMMARY

An all digital multi-axis, multi-input, multi-output pilot model flies five different tasks in aircraft of different classes while encountering turbulence represented by the Dryden spectral model. Six degree of freedom linearized aircraft equations of motion are used together with a generalized stability augmentation system.

The pilot model consists of two parts: (1) a decision maker and (2) a control action implementer. This decision maker selects the critical variable and predicts the error at action implementation. The control action implementer decides the magnitude of control to be applied and applies it.

This system has been successfully compared with hybrid/analog man-in-the-loop simulations of the F-5, A-7, T-33, and 707 aircraft, thus validating the all digital simulation and the decision and control pilot model.

INTRODUCTION

This paper will report the modelling of the function of the human pilot in complex multi-axis, multi-input, multi-output aircraft tracking tasks. Single-axis tracking tasks have been studied extensively [1, 11] and, generally, the concepts postulated for the multi-axis pilot function are extensions of single axis theory which assume the pilot is capable of active control of multiple axes simultaneously. Simulation data collected within the Flight Dynamics Laboratory and also by Northrop [2] will not support this hypothesis. Rather an urgency for action concept which implies control action on the axis most in need of correction seems more applicable. To test and demonstrate this concept, an all digital simulation of manned flight in turbulence employing this approach was developed. This required a sequential two part pilot model capable of decision making and control action. Of necessity, this introduces a non-linear, non-continuous, and time varying element as the model of the human controller. The analysis and simulation was quite extensive and included the pilot performing five specific tasks in different classes of aircraft. Just an overview of the pilot model and simulation will be presented in this paper which is a summary of one of the author's dissertation research [5]. A representative example of the

simulation is given for the landing task for the Boeing 707.

I. Aerodynamics

The equations of motion for the aircraft were represented by linearized perturbation equations written with respect to stability axes for the simulated aircraft. These equations and the definition of terms have been developed in many other sources [3, 4, 5] and only a representative set are presented here.

$$\begin{aligned}
 \dot{u} &= X_u u + X_\alpha \alpha - g\theta \cos \theta_0 \\
 \dot{\alpha} &= Z_u u + Z_\alpha \alpha + Z_{\delta e} \delta e - \frac{g\theta}{U_0} \sin \theta_0 + q \\
 \dot{q} &= M_u u + M_\alpha \alpha + M_{\delta e} \delta e + M_q q \\
 \dot{\theta} &= q \\
 \dot{\phi} &= p + r \tan \theta_0 \\
 \dot{\psi} &= r \sec \theta_0 \\
 \dot{\beta} &= Y_\beta \beta + Y_{\delta a} \delta a + Y_{\delta r} \delta r + \frac{g\phi}{U_0} \cos \theta_0 + \frac{g\psi}{U_0} \sin \theta_0 - r \\
 \dot{p} &= L'_\beta \beta + L'_p p + L'_r r + L'_{\delta a} \delta a + L'_{\delta r} \delta r \\
 \dot{r} &= N'_\beta \beta + N'_p p + N'_r r + N'_{\delta a} \delta a + N'_{\delta r} \delta r
 \end{aligned} \tag{1}$$

II. The Stability Augmentation System and Physical Actuators

In many aircraft the above airframe equations yield lightly damped and even unstable characteristics. To bring the aircraft within 8785 [8] specifications, a stability augmentation system is provided to improve basic system characteristics and responses. Considering δe_c , δa_c and δr_c as the commanded surface deflections, the pilot and the augmentation system join to yield

$$\begin{aligned}
 \delta r_c &= \delta r_{aug} + \delta r_p \\
 \delta a_c &= \delta a_{aug} + \delta a_p \\
 \delta e_c &= \delta e_{aug} + \delta e_p
 \end{aligned} \tag{2}$$

Here δr_p , δa_p , and δe_p are the pilot's commands and δr_{aug} , δa_{aug} , and δe_{aug}

are carefully chosen and blended feedback compensation. Readily measurable variables such as θ , q , \dot{q} , n_z , r , \dot{r} , p , ϕ , a_y and others [5, 6, 7] are generally used. The actual surface deflections often are obtained by feeding the commanded deflections through electro-mechanical servo actuators which are modeled by a first order lag such as

$$\dot{\delta r} = -\frac{1}{\tau} \delta r + \frac{1}{\tau} \delta r_c \quad (3)$$

and similarly for δe and δa .

III. The Turbulent Environment

To provide a quasi-realistic environment for flight, turbulence is introduced by using the Dryden Spectral Model given by [8] with implementation by Heath [9] and special considerations for implementation by Pollard and Hannen [10]. The recommended values of intensity were implemented as well as other desirable multiples to yield light, moderate, heavy and thunder-storm turbulence.

IV. A Decision and Control Multi Axis Pilot Model

A. The Decision Maker

Figure 1 shows a block diagram of the functions performed by the digital pilot during the decision making process. As can be seen the pilot scans his instrument display and notes the variables critical to his task and the rates at which they are changing. From this information he is able to predict (lead) the errors at some future time; in so doing the pilot accounts for the magnitudes of displacements he observes on his instruments and normalizes the results. After considering the relative time since he last acted on each variable, he ranks the variables as most critical independent of task. Task dependence is then added by relatively weighting each of the errors and finally the critical variable is chosen by relative comparison. Figure 2 shows the detailed diagram of the decision making process.

B. Control Action Implementation

The control action taken by the pilot is determined by judicious application of the initial value theorem and consideration of the physical characteristics of human process control. Figure 1 shows a general block diagram of the control action implementation. After the magnitude of control action is determined by the IVT, compensation for the aircraft being flown, which is in the form of a scale factor dependent on aircraft mass, is introduced. The failure of the pilot to accurately implement his desired control action is considered by much the same method as Kleinman, Baron, and Levison [11], although a minimum threshold value for the rms value of the remnant is introduced. The estimated value is then checked by a limiter for physical realism, and the control action applied after a pure time delay and accounting for

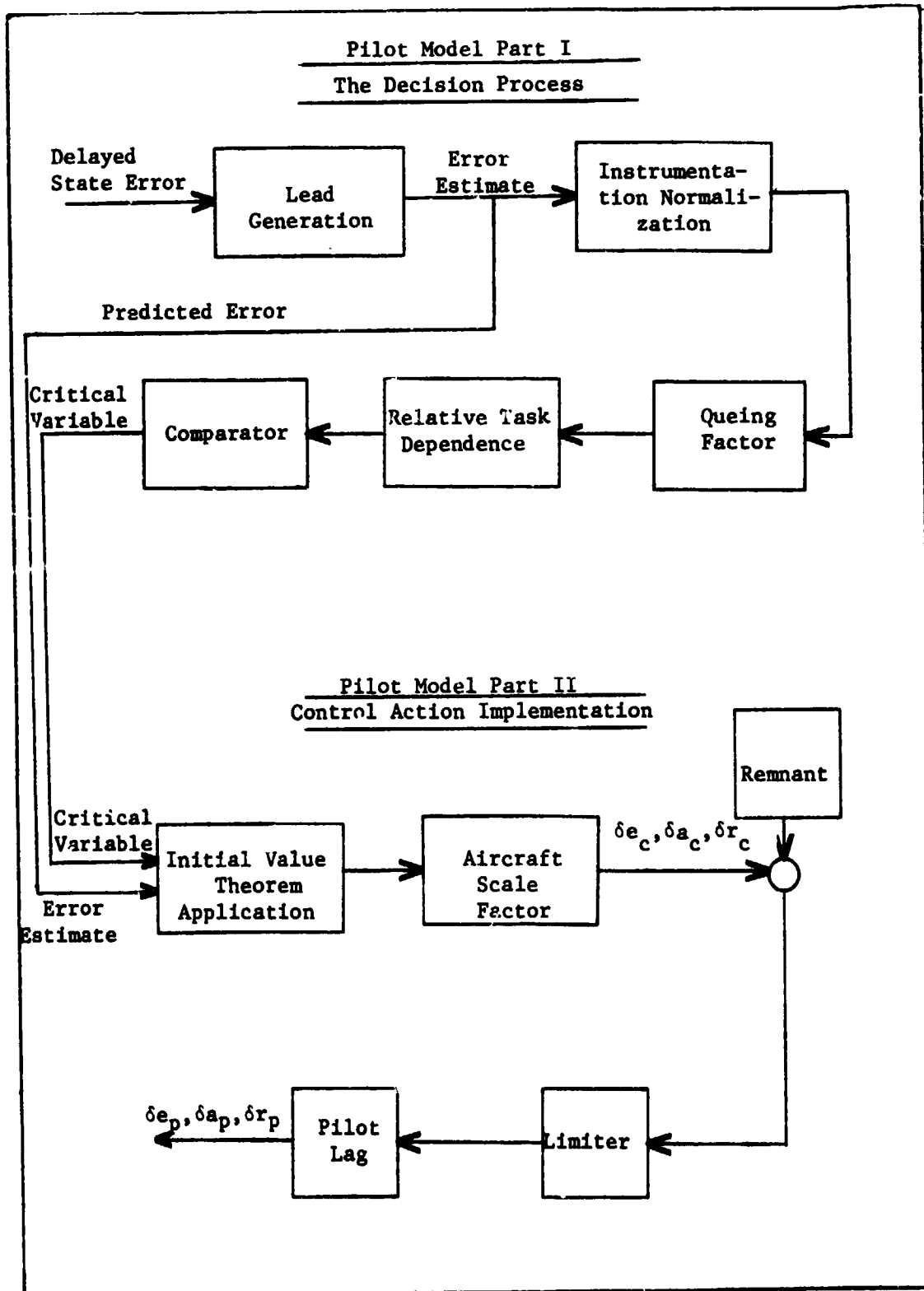


Figure 1. General Diagram of the Pilot Model

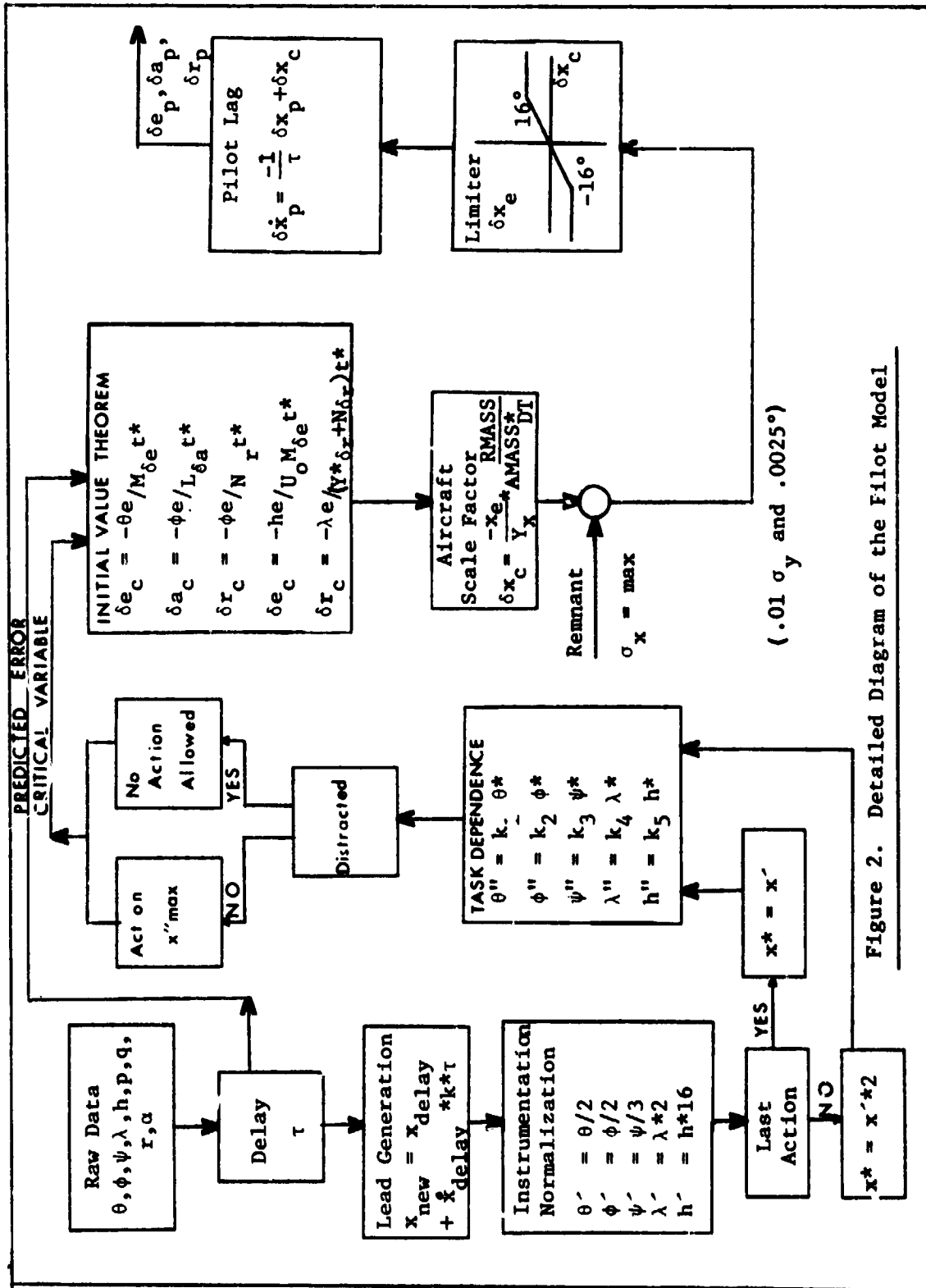
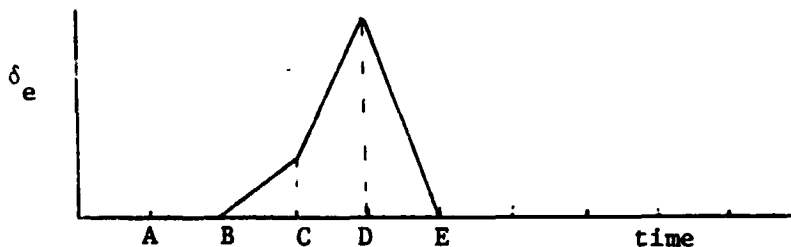


Figure 2. Detailed Diagram of the Pilot Model

for pilot lag. Figure 3 shows the typical control action sequence for an elevator command:



- A - Instruments scanned; decision making process begins.
- B - Decision process complete; control action begins.
- C - Desired control action initiated at B achieved; however further control action is still required.
- D - Sufficient control action observed; decision to return to trim complete.
- E - Control sequence complete; elevator returned to trim.

Figure 3. Control Action Sequence

Figure 2 presents a more detailed representation of the multi-axis control action implementation.

The initial value theorem is used as the primary method for control action determination. This theorem is applicable because the aircraft is kept in a transient state by the discontinuous and frequent control actions taken as the pilot divides his time among the axes.

The actual application of the initial value theorem is demonstrated here for a case where the pitch attitude has been determined the critical variable. An appropriate transfer function for $\dot{\theta}/\delta e$ is given by [12].

$$\frac{\dot{\theta}(s)}{\delta e(s)} = \frac{(M_{\delta e} + Z_{\delta e} M_w)s + (Z_{\delta e} M_w - M_{\delta e} A)}{(s^2 - (U_o M_w + Z_w + M_q)s + (M_q Z_w - U_o M_w))} \quad (4)$$

The Initial Value Theorem states

$$\lim_{t \rightarrow 0} f(t) = \lim_{s \rightarrow \infty} sF(s) \quad \text{if the limit exists.} \quad (5)$$

So equation (4) becomes

$$sF(s) = \frac{s\dot{\theta}_e(s)}{\delta e(s)} = \frac{sq(s)}{\delta e(s)} = \frac{(M_{\delta e} + Z_{\delta e} M_w) s^2 + (Z_{\delta e} M_w - M_{\delta e} Z_w) s}{s^2 - (U_w M_o + Z_w M_q) s + (M_q Z_w - U_w M_o)} \quad (6)$$

and taking the limit

$$\left. \frac{q}{\delta e} \right|_{t \rightarrow 0} = M_{\delta e} + Z_{\delta e} M_w \quad (7)$$

For most aircraft $M_{\delta e} \gg Z_{\delta e} M_w$ so that

$$\left. \frac{q}{\delta e} \right|_{t \rightarrow 0} \approx M_{\delta e} \quad \text{or} \quad q \approx M_{\delta e} \delta e \quad (8)$$

Now under the assumption the pilot wishes to reduce his pitch error to zero over the time t^* ,

$$\theta_e = - \int_0^{t^*} q_c dt \quad (9)$$

where

θ_e is the pitch error predicted

q_c is the commanded pitch rate (assumed constant over the time interval of interest)

and

t^* is the total time of application

Thus

$$q_c = - \frac{\theta_e}{t^*} \quad (10)$$

From (8)

$$M_{\delta e} \delta e = - \theta_e / t^* \quad (11)$$

and so the pilot's command can be expressed as

$$\delta e_c = - \theta_e / (M_{\delta e} t^*) \quad (12)$$

Discussion of the determination of t^* and other factors involved are given by Pollard [5].

V. The Time History Generation

The models of the aircraft, stability augmentation system, environment, and pilot model were integrated using a Cyber 74 digital computer. The state time history produced was sampled at a rate of 8 per second and time average statistics, plots, and maximum and minimum data points generated. A sample of the one page statistical output is given in Figure 4 for the 707 in power approach.

VI. Comparison of the Digital Simulation with a Hybrid Man in the Loop Simulation

Several landing approaches were made of each of two USAF pilots using a hybrid simulation at the Air Force Flight Dynamics Laboratory in a 707 simulator cockpit with simulated 707 aerodynamics. The results of the 707 study are thoroughly presented in Gressang, et al [13].

Of interest were ten flights by each pilot under IFR conditions with low turbulence present. The average standard deviations of each of the states for each pilot are shown by the triangle and star on the bar graphs of Figure 5. Additionally, ten approaches were made independently using the digital simulator and pilot model of this paper. These ten runs are shown by the circles on Figure 5. The tic marks represent actual extremes in the manned simulation. Agreement (verified by use of non-parametric statistical testing) is good except for q , δe and δr . The value of δr differs because the human pilots were trained to make lateral corrections using only aileron inputs while the digital pilot used both the rudder and aileron. The longitudinal problem is discussed in [5].

VII. Other Aircraft Considered and Other Applications

The model was also used with A-7, F-5, F-4, YQM-98, Y-33, and DC-8 aircraft with good consistent results matching various hybrid and analog man-in-the-loop simulations [5].

BOEING 707 FAA SIMULATION 2000 FT 50 DEGREES FLAPS

THE ASSIGNED TASK IS LANDING
 THE PARAMETERS USED IN THIS ANALYSIS WERE:
 PILOT DELAY .175 SECONDS. DISTRACTION RATE .10
 FLIGHT TIME 104.0 SECONDS. FLIGHT PATH ANGLE -3.0 DEGREES

XU = -.046 XA = 19.115 MASS= 5900. SPAN= 130.3 IAS = 233.
 ZU = -.001 ZA = -.597 ZDE = -.038 ALT = 500.
 G = 32.200 MA = -1.003 MDE = -.863 MQ = -.037 MADOT= -.271
 YI = -.035 YJR= .033
 LBETA= -1.628 LJR= .211 LDA = .141 LP = -2.026 LW = .610
 NBETA= .557 NJR= -.392 NDA = .011 NP = -.136 NR = -.248

AUGMENTATION SYSTEM PARAMETERS ARE
 TA = .010 TI = .50. TCOM = .010 TCOM2= .010
 KRAUG= .000 KPAUG= 0.00. KARI = 0.000 KC = 0.000
 KAZS = 0.00000 ELX = 25.000 GTHETA= 0.000 GPHI = 0.000

GUST PARAMETERS ARE SU= 2.200 SV = 2.200 SW = 1.600
 EXPECTED STANDARD DEVIATIONS ARE
 SUG= 2.200 SAG= .393 SQG= .323
 SPG= .428 SBG= .541 SNG= .380

VEHICLE IS UNDER PILOT CONTROL

VARIABLE	UNITS	MEAN	STD DEV	MINIMUM	MAXIMUM
THETA	(DEG)	.030	.529	-1.121	1.458
U	(FT/SEC)	.051	.914	-1.659	1.362
ALPHA	(DEG)	.003	.561	-1.449	1.743
Q	(DEG/SEC)	-.017	.342	-1.021	.989
DE	(DEG)	-.030	.524	-2.259	2.060
PSI	(DEG)	.007	1.162	-3.525	2.761
BETA	(DEG)	-.217	.931	-2.722	2.382
PHI	(DEG)	-.033	1.014	-2.724	2.081
R	(DEG/SEC)	-.007	.762	-2.520	1.313
P	(DEG/SEC)	.029	.789	-2.358	2.505
DA	(DEG)	.119	1.851	-5.616	7.305
DRAUG	(DEG)	-.000	.000	-.000	.000
JR	(DEG)	-.118	.823	-3.655	2.746
U GUST	(FT/SEC)	-.399	1.702	-4.243	6.422
ALPHA GUST	(DEG)	.037	.446	-.909	1.283
Q GUST	(DEG/SEC)	.008	.350	-.929	1.065
P GUST	(DEG/SEC)	.033	.444	-1.120	1.371
BETA GUST	(DEG)	.122	.515	-1.238	1.639
R GUST	(DEG/SEC)	.013	.571	-1.109	1.151
U	(FT)	-1.347	4.884	-14.594	11.622
H	(FT)	-.949	4.725	-13.846	11.301
LAMBDA	(DEG)	-.210	.781	-1.931	1.316
SVG =	2.09	SAG =	1.81		

THE NUMBER OF DECISIONS ON EACH VARIABLE WAS
 PITCH 171 ROLL 194 YAW 118 GLIDESLOPE 104 LOCALIZER 99 NO ACTION 72
 THE PILOT RATING IS 2.25

Figure 4. Digital Simulation Output

ORIGINAL PAGE IS
 OF POOR QUALITY

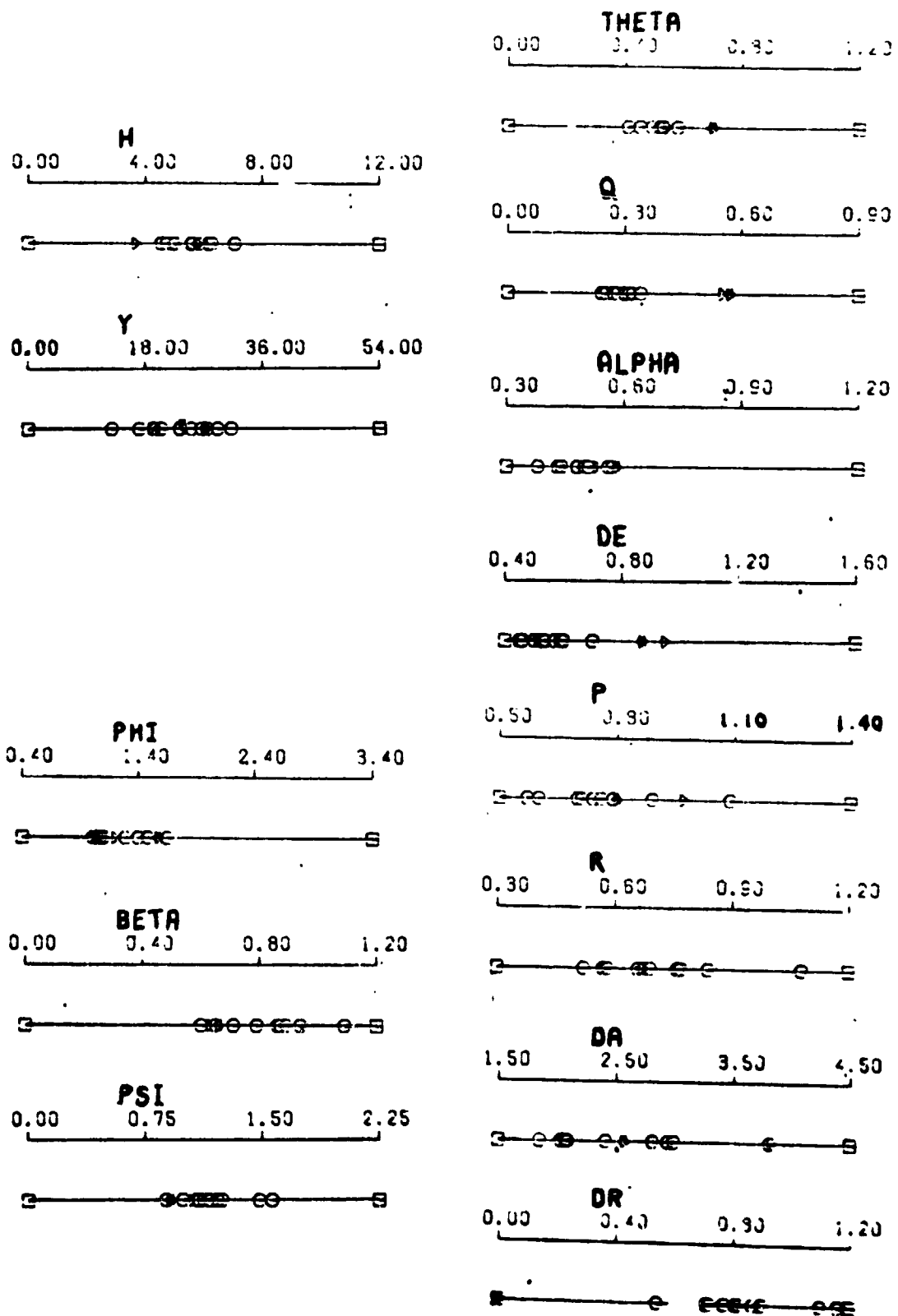


Figure 5. 707 Digital/Hybrid Simulation Comparison

Other applications considered for the program include aerodynamic data package checkout, stability augmentation system preliminary design and checkout, choosing and delimiting proposed manned simulation conditions, and the test of different aircraft under identical repeatable conditions.

VIII. Conclusions and Future Research Areas

All digital multi-axis, multi-input, multi-output piloted simulation can be performed readily and relatively inexpensively using the program developed. The need for expansion to include visual, aural, and kinematic effects is clear and proposed for future consideration.

REFERENCES

1. McRuer, D. and E.S. Krendall, Mathematical Models of Human Pilot Behavior, North Atlantic Treaty Organization, AGARDograph #188, November 1973.
2. Onstott, E., Multi-Axis Pilot Vehicle Dynamics During VTOL Flight, Northrop Corporation, Proceedings of the 10th Annual Conference on Manual Control, 9 - 11 April 1974.
3. McRuer, D., I. Ashkenas and D. Graham, Aircraft Dynamics and Automatic Control, Princeton, New Jersey, Princeton University Press, 1973.
4. Blakelock, J.H., Automatic Control of Aircraft and Missiles, New York, John Wiley & Sons, 1965.
5. Pollard, J.J., All Digital Simulation for Manned Flight in Turbulence, Air Force Institute of Technology, Doctoral Dissertation, DS/EE/75-1, Wright-Patterson AFB, Ohio, March 1975.
6. Teper, G., Aircraft Stability and Control Data, Systems Technology, Inc., Report #176-1, Hawthorne, California, April 1969.
7. Heffley, R. and W. Jewell, Aircraft Handling Qualities Data, Systems Technology, Inc., Report #1004-1, Hawthorne, California, May 1972.
8. Chalk, C.R., et al., Background Information and User's Guide for MIL-F-8785B(ASG), "Military Specification - Flying Qualities of Piloted Airplanes", Air Force Flight Dynamics Laboratory, AFFDL TR 69-72, Wright-Patterson AFB, Ohio, August 1969.
9. Heath, R., State Variable Model of Wind Gusts, Air Force Flight Dynamics Laboratory, AFFDL-FGC-TM 72-12, Wright-Patterson AFB, Ohio, July 1972.
10. Pollard, J., Digital and Analog Simulation of Linear Stochastic Differential Equations, Air Force Flight Dynamics Laboratory, AFFDL-TM-75-35 FGD, Wright-Patterson AFB, Ohio, October 1974.

11. Kleinman, D.L., and S. Baron, Analytic Evaluation of Display Requirements for Approach to Landing, NASA CR 1952, Bolt, Beranek, and Newman, November 1971.
12. -, Dynamics of the Airframe, Northrop Aircraft Inc., BUAER Report AE-61-4II, Bureau of Aeronautics, Dept of the Navy, September 1952.
13. Gressang, R.V., et al, A Low Visibility Landing Pilot Modeling Experiment and Data, Air Force Flight Dynamics Laboratory, AFFDL-TR-75-41-FGD, Wright-Patterson AFB, Ohio, December 1974.

* N75 23683

DISCRETE TIME MODELIZATION OF HUMAN PILOT BEHAVIOR

by Daniel CAVALLI and Dominique SOULATGES

Office National d'Etudes et de Recherches Aéronautiques (ONERA)
92320 Châtillon (France)

SUMMARY

This modelization starts from the following hypotheses : pilot's behavior is a time discrete process ; he can perform only one task at a time ; his operating mode depends on the considered flight subphase.

Pilot's behavior was observed using an electro-oculometer and a simulator cockpit, in the case where the vehicle model was a simplified Lunar Module.

A Fortran program has been elaborated using two strategies. The first one is a Markovian process in which the successive instrument readings are governed by a matrix of conditional probabilities. In the second one, strategy is an heuristic process and the concepts of mental load and performance are described.

The results of the two aspects have been compared with simulation data.

INTRODUCTION

A modelization of the human pilot has been undertaken at ONERA. Its purpose is to improve safety in flight. This goal led J.C. Wanner [1] to this classification of troubles in flight :

- perturbation sensitivity troubles,
- handling troubles (whenever a correction maneuver induces an unexpected deviation on another parameters),
- pilotability troubles (whenever pilot's workload prevents him to operate : overload or underload with vigilance loss).

Perturbation sensitivity and maneuverability levels can be evaluated at a very early stage (i.e. : draft) of a new aircraft design. However its pilotability can only be estimated by use of a flight simulator, which often means that it is quite too late for any change. This is why we hope to be able to test pilotability as early as the draft phase of the design.

This aim implies two major requirements. On the one hand, the robot will have to cope with any type of draft. Therefore it will have to be a learning program. On the other hand, as pilotability assessment is the desired result, pilot workload has to be mathematically formalized.

Following J.C. Wanner, flight may be divided into a sequence of "phases", the aim of each phase being a "long term" aim. Let us take for example the "climbing" phase : starting from 50 ft above ground, the aircraft, which has just taken off, has to reach its cruising altitude, following a given ground path.

Each phase itself may be divided into a sequence of "subphases", the aim of each being a "short term" aim. For example the ILS-descent phase may be divided into the following sequence

of subphases : localizer beam engagement, glide beam engagement, push over and final descent [fig. 1].

For each subphase, a nominal flight path can be selected by the pilot, taking into account atmosphere, aircraft and pilot status.

As the objective of a subphase is to enable correct execution of the following subphase, (short term safety concept), this objective is expressed in terms of constraints and relations upon a subset of flight parameters : the nominal flight path is given to the pilot by nominal values of these parameters which are called here "principal parameters" of the subphase. We have [1] nominal values of principal parameters for the final descent subphase which is the example to test the Fortran program. Nominal values for principal parameters and related admissible deviations are therefore selected by the pilot at the beginning of the subphase.

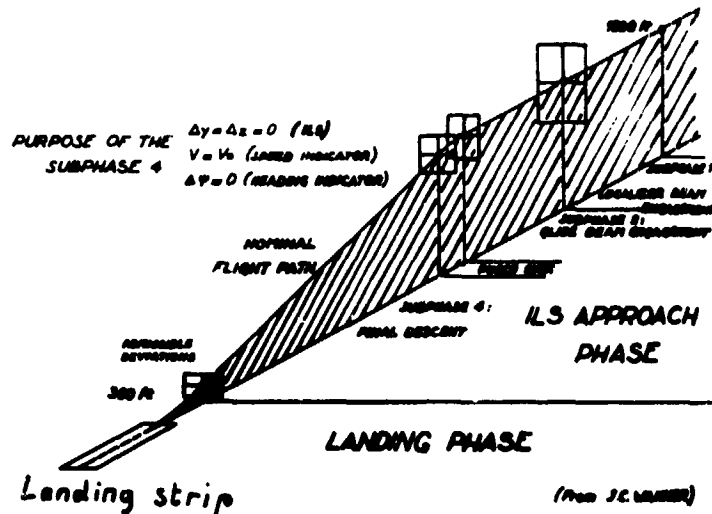


Fig. 1 - A mission for the human pilot.

Nominal values for principal parameters and related admissible deviations are therefore selected by the pilot at the beginning of the subphase.

VEHICLE MODEL

In order to work on simplified equations, the vehicle model selected for this study is not a plane but a simplified Lunar Module so that the aerodynamics effects are absent.

The vehicle has an axial thrust, F being the thrust level and mg its weight.

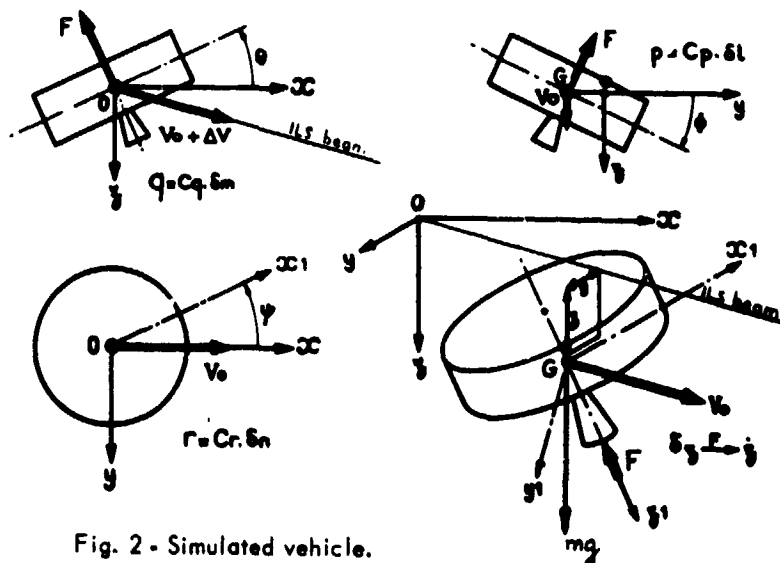


Fig. 2 - Simulated vehicle.

Oxyz is an inertial reference frame, Oz positive downwards, ILS beam being in the xOz plane. y and z represent lateral and vertical deviations from the ILS beam, V_0 is the desired velocity.

Gx, y, z , is a vehicle frame where ψ is the yaw angle, θ the pitch angle, Φ the roll angle. δl , δm , δn directly control, p , q , r velocities through controls efficiencies C_p , C_q , C_r .
 p , q , r being roll, pitch and yaw velocities in Gx, y, z axis.

For the altitude control, an automatic pilot is used which makes it possible to directly select \dot{z} from the throttle δz , through the F thrust and taking into account a given time constant τ .

HYPOTHESES AND EXPERIMENTATION APPARATUS

In this presented we did not use classical assumptions of the continuous pilot represented by transfert functions, we adopted another approach of a discrete behavior.

Human pilot behavior

The analysis of human pilot behavior shows that the pilot collects trajectory and immediate security data such as aircraft position, altitude, etc.. These data are accessible to the crew by various means :

- some of them can be read on the display,
- others are directly accessible to the pilot (for example : aircraft position with respect to landing strip when possible).

All these informations are collected by different sensors : eyes, ears, arms, legs, etc.

Eyes are double sensors : the central vision collects few but precise data while the peripheric vision collects numerous but not precise data.

From these elements an interpretation of human pilot behavior has been proposed by J.C. Wanner [1].

One datum collected by a sensor is used if and only if the brain asks for the information. This means that collecting simultaneously several informations is impossible, the brain asking only one or another at one time. Collected data are transmitted to the brain which, either by direct comparison with known situations or by computation using memorised programs, comes up to a decision.

This decision can be :

- to call for a new information,
- to act on one control,
- to wait.

The pilot's behavior is a time discrete process ; he can perform only one task at a time : instrument reading, decision making or action on one control.

For this study we shall exclusively take into account the central vision, which means that only one sensor will be used to collect informations from the display board.

Simulator cockpit

The requirement, for this study of knowing at any time which information is sought by the pilot has imposed the realisation of a somewhat peculiar display board. Some of the instruments have been split into several parts in order to associate only one information to a line of sight.

(For example : for ILS, the two informations have been separated). The electro-oculometer (EOM), which detects the eye's position in his orbit, enables us to know the line of sight on the condition that the various instruments are sufficiently far apart. As a consequence, the display board must be of relatively large size.

This display board includes seven dials related to the final descent subphase.

- yaw indicator ψ , roll indicator Φ , pitch indicator θ ;
- two instruments resulting from the ILS split : altitude deviation indicator z , lateral deviation indicator y ;
- a speed indicator V , an altimeter h .

The simulator cockpit includes also a seat four controls : δl : lateral control, δm : longitudinal control, δn : rudder control, δz : throttle.

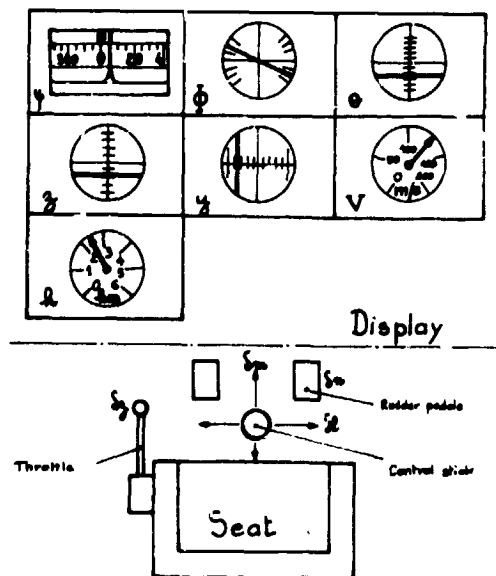


Fig. 3 - Simulator cockpit.

EOM equipment

Eye motion can be followed with an EOM equipment which includes seven electrodes on a box with battery and amplifiers. EOM measures voltages which are function of the relative position of the eyes with respect to the skull

EOM signals are plotted into two graphs : one corresponds to vertical eye displacement, the other to horizontal displacement. In both cases the measured voltage is proportional to the sine of eye rotation angles. Analysis of the two plots provides the identification of the dial read at any time.

EXPERIMENTATION

As a first experimental step, the simulated vehicle has been piloted by about ten (human) subjects. For this experiment, they did not know the meaning of each indicator or control. The only instruction they had was to set to zero deviations on the principal parameters indicated to them.

As soon as they were able to perform this, they were asked to explain by a graph how they thought the vehicle was.

Each of them explained his operating insight in terms of differentiation relations between parameters and between parameters and controls.

Then a second group of four subjects was selected. After a learning phase with tutor 30 questions were put to them [fig. 4]. The question was: "How to set the speed indicator to the right position V_0 ?". The answer interpretation is given in terms of differential relations. These relations obviously agree well with linearized equations of motion [fig. 5].

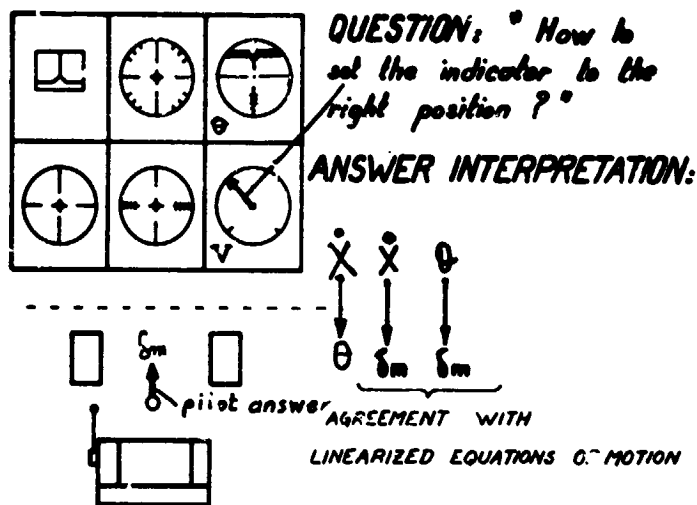


Fig. 4

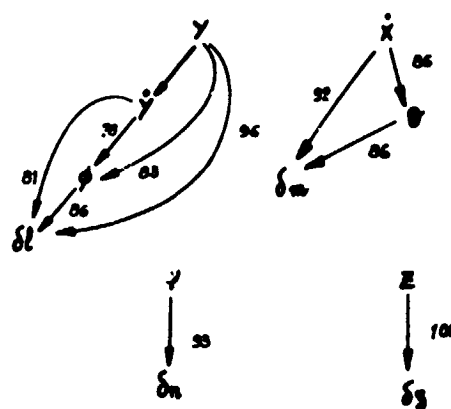


Fig. 5 - Operating insight (").

The result of the questionnaire for four subjects was expressed in terms of ratio of answers agreeing with linearized equations to total number of possible answers. These ratios are high. Therefore the robot will be able to use the linearized equations. Note that there is no coupling between these four families of parameters.

Levels in operating mode

Previous studies have led to the classification into three activity levels in the pilot's behavior. This classification is only a working hypothesis which seems close to the observed reality.

LEVEL	DEFINITION	AIM	COST
STRATEGY	CHOICE OF TACTICS	SHORT TERM SAFETY	MENTAL LOAD (DECISION)
TACTICS	ALGORITHMIC SEQUENCE OF ELEMENTARY ACTIONS.	IMMEDIATE SAFETY	MENTAL LOAD (MEMORISATION)
ELEMENTARY ACTIONS	.READ INDICATORS .WAIT .ACT ON CONTROLS		PHYSICAL LOAD

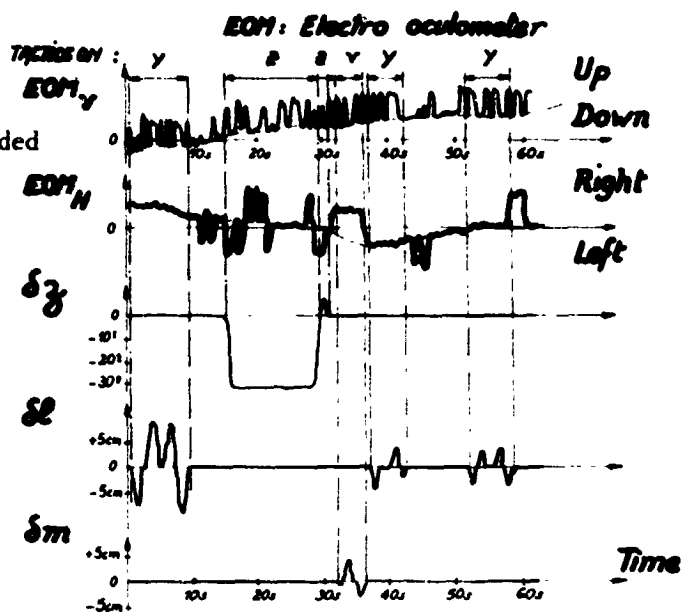
Fig. 6 - Levels in operating mode.

Data processing

The first data processing consisted into a reduction into tactics of tape-recorded actions on controls and EOM signals. For example, tactics on lateral deviation y , altitude deviation z , and speed V can be seen on the figure 7.

As a second step, mean fixation time on indicators, sequences of fixation reading, indicators frequency, deviations on principal parameters and action laws on controls were measured.

Fig. 7 - Subdivision into tactics.



MODELISATION

Program description

A robot program description is shown on the figure 8 where we can see the three levels of actions : strategy, tactics, elementary actions.

After initializations, the robot selects, using a strategy logic, a tactics to be executed, that is a parameter correction algorithm or the reading of an indication.

Then it expands selected tactics into a sequence of elementary actions, which are executed : read an indication, wait, act on control.

In fact, while the robot is waiting, it can begin the execution of another tactics before the end of this waiting period.

The number of memorized actions to be executed is considered as a memorization load indicator.

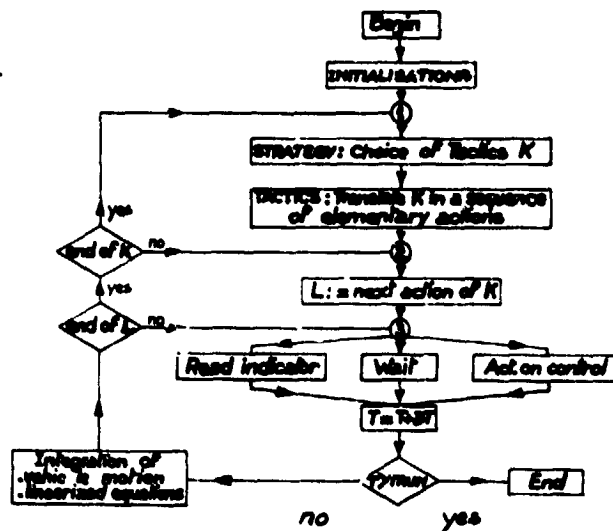


Fig. 8 - Program execution.

Time increment dT induces on the one hand a change in the robot's memorized situation according to the linearized equations (operating insight), and on the other hand a change in parameter values according to exact equations of motion.

This program has been run using two different strategies. The first one is a Markovian strategy, the second one a heuristic strategy. These two aspects will be described after the tactics presentation.

Correction tactics modelization

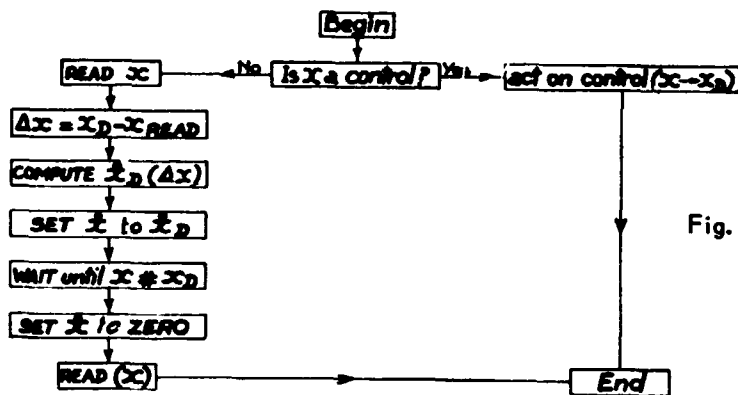


Fig. 9 - Setting parameter x to desired x_D (tactics on x).

A unique algorithm is used for all parameters. This is possible because each integration level is apparent, there is no damping and no coupling between families of parameters in the operating insight.

Then, to set any parameter x to desired value x_D , the sequence of elementary actions is the following :

- read x ,
- compute $\Delta x = x_D - x_{read}$,
- compute $\dot{x}_D(\Delta x)$ (control law),
- set (recursively by the same algorithm) x to x_D ,
- wait until x is near x_D ,
- set (recursively) \dot{x} to zero,
- read x to know whether the correct result is obtained or not.

Modeling of the Markovian strategy

For this strategy, reading of instruments depends upon two random processes as far as numerical simulation is concerned. The sequence of looked up dials is regarded as a Markov chain and the time interval between two successive readings is governed by a Poisson process.

The sequence of looked dials is governed by a matrix of conditional probability to read on instrument after another. This matrix is called here switch matrix. After every instrument reading, the value of a random variable determines, taking the switch matrix into account, which dial will be read next. This process is called switch law.

Reading of the dials has a variable rhythm which obeys to a law of Poisson, Mean Time Between Switches being noted MTBS. This time interval corresponds to the looking-time necessary to the simulated pilot to acquire one datum.

As regards parameters y and z it is necessary to evaluate their derivatives in order to elaborate an order. For this purpose, a second reading immediately follows the first, thus enabling a finite difference derivative computation. The time interval between the two readings obeys to a law of Poisson, Mean Time Between Reading being noted MTBR.

Let us come back to the switch process, which we said to be random. This is not always the case, as whenever one or several parameters exceed or have already exceeded, at reading time t , the respective preassigned levels, a deterministic process is used.

If only one parameter is in violation the switch matrix is temporarily modified so as to read the corresponding dial next.

If several parameters are simultaneously in the red, several dials are in competition : the detected one corresponds to the one having the highest probability of reading in the initial switch matrix.

The following phenomenon can be observed when using such a policy : the simulated pilot concentrates upon one parameter, letting others shift and diverge. This behavior is confirmed by experience on human pilots whenever a parameter goes off-bound, his attention usually goes to the corresponding dial, as his peripheral

vision enables him to simultaneously and approximately monitor all other dials ; whenever several parameters simultaneously diverge, a human pilot takes first care of the one which he thinks has a priority and meanwhile let others shift away.

The switch matrix has been experimentally elaborated using the simulator cockpit and the EOM equipment, in the final descent subphase case.

Tactics switch matrix
(matrix of conditional probability to read an instrument after another)

	γ	δ	ν	ψ	ϕ	θ	k
γ	0,04	0,23	0,37	0,12	0,33	0,10	0,19
δ	0,17	0,27	0,10	0,48	0,26	0,11	0,31
ν	0,00	0,07	0,03	0,02	0,07	0,44	0,11
ψ	0,03	0,19	0,01	0,23	0,03	0	0,01
ϕ	0,27	0,01	0,03	0,04	0,07	0,12	0
θ	0,04	0,04	0,52	0,04	0,10	0,00	0,01
k	0,07	0,19	0,16	0,07	0,06	0,07	0,27

$\sum = 1 \quad = 1$
Matrix obtained with EOM apparatus

- All parameters $X_i < L_i$
 \Rightarrow Instrument readings are governed by the switch matrix
 - One parameter $X_i \geq L_i$
 \Rightarrow Reading of X_i
 - Several parameters $X_i \geq L_i$
 \Rightarrow Reading of X_i which has the greatest probability in the switch matrix
- L_i : Level given in advance for each parameter X_i

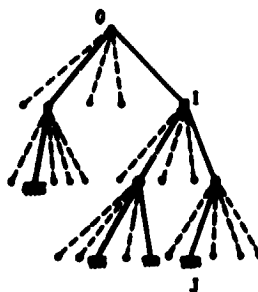
Fig. 10 - Markovian strategy.

Heuristical strategy

The robot has no access to the real shape and real situation of the vehicle. Its operating insight is only in agreement with linearized equations of motion.

The robot has a double task :

- overlooking the display,
- acting in order to keep the subphase principal parameters within their admissible range around the nominal vehicle flight path.



- Instantaneous Seriousness Assessment
- $$G(t) = \text{Max} \left\{ \left| \frac{\text{estimated deviations}}{\text{strained deviations}} \right| \right\}$$
- $$+ \sum_{\text{indicators}} h_{ix} \sqrt{|t_j - t_i|} \text{ reading of } \alpha$$
- Short term evaluation from I to a terminal node J :
- $$e(t) = \frac{1}{t_j - t_i} \sum_{x \rightarrow j} \frac{\Delta'_{ix}}{G(N)}$$
- Selected path: Path of maximum short term evaluation from 0.

Fig. 11 - Heuristical strategy : choice of a tactic.

From admissible deviations the robot computes strained deviations on principal parameters. It is then possible for the robot to compute an "instantaneous seriousness index". This index is the sum of two terms :

- the first one is the maximum ratio over principal parameters of estimated deviations to strained deviations ;
- the second one gives an idea of misinterpretation of the actual situation using standard deviation of a Brownian motion. Positive h_x represents the importance of x indicator reading. Misinterpretation grows with elapsed time since last reading time since last reading time of indicator.

These h_x and strained deviations have been experimentally computed during the experimental phase.

Let S_0 be the memorized situation within the operating insight at time t_0 . The robot can then use linearized equations of motion to obtain predicted situation S_1 at time $t_1 = t_0 + \Delta t_1$.

This prediction may be a conditional prediction. The robot is able to imagine that during the time Δt_1 it will execute tactics K setting to zero the deviation on parameter x .

Then, situation S'_1 is identical to S_1 , except for x which is now corrected and we have to read the indicators used by K at time t_1 .

Now, we are going to see how the robot uses these notions of seriousness and prediction in order to select the "best" tactics to be executed at anytime. Its choices are aimed at preserving short-term safety.

The robot is able to unfold a tree in which :

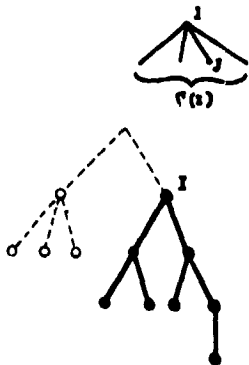
- root is an estimated status (of operating insight) at the present time.
- other nodes are predicted situations,
- arrows are heuristically pre-selected tactics.

Instantaneous seriousness index can be computed at each node.

Considering a constant predicted situation during time Δt_1 elapsed from I 's predecessor until I , the robot can compute short-term evaluation of any path from the root to any terminal node by weighting with a function of elapsed time the inverse of instantaneous seriousness indices.

The path corresponding to the best evaluation can then be selected and tactics related to the first arrow can be executed.

Short term evaluation is then used to compute a strain coefficient defining the work speed of the robot (i.e. control laws, mean fixation time). This strain coefficient is constant upon the next short-term evaluation (using the strategy).



. Conditional probability J given I :

$$p(J|I) = \frac{e(J)}{\sum_{K \in P(I)} e(K)}$$

. Cost of question J :

$$f(J) = \sum_{K \in P(J)} p(K|J) \log_2 \frac{1}{p(K|J)}$$

. Cost of I -root subquestionary:

$$g(I) = f(I) + \sum_{J \in P(I)} p(J|I) \cdot e(J)$$

. Cost of total questionary

$$e(I)$$

Fig. 12 - Heuristical strategy :
decision load.

Following Kalsbeek [2], a decision load measure can be taken as the informative cost of selection. Let the root probability be equal to 1. For every other node, the conditional probability for this node starting from its predecessors can be defined as :

$$p(J|I) = \frac{e(J)}{\sum_{L \in \Gamma(I)} e(L)}$$

we can then use the Questionary Theory [3] and define :

- the cost of a question,
- the cost of an I-root questionary,
- the cost of a questionary ;

the weighted sum of these costs upon the time gives a measure of decision load.

IDENTIFICATION

The numerical identification method is a weighted least mean square one, in which the minimized residual is the one between responses of simulated and human pilots.

In order to simplify this problem, various parameters of the numerical model have first been hand adjusted in order to obtain a rough coincidence between the two responses. An interactive graphic display has been used for this purpose. Both responses were visually compared and parameters interactively adjusted.

As an example let us take lateral piloting responses of numerical and human pilots (fig. 13).

A good coincidence is obtained during the first 15 seconds corresponding to an important effect on parameter y . Responses diverge after this interval of time but both of them are oscillating around zero.

A numerical identification of responses has been carried out for the Markovian strategy program. Following results have been obtained (fig. 14).

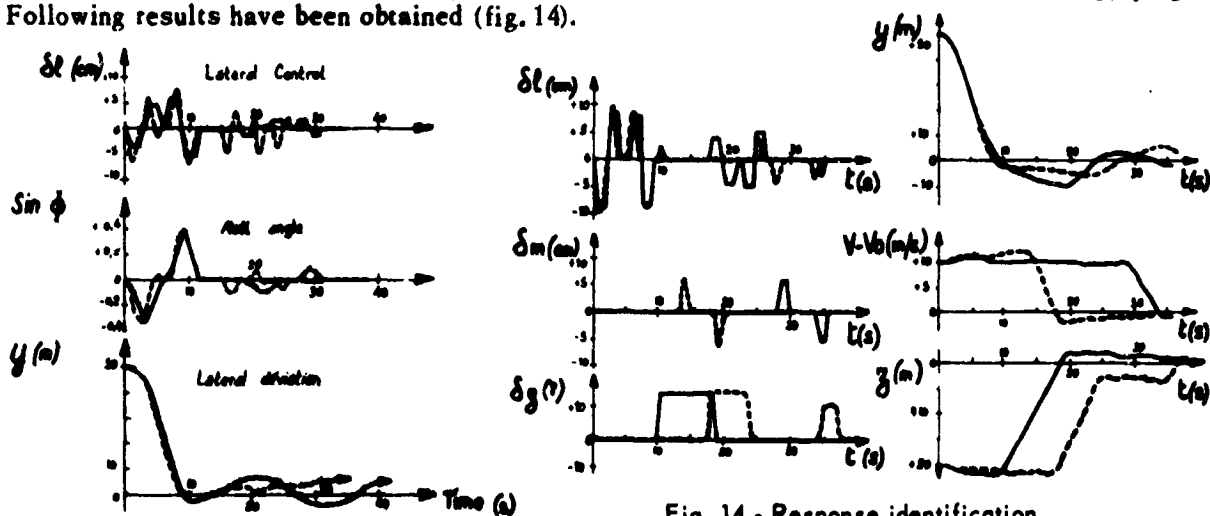


Fig. 13 - Identification of lateral response.

Fig. 14 - Response identification.

— Mathematical model - - - Human pilot

Note the non-coincidence in time of human and simulated pilot actions on controls. Nevertheless parameter responses do converge after some time.

Deviations seem important, but this is due to the fact that human and simulated pilots do not perform the corrections in the same order.

CONCLUSION

A numerical model of a human pilot behavior has been elaborated for the case of a simplified Lunar Module. In a first approach the pilot's strategy is regarded as a Markovian process, taking into account preassigned bounds on parameters. In a second approach the pilot's strategy has been modeled by the evaluation using the graph of predicted situations.

This program has been developed using the following basic ideas :

The pilot's behavior is a time-discrete process ; he can perform only one task at a time (instrument reading, decision making, action on one control, etc.); his operating mode depends on the considered flight subphase.

The program has fruitfully been checked against results of simulation using human pilots.

Contemplated follow-ons for this study include modeling of other flight subphases and other vehicles. The final and ambitious objective is to develop a general program, non-specific to a subphase nor to a vehicle.

REFERENCES

- [1] Wanner, J.C. : Pilotage et conception des avions. L'Aéron. et l'Astron. n° 40 (1973).
- [2] Kalsbeek, J.W.H. : On the Measurement of Deterioration in Performance Caused by Distraction Stress. Ergonomics 7. 187-195 (1964).
- [3] Soulatges D. : Théorie des Questionnaires : Modélisation de la charge mentale d'un pilote. N.T. ONERA n° 230 (1974).

N75 33684

HUMAN INTERACTION WITH AN INTELLIGENT COMPUTER
IN MULTI-TASK SITUATIONS*

William B. Rouse

Department of Mechanical and Industrial Engineering
Coordinated Science Laboratory
University of Illinois at Urbana-Champaign
Urbana, Illinois 61801

ABSTRACT

A general formulation of human decision making in multi-task situations is presented. It includes a description of the state, event, and action space in which the multi-task supervisor operates. A specific application to a failure detection and correction situation is discussed and results of a simulation experiment presented. Issues considered include static vs. dynamic allocation of responsibility and competitive vs. cooperative intelligence.

INTRODUCTION

In many systems, the human decision maker (DM) has responsibility for the simultaneous completion of several tasks. The DM's involvement in this multi-task situation may range from direct performance of all tasks to supervision of humans and/or machines who actually perform the tasks. In many cases, the DM's role falls somewhere between these extremes.

Realistic examples of multi-task situations include piloting an aircraft where the human can be an integral part of the control loop, yet only a monitor or supervisor of several other loops. Another example is the monitoring of industrial processes where the DM sits in a control room watching indicators of the states of the various processes being performed.

There are two classes of problems in such multi-task situations that are especially interesting to researchers in man-machine systems. One class concerns the workload placed on the DM. This workload increases with number of tasks, rate of performance, lack of similarity among tasks, and the DM's involvement with the individual tasks. If the level of the DM's direct involvement with individual tasks can be decreased then the number of tasks can be

*Partially supported by the United States Air Force Systems Command under Contract F33615-73-C-1238.

increased without an increase in workload.

As the DM becomes more of a supervisor, another interesting class of problems becomes significant. At any given time, the DM must choose whether to continue monitoring or supervising all tasks or, to divert his attention to one particular task. His motivation for diverting his attention may be that he feels some malfunction to have occurred or some desired state achieved. The problem faced by the DM is that, when he diverts his attention to a particular task, he necessarily must ignore the remaining tasks and therefore may miss some interesting events. The DM could be aided in this situation if there were some method for performing his overall duties while his attention was diverted. If an interesting event was detected, the DM could be notified or, if the abilities of the method were sufficient, decisions might be made without having to alert the DM.

Any system that can successfully make decisions that would normally be made by the DM can be called an "intelligent" system. Any realization of such a system would most likely be in terms of computer hardware and software. There are several interesting questions that arise when we consider human interaction with an intelligent computer in multi-task situations.

One especially interesting question concerns how intelligent the computer would have to be to yield significant benefits in the multi-task situation. In fact, the computer can utilize rather poor decision making procedures and still be of value. The reason is that if the computer were not performing the tasks the DM is ignoring (because he has diverted his attention to a particular task), those tasks would not be performed at all. In a later section of this paper, we will return to this point.

The other interesting questions center around how to interface the DM with an intelligent computer. How should responsibilities be allocated? What are the benefits and disadvantages of dynamic allocation? What are the effects of the DM's confidence in the computer and the feedback he receives about the computer's decisions? How should conflicts between the DM's decisions and the computer's decisions be resolved? Or, in other words, how can "competitive intelligence" be avoided and "cooperative intelligence" be promoted?

The purpose of this paper is to discuss the above issues in the context of some specific examples. We will proceed by first considering related work appearing in the literature. Next, a general formulation of the multi-task situation will be proposed. This is followed by an application of this formulation to a failure detection and correction situation. Finally, we comment on some of the general issues throughout the paper.

RELATED RESEARCH

Licklider has given us a general feeling for task allocation in man-

computer systems [1] and his discussion of information retrieval systems of the future illustrates specific applications of the ideas [2]. While Licklider's work has not solved all the problems in designing man-computer systems, his ideas appear to have motivated and affected ensuing research efforts.

Closely related to the topic of this paper is the supervisory control ideas of Sheridan. His paper with Ferrell [3] considers many of the issues arising when man and computer interact to perform a single, possibly remote, task. While Sheridan's work on supervisory sampling [4] and allocation of personal presence [5] is oriented toward single-task situations, the supervisor paradigm almost necessarily implies multi-task situations once we sufficiently understand single-task performance.

Of a more specific nature is Sender's information theory approach to modeling human multiple-instrument monitoring [6] and Carbonell's queueing theory approach to the same problem [7]. Carbonell's priority queueing model relates to our later discussion. While these authors were dealing with multi-task situations, neither considered the issues involved when a computer monitors the instruments that the DM is not, at the moment, considering.

While there is a great deal of literature that has implications for the design of man-computer systems [8], there is very little that considers interaction with intelligent computers in the sense that we defined intelligence earlier. Thomas and Pritsker [9] considered an instrument-nulling task where decision making responsibility was transferred between man and computer via a "manual" light telling the DM to take over the task. Corcoran and his colleagues [10] looked at man-computer cooperation in the classification of sonar signals. In this case the computer displayed its decision which the DM then incorporated with his own decision to reach a final choice. One especially interesting result was that, when the computer was very good at this classification task, the DM's portion of the performance degraded. This would appear to have serious implications in an operational system when the computer malfunctions.

Freedy's work [11,12] speaks directly to human interaction with intelligent machines. While he has dealt with single-tasks, these tasks have been multi-dimensional and the issues he raises are similar to some of those discussed in this paper. As with Thomas and Pritsker, he transfers responsibility between the DM and the computer via a single light. His emphasis has been on intelligent systems that "learn" by watching the DM and then can successfully perform the task without the DM's assistance.

Rouse [13] considered the DM in data smoothing tasks and suggested that the resulting model could be used to aid the computer in gaining an understanding of the task whereupon it could assume responsibility and, transfer control back to the human if it lost confidence. The interesting possibility here is that the computer could perform the task much better than DM because the computer would attempt to separate that portion of the DM's output that is useful from that portion attributable to the DM's suboptimality. However, this approach has not yet been reduced to practice.

GENERAL FORMULATION

In this section, we will mathematically describe the multi-task situation. Such a formulation will hopefully allow us to compare the DM's performance to optimal performance and perhaps study any systematic variations. Also, discussion of a possible mathematical formulation will ease the transition from verbal generality to specific examples.

Consider the multi-task situation as involving N processes. Some of these processes may involve control tasks for the DM while others may involve mostly monitoring. Each process is characterized by a state vector

$$\underline{x}_i = (x_{i1}, x_{i2}, \dots, x_{iM_i}) \quad (1)$$

and the entire state space is characterized by

$$\underline{X} = (\underline{x}_1, \underline{x}_2, \dots, \underline{x}_N). \quad (2)$$

While we usually think of state variables as quantifiable measures such as velocity, heading angle, etc., in many circumstances it may be appropriate to think of a state variable as indicating the presence or absence of some pattern or some social situation.

We will denote the DM's observation of the state space by \underline{Z} . The observation \underline{Z} is differentiated from the state \underline{X} to reflect possible partial and/or noisy observations. Upon obtaining an observation \underline{Z} , the DM must decide whether he should continue to observe or should divert his attention to process i . His motivation for diverting his attention to process i is based on his perception of the possibility of some event of set

$$\underline{e}_i = (e_{i1}, e_{i2}, \dots, e_{iL_i}) \quad (3)$$

having occurred that requires an action of set

$$\underline{a}_i = (a_{i1}, a_{i2}, \dots, a_{iK_i}). \quad (4)$$

His observation \underline{Z} leads to estimates of the form

$$p(\underline{e}_i | \underline{Z}) = p(e_{i1}, e_{i2}, \dots, e_{iL_i} | \underline{Z}) \quad (5)$$

and he must trade off the cost of ignoring this information against the cost of ignoring $N-1$ processes while he implements some action of set \underline{a}_i .

The costs of not monitoring the $N-1$ processes depends on what events may occur over the interval of interest. Denoting $t_{e_{ij}}$ as the time until the next occurrence of event e_{ij} and \underline{t}_{e_i} as the vector of event times associated with process i , then $f_i(\underline{t}_{e_i} | \underline{Z})$ is the joint probability distribution of event times for process i conditioned on the observation \underline{Z} . Then,

$$f(\cdot | \underline{Z}) = f(t_{e_1}, t_{e_2}, \dots, t_{e_N} | \underline{Z}) \quad (6)$$

is the joint distribution of event times for all processes. Based on (5), note there is possibly a significant probability of having event times equal to zero for events that have already occurred. Also note that this distribution as others to be mentioned may, in general, have time dependencies, but we have ignored them in this discussion.

The interval of interest is probabilistic and related to the time required to implement the desired action. Denoting $t_{a_{ij}}$ as the time required to perform a_{ij} and \underline{t}_{a_i} as the vector of action times for process i , then $g_i(\underline{t}_a | \underline{Z})$ is the joint probability distribution of action times for process i conditioned on the observation \underline{Z} . And,

$$g(\cdot | \underline{Z}) = g(t_{a_0}, t_{a_1}, \dots, t_{a_N} | \underline{Z}) \quad (7)$$

is the joint distribution of action times for all processes. In (7), t_{a_0} denotes the null action or continued monitoring.

Determination of the optimal allocation of supervisor attention depends on our choice of cost criterion. There are numerous possibilities and we will not advocate any particular form. However, we will note several interesting aspects.

One of these aspects is the planning horizon. Given a choice between continued monitoring (action a_0) for a period t_1 and diverting attention to a particular process for a period t_2 where $t_1 \ll t_2$, and assuming that actions once initiated cannot be preempted, a cost criterion that does not include effects of current actions on future costs will result in the optimal choice being continued monitoring. This results because actions are usually implemented for the purpose of future benefits which might not be realized within a short horizon.

Another interesting aspect is the cost associated with a false alarm in the sense that diverting attention to a particular process and finding that the chosen action was unwarranted results in no benefit yet still incurs costs due to ignoring the other $N-1$ processes. In this case, a "regrets" type cost function might be appropriate where the cost of a false alarm is the benefit that might have been gained if another action had been chosen.

If the DM can continue some form of monitoring even while he has diverted his attention, he can possibly prematurely terminate one action to implement another action with greater potential benefits. The possibility of such preemptive strategies would seem to greatly affect any optimal allocation of DM attention.

To illustrate the range of situations to which this problem formulation

can be applied, consider the college senior who is completing his undergraduate studies and must select among several job offers, graduate school opportunities, and continued monitoring of the possibilities. His observation \underline{Z} may include salary, job description, geographical location, climate, etc. The events of interest to him could be enjoyable work, salary increases, promotions, marriage, a home, etc. The possibility of these events occurring is characterized by his perception of $f(\cdot | \underline{Z})$. The time necessary to act with respect to any of the processes is characterized by $g(\cdot | \underline{Z})$. Except for the null action of continued monitoring, action times are liable to be of the order of a year. Also, false alarms afford very high penalties. Thus, the above formulation would predict a student choosing a_0 almost indefinitely. However, this does not occur indefinitely since each process may yield another event which we have not noted. This event is the rescinding of the offer or opportunity.

Combining subjective estimates of \underline{X} , $f(\cdot | \underline{Z})$, $g(\cdot | \underline{Z})$ and cost criterion parameters such as planning horizon and the cost of false alarms, the formulation discussed here has interesting possibilities for descriptive modeling of the human decision maker. However, the purpose of this paper is to discuss human interaction with an intelligent computer in this multi-task situation.

A computer could aid the DM in several ways. It could observe inaccessible states or filter \underline{Z} and yield $\hat{\underline{X}}$. It could make estimates of $p(e_i | \underline{Z})$, $i = 1, 2, \dots, N$ or calculate expected costs for alternative actions. However, such tasks require considerable knowledge of the processes and probability distributions. Also, such aids would not be considered intelligent in the sense that decisions normally allocated to the human were being performed.

The DM's main difficulty in the multi-task situation is the lack of time to perform all tasks adequately. The computer is much faster than the DM and can perhaps use this advantage to help make decisions. We will use an example to illustrate the benefits and difficulties of such an approach to aiding the DM.

AN EXAMPLE - FAILURE DETECTION AND CORRECTION

The DM's task is to monitor N processes looking for failures. When he detects a failure, he diverts his attention to the failed process and corrects the failure unless he feels the cost of ignoring the remaining $N-1$ processes exceeds the potential benefits of correcting the failed process. Failures arrive randomly and independently. Thus,

$$f(\cdot | \underline{Z}) = f_1(t_e) f_2(t_e) \dots f_N(t_e) \quad (8)$$

where $f_i(t_e)$ is exponential with mean θ_i . Similarly, the time to correct a failure is random and independently distributed yielding

$$g(\cdot | \underline{Z}) = g_1(t_a) g_2(t_a) \dots g_N(t_a) \quad (9)$$

where $g_i(t_a)$ is exponential with mean α_i . Assume, for the moment, that

failures unequivocally present themselves.

This task can be formulated as a queueing problem in a manner similar to that of Carbonell [7]. If we further assume that DM can sample, at no cost, the state of each queue at the end of each service epoch, then Cox and Smith [14] have shown the optimal strategy to be to correct the failure with highest C_i/α_i where C_i is the cost per unit time of delaying correction of the failure and the criterion function is expected cost. More recently, Harrison [15] has considered situations where future costs are discounted. In this case, the optimal policy can depend on the θ_i , $i = 1, 2, \dots, N$ as well as the holding costs and average action times.

A more realistic example is one where failures do not unequivocally present themselves. In queueing terms, this is a situation where one is not sure a customer is present. The author is not aware of any analytical solutions to this problem. Thus, we have resorted to simulation for studying this situation.

The simulation situation was as follows. The DM was monitoring N discrete time series which were generated using

$$x_i(k+1) = \phi x_i(k) + w_i(k+1), \quad i = 1, 2, \dots, N \quad (10)$$

where $\phi < 1$ and w is a zero-mean Gaussian white process. The processes were completely independent of each other.

Failures arrived randomly with average interarrival time of θ and were uniformly distributed across processes. When a failure occurred, the input to the failed process was zeroed. Thus, the manifestation of a failed process was its state asymptotically approaching zero.

One time unit was required to observe the current states of all N processes and one time unit was required to correct a failure if the DM chose to do so. Correction was taken to mean shutting the process off for diagnosis and repair. Thus, false alarms also resulted in a unit of downtime.

The objective of the task was to minimize average downtime per failure. The DM was modeled as having a perfect knowledge of the system, ϕ . He scanned his displays in the order $1, 2, \dots, N$. Upon observing a failed process, he detected the failure with probability $p(e_i | Z) = P$ for all i . He then corrected the perceived failures in the order in which they were detected. Upon correcting these failures, he then returned to monitoring. If he detected no failures, he continued monitoring.

The DM's unaided performance is summarized in Tables I and II. Unless otherwise noted, all simulation results are based on ≈ 1000 failures and 3 replications.

Note that performance degrades as N increases, θ decreases, and P decreases. The N effect is due to the fact that small N , with θ constant, results in queues of failures forming in processes. However, downtime does not

Mean Time Btw. Failures, θ	Probability of Detection, P		
	1.0	0.9	0.7
1.58	4.161 (0.045)	4.463 (0.052)	5.043 (0.122)
2.54	3.466 (0.038)	3.613 (0.019)	4.022 (0.030)
5.52	3.156 (0.010)	3.300 (0.019)	3.636 (0.022)

() = standard deviation

Average Downtime Per Failure: Unaided Human (N = 10)

Table I

Number of Processes, N	Probability of Detection, P		
	1.0	0.9	0.7
2	2.568 (0.010)	2.610 (0.026)	2.791 (0.035)
5	3.751 (0.037)	3.799 (0.088)	4.099 (0.066)
10	4.161 (0.095)	4.463 (0.052)	5.043 (0.122)

() = standard deviation

Average Downtime Per Failure: Unaided Human ($\theta = 1$)

Table II

accumulate any more rapidly with more than one failure. Also, while correction time increases with multiple failures, detection time decreases because the DM can detect multiple failures simultaneously.

In designing a computer aid for DM in this situation, we wanted to balance the computer's speed and/or parallel processing advantages over the human with a commensurate decrease in ability. Thus, the detection criterion employed by the computer is rather crude. The computer observes $x_i(k)$ and $x_i(k+1)$ for all i . If successive states of a process satisfy

$$|x_i(k+1)| - |x_i(k)| < 0 \quad (11a)$$

$$x_i(k+1)x_i(k) > 0 \quad (11b)$$

K times in a row, a failure is reported. Equations (11) utilize only the idea that the states of a failed process asymptotically approach zero. The criterion employs no knowledge of the system, ϕ . To compensate for this disadvantage, the computer was able to simultaneously detect and correct failures in all processes.

The computer's unaided performance is summarized in Table III. Note that the best value of K strikes a balance between misses and false alarms. As θ increases, the computer has increasing difficulty with false alarms and must increase K to avoid them. However, this results in large delays in detection and thus performance degrades as θ increases.

Now we want to consider the DM and computer performing this task together. We are combining a fairly knowledgeable but slow human with a computer that is a rather poor decision maker but is fast and/or a parallel processor. Note also that θ affects their respective performances in opposite ways.

We have considered four levels of man-computer interaction. They will first be discussed in general and then we will note the performance achieved with each type of interaction.

Case 1: No Cooperation

In this case, we simply allowed both decision makers to operate independently. Neither received any feedback about what the other was doing. In a sense, they competed to detect and correct failures.

Case 2: Computer Avoids Conflicts Without Feedback

Here the computer avoided becoming involved with the same process with which the DM was currently involved. However, no feedback was provided to the DM about what the computer was doing. Thus, they only competed over failures that DM has not yet started to correct.

Case 3: Computer Avoids Conflicts With Feedback

In this case, the computer avoided current conflicts as in Case 2, but also notified the DM of any actions taken that might affect the DM's choice of actions in the future. Thus, there was no competition in this case.

Case 4: Computer Preempts Human Decisions

Here the computer would preempt the human from making any decisions that it felt confident to make. It then shifted the DM's attention to situations for which it would not accept responsibility. It was assumed that the computer knew the set of actions planned by the DM and could preempt any of this set, leaving the remainder for the DM.

The performance resulting, with these levels of interaction is summarized in Table IV. All results are for 5 replications with $N = 10$, $\theta = 1$, and $P = 1.0$ unless otherwise noted. Multiple values of K are shown when the average downtime per failure between them was not significantly different at least at the 0.10 level. Other entries in the table are for the underlined values of K.

Mean Time Btw. Failures, θ	Detection Criterion, K							
	1	2	3	4	5	6	7	8
1.58	6.113 (0.044)	4.074 (0.061)	3.750 (0.127)	3.774 (0.053)	4.064 (0.074)	-----	-----	-----
2.54	-----	5.539 (0.145)	4.661 (0.059)	4.580 (0.038)	4.698 (0.040)	4.935 (0.056)	-----	-----
5.52	-----	-----	7.943 (0.050)	6.865 (0.096)	6.547 (0.104)	6.441 (0.187)	6.608 (0.059)	6.832 (0.096)

() = standard deviation

Average Downtime Per Failure: Unaided Computer (N = 10)

Table III

Level of Interaction	Detection Criterion, K	Downtime Per Failure	Computer		Human	
			Corrections Per Failure	False Alarms Per Failure	Corrections Per Failure	False Alarms Per Failure
1	5, <u>6</u>	3.808 (0.038)	0.456	0.374	0.544	0.293
2	4, 5, <u>6</u>	3.744 (0.016)	0.297	0.359	0.703	0.164
3	<u>4</u> , 5	3.487 (0.045)	0.391	0.736	0.609	0.000
4(P = 1.0)	<u>5</u> , 6	3.345 (0.026)	0.483	0.517	0.517	0.000
4(P = 0.7)	4, <u>5</u>	3.468 (0.009)	0.559	0.509	0.441	0.000
4(P = 0.4)	<u>4</u>	3.586 (0.076)	0.789	0.723	0.211	0.000
4(N = 5)	<u>3</u> , 4	2.716 (0.032)	0.753	0.354	0.247	0.000

() = standard deviation

Average Performance for Man-Computer System

Table IV

Case 1 resulted in performance slightly worse than could have been achieved by the computer alone while Case 2 resulted in significantly improved performance that was not significantly different than that possible with the unaided computer. This improvement was mainly due to fewer false alarms on the DM's part since the computer avoided conflicting with current DM actions. However, this did not avoid having the current computer actions conflict with future DM actions. This was avoided in Case 3 by giving feedback to the DM concerning the computer's actions.

With Cases 2 and 3, the computer's avoiding conflict with the DM results in the DM having to perform more of the corrections. This can be avoided by having the computer preempt any DM actions that it feels competent to perform. We see that this results in improved performance as well as fewer corrections on the part of the DM.

As the DM's probability of detection P decreases, decreasing the computer's detection criterion results in improved performance. The computer makes increasingly more corrections as P decreases.

As the number of processes N decreases, the computer's detection criterion is also lowered. However, this is somewhat of an artifact due to maintaining θ constant which effectively decreases the mean time between failure per process. Increasing the mean time between failure per process will dictate an increased K . Decreasing N while maintaining the θ per process should also require an increased K since the DM now has more time to devote to each process. However, we have not systematically studied any of these effects.

DISCUSSION AND CONCLUSIONS

From these simulation results, we can see that the computer's speed can significantly aid the DM even though the computer's decision making method was crude. Not only was system performance improved but the workload of the human, in terms of corrections per failure, was also decreased.

However, these benefits were not achieved with a static allocation of responsibility. The detection criterion K had to be decreased as the DM's detection probability decreased. Similarly an increased number of tasks would seem to indicate a decrease in K implying that more load is placed on the computer. Of course, to achieve this the computer would have to be able to monitor the DM's performance and determine what he was doing (i.e., how many tasks he was involved with).

We also found that the level of interaction in terms of feedback to man and computer about each other's actions, is important. With no feedback, competitive intelligence results and performance is inferior to that obtainable without the interaction. Increased feedback leads to cooperative intelligence and improved performance.

How might such feedback be provided? The simplest way to determine what the DM is doing is to ask him. However, this presents several problems not the least of which is the human having difficulty articulating what he is doing. Also, such communication might become a significant portion of the DM's workload. Some verbal input by the human might be desirable and a limited vocabulary natural language input seems feasible [16].

Another approach is to "watch" the DM and try to infer what he is doing and what he is planning to do. A possibility is model matching and using the parameters to predict perceptions [17]. Then, a knowledge of the structure of the task would be necessary to predict future actions. For example, someone who perceives a difficulty in a particular process is likely to request information relevant to that process and likely to select actions in the set associated with the process.

A third possibility is to use physiological measures such as the EEG to predict perceptions of events [18]. This would appear to offer tremendous advantages with respect to the workload on the DM since he might not have to overtly communicate with the computer.

Considering giving feedback to the DM about the computer's actions, there are also several possibilities. Visual displays are the most common forms of feedback, but there is a possibility of overloading the visual channel and thus, visual displays may have to be limited to status lights with low information transmission rates.

Auditory displays and more specifically natural language systems seem attractive and feasible [16] if noise problems do not make the speech inaudible.

Some of the above ideas are currently being investigated in terms of computer-aided decision-making for flight operations [19]. In this situation, artificial intelligence programs detect and correct failures in the aircraft fuel supply/engine subsystems. The pilot simultaneously attempts to control the pitch and bank of the aircraft and monitor the aircraft subsystems. Informal experiments with this system showed that competitive intelligence was, potentially, a serious problem. Some feedback on computer actions was provided via a series of status lights, but more feedback seemed necessary. One current effort [17] is looking at real time model matching as an approach to telling the computer what the pilot is doing.

From the results discussed here, it appears that a dynamic allocation of responsibility between man and computer has potential benefits. However, this benefit will not be realized if appropriate feedback cannot be provided to the man and computer without overloading the human with additional information. On the other hand, an inappropriately designed interface may be worse than having no computer aid at all.

REFERENCES

1. J. C. R. Licklider, "Man-Computer Symbiosis," IEEE Transactions on Human Factors in Electronics, Vol. 1, No. 1, pp 4-11, March 1960.
2. J. C. R. Licklider, Libraries of the Future, Cambridge, Mass.: MIT Press, 1965.
3. W. R. Ferrell and T. B. Sheridan, "Supervisory Control of Remote Manipulation," IEEE Spectrum, Vol. 4, No. 10, pp 81-88, October 1967.
4. T. B. Sheridan, "On How Often the Supervisor Should Sample," IEEE Transactions on Systems Science and Cybernetics, Vol. SSC-6, No. 2, pp 140-145, April 1970.
5. T. B. Sheridan, "Optimal Allocation of Personal Presence," IEEE Transactions on Systems Science and Cybernetics, Vol. SSC-6, No. 3, pp 242-244, July 1970.
6. J. W. Senders, "The Human Operator as a Monitor and Controller of Multidegree of Freedom Systems," IEEE Transactions on Human Factors in Electronics, Vol. HFE-5, No. 1, pp 2-5, September 1964.
7. J. R. Carbonell, "A Queueing Model of Many-Instrument Visual Sampling," IEEE Transactions on Human Factors in Electronics, Vol. HFE-7, No. 4, pp 157-164, December 1966.
8. W. B. Rouse, "Design of Man-Computer Interfaces for On-Line Interactive Systems," Proceedings of the IEEE, Special Issue on Interactive Computer Systems, Vol. 63, No. 6, pp 847-857, June 1975.
9. R. E. Thomas and A. A. E. Pritsker, "Decision Programming: A Model of Man-Machine Control," IEEE Transactions on Human Factors in Electronics, Vol. HFE-3, No. 1, pp 25-28, March 1962.
10. D. W. Corcoran, J. L. Dennett, and A. Carpenter, "The Cooperation of Man and Computer in Classification," Royal Naval Personnel Research Committee, London, England, AD-787 024, October 1970.
11. A. Freedy, F. C. Hull, L. F. Lucaccini, and J. Lyman, "A Computer-Based Learning System for Remote Manipulator Control," IEEE Transactions on Systems, Man and Cybernetics, Vol. SMC-1, No. 4, pp 356-363, October 1971.
12. A. Freedy, G. Weltman, and J. Lyman, "Interactive Aspects of a Man/Learning System Control Team," Proceedings of the 1972 IEEE Systems, Man and Cybernetics Conference, Washington, pp 135-140, October 1972.

13. W. B. Rouse, "A Model of the Human as a Suboptimal Smoother," Proceedings of the 1974 IEEE Decision and Control Conference, Phoenix, pp 647-654, November 1974.
14. D. R. Cox and W. L. Smith, Queues, London: Methuen, 1961.
15. J. M. Harrison, "Dynamic Scheduling of a Multiclass Queue: Discount Optimality," Operations Research, Vol. 23, No. 2, pp 270-282, March-April, 1975.
16. J. Martin, Design of Man-Computer Dialogues, Englewood Cliffs, NJ: Prentice-Hall, 1973, Chap. 4.
17. K. D. Enstrom, Real Time Adaptive Modeling of the Human Controller with Application to Man-Computer Interaction, MSIE Thesis in progress, University of Illinois at Urbana-Champaign.
18. L. R. Pinneo, "Persistent EEG Patterns Associated with Overt and Covert Speech," Bulletin of the Human Factors Society, Vol. 18, No. 2, pp 1-2, February 1975.
19. R. T. Chien, et. al., Computer-Aided Decision-Making for Flight Operations, Report No. 2, Coordinated Science Laboratory, University of Illinois at Urbana-Champaign.

75 33685

A MODEL FOR SIMULTANEOUS MONITORING AND CONTROL*

Renwick E. Curry
Man-Vehicle Laboratory, MIT; Consultant to ASI

David L. Kleinman
Department of Electrical Engineering, U. Conn.; Consultant to ASI

William C. Hoffman
Senior Project Engineer, Aerospace Systems, Inc. (ASI)

INTRODUCTION

Mathematical models of the human operator have been concerned primarily with his input/output characteristics and his adaptive behavior to sudden changes in the controlled element dynamics. Newer models have examined the ability of the human to detect failures when acting as a monitor (Reference 1). However, models for simultaneous monitoring and control (e.g., an aircraft pilot flying a split-axis approach) are almost non-existent. Such models are necessary for performing pilot task allocations and for coordinated design of display and control subsystems.

Flight test results of simulated instrument helicopter approaches conducted by the Langley Research Center (References 2-4) have shown the following:

- Constant speed approaches can be made quite comfortably by the pilots;
- Pilots cannot hover on situation displays alone;
- Pilots can hover with a flight director display, but feel uncomfortable because they do not have enough 'time' to monitor the situation displays.

MODEL DESCRIPTION

The proposed model is based on the above facts and similar results reported elsewhere. It is a lexographic model utilizing the optimal control representation of the human operator in the following way: The human gives first priority to the control tasks and tries to control the system to a desirable level of performance. Monitoring is then performed with any remaining attention. Thus, for a given fraction of attention dedicated to the control task, f_c , the pilot will adopt a control strategy to minimize the quadratic performance metric:

*Research sponsored by the NASA Langley Research Center, Contract NAS 1-13653 to Aerospace Systems, Inc., Burlington, Massachusetts.

$$J_c = \sum (\sigma_i / X_{i_{\max}})^2 \quad (1)$$

where σ_i is the rms value of the i^{th} performance variable X_i (state element, control input, etc.), and $X_{i_{\max}}$ is the maximum desirable value of X_i . The attention is allocated among the available displays to further minimize the performance metric, i. e.

$$\min(J_c) \text{ wrt } f_{c_i} \quad (2)$$

where

$$f_c = \sum f_{c_i} = \text{control workload}$$

f_{c_i} = fraction of attention on the i^{th} display element used for control.

Repeating this process for several values of control task workload f_c allows one to construct a system performance vs. workload curve, as illustrated for two systems in Figure 1.

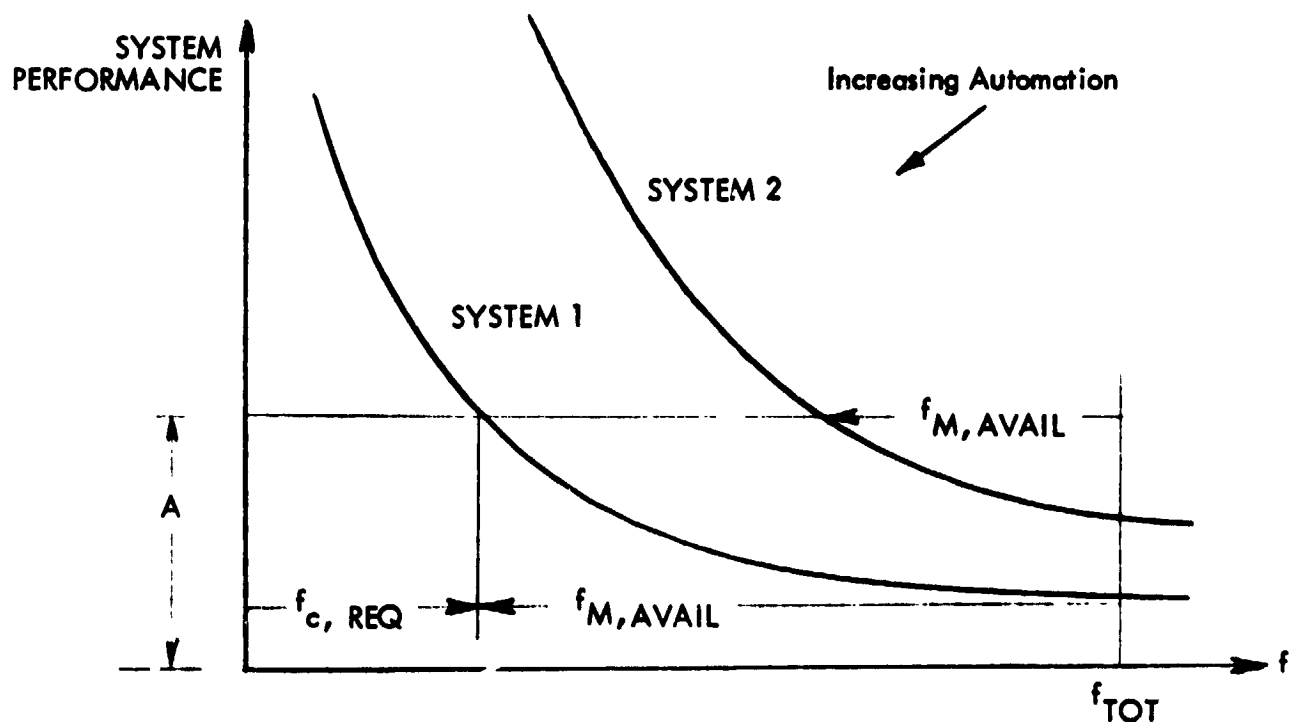


Figure 1. System Performance vs. Workload for Two Levels of Automation.

A common performance level ("A" in Figure 1) is chosen to compare all systems. The fraction of attention available for monitoring ($f_{M,AVAIL}$) is the difference between the fraction of attention required to control to this performance level ($f_{c,REQ}$), and the total fraction allowed for the task (f_{TOT}).

MONITORING MODEL CONCEPTS

The previous discussion has specified the metrics for control task workload and performance (f_c and J_c) and for monitoring workload (f_M). Several candidates for a monitoring performance metric and attention allocation criterion have been considered:

- Equal Attention

$$f_{M_i} = f_M / n_y \quad (3)$$

where n_y is the number of displays used for monitoring. This is equivalent to residual monitoring.

- Peak Excursion Monitoring

$$f_{M_i} \propto \text{PROB} [|y_i| > k \sigma_i] \quad (4)$$

where y_i is the displayed quantity, and $k \sigma_i$ is the displayed signal level which captures the pilot's attention.

- Generalized Quadratic Index

$$J_M = \frac{1}{m} \sum_{i=1}^m (\gamma_i \sigma_{e_i} / \sigma_{y_i})^2 \quad (5)$$

where the γ_i are weighting coefficients, $\sigma_{y_i}^2$ is the displayed signal variance, and $\sigma_{e_i}^2$ is the error variance in the Kalman estimate of y_i .

Depending on the choice of γ_i , the attention allocation strategy

$$\min(J_M) \text{ wrt } f_{M_i} \quad (6)$$

is optimal for

- Instrument Failure Detection
- Relative Estimation Errors
- Performance Assessment

Consequently, the monitoring performance index of Eq. (5) was chosen because of its generality, as well as its duality with the control task index of Eq. (1).

MATHEMATICAL SUMMARY

A brief summary of the mathematical aspects of the model is presented below. A full development will be contained in a later report to show in detail the duality between monitoring and control. For the control task, the dynamics of the system state x are expressed by the well known equation:

$$\dot{x} = Ax + Bu_c + Ew \quad (7)$$

with observations

$$y = Cx. \quad (8)$$

The optimal control cost can be separated into two parts, one of which depends on the fractions of attention, f_{c_i} :

$$J_c = J_c^0 + \text{tr} [L_e \Sigma L_e'] \quad (9)$$

where

$$L_e = \text{diag} (q_r^{1/2}) L_e^{A\tau} \quad (10)$$

L is the feedback control gain matrix, τ is the pilot's perceptual time delay (~ 0.2 sec), and Σ (the covariance of the Kalman Filter) obeys the Ricatti equation

$$0 = \Sigma A' + A\Sigma + EWE' - \Sigma C'V^{-1}C\Sigma \quad (11)$$

The observation noise covariance is related to the control fractions of attention by

$$V_i = \rho_i \sigma_i^2 / f_{c_i} N_i \quad (12)$$

where $\rho_i \approx 0.01$ and N_i is the random input describing function for indifference thresholds. The dependence of σ_i^2 on f_c is complicated by the Ricatti equation constraint, and in general

$$\sigma_i = g(f_{c_1}, f_{c_2} \dots) \quad (13)$$

The monitoring performance index is almost identical in form to Eq. (9) for the control performance index, i.e.,

$$J_M = J_M^0 + \text{tr} [C_e \Sigma C_e'] \quad (14)$$

where

$$C_e = \text{diag} \left(\frac{y_i}{\sigma y_i} \right) C_e^{A\tau} \quad (15)$$

and the covariance of estimation errors Σ obeys the same Riccati equation (11). However, the observation noise variance now includes the monitoring attention:

$$V_i = \rho_i \sigma_i^2 / (f_{c_i} + f_{m_i}) N_i \quad (16)$$

but σ_i and f_{c_i} are assumed constant when minimizing J_M with respect to f_{m_i} .

The iterative minimization of J_c and J_M are greatly facilitated by the following closed-form expressions:

$$\frac{\partial J_c}{\partial f_{c_i}} \approx \frac{V_i}{f_{c_i}} \text{diag} \left[G' \int_0^{\infty} e^{\hat{A}'\sigma} L_e' L_e e^{\hat{A}\sigma} d\sigma G \right] \quad (17)$$

$$\frac{\partial J_M}{\partial f_{M_i}} = \frac{V_i}{f_{M_i} + f_{c_i}} \text{diag} \left[G' \int_0^{\infty} e^{\hat{A}'\sigma} C_e' C_e e^{\hat{A}\sigma} d\sigma G \right] \quad (18)$$

where

$$G = \Sigma C' V^{-1} = \text{Kalman filter gain}; \quad A = \hat{A} - GC$$

A basic gradient optimization technique is used, but the gradients are projected onto the constraint hyperplanes:

$$\Sigma f_{c_i} = f_c \quad (19)$$

$$\Sigma f_{M_i} = f_M \quad (20)$$

SAMPLE RESULTS

The attention allocation scheme has been applied to the longitudinal control of a CH-46C helicopter in hover. Table 1 compares the predicted performance with and without a flight director. The results are very much in accord with the actual flight tests: When the flight directors are included, hovering performance is vastly improved and almost the entire attention capacity is devoted to the pitch and power flight director indicators.

Table 1. Helicopter Hover Task, Longitudinal Axis, Pitch Command Control System,
 $f_c = 0.3$

INSTRUMENT	σ_{y_i}		f_{c_i}/f_c	
	w/o FD	FD	w/o FD	FD
MAP	25.5 ft	16.6 ft	.35	.03
ALTIMETER	4.7 ft	4.7 ft	.17	.1
PITCH	1.0°	.7°	.03	.03
IVSI	1.4 fps	1.2 fps	.45	.13
δ_{D_x}	-	.13 in	-	.30
FD _h	-	.14 in	-	.40
δ_e	.13 in	.10 in		
δ_c	.25 in	.22 in		

CONCLUSIONS

Performance measures and workload metrics have been defined for both control and monitoring tasks conducted simultaneously. Systematic procedures have been developed for allocating attention among the available displays; this avoids the previously arbitrary choice of f_i . Work is continuing to further validate the model, to determine information requirements for different display and control systems, and to allocate pilot control and monitoring tasks between manual and automatic systems for a helicopter.

REFERENCES

1. Gai, E. G.; and Curry, R. E.: Failure Detection by Pilots During Automatic Landings: Models and Experiments. Paper A.5, XIth Annual Conference on Manual Control, NASA Ames Research Center, May 21-23, 1975.
2. Kelly, James R.; Niessen, Frank R.; and Sommer, Robert W.: Evaluation of a VTOL Flight-Director Concept During Constant-Speed Instrument Approaches. NASA TN D-5860, June 1970.
3. Garren, John F., Jr.; Kelly, James R.; Sommer, Robert W.; and DiCarlo, Daniel J.: Flight Investigation of VTOL Control and Display Concept for Performing Decelerating Approaches to an Instrument Hover. NASA TN D-6108, February 1971.
4. Kelly, James R.; Niessen, Frank R.; Thibodeaux, Jerry J.; Yenni, Kenneth R.; and Garren, John F., Jr.: Flight Investigation of Manual and Automatic VTOL Decelerating Instrument Approaches and Landings. NASA TN D-7524, July 1974.

1 N75 33686

DETECTION OF SYSTEM FAILURES IN MULTI-AXES TASKS

by Arye R. Ephrath

Man-Vehicle Laboratory

Massachusetts Institute of Technology

SUMMARY

The investigation has examined the effects of the pilot's participation mode in the control task on his workload level and failure-detection performance during a low-visibility landing approach. We found that the participation mode had a strong effect on the pilot's workload, the induced workload being lowest when the pilot acted as a monitoring element during a coupled approach and highest when the pilot was an active element in the control loop.

The effects of workload and participation mode on failure detection were separated. The participation mode was shown to have a dominant effect on the failure detection performance, with a failure in a monitored (coupled) axis being detected significantly faster than a comparable failure in a manually-controlled axis.

INTRODUCTION

In the last decade, a great deal of thought has been given to Category III landings and their implications. One area of intensive investigation centers around the role of the crew during the approach, and current thought is polarized around two extremes:

- a. The crew is in the control loop and flies the aircraft in accordance with instrument-generated steering signals.
- b. Steering signals are coupled directly into the autopilot, with the crew monitoring the system

It is axiomatic that a pilot should be capable of detecting and identifying failures in the automatic landing system accurately, reliably and with minimal time delay. To this end, extensive studies have been conducted in which the pilot was treated as a controlling element in a one-dimensional task; his decision processes (Schrenk, 1969) and his adaptive behavior following a sudden change in the controlled plant dynamics were investigated (Young *et al*, 1964; Phatak and Bekey, 1969). Other studies investigated the failure-detection performance treating the operator as a pure monitor (Gai and Curry, 1975). In reality, however, the pilot is faced with multi-axes, not single-axis, tasks; although models for interference among multiple control tasks have been derived (Levison, 1970), the interrelationships among simultaneous control and monitoring tasks are not yet well understood (Levison, 1971).

Young *et al* (*op. cit.*) found that in single-axis tracking tasks the human operator's performance as a failure detector was better when he was in the control loop; simulated Category III landing studies, on the other hand, have shown that the pilot's failure detection performance deteriorated when he was faced with manual control task, compared to the monitoring mode (Vreuls *et al*, 1968). When faced with split-axis tasks, pilots' monitoring and decision making were impaired (Monroe *et al*, 1968) and they sometimes completely overlooked the occurrence of a failure, presumably because of the increased workload associated with split-axis tasks (Gainer *et al*, 1967).

It has been recognized that when the the role of the human changes from monitoring to that of an active controller corresponding changes take place in his workload level (Ekstrom, 1962; Wewerinke). However, in pilot-performance studies to date these effects were completely confounded. It is the primary purpose of this investigation to separate these effects and to document pilot performance during a Category III landing as a function of the particular control mode at different workload levels. We wished to isolate and identify the effects on performance due to the variations in the control mode alone - and hence, variations in the operator's mode of behavior - apart from the effects on performance due to the variations in the workload level.

METHOD

As stated, the purpose of this research was the study of the pilot's short-term decisions regarding performance assessment and failure monitoring. We wished to investigate the relationship between the pilot's ability to detect failures, his degree of participation in the control task and his over-all workload level. Also, we wished our findings to be applicable to the general population of pilots who fly low-visibility approaches in commercial jet transport aircraft. To this end, this research consisted of an experimental investigation which was carried out in a static ground simulator and which utilized fifteen airline pilots as subjects.

The simulation capability included the ADAGE AGT/30 digital graphics computer and a fixed-base cockpit simulator. A mathematical model has been developed of a large transport aircraft in the landing approach flight envelope; the actual flight data of a DC-8 were used in the equations of motion, and the various parameters were later refined following a series of flight tests by a senior airline captain with considerable Boeing 707/123 experience. Non-linear phenomena such as ground-effect and stalls have also been included.

An integrated-cue flight director system has been designed for this simulator, providing the capability to land the simulated aircraft manually in zero-zero conditions in a relatively satisfactory manner. Also, a two-axis autopilot has been incorporated into the simulation which was capable of intercepting and tracking the Instrument Landing System (ILS), in either axis or in both axes, to touchdown. We also had the capability to add wind disturbances to the simulation to induce different workload levels. The wind gusts were modelled as filtered white noise with a cutoff frequency of $\pi/6$ rad/sec.

The mathematical model was programmed into the AGT/30 computer which was linked via multiplexer channels and sense lines to the cockpit simulator. The cockpit was a mock-up of the captain's crew station in a Boeing transport aircraft (Fig. 1). The windows were frosted to eliminate external visual ref-



Figure 1. Cockpit Simulator

erence.

The controls included an operational, spring-centered control column with a control wheel and rudder pedals, as well as four throttles, flaps, speed-brake and landing-gear levers and flight-director and autopilot controls.

Apart from engine instruments and marker-beacon lights the simulator was equipped with three CRT screens, mounted one each on the main instrument panel at the captain's and the first officer's stations and one in place of the weather radar screen. The screens were driven simultaneously by the ADAGE computer and presented the six standard flight instruments (Fig. 2): Airspeed, attitude-flight director indicator, altimeter, instantaneous vertical speed indicator, horizontal situation (HSI) and radio-magnetic (RMI) indicators, as well as a DME digital readout and glideslope deviation and course deviation needles. The CRT screens were driven by the computer at a rate of 24 frames per second which was sufficient to produce flicker-free images. The information was updated at a rate of 5/second.

To measure the pilot's workload, a "warning light"-type subsidiary task was selected for the research. It consisted of two small red lights mounted above each other outside the subject's peripheral vision field, and a rocker thumb switch mounted on the left horn of the control yoke.

The lights provided the stimuli. During the run the upper or lower light, with equal probability, was lit at a random time for a maximum of two seconds. A correct response by the subject consisted of turning the light off by a proper motion of the rocker thumb switch. The program recorded the number of times that the subject responded correctly to the warning light ("hits") and his response time (latency) for each response. Incorrect responses by the pilot, that is, not responding to an illuminated light or activating the switch the wrong way, were also counted and labeled as "misses".

A workload index was computed from these data as follows:

- a. As each stimulus was presented for a maximum of 2 seconds, the total response-time ratio RTR for both "hits" and "misses" was computed by

$$RTR = \frac{\text{cumulative latency } (\sum T_i)}{\text{Total number of stimuli} \times 2 \text{ sec}} \quad (1)$$

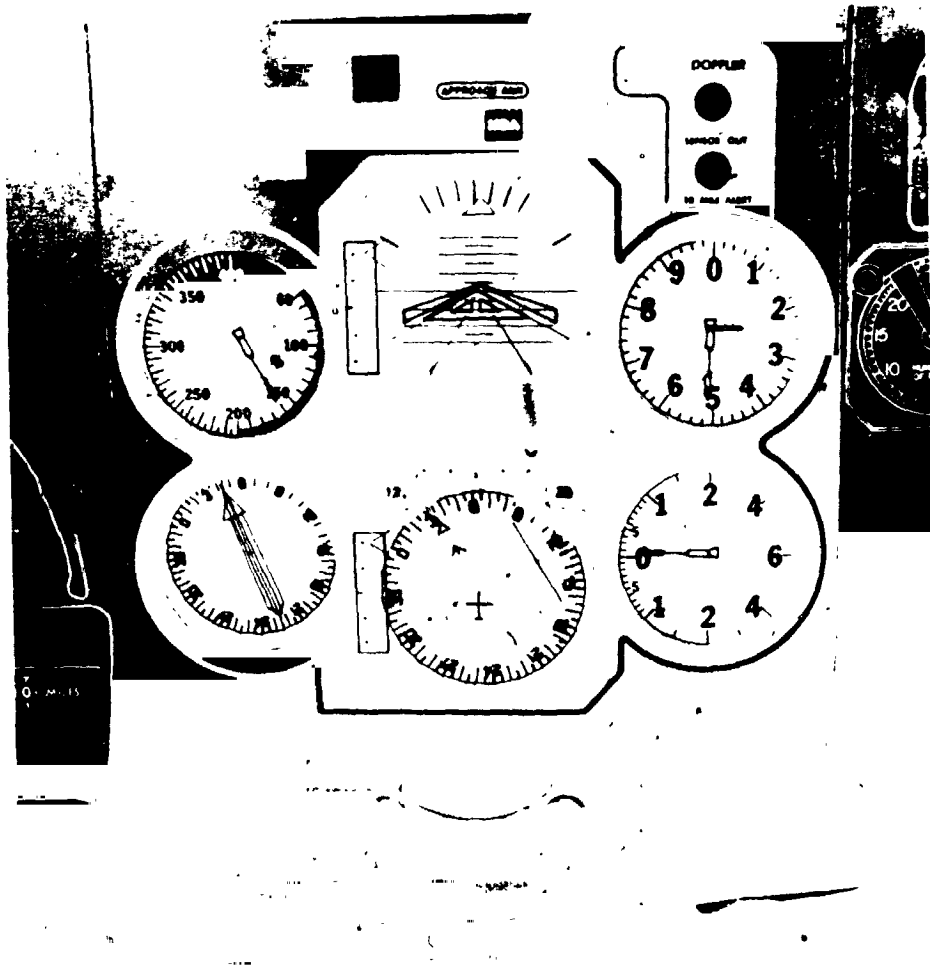


FIGURE 1. Instrument Panel

ORIGINAL PAGE IS
OF POOR QUALITY



FIGURE 1. BILL CUNYAN'S OFFICE BUILDING

ORIGINAL PAGE IS
OF POOR QUALITY

b. A miss-rate MR was computed by

$$MR = \frac{\text{Number of stimuli missed}}{\text{Total number of stimuli}} \quad (2)$$

c. A workload index WLX was then extracted using the best least-squares fit weighing coefficients

$$WLX = \frac{0.78 \text{ RTR} + 0.626 \text{ MR}}{0.78 + 0.626} \times 100 \text{ percent} \quad (3)$$

This measure of workload has been shown (Spyker *et al*, 1971) to be correlated with physiological predictors of workload with a correlation coefficient $\rho = 0.646$, significant at the $P < 0.005$ level.

d. Finally, we wished to eliminate differences between subjects which may have been caused by different subjects assigning different relative priorities to the primary tracking task and the subsidiary task. To this end the workload index of each subject was normalized, that is, a workload index of zero was assigned to the approach which resulted in the lowest workload measure for each subject and a workload index of 100 was assigned to the approach with the highest workload measure for the subject. The normalized workload index on approach i of subject j was then computed by

$$\text{Normalized } WLX_{ij} = \frac{WLX_{ij} - \min_i \{WLX_{ij}\}}{\max_i \{WLX_{ij}\} - \min_i \{WLX_{ij}\}} \times 100 \text{ percent} \quad (4)$$

Experimental Design

The experimental variables to be investigated in this study were the pilot's participation level in the piloting task, the workload induced by the control dynamics and by external disturbances, and the pilot's failure detection performance.

The experiment involved four levels of control participation:

- a. "Passive monitoring", with autopilot coupling in all axes, including autothrottle.
- b. "Yaw manual", with autopilot coupling in the pitch axis and autothrottle coupled.
- c. "Pitch manual", with autopilot coupling in the yaw axis only.
- d. "Fully manual".

There were three levels of wind disturbance:

- a. No wind.
- b. A 45° tailwind of 5 knots, gusting to 15 knots.
- c. A 45° tailwind of 10 knots, gusting to 30 knots.

Three failure conditions were used:

- a. No failure.
- b. Failure in the yaw axis. In this condition the autopilot, if coupled, or the flight director would steer the airplane away from the localizer course to intercept and track a course parallel to the nominal path but translated by a distance corresponding to one dot deviation (1.25°) at the point of failure occurrence. This resulted in a one-dot angular error about 100 seconds after the initiation of the failure. This type of failure was chosen, rather than a runaway failure, as it was quite subtle and therefore it provided a good measure of the limits of the pilot's failure detection capability.
- c. Failure in the pitch axis, which resulted in a one-dot deviation (0.35° of angular error) approximately 30 seconds after the occurrence of the failure.

Failures were presented only between the altitudes of 1800 and 800 feet; each approach was terminated either at touchdown or when a positive rate of climb has been established following the initiation of a go-around by the subject. The selection of the failure altitude was randomized, as was the selection of the direction of the failure (left-right in a lateral failure mode, up-down in a pitch failure mode). Workload levels and failure detection performance were investigated in separate experiments, to avoid possible contamination of failure detection data by the presence of a concomitant subsidiary task; the "no failure" condition was incorporated in the design so that the subjects

would not anticipate a failure on each and every approach.

RESULTS AND DISCUSSION

It seems clear from Figures 4 and 5 that the side-task scores were sensitive to variations both in the disturbance level and the participation mode. Indeed, analysis of variance under the hypothesis that the effects of the disturbance and of the participation were additive revealed that the variations in workload scores as a function of participation mode were significant at the $P \ll 0.01$ level and as a function of the severity of the disturbance - at the $P < 0.05$ level.

There was, however, no significant difference between workloads at the two low disturbance levels, namely, calm air and a quartering wind of five knots, gusting to fifteen knots. It was assumed, and it was verified by pilots' comments, that the components of the wind parallel and normal to the final approach path, 3.5 knots gusting to 10.6 knots, were not strong enough to induce workload significantly higher than that induced by piloting the simulated aircraft in calm air. Consequently, these two disturbance levels were combined in the analysis and the data were treated as if there were only two distinct disturbance levels, "low" and "high".

An additive model was used in the regression of workload scores on the disturbance levels and participation modes, to yield

$$WLX(P,D) = W_1(P) + W_2(D) \quad (5)$$

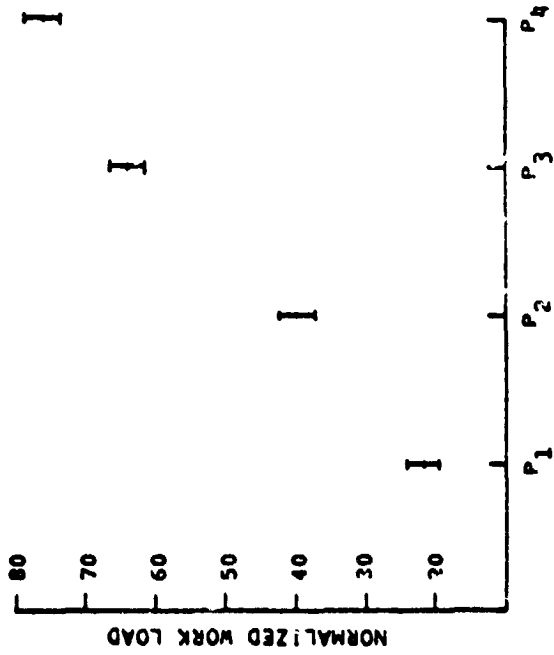
where WLX is the normalized workload score

P is the participation mode

D is the disturbance level

$W_1(P) =$ 18.7 for the fully-automatic mode
36.6 for split-axis, yaw manual mode
61.0 for split-axis, pitch manual mode
72.9 for the fully manual mode

and $W_2(D) =$ 0 for the "low" disturbance level
9.82 for the "high" disturbance level

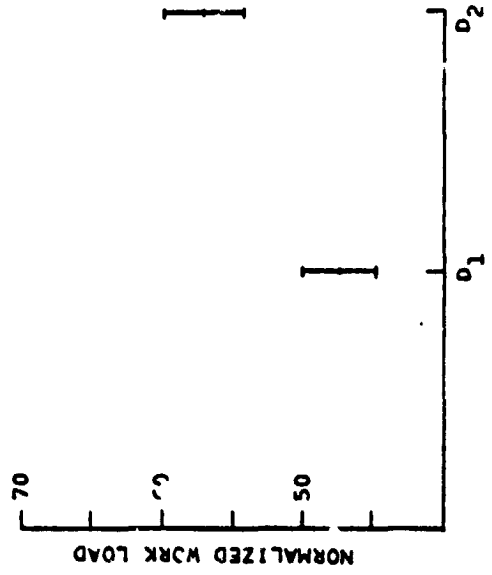


Normalized Workload Index at Four

Participation Modes

- P1 - Fully Automatic
- P2 - Split Axis, Yaw Manual
- P3 - Split Axis, Pitch Manual
- P4 - Fully Manual

Figure 4.



Normalized Workload Index at Two

Disturbance Levels

- D1 - Calm Air
- D2 - 10 kt. Wind, Gusting to 30 kt.

Figure 5.

These values yielded workload-participation mode correlation significant at $P < 0.001$ and workload-disturbance correlation significant at $P < 0.05$.

Detection performance was analyzed in terms of detection time and accuracy. Detection time was defined as the elapsed time between the occurrence of a failure and the verbal report by the subject that the failure has been detected and identified. Accuracy was measured by the fraction of failures that were missed altogether. We differentiated between approaches in which a failure went unreported but which resulted in a successful touchdown and approaches in which a failure was missed and which did not terminate in a successful landing because of gross error in the failed axis. The latter are shown in Tables 1 and 2; the numbers in parentheses represent the fraction of all missed failures, whether or not they resulted in a successful landing.

In all, 90 approaches were flown in which a longitudinal failure occurred; of these, 8 went unreported, 6 of which did not terminate in a successful landing. Of the 90 lateral failures presented, 9 were missed; of these, 6 did not terminate in a successful landing.

A very interesting pattern is obvious from Tables 1 and 2 and from Figures 6 and 7: All failures in an automatically-controlled axis were detected in consistently short times, between 9 and 17 percent of the failures which occurred in a manually-controlled axis were not detected at all, and the ones that were required considerably longer detection times. The difference between the mean detection times in an automatic and manual mode was highly significant at the $P < 0.01$ level.

We hypothesized that this difference in detection performance was due, in part, to the increased involvement of the pilot in the control task in the manual mode and, in part, to the increased workload levels associated with manual control; we set out to separate the individual effects of these factors on the failure detection performance.

In Figures 6 and 7 the mean detection times of pitch and yaw failures, respectively, are plotted as functions of the corresponding mean workload levels for the four participation modes. The following relationships are evident:

1. Detection times in a manually-controlled axis are longer than detection

TABLE 1
Fraction of Missed Longitudinal Failures
in Percent

Participation Mode	disturbance Level			Overall
	1	2	3	
Monitor	0.	0.	0.	0.
Control Yaw	0.	0.	0.	0.
Control Pitch	12.5 (12.5)	0. (14.3)	12.5 (12.5)	8.7 (13.0)
Manual Control	0. (12.5)	14.3 (14.3)	37.5 (37.5)	17.4 (21.7)
Overall	3.3 (6.7)	3.3 (6.7)	13.3 (13.3)	6.7 (8.9)

TABLE 2

Fraction of Missed Lateral Failures
in Percent

Participation Mode	Disturbance Level			Overall
	1	2	3	
Monitor	0.	0.	0.	0.
Control Yaw	25.0 (37.5)	14.3 (14.3)	12.5 (37.5)	17.4 (30.4)
Control Pitch	0.	0.	0.	0.
Manual Control	14.3 (14.3)	0.	14.3 (14.3)	9.1 (9.1)
Overall	10.0 (13.3)	3.3 (3.3)	6.7 (13.3)	6.7 (10.0)

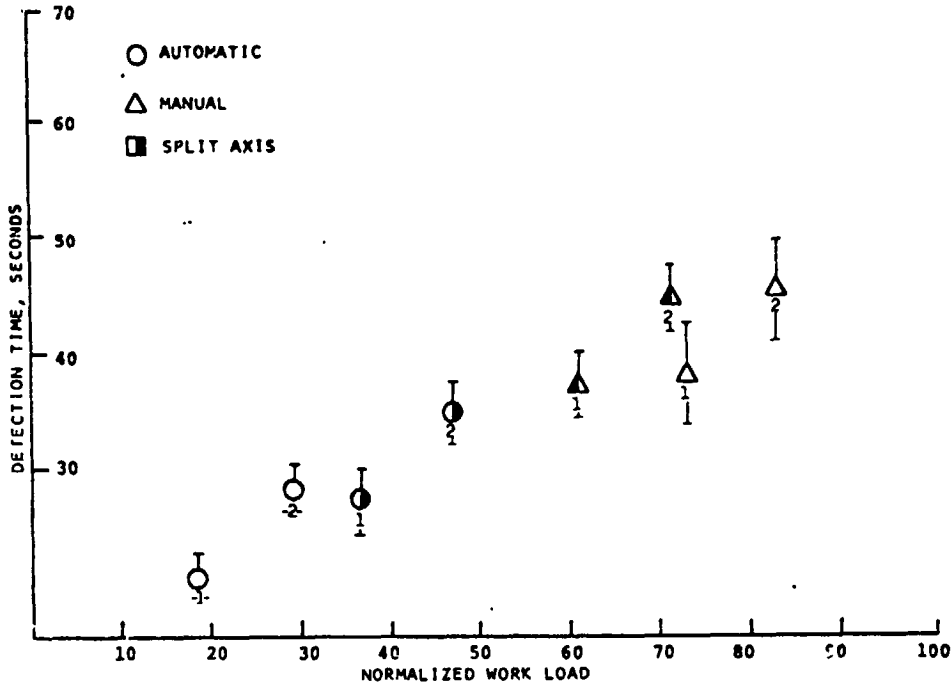


Figure 6. Mean Longitudinal Detection Times

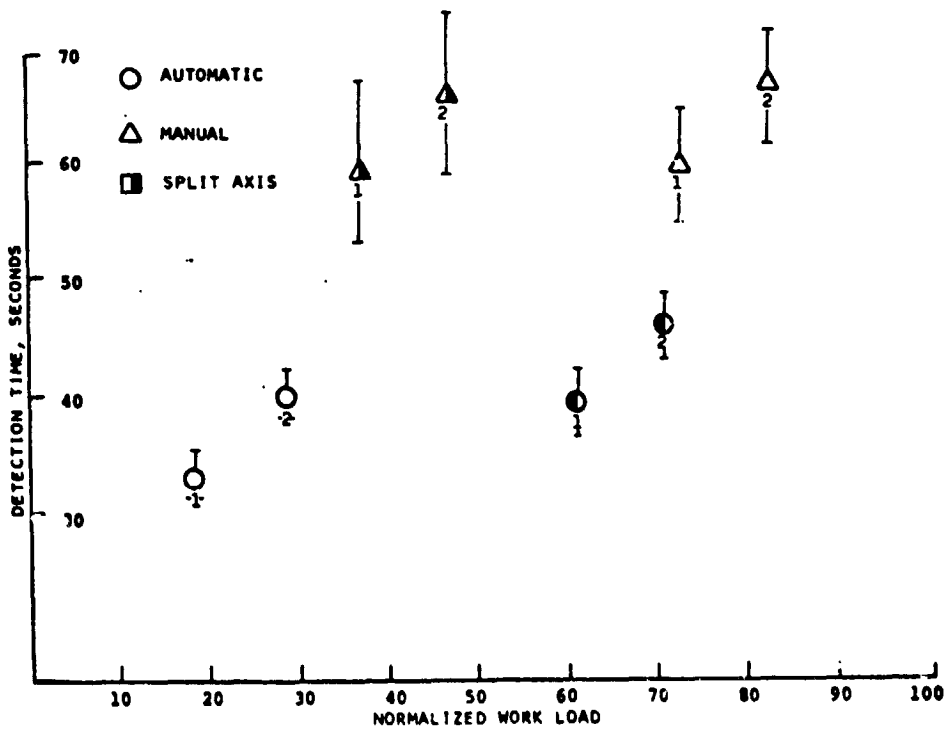


Figure 7. Mean Lateral Detection Times

times in an automatically-controlled axis.

2. Detection times for lateral failures are significantly longer than detection times for longitudinal failures at comparable workload levels.
3. Detection times increase in direct relationship to workload ($\rho = 0.322$ for $n=163$ pairs).

We assumed that the failure detection mechanism of the human operator acts similarly in both lateral and longitudinal axes; any difference in performance between these axes is due to differences in the plant dynamics and in display variables only, not to differences in processes internal to the operator. This assumption of equivalence between the lateral and longitudinal axes has been made, either explicitly or implicitly, by many investigators. It is based on the theory that the human behaves optimally with respect to his task (cf. Smallwood, 1967) in all axes, and that the operator adjusts his describing function to match the task (Young, 1969).

Longitudinal and lateral failure detection data were thus pooled; detection times were regressed on the type of failure (longitudinal or lateral) and on the control mode in the failed axis, with the workload index as a covariate, based on the following additive model:

$$T_{\text{detection}} = T_0 + \alpha(\text{control mode}) + \beta(\text{failed axis}) + \gamma(\text{workload}) \quad (6)$$

A solution was obtained for the regression coefficients α , β and γ :

$$T_{\text{detection}} = 20.9 + 16.5 \underline{M} + 15.4 \underline{A} + 0.10 \text{WLX} \quad (7)$$

where $\underline{M} =$ 1 if the failed axis is controlled manually

$\underline{M} =$ 0 otherwise

$\underline{A} =$ 1 if the failure occurs in the lateral axis

$\underline{A} =$ 0 if the failure occurs in the longitudinal axis

WLX = the normalized workload index

and $T_{\text{detection}}$ is measured in seconds.

The relationship is plotted in Figures 8 and 9 for longitudinal and lateral

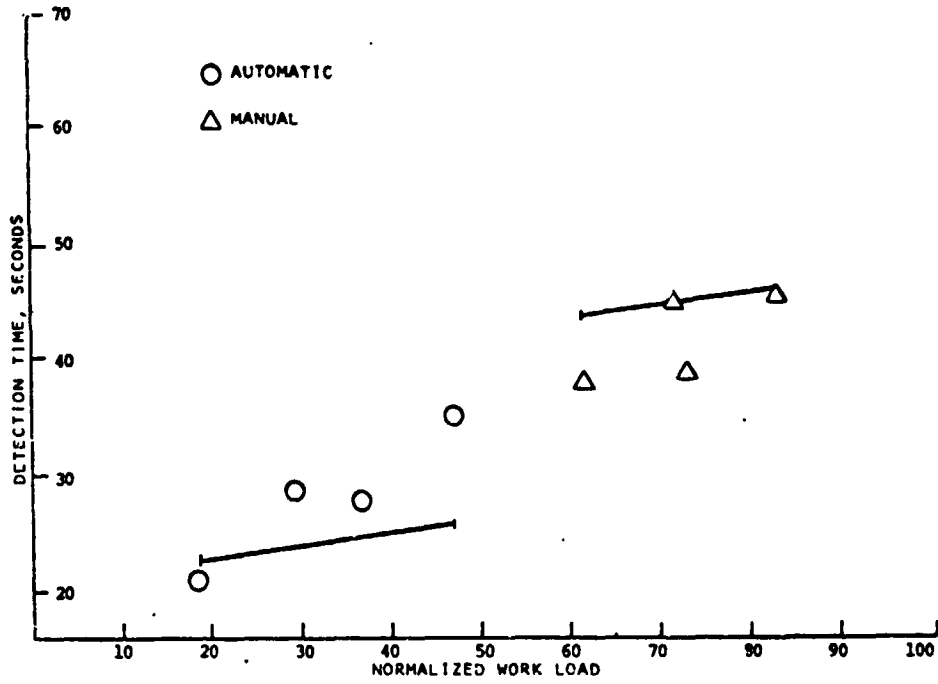


Figure 8. Predicted Longitudinal Detection Times

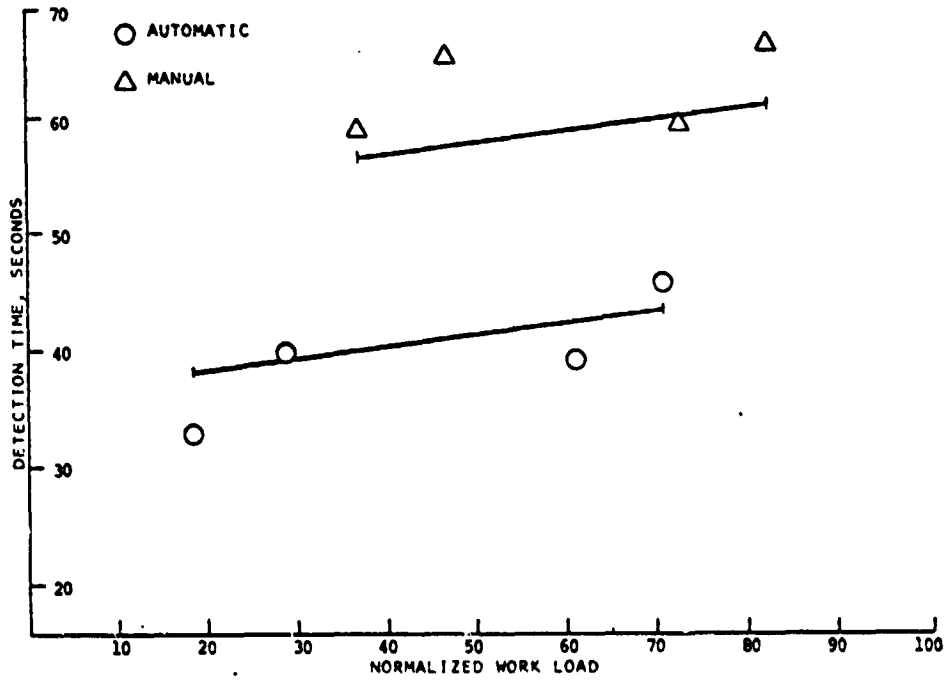


Figure 9. Predicted Lateral Detection Times

failures, respectively. Mean detection times at the corresponding mean workload levels are also shown for comparison. The model correlates well with the data, with $\rho_{n=163} = 0.531$, significant at the $P \ll 0.001$ level.

CONCLUDING REMARKS

Our goal in this research was to identify the participation mode and workload level which optimize the pilot's failure detection performance; this subject is treated in considerably more detail elsewhere (Ephrath, 1975).

Our results indicate quite clearly that a coupled, fully-automatic landing with the lowest possible workload is called for in Category III operations, with the crew monitoring the progress of the approach via cockpit displays: Failure-detection performance in all other control modes was unacceptable for commercial operations. Performance monitors and fault annunciators may alleviate the problem somewhat but they are inadequate at altitudes below 100 feet (Vreuls *et al*, 1968); also, they are not infallible, and additional warning lights and buzzers in the cockpit provide more opportunities for malfunctions and for crew confusion.

REFERENCES

- Ekstrom, P.J., *Analysis of Pilot Workloads in Flight Control Systems with Different Degrees of Automation*, IRE International Congress on Human Factors Engineering in Electronics, Calif., May 1962.
- Ephrath, A.R., *Pilot Performance in Zero Visibility Precision Approach*, Ph.D. Thesis, Massachusetts Institute of Technology, May 1975.
- Gai, E.G. and R.E. Curry, *Failure Detection by Pilots During Automatic Landings: Model and Experiments*, Annual Conference on Man-Machine Control, California, May 1975.
- Gainer, C.A. *et al*, *All Weather Landing Simulation for Category III Airborne*

Configuration: Flight Directors and Split Axis Control, Bunker-Ramo Corp. California, SRDS-RD-67-56/1, July 1967.

Levison, W.H., *A Model for Task Interference*, Annual Conference on Manual Control, Ohio, April 1970.

Levison, W.H., *A Control-Theory Model for Human Decision Making*, Annual Conference on Manual Control, California, June 1971.

Phatak, A.V. and G.A. Bekey, *Decision Processes in the Adaptive Behavior of Human Controllers*, IEEE Transactions on Systems Science and Cybernetics, V. SSC-5, 4:339-351, October 1969.

Schrenk, L.P., *Aiding the Decision Maker - A Decision Process Model*, IEEE Transactions on Man Machine Systems, V. MMS-10, 4:204-218, Dec. 1969.

Smallwood, R.D., *Internal Models and the Human Instrument Monitor*, IEEE Transactions on Human Factors in Electronics, V. HFE-8, 3:181-187, September 1967.

Spyker, D.A. et al, *Development of Techniques for Measuring Pilot Workload*, NASA CR-1888, 1971.

Vreuls, D. et al, *Pilot Failure Detection Performance with Three Levels of Fault Warning Information*, Bunker-Ramo Corp., California, SRDS-RD-68-9, February 1968.

Wewerinke, P.H., *Human Operator Workload for Various Control Situations*, National Aerospace Laboratory, N.L.R., Amsterdam, the Netherlands.

Young, L.R. et al, *The Adaptive Dynamic Response Characteristics of the Human Operator in Simple Manual Control*, NASA TN D-2255, 1964.

Young, L.R., *On Adaptive Manual Control*, IEEE Transactions on Man Machine Systems, V. MMS-10, 4:292-331, December 1969.

DRIVER DECISION-MAKING RESEARCH IN A LABORATORY SIMULATION

By R. Wade Allen, Stephen H. Schwartz, and Henry R. Jex

Systems Technology, Inc.
Hawthorne, California

SUMMARY

This paper reviews a simulation approach to the study of driver risk-taking behavior in a decision-making context. The objective is to differentiate between perceptual, psychomotor, and decision-making components of driving behavior. Tasks are set up in a decision-making context, with rewards and penalties applied as performance incentives. Expected value theory is used both to set up task conditions and as a means for data analysis and interpretation.

Simulation tasks were selected that would fit into a decision context and could be efficiently implemented. Signal light, obstacle avoidance, and curve negotiation tasks were chosen as representing a cross section of driving situations that would lead to an interesting, motivating driving scenario and cover a range of decision-making situations. The tasks were programmed to occur randomly and repeatedly in a simulated continuous drive.

Both performance and risk-taking behavior were measured for each of the tasks. Risk-taking behavior was consistent with an expected value decision-making model interpretation, and both performance and behavior show sensitivity to alcohol intoxication.

SESSION II
PHYSIOLOGICAL SYSTEMS

Chairman: WILLIAM H. LEVISON

75 33687

RECOGNITION OF STIMULUS DISPLAYS - AN ELECTROPHYSIOLOGICAL ANALYSIS

By Victor S. Johnston

New Mexico State University

SUMMARY

This study reveals that late components of evoked waveforms recorded from the frontal areas of the brain are correlated with an observer's interpretation of a stimulus display. The possible use of such signals as control inputs is discussed.

INTRODUCTION

The human brain is capable of a rapid but not instantaneous analysis of a stimulus display; that is, a finite period of time is required for the processes of identification and recognition. These processes impose temporal limitations on the rate of information flow across the machine-to-man interface and are vulnerable to disruption by a large number of environmental factors such as toxicants, stress and drugs. A knowledge of the basic physiological mechanism involved in the detection and recognition of a stimulus display offers a theoretical basis for a model of human performance capable of (a) predicting the interactive effects of a number of these environmental variables and (b) identifying possible physiological signals which may serve as reliable control inputs to machines.

Several experiments have suggested that the wave shape of stimulus-locked potentials may reflect a change in an observer's interpretation of a stimulus display. For example, John et al. demonstrated consistent differences in the late components of visual evoked potentials (VEP's) induced by two very similar stimuli, a square and a rotated square (diamond), irrespective of the

stimulus size. However, the interpretation of such experiments is difficult because the experimental procedure involves a change in the physical stimulus as well as a change in meaning. Physical attributes of a stimulus change the waveform of VEP's (references 2-7) so, in order to avoid confounding the meaning change with the physical stimulus change, it is necessary to keep the latter constant.

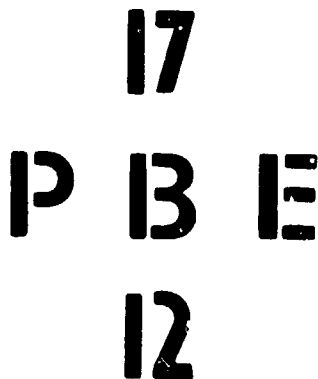


Fig. 1. Stimuli used in experimental procedures. Central stimulus is ambiguous. meaning of a constant stimulus by

adding a new association using a conditioning procedure, for example, pairing a visual stimulus with an auditory click (reference 8). However, any change in the VEP as a result of this may reflect enhanced arousal or attention rather than the meaning change per se. Modification of VEP's by such variables as expectancy, affect, uncertainty, or attentional state have been demonstrated in many situations (references 9-14). The conditioning procedure not only brings about a change in meaning but may also have a quantitative effect on one or more of these state variables. The difficulties inherent in equating both the physical stimulus and state variables may be circumvented by the use of a symbolic stimulus that has two or more distinct meanings depending on the context in which it is presented.

APPARATUS

The central symbol in Fig. 1 can be interpreted as "B" or "13," depending on its context. The stimulus-locked evoked potential for this symbol was recorded when it was embedded in the temporal context of other numbers or other letters.

The subjects were seven student volunteers with normal visual acuity. They were seated in an electrically shielded, sound-deadened enclosure looking directly at a translucent Plexiglas screen. A Kodak Carousel projector, fitted with a strobe light, back-projected stimuli onto the Plexiglas screen from an adjacent room. All stimuli subtended a 2° visual angle and were presented as white figures on a black background. The nonambiguous letter stimuli were equated in surface area with the nonambiguous number stimuli. The projector advance mechanism and strobe were under the control of a PDP8/e computer. The subject initiated a stimulus presentation by depressing a button with his left hand and, after a delay of 0.5 second to allow movement potentials to subside, the stimulus slide was projected for 10 μ sec.

PROCEDURE

A session consisted of 80 stimulus presentations. The three numerals shown in the column on Fig. 1 were presented separately, in a random temporal sequence, in number sessions. During letter sessions, a similar random sequence of letters shown in the row of Fig. 1 was presented. The ambiguous stimulus occurred 40 times and the nonambiguous stimuli 20 times each within a session. Each subject participated in eight sessions (four number and four letter) on the same day. Number and letter sessions were alternated for each subject, and the nature of the first session varied among subjects. The first two were warm-up sessions and served to familiarize the subjects with all stimuli.

Subjects were instructed that the task was concerned with the speed with which they could name numbers and letters. They initiated a stimulus presentation by depressing a button with their left hand, and a voice-operated relay detected the subjects' verbal response so that reaction time was monitored throughout the experiment. Before each session, subjects were informed

of the visual stimuli to be presented in that session. This also served to enhance the perceptual set for the ambiguous stimulus. Questioning after the experiment revealed that only one subject was aware that he had been calling the same stimulus by two different names according to its context. All the other subjects showed surprise when the relationship was pointed out to them.

Subjects were fitted with scalp electrodes located on the midline either 2.5 cm above the inion (occipital) or 2.5 cm above the nasion (frontal). The final subject had electrodes in both locations. Thus, four records were obtained from subjects with occipital electrodes and four from subjects with frontal electrodes. Corneorecinal potentials were reduced by providing the subject with a cross-hair fixation point, allowing self-presentation of the stimuli, and referencing the frontal electrode to the central terminal of a 40-kilohm potentiometer connected between a vertical electrooculogram electrode and the two earlobes (reference 15). Before the experiment, the potentiometer was adjusted until vertical eye movements could no longer be detected on the electroencephalographic recording. Occipital electrodes were referenced to the two earlobes.

Evoked potentials were amplified by Grass model 6A5 wide-band a-c amplifiers and, after being digitized at the rate of 500 points per second, they were stored in the PDP8/e computer. Each waveform, which contained 240 msec of data collected immediately after stimulus presentation, was averaged with others for the same stimulus for that subject and session. Four averaged evoked potentials, each the average of 20 stimulus presentations, were collected from each subject during each session. These waveforms were then transferred to magnetic tape for subsequent analysis on an IBM 360 computer.

RESULTS

Six sessions, four averaged waveforms per session, yielded a total of 24 averaged wave forms collected from the same electrode location on each subject. Of these, 12 were recorded following the presentation of the ambiguous stimulus. The data from each subject was analyzed on an IBM 360 computer by using the BMD-08M factor analysis program from the UCLA Biomedical package. Before analysis, all VEP's were adjusted to a zero mean. A principal components analysis and varimax rotation were performed on the 120 by 120 correlation matrix formed by the correlations among the 120 time points for "B" and "13." An excellent theoretical discussion of this procedure has been given by Donchin (reference 7). In all cases it was found that five eigenvalues accounted for between 80 and 95 percent of the total variance in the data. The corresponding eigenvectors were cross-multiplied by the original waveforms. In this way we can find which, if any, factors show a significantly different loading when the ambiguous stimulus is interpreted as "B" or as "13." This method has the advantage over cross-correlation or peak-to-peak measurement techniques in that it allows a temporal localization of differences, as well as a quantifiable assessment of statistical significance.

The analysis revealed that in the case of occipital recording, none of the four subjects showed any significant difference related to the context of the ambiguous stimulus: that is, none of the rotated eigenvectors were differentially loaded on "B" and "13" waveforms. In the case of frontal

recordings, three of the four subjects showed differential loadings on one or more factors. The subject with simultaneous recordings for occipital and frontal locations showed significantly different loadings on recordings from the frontal location and no difference in the occipital recordings.

Figure 2 shows an example of the eigenvectors extracted from frontal recordings for one subject, together with the "B" and "13" wave forms averaged over all experimental sessions. In this case, four factors accounted for more than 85 percent of the total variance. Only factor 2 (f2), which begins 160 msec after stimulus presentation, is differentially loaded on "B" and "13" ($U = 0$, $P < .002$). Frontal recordings for two other loading subjects also showed differential loading on a similar factor temporally located on this part of the wave form ($U = 0$, $P < .002$; $U = 1$, $P < .004$). This suggests that the most significant difference between "B" and "13" wave forms occurs in the late components, starting 160 msec after the stimulus. In addition, one frontal recording subject had a significantly different loading on a second factor which accounted for 5.9 percent of the variance ($U = 0$, $P < .002$). This factor (f4) was temporally located between 100 and 140 msec after stimulus presentation. Comparable factors in two other frontal recording subjects also showed a trend in this direction ($U = 8$, $P < .066$; $U = 7$, $P < .047$).

There was no significant difference between the reaction time to a "B" or a "13" over all subjects. This suggests that the observed differences in the wave forms cannot be accounted for by differences in the arousal level or attention of the subjects. Differences due to corneoretinal potentials are improbable since they were almost eliminated by the procedure described earlier, and it appears unlikely that differential eye movements would occur in response to a 10- μ sec flash of the same stimulus in the two different contexts.

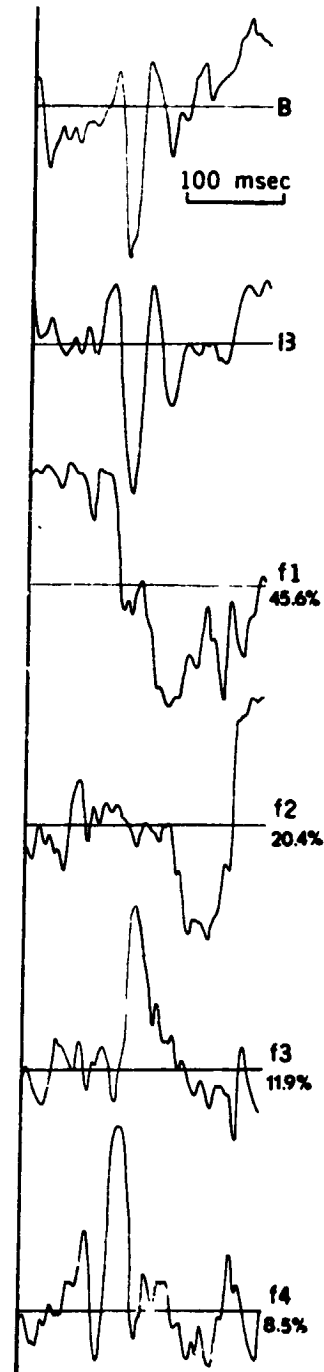


Fig. 2. Average "B" and "13" wave forms recorded from a frontal location on the same subject. First four rotated eigenvectors (f1 to f4) are shown for this subject, together with the percentage of the total variance accounted for by each factor. Peaks on vectors show time period when a component was most active.

C. 3

DISCUSSION

The results of this study, and others (references 16-17) suggest that late components of evoked responses recorded from the frontal areas of the brain are reliably correlated with an observer's interpretation of a stimulus display. Such electrophysiological signals are a potential source of control inputs at man-machine interfaces. A more complete knowledge of the spacial and temporal distribution is required for such signals to be reliably identified during a single stimulus presentation. One possible step in this direction is to make use of the observation that a missing event may be ambiguous, and evoked responses at the time of a missing stimulus allows an examination of the spacial and temporal distribution of meaning correlated changes in the absence of concurrent sensory input.

REFERENCES

1. John, E. R.; and Herrington, R. N.: Effects of Visual Form on the Evoked Response. *Science*, 1967, 155: 1439-1442.
2. Vaughan Jr., H. G.; and Hull, R. C.: Functional Relation Between Stimulus Intensity and Photically Evoked Cerebral Response in Man. *Nature (Lond.)* 1965, 205: 720-722.
3. Shipley, T.; Jones, R. W.; and Fry, A.: Evoked Visual Potentials and Human Color Vision. *Science*, 1965, 150: 1162-1164.
4. Bushbaum, M.; and Silverman, J.: Stimulus Intensity Control and the Cortical Evoked Response. *Psychosom. Med.*, 1968, 30: 12-22.
5. Regan, D.: An Effect of Stimulus Colour on Average Steady-State Potentials Evoked in Man. *Nature (Lond.)*, 1966, 210: 1056-1057.
6. Wicke, J. D.; Donchin, E.; and Lindsley, D. B.: Visual Evoked Potentials as a Function of Flash Luminance and Duration. *Science*, 1964, 146: 83-85.
7. Donchin, E.: A Multivariate Approach to the Analysis of Average Evoked Potentials. *I.E.E.E. Trans. bio-med Engin.*, 1966, BME-13: 131-139.
8. Begleiter, H.; and Platz, A.: Evoked Potentials: Modifications by Classical Conditioning. *Science*, 1969, 166: 769-771.
9. Sutton, S.; Braren, M.; Zubin, J.; and John, E. R.: Evoked Potential Correlates of Stimulus Uncertainty. *Science*, 1965, 150: 1187-1188.

10. Easton, R. G.; and Harter, M. R.: Effects of Attention and Arousal on Visually Evoked Cortical Potentials and Reaction Time in Man. *Physiology and Behavior*, 1969, 4: 283-289.
11. Chapman, R. M.; and Bragdon, H. R. Evoked Responses to Numerical and Non-numerical Visual Stimuli while Problem Solving. *Nature (Lond.)*, 1964, 203: 1155-1157.
12. Haider, M.; Spong, P.; and Lindsley, D. B.: Attention, Vigilance, and Cortical Evoked Potentials in Humans. *Science*, 1964, 145: 180-182.
13. Davis, H.: Enhancement of Evoked Cortical Potentials in Humans Related to a Task Requiring a Decision. *Science*, 1964, 145: 182-183.
14. Gross, M. M.; Begleiter, H.; Tobin, M.; and Kissin, B.: Auditory Evoked Response Comparison During Counting Clicks and Reading. *Electroenceph. Clin. Neurophysiol.*, 1965, 18: 451-454.
15. McCallum, W. C.; and Grey Walter, W.: The Effects of Attention and Distraction on the Contingent Negative Variation in Normal and Neurotic Subjects. *Electroenceph. Clin. Neurophysiol.*, 1968, 25: 319-329.
16. Begleiter, H.; Porjesz, B.; Yerre, C.; and Kissin, B.: Evoked Potential Correlates of Expected Stimulus Intensity. *Science*, 1973, 179: 814-816.
17. Begleiter, H.; and Porjesz, B.: Evoked Brain Potentials as Indicators of Decision-Making. *Science*, 1975, 187: 754-755.

A TWO-DIMENSIONAL TRACKER TO TEST AND EVALUATE PATIENTS
AFFLICTED WITH NERVOUS SYSTEM DISORDERS

Hugh P. Bergeron and James D. Holt
NASA-Langley Research Center

A two-dimensional tracking device for testing patients with known or suspected nervous system disorders has been designed and constructed. This paper explains the operation of the device, presents some tentative results, and suggests other potential uses of the device.

The tracker is a hand-manipulated device that uses two sliding rods to rotate two potentiometers. The output of the potentiometers are transformed into the x and y coordinates of a two-dimensional plane. The resultant transformation error in the x and y coordinates is calculated to be less than 1 percent. A measured error of about 2 to 3 percent was obtained from an operating prototype.

The prototype was used in initial tests at Duke University on both patients and normal subjects. Tracking tasks with various forcing functions were tried. Both the frequency and shape of the forcing function were varied. A difference in error of greater than 3 to 1 was obtained between a normal subject and a Parkinson patient.

The device has other potential applications. As a two-dimensional tracker it can perform as:

- (1) An x/y curve plotter.
- (2) A device to calculate the area under a random curve.
- (3) A device to calculate the area of an arbitrarily shaped two-dimensional shape.
- (4) In general, any x/y measurements in a two-dimensional plane.

The addition of a third potentiometer will allow the tracker to supply the x, y, and z coordinates of any random point in space that is within the predetermined construction limits of the device.

N75 33688

FREQUENCY MODULATED CUTANEOUS ORIENTATION FEEDBACK FROM ARTIFICIAL ARMS

by Moshe Solomonow, Amos Freedy and John Lyman

Biotechnology Laboratory, UCLA

SUMMARY

A model of the human arm, emphasizing the neuromuscular mechanisms of feedback control, has been constructed.

The various parameters and functions of physiological receptors in the feedback section have been classified into an automated category that can be incorporated in the prosthesis servo loop, and into a sensory category that should be communicated to the operator if control and dynamic performance are to be optimized.

A scheme for simultaneous display of two such sensory parameters, i.e., fingertip pressure and elbow position, has been developed, implemented and evaluated. The neurophysiological mechanism of such displays, and the feasibility of sensory transformation, is discussed in this paper.

INTRODUCTION

Upper limb rehabilitation can be approached from the systems point of view. The structural components of such a system consist of bones, nerves, muscles and sensors. The underlying principles of operation are classified into two categories: (1) effector (motor) and (2) effector (sensory).

The effector subsystem includes a multifunctional combination of the humerus, radius and ulnar and the hand phalanges linked and powered by the various arm and hand muscles and the structures of the shoulder and upper arm. Such a manipulator possesses 2 degrees of freedom at each joint; elevation and rotation of the shoulder; elbow flexion-extension and rotation, and wrist flexion extension and rotation. The basic arm structure serves the purpose of orienting the hand in any given point in three dimensional space.

The muscles powering the arm function as prime movers where agonist and antagonist elements, acting in dynamic synergy, cause a net deflection of a joint angle, and supporting agonistic/antagonistics that act in static synergy cause the fixation of the joint in space.

The hand possesses approximately 32 degrees of freedom, made possible by the many rotations of which the fingers are capable. In addition to the obvious motor capabilities of the hand, it serves as a multi-dimensional

affector channel. Although the sensory modalities of the hand do not differ from other somatic modalities, the quantity of the receptors is large, making the hand sensitive to kinesthetic and tactile stimuli such as temperature, touch, pressure, position, velocity, etc.

Control of such complex manipulator systems is derived from reflexes and synergy, in the lower motor neurons of the spinal cord, as well as from coordinated voluntary commands from the upper motor neurons of the brain.

Such a system is represented in the simplified diagram of Figure 1.

In Figure 1, α and α' are prime moving and supporting muscle sets, respectively. K is the electro-chemical gain provided by the neuromuscular junction in transferring neural signals of muscular motion. The golgi and spindle muscle receptors subserve position and force feedback, providing local stability. Gamma (γ) is the gain adjustment control of the muscle spindle. The feedback information from the hand is amplified by an arbitrary constant K' , representing the hand's increased sensitivity to sensory stimuli.

The feedback information is transmitted to the central nervous system (CNS), providing enlarged panoramic perception of various modalities as to the arm's state as well as its environment. Some of this information is also provided to the lower localized levels, as is obvious in various reflex activities, e.g., instinctive withdrawal from painful stimuli.

In cases of upper limb amputation, the losses include the associated elements of the severed arm, i.e., nerve axons, muscles, bones, and receptors.

Current reconstruction efforts at our laboratory utilize the correlation between the prime mover and supporting muscles at various arm joints, in conjunction with pattern recognition techniques, to yield an artificial controller as part of an adaptive aided prosthesis system. The system is externally energized, and uses myoelectric signals from shoulder muscles as control inputs.

In order to optimize the performance of such an adaptive aided system, the problem of reconstruction of an artificial sensory feedback information subsystem has been addressed.

A general description of the system is shown in Figure 2.

Sensory information, as illustrated in the models, subserves two functions:

1. Localized feedback to the spinal levels for purposes of reflex, and stability without reaching consciousness.
2. Perceptive type of feedback to the higher cortical sensory areas on both conscious and subconscious levels.

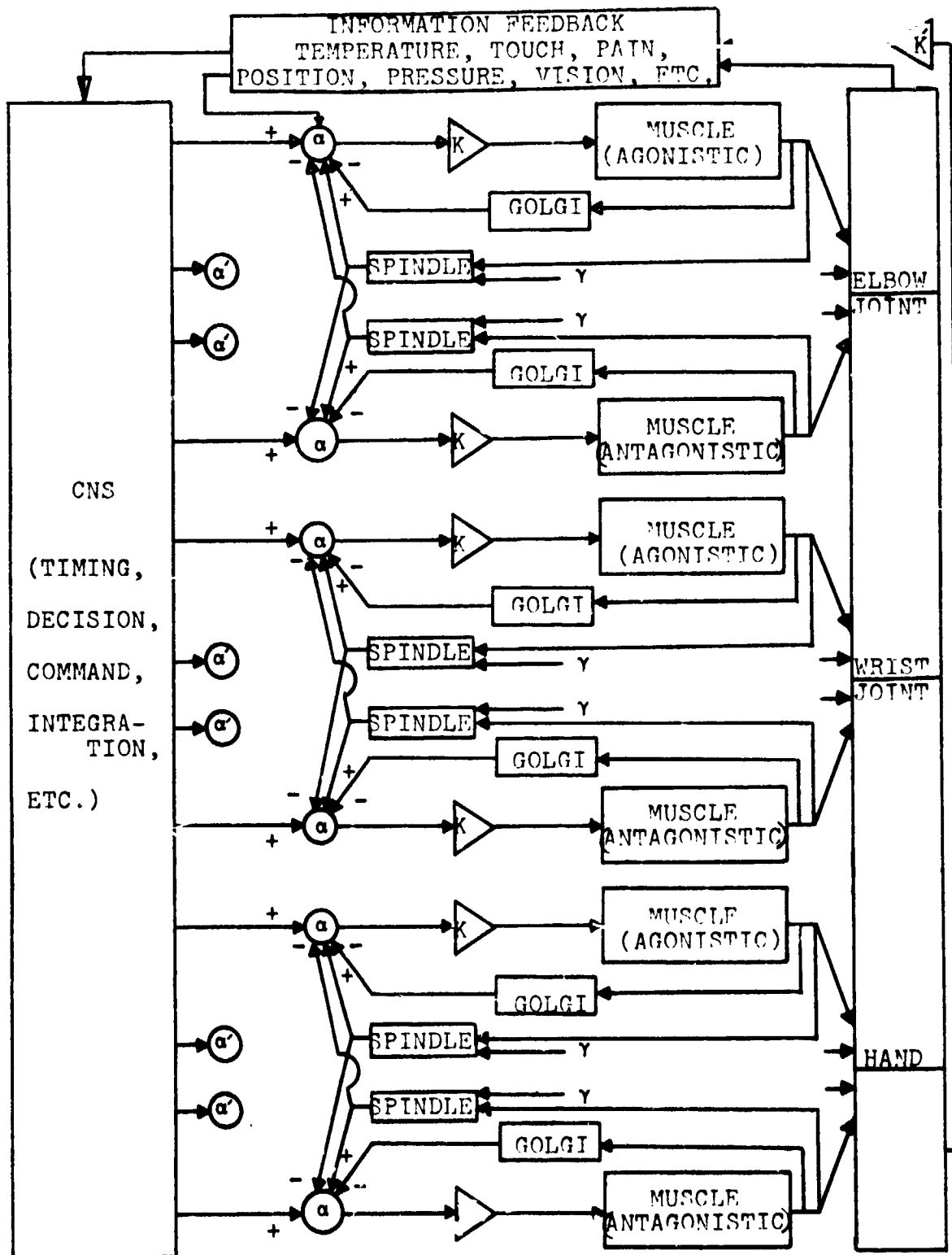


FIGURE 1
NEUROMUSCULAR MODEL OF THE HUMAN ARM.

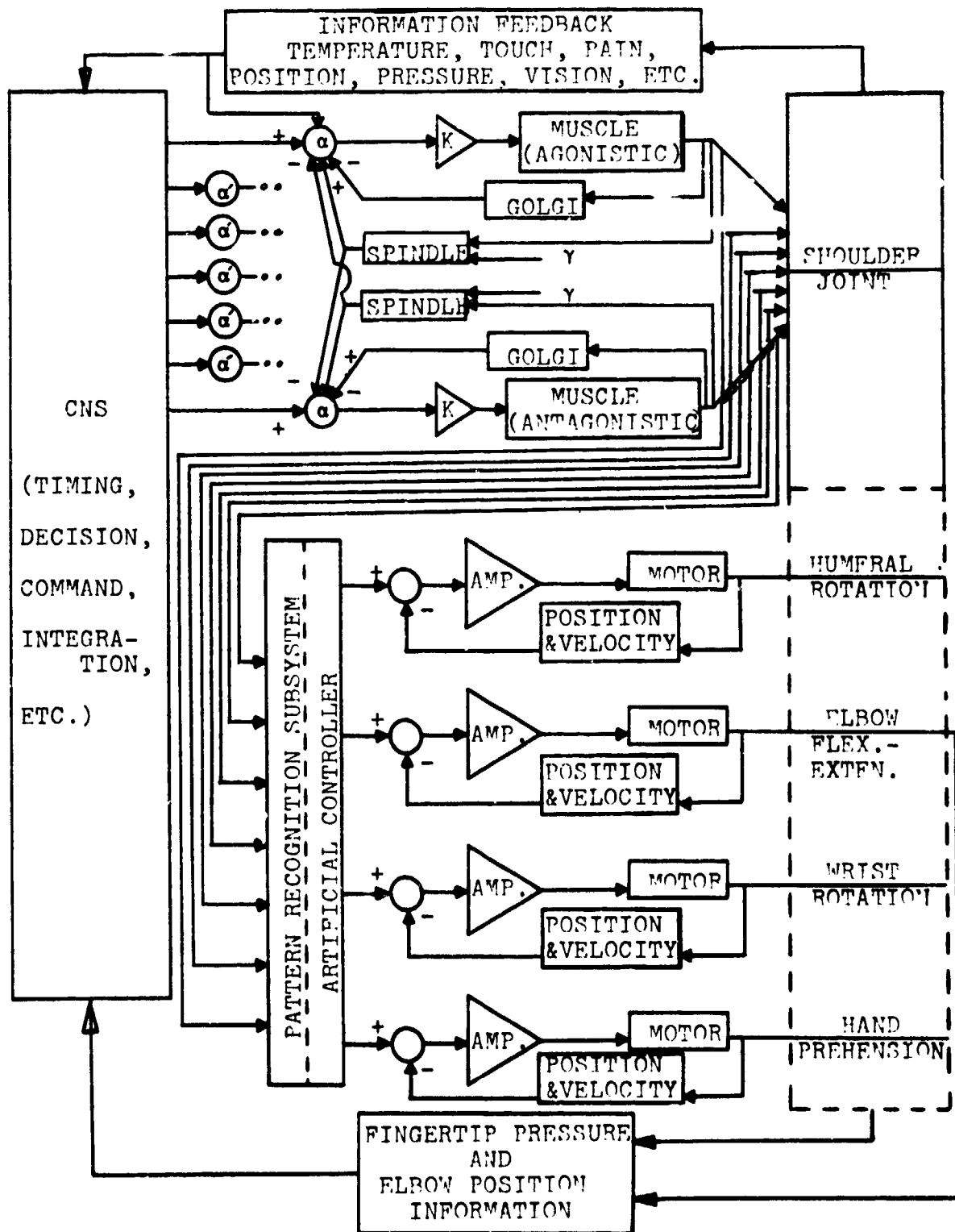


FIGURE 2
ADAPTIVE AIDED MODEL OF THE RECONSTRUCTED ARM .

Further narrowing of the problem is in order when the reflexive-stabilizing type of feedback in a prosthesis system is provided in the servo loop in the form of position or velocity feedback from the joints.

This report concerns the perceptive type of feedback responsible for the consciousness of the operator as to the state of the prosthesis and its environment, thereby establishing the necessary man-machine dialogue for the system.

APPROACH

The sensory information gathering and communication capability of the human upper limb is obviously formidable. Exact reconstruction of such information processing systems is beyond our reach, due to lack of proper technology to duplicate the detailed biological processes as well as the inability of the human operator to artificially perceive large quantities of tactile information in a subconscious manner.

The objective of our investigation was to attempt to provide an amputee with a two dimensional feedback system. The choice of parameters to be displayed was derived from the most useful feedback to an amputee in order to optimize his control of the prosthesis, namely, fingertip pressure and elbow position.

The underlying principles in the approach to the solution of this problem are the perceptive response of the human skin to electrical stimulation of variable frequency, as well as two point discrimination orientation and their relationships to fingertip pressure and elbow position, respectively.

The paper presented at the 1974 Annual Conference on Manual Control (Reference 1) described the design and implementation of a fingertip pressure sensory feedback system, using frequency variation from 10 to 100 pps proportional to pressure exerted by the fingers. The information was transferred to the amputee via cutaneous electrical stimulation. For convenience, the diagram of the system is presented in Figure 3.

Studies performed by Bach-y-Rita and Collins (Reference 2), in an effort to provide the blind with a tactile vision substitution, indicated that cutaneous receptors and their neural pathways are capable of carrying pictorial information to the brain. One of their systems consisted of a television camera linked to a commutator system activating an $n \times n$ matrix of vibrotactile stimulators mounted against the back of the blind subject. Experimentation on blind subjects revealed that within a short training period, the subjects were capable of interpreting such patterned stimuli as visual rather than cutaneous. The possibility that the central nervous system is capable of utilizing and modifying existing mechanisms to perceive such information is considered.

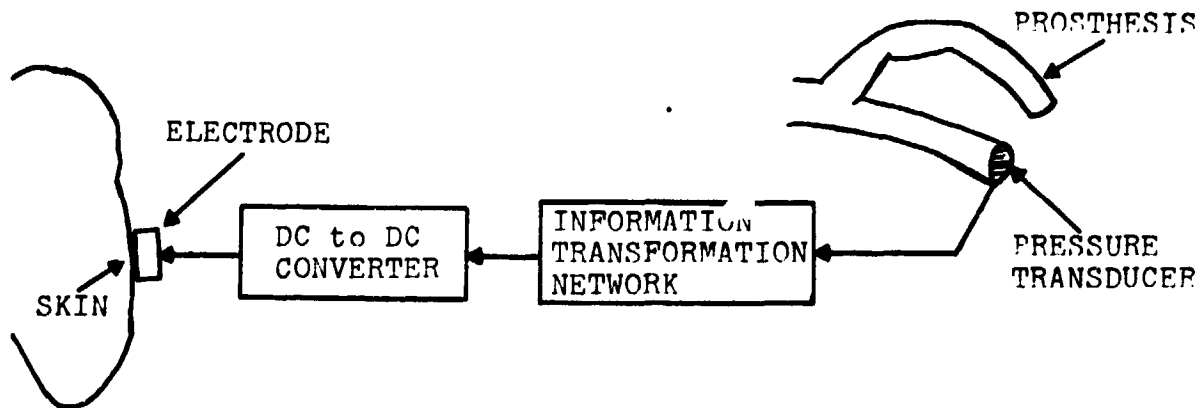


FIGURE 3
FINGERTIP PRESSURE SENSORY FEEDBACK SYSTEM.

Capitalizing on the above, as well as on the already proven frequency modulated approach, an integrated system was designed incorporating both fingertip pressure and elbow position. The system utilized electrical stimulation electrode arrays at the man-machine interface with multiple possibilities for two point discrimination angles. Such an arrangement attempted to create the subconscious "learned" neural image of the corresponding elbow angles.

Figure 4 provides a description of the system.

DESCRIPTION OF THE SYSTEM

Fingertip pressure was monitored by a Dynacon^(T) resistive rubber type transducer. Fingertip grasp on an object applied pressure on the transducer, and induced decline in resistance proportional to the pressure.

The variations in resistance controlled an information transformation network generating 100 μ sec duration pulses at a frequency range of 10 to 200 pps proportional to the control resistance.

A DC to DC converter was used to amplify the pulse amplitude up to 200 volts current regulated. The signal was then applied to concentric silver electrodes that could be cutaneously applied.

Elbow angle was monitored by a distributor subsystem in which 20^o increment deflections switched the signal to an adjacent channel connected to its corresponding electrode. The distribution network thus monitored elbow

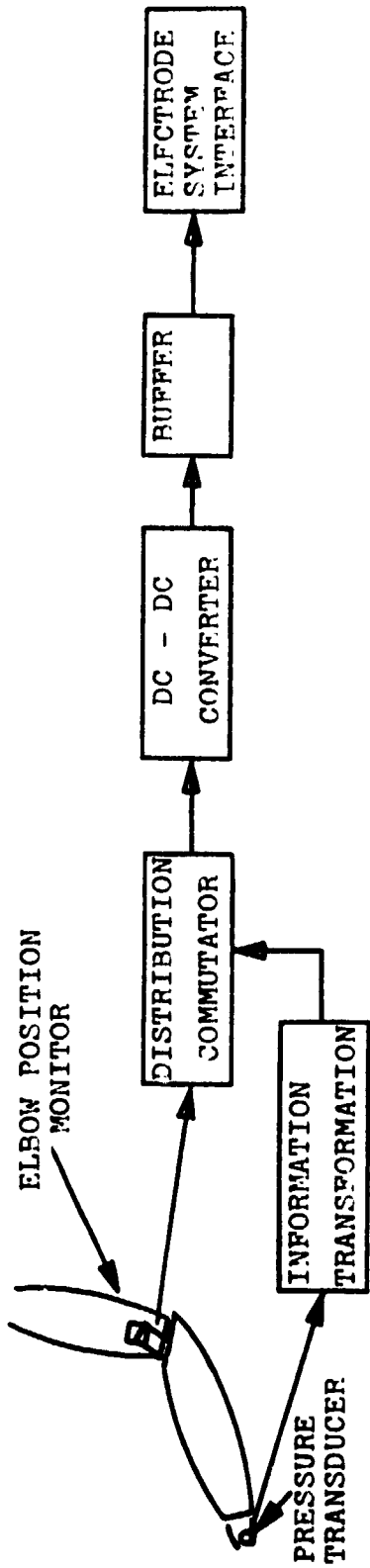


FIGURE 4
THE TWO DIMENSIONAL SENSORY FEEDBACK SUBSYSTEM .

angle changes of 20° increments by switching the FM signal derived from the fingertips of the hand to different electrode channels at different locations on the skin.

Two electrode sets were designed for the preliminary experiments: a circular set and a rectilinear set.

The circular electrode set consisted of eight electrodes at 20° increments mounted on a disc with a center electrode serving as reference; and the center electrode was on at all times.

The rectilinear set consisted of an array of eight electrodes mounted on a flexible plastic strap that was capable of adjusting to skin curvature, thus insuring reliable contact.

Figure 5 (a) and (b) illustrate the two electrode sets.

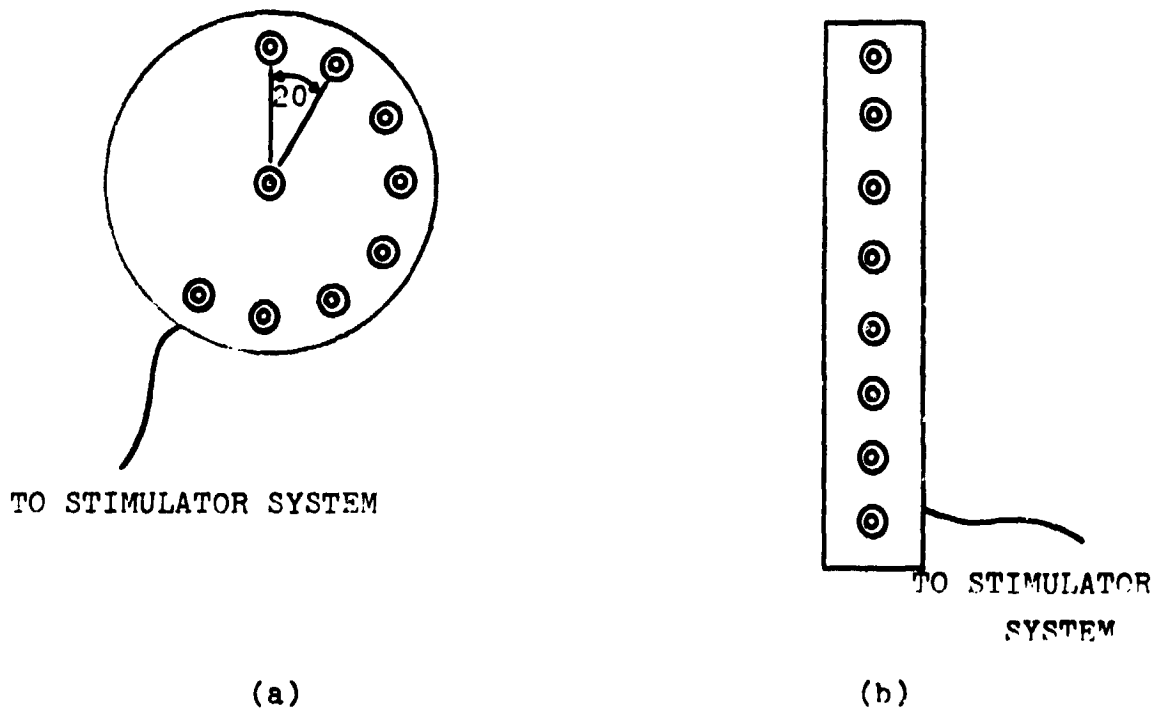


FIGURE 5
CIRCULAR AND RECTILINEAR ELECTRODE
INTERFACES.

Electrode system (a) at no motion drew a pictorial vector between the reference electrode and the electrode corresponding to the given elbow angle. Upon elbow motion, the adjacent electrode switched on, while the previous one turned off. Therefore, a new vector of a different angle was sensed by the skin, and correlated with the appropriate elbow angle.

Electrode system (b) had no reference electrode, and upon elbow motion upward (flexion), for example, the signal was switched to the rostral electrode corresponding to the given elbow angle.

If flexion of 60° was performed, the third electrode from the bottom switched on, which corresponded to resolution of 20° flexion per electrode. In addition, the transient switching of electrodes during gross motion, say 60° , indicated velocity of movement to the operator. The signal at each electrode was frequency modulated by the fingertip pressure transducer. Therefore, two pieces of information were simultaneously relayed to the amputee.

Since a certain amount of training is required for optimal perception and correlation of the coded information with real world sensory modalities, a training and evaluation apparatus was designed and implemented. The apparatus consisted of an artificial elbow joint, on which the distributor was mounted, as well as the pressure transducer and the information transformation network. The stimulus amplitude could be adjusted to a comfortable level for the amputee.

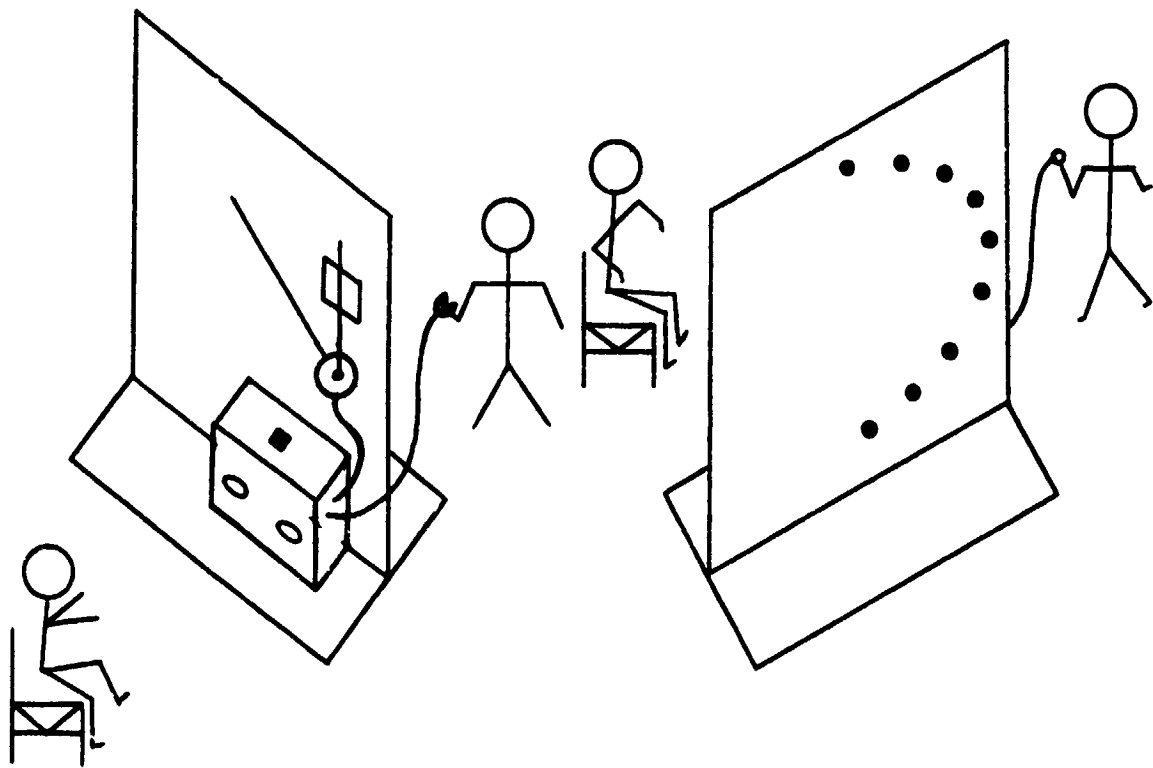
The system was mounted on one side of the partition (Side I) where the experimenter could change the control variables. The amputee was positioned on the other side of the partition (Side II), and was connected to the electrode system.

The experimenter, therefore, adjusted at will the elbow angles, and required the amputee to indicate the perceived angle on the partition. The perceived angle was then compared with the real angle by means of eight colored lights mounted on the amputee side of the partition, and switched on for comparison for each trial. Statistical data were then collected and analyzed as a measure of performance and utility of the system.

Figure 6 is a diagram of the training and evaluation apparatus.

EXPERIMENTAL PROCEDURES AND RESULTS

Four normal subjects were tested in a preliminary evaluation session. Each subject was placed initially on Side I of the testing assembly and was asked not to move his arm. The electrodes were applied to the cutaneous area of the forearm with elastic stockinette, using ECG paste on each electrode. The experimenter then adjusted the stimulus level to the comfort of the subject, and rotated the artificial elbow slowly in 160 degree excursions. The subject was asked to follow the stimulation pattern and correlate it



EXPERIMENTER'S SIDE
(SIDE I)

AMPUTEE'S SIDE
(SIDE II)

FIGURE 6
TRAINING AND EVALUATION APPARATUS.

with the observed artificial elbow positions. After 20 minutes or so, the subject was asked to move to Side II of the partition where he could no longer see the artificial elbow. The elbow was moved again and the subject was asked to indicate the position of the elbow by designating the light nearest the elbow position he perceived. The experimenter then identified the actual elbow position by switching on the correct light.

A second session made use of the alternative electrode system for comparison of perception performance. The preliminary evaluation showed major differences in perception and discrimination capability of the two electrode interfaces. The circular electrode interfaces provided the perception of change, apparently due to switching of the electrodes respective to elbow angle, but the subjects could not correctly indicate elbow angles, even if the elbow was returned to the initial reference angle. Also, the expected vectorial perception could not be realized, and the subjects indicated that they perceived change of stimulation location which could not be related to any elbow angle.

Removal of continuous stimulation from the center reference electrode did not vary the perception appreciably, and the circular electrode configuration in the form used was considered unsuitable for our application.

Experiments with the rectilinear electrode interface demonstrated excellent perceptual resolution and discrimination. Subjects training for 30 to 40 minutes were able to correctly indicate elbow angle up to the resolution limit of the test equipment (20° increments).

Predictions were correct for very rapid elbow motions as well as for slow ones. The transient "on" time of the electrodes for gross increments indicated direction of motion as well as velocity to the subjects.

In several instances, the experimenter increased the frequency of stimulation deliberately in order to evaluate the ability of the subjects to perceive two information pieces simultaneously. This had the perceived effect of more intense stimulus, but the discrimination was sharp enough so that no subject confused it with elbow position change.

This short preliminary evaluation demonstrated the potential of skin orientation stimulation, in combination with signal frequency modulation, as a practical means for relaying two useful channels of information to amputees. Further experiments are planned to incorporate amputee subjects to provide statistical data to indicate performance utility of such a feedback system and the necessary design criteria to make it clinically applicable. A future state will be to incorporate such a feedback system into a three degree of freedom above elbow myoelectrically controlled prosthesis. This prosthesis is now in final stages of development at our laboratory.

Acknowledgment: Primary support for this research was provided by the Veterans Administration, Contract VA# V101-(134)P121

REFERENCES

1. Solomonow, Freedy and Lyman, "General Approach to Generating Sensory Feedback Information from Upper Extremity Prosthetic Terminal Device," Proceedings of the 10th Annual Conference on Manual Control, Wright Patterson Air Force Base, Ohio, April, 1974
2. Bach-y-Rita and Collins, "Sensory Substitution and Limb Prosthesis," Advances in External Control of Human Extremities, Belgrade, Yugoslavia, 1970
3. Prior, R. and J. Lyman, "Electrocutaneous Feedback for Artificial Limbs," Biotechnology Laboratory Progress Report No. 54, UCLA School of Engineering and Applied Science Report UCLA-ENG-7459, Los Angeles, California, February 1974
4. Feimers, Stephen D., "The Testing and Evaluation of a Kinesthetic Feedback System for Amputees," Master's Thesis, Massachusetts Institute of Technology, 1969

N75 33689

ROLE OF STRETCH REFLEX IN VOLUNTARY MOVEMENTS

By Gerald L. Gottlieb and Gyan C. Agarwal

Department of Biomedical Engineering
Rush Medical College
Chicago, Illinois 60612

and

College of Engineering
University of Illinois at Chicago Circle
Chicago, Illinois 60680

SUMMARY

The stretch reflex is often described as a spinal servomechanism, a device for assisting in the regulation of muscle length. Observation of the EMG response to mechanical interruption of voluntary movements fails to demonstrate a significant role for spinal reflexes at 40 msec latency. Two functional responses with latencies of 120 msec and 200 msec, implying supraspinal mediation, are observed.

INTRODUCTION

The concept of a length regulating servomechanism elegantly fits the known neuroanatomy of the stretch reflex (Merton⁹). It provides a useful working hypothesis for investigating reflex function and has proved adaptable to our expanding experimental knowledge of reflex behavior. The demonstrated linkage of alpha motor and fusimotor coactivation enables the spindle to remain active during shortening and thus play a role in voluntary contraction (Granit⁴, Vallbo^{12a,b}). Nevertheless, the functional existence of such a mechanism has not been demonstrated.

A stretch reflex servomechanism, by virtue of its negative feedback topography, may perform two functions. It can reduce the sensitivity of muscle length to changes in external loading. It can also reduce that sensitivity to changes in intrinsic muscle performance factors. In either case, one of the key parameters of the reflex would be its "loop gain" or the amount of tension that it produces in response to a unit change in length.

On the basis of recordings from human peripheral nerves, Vallbo^{12c} has argued that the gain of the gamma loop appears to be inadequate to "constitute the main mechanism for load compensation with regards to muscle length". We have made a contrary argument based on evidence that the loop gain of the physiological system is a controlled variable that can be greatly increased by voluntary movement (Gottlieb, et al³, Gottlieb and Agarwal²).

Other evidence in favor of a gain controlled servomechanism for regulating muscle length during voluntary movement has been reported by Marsden, et al⁸.

The criterion for judging the presence and effectiveness of such a servomechanism in the regulation of voluntary movement may be found by observing reflex responses to experiment produced "errors" in movement. The onset of those responses should follow the development of error with latencies consistent with those of known spinal reflex responses.

METHODS

Each subject was seated and the right foot strapped to a plate which could rotate about a horizontal axis (figure 1). Foot angle was measured from a potentiometer and foot torque from strain gauges in the arm of the plate. A DC torque motor was connected by a gearbelt and pulley system to apply rotational torques to the foot.

Electromyograms were recorded from disc surface electrodes placed over the bellies of the soleus and anterior tibial muscles. These were amplified, full-wave rectified and filtered before recording (Gottlieb et al³).

The experiment consisted of asking the subject to make a rapid plantar-flexion upon perceiving a visual signal. The onset of the soleus EMG was detected and, after a fixed delay specified at the beginning of each experiment, used to trigger the motor servomechanism. This servo could be set to provide a specified mechanical impedance to foot rotation or to be a simple torque device to produce rotation of the ankle. In either case, interruption of the voluntary movement by activation of the motor would occur on a random basis in approximately one out of three movements.

Data from interrupted and uninterrupted movements was separated and individual records were aligned and averaged.

RESULTS

Figure 2 shows individual records. The upper curves are filtered soleus EMG (increasing downward) and in parts a-c, the associated unfiltered EMG. The lower curve shows foot angle. In all six cases, a torque step was applied to the foot just prior to (a) or immediately after (b-f) the onset of soleus contraction. This moment is indicated in the figures by an asterisk. In the first four cases, the motor briefly rotates the foot dorsally before being overcome by the voluntary contraction. In the latter two, the movement is transiently and abruptly halted but not reversed.

Record 2a shows that the stimulus is adequate to produce a strong reflex response. Only two (b and e) of the five records in which the stimulus was delivered after the onset of contraction show a similar reflex response. Records c, d and f show no reflex volley that is distinguishable from the ongoing voluntary level of activity.

The fact that the reflex response appears to be so labile under those conditions suggests that we examine ensemble average responses rather than individuals.

Figure 3 shows two experiments, the first in which the motor simulated a stiff spring, the second in which increased stiffness was augmented by a torque step. Figure 4 shows a second sequence of experiments with a torque step in a different subject. Figure 5 shows a third sequence in which the subject (same as 4) made deliberately slow, ramp-like movements of about one seconds duration.

DISCUSSION

The experiment shown in figure 3a,b shows evidence in favor of servo action of the stretch reflex. We see a divergence in the average EMGs which lags behind the angular divergence by an interval consistent with spinal reflex latencies. By contrast, the experiment in figure 3c,d shows a clear stretch reflex but not servo-like action. That is, there is but a brief and discrete reflex volley that appears as if superimposed upon the voluntary EMG with little or no additional alteration to the recruitment pattern in the early time interval. The sequence of experiments in figure 4 gives no evidence of either servo-like action or of spinal stretch reflex activity. A response in the EMG with a latency of approximately 120 msec is present, and this is also seen in the previous sequence. Data from two other subjects more closely resemble figure 4 than figure 3. All subjects had brisk and easily elicitable patellar and achilles reflexes.

The earliest studies of stretch reflex servo behavior by Hammond, et al⁶, examined a problem of postural maintenance. Their subjects were maintaining a fixed limb (arm) position and instructed to resist a mechanical disturbance. They showed two responses in the EMG, one with a latency consistent with spinal reflex delays and a second with a latency about three times longer (15-20 msec and 50-70 msec in the arm biceps). A similar experiment by Melville Jones and Watt⁷ with the gastrocnemius muscle found the same paired responses with latencies of 37 msec and 120 msec.

The more recent studies of Marsden et al⁸, examined an interrupted phasic movement. They found an EMG response which began after a spinal reflex latency and continued for at least 100 msec. The experiments by Hammond and Melville Jones and Watt are not directly comparable with Marsden's because the task given to the subjects was different. Hammond noted the dependence of his late response on the nature of the instructed

task. He observed that the second response could be reduced or abolished by verbal instruction while the first response could not.

In this light consider the data presented here. We see in one experiment, a short latency response blending in and continuous with the longer latency response. For the remainder however, we see only a long latency response. Reaction times (R.T.), measured from the onset of the visual command to plantarflex to the onset of the EMG and the response latencies (t) measured from the onset of the interrupting force are summarized in table 1. They show the long latency response to be approximately three times the spinal reflex latency and about six tenths of the initial reaction time.

A likely interpretation of this is that the late response is a supra-spinal "stretch reflex" similar to the late response seen by Hammond and to Melville Jones' Functional Stretch Reflex (FSR). It too is altered by verbal instructions. An alternative interpretation is that the 120 msec response is a second reaction time, produced by the same processes that produce the initial 200 msec reaction time but briefer because of the different, and presumably more intense, second stimulus. This cannot be refuted by the data presented here since 120 msec is about at the lower limit of possible reaction times but the hypothesis seems unlikely. For one thing, if the response is a simple reaction time then we should expect it to be longer than the initial reaction time because of the "psychological refractory period" first described by Telford¹¹.

Figure 5 shows the effects of interrupting a relatively slow voluntary movement and displays the foot torque and velocity as well. Activation of the motor causes a sudden rise in torque (the motor is acting like a spring) and a halting of the movement. The EMG shows a small burst of activity about 40 msec after activation but it is not visibly greater than the normal variations in soleus EMG shown in the uninterrupted record.

The halt is only momentary and the movement continues at a slower rate but with increasing muscle tension according to the force-velocity characteristics of the muscle. About 120 msec after the interruption there is another EMG burst which is sustained throughout the recording interval. The consequences of this are first a slight increase in the rate of tension development (note curvature in foot torque curve between 400 and 560 msec). Beyond 560 msec the torque motor saturates and the movement speeds up.

Looking closely at the EMG record, there is a third phase of soleus EMG about 200 msec after the interruption. In figure 5 this can be seen as a burst at $t = 480$ msec. Looking back in figure 4 the bursts starting at 120 msec post-stimulus last about 100 msec and are followed by a lower level of activity which is still higher than in the undisturbed case. Similar behavior is seen in figure 3. This third phase could well represent a different level of neural control with adequate time being present for conscious cortical influences to be exerted.

Recognizing the inherent variability of these EMG data it is premature to make firm statements based on them. In the data seen thus far however it seems possible to describe three phases in the EMG response to unexpected errors in a movement. A spinal stretch reflex phase of very variable intensity starting 40 msec post-stimulus and lasting up to 80 msec. A probable supraspinal reflex phase, the FSR in the 120-200 msec interval and a possibly voluntary response phase from 200 msec on.

The question of whether or not there is, in any functional sense, a stretch-reflex servo operating over spinal reflex arcs remains open. There may well be multiple functional reflex loops, one at the spinal level and others supraspinal (Eccles¹). When the motor system is performing a postural maintenance task only the latter are important. When a rapid movement is performed, most of the activity is planned in advance or preprogrammed. Corrections for errors in movement are handled at supraspinal levels. Slower (and more precise) movements are handled differently however (Nava and Stark¹⁰) by making use of the shorter spinal reflex arcs. Even fast movements may use this pathway if the errors are detected early enough in the movement.

These remain hypotheses however. We are as yet unable to show that the spinal stretch-reflex, either monosynaptic or polysynaptic, is an important mechanism in the execution of normal movement. The presence of servo-mechanism behavior operating over this pathway cannot be clearly demonstrated.

ACKNOWLEDGMENT

This work was supported in part by the National Science Foundation Grant # GK-37540 and by General Research Support Grant # RR-05477 from the National Institutes of Health.

REFERENCES

1. Eccles, J.C. The Inhibitory Pathways of the Central Nervous System, Thomas, Springfield, Illinois, 1969.
2. Gottlieb, G.L. and Agarwal, G.C. "Modulation of Postural Reflexes by Voluntary Movement. 2. Modulation at an Inactive Joint," J. Neurol., Neurosurg. and Psychiat., 36, 540-546, 1973.
3. Gottlieb, G.L., Agarwal, G.C. and Stark, L. Interactions between Voluntary and Postural Mechanism of the Human Motor System, J. Neurophysiol., 33, 365-381, 1970.
4. Granit, R. Receptors and Sensory Perception, Yale University Press, New Haven, 1955, pp. 191-276.

5. Hammond, P.H. An Experimental Study of Servo Action in Human Muscular Control, Proc. of Third Int. Conf. on Medical Electronics, 190-199, 1960.
6. Hammond, P.H., Merton, P.A. and Sutton, G.G. Nervous Graduation of Muscular Contraction, British Med. Bull., 12, 214-218, 1956.
7. Jones, G. Melville and Watt, D.G.D. Observation on the Control of Stepping and Hopping Movements in Man, J. Physiol., 219, 709-727, 1971.
8. Marsden, C.D., Merton, P.A. and Morton, H.B., Servo Action in Human Voluntary Movement, Nature, 238, 140-143, 1972.
9. Merton, P.A., Speculations on the Servo-Control of Movement, pp. 247-260 in The Spinal Cord, Ciba Foundation Symposium, Little, Brown & Co., Boston, 1953.
10. Navas, F., and Stark, L. Sampling or Intermittency in Hand Control System Dynamics, Biophys. J., 8, 252-301, 1968.
11. Telford, C.W. The Refractory Phase of Voluntary and Associate Responses, J. Exp. Psychol., 14, 1-36, 1931.
12. (a) Vallbo, A.B., Muscle Spindle Response at the onset of Isometric Voluntary Contractions in Man. Time Difference between Fusimotor and Skeletomotor Effects. J. Physiol., 218, 405-431, 1971.
12. (b) Vallbo, A.B., Single Unit Recording from Human Peripheral Nerves: Muscle Receptor discharge in Resting Muscles and During Voluntary Contractions. Neurophysiology Studies in Man, G.G. Somjen, (Ed.) pp. 283-295, Excerpta Medica, Amsterdam, 1972.
12. (c) Vallbo, A.B. Human Muscle Spindles Discharge during Isometric Voluntary Contractions. Amplitude Relations between Spindle Frequency and Torque. Acta Physiol. Scand., 90, 319-338, 1974.

TABLE I

The average reaction time (R.T.) measured from the visual signal to the onset of the EMG; and the interruption response time (t) measured from the activation of the torque motor to the onset of the response EMG. Standard deviations are in parentheses.

Exp.	N	R.T. (msec)	t (msec)
GCA016	22	180.7 (26.9)	135.7 (18.2)
GCA019	24	204.8 (32.4)	124.4 (10.2)
GLG010	16	214.6 (54.6)	120.0 (12.6)
GLG011	16	227.4 (34.6)	116.5 (9.4)
GLG012	16	229.4 (26.2)	130.0 (10.5)
GLG013	16	215.9 (25.6)	107.8 (12.2)
GLG014	15	208.8 (21.6)	121.4 (18.8)

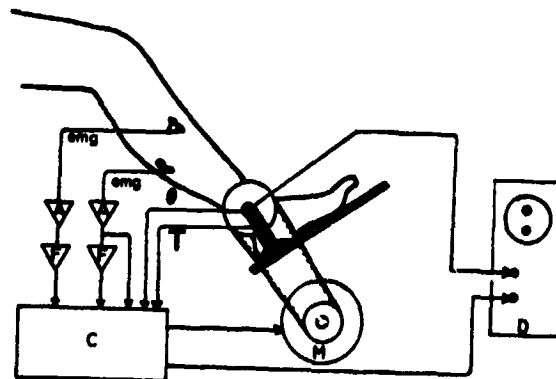


Figure 1

Apparatus-Motor (m) and crt display are under computer control.
 Electromyogram amplifiers (a) are Tektronix 2A61s (bandwidth
 60-600 Hz), filters (f) are third order averaging (10 msec).

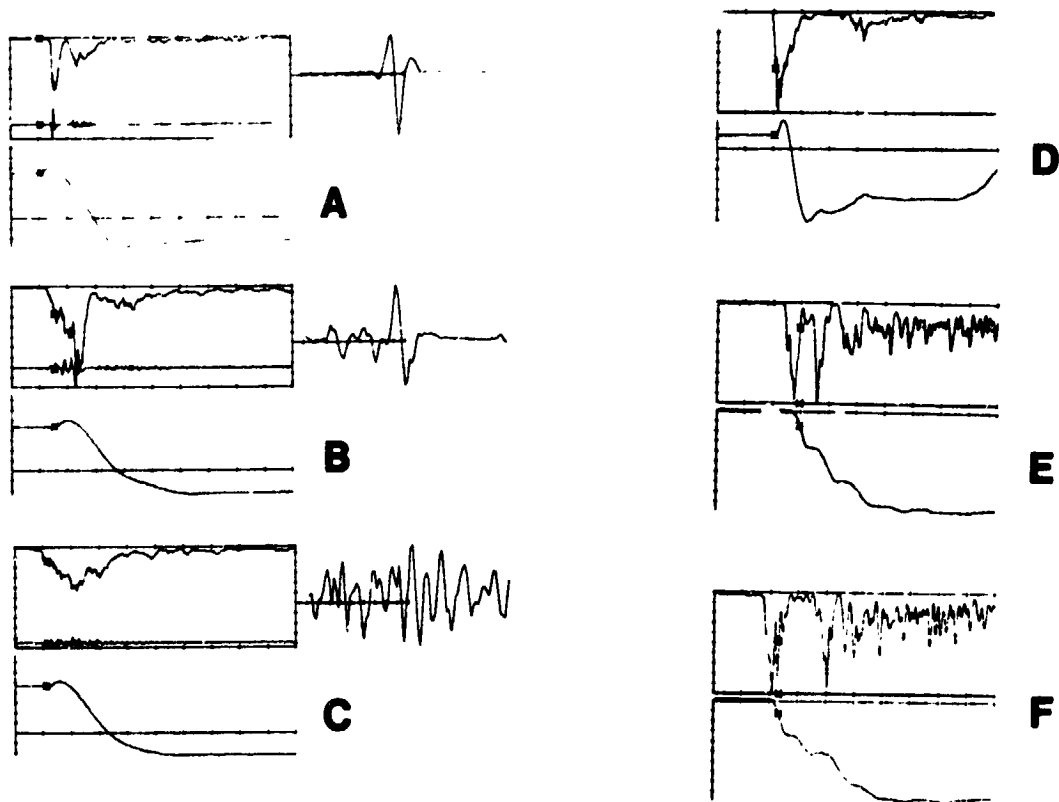


Figure 2

Typical data records - uppermost trace in each part is filtered soleus EMG increasing downward (arbitrary units). Lower trace in each part is foot angle with plantar-flexion plotted downward (range 20 degrees). Intermediate trace (parts a, b & c) is unfiltered soleus EMG. This EMG is shown on an expanded scale at right of those three parts. (a) Stimulus precedes voluntary movement showing adequacy of torque stimulus. Left time abscissa covers one second. Expanded scales at right are 100 msec and 8.0 mv. Subject GCA. (b) Stimulus triggered by voluntary EMG. Left time abscissa covers 0.5 seconds. Expanded scales at right are 100 msec. and 4.8 mv. Subject GCA. (c) Like b except expanded scales at right are 100 msec and 1.2 mv. Subject GCA. (d) Stimulus triggered by voluntary EMG. Left time abscissa one second. Subject BWF. (e and f) Like d. Subject GLG.

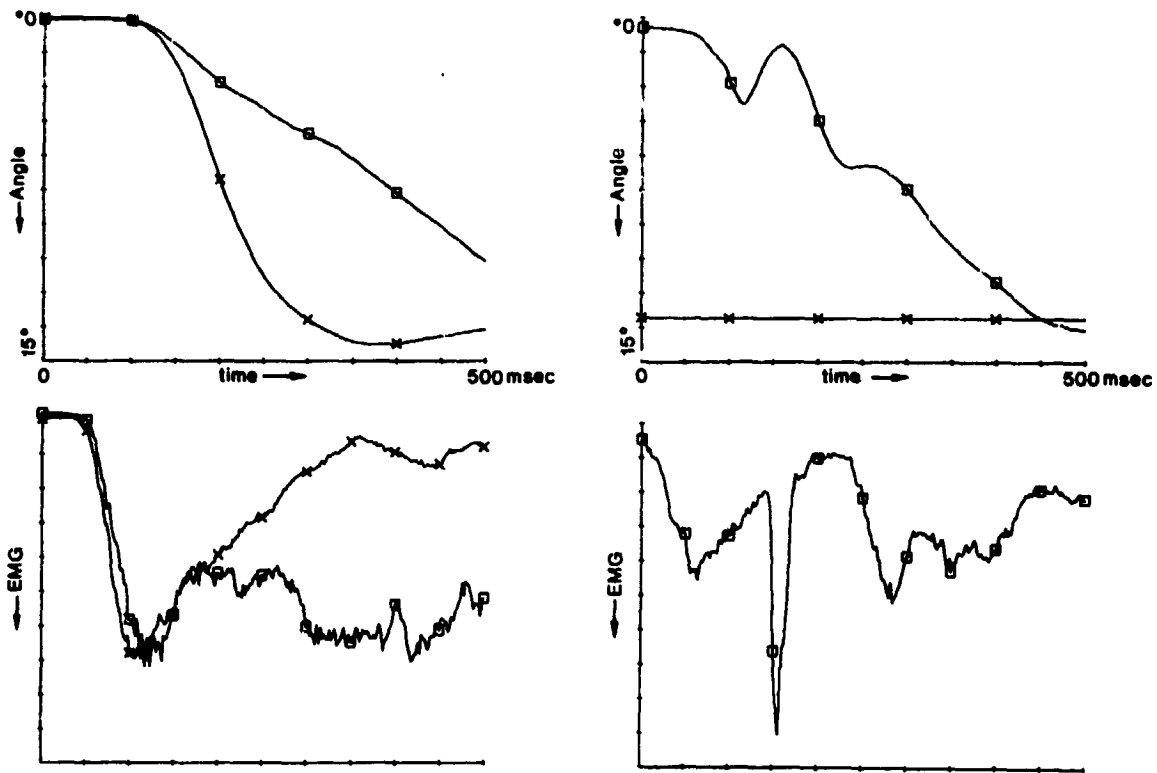


Figure 3

A - angle of the foot versus time, during voluntary plantarflexion of the ankle. The curve marked X is made without opposition by the motor (average of 64 movements). In the curve marked □, the motor resisted movement from its onset by simulating a stiff spring (average of 24 movements). The range of the plot is 15 degrees plantarflexed from neutral at the top of the graph. B - the average soleus, EMG, full-wave rectified and filtered for the movements in A. C and D correspond to A and B for an experiment in which the motor applied a step of torque to interrupt and briefly reverse the movement.

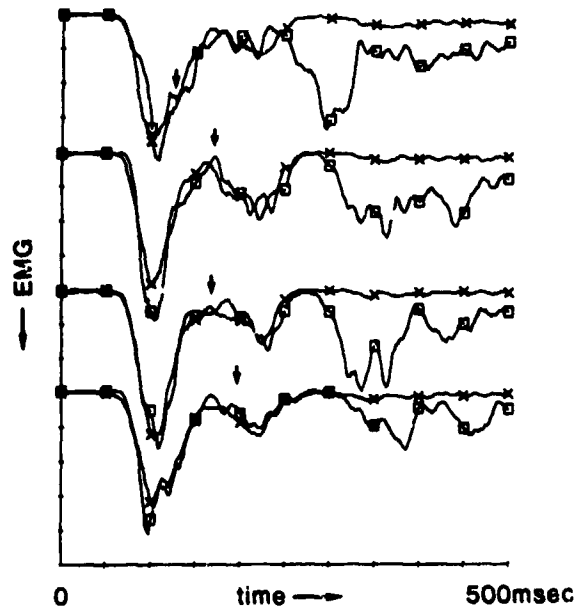
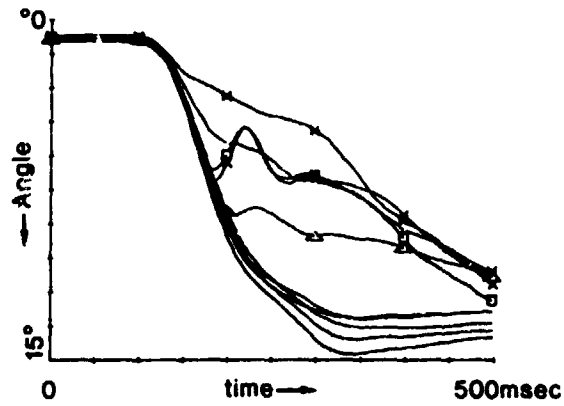


Figure 4

Average foot angle and soleus EMG records for movements interrupted at different angles. The EMG's in part B correspond, from top to the bottom, with the angle traces marked X (upper curve), \square , X (lower curve) and Δ respectively. Averages of interrupted movements have 16 records, uninterrupted averages have 37. The arrow above the EMG traces indicates the onset of the disturbing torque.

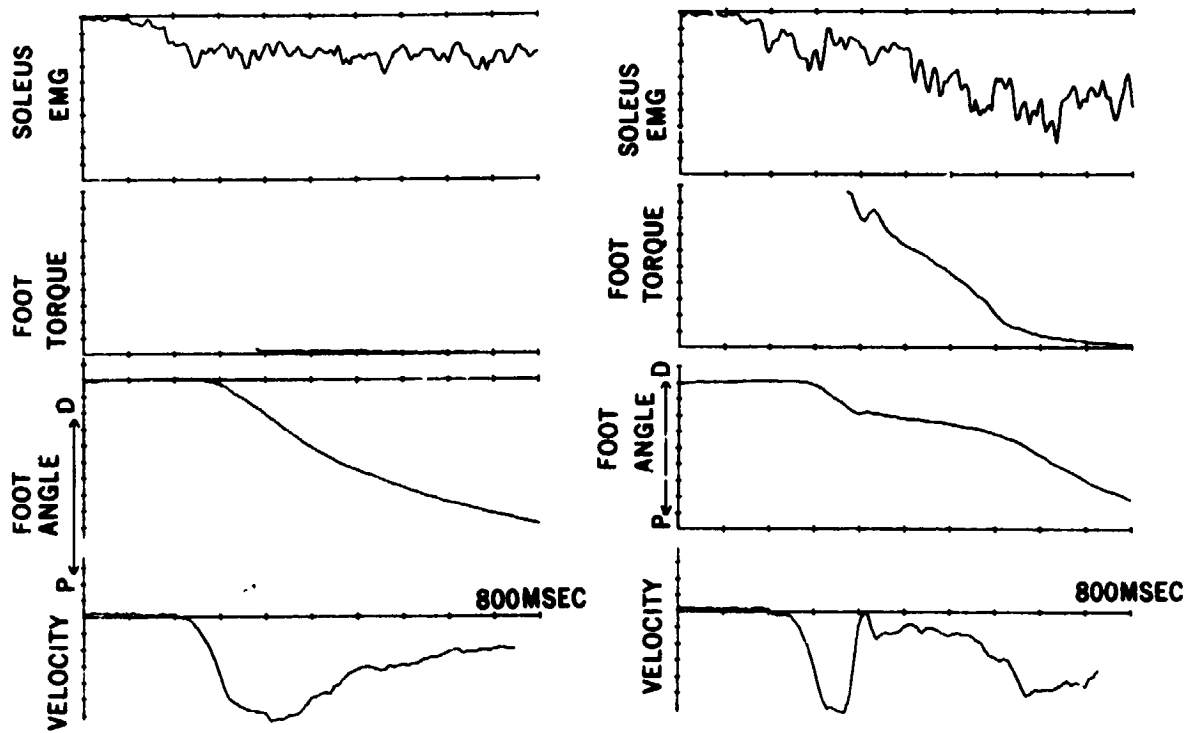


Figure 5

Average EMG, foot torque, foot angle and angular velocity for a slower voluntary plantarflexion. The uninterrupted record is an average of 25 movements. The interrupted record is an average of 10 movements.

N75 33690

HEAD-EYE TRACKING IN TWO-DIMENSIONAL PURSUIT TASKS

D. K. Shirachi* and J. H. Black, Jr.**

**Aerospace Medical Research Laboratory
Aerospace Medical Division
Air Force Systems Command
Wright-Patterson AFB, Ohio**

SUMMARY

Previous literature [1,2] devoted to head and eye movements has been primarily restricted to single-degree-of-freedom, horizontal movement investigations, with researchers possibly assuming that vertical and horizontal tracking characteristics are nearly identical.

The research presented in this report advances present knowledge of the neurological control systems for the eye and head by investigating dynamic eye and head rotations in two-degrees-of-freedom using band-limited, white noise stimuli, nominally wide field-of-view stimulus presentations of $\pm 10^\circ$ and power spectral analysis of the data to produce input-output transfer and coherence functions.

The authors determined the frequency response characteristics of these systems and investigated the linearity of the transfer functions in both coupled and decoupled vertical and horizontal stimulus-response reference axes and the amount of cross-axis coupling present in the system responses. A comparative study was also conducted to assess the differences in response characteristics between single-axis and dual-axis visual stimulation for the same subject.

INTRODUCTION

The purpose of this investigation into eye and head tracking at the Aerospace Medical Research Laboratory is to determine the applicability and dynamic performance of Visually Coupled Systems (VCS), control systems which are activated by head and/or eye movements with relevant feedback information displayed directly to the operator's visual field-of-view.

* National Research Council Resident Research Associate

** Captain, United States Air Force

Numerous potential applications of VCS to manned and unmanned aircraft flight control, fire control, target acquisition and reconnaissance have been proposed. Aside from in-the-loop control of sensors and weapons, head and eye line-of-sight measurements are being considered for selection and control of aircraft cockpit informational displays and as a means of updating onboard navigation systems. In addition, if real time knowledge of the operator's line-of-sight is coupled with information and special processing provided by a central data management system (e.g., an airborne data computer), VCS devices can display cues directly to the operator as to locations of targets, threats, checkpoints, runways, etc., in the real world.

The interest in head and eye directed control systems is based on the following considerations: for conventional manual control, use of the hands and feet has traditionally been reserved for vehicular attitude controls; the incorporation of head and eye control systems offer numerous additional control possibilities, including simultaneous secondary tasks without overloading or severely encumbering the operator; rapid, precise eye and head movement coordination is a natural physiological activity in man which is closely coupled to his perception and reaction to the environment.

EXPERIMENTAL APPARATUS

The experimental apparatus consisted of a Honeywell Remote Oculometer which computes the angular line-of-sight associated with dynamic eye movements and a Honeywell Helmet-Mounted Sight (HMS) to compute angular line-of-sight information for dynamic head movements.

The Honeywell Oculometer is a digital signal processor which extracts line-of-sight information from a scanned television vidicon field and determines pupil diameter and visual fixation angles by means of appropriate real time signal processing. Merchant, et al. [3] provide a detailed description of the operation and performance of this instrument.

The Honeywell HMS described in reference [4] computes head line-of-sight from information generated by scanning infrared light beams transmitted from fixed-coordinate "light fans" mounted beside the experimental subject and received by light sensors mounted on a helmet worn by the subject. An electronic computation unit outputs the horizontal and vertical coordinates associated with the head line-of-sight in accordance with a preliminary calibration operation.

The moving target stimuli for the eye and head pursuit tracking are generated by projecting a laser beam directed by an X-Y mirror galvanometer system onto a vertical viewing screen which subtends a visual angle of $\pm 20^\circ$ for both vertical and horizontal axes. The vertical and horizontal channels of the galvanometer system have independent input connections and

the stimuli consist of band-limited, Gaussian white noise which are uncorrelated between vertical and horizontal channels.

DATA ANALYSIS

The data analysis method chosen for investigation of the head and eye movement system dynamics was power spectral analysis [5], and the frequency information of the spectral analysis permitted a comparison of the authors' data with those in the literature [1,2]. Using power spectral analysis techniques, one may directly compute the system's linear, input-output transfer function and the coherence function which is a quantitative measure of the credibility associated with the computed linear transfer function.

It is assumed that the measured output response, $x(t)$, is the sum of an input stimulus, $u(t)$, multiplied by the system transfer function, h , plus an additive noise source, $n(t)$, which is uncorrelated with the input.

$$x(t) = h(t) u(t) + n(t)$$

$$E[n(t) u(t)] = 0; \quad 0 \leq t \leq T$$

Performing a Fourier transformation of the input and output variables and converting to power spectra

$$G_{ux} = H G_{uu} + G_{nx}$$

where

$u(t)$ = input time function

h = transfer function (time domain)

$x(t)$ = response time function

$n(t)$ = noise time function

G_{uu} = auto-power spectrum of $u(t)$

G_{ux} = cross-power spectrum of $u(t)$ and $x(t)$

G_{nx} = cross-power spectrum of $n(t)$ and $x(t)$

$E[]$ = expected value operator

Assuming that $n(t)$ is uncorrelated with $x(t)$ and $n(t)$ is zero mean, Gaussian noise, then the use of ensemble averaging for the auto- and cross-power spectra for many segments of frequency computations causes G_{nx} to approach zero. Therefore,

$$\overline{G_{ux}} = H \overline{G_{uu}}$$

and

$$H = \frac{\overline{G_{ux}}}{\overline{G_{uu}}}$$

where \overline{G} denotes the ensemble average.

The coherence function, γ^2 , is defined as

$$\gamma^2 = \frac{G_{ux}}{G_{uu} G_{xx}} ; \quad 0 \leq \gamma^2 \leq 1.0$$

where G_{xx} = auto-power spectrum of $x(t)$.

The coherence function is the proportion of input power contained by the output power spectrum and is a quantitative measure of the linear causal relationship between the input and output of a system.

Input-output cross-correlations were computed to determine the time delay of the output response relative to a given input stimulus. The lag time corresponding to the maximum value of the cross-correlation function is considered as the time delay of the measured input-output relationship.

RESULTS

The data presented here were recorded primarily from one subject and are considered to be a preliminary investigation of two-dimensional head and eye movement dynamics.

Eye Movement Responses

The eye transfer function for a single-axis stimulus is shown in Figure 1. Note that the gains for both vertical and horizontal axes are less than one for all frequencies investigated and that the horizontal gain is less than the vertical gain. The phase lag is linearly correlated with frequency with a correlation coefficient of 0.98, and this type of phase relationship corresponds to that for a time delay function.

The corresponding eye transfer function for dual-axis stimuli is shown on Figure 2. The gains are linear with frequency, and the vertical gain is much greater than the horizontal gain. It should be noted that the vertical to horizontal gain ratio is greater in the dual-axis case than the single-axis case. In dual-axis pursuit for this particular subject, the horizontal gain decreased and the vertical gain increased when compared to the single-axis case. The phase lag for the dual-axis case is also linearly related to frequency, but the dual-axis phase lag is approximately 20 degrees greater than the single-axis case for all frequencies.

The gain data for the dual- and single-axis stimuli do not agree very well with previously published results. Perhaps the primary source for disagreement is the fact that previous investigators compute the transfer function by the amplitude ratio between output response and input stimuli,

assuming that the output waveform is linearly correlated with the input waveform. The power spectral analysis assumes linearity between input and output; however, the coherence function computed in conjunction with the system transfer function indicates the validity of this linearity assumption at each computed frequency and therefore, indicates the frequency regions in which the linearity assumption is valid.

A typical coherence function is shown on Figure 3. It should be noted that the coherence is relatively large, indicating that the system can be approximated as a linear system up to a 1 Hz stimulus frequency. The mean values of the single-axis coherences are approximately 0.75 for both vertical and horizontal pursuit tasks, and the dual-axis coherences are approximately 0.84 for both axes (Table I). These results show a greater degree of linearity for the dual-axis case than the single-axis case. The cross-coupling coherence functions show a mean value of approximately 0.15 so that axis cross-coupling seems to have a minor effect on dual-axis responses (the cross-correlation function results also verified this conclusion).

The time delays (Table II) for single-axis eye pursuit of 110 milliseconds in the horizontal direction and 140 milliseconds in the vertical direction. The dual-axis case, on the other hand, shows delays of 180 milliseconds in the horizontal direction and 200 milliseconds in the vertical direction. Clearly, the dual-axis delays are longer than those for single-axis responses, and the vertical axis delays are slightly longer than the horizontal axis delays. The difference in delays between dual-axis and single-axis tracking may imply additional processing time required by a stimulus trajectory orthogonal component processor operating on the stimulus trajectory vectors to produce component stimuli in the vertical and horizontal directions during dual-axis pursuit tasks.

The equivalent time delays computed from the phase data under the assumption that the phase lag is produced only by a time delay factor for the single- and dual-axis cases agree with the time delays computed from the cross-correlation computations.

Head Movement Responses

The transfer function frequency graphs for single-axis head pursuit are shown in Figure 4. The vertical response gain is greater than the horizontal response gain; however, the gains for the head system are lower than those for the eye system for similar single-axis tracking. The phase lag is a linear function of frequency similar to the eye responses.

The dual-axis frequency response shows a higher gain than the horizontal response, and both the vertical and horizontal gains increase during the dual-axis task when compared to their single-axis counterparts. The phase lag is also a linear function of frequency just as in the other cases.

The single-axis response has approximately 15 degrees greater phase lag than the dual-axis response, and this trend is the reverse of that shown for the eye movement responses.

The dual-axis coherences (Table III) are greater than the single-axis coherences, and the horizontal coherence is greater than the vertical coherence for the dual-axis case.

The time delays associated with dual-axis performance are less than those for single-axis by approximately 50 milliseconds (Table IV). The time delays computed from the phase data are approximately 70 milliseconds less than those computed from the cross-correlation functions. However, this is not considered a serious discrepancy. The lower coherence values for head movements when compared to eye movements in similar pursuit tasks seem to indicate a slightly greater degree of nonlinearity for the head movement system, and this additional nonlinearity may account for the discrepancy between time delays as computed from the cross-correlation and phase lag results.

DISCUSSION

Eye Movement Responses

Prior to performing the experimental investigation presented here, the authors expected that much of the two-axis experimental data analysis would be a verification of previous reports. The eye frequency responses were expected to be of constant gain up to 1 Hz beyond which the gain would decrease with a rather steep negative slope. The present data indicate that the transfer function gain curve is nearly constant up to 1 Hz, and the coherence functions verify that the system is nearly linear up to a 1.5 Hz frequency (coherence values as low as 0.8 are acceptable for linearity assumption). The low values of coherence beyond 1.5 Hz cause a rejection of these transfer function computations; therefore, the authors feel that a linear transfer function is valid only up to a 1.5 Hz frequency.

The phase data seem to agree fairly well with previous reports, but the linear function of phase with frequency was unexpected since this result indicates that the phase lag was produced solely by a time delay factor. An excellent correlation of the time delays computed from the phase data with the cross-correlation time delays is certainly strong evidence for believing that the phase lag is only due to a time delay in the transfer function.

A longer time delay for dual-axis tasks suggests the possibility of an internal orthogonal axis component processor engaged in computing the horizontal and vertical axis components of the trajectory vector associated with the stimulus. The extremely small values for the coherence functions associated with cross-coupling of the vertical and horizontal

axis stimuli and responses also suggest this vector processor.

Thus, these experimental results suggest that the vertical and horizontal eye movement systems operate as independent control systems with very little cross-coupling between the orthogonal reference axes.

The coherence function indicates that the dual-axis responses have greater linearity than single-axis responses, suggesting that single-axis responses might have some prediction artifact in the response data due to the a priori knowledge that the stimulus is constrained to move on a single reference axis. The horizontal and vertical eye movement system responses for smooth pursuit seem to indicate that the transfer function consists of a gain term coupled to a time delay. The vertical and horizontal gains have different values with the vertical gain being larger than the horizontal gain.

Head Movement Responses

The important results from the head pursuit experiments are that the coherence functions and gains for the horizontal and vertical axes differ. Since the vertical coherence is less than the horizontal coherence, horizontal head position control is more linear than the vertical axis control. The coherence functions increase when switching from a single-axis pursuit mode to a dual-axis mode, and this is certainly a significant result.

Another unexpected result is that the delays for the dual-axis task is less than the single-axis task. In view of the eye data, one would expect the opposite trend to occur.

The fact that the time delays computed from the head pursuit phase data do not match the corresponding cross-correlation computed delays could be attributed to the slightly smaller coherence functions for the head as compared to the eye data.

FUTURE RESEARCH

As a result of the intent to specify design criteria for VCS and to test candidate hardware for suitability as control activators, further investigations are planned.

The authors intend to investigate the effects of stimulus field-of-view, stimulus bandwidth and, for the head pursuit system, effects of helmet weight. The final phase will be the formulation of models for the eye and head neurological control systems which are derived from both time and frequency domain analyses. It is anticipated that this model will be used to develop a human operator simulation for VCS controls to perform system

analysis evaluations of proposed VCS hardware configurations and to determine parametric changes in the human operator's performance when subjected to changes in the environment or control task.

REFERENCES

1. Bach-Y-Rita, P.; Collins, C.C. and Hyde, J.E.: The Control of Eye Movements. Academic Press, 1971.
2. Stark, L.: Neurological Control Systems. Plenum Press, 1968.
3. Merchant, J.; Morrissette, R. and Porterfield, J.L.: "Remote Measurement of Eye Direction Allowing Subject Motion Over One Cubic Foot of Space." IEEE Transactions on Biomedical Engineering, Vol. BME-21, No. 4, July 1974, pp. 309-317.
4. Ferrin, F.J.: "F4 Visual Target Acquisition System," Proceedings of A Symposium on Visually Coupled Systems: Development and Application, sponsored by Aerospace Medical Division, Brooks Air Force Base, Texas and 6570th Aerospace Medical Research Laboratory, Wright-Patterson AFB, Ohio. AMD-TR-73-1, September 1973, pp. 15-32. AD 916572.
5. Roth, P.R.: "Effective Measurement Using Digital Signal Analysis," IEEE Spectrum, Vol. 8, April 1971, pp. 62-70.

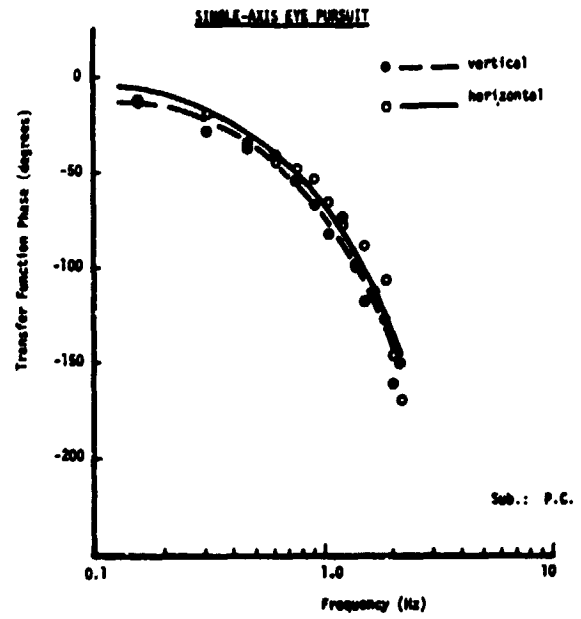
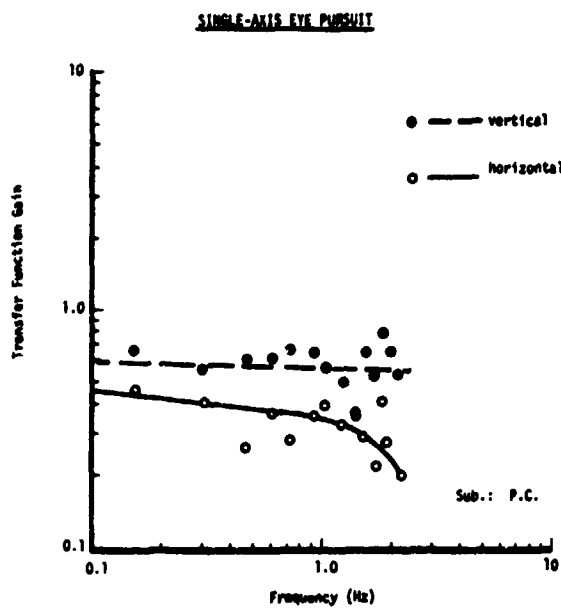


FIGURE 1

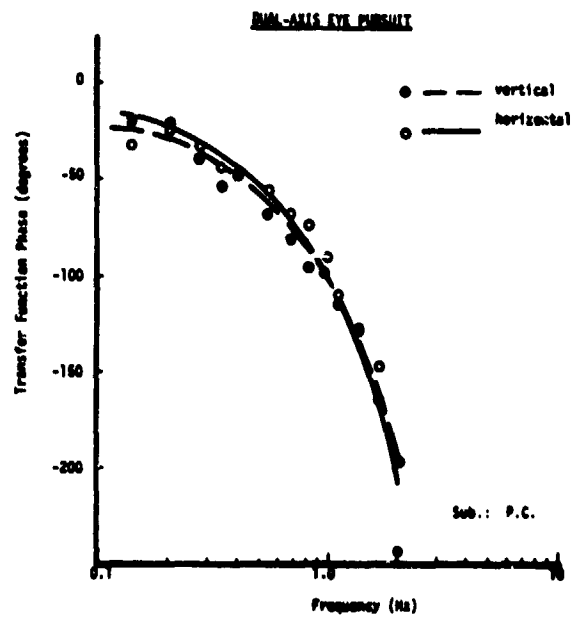
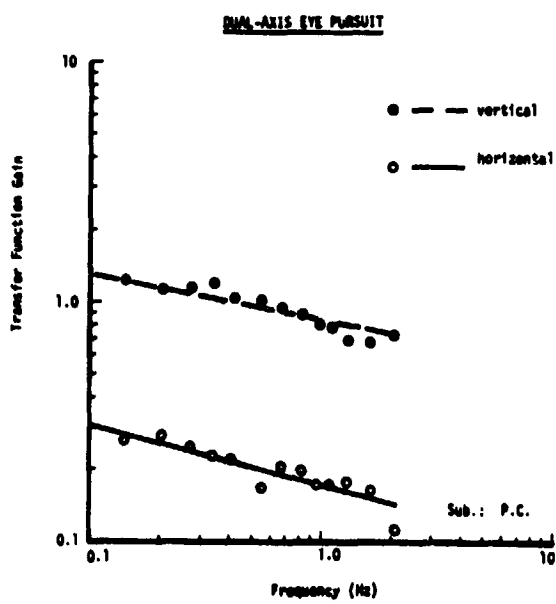


FIGURE 2

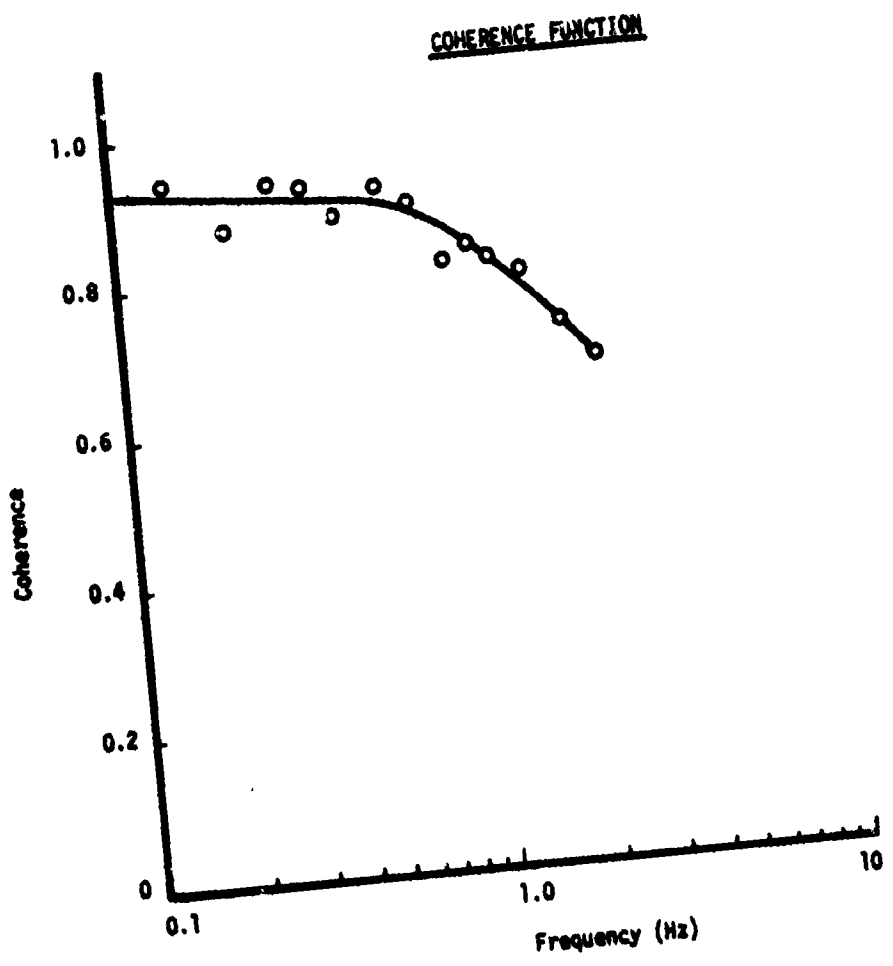
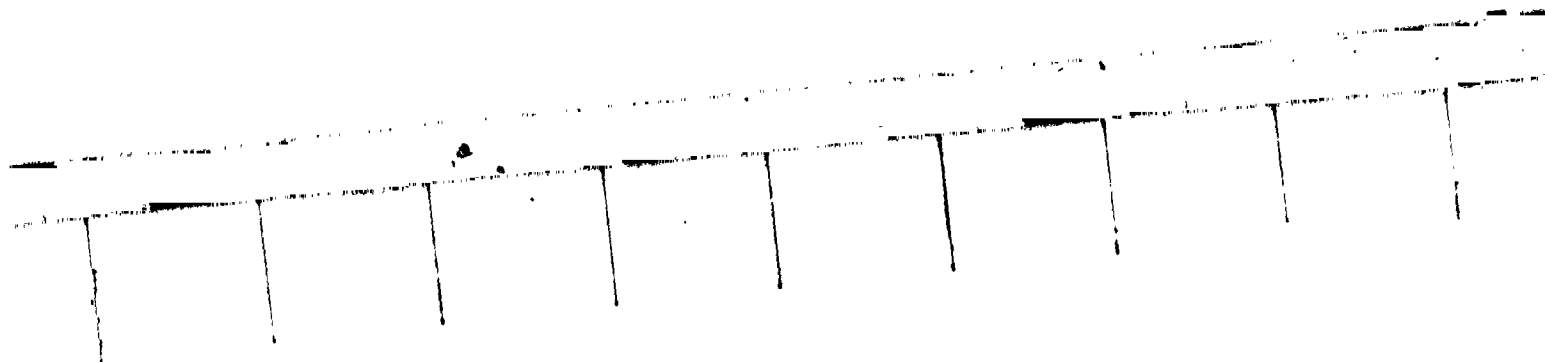


FIGURE 3

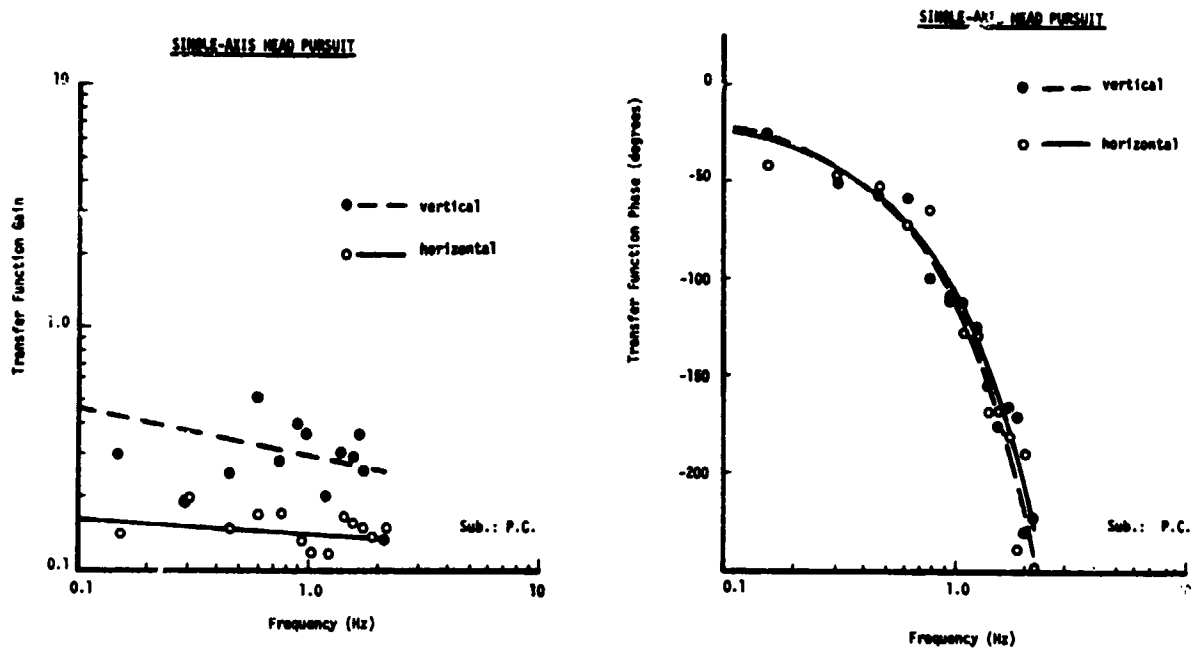


FIGURE 4

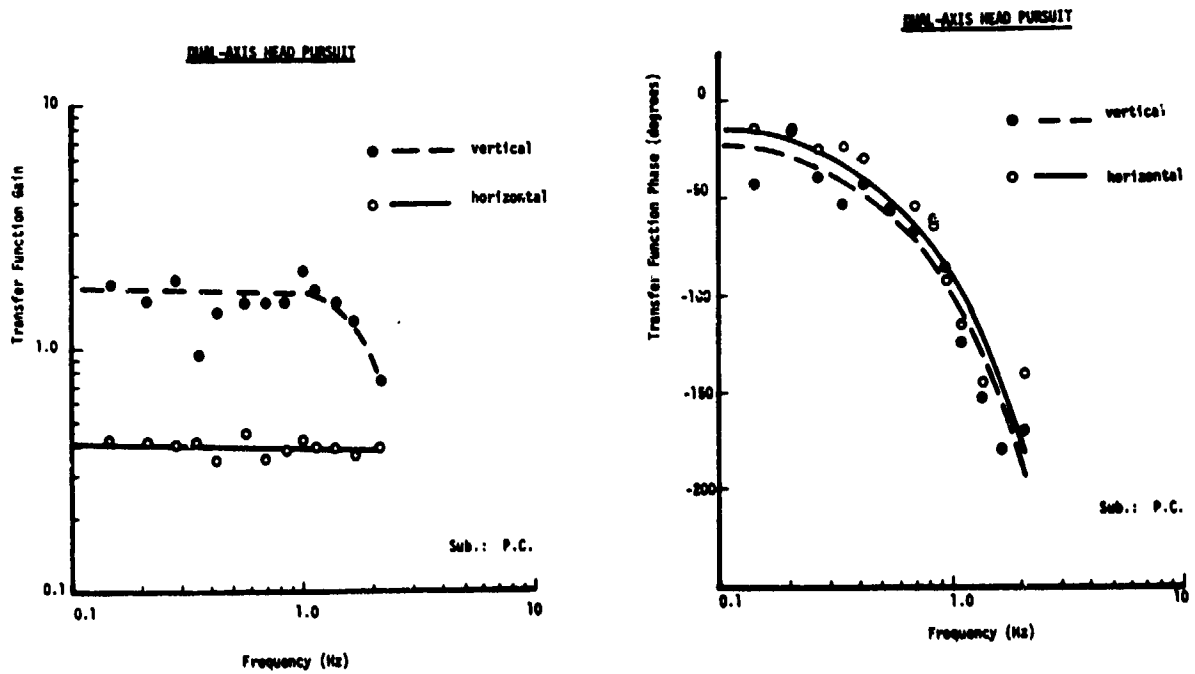


FIGURE 5

TABLE I. EYE PURSUIT COHERENCE

	MEAN	STD. DEV.	RANGE
Single-Axis:			
Horizontal	0.75	0.11	0.52 - 0.94
Vertical	0.74	0.15	0.46 - 0.93
Dual-Axis:			
Horizontal	0.83	0.12	0.44 - 0.91
Vertical	0.84	0.08	0.67 - 0.94

TABLE II. EYE PURSUIT DELAY

	Horizontal	Vertical
Single-Axis	110 msec.	140 msec.
Dual-Axis	180 msec.	200 msec.

TABLE III. HEAD PURSUIT COHERENCE

	MEAN	STD. DEV.	RANGE
Single-Axis:			
Horizontal	0.63	0.13	0.45 - 0.87
Vertical	0.53	0.12	0.31 - 0.67
Dual-Axis:			
Horizontal	0.82	0.07	0.63 - 0.89
Vertical	0.67	0.13	0.43 - 0.86

TABLE IV. HEAD PURSUIT DELAY

	Horizontal	Vertical
Single-Axis	280 msec.	290 msec.
Dual-Axis	240 msec.	240 msec.

N75 33691

EFFECTS OF LOW FREQUENCY VIBRATION OF A LIMB

by Gyan C. Agarwal and Gerald L. Gottlieb

Department of Biomedical Engineering
Rush-Presbyterian-St. Luke's Medical Center
Chicago, Illinois 60612

and

College of Engineering
University of Illinois at Chicago Circle
Chicago, Illinois 60680

SUMMARY

Low frequency oscillations (3 to 30 Hz) were applied on the ankle joint in plantarflexion-dorsiflexion rotation using a torque motor. The torque, the angular rotation and the evoked electromyogram from the gastrocnemius-soleus and the anterior tibial muscles were recorded.

Significant nonlinearities were observed in the angular rotation from 8 - 12 Hz. The following methods are used for data analysis: 1) two-cycle averaged response, 2) Fourier transform and 3) Fourier analysis at the driving frequency.

Important observations are: 1) resonance near 6 - 8 Hz, 2) slowly increasing amplitudes of oscillation near resonance, 3) self-sustaining oscillations after the motor is turned off, particularly in the fatigued limb, 4) distortion of angular rotation during which there are spontaneous recurrences of oscillation at the driving frequency.

INTRODUCTION

There has been a growing concern in recent years regarding the effects of vibration upon human operators. Nearly everyone is exposed at one time or another to some form of vibration and in fact, there are several million individuals (estimated 8 million in U.S. alone (Wasserman and Badger, 1973a) who throughout their working lives are continuously exposed to vibrational stresses: truck drivers, heavy construction machine operators, and hand tool operators, to name a few.

An individual may be subjected to whole body vibration or the vibrational stresses may be directed to one or more segments of the body. Long term exposures to vibration in workers produce many pathological and psychological syndromes (Taylor, 1974, Wasserman and Badger, 1973b).

Most studies on the effects of vibration have been limited to the effects of long term exposures and their clinical manifestations. Our knowledge of the direct effects of vibration on the human motor system is very limited. Vibration is a potent stimulus to the muscle spindles and therefore is quite capable of producing significant changes in the control and coordination of movements.

In this paper we will examine the effects of low frequency oscillation of a limb; rotation around the ankle joint. High frequency vibration (50 - 200 Hz) applied directly to the muscle belly or muscle tendon produces tonic vibration reflex and significantly alters the Hoffmann and tendon-jerk reflexes (Agarwal and Gottlieb, 1975, Hagbarth, 1973, Lance, Burke and Andrews, 1973).

METHODS

Experiments were done on six normal human subjects. The subject sat in a chair with his right foot strapped to a foot-plate which permitted only dorsiflexion-plantarflexion about the ankle joint. A schematic of the equipment used is shown in figure 1.

The plate is rotated by a D.C. torque motor via a gearbelt and pulley system for torque amplification. Constant tension springs (not shown in the figure) are also used to balance the downward gravitational force on the foot. With the motor off and the subject completely relaxed, the resulting joint position is defined as the zero angular position and this reference is provided as a fixed dot on a dual beam oscilloscope. The second beam is used to display his angular position.

The subject was instructed to maintain a constant mean force against the bias torque of the motor so that the oscillation is nearly symmetrical in plantar-dorsal amplitude of rotation with respect to the reference angular position.

Sinusoidal signals were superimposed on the mean torque level. Frequencies from 3 to 30 Hz were used. In some experiments, frequencies down to 1 Hz were used. The torque, the resulting angular rotation and rectified, filtered electromyograms from the surface of the gastrocnemius-soleus and the anterior tibial muscles were continuously recorded on a digital tape. The angle and the torque signals were sampled at a rate of 250 Hz and the filtered EMGs at a rate of 500 Hz.

The data was continuously recorded for 10 seconds or more at each frequency. After 10 seconds, we frequently recorded the data going through a stop, start and stop again of the modulating signal. The bias voltage was constant throughout the run. This allowed us to observe self-generated oscillations as discussed in the results section.

Whereas the applied torque signal was nearly a single frequency sinusoid, the angular rotation at certain frequencies had significant distortion. For this reason the following analyses were done.

1. Fourier coefficients at the fundamental frequency were obtained from the torque, the angular rotation and the EMG data for the first 10 seconds. The analysis was done for twenty half-second data records and the resulting numbers were averaged.
2. A two cycle time average was generated for a 10 second data record by taking successive intervals equal to twice the modulation period.
3. An average Fourier Transform was obtained by using five two-second data records with the incremental re-

3. (continued)
solution frequency of 0.4883 Hz.

In some experiments, vibration near the resonant frequency was applied continuously for 100 seconds or more to develop muscle fatigue and to observe the self-generated oscillations after the modulating signal of the motor was stopped.

RESULTS

The average wave shapes for the torque, angular rotation and the two EMG's are shown in figure 2 (A-H). The motor drive is $0.5 + 0.4 \sin 2\pi ft$ and the frequencies are 4, 5.5, 6, 6.5, 7, 10, 12 and 15 Hz. The corresponding Fourier Transforms are shown in figure 3 (A-H).

The two cycle averages and the fourier transforms indicate that the angular rotation at certain input frequencies (8 - 12 Hz) contains significant subharmonic and higher harmonic components. Other interesting features of this data are shown in figures 4 - 6.

Figure 4 shows the slowly increasing amplitudes of oscillation when modulation is turned on near the resonant frequency of 6.5 Hz. The peak EMG of the gastocnemius-soleus muscle also increases in amplitude as the oscillation builds up.

Figures 5 and 6 show the distortion in the angular rotation. In figure 5, the drive frequency is 11 Hz and the oscillation starts out at the same frequency with corresponding EMG. Due to the time varying changes in the muscle stiffness as the muscle contracts during each cycle, the nonlinear behavior becomes progressively dominant with alternate stretch cycles less effective. The EMG pulses are also at half the driving frequency.

In figure 6, the driving frequency is 10 Hz. The spontaneous recurrences of oscillation at the driving frequency (indicated by underlines) with corresponding 10 Hz frequency in the soleus EMG, are observed for a few cycles in between the periods of nonlinear oscillation.

Figure 6 also shows the free oscillation of the foot after the modulating signal to the torque motor is turned off as indicated by the arrow. This free oscillation for the first two seconds after modulation is stopped is at 6.15 Hz as determined by Fourier transform analysis.

Figures 2 - 6 clearly point out the nonlinear nature of the system. As a first order approximation, a linear systems analysis is attempted here. From the data, the Fourier coefficients at the driving frequencies are obtained and compared.

The compliance of the muscle is defined by taking the ratios of the angular rotation and the torque coefficients and using the following relation:

$$\begin{aligned} \frac{\Delta L}{\Delta F} &= \text{Compliance of the muscle} \\ &= \frac{\theta \times R}{59.29 \times 0.4667} \times \frac{1.9876 \times R}{\tau} \\ &= (\theta / \tau) \times 1.8 \times 10^{-3} \text{ meters/newton} \end{aligned}$$

The numbers in the expression are the scale factors to convert angular rotation in radians and torque in newton meters. R is the radius of action for the muscle. For plantar as well as for dorsal movements, this radius is roughly 5 cm., although it is a function of the foot angle (Hogins, 1969).

Figures 7 and 8 show the muscle compliance for six experiments when the amplitude of modulation is kept constant and the bias voltage is changed from -0.5 to 0.75 volts. For the relaxed foot with zero bias voltage, the resonant frequency is at 4 Hz. For tonically active muscle, the resonant frequency is around 5.5 to 6.25 Hz.

Figure 9 shows the phase lag of the angular rotation with respect to the input torque and the phase lag of the EMG with respect to the angular rotation for a drive of $0.5 + 0.5 \sin 2\pi ft$.

Figure 10 shows the muscle compliance for the case when the bias is kept constant at 0.5 volts and the amplitude of modulation is varied with values of 0.2, 0.4, 0.5 and 0.6 volts. At 0.2 volts modulation, the peaks in the compliance curve are at 9 and 12 Hz; at 0.4 volts modulation the peaks are at 6 and 6.5 Hz; at 0.5 volts modulation peak is at 6.25 Hz and at 0.6 modulation the peaks are at 6.25 and 9 Hz.

Figure 11 shows the compliance versus frequency of the data in figures 2 and 3. Also shown is the soleus EMG stretch gain of this data. It must be emphasized that this gain is defined by taking the ratios of Fourier coefficients at the drive frequency. The rectification of the EMG produces higher harmonics which are not accounted for in defining this ratio. Figure 12 shows the angle data at this drive of $0.5 + 0.4 \sin 2\pi ft$ similar to figure 9 for a different subject.

In figure 6, there is a self-sustaining oscillation of the ankle joint after the motor is turned off which lasts for several seconds. Figure 13 shows the fourier transform of 2 seconds of the data after the modulation is turned off. The torque and the angular rotation at the driving frequency of 10 Hz are 0.0055 newton meters and 0.13 degrees. The peak amplitude in

the Fourier transform is at 6.15 Hz. The nearest drive frequencies tested were 5.5, 6, 6.25 and 6.5 Hz. The resonant frequencies were 6 and 6.5 Hz.

DISCUSSION

Table I shows the Fourier coefficients of the data of figures 2 and 3. Note that the maximum oscillation is at 6 Hz and the minimum torque is at 6.5 Hz. Near the resonant frequency, the gastrocnemius-soleus EMG is also maximum. The nonlinearity of the data is quite pronounced near 10 - 12 Hz as shown in the Fourier transforms of figure 3.

The details for this nonlinear behavior have not yet been investigated. The generation of subharmonics at these frequencies is most likely due to time varying changes in the compliance of the contracting muscle. The compliance of the human arm as calculated from Wilkie's data is 0.5×10^{-3} to 1.5×10^{-5} meter/newton (Wilke, 1950; Gottlieb, et al, 1969). The compliance decreases as the tension increases. For a tendon jerk in the soleus muscle the time to peak twitch is also a function of tonic tension and varies from 180 - 220 msec being smaller for the plantarflexion (Agarwal, et al, 1970).

The slow build up in the amplitude of oscillation near the resonant frequency (see figure 4) is a common phenomenon in nonlinear systems. The 'jump' phenomenon has been reported near the resonant frequency of the wrist movement (Walsh, 1973, 1974). Joyce, Rack and Ross (1974) have observed resonance of the elbow joint near 8 - 12 Hz.

The self-sustaining oscillation as seen in figure 6 have been seen by Joyce et al (1974) in the wrist movement as well. Such oscillations are due to the regenerative effects of the feedback loop and imply instability of the loop.

Walsh (1973) and Joyce, et al (1974) did not study single frequencies and swept the frequency range in only a few seconds. As seen in figures 5 and 6, the nonlinear movements develop only after a few cycles and therefore these effects were not observed.

The phase angle between the soleus EMG and rotation in figures 9 and 12 can be mostly accounted for by the conduction time lag of about 55 msec around the neural loop. Below the resonant frequency, angular rotation lags the torque by 150-180 degrees. This phase relationship changes abruptly near the resonant frequency. Beyond the resonant frequency, this phase lag between θ and τ is about 30 degrees and approaches zero degrees near 30Hz.

Such sudden changes in phase are characteristic of marginally stable systems near resonance. This behavior coupled with the existence of self-sustaining oscillations which are emphasized with fatigue (in one experiment a subject continued to oscillate for 58 seconds until he finally halted it) is surprising. Conservative engineering design tends to emphasize stability and this normally characterizes our view of most physiological regulating

mechanisms.

An alternative view of many such regulators is that they are inherently unstable within some of their inner loops. Homeostasis is preserved however by the existence of outer loops which become active only near the boundaries of some allowable state space. Thus the inherent instability is not observed except in cases of pathology or perhaps in experiments such as described here. Certainly none of our subjects has ever had any history of neuromuscular illness nor have they any present complaints. None show ankle tremor and none have difficulty walking or driving. But all have experimentally demonstrated clonus. This is a most interesting paradox.

ACKNOWLEDGEMENT

This work was supported in part by a National Science Foundation grant # GK-37540 and by General Research Support Grant # RR-05477 from the National Institutes of Health.

REFERENCES

1. Agarwal, G. C., Berman, B. M., Lohnberg, P., and Stark, L., "Studies in Postural Control Systems. II. Tendon Jerk Input", *IEEE Trans. Systems Science and Cybernetics*, SSC-6, pp. 122-126, 1970.
2. Agarwal, G. C. and Gottlieb, G. L., "Effects of Vibration on Human Spinal Reflexes", in Motor System - Neurophysiology and Muscle Mechanism, M. Shahani (Editor), Elsevier, Netherland, 1975 (in press).
3. Gottlieb, G. L., Agarwal, G. C., and Stark, L., "Stretch Receptor Models. Single-Efferent Single-Afferent Innervation", *IEEE Trans. Man-Machine Systems*, Vol. MMS-10, pp. 17-27, 1969.
4. Hagbarth, D. E., "The Effect of Muscle Vibration in Normal Man and in Patients with Motor Disorders". In New Developments in Electromyography and Clinical Neurophysiology, J. E. Desmedt (Editor), Vol. 3, pp. 428-443, S. Karger, Basel, 1973.
5. Hogins, M. T., "Identification of the Human Ankle Control System" Ph.D. Thesis, University of Illinois at Urbana, 1969.
6. Joyce, G. C., Rack, P. M. H., and Ross, H. F., "The Forces Generated at the Human Elbow Joint in Response to Imposed Sinusoidal Movements of the Forearm", *J. Physiol.*, 240, pp. 351-374, 1974.
7. Lance, J. W., Burke, D., and Andrews, C. J., "The Reflex Effects of Muscle Vibration", in New Developments in Electromyography and Clinical Neurophysiology, J. E. Desmedt (Editor), Vol. 3, pp. 444-462, S. Karger, Basel, 1973.

8. Taylor, W. (Editor), The Vibration Syndrome, Academic Press, London, 1974.
9. Walsh, E. G., "Motion at the Wrist Induced by Rhythmic Forces", J. Physiology, 230, pp. 44P-45P, 1973.
10. Walsh, E. G., "Resonance at the Wrist-A Jump Effect", J. Physiol., 245, pp. 69P-70P, 1974.
11. Wasserman, D. E. and Badger, D. W., "Vibration and Its Relation to Occupational Health and Safety", Bull. New York Acad. Med., 49, pp. 887-894, 1973a.
12. Wasserman, D. E. and Badger, D. W., Vibration and the Worker's Health and Safety, Tech. Report #77, U. S. Department of Health, Education and Welfare, National Institute for Occupational Safety and Health, 1973b.
13. Wilkie, D. R., "The Relation Between Force and Velocity in Human Muscle", J. Physiology, 110, pp. 249-280, 1950.

TABLE I

Fourier coefficients of the data in figure 2. The motor drive was $0.5 + 0.4 \sin 2\pi ft$. FC denotes the Fourier coefficient at the drive frequency and DC is the average value.

FREQ	GS-EMG		Rotation	Torque		Compliance
	FC	DC	(deg) FC	(N.M) FC	(N.M) DC	(M/N) $\times 10^{-3}$
4	0.19	0.39	1.6	0.12	0.16	5.3
5	0.51	0.51	2.6	0.13	0.19	8.2
5.5	0.76	0.63	3.5	0.11	0.19	13.5
6	1.0	0.78	4.7	0.04	0.2	47.5
6.25	0.9	0.74	4.0	0.06	0.18	28.7
6.5	0.95	0.77	4.4	0.03	0.18	54.3
6.75	0.95	0.76	3.7	0.06	0.2	26.7
7	1.2	0.95	3.8	0.06	0.19	24.8
8	1.0	0.80	1.7	0.08	0.53	9.0
10	0.5	0.61	1.3	0.12	0.17	4.6
12	0.63	0.66	0.81	0.13	0.18	2.5
15	0.17	0.37	0.53	0.12	0.20	1.8
25	0.19	0.34	0.33	0.13	0.17	1.1
30	0.16	0.34	0.3	0.11	0.16	1.1

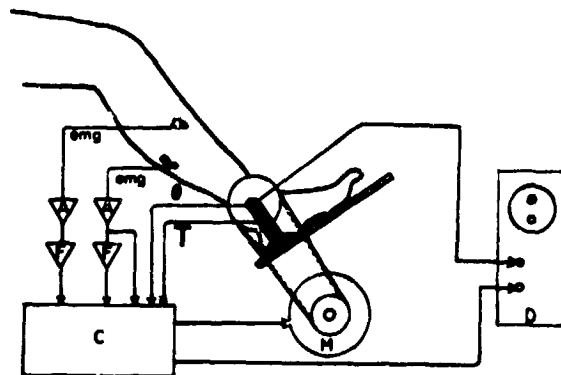


Figure 1

A schematic of the apparatus used for the forced oscillations of the ankle joint. The components are: D.C. Torque Motor (M) driven by a Bulova power amplifier, electromyogram is recorded using disc surface electrodes placed over the bellies of the soleus and anterior tibial muscles, EMG amplifiers (A) are Tektronix 2A61 (bandwidth 60-600 Hz), filters (F) are third order averaging (10 msec averaging time), display oscilloscope (D) is a dual beam Tektronix 502, digital computer (C) is S^oC-16.

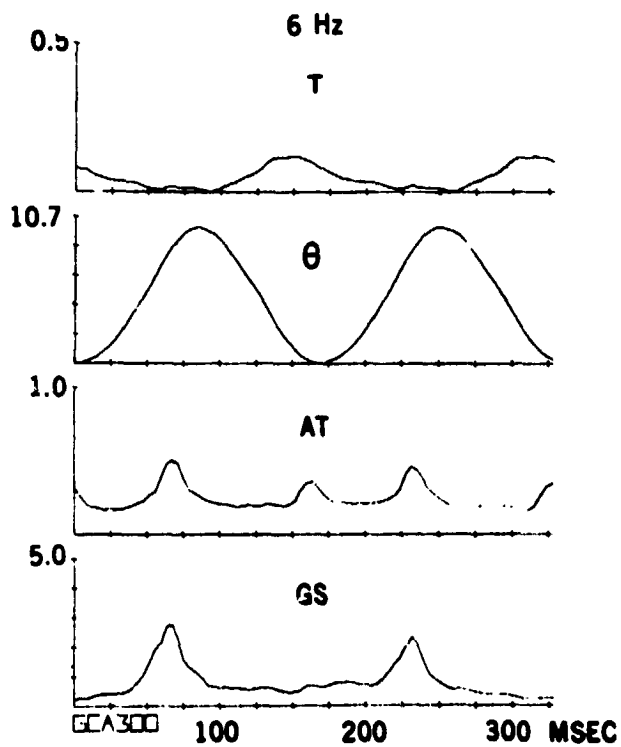
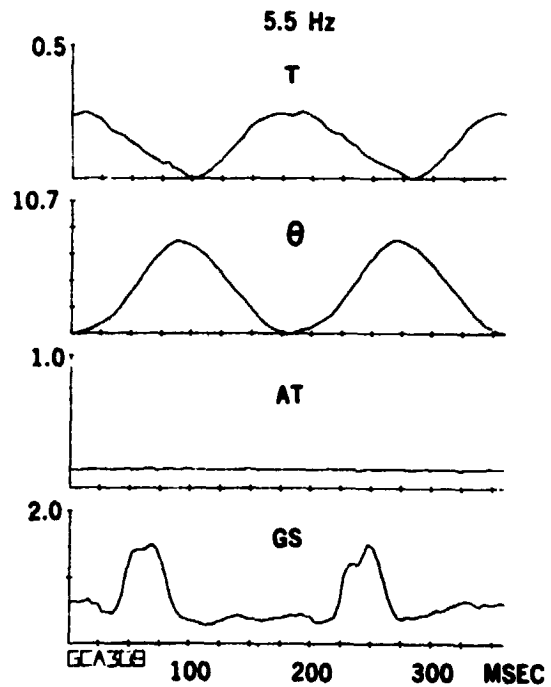
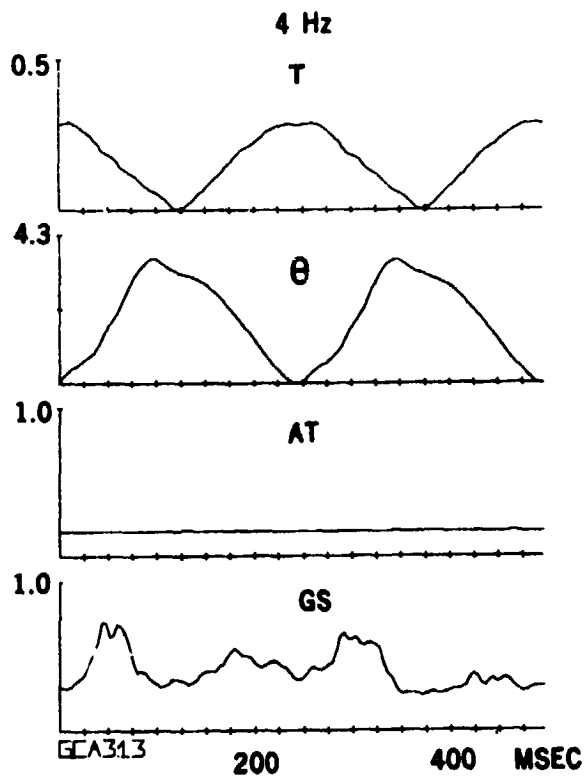


FIGURE 2 A,B,C

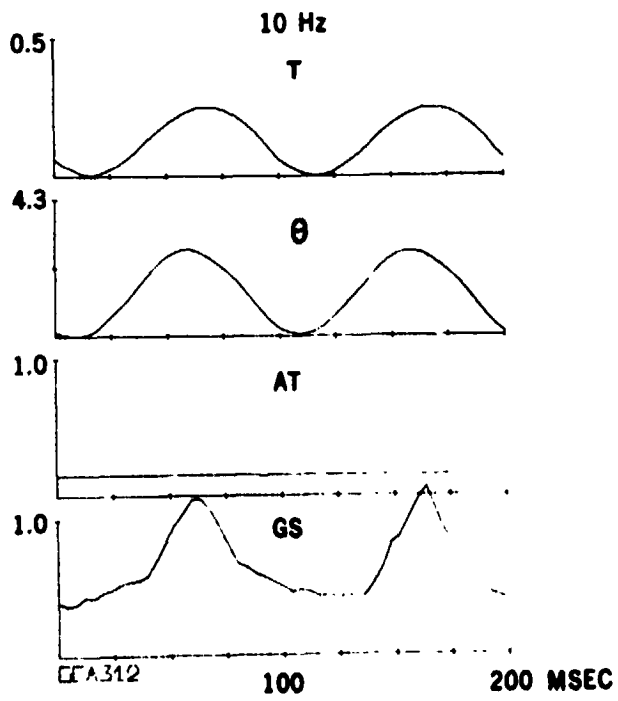
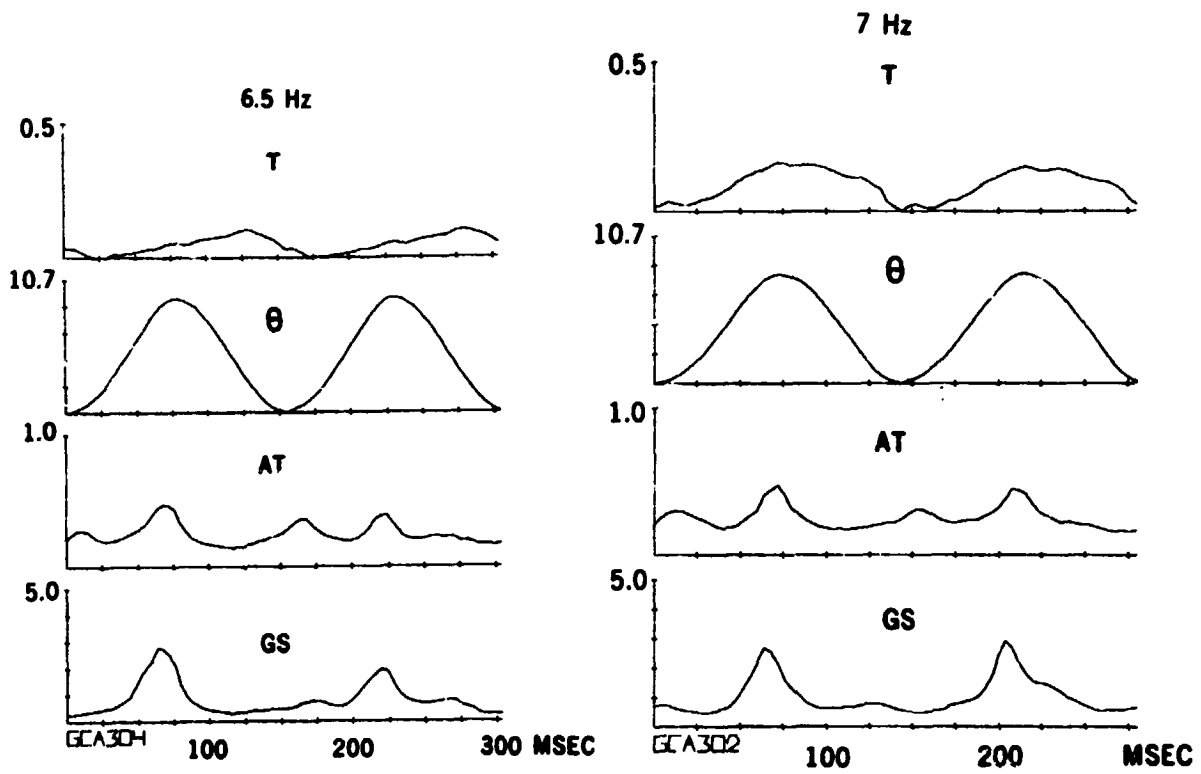


FIGURE 2 D,E,F

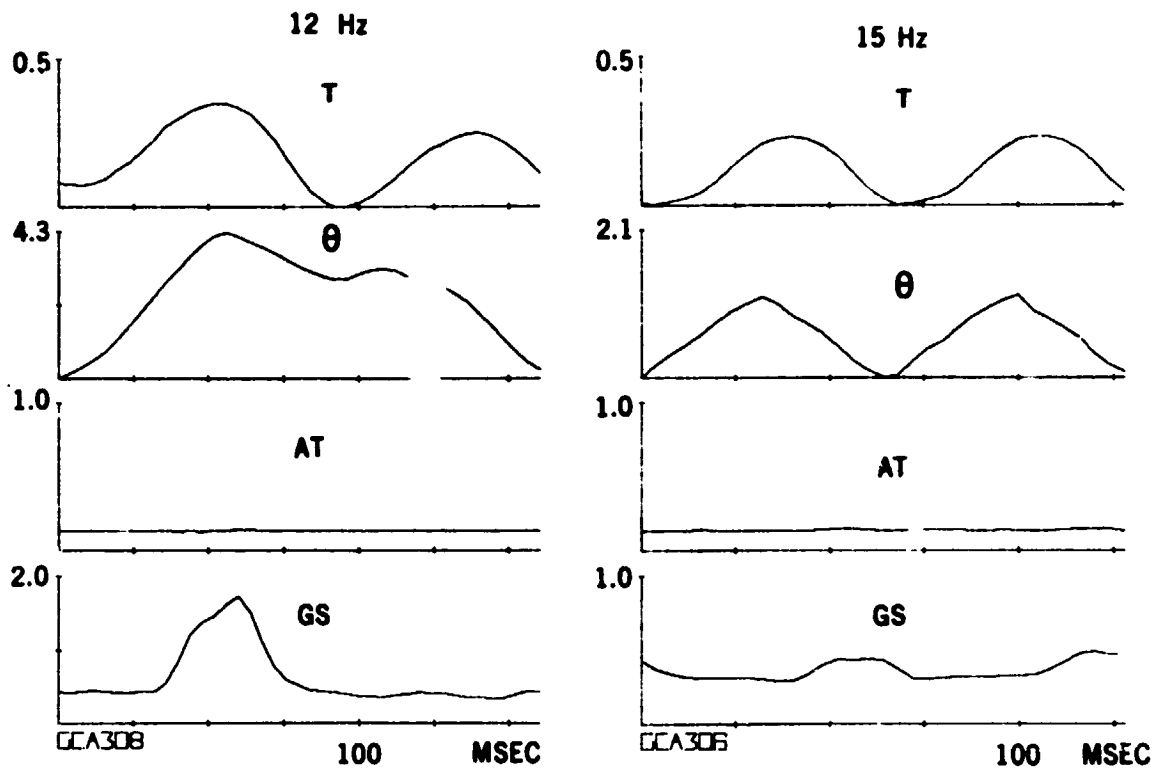


Figure 2

Two cycle averaged response at input frequencies of 4, 5.5, 6, 6.5, 7, 10, 12, and 15 Kz. The four traces from top to bottom in each part are torque in newton meters, foot angle in degrees, rectified and filtered EMG from the anterior tibial and the gastrocnemius-soleus muscles. The averaging was done for a 10 second data record by taking successive intervals equal to twice the modulation period. The drive was $0.5 + 0.4 \sin \omega t$.

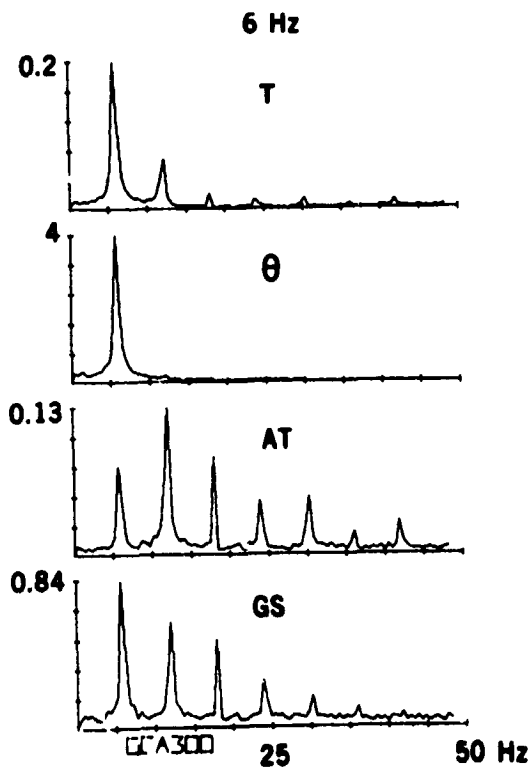
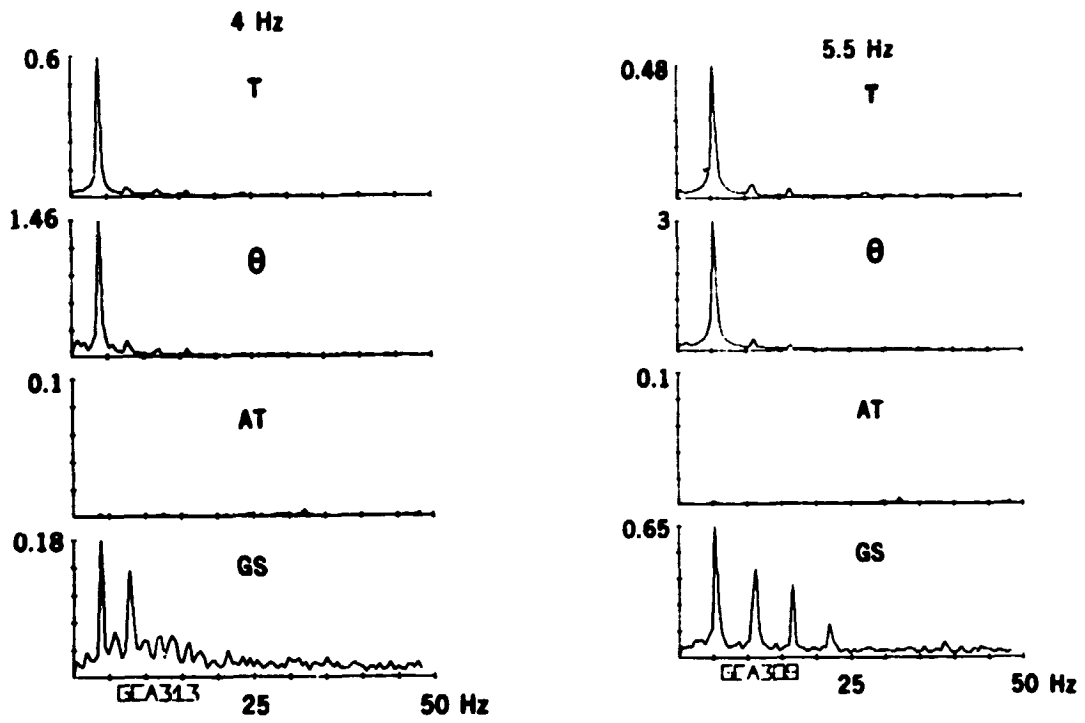


FIGURE 3 A,B,C

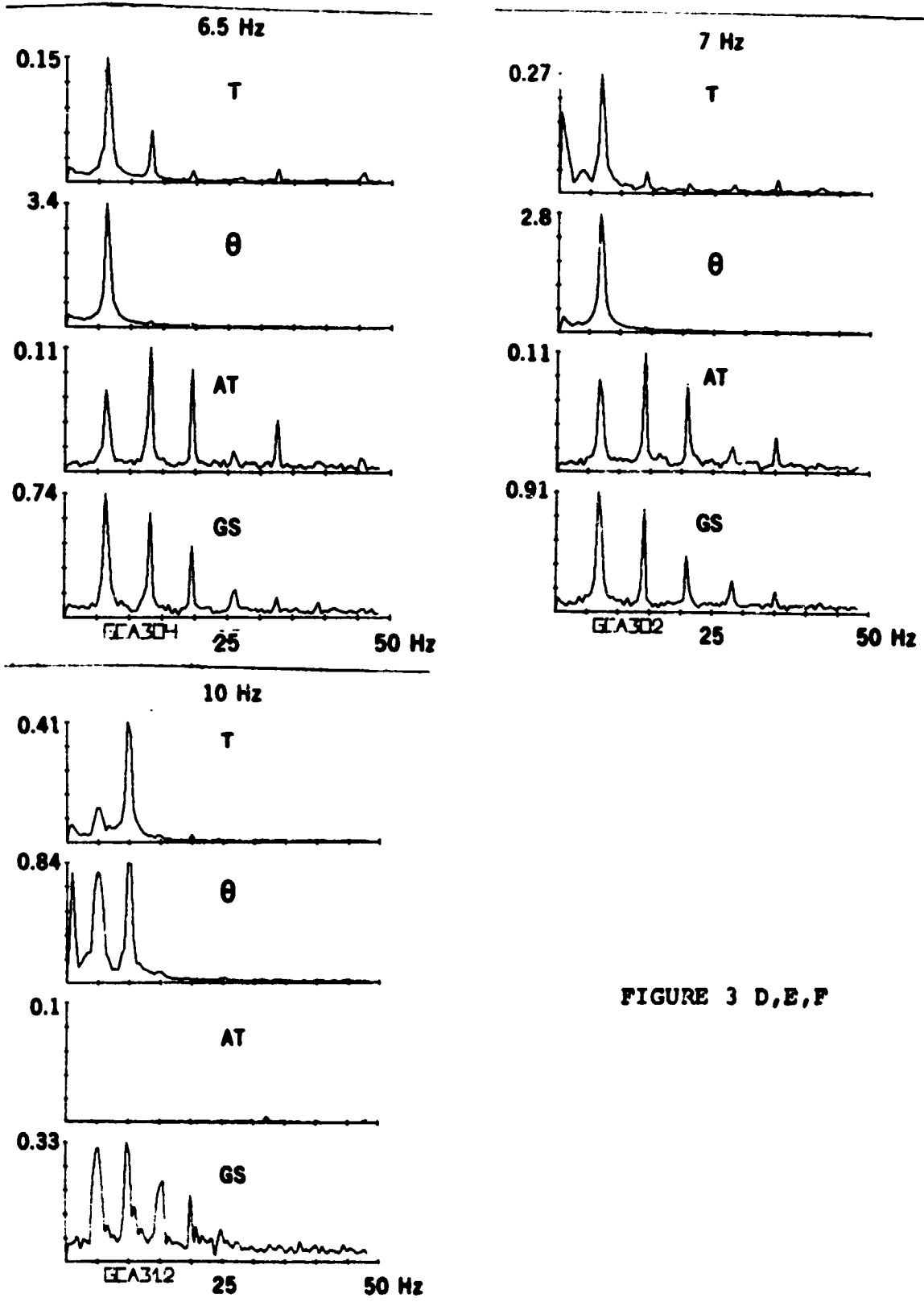


FIGURE 3 D,E,F

18

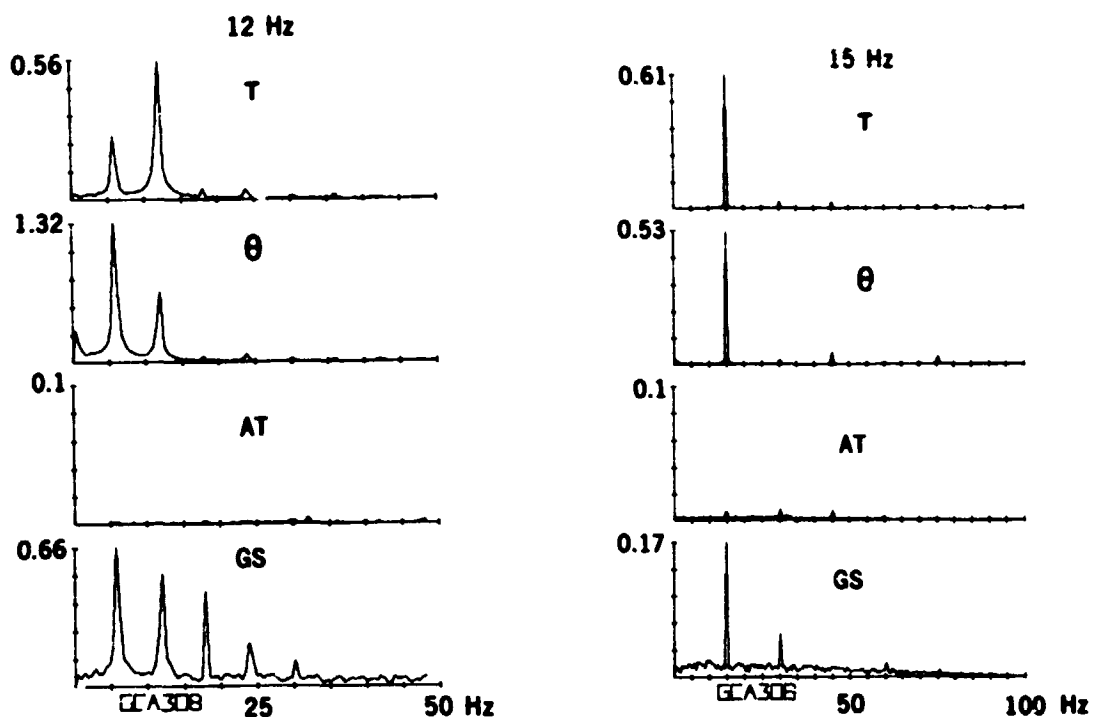


Figure 3

The averaged fourier transforms for five 2-second data records at input frequencies of 4, 5.5, 6, 6.5, 7, 10, 12, and 15 Hz. The four traces from top to bottom in each part are torque in newton meters, foot angle in degrees, rectified and filtered EMG from the anterior tibial and the gastrocnemius-soleus muscles. The drive was $0.5 + 0.4 \sin \omega t$.

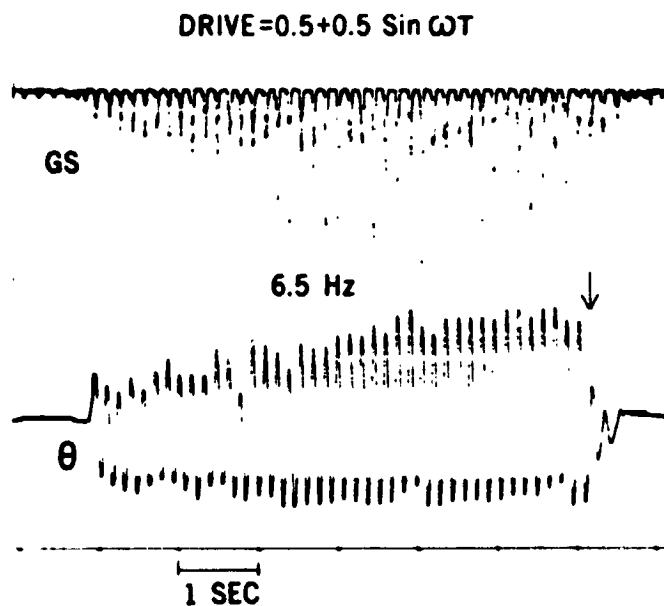


Figure 4

Slowly increasing amplitude of oscillation near the resonant frequency of 6.5 Hz. The upper trace is the EMG of the gastrocnemius-soleus muscle (rectified and filtered) and the lower trace is the angular rotation. The drive was $0.5 + 0.5 \sin \omega t$.

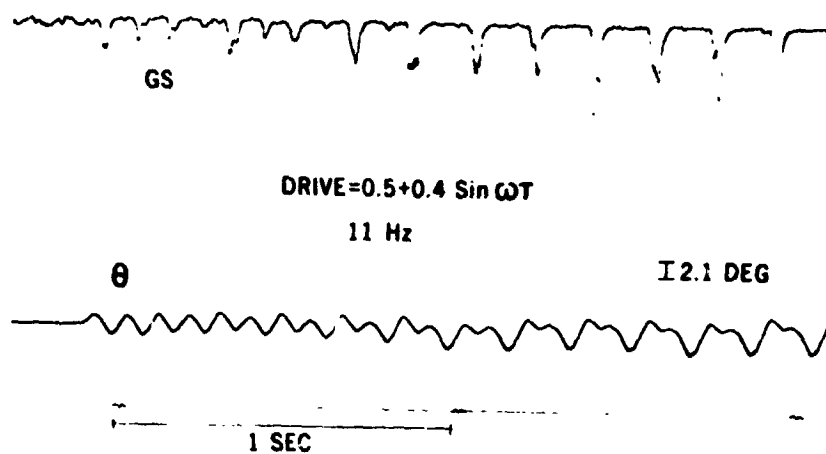


Figure 5

Forced oscillation of the ankle joint at 11 Hz. The drive was $0.5 + 0.4 \sin \omega t$. The upper trace shows the EMG activity of the gastrocnemius-soleus muscle (rectified and filtered) and the lower trace shows the angular rotation. The time markers are one second apart from left to right.

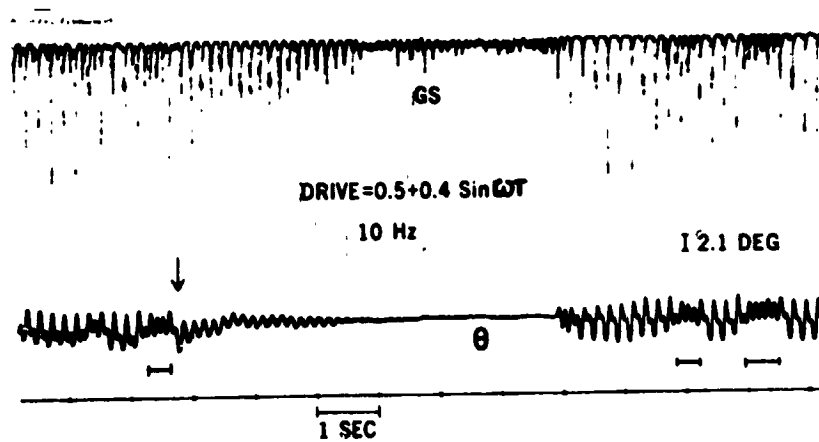


Figure 6

Forced oscillation of the ankle joint at 10 Hz. The motor drive was $0.5 + 0.4 \sin \omega t$. The upper trace shows the EMG activity of the gastrocnemius-soleus muscle (rectified and filtered). The lower trace shows the angular rotation. The time markers are one second apart from left to right. The arrow indicates the time when the modulation signal of the motor was turned off. The self-sustaining oscillation of the ankle joint continued for several seconds near 6.15 Hz. As the motor was turned on again, the non-linear waveform developed rapidly. The recurrences of 10 Hz oscillations in between the nonlinear response are indicated by line segments underneath the angle trace.

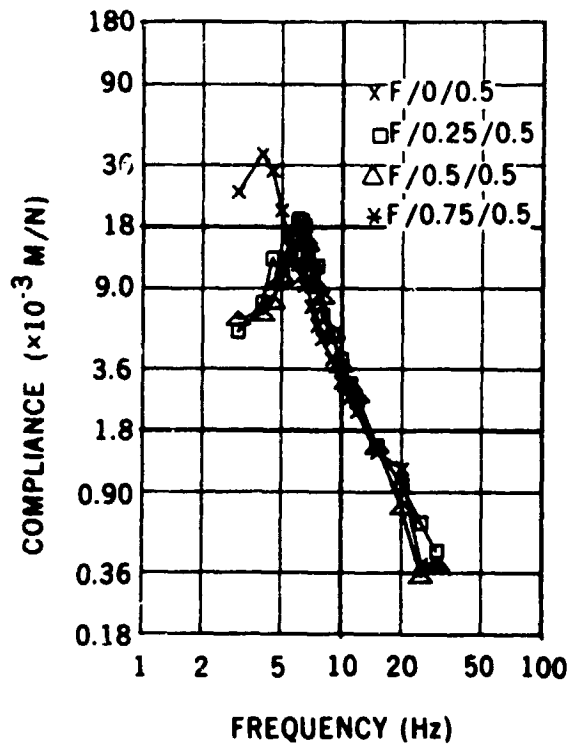


Figure 7

Effective compliance (angular rotation/torque gain) in meters/newton as a function of the input frequency. The amplitude of the modulation signal to the motor was kept constant at 0.5 volts. The motor bias voltages for the four cases were: x 0 volts, □ 0.25 volts, Δ 0.5 volts, and * 0.75 volts. For positive non-zero bias the gastrocnemius-soleus muscle was tonically active to maintain the zero angular foot position. The resonant frequencies for these four cases were 4, 5.5, 6.25, and 6.75 Hz, respectively. (Subject GLG)

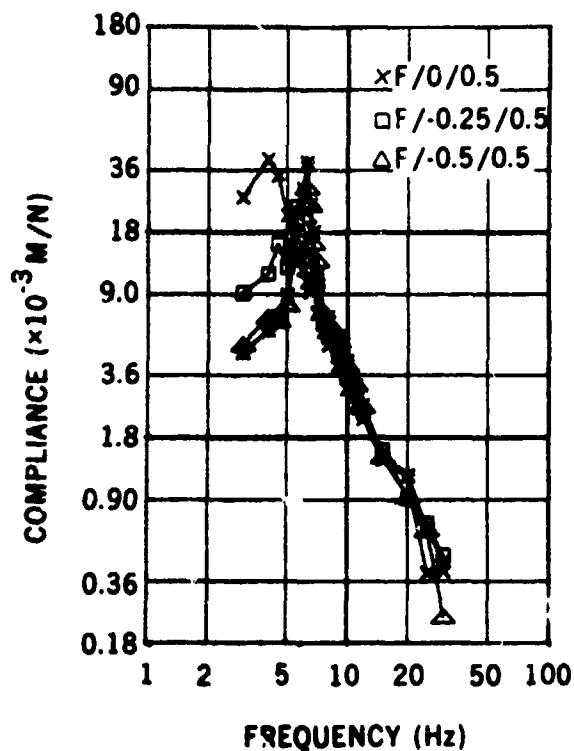


Figure 8

Effective compliance (angular rotation/torque gain) in meters/newton as a function of the input frequency. The amplitude of the modulation signal to the motor was kept constant at 0.5 volts. The motor bias voltages for the three cases were: x 0 volts, □ -0.25 volts, and Δ -0.5 volts. For negative nonzero bias the anterior tibial muscle was tonically active to maintain the zero angular foot position. The resonant frequencies for these three cases were 4, 6, and 6 Hz, respectively. (Subject GLG).

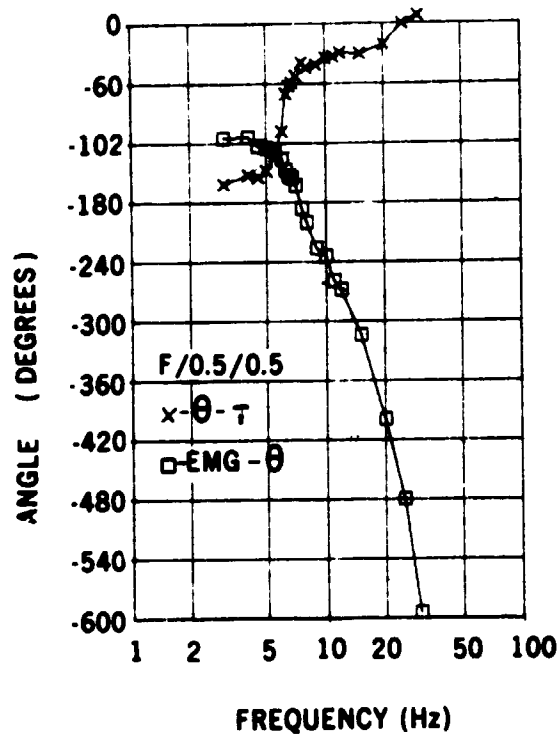


Figure 9

Phase angle between angular rotation and the applied torque (X) and between the soleus EMG and the angular rotation(□) as a function of the drive frequency. The phase relationship was calculated from the Fourier analysis. The motor drive was $0.5 + 0.5 \sin \omega t$. (Subject GLG).

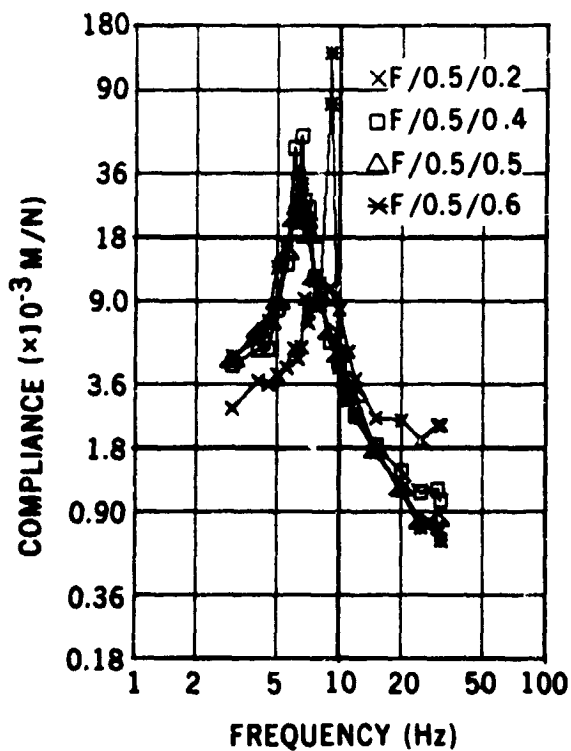


Figure 10

Effective compliance (angular rotation/torque gain) in meters/newton as a function of the drive frequency. The motor bias voltage was kept constant at 0.5 volts. The amplitude of the modulation signal for the four cases was: x 0.2 volts, □ 0.4 volts, △ 0.5 volts, and * 0.6 volts. The gastrocnemius-soleus muscle was tonically active against the motor bias to maintain the zero angular foot position. The resonant frequencies for these cases were: 6.75 and 8 Hz at 0.2 volts modulation, 6 and 6.5 Hz at 0.4 volts modulation, 6.25 Hz at 0.5 volts modulation, and 6.25 Hz and 9 Hz at 0.6 volts modulation. (Subject GCA).

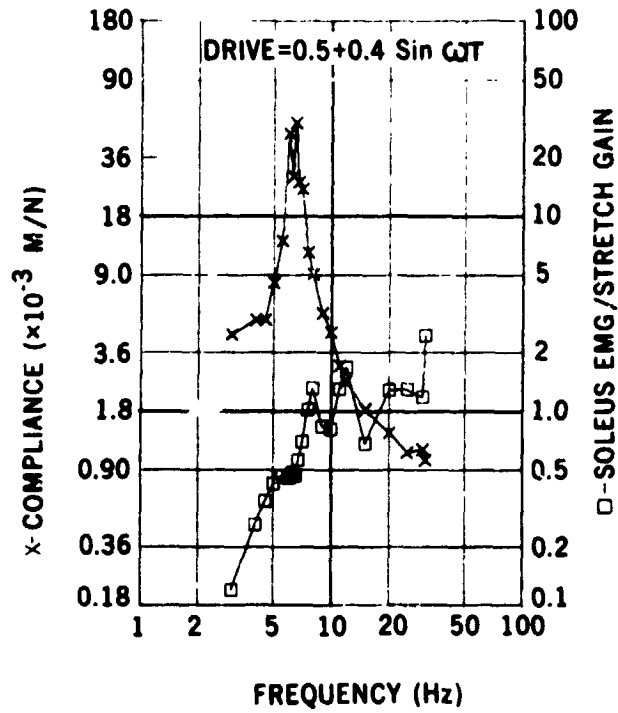


Figure 11

Effective compliance (X) and soleus EMG/stretch gain as a function of the input frequency. The motor drive was $0.5 + 0.4 \sin \omega t$. The compliance resonant frequencies are at 6 and 6.5 Hz. The soleus EMG/stretch gain peaks are at 8 and 12 Hz.

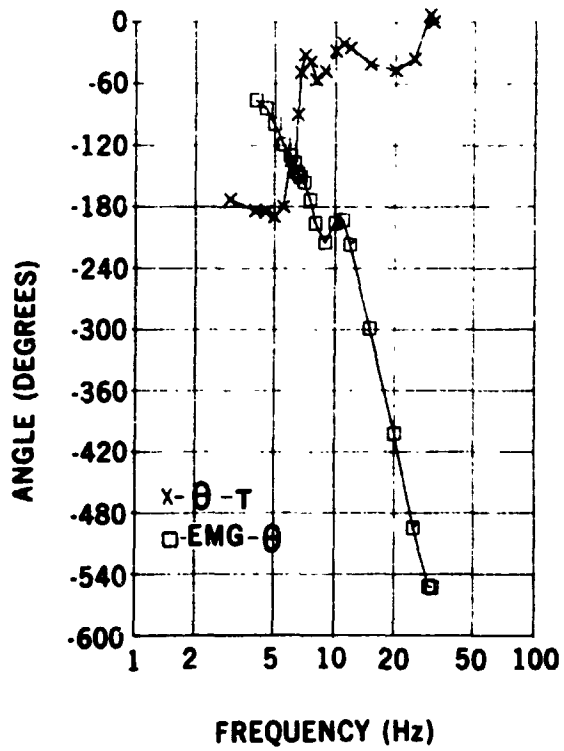


Figure 12

Phase angle between angular rotation and the applied torque (X) and between the soleus EMG and the angular rotation (□) as a function of the drive frequency. The motor drive was $0.5 + 0.4 \sin \omega t$. (Subject GCA)

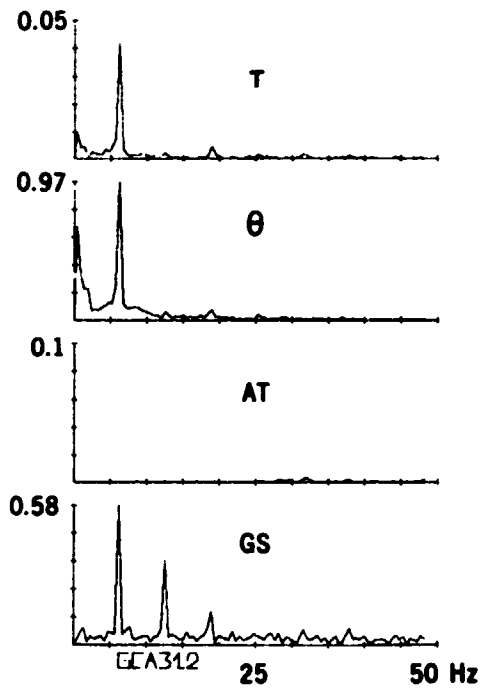


Figure 13

ier transform of the data for 2 seconds after the modulating motor signal is turned off as shown in Figure 4. The four traces from top to bottom are torque, angular rotation, EMG of anterior tibial and EMG of gastrocnemius-muscle. The frequency of the self-sustaining oscillation was 6.15 Hz.

SESSION III
CONTROLS AND DISPLAYS

Chairman: GARY P. BEASLEY

N75 33692

MANUAL CONTROL DISPLAYS
FOR A
FOUR-DIMENSIONAL LANDING APPROACH

James T. Silverthorn, 1st Lt USAF*
School of Aeronautics and Astronautics,
Purdue University, West Lafayette, Indiana

Dr. Robert L. Swain**
School of Aeronautics and Astronautics,
Purdue University, West Lafayette, Indiana

Six instrument rated pilots flew an STOL fixed base simulator to study the effectiveness of three displays for a four-dimensional approach. The three examined displays were a digital readout of forward position error, a digital speed command, and an analog display showing forward position error and error prediction. A flight director was used in all conditions. The feedback laws were designed using a combination of optimal and manual control theories. All test runs were for a "typical" four-dimensional approach in moderate turbulence that included a change in commanded ground speed, a change in flight path angle, and two standard rate sixty degree turns. Use of the digital forward position error display resulted in large overshoot in the forward position error. Some type of lead (rate or prediction information) was shown to be needed. The best overall performance was obtained using the speed command display. This display also received the best Cooper-Harper rating. It was demonstrated that curved approaches can be flown with relative ease. While four-dimensional approaches were described as difficult, the pilots were able to fly the approaches with sufficient accuracy to warrant further study.

*PhD Candidate
(Presently with Air Force Avionics Lab, Wright-Patterson AFB)

**Professor and Associate Head

PRECEDING PAGE BLANK NOT FILMED

SYMBOLS

U	Forward Speed (m/sec)
γ	Flight Path Angle (rad)
θ	Pitch Angle (rad)
α	Angle of Attack (rad)
β	Sideslip Angle (rad)
$\dot{\psi}$	Turn Rate (rad/sec)
ψ	Heading Angle (rad)
e_x	Forward Position Error (m)
e_y	Lateral Position Error (m)
e_z	Vertical Position Error (m)
δ_e	Elevator Deflection (rad)
δ_e^*	Flight Director Pitch Command
δ_a	Aileron Deflection (rad)
δ_a^*	Flight Director Roll Command
δ_t	Thrust Input (newtons)
δ_t^*	Speed Command
ω	Undamped Natural Frequency (rad/sec)
ζ	Damping Ratio
1/T	(Time Constant) ⁻¹ (rad/sec)
σ	Standard Deviation
g	Acceleration of Gravity (m/sec ²)

Subscripts

r	Reference Variable
e	Error Variable
p	Phugoid Mode
sp	Short Period Mode
dr	Dutch Roll
hp	High Pass Filter
u_g	Forward Gust
v_g	Lateral Gust
w_g	Vertical Gust

INTRODUCTION

The Microwave Landing System (MLS) will set the stage for three and four dimensional (4-D) approaches. This guidance system provides the means for noise abatement, wake avoidance, fuel savings, and increased airport capacity. This is because the landing approach can be altered from the present straight in approach to one that includes turns, changes in flight path angle, and changes in speed. Trajectories can be designed so that small aircraft can avoid the wake of larger craft; slower aircraft can "capture the beam" closer to the runway; and an added dimension to safety minimums can be incorporated.

This study looks at the practicality of a pilot flying a four dimensional approach. It attempts to answer the questions "How well can a pilot fly a 4-D approach?" and "Which of the displays examined results in the best performance?" Three-dimensional and 4-D approaches have been examined by other researchers, but most were concerned with synthesizing a trajectory and then seeing how well an autopilot could fly it (references 1-4). A limited number of studies have been directed toward pilot in the loop simulation. Several researchers have examined pilot tracking performance using a pictorial map or situation display while flying curved approaches. Such displays have become increasingly attractive with the development of computer generated graphics. Baty (reference 5) looked at the effect of prediction and map orientation on tracking performance during a 3-D approach. This display concept can also be extended to 4-D approach. The work by Kreifeldt and Wampe (reference 6) can also provide information about 4-D tracking performance. Three pilots flying STOL aircraft were required to merge with two other aircraft and cross an approach point at 30 second intervals. Each pilot was presented with an Air Traffic Situation Display showing all aircraft in the terminal area. The curved approaches and time interval control, while not purely 4-D in formulation, produce 4-D like trajectories. All these experiments demonstrate that a pictorial map display could be the answer for 4-D guidance. Anderson, Will, and Grantham (reference 7) performed a 4-D approach simulation where time (forward position) error and speed error are displayed digitally to the pilot. They found the pilots performed satisfactorily but their results were somewhat limited. The intent of Cunningham and Swaim (reference 8) was to use manual and optimal control concepts to design flight director gains for 4-D guidance. Pilot models were used to validate the design. This present study is, conceptually, a continuation of their work. Three displays are examined in terms of pilot tracking performance and preference in flying a 4-D approach. One display is a digital readout of forward position error (situation information only) and represents the lowest level of sophistication. The second display is a speed command display and is conceptually similar to a flight director. The third is an analog display showing situation and prediction information on a CRT. It would be the most difficult display to implement on an aircraft.

FOUR DIMENSIONAL APPROACH

One way to define a four dimensional approach is to specify where the aircraft should be as a function of time. This establishes a reference trajectory. Figure 1 is a four dimensional approach because the aircraft should be at each particular point on the trajectory at a particular time. The time function is determined by the reference velocity vector (the velocity time history the aircraft is desired to follow). This is done by specifying a reference forward speed (U_r), flight path angle (γ_r), and turn rate ($\dot{\psi}_r$). Error variables are then defined as the difference between the aircraft and the reference variable. That is:

$$\begin{aligned}U_e &= U - U_r \\ \gamma_e &= \gamma - \gamma_r = (\theta - \alpha) - \gamma_r \\ \dot{\psi}_e &= \dot{\psi} - \dot{\psi}_r\end{aligned}$$

Three position errors result from this reference trajectory. Forward position error (e_x), lateral position error (e_y), and vertical position error (e_z) are each the distance the aircraft is ahead of, to the right of, and below where it should be. The differential equations describing these variables are:

$$\begin{aligned}\dot{e}_x &= U_e = U - U_r \\ \dot{e}_y &= U \cdot (\psi_e + \beta) = U \cdot (\psi - \psi_r + \beta) \\ \dot{e}_z &= -U \cdot \gamma_e = U \cdot (\alpha - \theta + \gamma_r)\end{aligned}$$

where α , θ , and β are the aircraft angle of attack, pitch angle, and sideslip angle, respectively.

AIRCRAFT

The aircraft modeled in this study is the Breguet 941, a four engine turboprop, blown flap, STOL aircraft. It has been examined by McDonnell Douglas and is considered representative of future STOL aircraft.

Linearized aerodynamics are used to simulate the equations of motion. Small perturbations about some trimmed condition are assumed. Linear differential equations for these perturbation variables are then obtained by neglecting all higher order terms in the complete nonlinear equations. The trimmed condition assumed was a landing approach at 60 knots (100 ft/sec; 30.5 m/sec) on a $-7 \frac{1}{2}$ degree flight path with flaps deflected 98 degrees.

This aircraft is characterized by its low damping in the dutch roll and phugoid modes and an overcritically damped (two real roots) short period mode. A yaw damper is implemented to improve the dutch roll characteristics.

The equations used in this simulation, including the yaw damper, produce the following eigenvalues:

longitudinal	lateral
$\omega_p = .27 \text{ rad/sec}$	$\omega_{dr} = .81 \text{ rad/sec}$
$\zeta_p = .23$	$\zeta_{dr} = .53$
$1/T_{sp1} = 1.02$	$1/T_1 = .16$
$1/T_{sp2} = .80$	$1/T_2 = .66$

The forward, normal, and lateral gusts are simulated by gaussian white noise passed through first order low pass filters. The RMS level for these gusts is given by:

$\sigma_{u_g} = 7.5 \text{ ft/sec}$	$\sigma_{v_g} = 7.5 \text{ ft/sec}$	$\sigma_{w_g} = 5.0 \text{ ft/sec}$
$= 2.28 \text{ m/sec}$	$= 2.28 \text{ m/sec}$	$= 1.53 \text{ m/sec}$

The primary inputs available to the pilot are elevator and aileron deflections using a control stick and power changes using a throttle lever. Rudder pedals are also present but were not used to any great extent by the pilots. Because of the multi - airspeed, multi - flight path angle trajectory that is characteristic of a four dimensional approach (Figure 1), a flap change is required. The Breguet 941 flies the beginning portion of this approach with flaps deflected 75 degrees and transitions to 98 degrees flaps at the time of descent. To provide for this change, a two position flap switch is located in the simulator. Flap actuator dynamics are represented by a first order lag with a time constant of 3 seconds.

SIMULATOR DESCRIPTION

A photograph of the simulator is shown in Figure 2. The primary variables displayed are attitude and flight director commands on an attitude director indicator (ADI); vertical and lateral position errors on conventional ILS needles; forward position error using a digital readout; speed commands using a digital readout; and forward position error with error prediction on an analog display. These last three displays are the experimental variables for this study. In addition, the instrument panel includes indicators for airspeed, vertical velocity, compass heading, and angle of attack, along with an altimeter, tachometer, and needle-ball.

The feedback gains for the flight director were obtained using a combination of optimal and manual control theories. Optimal control was first used to find the gains that produced good step response and small deviations due to gusts. The gains were then adjusted so that the transfer function (δ^*/δ_e) (where δ^* is the flight director elevator or pitch command and δ_e is the pilot's elevator input) demonstrates the desired "K/s" behavior in the crossover region. This seems to have been an

effective technique because it resulted in favorable comments concerning the flight director from several of the pilots. The flight director aileron (roll) commands were obtained using the same technique. The feedback gains that resulted are:

$$\delta_e^* = -.0046e_x - .100 \dot{e}_x - .0443e_z - .082\dot{e}_z + 3.5\Theta_{hp} + 4.0\dot{\Theta}$$

$$\delta_a^* = -.0043e_y - .0722\dot{e}_y - 2.0 \phi_e - 2.4\dot{\phi} - 1.7\dot{\Psi}_e$$

where: $\Theta_{hp} = \{s/(s + 1)\} \cdot \Theta$; high pass (wash out) filter

$$\phi_e = \phi - \phi_r = \phi - U \cdot \Psi_r/g; \phi \text{ is roll angle}$$

It should be noted that the elevator command includes feedbacks from both the vertical and forward position errors. The forward position error term results in a pitch down command when the aircraft is behind where it should be. This is intuitively correct for pitching down will result in less drag and the aircraft will catch up to its desired position.

ILS needles are used to display lateral and vertical position errors. The task was to keep these needles nulled, just as for a normal ILS approach, even though this was a curved approach.

The "Digital Forward Position Error" display, shown in Figure 3, is positioned directly above the ILS needles. A positive number indicates that the aircraft is behind where it should be and the pilot should speed up. The display is incremented in steps of 10 feet (3.05 m) with a maximum of +2000 feet (+710 m) and is updated once per second.

A digital readout was used for three reasons. First, a DME is displayed digitally, and while a DME does not give position error, it does refer to a distance measurement in the forward direction. Secondly, today it seems that an increasing number of instruments are being implemented with a digital readout. And finally, a person can detect slow changes on a digital readout better than on an analog scale. This point needs explaining. Usually it is assumed that a digital readout is a poor source of rate information. This is true when the numbers are changing rapidly. But when the numbers are changing very slowly, as they should be if the pilot is making gradual changes, then I believe a digital display is a good source of rate information. For example, the pilot looks at his display and it says "+250." He scans back and if it says "+260" or "+270" he knows the approximate rate of change. When a pilot scans an analog display he can not detect such a small change as readily. It is difficult for an analog display to have both high sensitivity and a large dynamic range.

The "Digital Speed Command" display is shown in Figure 4. It gives speed commands just as the flight director gives pitch and roll commands. Furthermore, just as one should try to null the flight director, one should also try to null the speed command. It too is updated once per

second. In addition to the three reasons presented above, a "digital" display of speed command is desirable because it reinforces the correspondence between forward position error and speed command. In both cases a positive number means "catch up." Furthermore, a digital speed command avoids a problem that could develop using an analog version. The original plan was to use a third cue on the flight director, similar to the collective pitch command for helicopters. One would naturally expect this cue to move upward when additional power is commanded (throttle forward). The flight director pitch command moves upward for a pitch up command (stick back). This means the throttle would go forward and the stick back when the two cues went upward. The problem was avoided by making the speed command cue a digital command.

The feedback gains for the speed (throttle) command were designed in conjunction with the flight director pitch command using the same techniques. The transfer function (δ_t^*/δ_x), where δ_t^* is the speed command (throttle command) and δ_x is the pilot's throttle input, was designed to have a "K/s" behavior in its crossover region. Unlike the elevator crossover frequency of around 3 rad/sec, the throttle command has a crossover frequency of about .08 rad/sec. This lower crossover frequency is due to the slow response in the forward direction and results in less need for rapid throttle activity. The feedback law for the speed command is:

$$\delta_t^* = 730.e_z + 584.\dot{e}_z - 175.e_x - 1985.\dot{e}_x$$

The final display is the "Forward Position Error with Prediction." Shown in Figure 5, it is presented on a CRT directly below the ADI. An aircraft symbol is fixed in the center with a box showing where the aircraft should be. That is, if the box is ahead, then the aircraft is behind where it should be. Just as with the ILS needles, where the pilot flies to the needles, the pilot should fly to the box. Prediction (or rate) information is provided by the line extending from the aircraft symbol. The tip of the line represents where the aircraft will be with respect to the box in 30 seconds. If the rate of change of forward position error (e_x) is positive then the line will point forward. If the rate of change is negative, then the line will point backward. The idea is to have the line just touching the box. By doing this, the aircraft will catch up (or slow down) to where it should be in 30 seconds. This was found to be a good rate of response.

Finally, some description should be made of the autopilot used in this study. The autopilot provides a baseline for the pilot performance evaluation. There are many advantages of keeping the pilot in the loop. The question is, how much do you lose in terms of tracking accuracy by keeping him in the loop. This is answered by comparing the pilots' performance to that of an autopilot.

The autopilot design used for this study included elevator, throttle, and aileron inputs. Rudder inputs were also provided by an aileron-rudder interconnect. The feedbacks for these controls were almost identical to

those of the flight director and speed commands. The autopilot gains were in fact the gains resulting from the preliminary design stage, prior to adjusting to obtain a "K/s" behavior.

EXPERIMENT

This study attempts to answer the following questions. Which of the three displays examined results in the best pilot performance? What are the advantages and disadvantages of each display? How well can pilots perform using these displays compared to an autopilot? How difficult is it to fly a four dimensional approach?

The three displays discussed previously were used to answer these questions. They are:

Display

- D₁ - Digital Forward Position Error (Figure 3)
- D₂ - Digital Forward Position Error and Digital Speed Command (Figure 4)
- D₃ - Digital Forward Position Error and Forward Position Error with Error Prediction (Figure 5)

In all cases the flight director provided pitch and roll commands. In short, display D₁ is situation information only and represents a minimum addition to existing equipment. Display D₂ is situation with speed command and display D₃ is situation with prediction information.

Six instrument rated pilots performed in this study. Their experience varied from private, military, to commercial. The average total flight hours surpassed 1800 hours. A detailed description of the simulator, each display, the task, and the purpose of the experiment was first distributed to each pilot. The task was described as "continuously maintain the three position errors e_x , e_y , e_z as close to zero as possible." They were instructed to consider 300 feet (91.5 m) of forward position error to be of equal severity as two dots (80 feet; 24.4 m) of vertical error.

Each pilot spent from one to two hours getting acquainted with the simulator. Following this practice, one hour sessions were conducted using each of the displays. The order the displays were presented was varied to include each possible combination and is shown in Table 1. The first twenty minutes of each hour session was spent practicing with the particular display being examined. The next fifteen minutes the pilot flew at least five runs on a typical four dimensional approach. Maximum deviations of the three position errors were recorded as a means of determining his learning curve. When it appeared that the pilots performance reached a plateau, one additional run was made on the actual test trajectory (Figure 1). Then the six actual data runs were performed.

The pilot was given about ten seconds to get "in the loop." Data recording then began when the pilot had essentially zeroed out all the position errors that had accumulated. The researcher gave verbal instructions to the pilot at ten seconds into the data recording to "slow down to 60 knots" and sixty seconds to "start your descent and lower your flaps." At 100 seconds the run was completed.

During the actual test runs the three position errors were sampled ten times per second and converted to digital words. The root mean square (RMS) of each of these position errors was then computed off - line. Because the analysis was done after the session was over, no immediate results were available to the pilot. But because of the digital readout of forward position error, he was always aware of how well he was doing.

Each pilot was given a questionnaire at the completion of the experiment. It requested he list the advantages and the disadvantages of each display, any undesirable features of the simulation, and to assign a Cooper - Harper rating to each display.

RESULTS

The tracking performance in the forward, vertical, and lateral directions using the three displays is shown in Figure 6. Also shown is the performance with the autopilot engaged. The diamond represents the mean RMS position error and the dashed lines extend to the one sigma deviations. Analysis of variance was performed on each channel (forward, vertical, and lateral) independently and is shown in Table 2. The autopilot performance was not included in these analyses.

The differences in performance among the displays in both the forward and vertical directions were statistically significant. Examining the marginal means (Table 3) indicates that in the forward direction displays D_2 and D_3 were each significantly better than D_1 . In the vertical direction, D_2 was found to be better than D_1 or D_3 . While D_3 appears to be better than D_1 , the difference was not statistically significant. The above indicates that the pilots do equally well with displays D_2 and D_3 in controlling forward position error, but D_2 is superior in controlling vertical position error. In both cases, D_1 is the worst.

Both D_2 and D_3 are used primarily to control forward position error. The fact that no difference was found in the forward direction but a significant difference was found in the vertical direction is interesting. There are two possible explanations for this D_2 - D_3 difference. One is that the pilots were able to scan and interpret D_2 faster than they could D_3 . As a result the pilots could spend a greater percentage of their time following the ADI when D_2 was present than when D_3 was present. The closer one follows the flight director the smaller the excursions in vertical position error. This explanation is substantiated with pilot comments. Pilot P_1 stated that ". . . with the prediction display (D_3),

I found myself wanting to return to it after each scan. By diverting attention from the attitude indicator it creates a dangerous situation." Pilot P₃ mentioned that the position error with prediction display (D₃) promoted "instrument fixation." And finally, pilot P₄ stated that the digital speed command (D₂) required the least amount of scan time. This is in spite of the fact that display D₂ is located far to the left and requires a conscious effort by the pilot to scan. Display D₃ is located directly below the ADI. While D₃ is located where it should, D₂ is somewhat out of the field of view.

This difference in vertical position error can also be attributed to the digital speed command (D₂) containing terms involving forward and vertical position errors. Display D₃ contains no information concerning vertical position error. As a result, the pilots using D₂ are making throttle changes based on both vertical and forward position error whereas with D₃ the power changes are probably due to forward position error only. The actual reason for this difference in performance is quite likely a combination of these two explanations.

Significant differences were found among the pilots in all three position errors. This reflects both the tracking proficiency and conscious effort of the pilots. That is, some pilots were content with a slight position error while others tried hard to zero out any error.

A significant interaction between pilots and displays occurred in the forward and vertical directions. It was shown above that D₂ is generally superior to D₃. This interaction indicates that this generalization is not true for all the pilots. Two of the six pilots had a lower mean RMS vertical position error with D₃ than with D₂.

The pilots were asked to assign to each display a Cooper - Harper rating for the 4-D landing approach task with moderate turbulence and the aircraft as simulated. The means and standard deviations of these ratings is shown in Figure 7. Display D₂ required minimal to moderate pilot compensation; D₃ required moderate to considerable compensation; and D₁ required extensive compensation. This result is consistent with the tracking performance just presented. That is, D₂ is somewhat better than D₃ which is much better than D₁.

Another important criterion for determining the "best" display is the pilots' preferences and criticisms about the displays. In response to the question, "Compare the difficulty of flying this trajectory using the three displays with the difficulty of flying a conventional ILS approach," the pilots answers centered around:

Using display D₁ = more difficult

Using display D₂ = about the same

Using display D₃ = slightly more difficult

In addition, the pilots gave the following ratings and comments of the three displays:

Display D_1

- (1) Five pilots liked D_1 the least and thought they tracked worst with it.
- (2) "Amount of correction required is hard to determine."

Display D_2

- (1) Five pilots liked D_2 the best and felt they tracked best with it.
- (2) "Very useful"
- (3) "Definite advantage - gives good rate information and requires no interpretation" (stated by two pilots)

Display D_3

- (1) Four pilots thought D_3 was difficult to learn.
- (2) "Provides good rate information but not as easy to interpret and learn."
- (3) "Occasionally confusing"
- (4) "Enjoyed figuring out my own corrections from vector."

Referring to Figure 6, the autopilot performed approximately twice as well as the pilots in tracking the beam. Furthermore, the variation in autopilot performance is less than the pilots. This variation is represented by the small standard deviation or the consistency in performance as presented in Table 4. It should be reiterated that the purpose of this study was not to show that an autopilot is needed or not needed. The purpose was to see how well pilots could fly a four dimensional approach. The autopilot was used to provide a baseline to establish the difficulty of the task. In addition, by presenting the performance using an autopilot, one can observe how much tracking performance is lost by having the pilot in the loop.

While the autopilot performance seems to overshadow the pilots' performance, close examination of the position errors reveals how well they did. The mean RMS lateral position error (Table 3) was only 13.7 meters (45 feet) and the standard deviation only 3.9 meters (12.9 feet). These numbers become more impressive when considering that the primary difficulty in the task was controlling forward position error. Presumably, if this had been a 3-D approach where the pilot does not control forward position, the lateral performance would have been even better. In addition, this was achieved with no map display showing the trajectory nor with any cue indicating the start of a turn. The only lateral information available was lateral position error displayed on the localizer needle and roll flight director commands. This indicates the precision a pilot can fly a curved approach. A map display showing the trajectory and the runway is very

desirable however, to provide the pilot the terminal area situation information he needs.

The pilots were also very effective in controlling forward position error. The mean RMS forward position error was 25.5 meters (83.8 feet) and the standard deviation was 10.9 meters (35.6 feet). Furthermore, the maximum forward distance any pilot was off in 108 runs was only 113 meters (370 feet). With a forward speed of 60 knots (100 ft/sec; 30.5 m/sec) this distance corresponds to a 3.7 second time slot error. The mean time slot error was less than one second. This is much better than the accuracy required to make four dimensional approaches feasible.

The pilots found that following the flight director commands was sufficient to maintain small vertical and lateral position errors. As a result they scanned the ILS needles infrequently. This further substantiates the possibility for three and four dimensional approaches under manual control.

CONCLUSIONS

The pilots performed best when they were presented speed commands. The digital speed command display was given the best pilot rating and highest preference. The forward position error with prediction display was also effective, but not to the same extent as the speed command display. Some type of map display showing the trajectory, runway, position error and prediction is nevertheless desirable because it would provide the pilot the terminal area information he needs. Both a speed command display and a map display seem to be the best choice. In this way the pilots would have the control advantages of speed commands and the situation information of a map.

Curved (3-D) approaches appear to be fairly simple, at least from a control point of view. The pilots were able to stay very close to the desired trajectory. This is especially true in the lateral direction. The pilots agreed that controlling lateral position error was the easiest part of the task.

When rate information was available, the pilots were also able to keep the forward (time) error small. This supports the concept of four dimensional approaches. Pilot workload, maximum control deflections and state variable (pitch angle, angle of attack, and airspeed) excursions all need to be examined before the feasibility of four dimensional approaches can be fully ascertained.

When rate information was not available (digital forward position error display only), the pilots' performance deteriorated. There was large overshoot in forward position error because the pilots overcorrected. Their control actions were too late and too large due to the aircraft slow response and low damping in the forward direction. Some type of aiding (rate or prediction information) is needed.

REFERENCES

1. Farrington, F. Goodson, R., "Simulated Flight Tests of a Digitally Autopiloted STOL - Craft on a Curved Approach with Scanning Microwave Guidance," Paper 15-2. Proc. 1973 Joint Automatic Control Conference. Ohio Univ., Columbus, Ohio, June 1973, p 437 - 448.
2. Lee, H. Q., McLean, J. D., Erzberger, H., "Guidance and Control Techniques for Automated Air Traffic Control" Journal of Aircraft, Vol. 9, No. 7, July 1972, p 490 - 496.
3. Erzberger, H., Pecsvardi, T., "4-D Guidance System Design with Application to STOL Air Traffic Control" Paper 14-1. Proc. 1972 Joint Automatic Control Conference. Stanford Univ., Stanford, Calif., August 1972, p 445 - 454.
4. Foudriat, E. C., "Aircraft 4-D Constant Velocity Control System" Journal of Aircraft, Vol. 11, No. 6, June 1974, p 326 - 333.
5. Baty, D. L., "An Evaluation of a Predictor Used with Two Different Aircraft Map Display Orientations" Paper 17. 10th Annual Conference on Manual Control. Wright-Patterson AFB, Ohio, April 1974, p 397 - 426.
6. Kreifeldt, J. G., Wempe, T. E., "Future Terminal Air Traffic Management Concepts" Paper 21. 10th Annual Conference on Manual Control. Wright-Patterson AFB, Ohio, April 1974, p 477 - 501.
7. Anderson, W. W., Will, R. W., Grantham, C. "Study of Aircraft - Centered Navigation, Guidance and Traffic Situation System Concept for Terminal - Area Operation." NASA TN D-6992, November 1972.
8. Cunningham, T. B., Swaim, R. L., "Design of a Manual Control System for a STOL Aircraft on Microwave Landing System Curved Approaches" Paper 28. 10th Annual Conference on Manual Control. Wright-Patterson AFB, Ohio, April 1974, p 641 - 666.

Table 1 Order of Presentation of Displays

Pilot	Session		
	1	2	3
P ₁	D ₂	D ₁	D ₃
P ₂	D ₃	D ₂	D ₁
P ₃	D ₁	D ₂	D ₃
P ₄	D ₂	D ₃	D ₁
P ₅	D ₃	D ₁	D ₂
P ₆	D ₁	D ₃	D ₂

Table 2 Analysis of Variance

Source of Variation	Deg of Freedom	RMS Forward Position Error		RMS Vertical Position Error		RMS Lateral Position Error	
		Mean Square	F Ratio	Mean Square	F Ratio	Mean Square	F Ratio
Displays (D)	2	9000.	9.2**	744.	15.5**	79.	<1
Pilots (P)	5	4900.	5.0**	226.	4.7**	1720.	19.8**
DxP	10	2080.	2.1*	96.	2.0*	79.	<1
Within Replicates	90	972.		48.		87.	

* Significant at .05 level

** Significant at .01 level

Table 3 Summary of Results

	RMS Forward Position Error		RMS Vertical Position Error		RMS Lateral Position Error	
	Meters Mean	(Feet) Std Dev	Meters Mean	(Feet) Std Dev	Meters Mean	(Feet) Std Dev
Display D ₁	31.1 (102.0)	12.1 (39.6)	9.7 (31.8)	2.8 (9.2)	13.2 (43.4)	3.5 (11.5)
Display D ₂	22.7 (74.6)	10.4 (34.2)	6.9 (22.8)	1.8 (6.0)	13.9 (45.6)	3.0 (10.0)
Display D ₃	22.8 (74.8)	10.0 (32.7)	8.7 (28.6)	2.4 (7.9)	14.1 (46.3)	5.0 (16.3)
Autopilot	13.7 (45.0)	4.1 (13.5)	3.7 (12.0)	0.3 (1.0)	5.9 (19.3)	0.2 (0.8)
Pilot P ₁	27.9 (91.4)	12.1 (39.8)	8.5 (27.8)	2.2 (7.2)	14.8 (48.5)	2.4 (7.9)
Pilot P ₂	16.6 (54.3)	5.2 (17.1)	7.3 (23.8)	1.8 (6.0)	13.2 (43.4)	2.5 (8.3)
Pilot P ₃	25.9 (85.0)	11.8 (38.6)	7.8 (25.6)	2.5 (8.3)	9.2 (30.1)	1.7 (5.7)
Pilot P ₄	24.5 (80.5)	8.8 (28.9)	7.9 (26.0)	2.1 (7.0)	13.0 (42.6)	2.4 (7.9)
Pilot P ₅	31.7 (103.9)	12.5 (40.9)	10.3 (33.8)	3.5 (11.6)	13.8 (45.4)	3.3 (10.7)
Pilot P ₆	26.8 (87.8)	12.1 (39.7)	9.0 (29.5)	2.4 (7.8)	18.4 (60.4)	3.9 (12.8)
Total	25.5 (83.8)	10.9 (35.6)	8.4 (27.7)	2.4 (7.8)	13.7 (45.1)	3.9 (12.9)

Table 4 Minimum and Maximum RMS Errors

	RMS Forward Position Error		RMS Vertical Position Error		RMS Lateral Position Error	
	Meters Min	(Feet) Max	Meters Min	(Feet) Max	Meters Min	(Feet) Max
D ₁	13.7 (45)	60.1 (197)	3.7 (12)	16.5 (54)	7.6 (25)	22.2 (73)
D ₂	5.5 (18)	50.4 (165)	4.9 (16)	11.9 (39)	7.6 (25)	23.2 (76)
D ₃	8.9 (29)	54.4 (178)	5.2 (17)	16.5 (54)	6.4 (21)	29.3 (96)
Auto- pilot	8.9 (29)	18.6 (61)	3.0 (10)	4.0 (13)	5.5 (18)	6.1 (20)

Note: Minimums and maximums for D₁, D₂, D₃ are for 36 runs each
 Minimums and maximums for autopilot are 6 runs

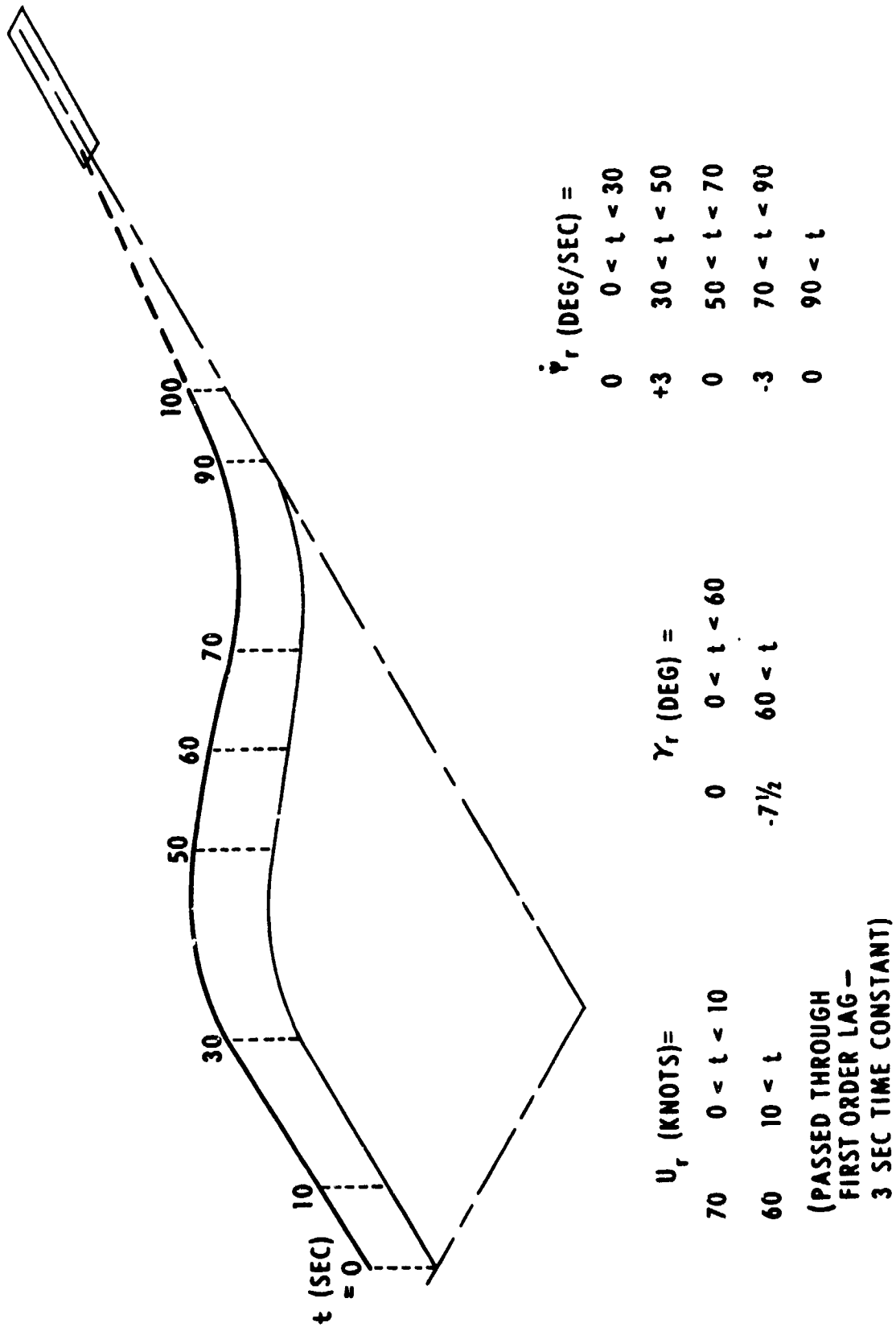


Figure 1 Four Dimensional Approach

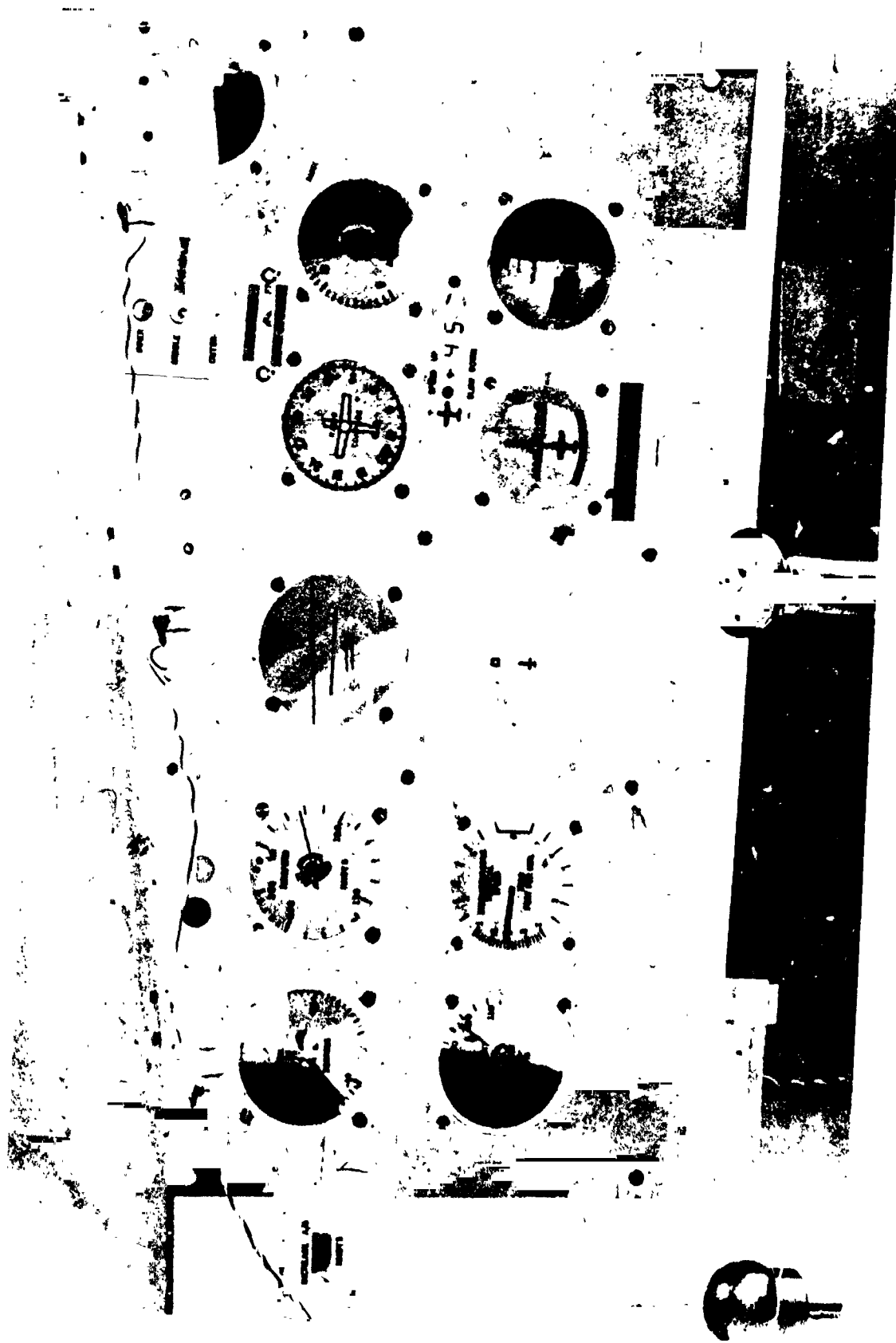


Figure 2 Cockpit Interior

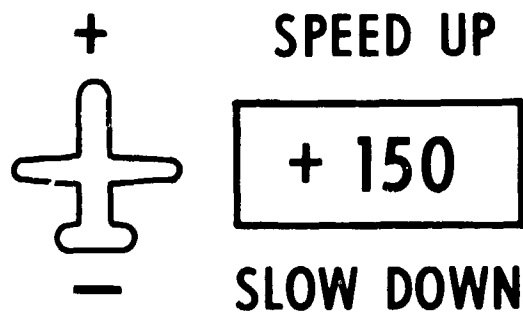


Figure 3 Digital Forward Position Error Display showing aircraft 150 feet behind reference trajectory

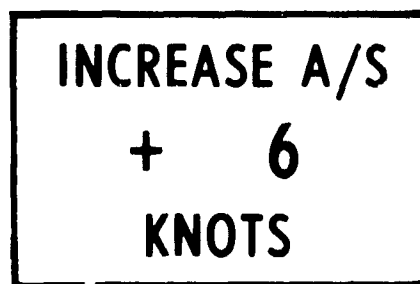


Figure 4 Digital Speed Command Display giving a "speed up by 6 knots" command

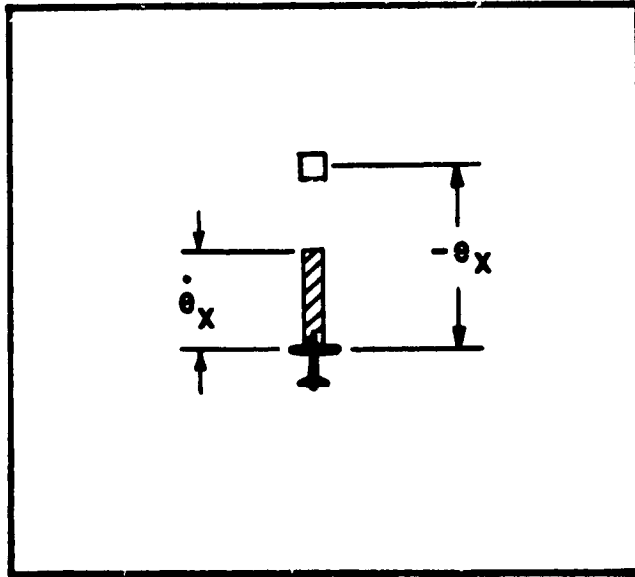


Figure 5 Forward Position Error with Prediction Display showing aircraft 150 feet behind reference trajectory and closing at the rate of 2.5 ft/sec

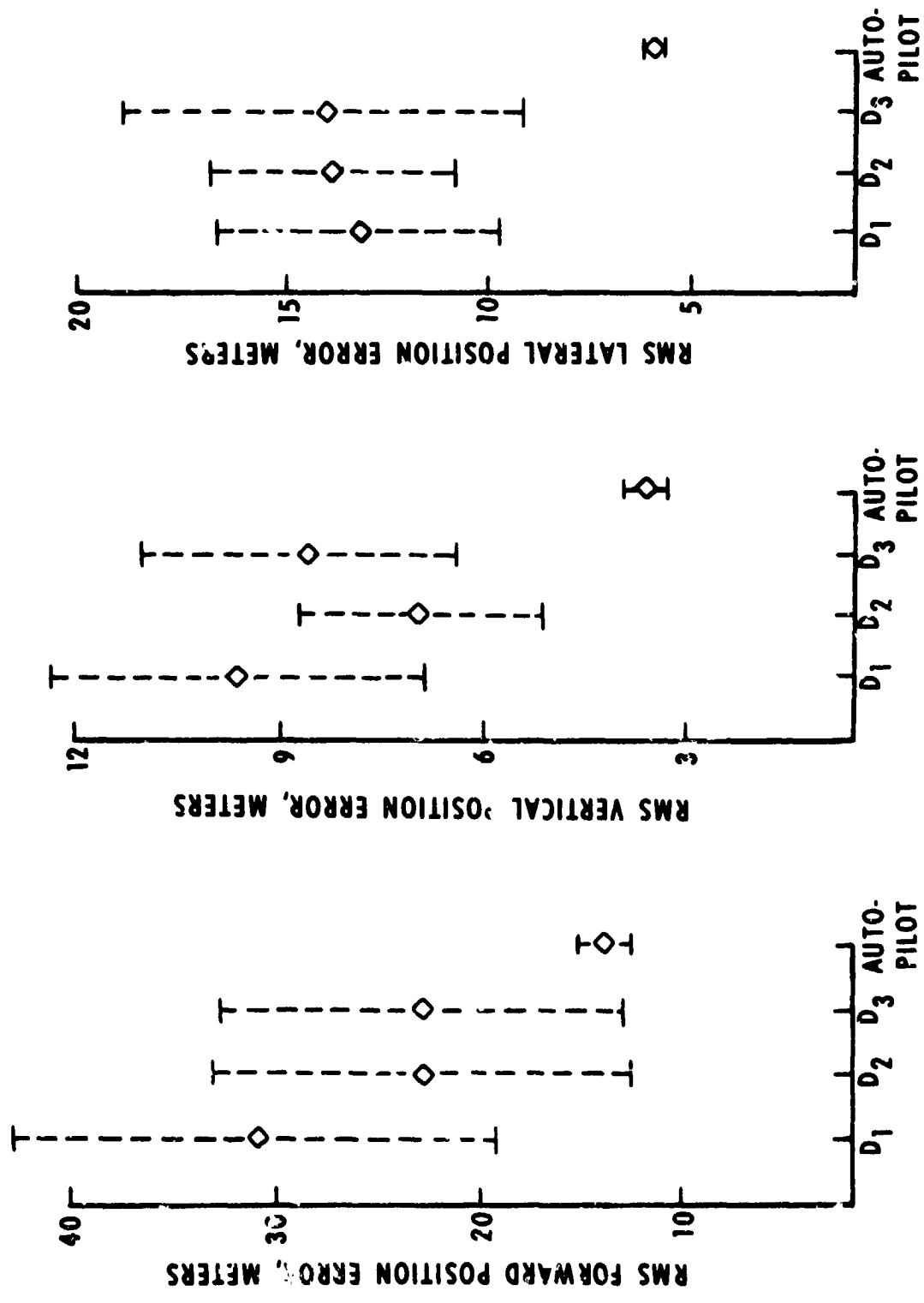


Figure 6 Pilot Performance for Each Display

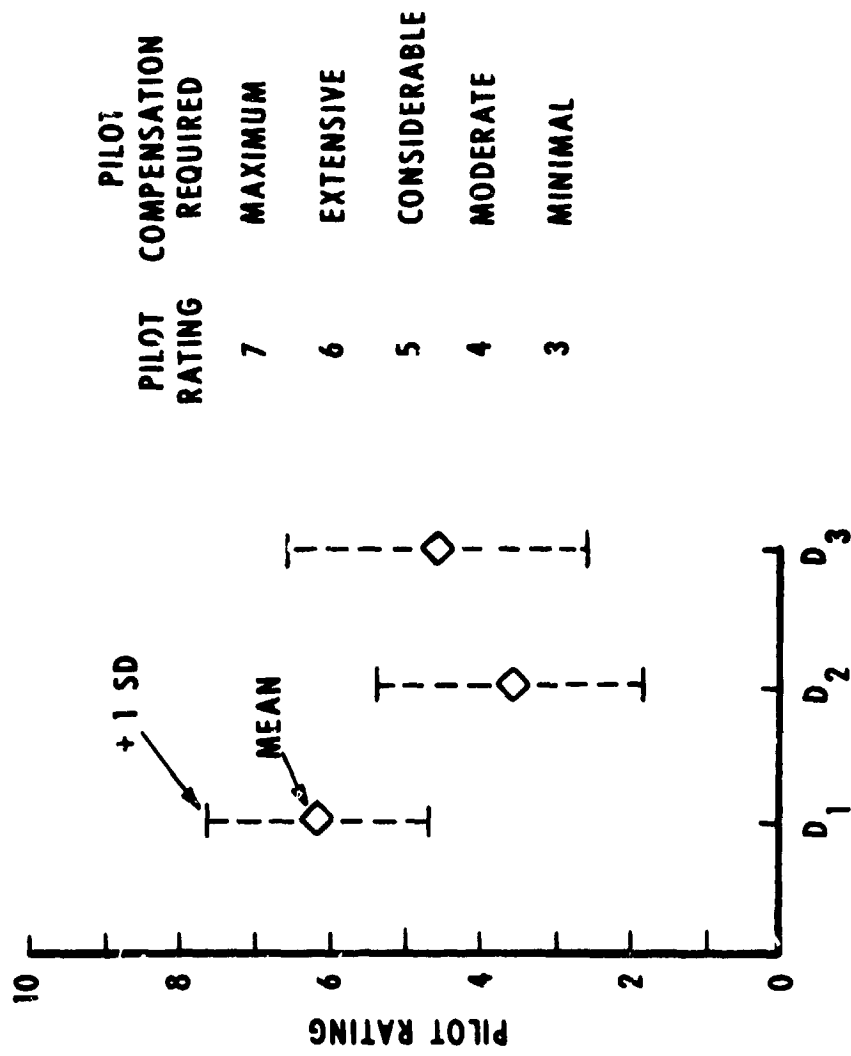


Figure 7 Cooper - Harper Ratings

N75 03693

SIMULATOR EVALUATION OF A PERSPECTIVE CLIPPED-POLE DISPLAY
AND A THRUST-VECTOR CONTROLLER FOR VTOL ZERO-ZERO LANDINGS

By M. R. Murphy and R. K. Greif

Ames Research Center, NASA, Moffett Field, CA 94035

SUMMARY

Five pilots participated in a simulator study to evaluate design features of a perspective clipped-pole display and a side-arm thrust vector controller for potential applications to VTOL zero visibility (zero-zero) landings.

The task was flown in a fixed-base, 3-degree-of-freedom, longitudinal simulation of a vectored lift-fan VTOL transport aircraft with variable, linearized aerodynamics, and consisted of a straight-in approach on a 10° approach slope, with optional hover and landing. The five pilots flew data runs with the basic perspective display, with the basic display plus digital airspeed, and with this latter combination plus digital altitude. The displays were presented on a CRT using digital vector techniques.

Objective measures were obtained for touchdown velocities and position, flight time, maximum thrust, and maximum deceleration; pilot opinion was also obtained. Analyses of objective measures by a t-test for related means showed significant learning effects, but did not show significant performance differences among display conditions. A mean longitudinal touchdown velocity of less than 4 knots, a mean vertical touchdown velocity of less than 1.22m/sec (4 ft/sec), and a mean longitudinal position error of approximately 15.24 m (50 ft), was attained during the final 10 trials of the experiment. The conclusion that adequate airspeed and altitude cues could be obtained from the glideslope and runway poles is supported by the absence of significant performance differences among display conditions. Both objective data and pilot opinion support the conclusion that the perspective clipped-pole display and thrust vector controller should be further researched for potential application to VTOL zero-zero landings.

INTRODUCTION

A future requirement for manual piloting of VTOL (Vertical Takeoff and Landing) aircraft in zero visibility (zero-zero) landings is assumed for three reasons: VTOL landing technology is at an early stage of development (ref. 1); the question of the capability to be provided for manual emergency takeover during potential future automatic landings has not been resolved; and manual control may result in more flexibility in operations than would fully automatic systems. Specific constraints for manual, zero-zero landing technology arise from the inherent absence of out-the-window visual contact and probable VTOL operational requirements such as: steep and/or curved approaches at decelerating speeds; highly precise energy management;

C-4

transition to hover; and high density, time-constrained flight environments. These projected operational requirements, in conjunction with the complex control requirements of VTOL aircraft, imply potentially high pilot workloads.

Based on the above considerations, a display concept (clipped-pole) and a control concept (thrust vector) were derived for potential application to VTOL zero-zero landing technology. The objectives of this study were to determine whether the display and control concepts should be further researched, and to evaluate specific design features of an implementation of these concepts.

DESCRIPTION OF DISPLAY

The display concept is based on the use of vertical poles, stroke-written on a CRT, to define a commanded approach slope, as is the SAAB pole-track display for the Viggen aircraft (ref. 2). The concept differs from that of the pole-track display in two important respects. First, the pole-track display presents a static perspective scene, while elements of the clipped-pole scene are clipped from view as they reach peripheral vision limits, as are real-world elements in a VFR flight. Second, the displayed view remains in true perspective relative to the changing position of the aircraft, and hence in relation to the pilot's eye-reference-point. Display elements were purposely kept simple; in addition to approach slope poles, only a runway outline, a horizon line, and constant-height runway edge poles were implemented in the display. The runway edge poles were added to provide a hover capability.

Figures 1 through 9 show views of the display during an approach and landing sequence. The digital presentation of indicated airspeed and altitude, shown at the top of the views, occurred only during a particular condition of the experimental design. The horizon is represented by the line at the top of the display; zero approach slope error is indicated when this horizon line and the imaginary line formed by the top of the approach slope poles are parallel. Figure 1 is a view of the display prior to approach slope capture and figures 2 through 5 show various approach slope error conditions during the approach, as indicated by the titles.

Figure 6 is a view taken just prior to transitioning to the guidance offered by the runway edge poles. When the pilot's eye is at 15.24 m (50 ft), the height of the runway edge poles, the horizon line is aligned with the tops of the poles. Figures 7 through 9, then, show a sequence below this point, ending near touchdown.

The 10° approach slope selected for this study intersected the runway at the runway centerpoint. Approach poles were spaced 76.20 m (250 ft) apart. The runway was 30.48 m (100 ft) wide and 152.40 m (500 ft) long. The 15.24-m (50 ft) high runway edge poles were spaced 30.48 m (100 ft) apart.

THRUST VECTOR CONTROLLER

A dual-action, left-hand controller was used for controlling thrust. The length of the controller arm commanded thrust magnitude and the arm angle commanded thrust angle. Controller arm angle and commanded thrust angle limits were 0° (controller forward to horizontal) to -120° (controller back to 30° past vertical). The controller, then, was like a miniature analog of the thrust vector. Figure 10 shows this controller in use. The pitch-attitude controller, shown being manipulated by the right hand, was not used in this experiment. Pitch attitude was stabilized at zero degrees for the neutral stick position, and the pilots were instructed to make all flight path corrections by the thrust vector controller.

METHOD

Simulation Facility and Task

The experimental task was flown in a fixed-base, 3-degrees-of-freedom, longitudinal (x, z, and θ) digital simulation of a vectored lift-fan VTOL transport aircraft with pitch attitude stabilization ($\omega_n = 2$ rad/sec, $\delta = 0.7$). The aircraft weighed 444,822 N (100,000 lb) and had a wing loading of 47788 N/m² (100 psf). The maximum available thrust-to-weight ratio was 1.5. Aerodynamics were linearized up to a stall angle of 20° . The engines had high bypass ratio ram drag characteristics and a first-order thrust response lag of 0.2 sec (to 63% steady-state). The pilot's eye-reference-point was 6.1 m (20 ft) forward of the center of gravity and 3.05 m (10 ft) above the ground at touchdown. Figure 11 shows the simulation chair cab and table 1 indicates the simplified equations of motion.

The task was to recover the aircraft from an initial idle thrust condition (decelerating aircraft), capture and fly the 10° approach slope, and decelerate and land at the center point of the runway pad. Hover was optional. Initial conditions for the task are indicated in table 2.

Experimental Design

Five pilots (2 commercial and 3 NASA) flew 60 data runs each, 30 during each of two sessions which were separated by a period of at least one day. After every block of 10 data runs, the pilots were given a rest period of 2 minutes. The 30 data runs on the first session for each pilot (blocks 1, 2, and 3) were flown with the basic perspective display and were intended to produce a plateau on the learning curve. The 30 data runs, comprising the second session for each pilot, were flown with the following display conditions: block 4, basic perspective display (a "refresher" of the first session); block 5, basic perspective display with a digital airspeed readout on the CRT; block 6, same as block 5 with the further addition of a digital altitude readout on the CRT.

Data were recorded for obtaining the following performance measures:

- Longitudinal velocity at touchdown (U_{TD})
- Vertical velocity at touchdown (W_{TD})
- Longitudinal position at touchdown (X_{TD})
- Total time to fly the approach (TIME)
- Maximum thrust-to-weight ratio used during the task
- Maximum longitudinal deceleration

all primary performance measurements were made in nonmetric units.

Altitude versus range and airspeed versus range were plotted and displayed to the experimenter by the computer in real-time, as shown for a sample data run in figure 12. Since Figure 12 represents a completed run; it also shows a printout of an ID (pilot and run number) and the first four of the performance measures described above.

Pilot opinion of the display, the overall task, and the controller was obtained by use of the twelve questions shown in table 3.

Procedure

Training - The pilots were not trained to any criterion level prior to starting the 60 data runs. They were, however, permitted from one to three familiarization runs prior to starting the data runs.

Instructions - The purpose of the experimental conditions was explained to the pilots prior to the first experimental session. The initial conditions, the aircraft, display, and task descriptive information, and the task performance criteria were reviewed before each session and were available to the pilots on briefing sheets at all times. The stated task was to "recover the aircraft from the low thrust condition and capture the approach slope and to "fly down the approach path, decelerate, and land at the center of the pad with horizontal and vertical velocities as low as possible."

The stated task performance criteria or guidelines were (1) "low horizontal velocity at touchdown (preferably less than 10 kts)", (2) "low vertical velocity at touchdown (preferably less than 1.52 m/sec (5 ft/sec))", (3) "minimum longitudinal position error at touchdown", (4) "low elapsed time from glideslope capture to touchdown", and (5) "minimum glideslope tracking error". Tradeoffs between these criteria, or guidelines, were left to the individual pilots.

Data Handling - In addition to the data shown in figure 12, which was recorded on magnetic tape, angle of attack, vertical velocity, vertical acceleration, thrust angle, thrust, and throttle position in percent were recorded on a strip chart.

RESULTS

Objective Measures

Group means and standard deviations and individual means were computed and plotted for the six performance measures of interest, as shown in figures 13 through 18. Performance measures are plotted on the vertical

scale as a function of the 6 sequential trial block, (10 trials per block).

Figures 13 and 14 show that mean performance met preferred criterion values immediately for longitudinal velocity and at around 30 trials for horizontal velocity, at touchdown. A mean longitudinal touchdown velocity of less than 4 knots, a mean vertical touchdown velocity of less than 1.22 m/sec (4 ft/sec), and a mean position error of approximately 15.24 m (50 ft) (see Figure 15) was attained during the final 10 trials of the experiment. Figures 13 and 14 also show that the standard deviations for the two most important measures, longitudinal and vertical velocities at touchdown, improved throughout the six trial blocks and reached values of about 1 kt. and 0.30 m/sec (1 ft/sec), respectively.

The trends shown in Figure 16 for flight time (i.e., the apparent decreases in mean time and in standard deviation during the first three blocks and the apparent increase in standard deviation during the latter three blocks) possibly reflect strategy changes. Figures 17 and 18 show almost constant levels in maximum thrust-to-weight ratio used and in maximum longitudinal deceleration over the six trial blocks.

T-tests for related means were calculated between particular trial blocks for group means of these six performance measures to test for effects due to learning and to experimental conditions. For $p \leq 0.10$, no effects due to experimental conditions were demonstrated for any of the six measures. This was an expected result, under the assumption that adequate airspeed and altitude cues could be attained from the approach slope and runway edge poles (i.e., that the addition of the digital readouts would result in reported strategy changes rather than performance improvement).

Learning effects were tested by comparing the means of combined data for blocks one and two with that for blocks 5 and 6. Learning was significant at $p \leq 0.05$ for only longitudinal and vertical velocities at touchdown. Longitudinal position at touchdown shows a learning trend; however this trend was significant only for $p \leq 0.25$. From figures 13 and 14 it is obvious that learning is also strongly demonstrated by decreases in variability for longitudinal and vertical velocities at touchdown.

Figures 13 through 18 also show the individual performance means and standard deviations for the five pilots. The commercial pilots, number 2 and 4, were airline pilots with considerable experience in conventional aircraft but with only approximately 40 h experience each in helicopters. Initial touchdown velocities were high for the commercial pilots but consistent with NASA pilots at the end of the experiment. Apparent tradeoff strategies of the two commercial pilots in attaining this end performance are indicated in the flight time and maximum longitudinal deceleration measurements: each started with fast approaches of about 55 sec; pilot 4 gradually increased his flight time, reaching times of about 100 sec at the end of the experiment; pilot 2 gradually decreased his flight time but used maximum decelerations throughout the experiment that would almost certainly be excessive for commercial passengers. Initially and consistently excellent performance is shown for pilot 1, the NASA pilot having the most experience with vectored lift-fan VTOL concepts. All NASA pilots had considerably more VTOL experience than the commercial pilots.

Approach slope tracking performance was recorded, as shown in figure 12, but has not been analyzed. Approach slope tracking performance was consistently good and figure 12 shows a typical example.

Pilot Opinion

General - Pilot opinion of the display, the overall task, and the controller was solicited by the questionnaire shown in table 3. Explanations of specific comments were also solicited. All pilots indicated that the display gave a feeling of realism to the task and that the task was easy to learn. Workload was rated as medium to high, the landing phase generally receiving a rating of higher workload than the approach phase. One pilot indicated that lags in the response to commanded thrust changes, especially, when controlling vertical velocity, contributed to a higher workload; although power management requirements to accomplish a combined low approach time and effective transition for landing (deceleration, etc) was most generally cited as responsible for the high workload. Special strategies that were used by the pilots generally were devised to cope with this power management requirement.

Controller - Only three of the five pilots rated the controller as adequate; all pilots suggested improvements. Vector angle detents were suggested at 0° for hover and at selected positions for controlling lift and forward thrust. Vertical movements of the controller for precise changes in lift were reported to be difficult, and one pilot attributed pilot-induced oscillations (PIOs) in the vertical plane during landing to this difficulty. One pilot also suggested inclining the controller forward by approximately 20° . However all objections to the controller appeared to be correctable with minor changes in design and technique.

Altitude Cues - Pilots unanimously agreed that the approach slope poles gave adequate height cues during the approach but that the runway edge poles did not give adequate height cues during landing. Actually it was the inability to see a sufficient number of poles when over the landing point that was cited as the reason for this landing problem. Improved runway surface marking and extension of the poles beyond the end of the runway were suggested in order to improve landing performance.

The addition of a digital readout of altitude was not thought to alter either workload or accuracy during the approach; however, opinion was less unanimous with respect to the landing phase. Three pilots thought that the digital readout improved performance during the last few meters of altitude, enabling reduced vertical velocity at touchdown. The remaining two pilots did not think that the digital altitude readout affected their landing performance.

Airspeed Cues - There was general agreement that useful cues as to relative airspeed were obtained from the approach slope poles during the approach, although it was pointed out by two pilots that small changes in airspeed could not be perceived. Two of the pilots also thought that adequate airspeed cues could be attained from the runway edge poles during landing. Complaints and suggestions from the remaining three pilots indicated problems essentially identical to those for attaining altitude cues from the runway poles as discussed above.

All pilots thought that some improvement in performance was obtained by adding a digital readout of airspeed. Some specific reasons suggested for improved performance were: enabled better control of longitudinal velocity at touchdown, and enabled more precise planning for reduction of airspeed during transition to hover. One pilot did indicate, however, that

attempted use of the readout during the landing phase aggravated his problem with PIOs due to interrupting his concentration on the visual perspective scene.

CONCLUDING STATEMENTS

Touchdown performance exceeded the velocity criteria: mean longitudinal velocity was less than 4 knots, mean vertical velocity was less than 1.22 m/sec (4 ft/sec), and mean position error was about 15.24 m (50 ft) during the final 10 trials. The standard deviations for these final touchdown velocities were approximately 1 kt and 0.30 m/sec (1 ft/sec). No significant improvements in performance were evidenced through adding digital airspeed and altitude to the display. This finding and pilot opinion support the conclusion that adequate airspeed and altitude cues for accomplishing the task are obtained from approach slope and runway edge poles, although design improvements were recommended for runway edge poles and surface markings. The side-arm thrust vector controller was generally rated as adequate, although minor human engineering improvements were suggested. Power management requirements to accomplish a combined low approach time and effective transition for landing was cited as contributing to medium and high workload ratings. Further research on the display and controller is recommended.

REFERENCES

1. Beyer, R., Bondurant III, R. A.; Huddleston, J. H. F.; McGregor, D. M.; Sterk, F. J.; and Walters, D. J.: V/STOL Displays for Approach and Landing. AGARD Rept. 594, 1972.
2. Frieberg U: Basic Considerations about Scale One-to-One Head Up Displays. Paper presented at The Technical Symposium of the Society of Experimental Test Pilots, European Section, Luzern, 1971.

TABLE 1. - SIMPLIFIED EQUATIONS OF MOTION

$$\dot{q} = \left[C_m(\alpha) q_o \frac{g}{W/S} \frac{\bar{C}}{k^2} \right] + \left[\frac{M_\delta}{I_y} \delta + \frac{M_q}{I_y} q + \frac{M_\theta}{I_y} \theta \right]$$

$$\dot{u} = \left[\left(-C_D(\alpha) \cos \alpha + C_L(\alpha) \sin \alpha \right) q_o \frac{g}{W/S} \right] + \left[\frac{T}{W} \cos \alpha_T g \right] - \left[g \sin \theta + qw \right]$$

$$\dot{w} = \left[\left(-C_L(\alpha) \cos \alpha - C_D(\alpha) \sin \alpha \right) q_o \frac{g}{W/S} \right] - \left[\frac{T}{W} \sin \alpha_T g \right] + \left[g \cos \theta + qu \right]$$

where:

$$C_m = C_{m_o} + \left(\frac{C_m}{C_L} \right) C_L, \frac{C_m}{C_L} = -0.1$$

$$C_D = C_{D_o} + \frac{C_L^2}{\pi R}, C_{D_o} = .1$$

$$C_L = C_{L_o} + C_{L_\alpha} \alpha, C_{L_o} = 0, C_{L_\alpha} = 0.1 \left(\frac{R}{R+3} \right), R = 5$$

Note: brackets in equations of motion enclose aerodynamic forces and moments; propulsive, control and stabilization forces and moments; and gravity and coupling terms, respectively.

TABLE 2. - INITIAL CONDITIONS

Airspeed	= 100 kts
Altitude	= 0.305 km (1000 ft)
X-range	= 1.706 km (5600 ft)
Attitude	= 0°
Trim	= 10° angle-of-attack
Thrust magnitude	= minimum
Thrust angle	= 90°

TABLE 3. - EVALUATION QUESTIONNAIRE

1. Did display give a feeling of realism?
2. Was the task (easy, a little difficult, difficult) to learn?
3. Was workload (high, medium, low) after learning the task?
4. Did you use any special strategy?
5. Did flight path poles give an adequate height cue during approach?
6. Did runway poles give an adequate height cue for landing?
7. Did inclusion of a digital readout of altitude improve performance or workload?
8. Did flight path poles give an adequate airspeed cue during approach?
9. Did runway poles give an adequate airspeed cue for landing?
10. Did inclusion of a digital readout of airspeed improve performance or workload?
11. Was controller adequate?
12. Additional comments:



Fig. 1. Prior to Capture.

Fig. 2. Below Approach Slope.



Fig. 3. Above Approach Slope.

Fig. 4. Near-Zero Approach Slope Error.



Fig. 5. - Below Approach Slope.

Fig. 6. - Near Transition to Runway Poles.

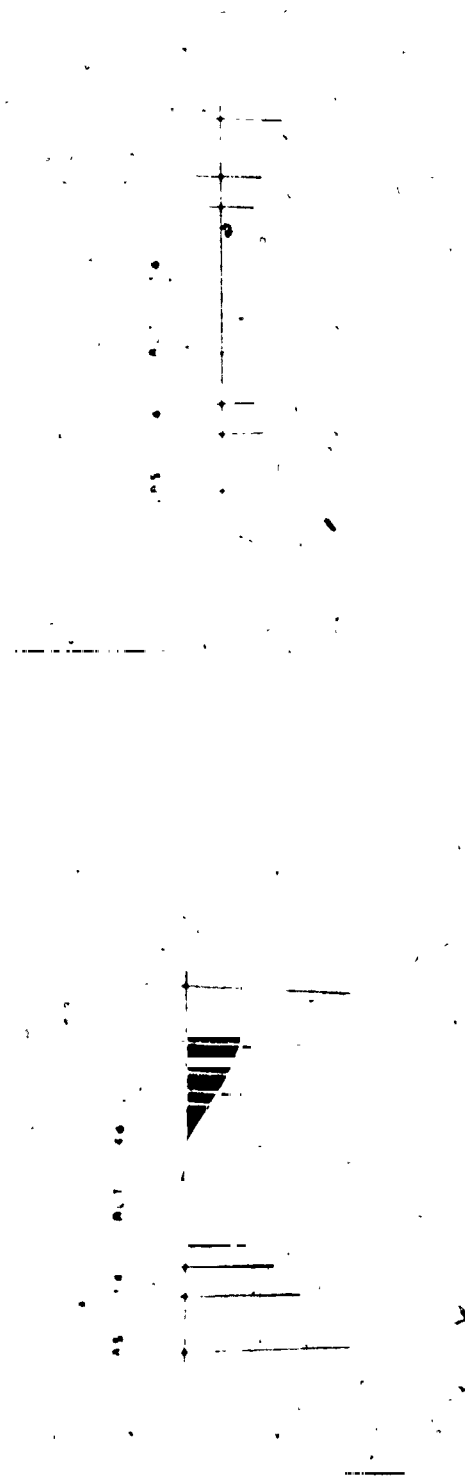


Fig. 7. - Above Runway.

Fig. 8. - Descending, Near Longitudinal Center.



Fig. 10. - Thrust Vector Controller.

Fig. 9. - Near Touchdown.



Fig. 11. - Simulation Chair Cab.

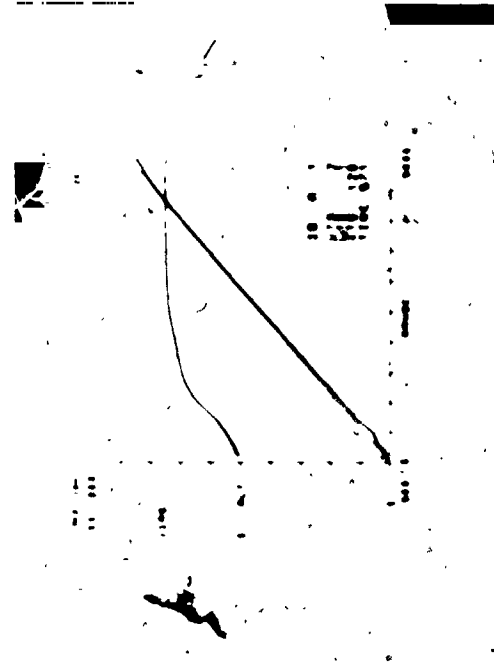


Fig. 12. - Altitude and Airspeed versus Range.

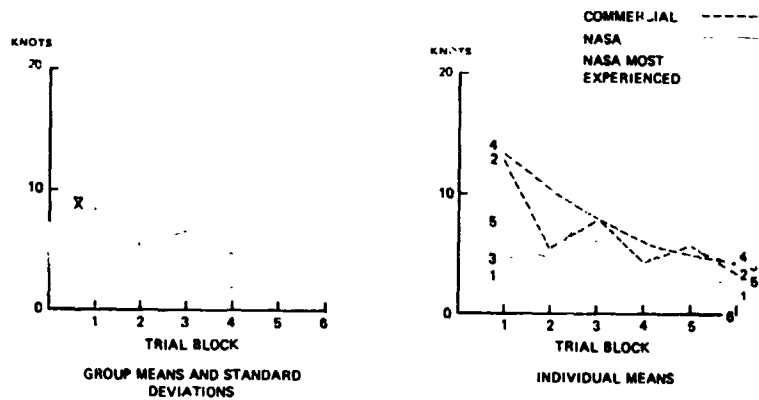


Fig. 13. - Longitudinal Velocity at Touchdown (Absolute).

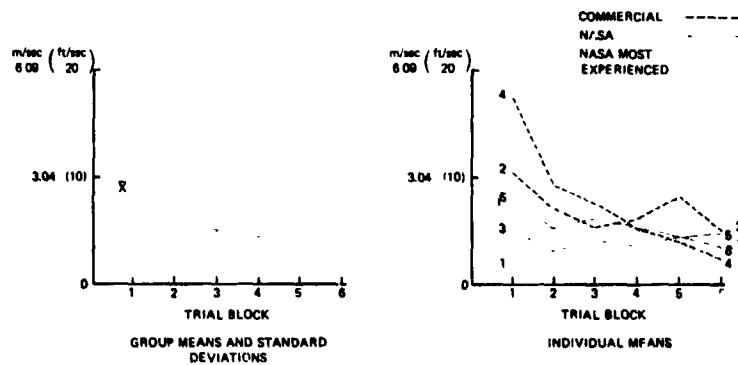


Fig. 14. - Vertical Velocity at Touchdown.

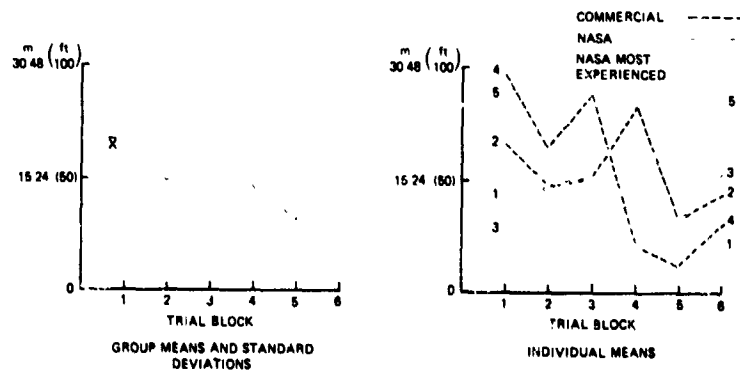


Fig. 15. - Longitudinal Position at Touchdown (Absolute Error).

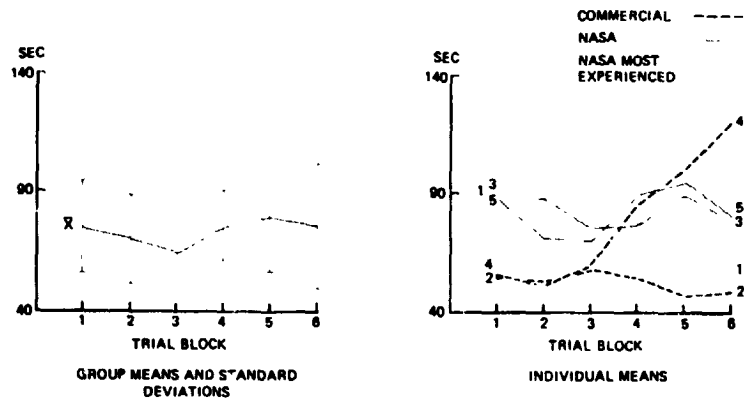


Fig. 16. - Flight Time.

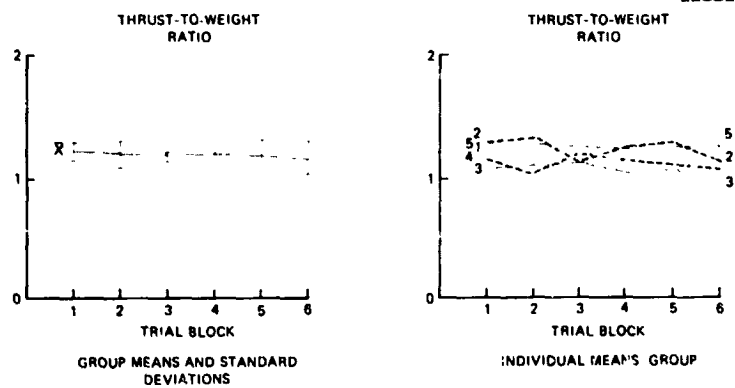


Fig. 17. - Maximum Thrust to Weight Ratio.

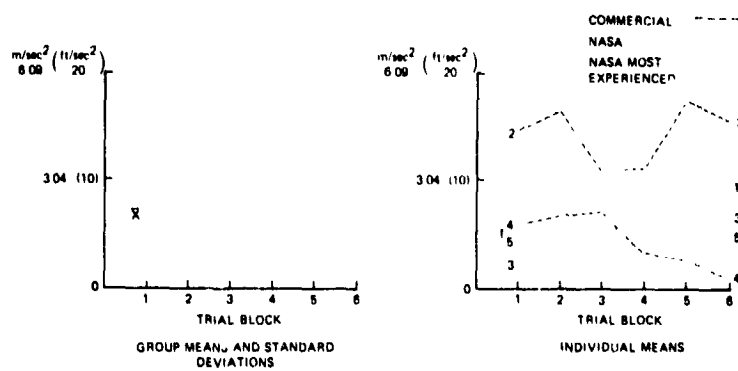


Fig. 18. - Maximum Longitudinal Deceleration.

INFORMATION AND DISPLAY REQUIREMENTS FOR
AN INDEPENDENT LANDING MONITOR*

By J.S. Karmarkar, J.A. Sorensen, and A.V. Phatak
SYSTEM CONTROLS INC.

ABSTRACT

Advanced transport aircraft in a dense, highly automated air traffic control environment, projected for the 1980's, will necessarily have an automatic landing capability. This trend towards increased automation, together with increased equipment and maintenance costs, has motivated a rethinking of the purpose of automation and the role of the crew. The problem, addressed in this paper, concerns the conceptual design of an Independent Landing Monitor (ILM), in terms of information and display requirements.

Functionally, the ILM system is designed to aid the crew in assessing whether the total system (e.g., autoland, avionics, aircraft, ground navigation aids, external disturbances) performance is acceptable, and otherwise to provide adequate information to enable them to select the least unsafe of the available alternatives. Economically, this concept raises the interesting possibility of reducing the primary autoland system redundancy and associated equipment and maintenance costs. The required level of safety for the overall system is maintained by upgrading the backup manual system via the ILM.

This paper presents an ILM design methodology to meet safety requirements, using the optimal control pilot model and covariance propagation methods. System implementation requirements in terms of displays, computers, sensors and logic for detecting an abnormal condition are also presented.

* Research supported by NASA Langley Contract NAS1-13490

N75 22694

LAGGED LOW ORDER CONTROL SYSTEMS WITH POWERED CONTROLS

By E.C. Poulton

Medical Research Council, Applied Psychology Unit, Cambridge, England

SUMMARY

We are all basically position control people because the world we grow up in is position control. With powered controls, a high order control system can be changed to a lower order control system with a lag, which is better suited to our position control skills and strategies. Separate groups of untrained men were trained on an acceleration control system, or on a rate control system with an exponential lag of either .5, 2, or 4 sec. Acquisition time was reliably shorter with all the lagged rate control systems than with the unlagged acceleration control system.

The advantage of the lagged rate control systems may not be found if skilled operators are used who are highly trained on the acceleration control system. Also the advantage may not be found if everyone performs all the conditions in a balanced or random order, because asymmetrical transfer effects and range effects introduce bias. To obtain an unbiased comparison, separate groups of untrained people need to be trained on each condition. Examples are given of 2 range effects, and of an asymmetrical transfer effect.

INTRODUCTION

Children develop in a world of position control. They reach for things. They move things about. This is all position control. Inevitably it is the compatible form of control for everyone, because they learn it first. It is not until children start steering vehicles that they meet acceleration control systems. Learning to cope with high order control systems has to be grafted onto the skills and strategies acquired in a world of position control. It never becomes fully compatible with our basic position control skills and strategies.

In simple vehicles, the controls are connected directly to the control surfaces. If the control system of the vehicle is approximately third order like the control system of an aircraft, the man has to move the controls in a pattern appropriate to the third order control system.

Powered controls can relieve the man of the necessity of doing this. They can provide him with a control system more suited to his basic position control skills and strategies. Instead of the third order control system of an aircraft, the man can be given a lagged rate aided control system with position and rate orders of control. To make such a radical change worth considering, there has to be a large difference in the man's performance with the existing control system and with the proposed new control system. This presents several difficulties.

One difficulty is that skilled trained operators are pretty good at tracking with their conventional control system. People who are not good at it get thrown out during training. Skilled operators are not likely to perform very much better with a lagged rate aided control system than with a conventional control system of higher order. They may even perform worse if they are not used to tracking with a lagged rate aided control system. An experimenter should not use skilled trained operators if he wants to demonstrate a large difference between an existing control system and a new system.

There is still a transfer of training difficulty if the two control systems are compared using specially trained people. The usual experimental design is AB-BA. One group practices first with the conventional control system and then transfers to the rate aided control system. Another group performs the two conditions in the reverse order. The difficulty with the AB-BA design is that transfer between the two conditions is not likely to be equal in both directions. Asymmetrical transfer may reduce the size of the difference between the two control systems. To obtain an unbiased assessment of the difference, it is necessary to use 2 separate groups of people, each of whom performs throughout with only a single control system. The late George Briggs used separate groups, but it is not the usual custom. I shall be returning to this point later.

A third difficulty is mentioned by Chapanis in reference 1. To convince engineers, the experimenter has got to use a measure which is relevant to them. The measure we used was the size of the exponential lag in the lower order control system which was required to degrade performance to the level with the conventional higher order control system. This is a novel approach, but it was accepted by the engineers.

ACCELERATION CONTROL VERSUS LAGGED RATE CONTROL

Figure 1 illustrates the 2 control systems which we used, a lagged rate control system on the left, a conventional acceleration control system on the right. The top section of this figure shows the movements of the control. The middle section shows the corresponding rate of the

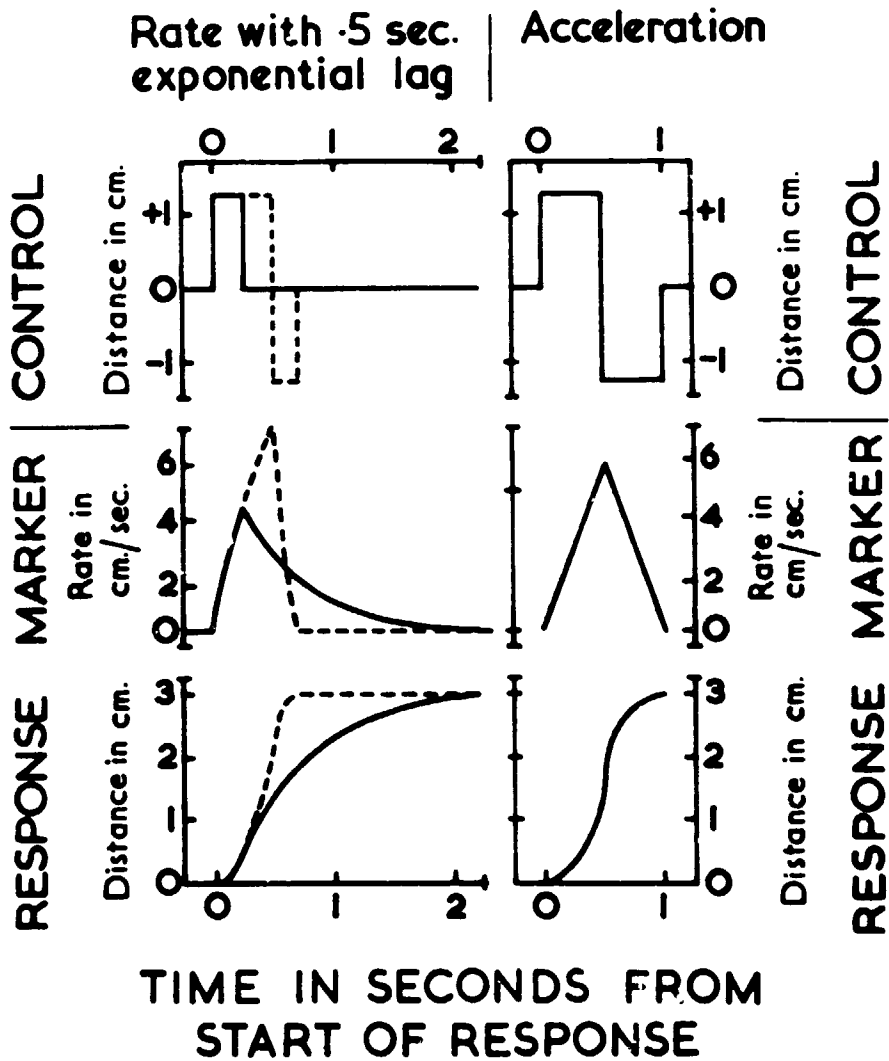


Figure 1. The theoretical control movements required to acquire a target with an acceleration control system and with a rate control system with a .5 sec. exponential time lag. (Tickner and Poulton, reference 2, figure 1.)

response marker. The bottom section shows the position of the response marker. Time goes from left to right.

With the acceleration control system on the right, 3 control movements are required to step the response marker from one position to another. With the lagged rate control, 2 control movements will do if the man is not in a hurry. This is illustrated by the unbroken functions on the left of the figure. If the man is in a hurry, he can use 3 control movements corresponding to the 3 control movements with the acceleration control system. This is illustrated by the broken functions. So the lagged rate control system is the more versatile system, because it offers two alternative strategies.

Table 1 shows the advantage of 4 lagged rate control systems over a pure acceleration control system. The task simulates gathering a missile and directing it towards a target. Tracking is in 1 dimension using a thumb joystick. After a warning, a target circle of 3 mm diameter jumps 3 cm to the left. The man has to acquire the target with a dot of 1 mm, and hold it inside the target for 2 sec. Travel time is the time before the dot remains within an imaginary outer target circle of 6 mm diameter. Adjustment time is the additional time before the dot remains within the target circle of 3 mm diameter. Each condition is performed by a separate group of from 5 to 15 naval enlisted men. They have 10 trials daily for 8 days. The results are the averages of the last 4 days.

Table 1. Acceleration control and lagged rate control

Order of control	Exponential lag (sec)	Maximum initial acceleration (cm/sec ²)	No. of men in group	Average acquisition time (sec)	
				Travel	Adjustment
Acceleration	0	12	12	5.3	6.6
Lag ed rate	2	12	5	5.5	2.7 ^b
	.5	15	6	2.8 ^a	2.4 ^b
	2	5	11	3.3 ^a	3.4 ^b
	4	2.5	15	4.5	3.4 ^b

Results from Tickner and Poulton, reference 2.

^{a b} Lagged rate control reliably quicker than acceleration control (p < .05 or better)

The top row of table 1 is for the unlagged acceleration control system. The second row is for a lagged rate control system. It has the same maximum initial acceleration of 12 cm/sec.², but it has an exponential time lag as long as 2 sec. Adjustment time is reduced reliably ($p < .02$) with the lagged rate control system by almost 4 sec., from 6.6 to 2.7 sec. This is a major advantage in acquiring a target with a missile.

The bottom three rows of table 1 give the results for 3 other lagged rate control systems. The exponential time lags range from .5 to 4 sec. Compared to the acceleration control system, adjustment time is reliably shorter with all the lagged rate control systems. This is because the small adjustments which place the dot in the center of the target circle require only 2 control movements, instead of the 3 control movements required with the acceleration control system.

The middle row of the table is for a lagged rate control system with a maximum initial acceleration of 15 cm/sec.², which is a little larger than for the unlagged acceleration control system. The exponential time lag is .5 sec. Here travel time also is reliably reduced ($p < .001$) by 2.5 sec., from 5.3 to 2.8 sec. This is because the man can afford to move his spot more quickly without risking a large overshoot.

The reduced travel time is not due to the slightly larger maximum initial acceleration. This is shown by the condition in the row below. Here the maximum initial acceleration is only 5 cm/sec.². The exponential time lag is 2 sec. Yet travel time is again reliably ($p < .05$) shorter than for the acceleration control system, 3.3 sec. compared with 5.3 sec.

Table 1 shows that the 4 lagged rate control systems all give quicker acquisition than the unlagged acceleration control system. This is what we predicted would happen.

A RANGE EFFECT FOR CONTROL SYSTEM DYNAMICS

The results in table 1 are for separate groups of men. We would not expect to obtain these results if we use the same men for all conditions. Giving the same men more than one condition produces asymmetrical transfer effects or range effects which bias the results. We do not waste our time doing this. So I shall have to use other people's results to illustrate the point.

The results in figure 2 are from Searle at the Naval Research Laboratory Washington D.C. in 1951, reference 3. Average error is plotted against the amount of acceleration aiding X, of a rate aided control with

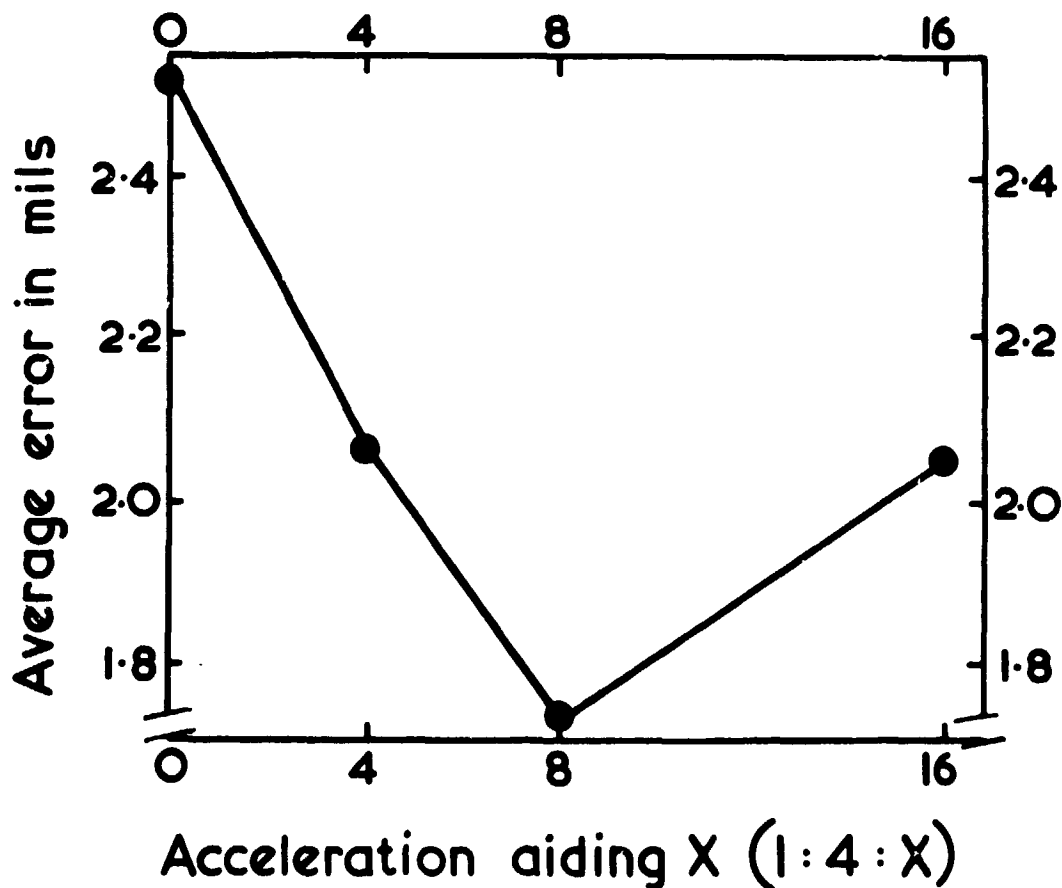


Figure 2. The average tracking error when alternating between control systems with aiding ratios 1:4:0, 1:4:4, 1:4:8 and 1:4:16. Tracking is compensatory, and in one dimension. The track comprises frequencies of 10, 6.7 and 4 cycles per min., of unspecified amplitudes. There are also 2 easier tracks with the higher frequencies more attenuated. A block of trials comprises 6 periods of 45 sec. Each of the 8 men has 6 blocks of trials with each of the 4 control systems, 2 blocks on each of the 3 tracks. The total of 24 blocks of trials for each man is arranged in an order which is balanced over the group of 8 men. The results for the 2 easier tracks are similar, but the average errors are smaller. (Results from Searle, reference 3.)

aiding ratios 1:4:X. The same 8 enlisted men perform with all the 4 control systems in a balanced treatments design which is effectively repeated 6 times. So there is plenty of opportunity for transfer between conditions to produce a range effect.

Reliably the best performance is given by the acceleration aided control system with the intermediate aiding ratio of 1:4:8. It is reliably better than both the aiding ratio of 1:4:4 and the aiding ratio 1:4:16 ($p < .01$). This is a range effect, produced by the within subjects experimental design. It fits a transfer of training model. Transfer is greatest between the conditions which are most similar, and least between the conditions which are very different. So the acceleration aiding condition 1:4:8 benefits most. The man learns to use a strategy in all conditions which is most appropriate to this middle of the range condition.

Acceleration is analogous to inertia. Reference 4 shows that increasing the proportion of acceleration or inertia always degrades performance in tracking with a control stick, if the experiment is properly designed with separate groups of people for each condition.

Searle's experiment shows exactly the opposite effect. On the left of figure 2 the control is pure rate aid, 1:4:0. Yet it gives more error than any of the acceleration aided control systems. This is because the strategy which is most appropriate to the acceleration aided control system with the aiding ratio 1:4:8, is not appropriate for the pure rate aided control system. The man tends to use this common strategy for all 4 conditions. So he performs best with the acceleration aiding ratio 1:4:8, and worst with the pure rate aided control system.

To obtain an unbiased comparison between the 4 conditions, it is necessary to train a separate group of untrained people on each condition.

ASYMMETRICAL TRANSFER BETWEEN EXPONENTIAL LAGS

Figure 3 shows an asymmetrical transfer of training effect when tracking with a position control system and exponential lags. The data come from Marvin Levine at Wright Patterson Air Force Base in 1953, reference 5. Mean percent time on target is plotted against blocks of 5 trials, each of 60 sec. Each function is from a separate group of 10 students, so you can see the asymmetrical transfer effect developing.

The unfilled points at the top represent practically no lag, .015 sec. The filled points at the bottom represent the longest exponential lag of 3.0 sec. The first 2 points on the left show the initial matching of the groups of students, either on the unlagged condition or on the 3.0 sec. lag condition.

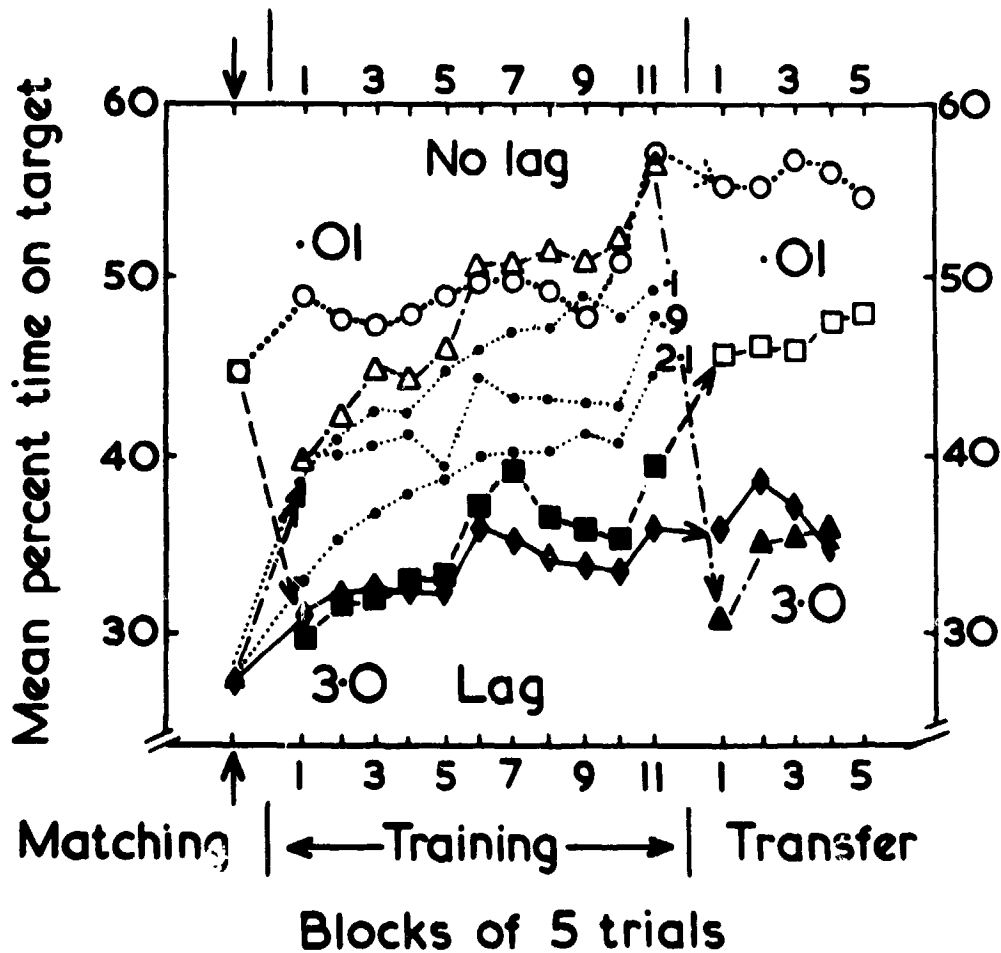


Figure 3. The average time on target when tracking with a position control and exponential lags of .015 ("no lag"), .1, .9, 2.1 and 3.0 sec. Tracking is compensatory and in one dimension. The track comprises frequencies of 11, 5 and 3 cycles per min. of equal amplitude. A block of trials comprises 5 periods of 60 sec. Each function represents a separate group of 10 students. The students start with a block of matching trials, on either the .015 sec. lag or the 3.0 sec. lag. This is followed by 11 training blocks with one of the 5 lags. Finally for 4 of the groups there are 4 or 5 transfer blocks with the original .015 sec. or 3.0 sec. lag. (Results from Levine, reference 5.)

The unfilled circles at the top represent a group which tracks throughout without lag. As you would expect, it has the longest time on target. The filled diamonds at the bottom represent a group which tracks throughout with the 3.0 sec. lag. It has the shortest time on target.

The triangles represent a group which has 5 matching trials with the 3 sec. lag, and then trains without lag. It takes 30 trials without lag before it catches up with the group which always tracks without lag.

The squares represent a group which has 5 matching trials without lag, and then trains with the 3.0 sec. lag. It catches up almost at once with the group which always tracks with the 3 sec. lag. But after 50 trials with the lag, it performs relatively badly when the lag is removed. And it hardly improves during the 25 transfer trials.

The group represented by triangles has 50 trials without lag, and then transfers to the 3 sec. lag. It does not do very well on the first block of 5 transfer trials. But after 20 trials it performs as well as the group which always tracks with the 3 sec. lag.

Figure 3 shows that after the first few transfer trials, training on the unlagged control system is as effective on transfer to the lagged control system as training all the time on the lagged control system. There is then 100% positive transfer. But prior training on the lagged control system is actually a disadvantage on transfer to the unlagged control system. The 5 transfer blocks of the group represented by the unfilled squares lie below the first 5 training blocks of the group represented by the unfilled circles. This is negative transfer. The students do better on the unlagged control system when they have had no prior training.

There is positive transfer from the unlagged condition to the lagged condition. But there is negative transfer from the lagged condition to the unlagged condition. If people are given the 2 conditions alternately, they will perform relatively badly without lag, but much as expected with the lag. So the disadvantage of the lag will be less than it should be.

To show the full true effect of the lag you need separate groups of people for each condition: the circles at the top of the figure on the left, the diamonds at the bottom. The effect of the lag appears smaller if you compare simply the unfilled squares on the right of the figure with the filled triangles on the right. If people change from one value of lag to another often enough, the effect of the lag may disappear completely.

The small dotted functions show the results of extra groups of 10 students who perform with lags of .1, .9 and 2.1 sec. The longer the lag, the shorter the time on target. This is in line with the results of other experiments on exponential control lags (reference 4).

With sine wave tracks like the one used by Levine, exponential control lags have 2 disadvantages. One disadvantage is the lag. The other disadvantage is the reduced transmission or control output at the higher frequencies. The results in the figure are probably due to a combination of the 2 disadvantages. Unfortunately Levine does not say what his maximum control output is. So one cannot tell how much of the reduction in time on target is due to the limit on the control output, and how much is due to the actual lag.

A RANGE EFFECT FOR CONTROL OUTPUTS

Figure 4 illustrates a range effect produced by giving 4 exponential lags each combined with 4 control gains, all to the same 8 people. The data come from Marty Rockway at Wright Patterson Air Force Base in 1954 (reference 6) a year after Levine's experiment. Time on target is plotted against the exponential time lags. Each function is for a separate control gain.

The longest time on target is given by the longest exponential time lag, although the difference between this point and the best performance with the .3 sec. lag is not statistically reliable. This quite ridiculous result is produced by the range effect for the control outputs, which swamps the effect of the actual lag in the confused experimental design.

Rockway's track comprises 3 equal amplitude sine waves of 11, 5 and 3 cycles per minute (cpm). In tracking sine waves, exponential time lags reduce the transmission of the control. The reduced transmission can be offset by increasing the control gain. Table 2 shows the product of the transmission at the top track frequency of 11 cpm times the control gain. The values of control output run from 9.4 at the top on the left to .29 at the bottom on the right. The values which give the longest time on target with each exponential time lag are underlined. They range between 2.9 and 1.7. They are all close to the mean value of 2.6.

With outputs less than 1.0, the man cannot follow the top track frequency. So his time on target is bound to be shorter. With very large outputs the man is also at a disadvantage, because a small error in the movement of the control will put him outside the target area.

There is bound to be an optimum output somewhere between these 2 extremes. But where the optimum is found to lie, depends upon the range of outputs selected by the experimenter. The optimum found tends to lie nearer to the middle of the range of outputs than it would if separate groups of people were used for each output. This is because the man tends to track in all conditions as if he has a control output of about the average size. The range effect for control outputs in figure 4 swamps the effect of the lags.

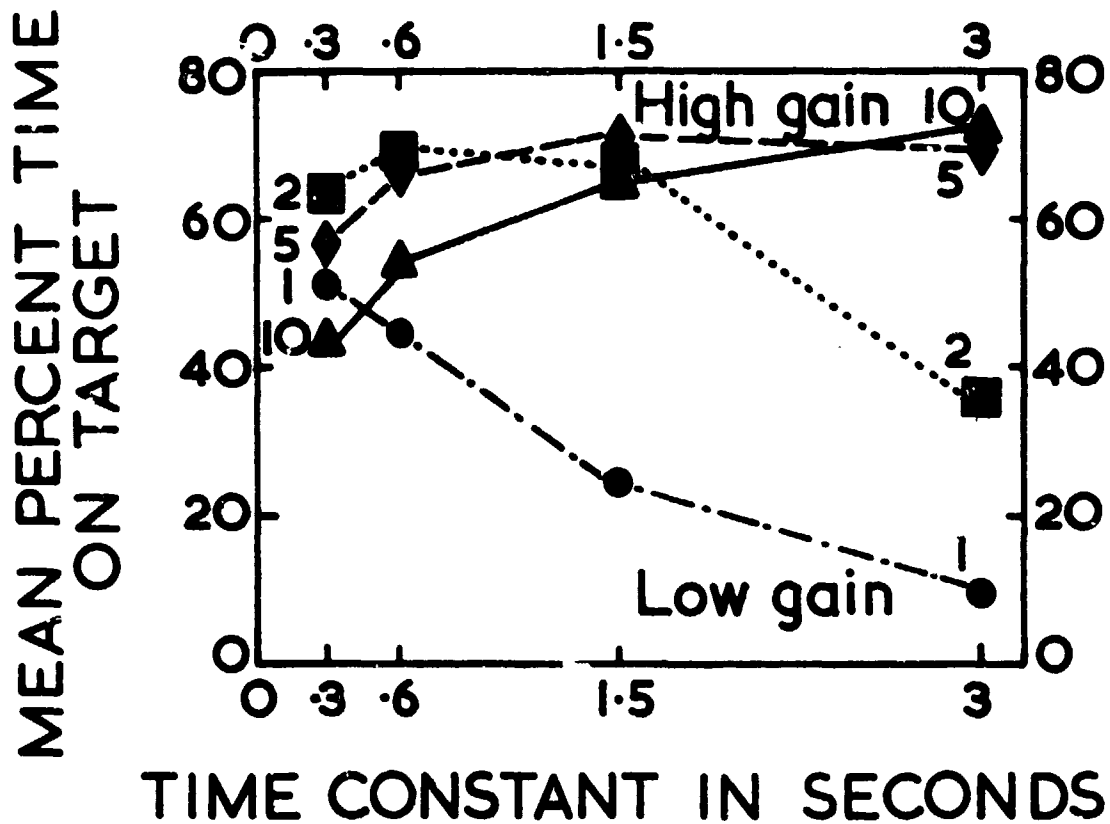


Figure 4. The average time on target when alternating between exponential lags of .3, .6, 1.5 and 3.0 sec. The task is similar to the task of figure 3, except that tracking is in 2 dimensions. The 16 combinations of 4 lags and 4 control gains are presented in balanced orders to each of 8 practiced people. The experiment is repeated the next day with the conditions in the reverse order. (Reference 4, figure 17.4, showing results from Rockway, reference 6.)

Table 2. Control output at 11 cycles per minute in Rockway's experiment (reference 6)

Control gain	Exponential lag in seconds			
	.3	.6	1.5	3.0
10	9.4	8.5	5.1	<u>2.9</u>
5	4.7	4.3	<u>2.6</u>	1.5
2	<u>1.9</u>	<u>1.7</u>	1.0	.58
1	.94	.85	.51	.29

Note. Control output = transmission at 11 cpm X gain

Again the range effect fits a transfer of training model. Transfer is greatest between the control outputs which are most similar, and least between the control outputs which are very different. So the control outputs of about 2.6 in the middle of the range benefit most.

This is another range effect like Searle's range effect for acceleration aiding in figure 2. Reference 4 gives numerous examples of asymmetrical transfer effects and range effects. The biased results which they produce have to be discarded in sorting out the contradictions in the literature.

CONCLUDING REMARKS

The example in figure 1 and table 1 of changing a powered acceleration control to a rate control with an exponential lag is only an illustration. A missile is easier to control if it has a position term in addition to a rate term, and so is rate aided.

In the future the greatest gains will probably come from changing the powered control systems of aircraft to make them more compatible with the pilots. When flying down the glide path in coming in to land, the aircraft may be blown sideways by a sudden gust. The pilot requires a minimum of 4 stick movements to step his aircraft back again to the middle of the glidepath. This could be reduced to 2. It would greatly reduce the pilot's workload.

In reference 7 Norman Walker shows that when under stress, even a pilot is less likely to make large errors if he has a lagged rate control system than if he has an acceleration control system.

ACKNOWLEDGEMENTS

The author is grateful to Dr. Alan Carpenter for help in computing the control outputs of table 2, and to Mr. Ron Speight for commenting on a draft of the manuscript. The experimental subjects were supplied by the British Royal Navy. The work forms part of a program of research for the Medical Research Council's Army Personnel Research Committee.

REFERENCES

1. Chapanis, A.: The relevance of laboratory studies to practical situations. Ergonomics, 1967, 10, 557-577.
2. Tickner, A.H.; and Poulton, E.C.: Acquiring a target with an unlagged acceleration control system and with 3 lagged rate control systems. Ergonomics, 1972, 15, 49-56.
3. Searle, L.V.: Psychological studies of tracking behavior: Part IV - The intermittency hypothesis as a basis for predicting optimum aided-tracking time constants. U.S. Naval Research Laboratory Report 3872, Washington D.C., 1951.
4. Poulton, E.C.: Tracking skill and manual control. New York: Academic Press, 1974.
5. Levine, M: Transfer of tracking performance as a function of a delay between the control and the display. USAF Wright Air Development Center, Technical Report 53-237, Wright-Patterson Air Force Base, Ohio, 1953.
6. Rockway, M.R.: The effect of variations in control-display ratio and exponential time delay on tracking performance. USAF Wright Air Development Center, Technical Report 54-618, Wright-Patterson Air Force Base, Ohio, 1954.
7. Walker, N.K.; and Burkhardt, J.F.: The combat effectiveness of various human operator controlled systems. U.S. Naval Ordnance Test Station, PO 60530/4030 Y 3664-65, AD 373246, 1965.

N75 33695

RESULTS OF A FLIGHT INVESTIGATION OF CONTROL-DISPLAY INTERACTIONS
FOR VTOL DECELERATING DESCENDING INSTRUMENT
APPROACHES USING THE X-22A AIRCRAFT*

By J. V. Lebacqz and E. W. Aiken

Calspan Corporation
Buffalo, New York 14221

ABSTRACT

The third flight research program using the variable stability X-22A aircraft was undertaken to investigate control, display, and guidance requirements for VTOL instrument transitions. The primary purpose of the experiment was to provide meaningful data related to the interaction of aircraft control system and pilot display characteristics on pilot rating and performance during a steep decelerating descending transition from a representative forward velocity (100 kt) to the hover under simulated instrument conditions. Thirty-seven evaluations were performed of combinations of five generic display presentations, ranging from position-information-only to four-axis control directors, and five levels of control augmentation systems, ranging from rate-augmentation-only to decoupled velocity responses and automatic configuration changes. Primary results of the program include the demonstration of an inverse relationship between control complexity and display sophistication, as was hypothesized in the experiment design, and the definition of acceptable and satisfactory control-display combinations.

NOTATION

- m_c , $(1/I_y) (\partial m/\partial \dot{\alpha})$ dimensional pitch moment derivative,
(rad/sec²)/($\dot{\alpha}$)
- n_x Body X-axis acceleration, ft/sec²
- n_z Body Z-axis acceleration, ft/sec²
- p Body axis roll rate, deg/sec
- q Body axis pitch rate, deg/sec
- r Body axis yaw rate, deg/sec

*Performed under Contract N00019-73-C-0504 for the United States Naval Air Systems Command and the NASA Langley Research Center.

t	Time, seconds
u	Body X-axis velocity, ft/sec
w	Body Z-axis velocity, ft/sec
X,Y,Z	Components of ground-referenced translation position, ft
$\dot{X}, \dot{Y}, \dot{Z}$	Components of ground-referenced translation rate, ft/sec
$X_{()}$	Dimensional body X-force derivative, (ft/sec ²)/()
$Z_{()}$	Dimensional body Z-force derivative, (ft/sec ²)/()
$\Delta_{()}$	Perturbation of () = current value minus initial value, ()
δ_{ES}	Longitudinal stick position, inches
δ_{CS}	Collective stick position, degrees
δ_{AS}	Lateral stick position, inches
δ_{RP}	Rudder pedal position, inches
$\epsilon_{()}$	Error in () = commanded value minus actual value, ()
ζ	Damping ratio of second order characteristic roots
θ	Body pitch attitude, degrees
θ_{WO}	Washed-out pitch attitude signal, degrees
λ	X-22A duct angle, measured from horizontal, degrees
τ	Time constant of first order response, seconds
ϕ	Body roll attitude, degrees
ω_n	Undamped natural frequency of second order roots, rad/sec

Abbreviations:

AGL	Above Ground Level
IFR	Instrument Flight Rules
PR	Pilot Rating (Cooper-Harper)
VSS	Variable Stability System

INTRODUCTION

The development of an instrument landing capability for V/STOL aircraft is a prerequisite for the extension of VTOL operations into restricted areas in all weather conditions. To provide this capability, problems must be solved which are more difficult than the corresponding problems for CTOL aircraft, because the landing approach now involves not only control of the spatial position of the aircraft but also precise control of a non-constant total velocity; this task requires active use of at least one additional controller, and furthermore requires additional information to the pilot concerning the increased dimensions of his task. The pilot's control problem is exacerbated by the generally degraded flying qualities encountered as the dependence on powered lift increases, and, in VTOL configurations different than the helicopter, by an additional control requirement related to the conversion from forward flight to powered lift (e.g. wing tilt, rotor tilt, jet thrust vectoring).

It is clear, therefore, that studies of the VTOL instrument landing approach problem must consider both the definition of required levels of information presentation for the pilot and the determination of required degrees of stability and/or control augmentation for the aircraft. An excellent summary of this problem and recommendations for future research are given in the AGARD Advisory Report on V/STOL display requirements for landing (Reference 1). In this discussion of necessary research, the AGARD Working Group placed a high priority on determining the interplay between display and control complexities. This interplay is schematically illustrated in Figure 1, taken from Reference 1. The hypothesis is that an inverse relationship exists for a given pilot rating level between control complexity and display sophistication; the problem is to quantify to some extent these two axes and attempt thereby to define satisfactory or adequate combinations.

The general goal of the flight research experiment discussed in this paper was therefore to examine combinations of generic levels of displayed information and types of stability/control augmentation. Since the scope of the flight program was relatively limited, extensive theoretical analyses and exploratory ground simulations were conducted during the design phase. Some of these analyses were discussed at a previous Annual Conference on Manual Control, and will not be repeated here (Reference 2); Reference 3, which may be considered a complement to this paper, outlines the relationship of the resulting experiment design to previous work in this area. The details of this design and the conduct of the evaluation flights are described in the next two sections of this paper; the following section discusses the principal pilot rating results, and the final section presents some of the conclusions drawn from the experiment.

DESIGN OF THE EXPERIMENT

General

The primary purpose of this experiment was to provide meaningful data related to the interaction of aircraft control system and pilot display characteristics on pilot rating and performance during a steep decelerating descending transition from a representative forward velocity (~100 kt) to the hover under instrument conditions. Accordingly, the experiment was designed to investigate combinations of several types of control system/stability augmentation characteristics with display presentations of varying sophistication, with the objective being the definition of satisfactory or acceptable combinations through the use of Cooper-Harper pilot ratings and measured performance and workload indices. In order to reduce the scope of the investigation to a manageable level, it was necessary to select from the many factors involved in ascertaining guidance, display, and control requirements those that were of major importance as variables (Reference 4). The characteristics of the resulting selections are summarized in the succeeding subsections.

Guidance Characteristics

In the context of this experiment, the term "guidance" is defined as the processing of raw X,Y,Z position data telemetered to the aircraft from a tracking radar to obtain information concerning positions and velocities and to derive the desired command relationships. It is important to recognize that the VTOL terminal area problem generally requires knowledge of, and commands for, both translational rates and positions, either for display to the pilot to aid him in the deceleration or for processing by an automatic control system to perform this operation for him. In the X-22A application, the derivation of the required status and command information was performed entirely onboard the aircraft, and was therefore essentially independent of the equipment used to provide the raw X,Y,Z data. For this experiment, neither the raw information (e.g. altitude, azimuth, and elevation information instead of X,Y,Z) nor the derived command relationships were considered as variables to be altered for investigation; the guidance relationships were designed and verified in extensive ground simulations and held fixed for the flight experiment.

The first processing of the data is the estimation of smoothed translational positions and rates relative to a hover point and selectable approach course direction by complementary filtering of the radar position data and aircraft linear accelerometer outputs. This method is similar to that discussed in Reference 5; the filter is second order and provides signals for both smoothed position and velocity in an earth-referenced axis system. A coordinate transformation to provide the positions and rates in an aircraft-heading-referenced axis system operates on these signals so that the information is available in either axis system for display to the pilot as required.

With the positions and velocities available, the next function of the guidance system is the generation of command information. For the descending decelerating approach task with a VTOL aircraft, the following types of commands are required:

- Longitudinal velocity as a function of range (deceleration profile)
- Lateral velocity as a function of lateral position
- Aircraft configuration change as a function of commanded velocity
- Vertical position as a function of range (glide slope)
- Vertical velocity as a function of range

A complete discussion of the characteristics of all these commands is beyond the scope of this paper, and the reader is referred to Reference 4 for detailed information. Since the implementations of the deceleration profile and configuration change commands in this experiment are significant new developments, however, they will be qualitatively described here.

A fundamental problem which must be addressed for VTOL decelerating approaches is the fact that the magnitude of the along-track wind velocity component can be a significant fraction of the commanded aircraft velocity, and in fact becomes comparable as the hover point is approached. If the commanded aircraft velocity is ground-referenced for the entire approach, then acquisition airspeed will vary from approach to approach, which complicates the pilot's task; more importantly, VTOL aircraft generally have relatively narrow corridors of acceptable airspeed/configuration (thrust tilt)/rate of descent combinations, and forcing differing airspeeds may violate these boundaries. One solution to the problem, proposed in Reference 6, is to refer the approach path and deceleration profile to the air mass by using either ground or aircraft measured wind velocity information to compute the transformation from ground-referenced to air-referenced coordinates. This technique ensures that both the path and the deceleration are always the same with respect to the air, thereby maintaining the aircraft within its allowable transition corridor. As a result, however, the ground track (approach angle, flare point) varies with different winds; in addition, in or near the hover it is velocity with respect to the ground, both longitudinally and laterally, which must be controlled, and the commands should therefore be ground-referenced at this point.

For the X-22A experiment, therefore, the implementation of the velocity commands was to divide the approach into two parts, and consisted of commanding: (1) airspeed and aircraft heading during localizer and glide slope acquisition, and (2) ground speed components parallel and perpendicular to the desired course during deceleration and hover. The airspeed and course commands are predicated upon the fact that the LORAS airspeed measuring system of the X-22A gives longitudinal and lateral components of airspeed

relative to the aircraft heading axis, which, in conjunction with the ground-referenced rates from the complementary filters, allows determination of the wind speed and direction. This information is used to command a constant airspeed (100 kt) and to derive an aircraft heading command to achieve the desired course by accounting for along-track and cross-track wind components; Reference 4 derives the commands, which are summarized in Table I as the resulting ground-speed commands "before switching" referred to the aircraft axes.

For the "after switching" part of the approach, the ground velocity parallel to the desired course is commanded based on a constant deceleration (0.05g) with a linear decrease to zero during the final 100 ft, and the component perpendicular to the course as a linear function of lateral position (see Table I). The parallel component command is implemented as a zero-wind velocity profile versus range on a function generator in the aircraft; this implementation serves a dual purpose of providing the "after switching" commands and also of defining the point at which the switching in command logic takes place. If the along-track wind component is a headwind, the ground speed for a commanded 100 kt airspeed will be less than the zero-wind ground-speed command until some point after the zero-wind deceleration initiation. The switching logic therefore works by subtracting the measured ground speed from the zero-wind command: while this difference is positive, the airspeed/course commands are used; when it first goes to zero, the switch is made to parallel and perpendicular ground speed commands for the remainder of the approach. As implemented for the X-22A experiment, this logic is constrained to cases in which a headwind is present, but the extension to include tailwinds is straightforward.

The other guidance implementation worth emphasizing is the configuration change command. VTOL configurations different than the helicopter require substantial configuration changes to convert from forward flight to powered lift in the hover. For jet-lift aircraft (e.g. Harrier AV-8A, Dornier DO-31), the conversion process can be quite flexible, since allowable combinations of thrust inclination and airspeed are relatively unconstrained; for aircraft types such as tilt-duct, tilt-wing, and tilt-rotor, however, a fairly narrow corridor of combinations exists to avoid buzz or buffet. It may be necessary, therefore, to provide the pilot with director information to perform the configuration change safely for these types of aircraft. In a more general sense, the conversion process for any VTOL type may overload the pilot without some information to help him perform it, and hence a configuration change command may be required.

For the X-22A aircraft, the center of the allowable transition corridor is well approximated by a linear relationship between duct angle and flight velocity, which simplifies the implementation but is not required. The configuration change command consisted of a commanded duct angle as a function of commanded ground speed parallel to the course, which was implemented with a balance-and-hold circuit to begin functioning at the switch to ground-speed commands. This implementation means that the conversion from the forward flight configuration will be initiated at ranges which vary with the amount of headwind present; since the conversion rate is the same for all

situations (same deceleration required), the result is that the final duct angle at hover will vary according to headwind, thereby maintaining air-speed-configuration within the allowable corridor. A more thorough discussion of the implementation is contained in Reference 4.

Display Characteristics

One of the two major variables of this experiment was information display sophistication, the characteristics of which will be discussed in this subsection. In the context of this experiment, display "sophistication" comprises a hierarchy of information levels displayed to the pilot in an ergonomically acceptable fashion.

Various independent efforts have been made to establish the information requirements of the pilot of a VTOL aircraft during an instrument approach to the hover: for example, a NASA study (Reference 7), a JANAIR-sponsored program (Reference 8), and the report of an AGARD Working Group (Reference 1). Because of the plethora of information required by the pilot for the stabilization and control of even a highly-augmented VTOL aircraft during a landing approach, conventional electromechanical instruments have been judged unsuitable for the task due to the excessively high mental workload required for the gathering of information and the subsequent decision-making process (Reference 1). The need for an integrated information display has been established for the helicopter by NASA Langley Research Center's VTOL Approach and Landing Technology (VALT) Program (Reference 9) and for the vectored-thrust VTOL aircraft by the results of a preliminary X-22A ground simulator study (Reference 10). The cathode-ray tube (CRT) is the best existing display device for the high data density required in integrated displays and hence was selected as the basis for the X-22A's electronic display system, described in more detail in Reference 4.

A schematic diagram of the evaluation pilot's instrument panel is given in Figure 2. The primary instrument is the electronic CRT which presents integrated vertical and horizontal information in formats which may be varied during flight; major auxiliary information consists of a radar altimeter with both analog and digital readout, a LORAS longitudinal air-speed tape instrument, a light for configuration change director information, a conventional electromechanical ADI including three-axis flight director elements, a duct angle instrument and conventional RMI, IVSI, and barometric altimeter instruments.

The major display variable in this experiment was the electronic display format. Brief investigations of the effects of a separate control director display on the ADI and of the lack of a configuration change director were also conducted in flight. The intent of the variation in the electronic display format was to present the pilot three generic levels of displayed information. They were:

- ED-1: position and commanded position

- ED-2: position, commanded position, velocity and commanded velocity information
- ED-3: position, commanded position and velocity, with longitudinal (δ_{E3}), lateral (δ_{A3}), and collective (δ_{C3}) control director information

From a practical viewpoint, the hypothesized reduction in pilot workload caused by the increasing levels of displayed information must be balanced against the increasing cost of deriving that information from more sophisticated sensors through more complex data processing. The results of this experiment provide a valid basis for the pilot-oriented portion of that trade-off. The least sophisticated display format, ED-1, presents the pilot raw aircraft position in three dimensions; although probably unacceptable for less complex control systems, this format may be sufficient if the pilot is provided with augmented control of the aircraft velocity vector. The ED-2 format is of the type espoused by T. Dukes for attitude-stabilized helicopters (References 11 and 12)*. The ED-3 format represents an attempt to achieve the integration of command and status information recommended as a result of NASA's VALT Program to date.

Very little has been written about the philosophy of integrated display design. However, it was the intent from the outset to present the various electronic display formats to the pilot in as favorable a manner as possible so that any display-related deficiencies would be a result of lack of information and not of display design problems. Therefore many of the integrated display principles of Dukes (Reference 11) and Young (Reference 13), based upon experimental results, were applied to the design of the three basic electronic display formats. In particular, the following guidelines were adopted:

- Aircraft-referenced display — The aircraft symbol is fixed and the other displayed information moves with respect to this reference.
- Error display — The guidance information is presented in the form of errors rather than as absolute values where possible.
- Explicit display of rates — No attempt is made to have the pilot estimate absolute or error rates implicitly by the rate of change of a position symbol on the display. When rates are displayed, they are displayed explicitly.

*The authors wish to express their appreciation to Messrs. T. Dukes and D. Carter of Princeton University for the loan of the ICL symbol generator during the design phase of this experiment and for their technical contributions concerning the ITED format and symbology.

- Display of lead information — When rate information is displayed, its function is to lead the position symbol to aid the pilot in his prediction of a future aircraft state.
- Symbol response to control input — The location of a symbol and the sense of its motion are selected to be compatible with the location and motion of its primary controller.
- Scaling of the displayed parameters — The scaling of the various symbol motions is selected so as to be acceptable to the pilot while not significantly degrading overall system performance. A relatively simple display with fast-moving symbols may appear "cluttered" to the pilot while a more complex display with slow-moving symbols may be acceptable to him but may also result in a relatively poor total system performance.

The choice of symbology, although not as significant as the previous considerations, is important insofar as it relates to the ability of the pilot to decode the information as it is presented to him. He must never be in doubt about the status of his aircraft because of momentary confusion about the meaning of a particular symbol. An extensive literature survey, opinions of Calspan's pilot/engineers, and the results of preliminary ground- and in-flight simulation were all used to decide upon the final version of the electronic display symbology (Figure 3). The techniques used to display the required information were drawn primarily from two sources and modified as required; for example, the aircraft symbol and horizontal velocity vector are based upon Dukes' helicopter display work (Reference 12) while the expanding landing pad symbol was used as part of the RAE display format evaluated in the CL-84 Tripa-tite Program (Reference 14).

The design of a display format also involves a careful consideration of the mission of the pilot/aircraft system. In this case the evaluation task was an instrument approach to the hover with no breakout to visual conditions. Therefore the emphasis of the display design process was placed upon the most crucial portion of the task, the precision hover.

The synthesis of the logic driving the control director elements of the ED-3 display format constituted a major portion of the display design process. The principles which guided the control director design were:

- Design condition — The precision hover was the critical portion of the task and hence the design condition for the control director.
- Simplified logic — An attempt was made to minimize the need for logic switching, error limiting, and gain scheduling.

- Use of manual control theory — The response of the director elements to control inputs must be acceptable to the pilot and yet not significantly degrade overall system performance.
- Four-axis director — Each director element commanded a single control input; therefore, in general, four director elements were required for the task: longitudinal stick, lateral stick, collective stick (thrust magnitude), and duct angle (thrust direction).

The final version of the control director logic was a result of preliminary analysis, extensive ground simulation, and in-flight testing. Based upon the experience of NASA Langley (Reference 15) it was decided to use the "control command" instead of "control demand" version of control directors (Reference 7) for the longitudinal, lateral, and collective controllers. Basically, this decision eliminated control position as a possible feedback variable to the display; therefore the proper airplane response, not control input, was required to center each control director element. Many techniques for control director design based upon the theory of manual control were examined (see, for example, Reference 2). A technique, based upon classical control theory, used by Systems Technology, Inc. (STI) (Reference 16, for example) was finally adopted. The technique involves the fulfillment of several guidance- and pilot-oriented requirements. The pilot-oriented requirements are based upon the STI "crossover" pilot model; basically, the director element must be designed so as to respond in a manner proportional to the integral of the pilot's control input in the region of potential crossover frequency in order to ensure pilot acceptability and good closed-loop system characteristics for a wide range of pilot gains.

The three control director elements on electronic display format ED-3 are:

- Horizontal bar (HBAR) — longitudinal stick (δ_{ϵ_s}) command
- Vertical bar (VBAR) — lateral stick (δ_{Δ_s}) command
- Vertical tab (VTAB) — collective stick (δ_{c_s}) command

HBAR and VBAR are implemented as "fly-to" commands while VTAB represents a "fly-away" command; that is, HBAR down and VBAR right command forward and right center stick inputs respectively, while VTAB down requires an up collective input. In general the HBAR and VBAR control director logic is expressed as follows:

$$\text{HBAR} = K_x \epsilon_x + K_\theta \theta_{WO} + K_q q$$

$$\text{VBAR} = K_y \epsilon_y + K_\phi \phi + K_p p$$

The one exception to the above logic is that, when the heading hold (HH) directional mode is selected, the roll angle feedback to VBAR is washed-out

with a three second time constant to avoid standoff errors due to wing-down approach s. The values for the director gains vary as a function of generic controlled vehicle characteristics; these gains are presented in Table II. VTAB is generated as follows:

$$VTAB = K_3 \epsilon_z + K_3(\lambda) \epsilon_z$$

The VTAB gain K_3 is made an increasing function of duct angle to compensate for the decreasing vertical damping of the basic X-22A with increasing duct angle. The values for the VTAB gain are also presented in Table II.

The fourth control director element, the configuration change director (or ITVIC - Independent Thrust Vector Inclination Command), was developed in the ground simulator and implemented in the form of a light on the evaluation pilot's instrument panel to give ON-OFF duct rotation commands. This type of control director corresponds to the nature of the duct angle controller, a switch on the collective stick which drives the ducts at a constant 5 deg/sec rate when activated. During the deceleration portion of the task, the ITVIC light is ON when a commanded duct angle (λ_c) exceeds the actual duct angle (λ) by three degrees. The commanded duct angle is a linear function of the commanded ground speed and hence a function of range to the hover point. When the ducts are rotated to reduce the duct angle error to 0.5 degree, the light is extinguished. This particular value of hysteresis in the ITVIC logic was chosen to command a sufficient number of duct rotations so as to minimize the pitch attitude oscillations required for vernier velocity control during the deceleration, and yet few enough rotations to minimize the pilot's dwell time on this portion of the display as well as to reduce the number and magnitude of the pressure transients in the duct drive hydraulic system.

Two variations on the basic electronic display formats were also evaluated. Format ED-2+ was added as a result of preliminary flight testing which indicated the need for a collective control director due to the high pilot workload required in the control of vertical errors. Format ED-1/FD consisted of the ED-1 electronic display and three-axis control director information displayed on the electromechanical ADI; this display configuration corresponded to NASA Langley's CH-46 format (Reference 15) and was included both to verify their results and to reinforce the requirement for integrated displays. A brief investigation of the effects resulting from the absence of a configuration change director was also conducted to verify the results of a preliminary simulator study which indicated an intolerable pilot workload without it. The final electronic display formats are presented in Figure 3; a more detailed explanation of the symbology, emphasizing the generic levels of information, is given in Table III.

Two alterations in the display formats occur at or near the hover under pilot control. The push-button control which selects the automatic turn coordination (ATC) or the heading hold (HH) directional modes also selects the reference frame for the horizontal situation display. When ATC is selected, an approach course-referenced system is used for the display of horizontal position and velocity; this system is illustrated in Figure 3.

When HH is selected near the hover, an aircraft heading-referenced system is used in which the tail of the aircraft symbol is fixed and the landing pad/approach course symbol both translates and rotates to indicate position and orientation. The heading-referenced display proved to be more effective in conveying to the pilot the information required for the precision hover; however the earth-referenced system was preferable for the approach. A second format variation for the hover task was a discrete increase in sensitivity of the velocity vector and velocity command diamond selected by the pilot by voice command to the radar operator; in this "hover mode" the scaling of the vector and diamond was 5 kt/cm while the approach scaling was 20 kt/cm. Both of the above display variations resulted from preliminary flight testing of the display formats.

Control System Characteristics

The other major design variable of this experiment was the degree of stability and/or control augmentation provided to the aircraft. The intent during the design of the augmentation systems was to examine generic levels of complexity to aid the design of future augmentation schemes, and so the characteristics of each were chosen to be "good" in the sense of compliance with MIL-F-83300 (Reference 17) when possible, with verification of the control forces and sensitivities being made during the preliminary ground simulations. The baseline system was selected to be an attitude command augmentation system similar in concept and characteristics to that used by NASA-Langley (Reference 9); systems both less complex and more complex were then designed consistent with past design practice and projected possibilities. The five resulting control systems are described in the following paragraphs; salient characteristics of them are listed in Table IV.

Rate Augmentation. This control system represents the minimum control and stability augmentation system complexity considered feasible for V/STOL aircraft. In particular, the system was mechanized as rate SAS only, with pitch, roll, and yaw rate stabilization approximately equal to the basic X-22A SAS chosen as a representative level. Although the resulting dynamic characteristics through transition were therefore dependent on the X-22A aerodynamics and hence not completely general, these characteristics are representative of this class of V/STOL aircraft, and the results for these configurations therefore provide a suitable base for minimal augmentation complexity. Duct rotation is manual.

Attitude Command Augmentation. This system is the baseline configuration chosen to be similar to that used in the NASA-Langley experiments (Reference 9). The directional axis is dual mode, selectable by the pilot; one mode is automatic turn following (zero sideslip) implemented by feeding back lateral velocity and washed-out yaw rate in the directional channel, and the other mode is yaw-rate-command-heading-hold, implemented by closing a heading loop in the directional channel, removing the washout on yaw rate, and using a proportional-plus-integral filter on the rudder commands. Both the pitch and roll axes provide attitude command responses, although the implementations were different. In the pitch channel, the

aircraft was highly attitude augmented ($\omega_n \approx 4.0$ rad/sec at hover) to minimize turbulence response and coupling inputs from the collective; the pitch stick commands were then shaped through a second-order pre-filter "model", with feedforward gains on stick input, model pitch rate, and model pitch attitude used to ensure second-order aircraft response. The prefilter characteristics ($\omega_n = 2.0$ rad/sec, $\zeta = 0.7$) were chosen to be consistent with "good" short-term longitudinal response characteristics as determined in an earlier X-22A experiment (Reference 18). In the lateral channel, system limitations precluded a similar implementation, and so attitude augmentation only, of a lower level, was used ($\omega_n \approx 2.0$, $\zeta \approx 0.5$ at hover). Again, duct rotation is manual.

Pitch Attitude Command/Roll Rate Command. This system is identical to the attitude command system described above except that an integral-plus-proportional prefilter is added to the roll stick input to provide a rate-command-attitude-hold roll response. Although the emphasis of this experiment was on localizer and glide slope tracking through deceleration rather than initial acquisition, it was recognized that roll attitude command is generally disliked by pilots for gross maneuvering because of the necessity to hold a constant force while performing a turn. The purpose of this control configuration was therefore to ascertain if tracking and hover performance would be the same for roll rate command and attitude command. As with the baseline control system, duct rotation was manual.

Automatic Duct Rotation. This control system represents an increase in complexity from the baseline attitude command system by making the duct rotation automatic instead of manual. The pitch, roll, yaw, and collective stick implementations and response characteristics are identical to those of the attitude command configuration. The automatic rotation is provided by feeding the ITVIC director signal to the duct rotation system. It should be noted that, conceptually, the elimination of the manual configuration change provides a situation comparable to the helicopter instrument approach studies of Reference 9.

Decoupled Velocity Control. This control system was the most complex investigated, and in fact is only one step away from a fully automatic system. The intent of the design was:

- To provide decoupled responses to collective stick (vertical velocity with respect to the ground) and duct angle (longitudinal velocity with respect to the ground) over the full range of duct angles from forward flight to hover.
- To provide augmented damping and hence improved aircraft responses in vertical and longitudinal velocity.
- To minimize pitch attitude input requirements through the transition.

In order to meet the design goals, the vertical and longitudinal velocity

errors as determined by the guidance system were used in feedback loops in the control system in addition to the conventional aircraft quantities. Some degree of decoupling and augmentation was sacrificed in an effort to avoid the necessity of programming all the feedbacks and cross-gearings as a function of duct angle, and in fact in the final design only one programmed cross-gearing (collective to pitch stick) was used. This system again employs automatic duct rotation. Details of the design are contained in Reference 4; a summary of the implementation is given in Table V.

CONDUCT OF THE EXPERIMENT

Equipment

The U. S. Navy X-22A V/STOL aircraft was used as the in-flight simulator for this experiment (Figure 4). This aircraft has a Calspan-designed four-axis (pitch, roll, yaw, thrust) VSS which enables it to reproduce a wide variety of aircraft dynamic characteristics; details of the X-22A and its VSS are covered more fully in Reference 19. For this program, the VSS capabilities were considerably enhanced by the addition of a Calspan-designed-and-fabricated on-board analog computer (Reference 20), which performed all of the guidance and some of the control system functions discussed earlier in this paper. Both experimental and flight safety data were telemetered to the Mobile Data Monitoring System and Digital Data Acquisition System developed expressly for the X-22A by Calspan (Reference 21). In addition, the X-22A Ground Simulator was used extensively as a design tool during the initial stages of the experiment (References 10, 22).

To provide a variable display capability, a Calspan-designed-and-fabricated analog symbol generator in conjunction with a 5" Kaiser CRT were added to the aircraft (References 20, 23). The programmable symbol generator is capable of producing as many as 32 different calligraphic symbols, and combines the simplicity and ease of programming available in an analog computer with an in-flight flexibility exceeding that of more complex digital devices. Ten combinations of the thirty-two output channels can be individually blanked through the use of switches in the cockpit; additionally, a display mode switch selects different inputs to the symbols to provide either an approach-course-up or heading-up reference for the display format. These capabilities are very important for in-flight research experiments, as different display presentations may be evaluated during flight without landing and reprogramming the symbol generator.

For this experiment, the raw X,Y,Z position data were provided by an AN/SPN-42T1 precision tracking radar manufactured by the Bell Aerospace Company. These data were obtained by resolving elevation, azimuth, and range information from the radar into X,Y,Z components relative to one of five selectable approach course directions; these components were then telemetered to the aircraft for processing on-board. As was discussed earlier, the guidance computations performed on the analog computer in the aircraft were essentially independent of the AN/SPN-42T1 equipment; the only exception was the necessity to perform a scale change to ensure sufficient resolution in the

X and Z radar data in hover because of the limited digital word length (and hence scaling per "bit") of the telemetry uplink in the AN/SPN-42T1. Details concerning this scale change, and other characteristics of the radar system, are contained in Reference 4.

Evaluation Task and Procedure

To obtain valid flying qualities data in the form of pilot ratings and comments, careful attention must be given to defining, for the evaluation pilot, the mission which the aircraft/display/pilot combination will perform and the conditions in which it will be performed. For this experiment, the simulated aircraft was defined to be a vectored-thrust VTOL transport with all-weather capability performing terminal area operations; the aircraft was considered to be a two-pilot operation to the extent that the evaluation pilot was relieved of secondary duties (e.g. communications) during the performance of the mission.

The specific tasks to be accomplished for each evaluation consisted of two fully-hooded instrument approaches from 100 kt to the hover; at the conclusion of the second approach, vertical airwork and an actual hooded landing were options available to the pilot. The elements of the approach are shown in Figure 5 and summarized below:

- level flight localizer acquisition (1700 ft AGL, 100 kt)
- constant speed glide slope acquisition (7.5 degrees) at approximately 12,000 ft range
- constant deceleration (.05g) on the glide slope, commencing at a range dependent on headwind (zero-wind range approximately 8000 ft)
- flare to level final approach commencing at approximately 800 ft range, final altitude 100 ft, deceleration continuing to hover
- hover at 100 ft above simulated pad, vertical airwork as desired.

It should be noted that this approach task was chosen to provide a representative level of difficulty, and was not designed to exploit or to avoid either capabilities or limitations of the X-22A. In particular, the constant deceleration profile is a more demanding task for the pilot/aircraft/display system than one "optimized" to a particular aircraft (e.g. constant attitude for helicopters), but operational use of VTOL aircraft may require that they all follow identical deceleration profiles, and constant deceleration is reasonable from an implementation point of view and provides a realistic operational task.

Upon completion of the two instrument approaches, the pilot made

comments with reference to a detailed comment card which directed his attention to the characteristics of the display, control system, and his performance which were of interest. He then assigned a Cooper-Harper pilot rating (Reference 24) to the aircraft/display configuration as evaluated, although actual landings were not to be weighted into the rating, and also assigned a turbulence effect rating, the purpose of which is primarily to give the analyst a qualitative indication of how much the ambient turbulence affected the evaluation.

EXPERIMENT RESULTS

Data obtained in this flight experiment consist of pilot ratings and commentary for each configuration, measurements of performance indices, control usage data, and aircraft response calibration records. The calibration records are used to verify the simulated dynamics by application of a digital identification technique developed for the X-22A (Reference 25); an example longitudinal case is shown in Figure 6. This paper will discuss the pilot rating data and their implications; analyses of performance indices and more detailed discussions of other results are given in Reference 4.

General Results

Figure 7 summarizes the bulk of the pilot rating data obtained on a "plot" of display sophistication versus control complexity. This means of presenting the data is chosen to facilitate comparison of trends with the AGARD graph in Figure 1; it is emphasized that the axes are ordinal rather than interval, and that the approximate iso-rating lines refer only to the data specifically on the figure as a device to emphasize the interactive effects. The data on this figure represent evaluations performed when crosswinds were not considered a major influence on the evaluation — repeat evaluations chosen to emphasize the important effects of crosswinds will be discussed separately.

Consider initially those configurations for which the pilot rating indicates satisfactory system performance ($PR \leq 3.5$). In a general sense, the most apparent result is the demonstration of the hypothesized interaction between control complexity and display sophistication: as the level of augmentation and/or automation increases, the required display presentation decreases from full integrated control director information to velocity (and velocity command) information both vertically and horizontally. It is apparent also that, for a satisfactory system, the display must include velocity status information, a result which corresponds to Dukes' findings (Reference 12); this requirement is primarily hover-oriented, and is a function of the need to know translational drift velocities accurately for touchdown. In the NASA-Langley experiments, touchdowns were performed without velocity status information, using only control-director and horizontal position information, but the conclusion was that the system "was not adequate for operational use" (Reference 9); the corresponding configuration in

this experiment was the ED-1 display and control director information on the ADI needles with the attitude command control system, and the pilot rating of 7 corroborates the unacceptability of this combination.

Within those configurations considered satisfactory, several important points should be noted. First, pitch and roll control directors are not required for satisfactory performance with an attitude command system as implemented in this experiment; although Dukes' helicopter simulations demonstrate a similar conclusion for the hover task, until this X-22A experiment it was thought that full control command information would be required for satisfactory decelerating instrument approaches (Reference 9). Second, note that when the pilot is relieved of performing the configuration change (Auto λ), the necessity for a collective stick director for vertical control is removed; pilot comments indicate that the automatic duct rotation allowed him to concentrate more thoroughly on the vertical task, and that vertical position and rate errors then were sufficient for satisfactory control. If the pilot must perform the configuration change manually, however, the collective director is necessary to reduce the workload in that axis; in general, control of vertical velocity is a demanding task in VTOL aircraft because of the changing effects of thrust magnitude with configuration and velocity as well as, for the task used in this experiment, the requirement to arrest the rate of sink at 100 ft AGL while still decelerating. The tradeoff between display sophistication and level of automaticity is quite evident in this control axis. Finally, note that, as long as velocity information is given to the pilot on the display, no trend of pilot rating with display sophistication is evident for the decoupled velocity control system. This result indicates the advantage of providing the pilot with augmented and decoupled control over the two velocity components of major interest plus eliminating the need for manual configuration changes; if "good" airplane response characteristics relative to the task are provided, the details of the displayed information become less important to satisfactory system performance.

Turning to those combinations rated adequate but unsatisfactory ($3.5 \leq PR \leq 6.5$), the data are useful primarily for noting trends as either display sophistication or augmentation complexity is reduced from the level required for a satisfactory system. First, note that acceptable system performance is possible with rate augmentation only (when the effects of crosswinds are not important) if the display includes integrated full control director information. Such a combination is unsatisfactory primarily because of attitude control problems in the hover, even with the stabilization commands provided by the pitch and roll directors; pilot comments indicate a tendency to overcontrol in pitch when attempting to move around the landing pad, and a preference for force feedback from the controls to help know the attitude. Roll attitude control problems in hover also account for the degradation in rating when the pitch and roll control directors are removed from the display for the pitch attitude/roll rate command control system. Difficulties in maintaining precise control of vertical velocity and glide slope are responsible for the degradation when the collective stick director is removed with the attitude command system (going from ED-2+ to ED-2); as indicated earlier, vertical control is a demanding task which requires

increased display sophistication when the configuration change must be performed manually.

Considering finally those combinations considered inadequate for the task ($PR > 6.5$), two important results are apparent. First, rate augmentation only is unacceptable if pitch and roll control directors are not provided; as would be expected, control of pitch and roll attitude during the deceleration and hover requires an intolerable level of pilot compensation if stabilization commands are not explicitly provided. Second, the lack of displayed velocity information (ED-1) is unacceptable even with a high degree of automation and augmented aircraft translational velocity responses. The requirement for explicit velocity information is hover-oriented, as pilot comments indicate that the precision of control necessary for touch-down must include displayed velocity information for even an acceptable situation to exist.

Effects of Crosswinds

Although acceptable system performance for the rate augmentation/full control director combination had been predicted by the ground simulations prior to flight and verified in flight when low headwinds were present, pilot comments in the evaluations noted that control of heading, without the dual-mode directional system used in the more complex augmentation schemes, required additional attention in the hover. This problem would be exacerbated if the pilot were required to perform large heading changes in the hover to line up with the wind, and so selected repeat evaluations were performed with a pure crosswind of approximately 10 kt. The resulting data are shown in Figure 8. As can be seen, the rate augmentation control system is now unacceptable even with full control director information. This degradation is a result of the pilot being unable to point the aircraft into the wind during the hover and the concomitant drift velocities that are generated. Note that no degradation was observed for the attitude command system in crosswinds, because the turn-following (zero sideslip) mode of the directional control channel pointed the aircraft into the wind automatically. It is possible that a display of wind direction information to the pilot could largely alleviate this problem for the rate augmentation control system; although this additional information can be derived by the onboard LORAS airspeed sensors, the inclusion of it was not investigated in this experiment. Without this information, the control system must perform the pointing function to achieve a satisfactory or acceptable system.

Effects of ITVIC

The data presented in Figures 7 and 8 and discussed in the preceding subsections were all obtained using the Independent Thrust Vector Inclination Command (ITVIC) director light, either to command the pilot to perform configuration changes when manual duct rotation was required, or as status information when the evaluation configuration included automatic rotation. Although it had originally been planned to devote several repeat evaluations to investigating the effects of removing the ITVIC signal, in

fact only two such evaluations were necessary to demonstrate its usefulness, and further investigation would have been pointless. The two configurations used for this check both had the baseline attitude command control system, one with the full control director display (ED-3) and one with the velocity command display (ED-2). In each case, the configuration was rated marginally acceptable (PR = 6); for the control director format, this degradation is from a system that is satisfactory with the ITVIC. The pilot comments indicate that the increased compensation required to derive configuration change command information from either the control director or the velocity command diamond increased the workload considerably and degraded tracking performance, particularly in the vertical plane.

CONCLUDING REMARKS

The experiment described in this paper was performed using the X-22A variable stability V/STOL aircraft, which is capable of changing both stability/control characteristics and display presentations in flight. Although some of the dynamic situations simulated in this flight program are dependent on the basic aerodynamic characteristics of the X-22A, these characteristics are representative of this class of vehicle; the guidance and display conceptual developments are largely independent of the actual aircraft employed.

General conclusions which may be drawn from the successful completion of this flight program are:

- Descending decelerating approach transitions from forward flight to the hover may be performed by VTOL aircraft under instrument conditions given satisfactory control and display system characteristics as defined by this experiment.
- A tradeoff between control augmentation complexity and display presentation sophistication exists for generic levels of each.

Specific results pertinent to the effects of the control system and display variables investigated in this experiment lead to the following conclusions:

- Satisfactory task performance is achieved without pitch and roll control directors, for manual configuration changes, with the Independent Thrust Vector Inclination Command (ITVIC), if an attitude command system in pitch and roll and a dual-mode yaw command system is implemented. No effect of crosswinds on the ratings for this combination was observed.
- Pilot comments for all the control systems investigated express a preference for a control-force-aircraft-attitude relationship in both pitch and roll for instrument hover. This conclusion might be qualified by the fact

that the attitude presentation on the electronic display was difficult to interpret; nonetheless, the comments indicate a desire to obtain the attitude information through control forces rather than visual scanning.

- For VTOL aircraft like the X-22A with low natural height damping in and near the hover, a thrust magnitude director is required for satisfactory task performance if the pilot must also perform configuration changes. Relieving the pilot of the configuration change job allows increased attention to the vertical tracking task and removes the requirement for a control director in that axis.
- The minimal level of displayed information must include translational velocity information to obtain acceptable performance, regardless of the level of control augmentation to the extent investigated in this experiment. This requirement is primarily hover-oriented, and reflects the pilot's dislike of having to obtain translational rates implicitly from the movement of symbols on the display.
- Rate augmentation alone is unacceptable for the task investigated unless full control director information is provided. Although performance with the rate system became unacceptable in crosswinds even with full director information, it is possible that an improved attitude presentation and the addition of wind direction information would provide an acceptable, although still unsatisfactory, system.
- Decoupling and augmenting the longitudinal and vertical velocity responses to control inputs considerably enhanced task performance, and tends to eliminate the trends of pilot rating with display sophistication in the configurations where ground velocity is explicitly displayed.
- The Independent Thrust Vector Inclination Command (ITVIC) director for manual configuration changes was required to achieve satisfactory system performance.
- A simple implementation of airspeed-grounds speed command and tracking switching was shown to be valuable as a means of maintaining aircraft parameters within the allowable transition corridor.

REFERENCES

1. Anon.: Displays for Approach and Landing of V/STOL Aircraft. AGARD Advisory Report No. 51, November 1972.
2. Chen, R. T. N.; Lebacqz, J. V.; and Aiken, E. W.: A Preliminary Look at Flight Director Design Philosophies for Application to a VTOL Landing Approach Flight Experiment. 10th Annual Conference on Manual Control, Wright-Patterson AFB, Ohio, April 1974.
3. Lebacqz, J. V.; and Aiken, E. W.: A Flight Investigation of Control, Display, and Guidance Requirements for Decelerating Descending VTOL Instrument Transitions Using the X-22A Variable Stability Aircraft. 31st Annual National Forum of the American Helicopter Society, Washington, D. C., May 1975.
4. Lebacqz, J. V.; and Aiken, E. W.: A Flight Investigation of Control, Display, and Guidance Requirements for Decelerating Descending VTOL Instrument Transitions Using the X-22A Variable Stability Aircraft. Draft to be submitted to the Naval Air Systems Command, August 1975.
5. Niessen, F. R.: A Low-Cost Inertial Smoothing System for Landing Approach. NASA TN D-7271, June 1973.
6. Hindson, W. J.; and Gould, D. G.: Modification of V/STOL Instrument Approach Geometry as a Means of Compensating for Along-Track Wind Effects. NRC, NAE LR-573, January 1974.
7. Gracey, W.: Comparison of Information Display Concepts for Landing of VTOL Aircraft. NASA TN D-4861, November 1968.
8. Wolf, J. D.: Display and Related System Requirements for IFR Steep Approach: Final Report. JANAIR Report 711106, January 1972.
9. Kelley, J. R., Jr. et al: Flight Investigation of Manual and Automatic VTOL Decelerating Instrument Approaches and Landings. NASA TN D-7524, July 1974.
10. Aiken, E. W.; and Schuler, J. M.: A Fixed-Base Ground Simulator Study of Control and Display Requirements for VTOL Instrument Landings With a Decelerating Approach to a Hover. Calspan Report No. AK-5113-F-2, February 1974.
11. Dukes, T. A.: An Integrated Display Concept for Helicopter and VTOL Aircraft. 25th Annual National Forum of the American Helicopter Society, Washington, D. C., May 1969.
12. Dukes, T. A.; Keane, W. P.; and Tsubanos, C. M.: Image and Superimposed Symbology - An Integrated Display for Helicopters. 29th Annual National Forum of the American Helicopter Society, May 1973.

13. Young, L. R.: Integrated Display Principles and Some Applications to V/STOL Aircraft. AGARD Conference Proceedings No. 96 on Guidance and Control Displays, February 1972.
14. Barrett, J. N.; and White, R. G.: The Flight Development of Electronic Displays for V/STOL Approach Guidance. AGARD Conference on the Guidance and Control of V/STOL Aircraft and Helicopters at Night and in Poor Visibility, Stuttgart, Germany, May 1974.
15. Kelley, J. R.; Niessen, F. R.; and Garren, J. F., Jr.: A Manual Control Approach to Development of VTOL Automatic Landing Technology. Preprint No. 742, 29th Annual National Forum of the American Helicopter Society, Washington, D. C., May 1973.
16. Klein, R. H.; and Clement, W. F.: Application of Manual Control Display Theory to the Development of Flight Director Systems for STOL Aircraft. AFFDL-TR-72-152, January 1973.
17. Anon.: Military Specification — Flying Qualities of Piloted V/STOL Aircraft. MIL-F-83300, December 1970.
18. Schuler, J. M.; Smith, R. E.; and Lebacqz, J. V.: An Experimental Investigation of STOL Longitudinal Flying Qualities in the Landing Approach Using the Variable Stability X-22A Aircraft. 28th Annual Forum of the American Helicopter Society, Washington, D. C., May 1972.
19. Lebacqz, J. V.; Smith, R. E.; and Radford, R. C.: A Review of the X-22A Variable Stability Aircraft and Research Facility. Calspan Report No. AK-5130-F-2, February 1974.
20. Beilman, J. L.; Gavin, T. J.; and Till, R. D.: In-Flight Research Applications of an Analog Computer and Symbol Generator to Determine Display and Control Requirements for VTOL Instrument Landings. 21st International Instrument Symposium, Philadelphia, Pa., May 1975.
21. Beilman, J. L.: An Integrated System of Airborne and Ground-Based Instrumentation for Flying Qualities Research with the X-22A Airplane. 28th Annual National Forum of the American Helicopter Society, Washington, D. C., May 1972.
22. Gavin, T. J.; and Till, R. D.: X-22A Fixed-Base Ground Simulator Facility. Calspan Report No. AK-5113-F-1, October 1973.
23. Lebacqz, J. V.; and Aiken, E. W.: The X-22A Task III Program: Control, Guidance, and Display Requirements for Decelerating, Descending VTOL Instrument Approaches. Advanced Aircrew Display Symposium, NATC, Patuxent River, Md., April 1974.
24. Cooper, G. E.; and Harper, R. P., Jr.: The Use of Pilot Rating in the Evaluation of Aircraft Handling Qualities. NASA TN D-5153, April 1969.

25. Lebacqz, J. V.: The Efficient Application of Digital Identification Techniques to Flight Data From a Variable Stability V/STOL Aircraft. AGARD Flight Mechanics Panel Specialists' Meeting, NASA-Langley, Hampton, Va., November 1974.

TABLE I
HORIZONTAL VELOCITY GUIDANCE COMMANDS

VELOCITY COMMANDS	BEFORE SWITCHING (AIRSPEED/COURSE TRACKING)	AFTER SWITCHING (DECELERATION TO HOVER)
EARTH-REFERENCED	$\dot{x}'_{ec} = -\dot{x}'_{hc} \cos \psi + \dot{y}'_{hc} \sin \psi$ $\dot{y}'_{ec} = \dot{x}'_{hc} \sin \psi + \dot{y}'_{hc} \cos \psi$	$\dot{x}_{ec} \cong \begin{cases} -1.13 \sqrt{x_e} & , x_e > 0 \\ 1.13 \sqrt{ x_e } & , x_e < 0 \end{cases}$ $\dot{y}_{ec} = -.064e$
A/C HEADING-REFERENCED	$\dot{x}'_{hc} = \dot{x}_h - \Delta u$ $\dot{y}'_{hc} = -.064e - \dot{y}_e + \Delta u \sin \psi + \dot{y}_h$	$\dot{x}_{hc} = -\dot{x}_{ec} \cos \psi + \dot{y}_{ec} \sin \psi$ $\dot{y}_{hc} = \dot{x}_{ec} \sin \psi + \dot{y}_{ec} \cos \psi$

NOTATION: ψ = aircraft heading with respect to approach course
 $()_e$ = approach course (earth)-referenced quantity
 $()_h$ = aircraft heading referenced quantity
 $()_c$ = command quantity
 $()'$ = a "before switching" quantity

TABLE II
CONTROL DIRECTOR LOGIC

DIRECTOR ELEMENT	VARIABLE	FULL SCALE SIGNAL				DECOUPLED VELOCITY CONTROL
		RATE AUGMENTATION	ATT/RATE AUGMENTATION	ATTITUDE AUGMENTATION	AUTO λ	
HBAR	ϵ_x	± 33 (ft/sec)	33	33	33	33
	θ_{wo}	± 37 (deg)	75	75	75	--
	ρ	± 230 (deg/sec)	230	230	230	--
VBAR	ϵ_y	± 42 (ft/sec)	42	42	42	42
	ϕ	± 20 (deg)	20	110	110	110
	ρ	± 67 (deg/sec)	38	296	296	296
VTAB	ϵ_z	± 100	100	100	100	100
	$\epsilon_z (\lambda = 0)$	± 50 (ft/sec)	50	50	50	250
	$(\lambda = 90^\circ)$	± 10 (ft/sec)	10	10	10	50

TABLE III
GENERIC LEVELS OF DISPLAYED INFORMATION

DISPLAY FORMAT	ATTITUDE	POSITION		VELOCITY		CONTROL DIRECTORS
		VERTICAL	HORIZONTAL	VERTICAL	HORIZONTAL	
ED-1	Pitch and roll: horizon bar and fixed indices (10° increments). Yaw: tail of fixed a/c symbol with respect to approach course.	Altitude error diamond and fixed indices (50 foot increments). Diameter of landing pad increases with decreasing altitude (2 cm diameter at 100 feet).	Position of fixed a/c symbol with respect to translating landing pad and approach course. Increasingly sensitive scaling with range (100 ft/cm in hover). Three range markers indicate important points of approach.	None	None	None
ED-2	Same	Same	Same	Left-hand circle indicates deviation from commanded descent rate. Increasingly sensitive scaling with duct angle (5 ft/sec/div at $\lambda = 90^\circ$) (25 ft/sec/div at $\lambda = 0^\circ$).	A/c ground velocity vector and velocity command diamond (20 kt/cm). Right-hand velocity error circle with respect to fixed index (± 50 ft/sec/cm).	None
ED-2*	Same	Same	Same	Collective control director (VTAB)	Same	VTAB only
ED-3	Same	Same	Same	VTAB	Same as ED-2 with no velocity command diamond.	Longitudinal, lateral and collective control directors (HBAR, VBAR, and VTAB respectively).

TABLE IV
APPROXIMATE ATTITUDE TRANSFER FUNCTIONS IN FORM $K(\frac{1}{s})[\zeta; \omega]$

	PITCH ATTITUDE TO δ_{ES}	ROLL ATTITUDE TO δ_{AS} (TURN-FOLLOW)
ATTITUDE COMMAND:	Filter \leftrightarrow Aircraft	
0 kt:	$\frac{.40(.17)(.25)}{[.7;4.0] (.17)(.29)[.76;4.13]}$	$\frac{.85(.22)(2.63)}{(.36)(2.63)[.30;2.2]}$
100 kt:	$\frac{.40(.1)(.79)}{[.7;4.0] (.09)(.62)[.68;4.58]}$	$\frac{.85[.60;2.72]}{[.75;1.90][.50;3.12]}$
ATT/RT COMMAND:	Filter \leftrightarrow Aircraft	Filter \leftrightarrow Aircraft
0 kt:	$\frac{.40(.17)(.25)}{[.7;4.0] (.17)(.29)[.76;4.13]}$	$\frac{(2) .35(.22)(2.63)}{(0) (.37)(2.63)[.50;2.18]}$
100 kt:	$\frac{.40(.1)(.79)}{[.7;4.0] (.09)(.62)[.68;4.58]}$	$\frac{(2) .35[.60;2.72]}{(0) [.90;1.90][.55;3.12]}$
RATE AUGMENT.		
0 kt:	$\frac{.40(.17)(.25)}{(.17)(3.06)[.19;.46]}$	$\frac{.35(.26)(1.6)}{(1.7)(2.5)[.11;.58]}$
100 kt:	$\frac{.40(.097)(.79)}{(.18)(-.15)[.93;2.56]}$	$\frac{.35[.86;1.31]}{(.22)(3.54)[.79;1.36]}$

TABLE V
DECOUPLED VELOCITY CONTROL
SYSTEM DESIGN

FEEDBACK VARIABLES	PITCH GAIN (in/unit)	COLLECTIVE GAIN (deg/unit)
ϵ_z (ft/sec)	-0.195	0.07
$\epsilon_{\dot{z}}$ (ft/sec)	0.19	0.52
$\Delta\theta$ (deg)	-0.67	-0.236
q (deg/sec)	-0.33	-0.037
ϵ_{λ} (deg)	0.2	-0.145
FEEDFORWARD VARIABLES		
δ_{ES} (in)	5.73	—
δ_{CS} (deg)	3.84 ($\lambda = 0$) ↓ 0.0 ($\lambda = 90^\circ$)	2.26

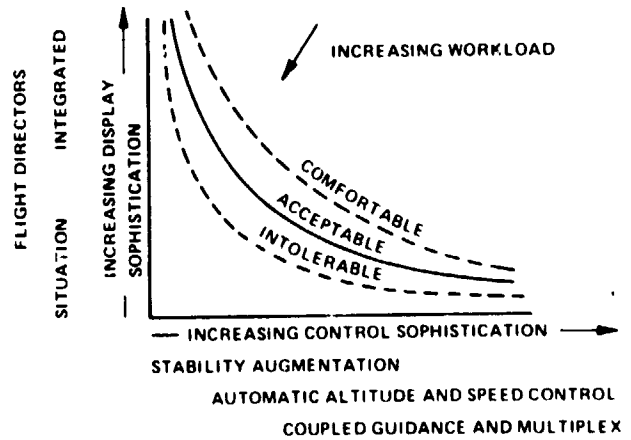


Figure 1 TRADE-OFF BETWEEN DISPLAY AND CONTROL SOPHISTICATION (FROM REFERENCE 1)

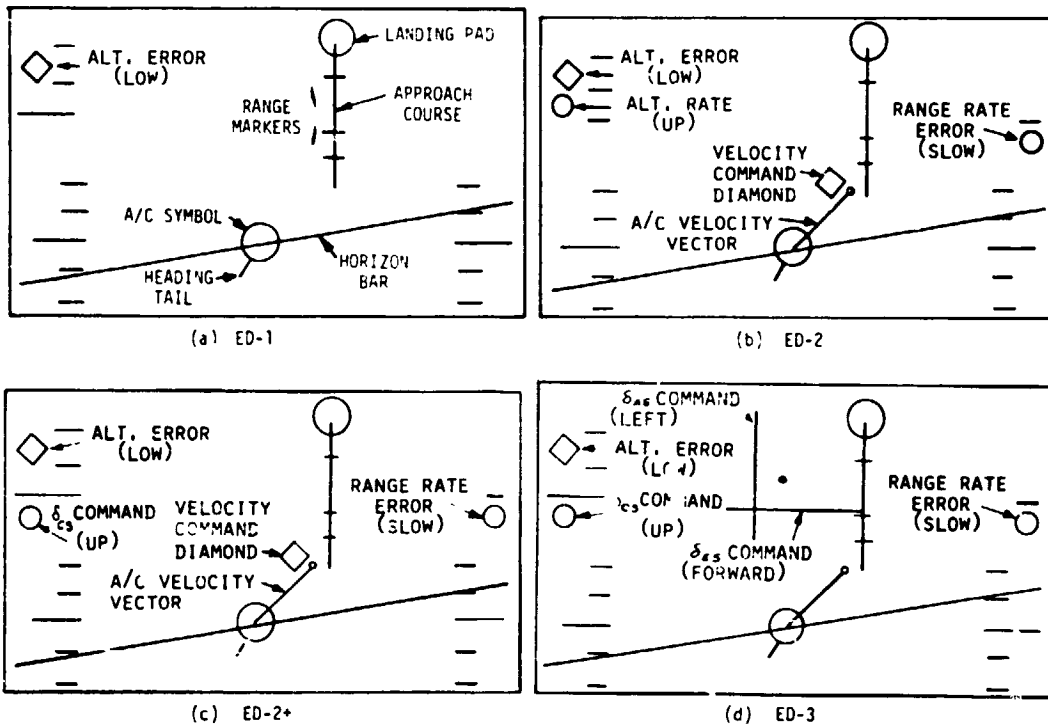


Figure 3 ELECTRONIC DISPLAY FORMATS

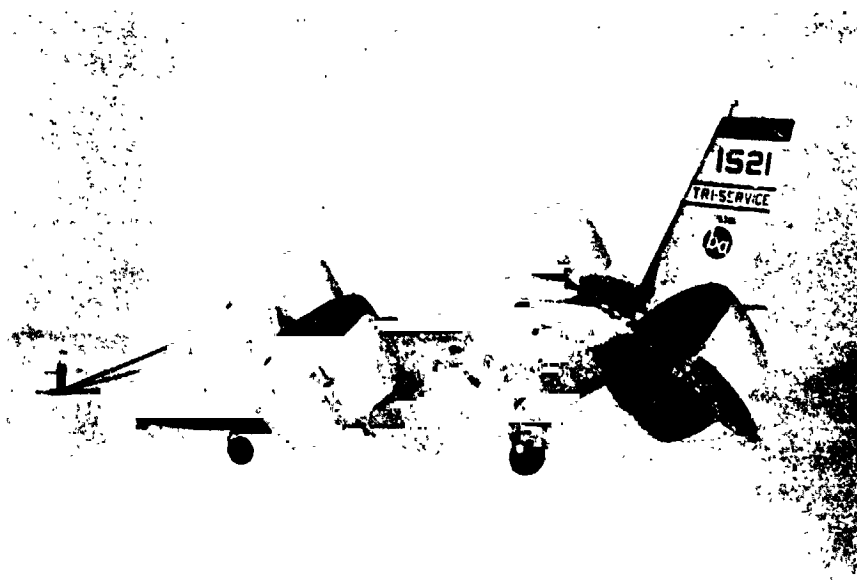


Figure 4 U.S. NAVY VARIABLE STABILITY X-22A

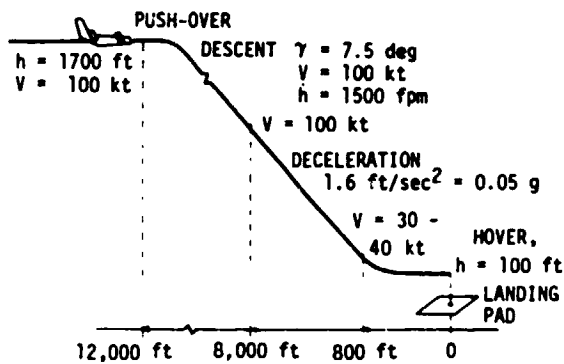


Figure 5 EVALUATION TASK

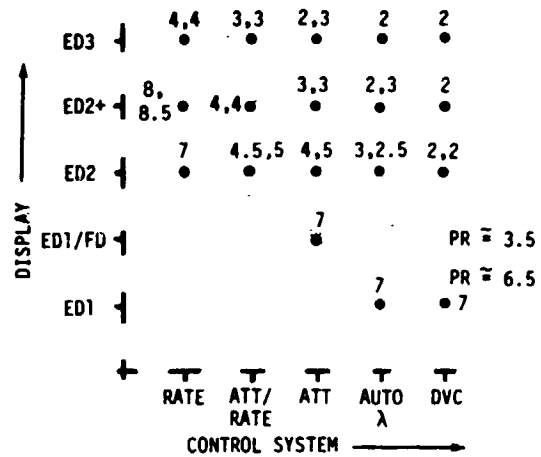


Figure 7 PILOT RATING DATA (WITH ITVIC, NO CROSSWIND EFFECT)

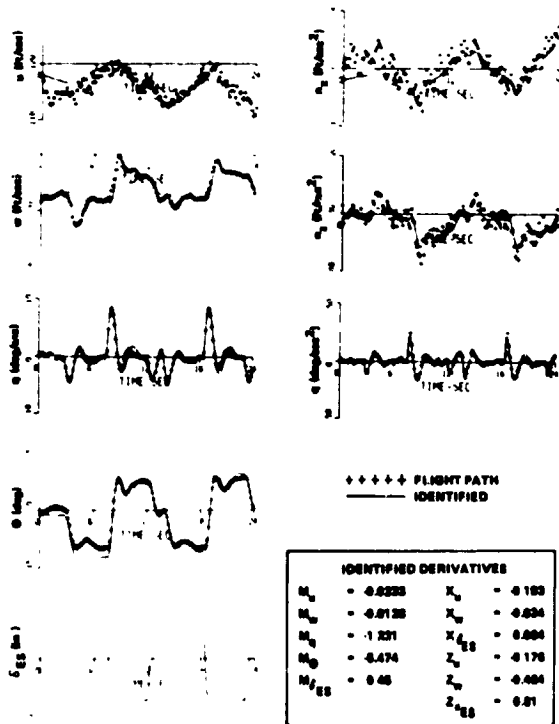


Figure 6 IDENTIFICATION RECORD

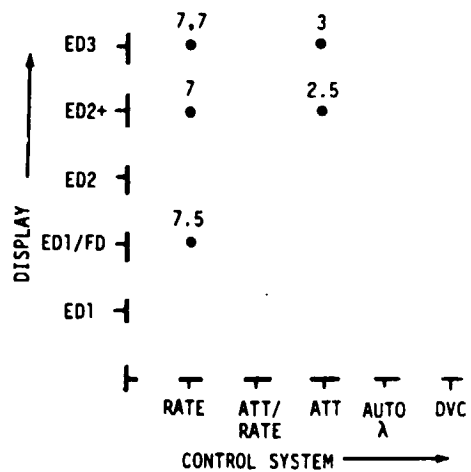


Figure 8 EFFECT OF CROSSWIND ON PILOT RATING DATA (WITH ITVIC)

N75 33696

A SIMULATOR STUDY ON INFORMATION REQUIREMENTS
FOR PRECISION HOVERING

Lt. James L. Lemons, USAF
Aeronautical Systems Div., WPAFB

Theodor A. Dukes
AMS Dept., Princeton University

ABSTRACT

A fixed base simulator study of an advanced helicopter instrument display utilizing translational acceleration, velocity and position information is reported. The simulation involved piloting a heavy helicopter using the Integrated Trajectory Error Display (ITED) in a precision hover task. The test series explored two basic areas. The effect on hover accuracy of adding acceleration information was of primary concern. Also of interest was the operators' ability to use degraded information derived from less sophisticated sources. An example of such degraded information is properly weighted attitude and angular acceleration instead of translational acceleration.

Three conclusions were reached in the course of the study. The addition of translational acceleration to a display containing velocity and position information did not appear to improve the hover performance significantly. However, displayed acceleration information seemed to increase the damping of the man-machine system. Finally, the pilots could use translational information synthesized from attitude and angular acceleration as effectively as perfect acceleration.

INTRODUCTION

The addition of a velocity vector to a display showing position error information significantly improves pilot performance in VTOL aircraft precision tasks (Ref. 1). Exploratory tests of a display utilizing acceleration information, in addition to velocity and position information, elicited favorable pilot comments. The usefulness of adding acceleration information to a display was therefore studied. In addition to the choice of the displayed variables it is important to consider realistically the sources of the information to be displayed. If information from relatively inexpensive sources can be used without a degradation in pilot performance, savings in system cost and complexity may be possible. This possibility, the use of a degraded information source, was explored in the simulator experiments described in this paper. The degraded translational information was derived from attitude related quantities. The study involved fixed base simulation of a heavy helicopter at hover and an experimental display. Below, the description of the display and its modes is followed by a discussion of the

derivation of the desired translational quantities. The helicopter control system and other details of the study are presented next. Finally, the results of the experiments are shown and discussed. A detailed account can be found in Reference 2.

SYMBOLS

B_1	cyclic control input
g	acceleration of gravity
$M()$	moment derivative
q	pitch rate
s	Laplace transform variable
u, v, w	velocity components along aircraft axes
$X()$	force derivative (x-axis)
$\Delta()$	perturbation
ϕ	roll angle
θ	pitch angle

DISPLAY

The Integrated Trajectory Error Display (ITED) developed at Princeton University* was used as the experimental display. The ITED is an abstract analog display which combines horizontal and vertical flight information for presentation on a CRT. A description of the ITED superimposed on an image display can be found in Reference 3.

The display is divided into three areas (Figures 1 and 2). The central area contains information in the horizontal plane: position, velocity, and acceleration. The vertical information band at the left of this area contains the variables needed for altitude control. In the outer bands an artificial horizon provides pitch and roll information. The display was used in two different modes: first, with available ground based position information and second, without such position information.

When used with ground referenced position information, in the "Reference Mode", the display's coordinate system is centered in the aircraft, but has an earth fixed orientation (Figure 1). As a result, the crosshair representing

*This work was supported by the Avionics Laboratory of USA-ECOM at Ft. Monmouth, N.J.

the nominal position moves fore, aft, left, and right across the display only in response to position changes. The helicopter symbol and the velocity and acceleration symbology are central in the Reference Mode. The location of a circle representing the rotor remains fixed; a straight line attached to the edge of the circle represents the tail of the aircraft, rotating in response to yaw changes. The velocity vector (solid line) originates at the center of the rotor. The acceleration vector (small circle) has as its origin the end of the velocity vector and its tip is represented by a small circle. In the airborne format, the display symbology is superimposed on a video image of the terrain. The simulation of a landing pad and a horizon line were added to the symbology as a substitute for an image display.

When ground based position information is not available, the "Marker Star" mode of the display is used, also superimposed on a visual image (Figure 2). The Marker Star represents a stabilized direction in space. It moves on the CRT screen, compensating for the aircraft body angles (in the simulation, the star's motion did not include compensation for roll because, with the small roll angles encountered in hover, their effect was minimal because of the small down-looking angle). As a result of the compensation, the Marker Star can be used as a terrain marker. The pilot can bias the star as desired to "illuminate" a terrain feature of his choice. The star moves with respect to the terrain feature only as the aircraft translates, except for motion along the stabilized beam. The pilot may use this display mode in approach by keeping the terrain feature illuminated while maintaining a desired rate of descent or he may use it in hover by holding altitude and keeping the terrain feature illuminated. The acceleration and velocity vectors are displayed in the same manner as in the Reference Mode.

In both display modes, the vertical information band contains a diamond that moves in response to altitude changes. The vertical velocity vector originates from the center of the diamond. Along the left margin of the vertical band, a small ellipse serves as a torque indicator. Two lines in the outer bands serve as an artificial horizon. From horizontal to the points where the roll reference lines meet the vertical field lines represents ± 20 degrees of roll. Pitch angle is indicated by the cusp of the roll reference triangle on a pitch scale with two-degree increments. At the top of the display is a turn and bank indicator. The display gains for position, velocity, and acceleration were chosen based on previous tests. The scale factors were: horizontal position 12.5 ft/in; horizontal velocity 5 ft/sec/in; acceleration 2 ft/sec²/in; vertical velocity 10 ft/sec/div; altitude 10 ft/div.

DISPLAY INFORMATION

Attitude based information, being readily available and simple to derive, was chosen as an example of a degraded source for translational information. In hover, the translational accelerations of the aircraft result from the tilt of the thrust vector (Figure 3). This tilt has two components. The first, of course, is associated with the aircraft's attitude. The ratio of

the resulting translational acceleration to the attitude of the body, assuming small attitude changes, is:

$$\frac{\dot{u}}{\dot{\theta}} = \frac{\dot{v}}{\dot{\phi}} = \frac{g}{57.3} = .562 \frac{\text{ft/sec}^2}{\text{deg}}$$

The second component of the tilt of the thrust vector is caused by control inputs, gust disturbances, and other factors. This additional component of the thrust vector tilt is also associated with the moment balance and therefore with the angular accelerations of the body. The ratio of additional linear acceleration to the additional component of thrust tilt can be approximated by the ratio of a given translational acceleration to the cyclic pitch causing that acceleration with the aircraft attitude unchanged. Referring to the linearized longitudinal acceleration equation, neglecting gusts,

$$s\Delta u = X_u \Delta u - g\Delta\theta + X_w \Delta w + X_{B_1} \Delta B_1$$

it can be seen that one degree of cyclic input yields a linear acceleration of $X_{B_1}/57.3 \text{ ft/sec}^2$. The same cyclic pitch input causes a pitching moment, hence an angular acceleration. Referring to the linearized pitching moment equation,

$$s\Delta q = M_u \Delta u + M_q \Delta q + M_w \Delta w + M_{B_1} \Delta B_1 + M_{\theta_c} \Delta \theta_c$$

one degree of cyclic yields $M_{B_1} \text{ deg/sec}^2$ in angular acceleration. The relationship between longitudinal translational acceleration and angular acceleration caused by control inputs is:

$$\frac{\dot{u}}{\dot{\theta}} = \frac{X_{B_1}/57.3}{M_{B_1}} = 0.13 \frac{\text{ft/sec}^2}{\text{deg/sec}^2}$$

In the lateral case, if the lateral acceleration caused by the tail rotor is neglected, the same approximation yields

$$\frac{\dot{v}}{\dot{\phi}} = \frac{Y_{A_1}/57.3}{L_{A_1}} = 0.014 \frac{\text{ft/sec}^2}{\text{deg/sec}^2}$$

The approximate relationships between translational and angular accelerations are based on the assumption that moments and forces caused by perturbations in aerodynamic variables are related in a similar ratio as those caused by cyclic control inputs. An implied assumption is also that moments caused by collective input changes are negligible.

The approximate linear accelerations may be derived from an attitude

gyro and from angular accelerometers. They may be integrated to obtain an approximate short term velocity vector, but the attitudes must be passed through high-pass filters in order to accommodate variable wind conditions and slow speed changes near hover. The assumption was made that adequate averaging time was available so that a low frequency source of velocity such as doppler radar or differentiated position could be utilized to obtain long term velocity. Low-pass filtered perfect velocity was used to simulate such a source. Final adjustments of gains were made to achieve a best match with perfect velocity. The final circuit for longitudinal and lateral information processing are shown in Figure 3.

SIMULATION

The VTOL vehicle simulated was the Sikorsky CH53 at hover. It was simulated using a linearized small perturbation model with two alternative control systems. The ASE control system used attitude and rate feedback while the HAS system used attitude, rate, and translational velocity feedback. In addition, altitude and heading hold systems were provided. Gust inputs were generated from low-pass white noise with a corner frequency of .3 rad/sec, a mean of zero, and an rms value of 6 ft/sec.

The test subjects were three US Army test pilots, two of them have had previous experience with the display. There were no significant differences in performance among the three subjects. Each pilot performed two replications of each test cell. The set of test variables was; two displays (the Reference Mode and the Marker Star mode), two control systems (ASE and HAS), and three sources of acceleration and velocity (perfect, attitude augmented with angular acceleration, and attitude only).

RESULTS AND DISCUSSION

The study sought answers to two questions. First: Does the addition of explicit acceleration information to a velocity and position error display significantly improve pilot performance? Second: Can degraded information sources be used for acceleration and velocity display without degrading the hover performance?

The performance measures were RMS position errors and RMS attitude rates. Figure 4 shows the longitudinal and the lateral position errors in the cells using the Reference mode, indicating also the 90% confidence intervals on the means. There are no statistically significant differences at the 1% level among the cells using ASE control or among cells using the HAS, with the exception of cell 6, displaying position errors only. Especially notable is the lack of difference between the cells of perfect and of attitude derived velocity and acceleration (e.g., cells 7 and 16).

Figure 5 presents the longitudinal and the lateral positioning accuracies using the Marker Star Mode. The general differences in magnitude between the longitudinal and lateral errors is caused by the differences in the perceived translational errors. Because of the forward and down looking angle represented by the Marker Star, a certain translational error causes a much larger angular displacement laterally than longitudinally. It can be seen that the addition of acceleration information or the degradation of information quality does not have any significant effect on the RMS position accuracy.

Figure 6 shows the RMS pitch and roll rates in the Reference Mode. Cells 11 and 13 are significantly different at a 1% level of significance. They use the same degraded information sources, but only in cell 11 is the acceleration vector displayed. The differences between cells 7 and 9 show a similar trend, though only at a lower significance level. Note that there are no statistically significant differences in either axis among cells 11, 16, 15, 10, 7; they all display the acceleration vector but use different information sources. When using the ASE control, addition of the acceleration vector distinctly reduces the attitude rates; the degradation of the information quality has no significant effect on the attitude rates.

In the simulated HAS control system, the result is not so unambiguous. This control system is asymmetric in that it is apparently better damped in pitch than in roll. As a result, there are no significant differences in pitch rate among cells 1, 3, 5, or 6. (Figure 6). In the lateral case, the difference between cell 1 and cell 3, while not statistically significant at the 1% level, does indicate a decreased attitude rate with the addition of acceleration information.

Figure 7 shows the RMS pitch and roll rates using the Marker Star mode of the display. Comparing the cells with and without acceleration information from the same source (2 and 4; 12 and 14; 17 and 18) a consistent trend can be observed indicating a reduction of attitude rates with the acceleration added, with the exception of the pitch rate using the HAS system with its tight pitch attitude loop. The amount of the reduction, however, is only less than 30%.

CONCLUSIONS

Under the test conditions described in the text, addition of acceleration information does not significantly improve a pilot's RMS error performance in hover; however, acceleration information does reduce the RMS attitude rates, but not by a large factor. Degrading displayed information quality (by deriving approximate velocities from attitudes and position components) does not degrade pilot performance significantly with either display tested.

REFERENCES

1. Dukes, T.A.: Helicopter Station Keeping. USA ECOM TR-02412-9, September 1972.
2. Lemons, J.L.: A Study of the Effect of Displayed Acceleration Information on VTOL Hover Performance. Princeton University M.S.E. Thesis, Princeton Report No. 1183-T, September 1974.
3. Dukes, T.A., Keane, W.P., & Tsubanos, C.M.: Image and Superimposed Symbology - An Integrated Display for Helicopters. American Helicopter Society 29th Annual National Forum, Preprint No. 724, May 1973.

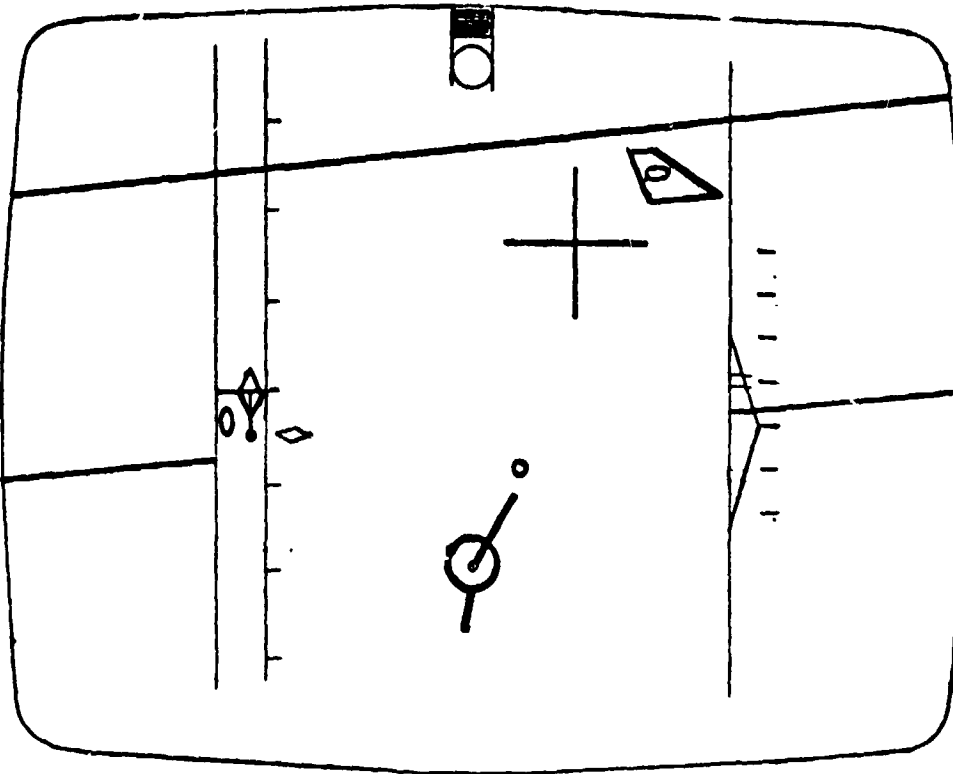


Figure 1. Display, Reference Mode

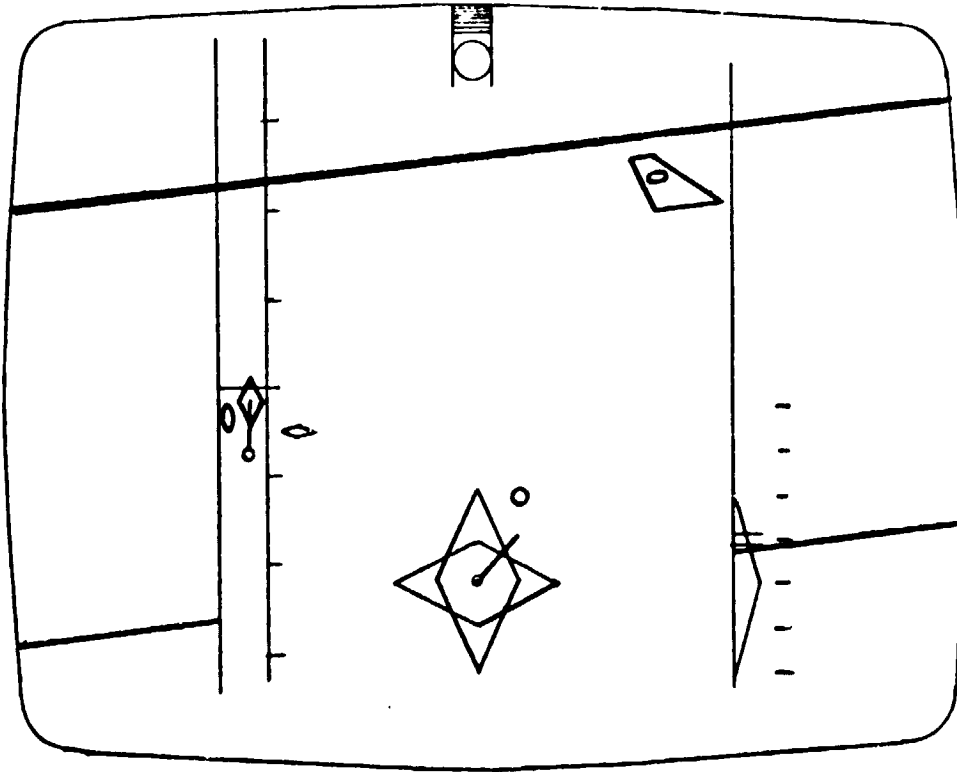


Figure 2. Display, Marker Star Mode

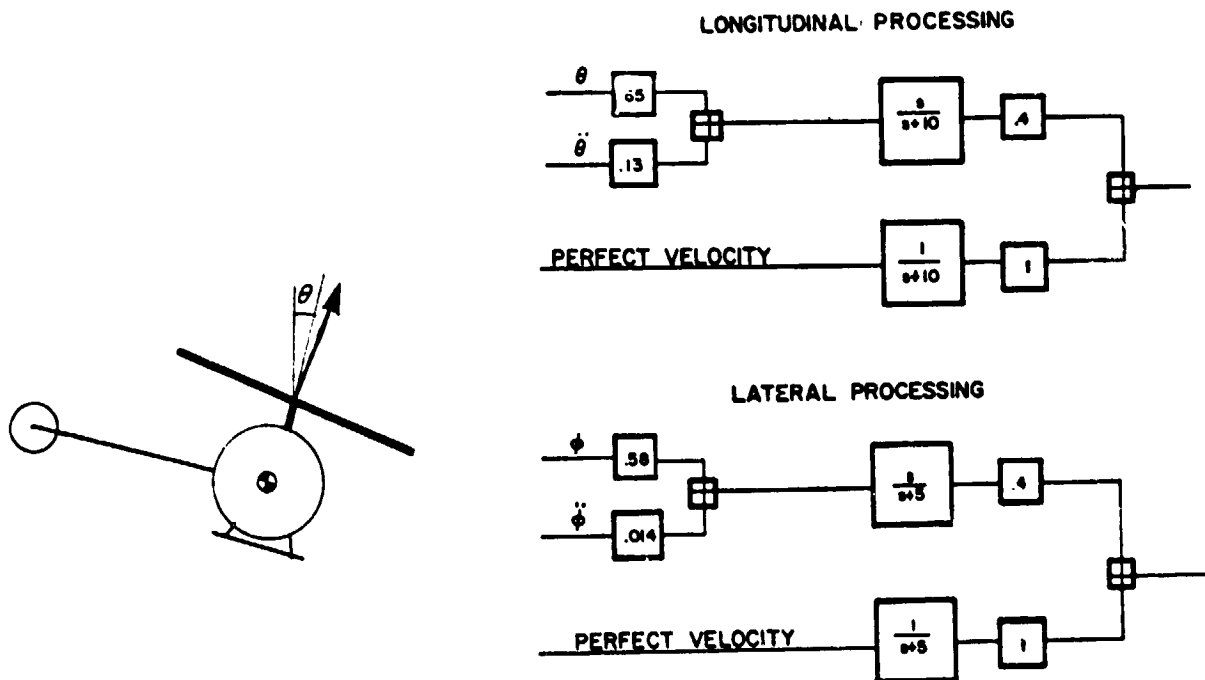


Figure 3. Information Processing

RMS POSITION ACCURACY
Y-AXIS - REFERENCE MODE
90% Confidence Interval

RMS POSITION ACCURACY
X-AXIS - REFERENCE MODE
90% Confidence Interval

Key Perf - Perfect Information
AA - Angular Acceleration plus Attitude
Att - Attitude only
--- - No Information Displayed
] - Average Position and Confidence Interval

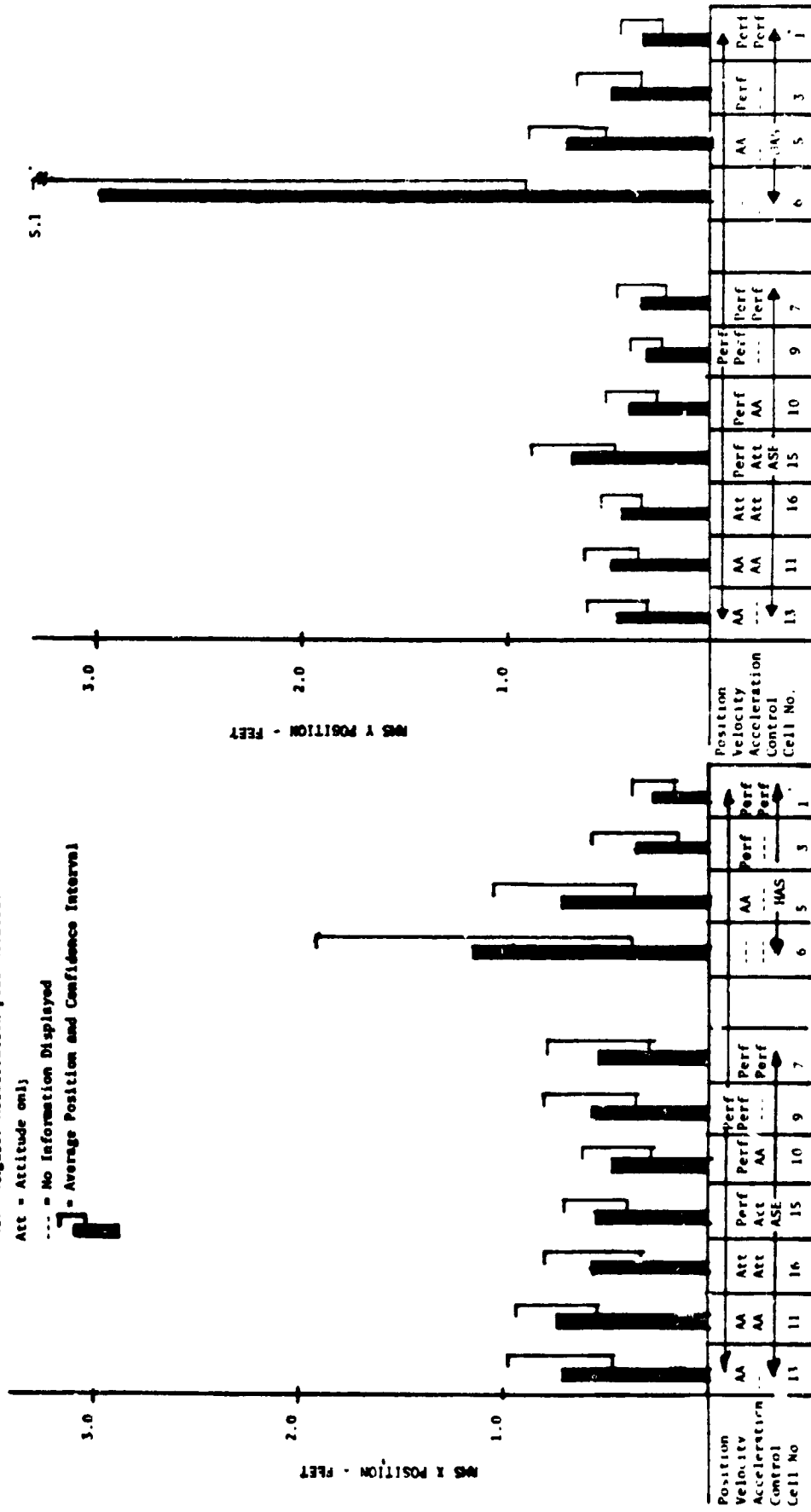
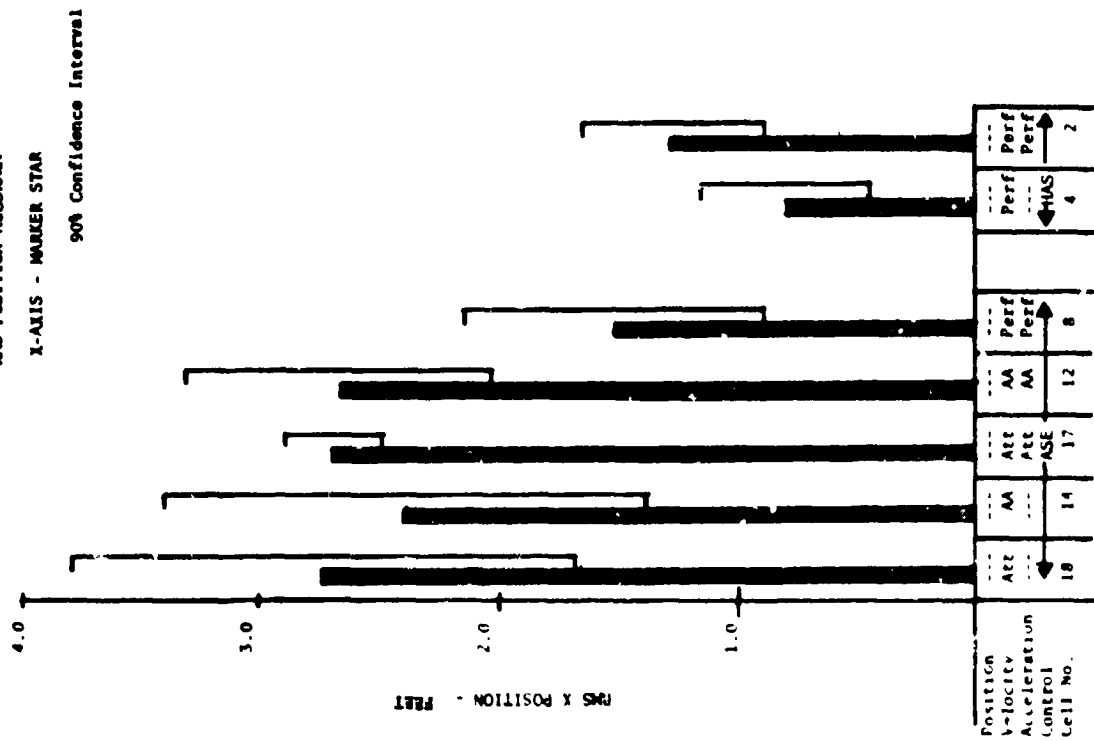


Figure 4. Position Errors, Reference Display Mode

RMS POSITION ACCURACY
X-AXIS - MARKER STAR
90% Confidence Interval



RMS POSITION ACCURACY
Y-AXIS - MARKER STAR
90% Confidence Interval

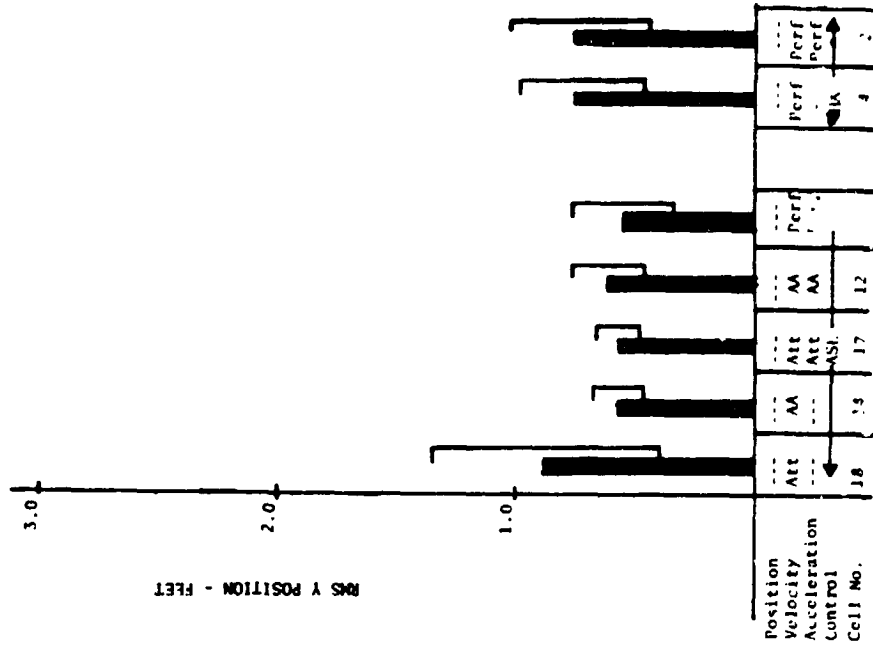


Figure 5. Position Errors, Marker Star Display Mode

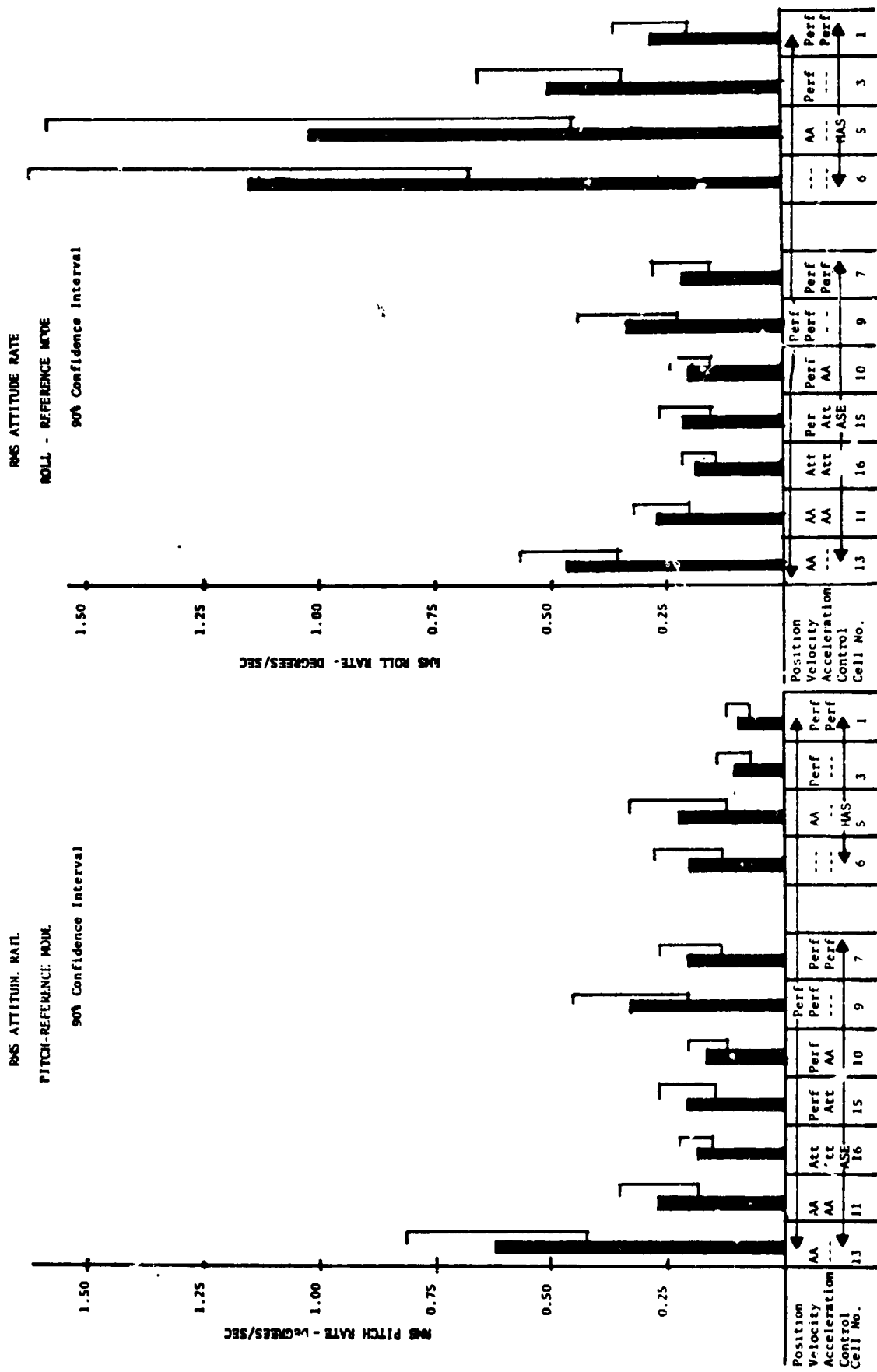


Figure 6. Attitude Rates, Reference Display Mode

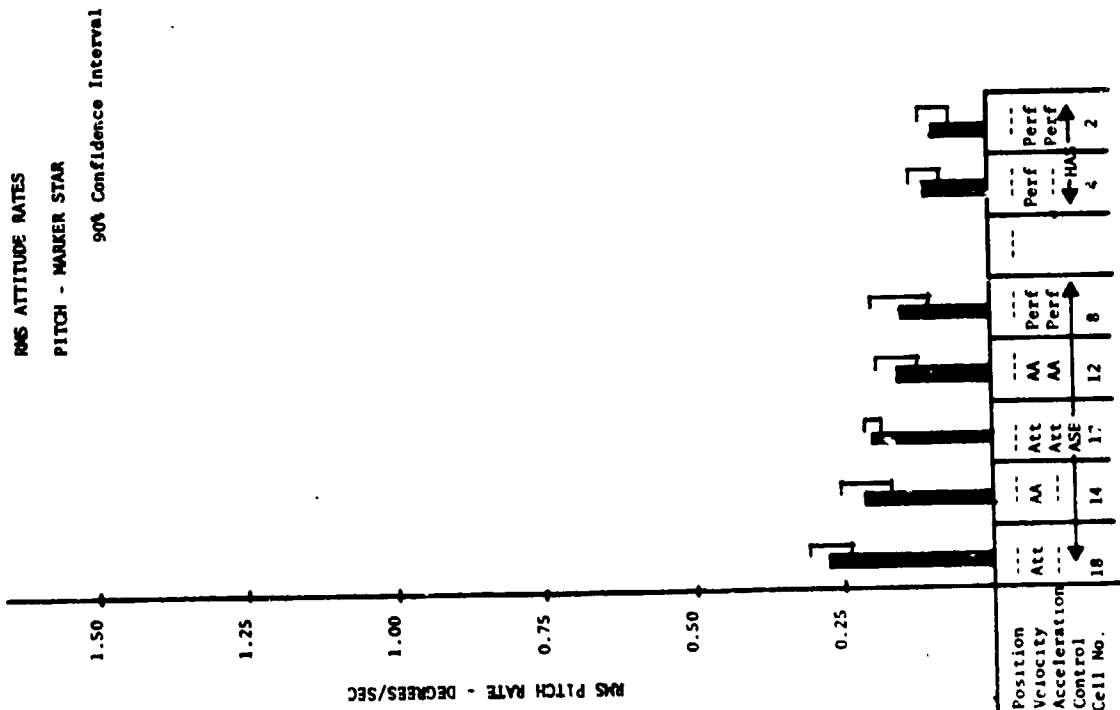
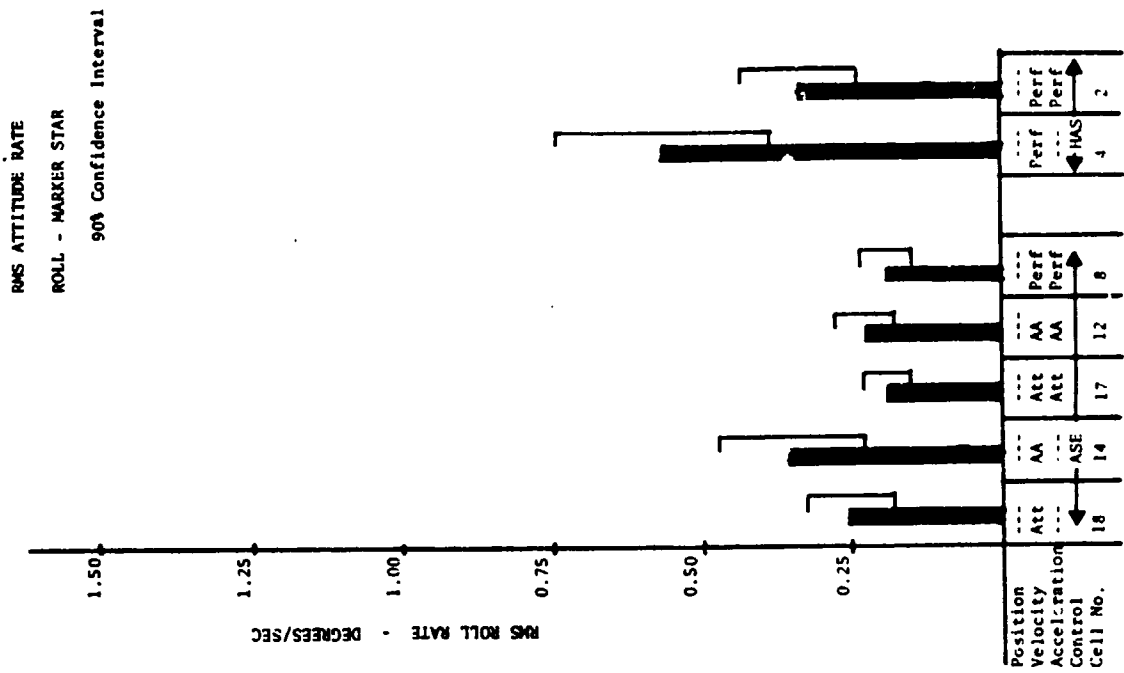


Figure 7. Attitude Rates, Marker Star Display Mode

MOTION-BASE SIMULATOR TESTS OF LOW FREQUENCY AIRCRAFT MOTION
ON THE PASSENGER RIDE ENVIRONMENT

Hugh P. Bergeron and James D. Holt
NASA-Langley Research Center

A large amplitude motion-base simulator, the NASA/Langley Real-Time Dynamic Simulator (RDS), was used to investigate passenger ride quality acceptance of low frequency aircraft motion. The motion simulated had been previously measured during routine airline operations. Passenger subjective ratings of the simulated motion were obtained and compared to ratings obtained from actual aircraft flights.

Subjects used in the simulation consisted of both naive subjects (that is, subjects that had never previously participated in any ride quality tests) and experienced subjects (subjects that had been previously tested in various aircraft ride environments). Each subject was tested at least twice. Three of the experienced subjects were tested up to 20 times.

The results indicate that:

- (1) Simulator motion can be used for evaluating low frequency aircraft motion in passenger ride quality tests.
- (2) The aircraft motion which produces motion sickness can be realistically simulated.
- (3) A small number of experienced subjects can be used to represent larger numbers of naive subjects.
- (4) Repeated runs with experienced subjects show no apparent run-to-run bias.

N75 33697

**A MODEL-BASED ANALYSIS OF A DISPLAY FOR
HELICOPTER LANDING APPROACH**

Ronald A. Hess and L. William Wheat

Abstract

A control theoretic model of the human pilot was used to analyze a baseline electronic cockpit display in a helicopter landing approach task. The head-down display was created on a stroke-written cathode-ray-tube and the vehicle was a UH-1H helicopter. The landing approach task consisted of maintaining prescribed groundspeed and glideslope in the presence of random vertical and horizontal turbulence. The pilot model was also used to generate and evaluate display quickening laws designed to improve pilot-vehicle performance. A simple fixed-base simulation provided comparative tracking data.

Nomenclature

$u(t)$	groundspeed deviation from nominal 60 kt approach speed ft/sec
$\theta(t)$	pitch attitude deviation from trim, rad
$h(t)$	deviation from nominal -6° approach glideslope, ft
$\delta_B(t)$	cyclic control stick motion, ft (measured at pilot's hand)
$\delta_C(t)$	collective control stick motion, ft (measured at pilot's hand)
$u_1(t), u_2(t)$	optimal control motions before pilot's time delay and neuromuscular dynamics are encountered, ft

I. Introduction

Few, if any, V/STOL aircraft have effective poor weather capability, particularly as regards landing in restricted sites. Fundamental to this problem is the fact that existing cockpit displays are inadequate for V/STOL approach and landing. Electronic displays show potential for improving this situation. Unfortunately, the full potential of such electronic devices has seldom been exploited by the use of dynamic models of the pilot-display-vehicle system.

In this preliminary study, a control theoretic model of the human pilot was used to analyze longitudinal pilot-vehicle performance in a helicopter landing approach when an electronic display was providing control/guidance information. The pilot model was also used to provide preliminary quickening laws, and was then called upon to evaluate the effectiveness of these laws in the landing approach task. The analysis was followed by a brief fixed-base simulation study which provided comparative root-mean-square (RMS) tracking data.

II. Control Theoretic Model

The pilot model utilized in this study is nearly identical to that offered by Kleinman, Baron and Levison [1]. The fundamental hypothesis behind the control theoretic model is that, subject to his inherent limitations, the well-trained, well-motivated pilot behaves in an optimal manner. The pilot's control characteristics can be modeled by the solution of an optimal linear control and estimation problem, with certain "modifications". These modifications are summarized as follows:

- (1) Time Delay A pure time delay is included in each of the pilot's control outputs.
- (2) Neuromuscular Dynamics Each output neuromuscular system is modeled as a first-order lag, or, equivalently, control rate appears in the quadratic index of performance.
- (3) Observation and Motor Noise Each variable which the pilot observes from his display is assumed to contain pilot-induced additive white noise which scales with the variance of the observed variable. Each control output is assumed to contain pilot-induced additive white noise which scales with the variance of the control.
- (4) Rate Perception If a variable is displayed explicitly, the pilot also perceives the first derivative of the variable but no higher derivatives. The first derivative of the displayed variable is also noise contaminated.

(5) Index of Performance The index of performance for the optimization procedure is chosen subjectively by the analyst to mirror what he believes to be the task and control objectives as perceived by the pilot.

The placement of the pilot time delay at the control output constitutes the only major deviation from the model of Kleinman, et. al. Here, the delay is represented by a second-order Pade' approximation and is treated as part of the plant dynamics. The model of [1] subsumes the delay into the observation process. The only advantage which the Pade' approximation affords is that it allows direct use of existing computational algorithms for the solution of optimal estimation and control problems.

Figure 1 is a block diagram representation of the pilot-display-vehicle system. Table I lists the baseline pilot model parameters chosen for this analysis. Weighting coefficients for the index of performance were selected on the basis of subjective judgment of the allowable deviations of the variables included in the index [2].

III. Vehicle Model

The UH-1H helicopter was the vehicle chosen for study. This single-engine, single-rotor utility helicopter weighs approximately 8500 lbs in the flight condition studied here. The particular vehicle modeled did not have a stabilizer bar, a device attached to the rotor hub which provides pitch and roll damping. In the configuration studied, the vehicle's handling qualities were marginal, with phugoid and short-period characteristics of $\zeta_p = -.15$, $\omega_p = .41$ rad/sec; $\omega_{sp} = .85$, $\omega_{sp} = 1.05$ rad/sec. Note the relatively large undamped natural frequency of the unstable phugoid mode. The reason for choosing an unaugmented vehicle was to determine the extent to which increased display sophistication alone could improve pilot-vehicle performance.

The nominal flight path was a -6° glideslope at constant 60 kt (101.34 ft./sec) groundspeed. The vehicle was exposed to random vertical and horizontal turbulence whose power spectral densities are given in Table 2. Only longitudinal motion was considered.

IV. Display

Figure 2 is a representation of the display symbology and baseline gains for the longitudinal approach task. In the quickened configuration, the pitch attitude and glideslope deviation symbols were quickened in a manner to be described. The nominal eye-to-display distance was 2.5 ft. The display itself was 6.5 in wide and 7.5 in high. Display symbology for lateral-directional control was not pertinent to the study and was not generated in the simulation to be described. Due to the nature of the groundspeed deviation

symbology, it was assumed in the analysis that groundspeed deviation rate was not perceived by the pilot.

V. Model for Task Interference

Reference [3] describes the model for task interference used in this study. In contrast to the situation in which the pilot need only concern himself with a single task, e.g., control of pitch attitude, task interference implies the pilot tracking behavior and performance which accompany shared attention, e.g., control of both pitch attitude and glideslope deviation. The model for task interference used here does not imply pilot scanning behavior. The assumptions implicit in the model are:

- (1) Multiple tasks are performed in parallel, not in sequence.
- (2) The pilot has a relatively large, fixed number, N, of "information processing channels" to distribute among his various tasks.
- (3) Each of these channels is perturbed by a white Gaussian noise process, uncorrelated with all other noise processes and system variables. The noise levels are proportional to signal variance.
- (4) The noise/signal ratio for any display is inversely proportional to the percentage of the N channels which the pilot devotes to that display.
- (5) The pilot allocates the N channels so as to minimize the index of performance defined in the modeling procedure.

Just as in [4], the effects of task interference were modeled as an increase in the nominal noise/signal ratios given in Table 1, for each displayed variable. Thus,

$$\rho_i = \rho \cdot \frac{1}{f_t} \cdot \frac{1}{f_s} \cdot \frac{1}{f_i}$$

where

- ρ_i = noise/signal ratio associated with the i^{th} displayed quantity when attention is being shared.
- ρ = noise/signal ratio associated with "full attention" to the i^{th} display
- f_t = fraction of attention devoted to the control task as a whole.
- f_s = fraction of attention devoted to sub-task s, e.g., longitudinal control.

f_i = fraction of attention devoted to the i^{th} displayed quantity in sub-task s , e.g., control of pitch attitude in the longitudinal sub-task.

Table 3 summarizes the range of values which the task interference parameters assumed in this study.

VI. Performance Measures

The primary performance measures for the pilot-vehicle analysis were (1) RMS deviations of vehicle motion variables from the nominal approach values (2) pilot RMS control activity, i.e. RMS values of longitudinal cyclic and collective control motions (3) probability of a "missed approach." A missed approach was defined as one in which the groundspeed and glideslope deviations were not within a "window" defined, somewhat arbitrarily, by groundspeed excursions of ± 10 ft/sec and glideslope excursions of ± 10 ft at any time in the landing approach. These values approximate the longitudinal dimensions of the Category II window [5]. Due to the stationary statistical nature of the problem the amplitude distributions of the vehicle motion variables are invariant along the approach path. Hence, the introduction of the minimum decision altitude, normally associated with the Category II window, is somewhat artificial in this analysis.

Since the variables in the pilot-vehicle analysis are assumed to possess zero-mean Gaussian amplitude distributions, the probability of the groundspeed and glideslope deviations being outside the window at any instant of time is simply

$$P = 1.0 - \int_{-10}^{10} \int_{-10}^{10} p(u,h) du dh$$

where $p(u,h)$ is the bivariate Gaussian probability density function for the groundspeed and glideslope deviations. $p(u,h)$ is uniquely determined once the variances of u and h and the covariance of u and h are known.

In addition, the analysis produced pilot "transfer functions" which were utilized in deriving the quickening laws. The ten transfer functions related the cyclic and collective pilot outputs to the five vehicle motion variables which constituted the displayed and perceived quantities.

VII. Results - Analysis

Figure 3 shows the results of the allocation of attention study using the model for task interference. For the two display configurations studied,

roughly a 50-50 allocation of attention between attitude and altitude display elements was found to be optimum.

Figure 4 indicates the probability of a missed approach, as a function of f_{τ} , for the two display configurations. The marginal vehicle handling qualities make their presence known in the relatively large probability of a missed approach for full attention to the control task with the baseline display.

Figure 5 represents the $j\omega$ -Bode diagrams for three of the ten pilot transfer functions. For purposes of clarity, the Bode diagrams were drawn without the pure time delay and neuromuscular dynamics. The transfer functions relate the optimal control motions $u_1(t)$ and $u_2(t)$ (see Figure 1) to the five vehicle motion quantities which constitute the displayed and perceived variables. A comparison of the Bode diagrams for all the transfer functions reveals that all but two can be approximated by pure gains for $\omega < 10$ rad/sec. Figure 5 shows the $u_1/\dot{\theta}$, u_2/h and u_1/h transfer functions, the latter of which is typical of the two functions not amenable to pure gain approximation. Note that, in the case of $u_1/\dot{\theta}$ and u_2/h , the magnitude curves remain reasonably flat for $\omega < 10$ rad/sec while the phase curves remain near 0° and -180° , respectively, in the same frequency range. Had the time delay and neuromuscular dynamics been included in the diagram, these simplifying approximations may not have been discovered.

The gain approximations allow one to quickly ascertain the extent to which the motion variables θ , $\dot{\theta}$ and u effect the cyclic control and the extent to which h , \dot{h} and $\dot{\theta}$ effect the collective control. Figure 6 was obtained by multiplying the predicted mean square values of the pertinent motion variables by the square of the respective transfer function gain approximations and then normalizing with respect to the largest product for each control. Thus, the bars in Figure 6 can be thought of as representing the approximate relative power in each control due to each of the motion variables shown. The remaining variables (h and \dot{h} in the cyclic, u and θ in the collective) can be shown to make smaller respective power contributions than u in the cyclic and $\dot{\theta}$ in the collective.

VIII Quickening Laws

Figure 6 implies that the cyclic control motion is dominated by $\dot{\theta}$ and θ and that the collective control motion is dominated by \dot{h} and h . This suggests that driving the pitch and glideslope deviation display elements by a weighted sum of pitch deviation and deviation rate, and glideslope deviation and deviation rate could result in improved pilot-vehicle performance. Driving the display elements in such a manner is referred to as quickening. Note that, in the baseline configuration, the pilot must perceive the time derivatives of pitch and glideslope deviations from the display element motion and use the perceived rates along with the display element displacement to create control motion. In the proposed quickened display, the weighted summing of perceived rate and displayed displacement would be obviated.

In the quickened display, the pitch attitude and glideslope deviations symbols were driven according to the laws

$$\theta' = \theta + K_{\theta} \dot{\theta}$$

$$h' = h + K_h \dot{h}$$

where θ' and h' represent the quickened pitch attitude and glideslope deviations, respectively. K_{θ} and K_h were obtained from the relative magnitudes of the pure gain approximations for the u_1/θ , $u_1/\dot{\theta}$ and the u_2/h , u_2/\dot{h} transfer functions respectively. The quickening results indicated in Table 4 and Figures 3 and 4 were obtained by implementing the control theoretic pilot model with the quickened display.

IX. Conclusions - Analysis

As Table 4 indicates, the RMS performance improvements obtained with the quickening are modest. Figure 4 shows significant but not overwhelming improvement in terms of the probability of a successful approach. These results are analytic predictions of the limited success one will have in trying to improve pilot-vehicle performance by display sophistication alone. In order to achieve better performance, say in terms of the probability of a successful approach, another avenue must be explored, i.e. artificial stability augmentation. The stabilizer bar on the standard UH-1 helicopter, of course, serves just this purpose.

X. Simulation

A simple fixed-base pilot-in-the-loop simulation of the longitudinal task was conducted on the Naval Postgraduate School's hybrid computer. The vehicle dynamics were simulated on the analog computer, the displays were generated on a stroke-written cathode-ray-tube graphics terminal with the digital computer driving the display elements.

Two subjects, one a UH-1 pilot, another a non-pilot, were used to generate a complete set of RMS performance measures. The turbulence was simulated by sums of sinusoids. The amplitudes and frequencies of the sinusoids were chosen to match the frequency distribution of power in the appropriate spectra of Table 5.

After considerable informal training, each subject received a formal training session in which he used the baseline and quickened displays for 90 sec runs apiece. In the formal data sessions, each subject used each display for ten 90 sec runs. The data sessions went as follows:

The baseline was flown for seven runs, followed by the quickened for seven. Then the quickened was flown for three runs followed by the baseline for three. Five of the "best" runs for each display were then selected as follows: For the ten data runs for each display, mean scores were computed for each of the RMS performance measures (u , θ , $\dot{\theta}$, h , δ_B , δ_C). Then, each RMS score for each display and run was normalized by dividing it by the respective mean RMS score. The normalized RMS scores were then summed to provide a single scalar index of performance for each display and run. The data in Table 5 represents the means and standard deviations of the RMS scores for the runs with the five lowest indices of performance for each display. Also shown in the table are the sinusoids which simulated the atmospheric turbulence.

Figures 7 and 8 graphically portray the performance data of Table 5 for subjects 1 (pilot) and 2 (non-pilot). Also indicated are the model predictions which best correlate with the data. These predictions are from the $f_t = .25$ data in Table 4.

XI. Results and Conclusions - Simulation

As the averaged performance data of Figures 7 and 8 indicates, the display quickening resulted in lower mean RMS scores for each motion and control variable for both subjects. The necessity of using the model data for the largest noise/signal ratio is probably due to the low RMS performance predictions which the model generated in the absence of indifference thresholds on the displayed or perceived variables.

XII. Conclusions - General

Based upon the analysis and simulation just described, the following conclusions can be drawn:

- (1) The quickening laws analytically obtained by the control theoretic pilot model yield significant improvements in RMS performance for the vehicle and task studied here.
- (2) Even an approximate determination of the relative amount of power in each control output which is associated with each displayed or perceived vehicle motion variable appears to be a very useful step in the pilot-vehicle analysis. In this study, the comparison pointed out
 - (a) the desirability of display quickening
 - (b) the vehicle's marginal handling qualities by predicting the extent to which perceived pitch rate and glideslope rate deviations would be employed in controlling the vehicle.

(3) For the vehicle and task studied here, increased display sophistication should give way to improved stability augmentation. Although the performance increments obtained were significant, performance is probably still deficient, particularly as regards the probability of a missed approach.

(4) Analysis using the control theoretic pilot model and simple fixed-base simulation are complementary tools in the evaluation-design process. While quite accurate a-priori modeling has been accomplished [6], the availability of simulation data is invaluable, particularly in iterative refinement of the pilot model.

References

- [1] Kleinman, D. L., Baron, S. and Levison, W. H., "An Optimal Model of Human Response, Part I: Theory and Validation," Automatica, Vol. 6, pp. 357-369, May 1970.
- [2] Levison, W. H., "A Model-Based Technique for the Design of Flight-Directors," Proc. 9th Annu. Conf. Manual Control, pp. 163-172, May 1973.
- [3] Levison, W. H., Ilkind, J. H. and Ward, J. L., "Studies of Multi-variable Manual Control Systems, A Model for Task Interference," NASA-CR-1746, May 1971.
- [4] Baron, S. and Levison, W. H., "A Display Evaluation Methodology Applied to Vertical Situation Displays," Proc. 9th Annu. Conf. Manual Control, pp. 121-132, May 1973.
- [5] Graham, D., Clement, W. F. and Hofmann, T. G., "Investigation of Measuring Systems Requirements for Instrument Low Visibility Approach," AFFDL-TR-70-102, Feb. 1971.
- [6] Kleinman, D. L. and Baron, S., "Analytic Evaluation of Display Requirements for Approach to Landing," NASA-CR-1952, Nov. 1971.

Table 1
Pilot Model Parameters

Time Delay	e^{-Ts}	$\tau = 0.2 \text{ secs}$
Neuromuscular System	$\frac{1}{T_N s + 1}$	$T_N = 0.2 \text{ secs}$
Observation Noise	V_{z_1}	$V_{z_1} = \rho \pi E \left[z_{p_1}^2(t) \right]$ $\rho = .01 \text{ (full attention)}$
Motor Noise	V_{m_1}	$V_{m_1} = \rho' \pi E \left[u_1^2(t) \right]$ ρ'
Index of Performance	J	$J = \lim_{T \rightarrow \infty} \frac{1}{T} \int_0^T \left[\frac{u^2(t)}{u_M^2} + \frac{\dot{\theta}^2(t)}{\dot{\theta}_M^2} + \frac{h^2(t)}{h_M^2} + \frac{u_1^2(t)}{u_{1M}^2} + \frac{u_2^2(t)}{u_{2M}^2} \right] dt$ $u_M = 10 \text{ ft/sec}$ $\dot{\theta}_M = .04 \text{ rad/sec}$ $h_M = 10 \text{ ft}$ $u_{1M} = 0.5 \text{ ft}$ $u_{2M} = 0.5 \text{ ft}$

Table 2
Turbulence Models

Vertical Turbulence

$$\phi_{w_g w_g}(\omega) = \frac{2\sigma_w^2 L_w}{U_o} \frac{1}{1 + \left(\frac{L_w \omega}{U_o}\right)^2} \text{ ft}^2 \text{ rad/sec}^2$$

$$\sigma_w = 5 \text{ ft/sec}$$

$$L_w = 100 \text{ ft}$$

$$U_o = 60 \text{ knots (101.3 ft/sec)}$$

Horizontal Turbulence

$$\phi_{u_g u_g}(\omega) = \frac{2\sigma_u^2 L_u}{U_o} \frac{1}{1 + \left(\frac{L_u \omega}{U_o}\right)^2} \text{ ft}^2 \text{ rad/sec}^2$$

$$\sigma_u = 5 \text{ ft/sec}$$

$$L_u = 600 \text{ ft}$$

Table 3

Task Interference Parameter Ranges

ρ	.01	observation noise/signal ratio for full attention
f_t	1.0 + 0.25	fraction of attention to entire control task
f_s	0.5	fraction of attention to longitudinal sub-task
f_1	0.25 + 0.75	fraction of attention to attitude-airspeed display of longitudinal sub-task [†]
f_2	0.75 + 0.25	fraction of attention to glideslope display of longitudinal sub-task

[†] Since airspeed symbology is effectively integrated with the aircraft symbol in the display, no attention sharing is assumed between pitch attitude and airspeed.

Table 4
Model Performance Predictions

f_t	<u>Baseline Display</u>			<u>Quickened Display</u>		
	1.0	0.5	0.25	1.0	0.5	0.25
σ_u (ft/sec)	.881	1.50	2.69	.666	1.23	2.45
σ_w (ft/sec)	2.94	3.75	5.11	2.24	3.02	4.39
$\sigma_{\dot{\theta}}$ (rad/sec)	.0109	.0147	.0204	.00829	.0118	.0178
σ_{θ} (rad)	.0104	.0158	.0259	.00795	.0128	.0231
σ_h (ft)	1.81	2.55	4.01	1.34	2.01	3.36
σ_{δ_B} (ft)	.0276	.0300	.0335	.0256	.0277	.0311
σ_{δ_C} (ft)	.0513	.0569	.0675	.0460	.0511	.0611

Table 5

Simulation Performance Data

Subj.	<u>Baseline</u>		<u>Quickened</u>		<u>Turbulence</u>	
	1	2	1	2		
σ_u (ft./sec)	5.58 [†] 1.55 ^{††}	2.60 .627	3.91 .653	1.86 .713	$\left. \begin{matrix} u_g \\ w_g \end{matrix} \right\} = \sum_{i=1}^5 A_i \sin \omega_i t$	
$\sigma_{\dot{\theta}}$ (rad/sec)	.0505 .00482	.0269 .00291	.0169 .00159	.0121 .00134	$\frac{u_g}{g}$	$\frac{w_g}{g}$
σ_{θ} (rad)	.0471 .00462	.0292 .00403	.0182 .00614	.0197 .00389	$A_1 = 4.472$	$A_1 = 4.472$
σ_h (ft)	9.31 1.04	5.51 .423	6.88 .949	4.79 .902	$A_2 = 3.536$	$A_2 = 3.536$
σ_{δ_B} (ft)	.0534 .00522	.0259 .00335	.0247 .00269	.0127 .00125	$A_3 = 2.236$	$A_3 = 2.236$
σ_{δ_C} (ft)	.0529 .00642	.0373 .00712	.0401 .00514	.0292 .00501	$A_4 = 2.738$	$A_4 = 2.738$
					$A_5 = 2.236$	$A_5 = 2.236$
					$\omega_1 = .070$	$\omega_1 = .420$
					$\omega_2 = .210$	$\omega_2 = 1.260$
					$\omega_3 = .350$	$\omega_3 = 2.100$
					$\omega_4 = .768$	$\omega_4 = 4.608$
					$\omega_5 = 1.765$	$\omega_5 = 10.050$

† mean

†† standard deviation

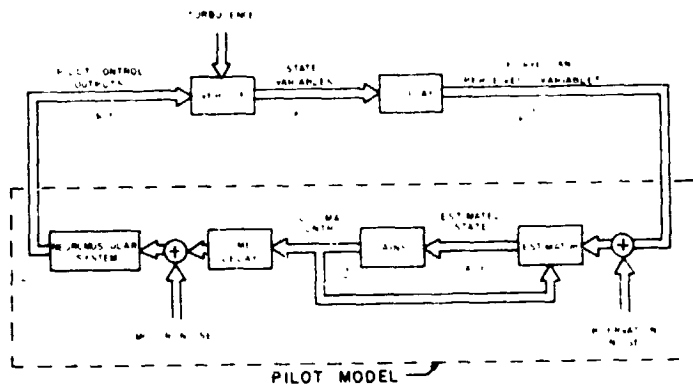
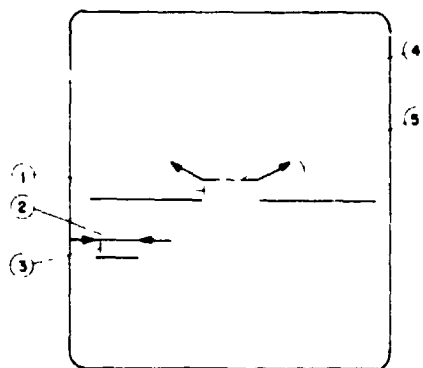


Figure 1 Block Diagram for Pilot-Display-Vehicle System



- ① PITCH ATTITUDE θ , 20 DEG/IN
- ② GLIDESLOPE REFERENCE
- ③ GLIDESLOPE DEVIATION h , 50 FT/IN
- ④ AIRCRAFT REFERENCE
- ⑤ GROUNDSPED DEVIATION u , 0.5 KTS/DEG

Figure 2 Display Symbology

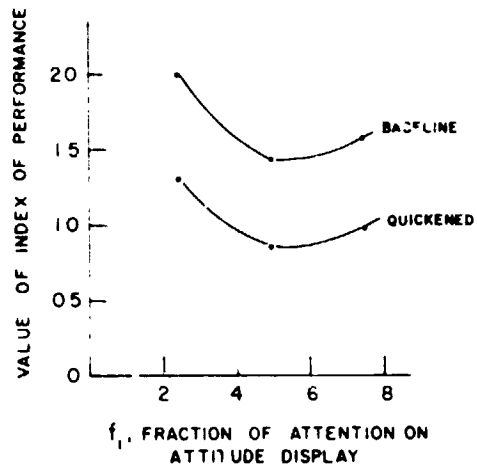


Figure 3 Allocation of Attention Results

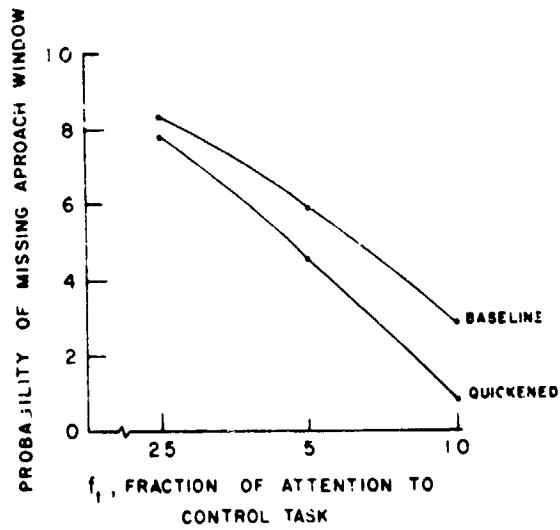


Figure 4 Probability of Missed Approach

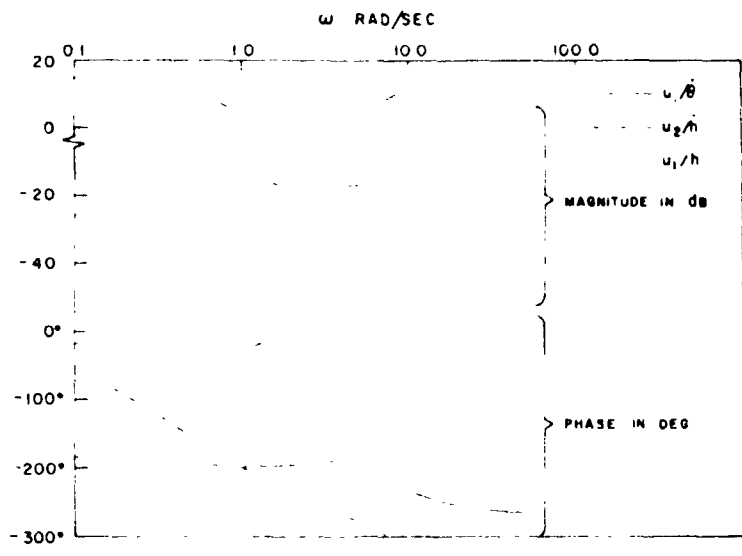


Figure 5 Representative Pilot Transfer Functions

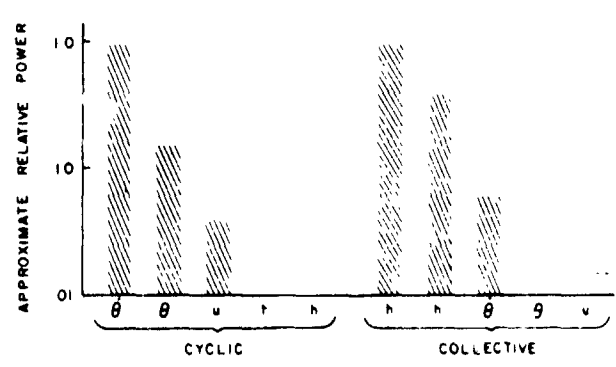


Figure 6 Vehicle Motion Variable - Pilot Control Motion Relationship

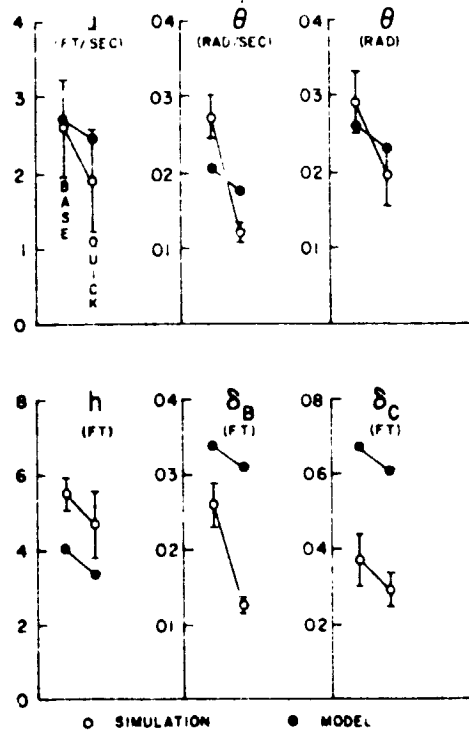


Figure 7 Performance Data, Subject 1

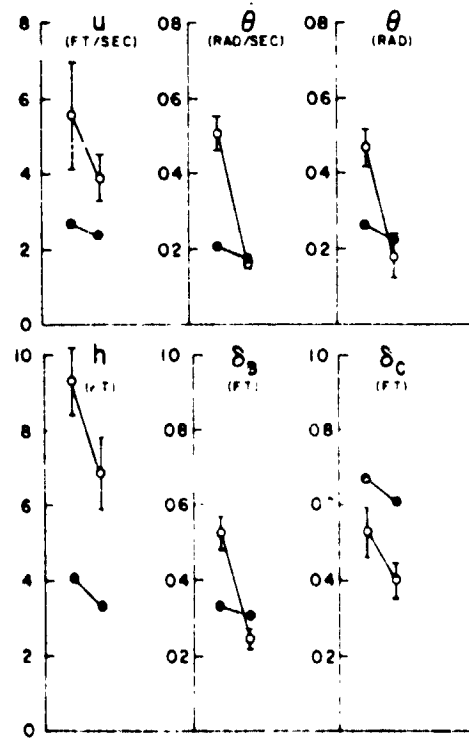


Figure 8 Performance Data, Subject 2

N75 23698

SIMULATION OF MAN-MACHINE INTERACTION

ON SHUTTLE PAYLOAD MANIPULATOR

By R. O. Hookway and R. S. Jackson

Martin Marietta Corporation
Denver, Colorado

SUMMARY

The main objective of this simulation was to evaluate the feasibility of a simplified control system for a remote manipulator for Space Shuttle payloads. The motion commanded by the operator through the control system to the six-degree-of-freedom manipulator approximates that of a backhoe. Compatibility of low arm damping, heavy payloads, small clearances in the shuttle cargo bay and stringent mission timelines were evaluated. The effects of various devices to enhance visual cues were evaluated.

The simulation was flown both by test pilots and by non-pilot personnel. Phase I of the simulation was capture of a payload flying free in space relative to the Shuttle; Phase II was simulation of cargo stowage into a mockup of the Space Shuttle cargo bay. A Shuttle remote manipulator control station mockup including TV monitors and hand controllers is used in the simulation. Results evaluating various parameters of the control system and the task, including arm flexibility, are presented.

INTRODUCTION

Teleoperators of varying degrees of complexity are expected to aid future exploration and activities in space (reference 1). Of immediate interest is the Shuttle-Attached Manipulator System (SAMS). Figure 1 shows one concept of the SAMS. References 2 and 3 discuss other SAMS concepts. Major subsystems of the SAMS are: (1) a mechanical arm articulated at the shoulder, elbow, and wrist; (2) an end effector and TV camera on the wrist; (3) an arm control computer; (4) a TV viewing system from which visual cues are obtained for remote arm operation; and (5) control input devices such as hand controllers.

References 2 through 5 present detailed tradeoff studies on each of these major subsystems, which can be configured in various ways. If an articulated arm is used, the optimum configuration might be considered to consist of a 7 DOF arm (see reference 2, page 90) with digital computer-aided control. The control philosophy for this case would consist of control laws that include such features as (1) a zero cross-coupling joint command distribution law; (2) joint rate saturation avoidance; (3) payload, arm, and shuttle collision avoidance; (4) command resolution along the appropriate TV coordinate viewing

system; (5) preselected trajectories and automatic positioning of the arm; (6) force feedback calculations for the master arm or hand controllers; (7) compensation for arm structural bending; and (8) mode selection and coordinate system indexing of command signals. The distribution law for this type of control is derived by applying the method of Lagrange multipliers to the problem of minimizing a performance index while satisfying the conditions for zero cross-coupling. A typical performance index is the sum of an optimization criterion (e.g., the sum of the squares of the joint rates, weighted singularity avoidance, joint stop avoidance, and collision avoidance functions). Reference 6 describes the mathematics of a similar joint command distribution law.

A preliminary computer timing and sizing estimate was done for the digital system described above. Memory requirements were found to be 11,611 words and thruput was estimated at 43,650 operations per second.

The digitally controlled 7 DOF SAM offers many obvious operational advantages, but it is at the high end of the manipulator spectrum in terms of both performance and cost. Driven by cost requirements, Martin Marietta has performed detailed design studies on an austere SAM system consisting of one 6 DOF arm, control laws simple enough to be implemented with analog electronics, and using simple hand controllers. The simplified arm control laws are illustrated in Figure 2.

Control commands are rate commands proportional to hand controller displacement. These commands are generated from two hand controllers, one for end effector translational velocity and one for end effector rotation rate. The output of the translation hand controller feeds into the control law which is designed so that a backhoe-type motion of the wrist results. (The simplified system operates in spherical coordinates and the digitally controlled arm operates in Cartesian coordinates.) Displacement of the rotation hand controller causes corresponding rotation rates of the wrist pitch, roll, and yaw joints.

The backhoe motion makes it convenient to electrically slave the shoulder pitch, elbow pitch, and wrist pitch joint commands, thus greatly simplifying the control law. The backhoe motion can also be viewed as a simulated telescopic motion because a translation command in the "X" direction causes the wrist to extend or retract along a straight line between the shoulder and wrist. The control system diagram (Figure 2) shows implementation of the control law. Switch H holds the pointing direction of the end effector constant as shoulder yaw and wrist elevation (γ) change. This mode, called the Hawk Mode, is used during the payload retrieval task.

The simplified nature of this SAM system raised some questions about its utility. Could the operator cope with the backhoe type motion in general; more specifically, could the operator tolerate the mismatch between TV viewing coordinates and command coordinates that exists in varying degrees during the payload capture task? A man-in-the-loop simulation, as described in the next section, was used to evaluate these questions.

SIMULATION DESCRIPTION

The man-in-the-loop simulations were performed in our Space Operations Simulator, a montage of which is shown in Figure 3. The operator's control station is shown at the upper left. Although considerable window area is shown, the operator's only view of the payload and cargo bay area is through closed circuit TV. The view from a camera mounted near the arm shoulder was presented on the CRT on the left of the console, and the view from a camera mounted on the wrist was presented on the CRT to the right of the other CRT. These two CRTs are more clearly shown in the closeup of the control console.

Also shown in the closeup are the translation and rotation hand controllers at the left and right sides of the control panels. To the right and slightly above the rotation controller is the pan and tilt switch which was used to make occasional adjustments to the shoulder camera line of sight. Directly above the CRTs is a digital voltmeter on which was displayed the difference between ψ_s and ψ_w .

The wrist end of the simulated arm can be seen in the upper right inset of Figure 3. The yoke, which simulates the wrist, is attached to a carriage which is computer-driven to translate in three degrees of freedom. Thus, the carriage motion simulates the backhoe type extension/retraction of the arm. In addition to the rigid body motion of the arm, the computer which drove the arm was programmed to simulate arm structural dynamics by placing bending dynamics quadratics of the form

$$\text{OUT/IN} = \omega_n^2 / (s^2 + 2\xi\omega_n s + \omega_n^2)$$

in series in the simulation as shown in Figures 4 and 5. Consider that a hand controller command might be given that would cause the payload cg position to change one foot in X. For the rigid arm, this response would appear as shown in Figure 6a; for the flexible arm the response would appear as shown in Figure 6b. The frequencies involved are well within the operator's bandwidth, although some are so low that the operator must learn to wait for one command to be absorbed before making another command. Arm structural dynamics are for an arm with an equivalent stiffness of 2.65 lb/in. In the simulation, the payload center of gravity is offset longitudinally from the payload/end effector attachment point. Thus, a payload roll oscillation is generated due to Y_{HC} commands. The above structural dynamics are greatly simplified over the actual case. Actually, for each hand controller displacement there are six degrees of freedom of payload cg motion (three translation and three rotation) and there are six predominate structural modes. Thus, in reality there are $6^3=216$ oscillatory motions that would make up a complete simulation.

We also performed a large scale, unmanned digital simulation of the Shuttle Orbiter with an attached 65,000 lb payload to verify that the response shown in Figure 6b is typical. The digital program simulated the complete nonlinear large angle dynamics of a cluster of n hinged bodies based on Hooker-Margulies equations.

The model payload bay and the payload are also shown in Figure 3. A large shuttle payload was simulated representing a 50-foot long payload having a diameter of 15 feet. In the real world, the clearance on each side of the cargo as it is lowered into the payload bay is only four inches (0.8 inches in the simulation world!).

The backhoe control laws shown in Figure 2 were programmed in the simulation using the gains shown in Table 1.

TABLE 1 SAMS CONTROL SYSTEM GAINS

<u>Symbol</u>	<u>Definition</u>	<u>Absolute Values</u>	
K_1	Azimuth Rate Command Gain	0.082 (1.43)	rad/sec/m/sec (deg/sec/ft/sec)
K_2	Elevation Rate Command Gain	0.082 (1.43)	rad/sec/m/sec (deg/sec/ft/sec)
K_3	Extension Rate Command Gain	0.082 (1.43)	rad/sec/m/sec (deg/sec/ft/sec)
K_4	Wrist Pitch Rate Command Gain	0.57	No units (no units)
K_5	Wrist Yaw Rate Command Gain	0.785	No units (no units)
K_6	Wrist Roll Rate Command Gain	1.0	No units (no units)

The simulation of payload retrieval was conducted in two phases. Phase I simulated capture of the free-flying payload. Phase II simulated stowing the captured payload in the cargo bay of the Orbiter.

Phase I simulated the payload approaching the Orbiter from the front with a relative velocity of 0.25 ft/sec. The SAMS operator test subjects were instructed to do the basic task of inserting the end effector into the payload receptacle. This task was done by watching the TV monitors--showing views from the wrist and shoulder TV cameras. Hand controllers were used to guide the end effector to payload capture.

Based on the coordinate system of Figure 2, the initial position of the payload attachment point relative to the shoulder was $X = 9.0$ ft, $Y = 31.4$ ft, and $Z = -18.0$ ft. The initial position of the end effector was $X = 0.0$ ft, $Y = -27.3$ ft, and $Z = -21.0$ ft. Initial arm angles were $\psi_s = -90$ deg,

$\theta_s = +90$ deg, $\theta_E = -106$ deg, $\theta_w = -11.6$ deg, $\psi_w = 40$ deg, and $\phi_w = 40$ deg.

That is, the payload was approaching on a trajectory parallel to the Orbiter X-axis and nine feet outboard and ten feet above the end of the manipulator.

Overall Orbiter mission timelines required that capture of the payload be completed in 170 seconds. To aid the operator in pacing the task, warning lights were built into the console. A yellow light came on at 110 seconds, followed by a red light at 170 seconds.

Phase II was divided into two functional parts. The first part, Phase IIA, consisted of translating the payload from a position above the payload bay to partial insertion into the bay. The second part, Phase IIB, was translation through the remaining 2 or 3 feet down into the bay to final pin seating. When these simulations were performed, the location of the pin seats and the design of the pins were still very preliminary. Therefore, it was assumed that there would be two such seats located on the centerline of the floor of the cargo bay. It was also assumed that the payload would be equipped with a pair of tapered pins. The initial conditions made the payload appear to be pitched down and yawed right roughly 45 degrees relative to the cargo bay.

One TV camera was the forward payload bay camera and the other camera pointed along the cargo bay floor at the seats and pins. The wrist camera was not used in Phase II since its view in this mode is completely obscured by the payload.

To improve depth perception, a cauted mirror was added to show the relative force and aft displacement of the pin relative to the hole. In addition, two sets of flexible whiskers were installed. A short set was installed forward of the aft seat and a set of taller whiskers was installed aft of the aft seat as shown in Figure 7. Thus, if the pin obscured the whiskers, the payload was too far forward; as the pin passed through the whiskers they deflected and clearly indicated the direction in which the payload must be moved.

SIMULATION RESULTS

Phase I - Payload Retrieval - Three test operators were used in this phase of the evaluation of the feasibility of the control laws. Operator 1 was the engineer who conceived the control laws; operators 2 and 3 had no previous exposure to the control law concepts. Each operator was given identical 30-minute training and familiarization periods. It was anticipated that two factors, (1) relative velocity between payload and orbiter, and (2) the arm structural dynamics, would strongly affect the results. Therefore, each operator made runs with the following configurations:

<u>Subtask Designation</u>	<u>Relative Velocity Feet per Second</u>	<u>Arm Structural Dynamics</u>
A	0	rigid
B	0	per Figure 5
C	0.25	rigid

<u>Subtask Designation</u>	<u>Relative Velocity Feet per Second</u>	<u>Arm Structural Dynamics</u>
C _A	0.25	rigid, without Hawk
D	0.25	per Figure 5
E	0.125	rigid

A run was graded as a success if the end effector was inserted in the payload in the allowable time without bumping the payload on the way in. A run was graded as a failure when the payload was bumped by the end effector before it was inserted or when 170 seconds had passed without insertion.

Phase I results are given in Tables 2, 3, and 4. For the rigid arm, the effect of relative velocity can be evaluated by comparing runs A, C, and E. For the flexible arm, the effect of relative velocity can be evaluated by comparing runs B and D. For two values of relative velocity, the effect of unloaded arm structural dynamics can be evaluated by comparing runs A and B with each other and by comparing runs C and D with each other. The most positive result of this phase of the feasibility simulation is that the capture task was easily learned and readily performed in much less than the allowable time. The allowable time was 170 seconds whereas the overall average (all operators, all test conditions) required time was only 93.8 seconds.

It was found that two other factors (other than the 170 second operational limit) made it desirable to do the capture task rapidly. First, if the capture task was not completed in a reasonable amount of time, the axes of the wrist TV system become misaligned with the hand controller axes as shown in Figure 8. Once the TV axes become too misaligned (more than about 45 degrees) with respect to the hand controller axes, the task was lost to the test operators. To help circumvent this difficulty, the Hawk Mode was implemented via switch H in Figure 2. This mode of operation proved to be very helpful, but only limited test data were taken with it.

The second factor affecting time is the necessity to allow some braking distance. That is, if the capture task was not completed before the arm became nearly fully extended, little or no braking distance remained.

Phase II - Payload Stowage - The data of Tables 5, 6, and 7 showed the extreme difficulty of successfully stowing the large payload without exceeding the mission time constraint of five minutes. For the rigid arm, the average stowage time for the three test operators was 6.83 minutes. When the arm flexible modes were added to the simulation, the average stowage time was increased to 9.42 minutes. These are total times for both phase IIA and IIB.

Furthermore, Tables 5, 6 and 7 made it apparent that, unless the wrist yaw axis was parallel to the payload bay yaw axis, the payload could not be stowed without many collisions with the orbiter structure. Therefore, a

black stripe was painted on the payload to indicate the wrist yaw angle. This visual cue was very effective and was used throughout the ensuing data-taking runs. The experimental data implies that with adequate timing and with greatly increased arm structural damping, Phase IIA could be completed within five minutes; but because of the arm structural dynamics and because of the small structural clearances, additional time is required for final pin seating. With the rigid arm, the complete task can be done in five minutes or less.

The relationship between task time and arm damping and frequency is plotted in Figure 9. The frequency multiplication factor, K , multiplied all of the structural frequencies. Figure 9 shows that the structural frequency needs to be increased by roughly a factor of 4 to meet a five-minute task time constraint. The structural frequencies are proportional to \sqrt{k} , $\omega_n \propto \sqrt{k}$ and $4\omega_n \propto \sqrt{16k}$, so a four-fold increase in frequency requires that the arm stiffness be increased 16 times. An arm stiffness of approximately $(2.65 \frac{\text{lb}}{\text{in.}}) (16) = 42.4 \text{ lb/in.}$ is difficult to realize within practical structural design.

On the basis of these preliminary tests, it seems that several steps must be taken to successfully carry out stowage of the largest Orbiter payloads. The arm stiffness and damping must be increased as much as possible over the values used in these simulations. Since there is a practical upper limit to damping and stiffness, the design of the cargo bay stowage system should include energy absorbing devices which allow bumping between the cargo and the stowage system. Furthermore, the cargo stowage system should be designed to assist in drawing the cargo down to the final seated position.

CONCLUSIONS

Capture Task

1. The backhoe control laws of SAMS are easily mastered (both for the capture task and the stowage task).
2. The Hawk Mode greatly aided capturing a free-flying payload within the time constraints of the mission timeline.

Stowage Task

1. Added visual cues from a stripe painted on the end of the payload made it possible for operator to minimize collisions between the payload and the Orbiter cargo bay.
2. Shock absorbers are desirable to minimize effect of payload-orbiter collision during final stages of the stowage task.
3. Depth perception aids; e.g., whiskers and mirrors, are desirable.

4. Cooperative pin receptacles which assist in drawing payload down to final seated position are desirable.
5. For the length of arm used in this study, successful stowage of the largest payload requires a much stiffer arm than it may be practical to obtain.

REFERENCES

1. Deutsch, S., and Heer, E.: "Manipulator Systems Extend Man's Capabilities in Space." *Astronautics and Aeronautics*, Volume 10, No. 6, June, 1972.
2. Smith, G. W., and DeRocher, W. L.: "Shuttle Payload Accommodation System Teleoperator." *Remotely Manned Systems (Exploration and Operation in Space)*, Proceedings of the First National Conference, Page 85ff, California Institute of Technology, 1973.
3. Brodie, S. B., and Johnson, C. H.: "Preliminary Design and Simulation of a Shuttle-Attached Manipulator System." *Remotely Manned Systems (Exploration and Operation in Space)*, Proceedings of the First National Conference, Page 105ff, California Institute of Technology, 1973.
4. "Configuration and Design Study of Manipulator Systems Applicable to the Free-Flying Teleoperator." Final Report, MCR-74-171, July, 1974. NAS8-30266. Martin Marietta Corporation, Denver Division, Denver, Colorado 80201.
5. "Preliminary Design of a Shuttle Docking and Cargo Handling System," Final Report, MSC 05218, December, 1971. NAS9-11932. Martin Marietta Corporation, P. O. Box 179, Denver, Colorado 80201.
6. Whitney, D. E.: "The Mathematics of Coordinated Control of Prosthetic Arms and Manipulators." *Transactions of the ASME, Journal of Dynamic Systems, Measurement, and Control*, Volume 94, Series G, No. 4, December, 1972.

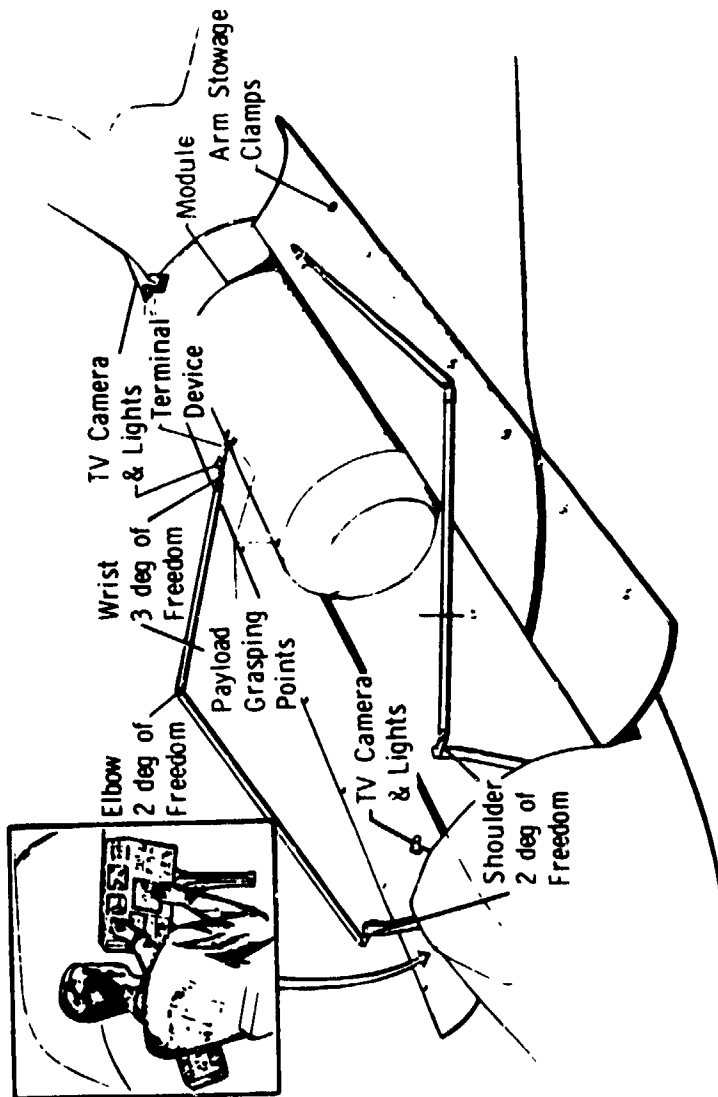


Figure 1 Shuttle Attached Manipulator System (SAMS)

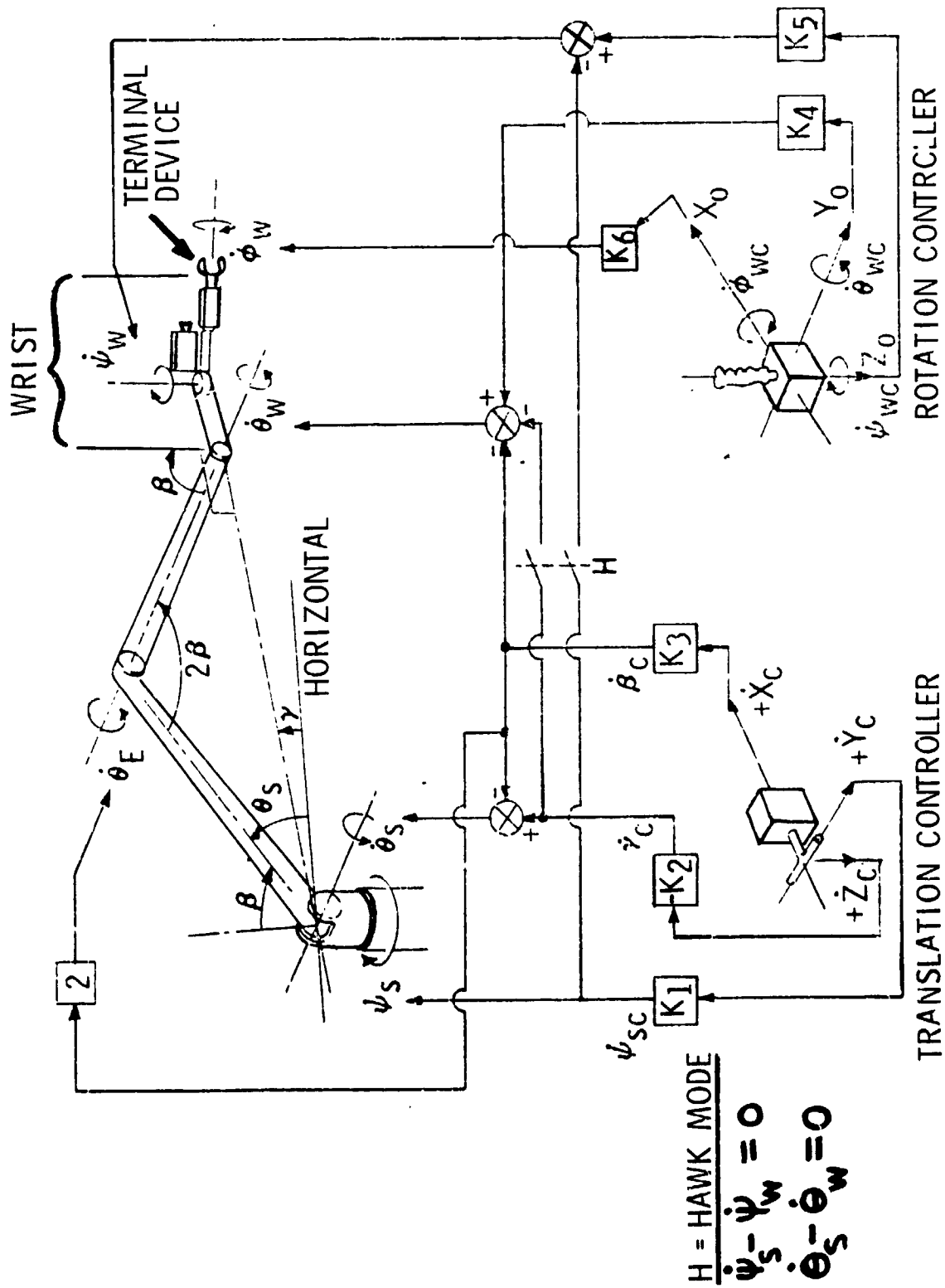


Figure 2 Backhoe Control System Diagram

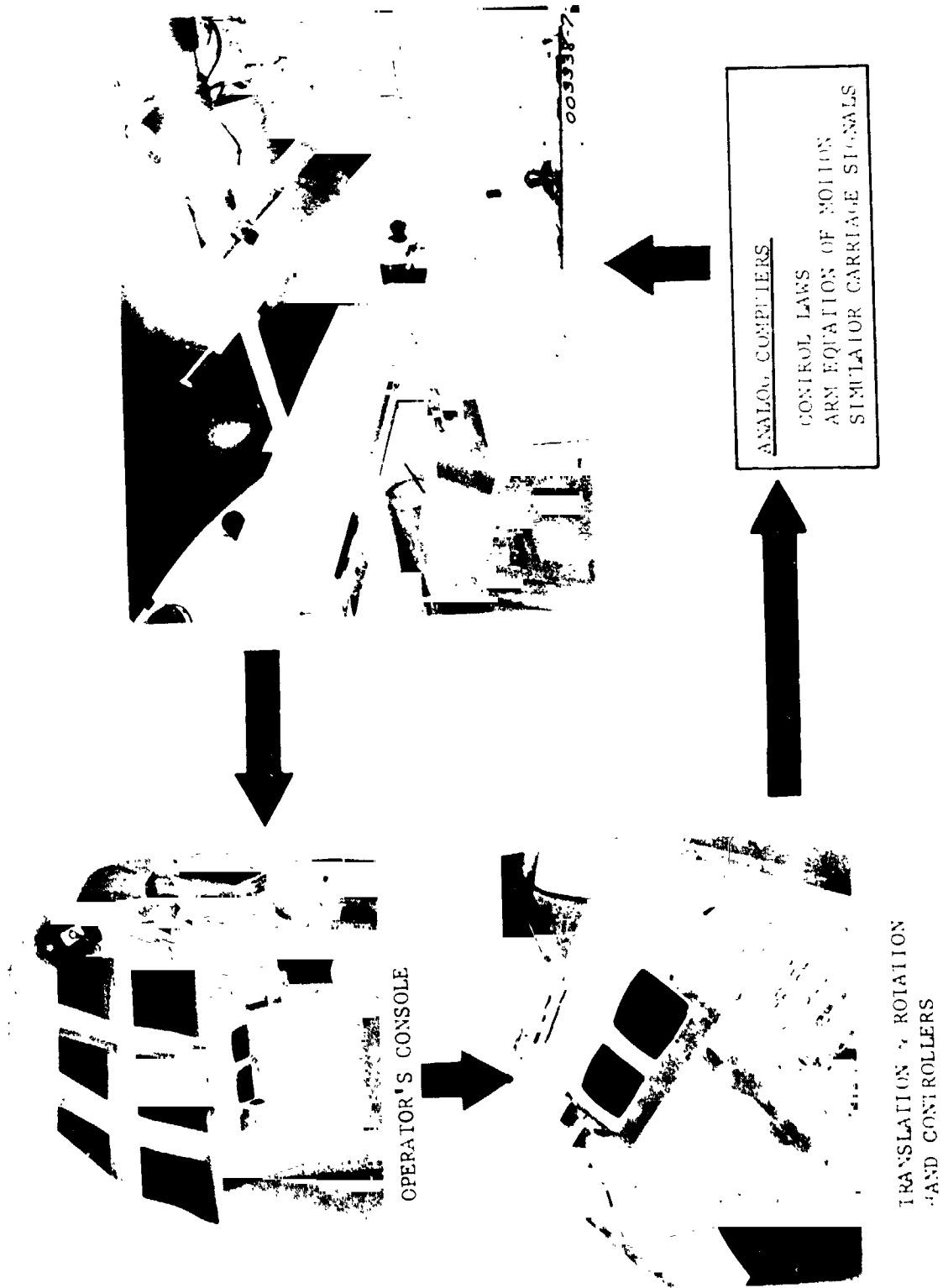


Figure 3 SAMS Simulation Setup

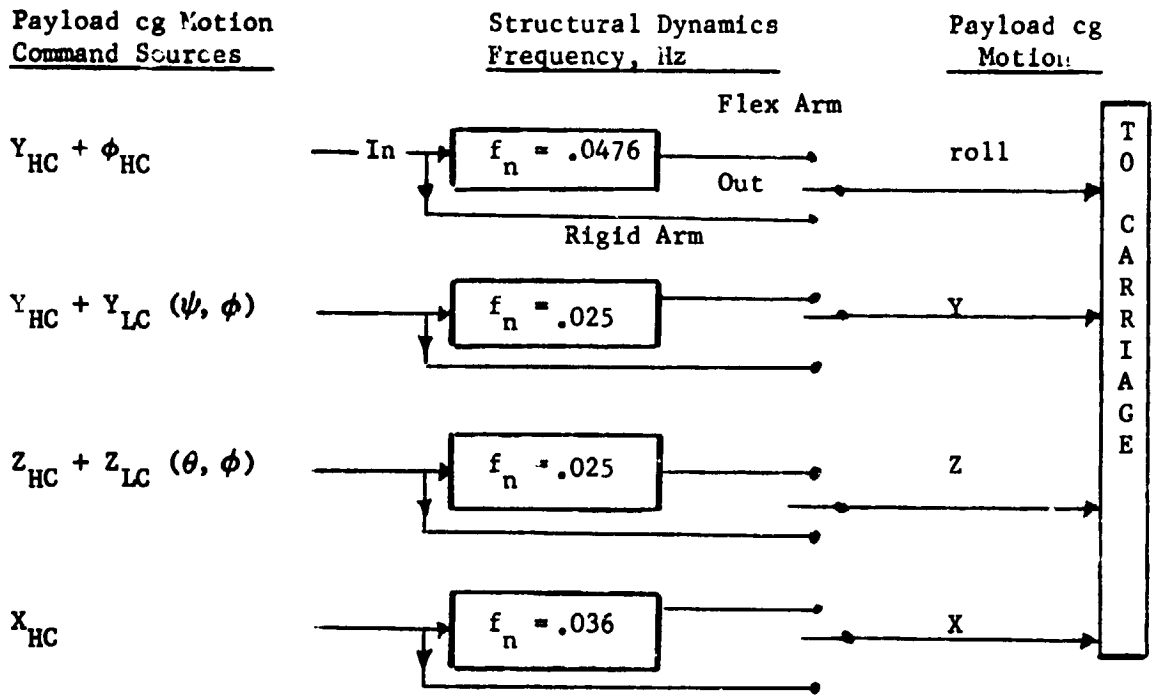


FIGURE 4 LOADED ARM STRUCTURAL DYNAMICS

Unloaded Arm Structural Dynamics

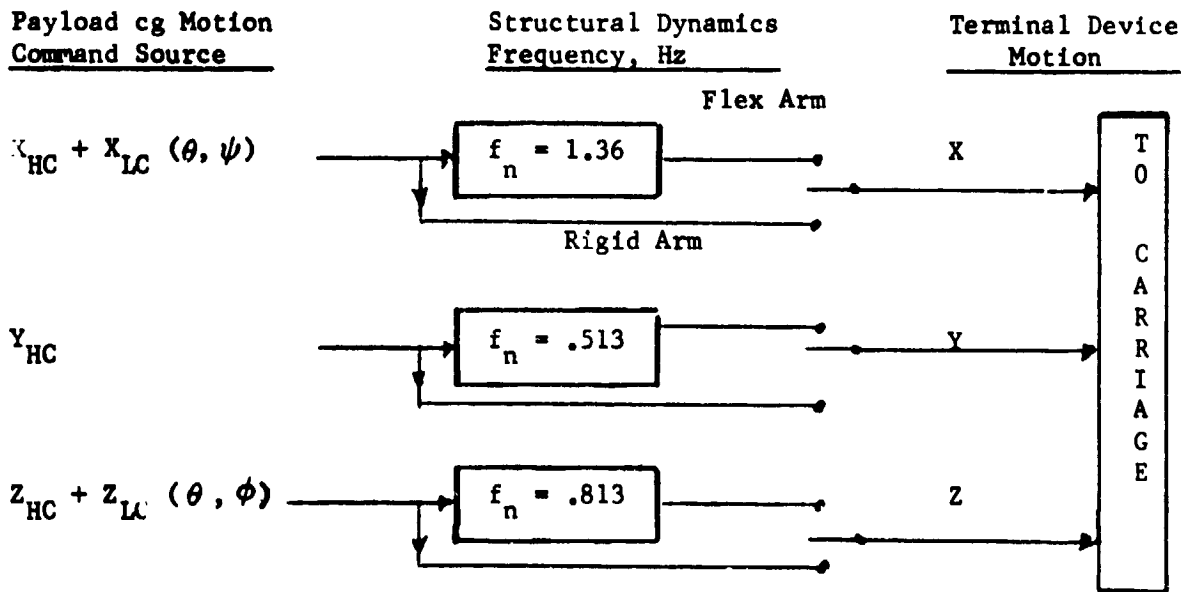


FIGURE 5 UNLOADED ARM STRUCTURAL DYNAMICS

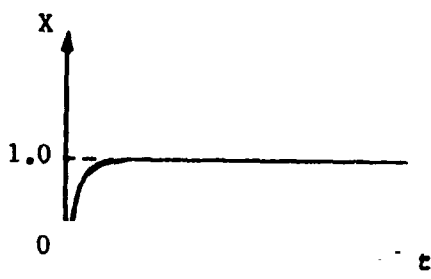


Figure 6a

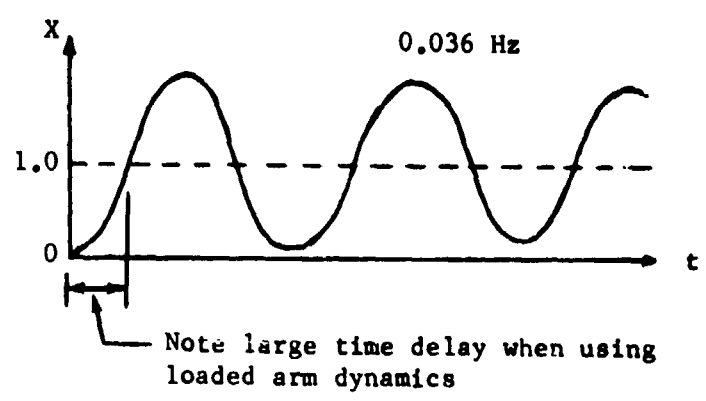
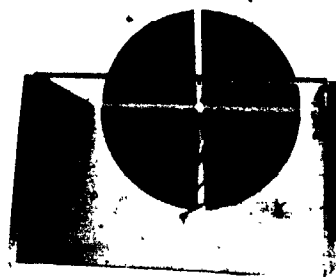


Figure 6b

Figures 6a,6b. Rigid Arm And Flexible Arm Response

VERTICAL ALIGNMENT
STRIPE AIDS
DETERMINATION OF
WRIST YAW ANGLE



AFT PIN SEAT,
MIRROR, WHISKERS
FOR DEPTH PERCEPTION

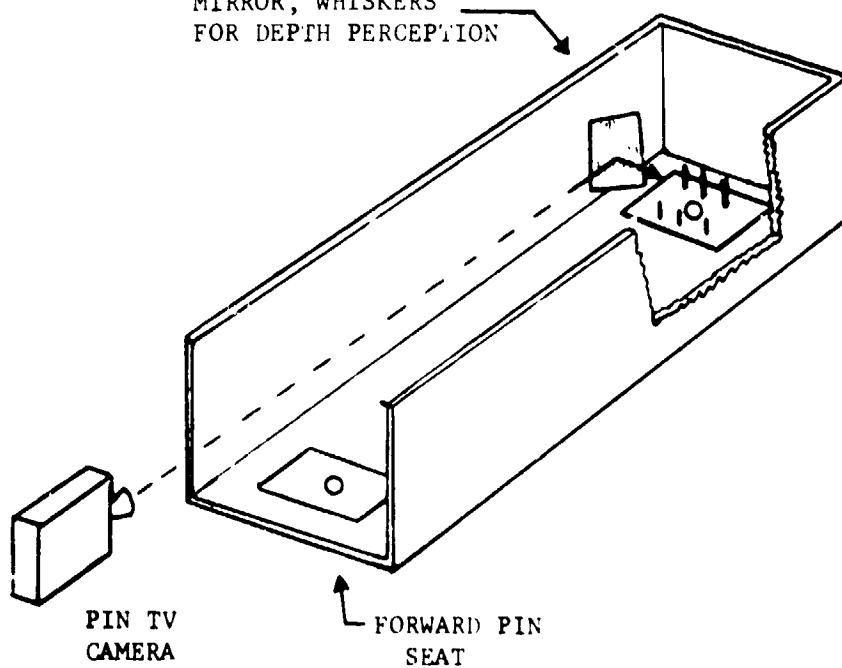
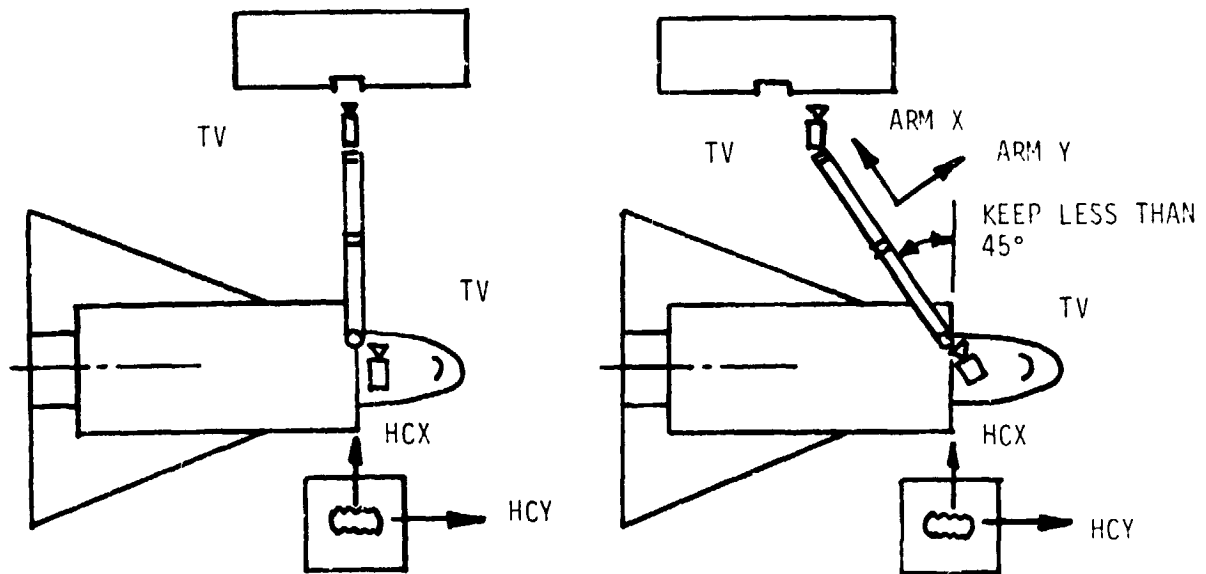


Figure 7 Visual Stowage Aids



ALIGNMENT OF WRIST TV AND HAND CONTROLLER AXES MAINTAINED IF PAYLOAD CAPTURE COMPLETED QUICKLY. X AND Y COMMANDS UNCOUPLED.

IF MISALIGNMENT OF TV AND HAND CONTROLLER AXES APPROACHES 45 DEG, OPERATOR IS SLOWED DOWN BY HAVING TO ESTIMATE COMBINED X AND Y COMMANDS.

Figure 8 Effect of Shoulder-Wrist Misalignment

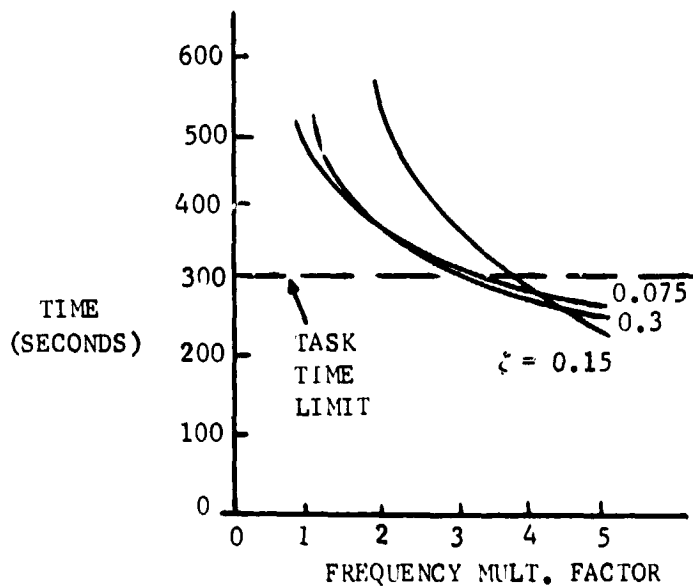


Figure 9 Effect of Arm Frequency and Damping on Performance of Stowage Task

TABLE 2 FREE-FLYING PAYLOAD CAPTURE TASK - OPERATOR 1

Run Description	R U N S	Time Req. Min: Sec	Arm Condition at Capture						S* or F**	COMMENTS
			Degrees			Feet				
			ψ_s	θ_s	θ_E	X	Y	Z		
A No relative velocity No arm structural dynamics	IC	-	- 90	90	-106	0	-27.3	-21.0	-	No depth perception
	1	1:50	- 72	80	- 99	9.0	-31.5	-18.0	S	
	2	1:25	↑	↑	↑	↑	↑	↑	S	
	3	1:22	↑	↑	↑	↑	↑	↑	S	
	4	1:29	↑	↑	↑	↑	↑	↑	S	
	5	1:28	↑	↑	↑	↑	↑	↑	S	
	AV	1:31							-	
B No relative velocity Unloaded arm dynamics	6	1:45							S	Structural dynamic seem- ed to be af- fecting con- trol when large hand controller dispersions were used.
	7	1:22							S	
	8	1:31							S	
	9	1:25							S	
	10	1:22	↓	↓	↓	↓	↓	↓	S	
	AV	1:29	- 72	80	- 99	9.0	-31.5	-18.0	-	
C Relative velocity No arm structural dynamics	11	1:37	-115	77	- 92	-15.0	-31.5	-18.0	S	No comments
	12	1:05	-101	71	-100	- 6.6	↑	↑	S	
	13	1:15	-102	71	-101	- 8.4			F	
	14	0:45	-102	85	-102	- 2.4			S	
	15	1:05	-102	80	- 99	- 8.4			S	
	AV	1:09	-104	77	- 99	-88.2			-	
D Relative velocity Unloaded arm struc- tural dynamics	16	1:07	-102	80	-102	- 8.4			S	Operator does not seem as confident, although he did have bet- ter entries when he was successful
	17	0:55	- 95	81	-102	- 3.6			F	
	18	0:61	-100	80	-101	- 6.3			S	
	19	1:22	-110	79	- 99	-12.0			F	
	20	1:02	-100	81	-101	- 6.6			S	
	AV	1:05	-101	80	-101	- 7.4			-	
E Relative velocity re- duced by ½. No arm structural dynamics	21	1:08	- 88	85	-106	+ 0.6			S	Operator said that this task was very easy
	22	0:59	- 85	81	-102	+ 0.6			S	
	23	1:12	- 90	82	-101	- 0.3			S	
	24	0:59	- 86	81	-101	+ 0.3			S	
	25	0:60	- 89	82	-106	+ 0.3	↓	↓	S	
	AV	1:04	- 88	82	-104	+ 0.3	-31.5	-18.0	-	

*S = Success; **F = Failure

TABLE 3 FREE-FLYING PAYLOAD CAPTURE TASK - OPERATOR 2

Run Description	R U N S	Time Req. Min: Sec	Arm Condition at Capture						S* or F**	COMMENTS
			Degrees			Feet				
			ψ_s	θ_s	θ_E	X	Y	Z		
A No relative velocity. No arm structural dynamics	IC	-	- 90	90	-106	0	-27.3	-21.0	-	Approximately 14 degrees wrist yaw.
	1	2:13	- 72	80	- 99	9.0	-31.5	-18.0	S	
	2	1:27	↑	↑	↑	↑	↑	↑	S	
	3	1:37	↑	↑	↑	↑	↑	↑	S	
	4	2:05	↑	↑	↑	↑	↑	↑	S	
	5	1:20	↑	↑	↑	↑	↑	↑	S	
AV	1:45							-		
B No relative velocity. Unloaded arm structural dynamics	6	1:45	↓	↓	↓	↓	↓	↓	S	No comments.
	7	1:35	↓	↓	↓	↓	↓	↓	S	
	8	1:15	↓	↓	↓	↓	↓	↓	S	
	9	1:53	↓	↓	↓	↓	↓	↓	S	
	10	1:24	↓	↓	↓	↓	↓	↓	S	
	AV	1:34	- 72	80	- 99	9.0	-31.5	-18.0	-	
C Relative velocity. No arm structural dynamics.	11	3:00	-135	70	- 86	-30.0	-25.8	-19.8	F	Too much time. Gently hit left edge of target.
	12	1:05	- 99	82	-100	- 6.0	-31.2	-18.0	F	
	13	2:34	-130	62	- 76	-27.3	-31.5	-18.0	S	
	14	1:17	-105	80	- 98	- 9.0	↑	↑	S	
	15	0:45	-90	82	-100	- 0.6	↑	↑	S	
	AV	1:44	-112	75	- 92	-14.6			-	
D Relative velocity. Unloaded arm structural dynamics.	16	2:25	-110	80	- 99	-10.5			F	Hit target. Hit target. Too much time. Hit target.
	17	0:47	- 91	81	-100	- 3.0			S	
	18	2:40	-120	75	- 92	-18.0			F	
	19	3:00	-120	75	- 90	-21.0			F	
	20	1:40	NA	NA	NA	NA			F	
	AV	2:06	-110	78	- 95	-13.1			--	
E Relative velocity reduced by 1/2. No arm structural dynamics.	21	1:13	- 90	81	-100	0			S	All very smooth.
	22	1:35	- 91	80	-100	- 3.0			S	
	23	1:02	- 86	81	- 99	0.6			S	
	24	2:18	-101	80	- 99	- 8.7			S	
	25	0:55	- 82	82	-100	3.0	↓	↓	S	
	AV	1:25	- 90	81	-100	- 1.6	-31.5	-18.0	-	

*S = Success; **F = Failure

TABLE 4 FREE-FLYING PAYLOAD CAPTURE TASK - OPERATOR 3

Run Description	R U N S	Time Req. Min: Sec	Arm Condition at Capture						S* or F**	COMMENTS
			Degrees			Feet				
			ψ_s	θ_s	θ_E	X	Y	Z		
A No relative velocity. No arm structural dynamics.	IC	-	-90	90	-106	0	-27.3	-21.0	-	Got too close to target. No depth perception.
	1	0:50	-72	80	-99	9.0	-31.5	-18.0	S	
	2	0:38	↑	↑	↑	↑	↑	↑	S	
	3	0:43	↑	↑	↑	↑	↑	↑	S	
	4	0:39	↑	↑	↑	↑	↑	↑	S	
	5	0:50	↑	↑	↑	↑	↑	↑	F	
AV	0:44							-		
B No relative velocity. Uploaded arm structural dynamics.	6	0:56	↓	↓	↓	↓	↓	↓	S	No comments.
	7	0:57	↓	↓	↓	↓	↓	↓	S	
	8	0:41	↓	↓	↓	↓	↓	↓	S	
	9	0:34	↓	↓	↓	↓	↓	↓	S	
	10	0:36	↓	↓	↓	↓	↓	↓	S	
	AV	0:45	-72	80	-99	9.0	-31.5	-18.0	-	
C Relative velocity. No arm structural dynamics.	11	0:59	-95	81	-100	-4.8	↑	↑	S	No comments.
	12	0:53	-92	81	-100	-3.0	↑	↑	F	
	13	0:44	-90	81	-100	-0.9	↑	↑	S	
	14	0:48	-90	82	-100	-3.0	↑	↑	S	
	15	0:36	-86	84	-100	0.3	↑	↑	S	
	AV	0:48	-91	82	-100	-2.3	↑	↑	-	
CA Same as C, but without Hawk mode.	11A	0:50	-90	82	-100	-3.0	↑	↑	F	2° Misalign 0° " 8.45° " 1.2° " 1.5° "
	12A	0:34	-89	82	-100	0.3	↑	↑	S	
	13A	0:39	-90	84	-100	0.0	↑	↑	S	
	14A	0:50	-91	83	NA	-3.0	↑	↑	S	
	15A	0:49	-91	82	-100	-3.0	↑	↑	S	
	AV	0:44	-90	83	-100	-1.7	↑	↑	-	
D Relative velocity. Unloaded arm structural dynamics.	16	0:38	-90	81	-100	-0.3	↓	↓	S	No comments.
	17	0:38	-90	82	-100	-0.3	↓	↓	S	
	18	0:51	-92	80	-100	-3.0	↓	↓	S	
	19	0:34	-85	81	-100	0.6	↓	↓	S	
	20	0:34	-85	82	-100	0.6	↓	↓	S	
	AV	0:39	-88	81	-100	-0.5	-31.5	-18.0	-	

*S = Success; **F = Failure

TABLE 5
CARGO STOWAGE TASK -
OPERATOR 1, NO ADDED VISUAL AID

RUN DESCRIPTION	R U N S	ARM STRUCT. DAMPING RATIO	TIME MIN: SEC.	COMMENTS
Rigid Arm	1	-	6:40	Operator used forward bay camera for depth cues (X), in runs 1 through 4. Bumped 1 side, 3 back probe, 2 front probe.
	2	-	4:20	Bumped 2 on side, 4 back probe, 4 front probe. Touched left side and stayed there for a long time.
	3	-	4:42	Bumped 3 on left side, 1 front probe.
	4	-	4:04	Bumped 1 left side, 1 right side, 1 front probe, 1 back probe. Touched right side and stayed along it for approximately 20 seconds.
	5	-	4:43	Cargo bay pin camera is being used for depth cues along bay X. Bumped 5 back probe, 1 left side, 3 front probe.
Loaded Arm Structural Dynamics	6	.3	12:51	Bumped a number of times. Hit hard and had to hold simulation.
	7	.7	8:00	Phase IIA time 5 minutes. Bumped 2 rear probe, 1 left front.
	8	.7	8:26	Phase IIA time 4 minutes. Bumped 4 rear probe, 2 front probe, 3 right front. Seemed to lose partial control after he was almost in. Hit hard once on right front.

TABLE 6
CARGO STOWAGE TASK -
OPERATOR 2, NO ADDED VISUAL AIDS

RUN DESCRIPTION	R U N S	ARM STRUCT. DAMPING RATIO	TIME MIN: SEC	COMMENTS
Rigid Arm	1	-	5:30	Phase IIA time - 3:15. No bumps, very good run.
	2	-	13:00	Phase IIA time 3:30. Bumped 6 back probe, 6 right side, 2 left side, 3 front probe. Got very confused due to lack of depth perception.
Loaded Arm Structural Dynamics	3	.3	10:25	Bumped 5 left side.
	4	.3	10:35	Bumped 4 left, 1 back probe.
	5	.7	9:38	Phase IIA time 8:00. Bumped 4 left.
	6	.7	8:37	Phase IIA time 6:30. Bumped 4 left.

TABLE 7
 CARGO STOWAGE TASK -
 OPERATOR 3, NO ADDED VISUAL AIDS

RUN DESCRIPTION	R U N S	ARM STRUCT. DAMPING RATIO	TIME MIN: SEC	COMMENTS
Rigid Arm	1	-	8:00	Bumped 1 right, 1 back probe.
	2	-	4:43	Phase IIA time - 3:00. Touched rear of cargo bay.
Loaded Arm Structural Dynamics	3	.3	10:51	Phase IIA time - 7:00. Bumped 1 rear probe, 2 left, 6 right.
	4	.3	8 14	Phase IIA time - 7:00. Bumped 2 left, 3 right, touched rear of bay with probe.
	5	.7	8:15	Phase IIA time - 6:15. Bumped 3 left, 2 right, touched rear of bay with probe.
	6	.7	7:25	Phase IIA time - 5:00. Bumped 2 left, 1 back probe, 1 front probe.

N75 33699

Unique Wide Field of View

Visual Simulation

John Niemela

U.S. Army Avionics Laboratory

Fort Monmouth, New Jersey

SUMMARY

Visual simulations are required to support investigations of the man-machine aspects of helicopter nap-of-the-earth flight. The visual simulation requirements are discussed vis-à-vis available technology. A wide field of view of the world outside the cockpit is necessary to provide adequate visual cues to the pilot. A unique design is described employing three TV monitors, collimating lenses, and electronics to selectively display a wide field of view without the use of a costly wide angle optical probe.

INTRODUCTION

Systems which will enable a helicopter to be effectively operated in nap-of-the-earth (NOE) flight are of current interest to the Army. NOE flight is helicopter operation as close to the earth's surface as vegetation, obstacles, and terrain will safely allow. During this type of flight the rotor tip-path plane is usually below treetop level as portrayed in Figure 1.

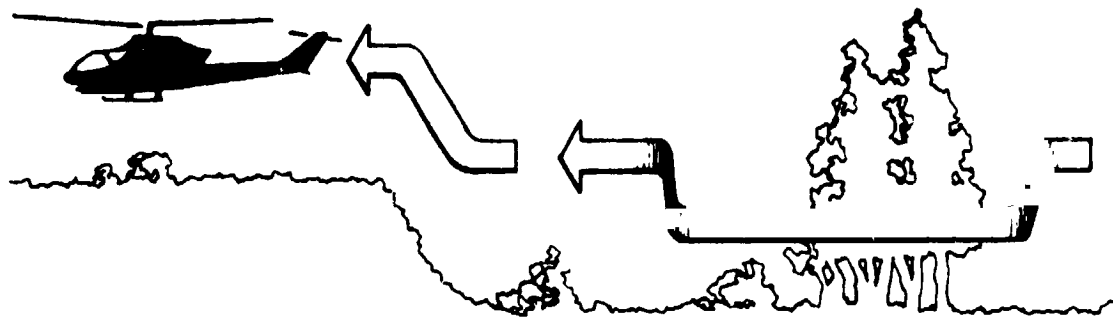


Figure 1. Helicopter Nap-of-the-Earth Flight.

Mean altitudes in these missions are typically between 5 and 15 meters, depending on terrain. It is anticipated that battlefield vulnerability will necessitate extensive NOE flight in future combat operations.

Effective NOE operation requires that the aircrew, particularly the navigator, be geographically oriented at all times in the course of a mission. To improve man-machine navigation system performance in both day and night operations, several navigation display concepts have been considered.

The elements of the man-machine navigation system are shown in Figure 2.

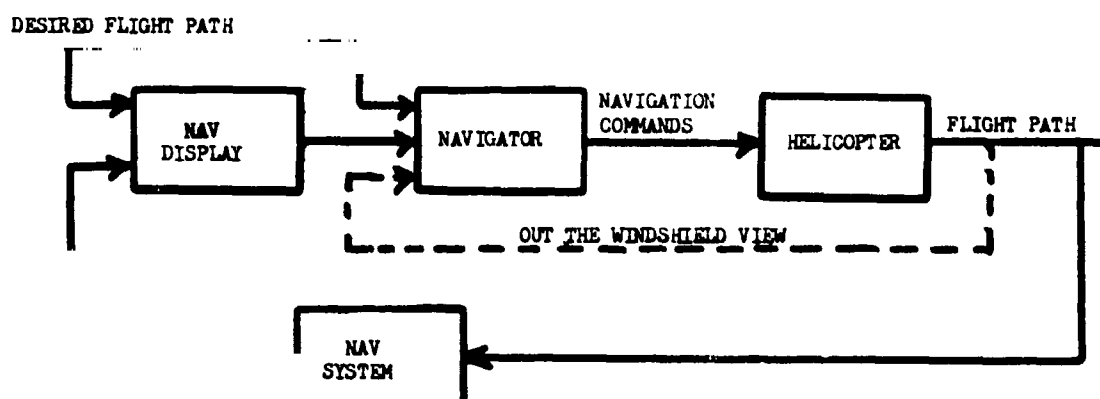


Figure 2. Man-Machine Navigation System.

The navigator compares the desired nominal flight path as indicated on a hand held map or navigation display with the actual course as indicated on the navigation display. These flight paths are compared with the observed out-the-helicopter-windshield scene and corrective commands are introduced to the system.

The element that is of current interest for NOE flight is the navigation display. Several general categories have been considered including the direct view map display, the projected map display, and several types of electronic map displays. A simulation of the navigation aspects of NOE flight was configured to investigate the suitability of these devices in a controlled environment.

SIMULATION REQUIREMENTS

The first general requirement for this simulation is for a wide field of view. Pilots with extensive experience in NOE flight state that the navigator detects and recognizes natural and man-made features by continually scanning left and right as the helicopter proceeds on a NOE flight. The

navigator utilizes a field of view of nearly 180° though only a limited portion at one time. It is apparent, therefore, that a field of view close to 180° is required for this simulation.

The second requirement is for a large and unrestricted geographical area of coverage. To measure the performance of the man-machine navigation system, the simulation must afford the opportunity for the navigator to become geographically disoriented or "lost". The simulation must, therefore, represent a reasonably large geographical area and be essentially unrestricted in movement over this area.

The final general requirement for this particular simulation is that it be compatible with night vision goggles. One of the more difficult NOE missions is night operations. During these flights it is expected that the navigator will operate with night vision goggles. The visual simulation must be, therefore, compatible with night vision goggles.

CANDIDATE APPROACHES

Several general categories of visual simulation exist including film, computer generated, and scale model techniques. Several previous navigation simulations have employed motion pictures to simulate the outside of the cockpit visual world. The flight path is, of course, severely constrained by this approach. Another film technique involves the use of a variable anamorphic lens. Though this technique allows some freedom, the flight path is not unrestricted.

Current computer generated visual simulations have been successful for terminal area applications. These simulations are geographically small and geometrically regular. However, the NOE navigation simulation requires that a relatively large geographical area of very irregular geometry including hills, streams, and ponds, be portrayed.

A third category of visual simulations is the scale model. One type of scale model employs a point light source which projects through a translucent model onto a screen. Point light source visual systems are effective for flat terrain but are not useful in simulating rough terrain. Since terrain contour is an important navigation cue in NOE flight, the point light source technique cannot be used.

The terrain model with servo-driven optical probe, orthicon tube, and TV monitor with collimating lens is the remaining alternative. The current simulation employed these conventional elements in an unconventional manner as shown in Figure 3. In this system, a wide field of view visual simulation is achieved without the expense of a wide angle optical probe.*

*The system concept for this simulation was suggested by W.J. Kenneally of the U.S. Army Electronics Command.

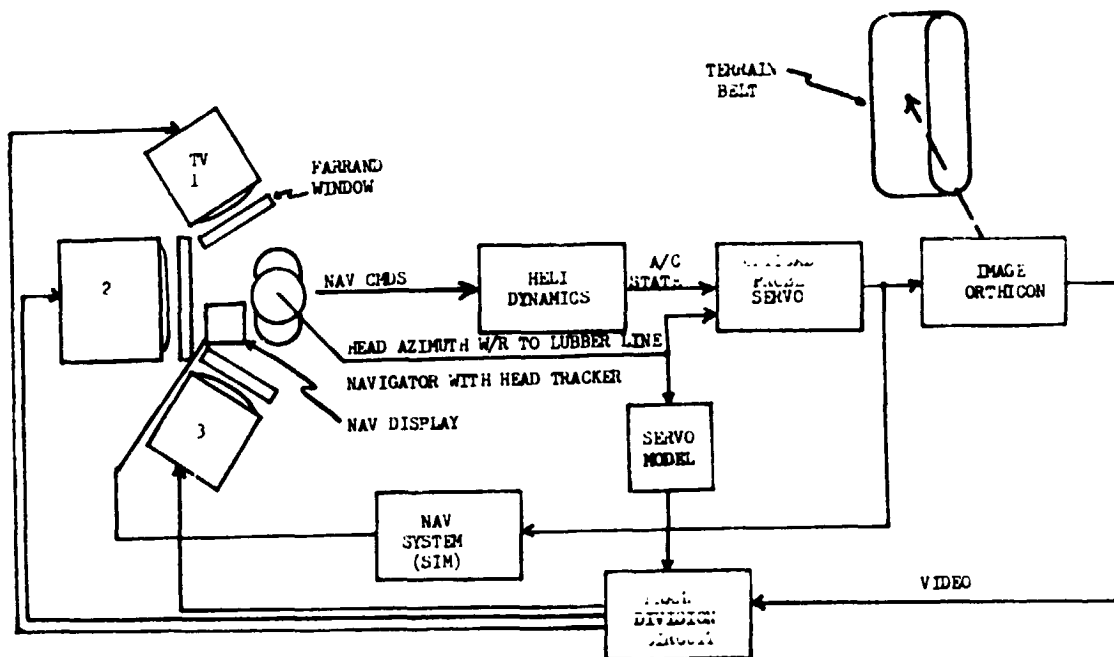


Figure 3. Visual Simulation Configuration.

SIMULATION DESCRIPTION

Examining the system simulated and referring to the block diagram of the man-machine navigation system in Figure 2, a wide field of view simulation provides the outside the cockpit visual cues. The map display is driven by the optical probe's servo follow-up on the terrain belt through the simulated navigation system. The navigator compares the outside of the windshield scene with the navigation display to generate corrective commands. These commands are entered through an audio link to the pilot who controls the helicopter, or directly if the navigator also performs the pilotage functions. These commands reach the optical probe servo through the model of the aircraft dynamics.

The visual simulation can be understood by proceeding step by step upstream from the navigator's eye. The outside world is viewed through three Farrand "pancake" windows which provide a collimated image of three TV monitors positioned behind the lenses. The monitors display that portion of the terrain belt corresponding to the helicopter's heading biased by the navigator's head orientation with respect to the helicopter. This is accomplished by the "Frame Division Circuit" which displays the optical probe's 50° by 40° image on the TV monitor or portion of each monitor faced by the navigator. A head tracker mounted on the navigator's helmet drives

the frame division circuit. A model of the optical probe's azimuth serv. drive dynamics is inserted between the head tracker and frame division circuit to prevent the orientation of the scene displayed from leading the scene viewed by the optical probe.

The result of this simulation is that as the navigator scans across the 180° field of view, a 50° scene corresponding to his head orientation is continuously moved across the three lens-monitor systems. The physical layout of the lenses is shown in Figure 4. The apparent claustrophobi



Figure 4. Layout of Collimating Lenses.

effect of having the lenses in proximity to the subject is eliminated by the collimated image. The TV images were adjusted in size and position such that they slightly overlapped from adjacent TV-lens systems. The only obstructions were the lens frames. It is difficult to appreciate the effect of the selective wide field of view simulation without a demonstration. This configuration, though by no means the final word in visual simulations, is the first developed to meet helicopter NOE navigation requirements.

N75 33700

**TEST PROCEDURES AND PERFORMANCE MEASURES SENSITIVE
TO AUTOMOBILE STEERING DYNAMICS**

By Richard Klein, Duane McRuer, and David Weir

Systems Technology, Inc.
Hawthorne, California

SUMMARY

A maneuver complex and related performance measures used to evaluate driver/vehicle system responses as effected by variations in the directional response characteristics of passenger cars are described. The complex consists of normal and emergency maneuvers (including random and discrete disturbances) which, taken as a whole, represent all classes of steering functions and all modes of driver response behavior. Measures of driver/vehicle system response and performance in regulation tasks included direct describing function measurements and rms yaw velocity. In transient maneuvers, measures such as steering activity and cone strikes were used.

INTRODUCTION

This paper presents an introduction to a major two-year research program (Ref. 1) conducted for the National Highway Traffic Safety Administration to evaluate closed-loop driver/vehicle response relationships and to identify optimum vehicle directional dynamic characteristics in normal and emergency driving situations. We will describe here the vehicle dynamic variables, the test procedures utilized, and the performance measures found to be sensitive to the changes in vehicle directional mode (i.e., steering) dynamics. Companion papers deal with more specific results and comparisons.

The primary objectives of the program were to identify optimum driver/vehicle systems and the sensitivity of these optima with respect to vehicle parameter changes; to identify significant maneuvers which exhibit sensitivity to changes in the vehicle dynamic variables; to correlate subjective driver opinion ratings and objective performance measures; and to establish an archival data base so that other researchers might be able to further analyze the data for these or other purposes. Besides these major purposes there were peripheral objectives, such as the assessment of effects due to long-term driving duration, and comparison of the results obtained with production vehicles, etc. To accomplish these objectives a three-pronged approach of analysis, simulation, and full-scale field tests was adopted. The analysis applied man/machine system theory to guide the experiments and to interpret, rationalize, and generalize the experimental findings. The fixed-base simulation served as a pilot-experimental prelude to the field tests and also permitted the coverage of a broader spectrum of vehicle dynamics than could be accommodated full scale.

The full-scale field tests expanded on and further verified the hypotheses developed analytically and on the simulator about the nature of driver/vehicle system interactions. The full-scale tests were divided into an exploratory and a validation series. These were, respectively, an examination of many configurations with one driver and an examination of a few configurations with many drivers.

VEHICLE DYNAMICS

The dynamic properties of interest in this program were restricted to steering control of the directional motions at constant speed. For these conditions the rolling and yawing motions of an automobile in response to steer angle and side load aerodynamic disturbances may be represented in matrix form by:

$$\begin{bmatrix} s - Y_V & \frac{m_{se}}{m} s^2 - Y_\phi & U_0 - Y_r \\ \frac{m_{se}}{I_\phi} s & s^2 - L_p s - L_\phi & \frac{I_{\phi z}}{I_\phi} s + \frac{m_{se}}{I_\phi} U_0 \\ -N_V & \frac{I_{\phi z}}{I_{zz}} s^2 - N_\phi & s - N_r \end{bmatrix} \begin{bmatrix} v \\ \phi \\ r \end{bmatrix} = \begin{bmatrix} Y_{\delta_w} & Y_{v_g} \\ 0 & L_{v_g} \\ N_{\delta_w} & N_{v_g} \end{bmatrix} \begin{bmatrix} \delta_w \\ v_g \end{bmatrix} \quad (1)$$

The meaning of the symbols, the axis system used, and the complete derivation of these equations is given in Ref. 2. The eigenvalues of the matrix of Eq. 1 ordinarily consist of a very lightly damped quadratic pair which represents primarily rolling motions, and a pair of roots, which may or may not be coupled into a quadratic, primarily associated with heading and lateral path changes. Reference 2 shows that the roll quadratic pair is almost always nearly cancelled by similar numerator quadratics in the transfer functions which relate side velocity and yawing velocity to steer inputs. In other words, the dynamic roll mode is only very slightly excited in steering maneuvers in ordinary cars, although a certain amount of steady-state roll will be present in turning maneuvers. This implies a dynamic decoupling of roll from the other lateral-directional degrees of freedom. If it is assumed that the yawing and side velocity modes are uncoupled from the rolling mode or, alternatively, that the rolling degree of freedom is suppressed or negligible, then Eq. 1 reduces to a two-degree-of-freedom set shown by Eq. 2:

$$\begin{bmatrix} s - Y_V & (U_0 - Y_r) \\ -N_V & (s - N_r) \end{bmatrix} \begin{bmatrix} v \\ r \end{bmatrix} = \begin{bmatrix} Y_{\delta_w} & Y_{v_g} \\ N_{\delta_w} & N_{v_g} \end{bmatrix} \begin{bmatrix} \delta_w \\ v_g \end{bmatrix} \quad (2)$$

When the stability derivative values in this equation are adjusted to a two degree-of-freedom context, i.e., considered as effective values, then the directional dynamics are reasonably well approximated by the Eq. 2 relationships. They are excellent for the primary situations investigated in the present program, not only for the reasons cited above but also because the roll degree of freedom was mechanically suppressed to the extent possible practically. This was in accordance with the project objective to study the vehicle dynamic behavior for essentially non-rolling directional control.

An elemental directional response variable of primary interest in driver vehicle system control is the yawing velocity, r . A convenient way to describe the yawing velocity response to nominal steering inputs is via the system transfer function, r/δ_{sw} . This can be obtained by manipulation of Eq. 2,

$$\begin{aligned} \frac{r}{\delta_{sw}} &= G_s \frac{r}{\delta_w} = G_s G_{\delta_w}^r = \frac{G_s N_{\delta_w} \left[s + \left(-Y_v \frac{V_{\delta_w}}{N_{\delta_w}} N_v \right) \right]}{[s^2 - (Y_v + N_r)s + (U_0 - Y_r)N_v + Y_v N_r]} \\ &= \frac{G_s N_{\delta_w} (s + 1/T_r)}{s^2 + 2(\zeta\omega)_1 s + \omega_1^2} \\ &= \frac{G_s N_{\delta_w} (1/T_r)}{[\zeta_1, \omega_1]} \end{aligned} \quad (3)$$

where

- G_s = Steering system gain
- N_{δ_w} = Yawing acceleration steering coefficient
- T_r = Lead time constant of yaw velocity response to steer input; yaw time constant for short
- ζ_1 = Damping ratio of directional mode
- ω_1 = Undamped natural frequency of directional mode
- s = Laplace operator

The frequency and damping ratio of the denominator roots can be plotted on the complex plane in polar coordinates (ρ, θ) where $\rho = \omega_1$ and $\theta = \cos^{-1} \zeta_1$ or in rectangular coordinates (x, y) where $x = -\zeta_1 \omega_1$ and $y = \omega_1 \sqrt{1 - \zeta_1^2}$. Figure 1 is an example of the complex plane representation of four different yaw velocity to steering wheel transfer functions. For vehicles which do not depart too far from a neutral steering condition the directional damping ζ_1 is just

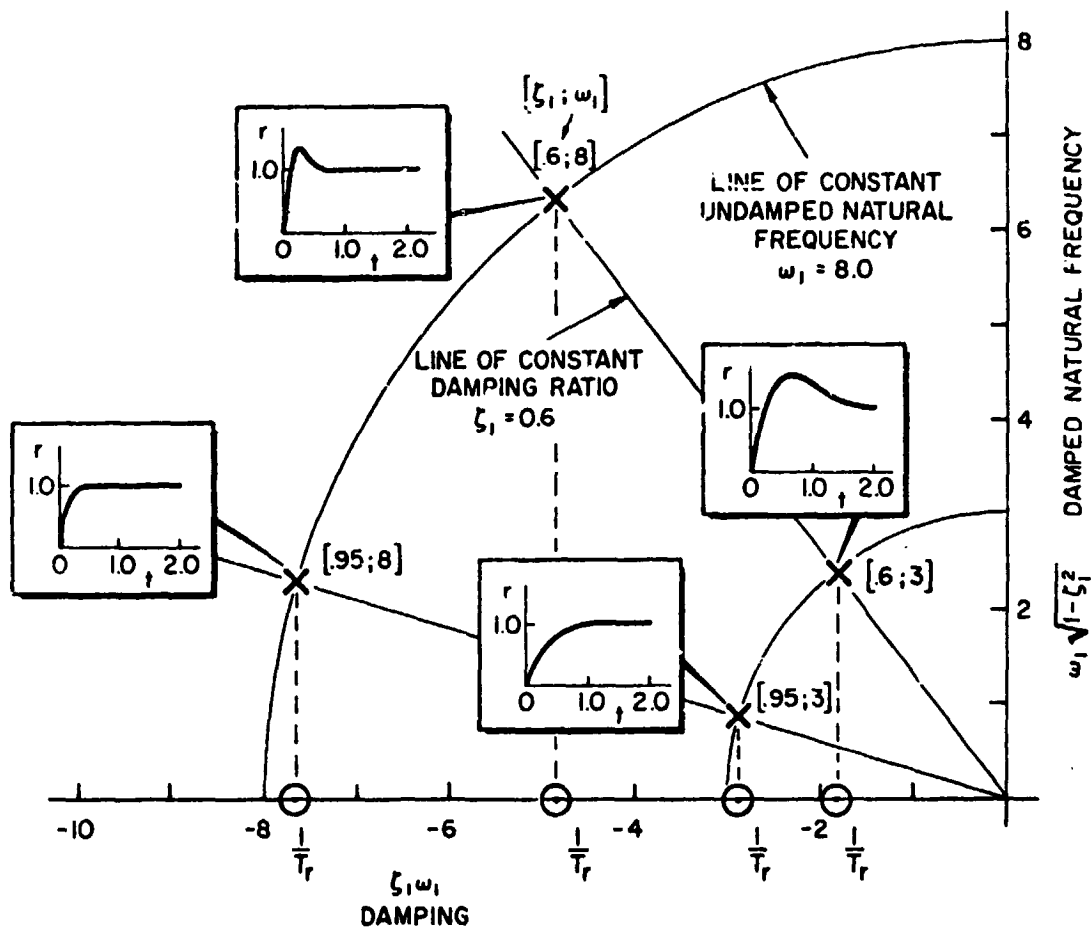


Figure 1. Complex Plane Representation of Vehicle Configurations

slightly less than the inverse yaw time constant, $1/T_r$. Normalized yawing velocity time responses to a step wheel input have been computed for these conditions and are shown alongside the respective transfer function poles (X). Notice that the higher frequency configurations respond more rapidly, and the amount of overshoot depends on both the damping ratio and the value of the numerator yaw time constant T_r . Lower frequency configurations rise more slowly and may be thought of as having a compressed time scale. A third dimension, not shown in Fig. 1, is the magnitude of the response; this is scaled by the steering system gain. These four variables of the directional response, i.e., yaw time constant (T_r), steering ratio ($1/G_s$), directional damping ratio (ζ_1), and directional frequency (ω_1) were the vehicle variables of the test program.

The directional dynamics tested are summarized in Table 1. In all cases the vehicle itself was a 1974 Chevrolet Nova hatchback, with the dynamics adjusted by a variety of mechanical and servomechanical means.

TABLE 1. SUMMARY OF VEHICLE DIRECTIONAL DYNAMIC CHARACTERISTICS AT 50 MPH

CONDITIONS TESTED		VEHICLE DYNAMICS			GAINS	
EXPLORATORY SERIES	VALIDATION SERIES	INVERSE YAW TIME CONSTANT $1/T_r$	DAMPING RATIO ζ_1	NATURAL FREQUENCY ω_1	STEADY-STATE STEER ANGLE GAIN $r/\delta_w _{ss}$	STEERING RATIO $1/G_s$
✓		2.25	0.83	2.6	5.3	19, 15, 10
✓		2.25	1.0	2.25	8.1	25, 19, 15
✓	✓	3.0	0.62	3.9	3.0	19, 15, 12, 9
✓		3.0	0.71	3.4	4.0	25, 19, 15, 10
✓	✓	3.0	0.75	3.5	4.5	25, 19, 17, 15, 10
✓		3.25	0.80	3.7	5.2	25, 19, 15, 10
✓		4.0	0.97	4.1	7.4	25, 19, 15
✓	✓	4.0	0.77	4.5	4.7	25, 19, 14, 12
✓	✓	5.0	0.57	5.8	2.6	19, 17, 15, 11
✓		5.0	0.81	5.4	5.0	30, 19, 15, 10
✓		5.0	0.91	5.2	7.4	25, 19, 15

MANEUVER COMPLEX

In setting up the maneuver complex and driving scenario to be used in the test series, three criteria were paramount. These were:

- Representative maneuvers. The maneuver complex should contain sufficient elements to provide a representative cross section of steering functions and maneuvers. The total should be inclusive of fair weather, sub-limit performance steering operations.

- Driver behavior. The maneuver complex should contain tasks which evoke all modes of driver control. These are to include:
 - Compensatory — regulation and command following.
 - Dual-mode (pursuit or precognitive combined with compensatory behavior) — course segments with sufficient preview to permit pursuit behavior and course segments with a distinct starting point which can be accomplished at a high level of skill.
- Tie-in maneuvers. Some maneuvers in the sequence should permit tie-ins with steering tests used by other investigators.

A final criterion was that the maneuver complex be such that it could be set up within the physical confines of the test area.

Table 2 lists the initial series of test maneuvers for the nominal driving scenario used in the test program. Listed alongside each maneuver is the associated steering function and the most likely driver control mode evoked.

TABLE 2. NORMAL DRIVING MANEUVER COMPLEX

NAME OF MANEUVER	STEERING FUNCTION	DRIVER CONTROL MODE	NOMINAL SPEED
Precision Lane Tracking	Precision course control	Compensatory	30
Highway Lane Regulation	Routine lane following	Compensatory	50
Random Disturbance Regulation	Steady-state regulation (external input)	Compensatory	50
Step Disturbance Regulation	Transient regulation (external input)	Compensatory	50
Double Lane Change	Normal command change	Dual Mode (Precognitive)	30 and 50
Emergency Lane Change	Evasive command change	Dual Mode (Precognitive)	30
Unexpected Obstacle	Unexpected command change	Dual Mode (Precognitive)	30

A second set of maneuvers was used to represent a high workload level and to exacerbate differences in driver skill levels. These maneuvers included a high-speed (50+ mph) slalom and high-speed (45-60 mph) double lane change such as used by driving schools, manufacturers, and the automotive press. A low-speed (30 mph) random slalom was also included and is a variation of the

conventional low-speed slalom used by other researchers. The random slalom consisted of randomly spaced pylons at 60, 120, 180, and 240 ft intervals. When run at a constant speed this maneuver exercised the vehicle's directional response capability at various lateral g levels.

Four of the maneuvers shown in Table 2 were particularly sensitive to the changes in vehicle dynamics varied in the test program or to driver behavioral differences. These four maneuvers were highway lane regulation, the double lane change, the emergency lane change, and the unexpected obstacle. These will be described in more detail below, first outlining the procedures involved in each and then the types of performance measures obtained.

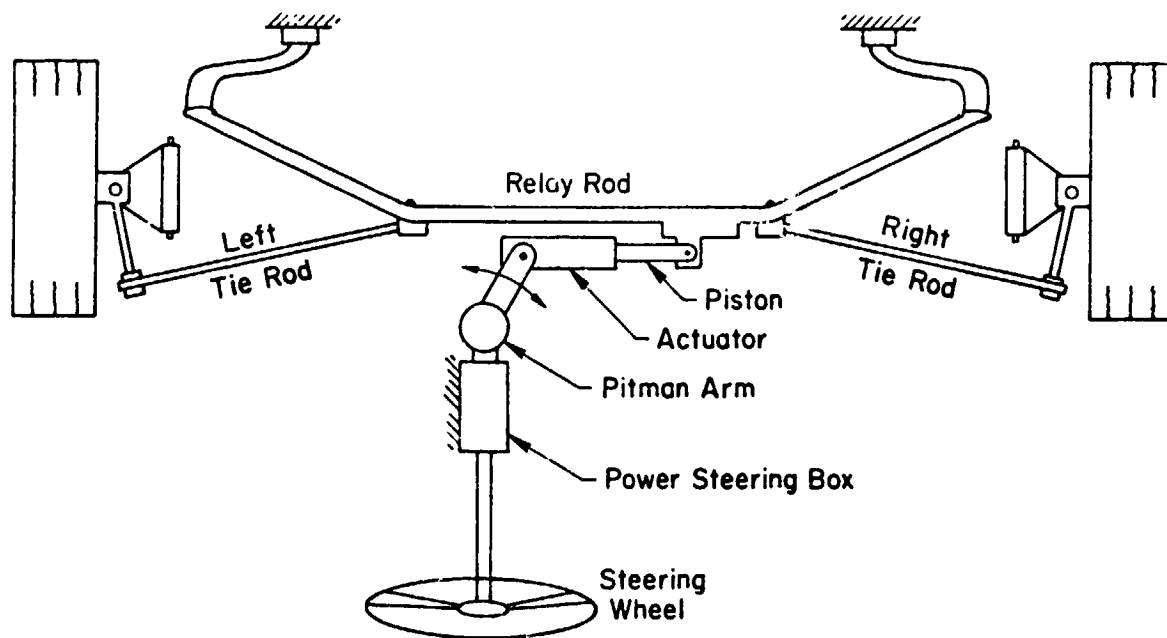
KEY MANEUVERS

The regulation task, or compensatory tracking task, is a maneuver that requires the driver to maintain position within a lane on a straight stretch of highway in the presence of a simulated gusting crosswind. The simulation of the crosswind was accomplished as one function of the special steering apparatus shown in Fig. 2. This was a linear electrohydraulic servo inserted in the front suspension between the driver's steering wheel and the tie rod that actually moves the front tires. In effect, it acted as an extensible link to the Pitman arm of the steering system. With no external input to the steering servo, the front steer angle is moved via the conventional steering linkage, composed of the power steering box, Pitman arm, relay rod, and tie rods. Because of the series connection the extensible link acts as a summing junction for the mechanical input applied via the steering wheel and the electrical input applied from the instrumentation system.

The servo performed three functions in the tests introduced here. First, by moving the tires as functions of vehicle motion quantities, such as lateral acceleration or yaw rate, different levels of oversteer or understeer could be achieved. Second, the steering wheel position could be fed forward to change the steering ratio. Both of these functions are similar to those available in other variable stability (Refs. 3 and 4) and variable characteristic (Refs. 5 and 6) automobiles. The third function was to insert disturbance inputs. These were either a step steer, which appeared to the driver as a blown tire or running off the edge of a lane, or a random-appearing signal which was the basis for the regulation task itself. The random input is composed of the sum of five sine waves at different amplitudes and frequencies such that it appears to the driver as if the car is in a gusting crosswind condition. The regular power steering box provided sufficient isolation between the servo and the driver so that this disturbance was not reflected into the steering wheel.

The second sensitive maneuver was a double lane change in which the driver had to switch from one 9 ft lane to another 9 ft lane at 50 mph through a 1 ft entry gate. He then had to repeat the maneuver in reverse to return to the original lane.

The third maneuver, an emergency lane change, incorporated some unexpected event aspects. It was based on three conventional traffic lights suspended



FEEDBACKS

- Lateral Acceleration
- Yaw Rate

FEEDFORWARD

- Steering Wheel

DISTURBANCE INPUTS

- Step
- Random

Figure 2. Functional Schematic of Variable Front Steering Servo

across three adjacent 12 ft lanes. Entry was at 50 mph, in the center lane, with all three traffic lights green. Upon tripping a pressure-sensitive roadway switch with the front tires, two of the three green lights were switched to red, at which point the driver had to determine which lane remained green, maneuver the car through that lane, and then back to the original lane. There were approximately 2 seconds from the time the car tripped the switch until the car was directly underneath the lights.

The fourth key maneuver was the unexpected obstacle. This utilized a full-size side view photograph of a car mounted on a movable styrofoam sheet. The subjects were all unaware that the "obstacle," prepositioned off the side of the road, would in fact come out into their lane.

PERFORMANCE MEASURES

In each of the above maneuvers, performance measures were obtained that were sensitive to the changes in vehicle dynamics. These measures can be classified under four general categories. First were driver response measures, such as describing functions. Second were vehicle motion performance measures, such as mean square values, peak values, and exceedences of key variables. Third were track scores, such as cone hits, timing throughout the test circuit, and speed deviations in specific maneuvers; and last were subjective driver ratings of each different vehicle which were to be correlated with the three previous objectives measures.

For the driver describing function measures, very repeatable driver/vehicle describing functions such as shown in Fig. 3 were obtained. These results were usually based on two or three runs per driver at 50 mph. The plot in Fig. 3 shows the combined open-loop driver/vehicle describing function denoted by $Y_p^*G_{sw}^*$. The driver and vehicle dynamics were not separated since changes in such key parameters as crossover frequency, phase margin, and effective time delay could, in themselves, be correlated with the changes in vehicle dynamics. Associated with the describing function measures were rms yaw velocity excursions and driver opinion ratings of the regulation task.

For the emergency lane change and double lane change maneuvers, steering activity measures and safety-relevant lane exceedences (as measured by cone strikes) were sensitive indicators of vehicle dynamic differences. An example of the steering activity measure is shown in Fig. 4. This shows steering wheel activity, steering wheel rate, lateral acceleration, and yaw velocity for each one of three different vehicle dynamic configurations. On the lefthand side is a very slowly responding car having $1/T_r = 2.25 \text{ sec}^{-1}$. On the righthand side is a more rapidly responding car with $1/T_r = 5 \text{ sec}^{-1}$. Comparing the steering wheel angle trace on the left to the one on the right it can be seen that there is much more steering activity and a much less repeatable signature for the slowly responding car than for the rapidly responding car. This characteristic is apparent in the other three traces also. From these traces it was possible to determine steering wheel reversals, peak steering wheel rates, and rms steering wheel activity as a function of vehicle dynamic response given by $1/T_r$.

The cone strike measures are shown in Fig. 5. These data are for the emergency lane change maneuver at 30 mph and show the percent of runs in which the driver exceeded the lane boundary. Exceeding the lane boundary was noted by either hitting or knocking over cones that delineated the maneuver lanes. This plot shows the changes in cone strikes as a function of four different vehicle configurations (noted along the bottom as A, B, C, and D) and by subject sex since this turned out to be an important variable. From this plot it can be seen that the cone strike measures are sensitive to changes in vehicle dynamics. A side result was that the female subjects, in all cases, exhibited a higher percentage of lane exceedences than male subjects.

For the last maneuver, the unexpected obstacle, we were not able to correlate any performance measures with the changes in vehicle dynamics since only the first exposure to the obstacle is representative of the unexpected or

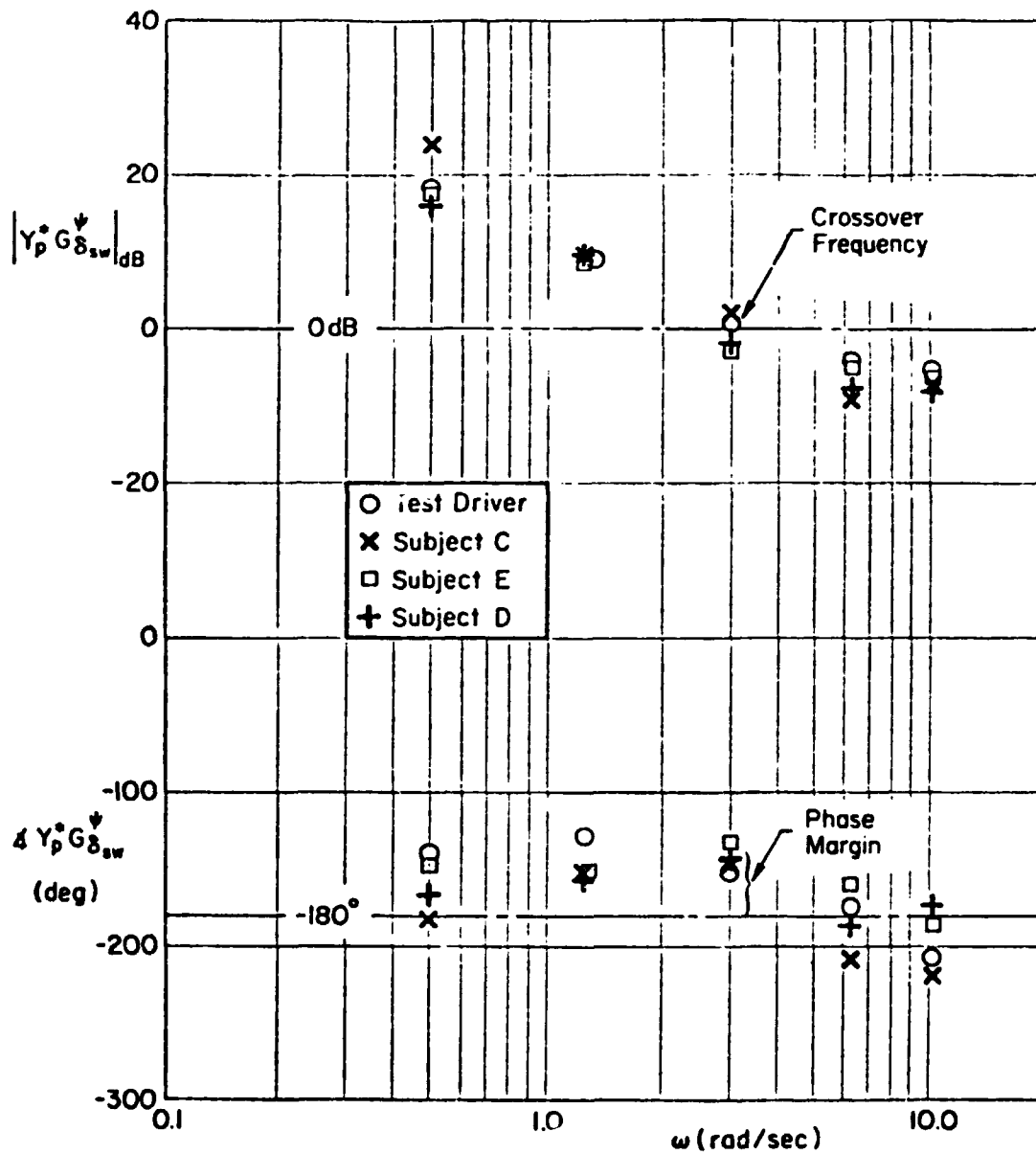


Figure 5. Driver/Vehicle Describing Function Comparison of Test Driver and Three Typical Subjects for Configuration B

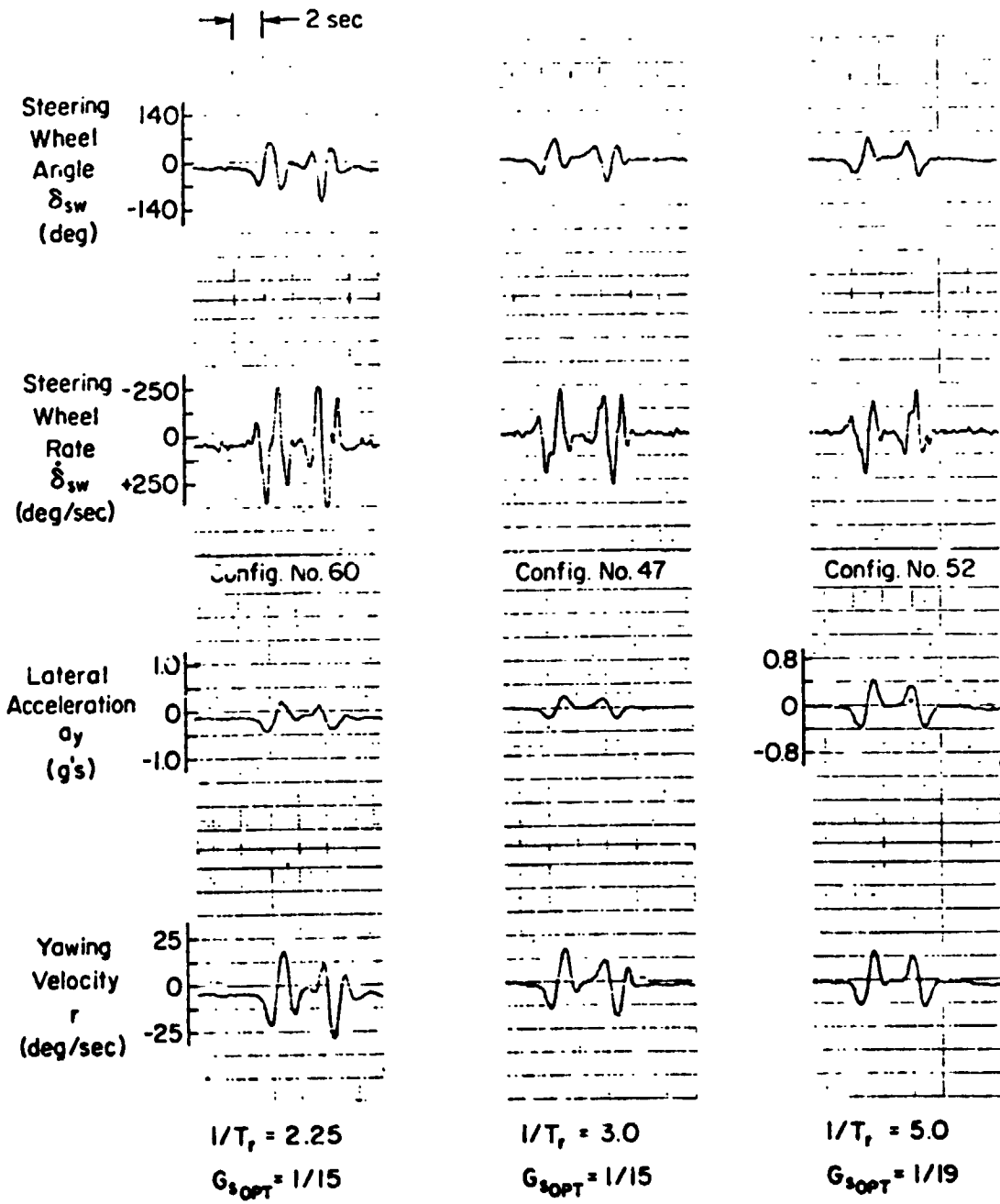


Figure 4. Comparison of Steering Activity and Vehicle Response for Three Vehicle Configurations in the 50 mph Double Lane Change Maneuver

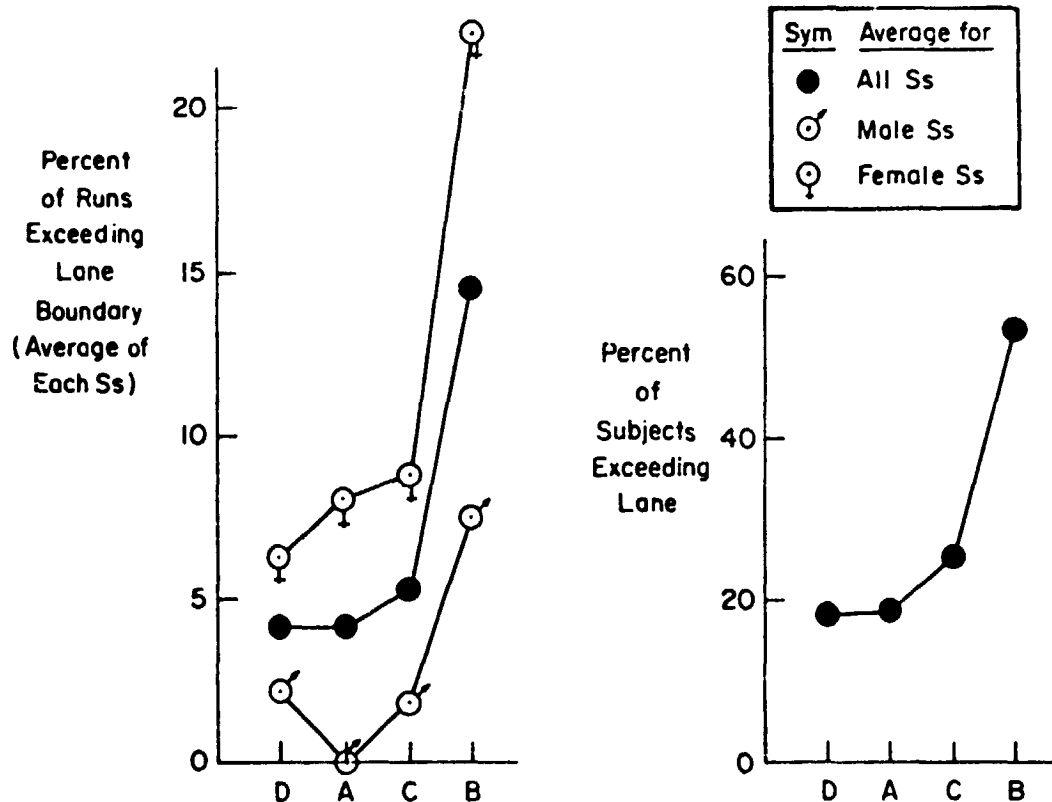


Figure 5. Cone Strike Measures for Emergency Lane Change Maneuver (30 mph)

emergency actions of the driver. This maneuver, however, showed large qualitative differences among the drivers.

Analyses and conclusions derived from the tests using these maneuvers allowed us to derive tentative boundaries for vehicle dynamic characteristics that required the least amount of driver lead equalization, produced the best closed-loop driver performance in all tasks, and were rated good from the standpoint of required workload. A summary of the primary conclusions (documented in Ref. 1) are as follows.

1. Measurements of closed-loop driver response characteristics in full-scale road tests showed crossover frequency, phase margin, response latency, and closed-loop damped natural frequency to be important driver response parameters. These results were compatible with previous driver/vehicle theory and models in terms of driver steering gain adjustments and the generation of lead equalization.

2. The key vehicle parameters were the overall steering gain of the car, i.e., the gain between the steering angle and the resulting yaw velocity response of the car and the closed-loop path mode time constant which is reflected by the yaw time constant, T_r . Of less importance were the directional mode frequency, ω_1 , and damping ratio, ζ_1 .
3. The key maneuvers were the regulation task (for measurement of closed-loop driver response characteristics), the double lane change (for measurement of the transient driver characteristics), and the emergency lane change (which was representative of an unexpected or emergency-type situation).
4. Key measures for these tasks were driver dynamic performance (describing functions), steering wheel activity, lane exceedences (as measured by cone strikes), yaw velocity dispersion, and driver opinion ratings.

In companion papers, these general conclusions are described more quantitatively.

REFERENCES

1. McRuer, Duane T.; and Klein, Richard H.: Automobile Controllability — Driver/Vehicle Response for Steering Control. Vol. I: Summary Report, DOT HS-801 406. Vol. II: Supporting Experimental Results, DOT HS-801 407. Nov., 1974.
2. Weir, David H.; Shortwell, Charles P.; and Johnson, Walter A.: Dynamics of the Automobile Related to Driver Control. SAE Paper 680194, Feb. 1967.
3. Segel, Leonard; and Bundorf, R. Thomas.: The Variable-Stability Automobile. SAE SP-285, Nov. 1965.
4. Kasselmann, J. T.; and Keranen, T. L.: Adaptive Steering. Bendix Technical Journal, vol. 2, no. 3, Autumn 1969.
5. Sweatman, P. F.; and Joubert, P. N.: The Melbourne University Variable Characteristic Car. Proc. Sixth Conf. Australian Road Research Board, 1972.
6. Sweatman, Peter: The Design of a Variable Characteristic Vehicle and Its Use in Driver Control Studies. Ph.D. Thesis, Univ. of Melbourne, Apr. 1973.

ACKNOWLEDGMENT

This research was supported by the National Highway Traffic Safety Administration under Contract DOT-HS-349-3-762.

N75 33701

AN INTERACTIVE DRIVING SIMULATION FOR DRIVER
CONTROL AND DECISION-MAKING RESEARCH

By R. Wade Allen, Jeffrey R. Hogge,
and Stephen H. Schwartz

Systems Technology, Inc.
Hawthorne, California

SUMMARY

Simulation is becoming an increasingly important tool in driving research. This paper describes display techniques and equations of motion for a relatively simple fixed-base car simulation. The vehicle dynamics include simplified lateral (steering) and longitudinal (speed) degrees of freedom. Several simulator tasks are described which require a combination of operator control and decision making, including response to wind gust inputs, curved roads, traffic signal lights, and obstacles. Logic circuits are used to detect speeding, running red lights, and crashes. A variety of visual and auditory cues are used to give the driver appropriate performance feedback.

The simulated equations of motion are reviewed and the technique for generating the line drawing CRT roadway display is discussed. On-line measurement capabilities and experimenter control features are presented, along with previous and current research results demonstrating simulation capabilities and applications.

BACKGROUND

Simulation of manual control tasks is desirable for a number of reasons. It is often less expensive than working with the real system, more variables are available for manipulation, and critical real-world situations (e.g., emergencies, performance limits, etc.) can be simulated in relative safety. Dynamic simulations of aircraft are common and quite sophisticated (Ref. 1), and can be justified because of the high cost and relative danger inherent in aircraft operations. Although the automobile represents a relatively inexpensive system, accidents are a major and expensive problem which justifies simulation for research and training purposes.

The simulation described in this paper is an inexpensive fixed-base system, with a fully interactive dynamic display that responds appropriately to driver steering and speed control actions (as opposed to canned film simulators, Ref. 2). Simulator capability requirements were evolved out of past research on automobile dynamics (Ref. 3) and driver control theory (Refs. 4 and 5). Application of simple automobile dynamics in a simulation were originally developed in collaboration with the UCLA Institute for Traffic and Transportation Engineering (Ref. 6).

Based on the above work, a more elaborate simulation was developed for use in a study of the effects of alcohol on driver control sponsored by the National Highway Traffic Safety Administration (NHTSA) (Ref. 7). This simulation has recently been further modified, including the addition of a relatively sophisticated roadway display, to accommodate NHTSA-sponsored research on alcohol effects on driver decision making. The present simulator configuration has a rich variety of visual and auditory cues, and readily modifiable lateral and longitudinal equations of motion, which should prove valuable in a wide range of applications including driver control and decision-making research, and driver training in normal and emergency situations.

SIMULATION

A block diagram of the major simulation elements is shown in Fig. 1. An actual car cab and controls are used along with an electronically generated

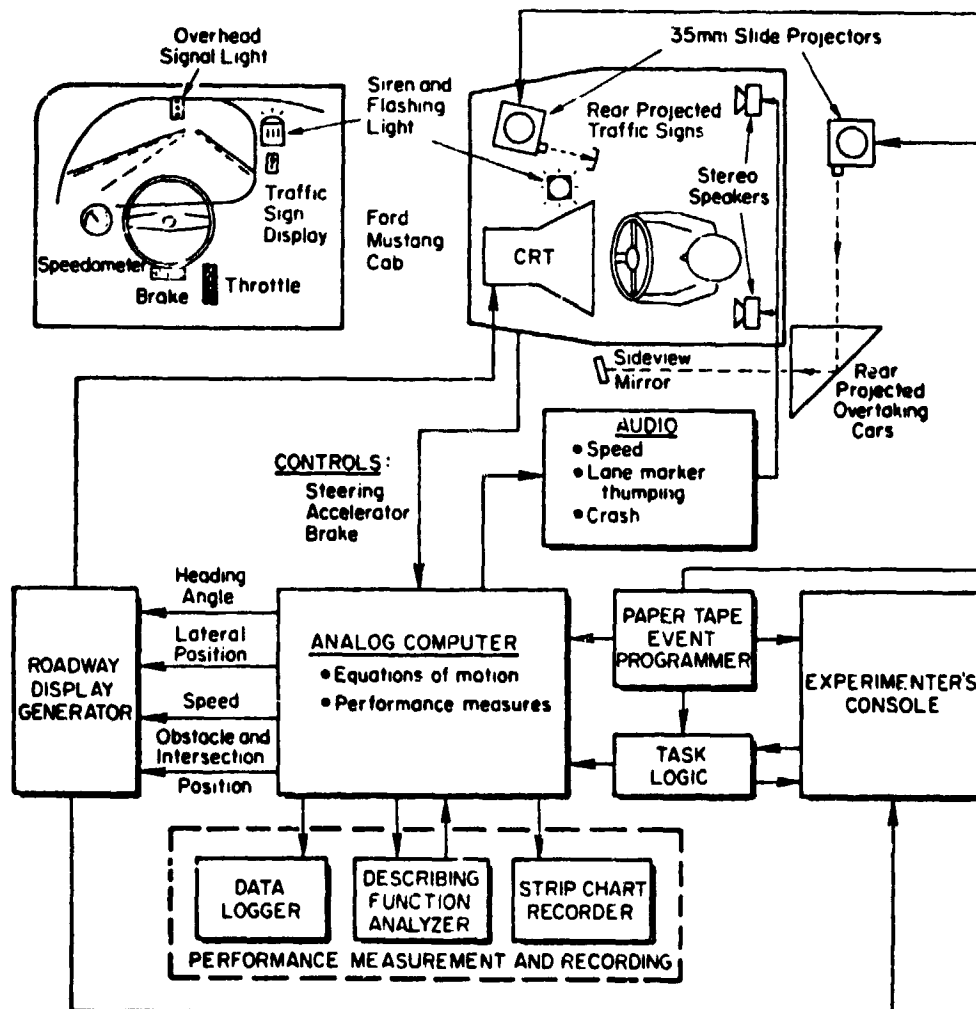


Figure 1. Simulator Block Layout

CRT roadway display. Additional displays include slide-projected road signs and adjacent traffic, a variety of auditory cues (speed, lane marker bumps, crashes), and a siren and flashing red light for traffic violations.

Car equations of motion are programmed on an analog computer. Forward speed is controlled by accelerator and brake inputs to a longitudinal speed equation. Dashed lane markers on the display move proportional to speed, which is also displayed on a circular 4 in. speedometer and as an auditory cue with frequency proportional to speed. Apparent car translation and heading display motions are controlled by steering inputs to a two-degree-of-freedom set of speed variable equations, and provision is made for simulating disturbances due to wind or road roughness.

A variety of tasks as described below can be controlled through task logic from either a punched paper tape programmer or experimenter's console which also allows performance monitoring and measurement.

Display

The roadway display is generated with special purpose electronic circuits, which are controlled by car motion variables generated on the analog computer, and displayed at $2/3$ scale on a 10" x 12" CRT. The circuitry generates line drawings of up to eight symbols at a repetition rate of 125 times per second which provides a smooth responding and flicker free image.

The display format basically consists of two 12 ft lanes bounded by 2.5 ft shoulders as shown in Fig. 1. Display computations are initially done in the horizontal plane where lines are straight and parallel, an obstacle is circular, and all points on the ground plane move at the same apparent speed. All symbols are then multiplexed and the correct geometric transformation applied to give the proper apparent road perspective in the display plane as illustrated in Fig. 2. At this point a horizontal display deflection proportional to the square of distance down the road can also be applied to give apparent roadway curvature.

The dashed lines are achieved by modulating the CRT intensity input with the square wave output of a multi-vibrator circuit. The circuit is configured to move the dashed lines one dash length at the car speed, then reset rapidly to give the illusion of apparent dashed line motion. Intensity of the display elements is also reduced as a function of distance down the road to give the illusion of distance. This electronic display concept provides a simple means for generating clean sharp images that respond instantly and smoothly to driver control actions, thus avoiding the dynamic problems and expense associated with computer-generated and terrain model display approaches (Refs. 6 and 8).

Decision Tasks

The above simulation capabilities are combined to present driving situations requiring the driver to decide among alternate control actions. These driving

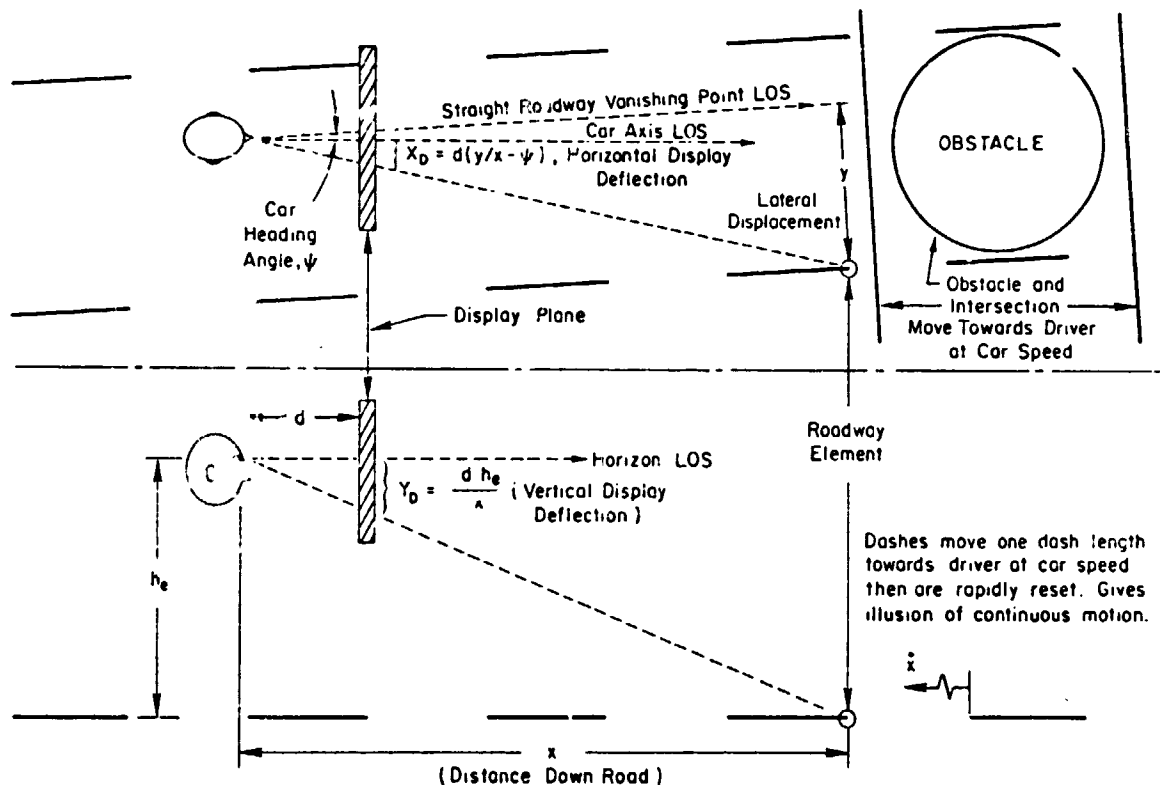
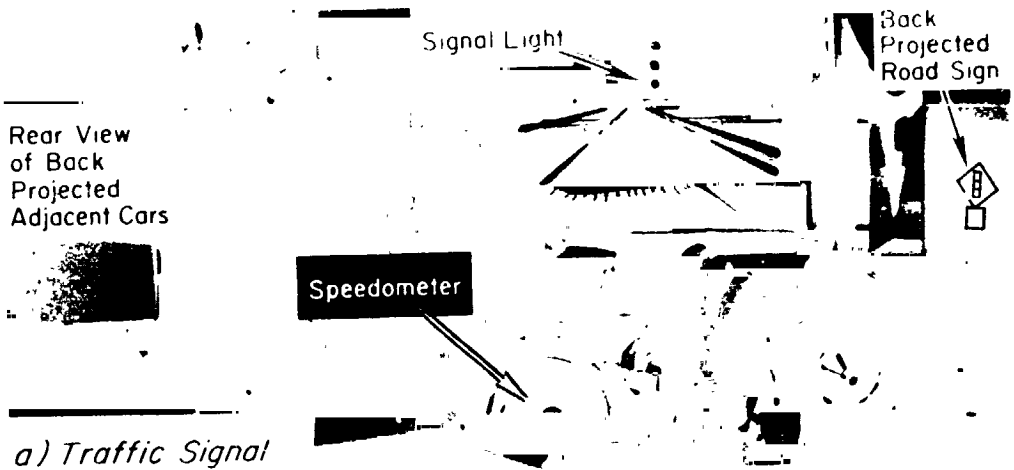


Figure 2. Roadway Ground Plane Transformation to Display Coordinates

situations are controlled by the paper tape programmer with presentation rate proportional to speed in a typical driving scenario as described below:

1. Traffic Signal — This task combines a model signal light and displayed intersection as shown in Fig. 3a. The intersection moves as a function of forward speed. The intersection initially appears at a distance of 300 ft (the maximum length of the displayed roadway) accompanied by the green (lower) light. The amber light is turned on for 3 sec at an intersection distance computed from car speed to give a commanded time interval for "making" the light (i.e., for higher speeds the intersection is triggered at larger distances from the car).
2. Unexpected Obstacle — In this task a stationary circular object at the right side of the road moves into the right lane as shown in Fig. 3b. In this situation the subject can either stop or drive around the obstacle. The task is further complicated by the possible presence of an interfering car in the left lane as projected on a rear screen and observed through the side view mirror. The obstacle road entry distances and adjacent cars are arranged to give a variety of conditions requiring either stopping or steering.



1968-1969

ORIGINAL PAGE IS
OF POOR QUALITY

3. Curved Road — This task is preceded by a projected curve warning sign followed in a short distance by the curved road as shown in Fig. 3c. The curvature increases to a peak value then recedes back to a straight road. Due to a limit placed on the car's tire slip angle, the maximum point of curvature cannot be negotiated any faster than 50 mph or else the car will skid off the road. This task thus requires combined steering and speed control for successful completion.
4. Overall Drive Scenario — The above tasks are presented to the subject in random order during a 15-20 minute drive controlled by the paper tape programmer. Various amber light and obstacle distances are included to induce a range of stopping, accelerating, and steering behavior. A violation circuit can also be activated by the programmer to detect speeding and red light violations at certain defined points in the scenario.

Crashes and violations during the drive scenario are determined automatically by logic circuits and logged on a pen recorder, and immediate feedback can be given to the subject via buzzers for crashes and a flashing red light/siren combination for violations. A variety of other performance measures is available as pen recordings including car variables such as speed and lane position and driver variables such as steering, accelerator, and brake activity. Additional instrumentation also allows the measurement of eye movements, heart rate, and other objective driver performance parameters including describing functions of steering control.

The experimenter's console shown in Fig. 4 is provided to give immediate feedback on task configuration and subject behavior. The console also allows the experimenter to independently initiate the various tasks described above during indoctrination and training sessions.

Control Tasks

A block diagram of the steering and speed control tasks is shown in Fig. 5. The driver's steering actions are processed by lateral vehicle steering dynamics and kinematic equations to give vehicle heading and position relative to the roadway (which may be curved). These variables then provide inputs to the roadway display. Similarly, throttle inputs to the longitudinal dynamics determine vehicle speed which is displayed to the driver visually via the roadway display and speedometer and aurally from the audio system.

Disturbance or inputs can be applied to the lateral and speed control loops in order to increase the driver's workload and provide stimuli for driver response measurements. A disturbance combined with the driver's steering signal acts much like wind gusts and provides a simple means for measuring the driver's compensatory steering response dynamics under constant speed conditions (Ref. 9). In an analogous fashion a disturbance can be combined with

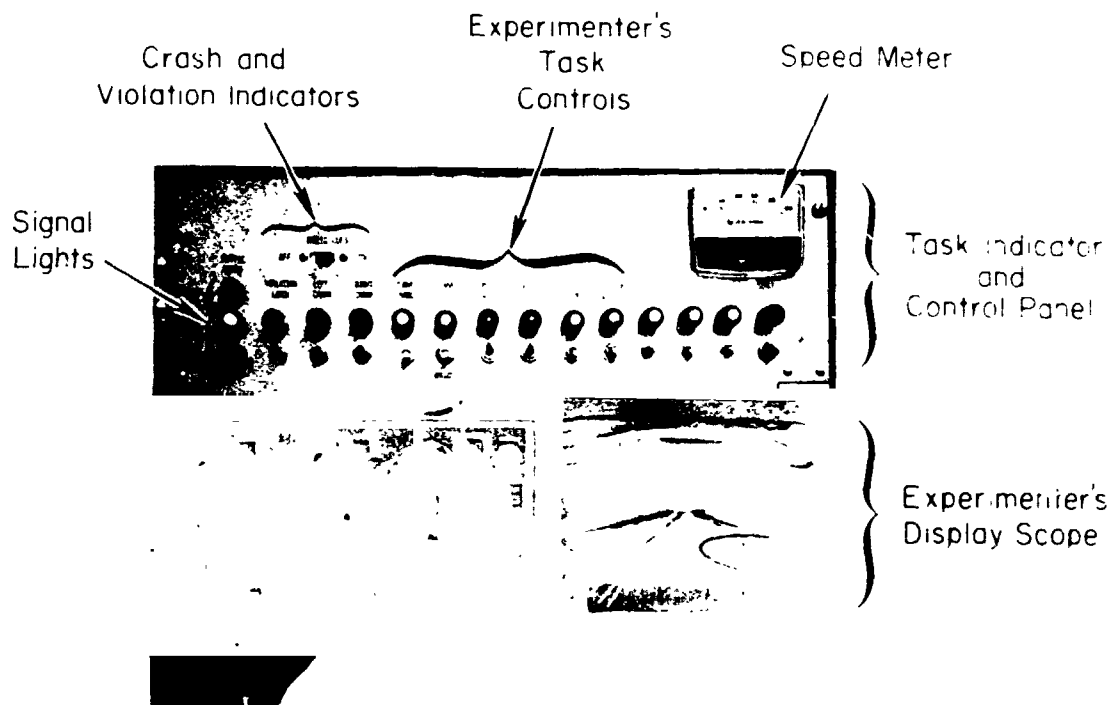


Figure 4. Experimenter's Console

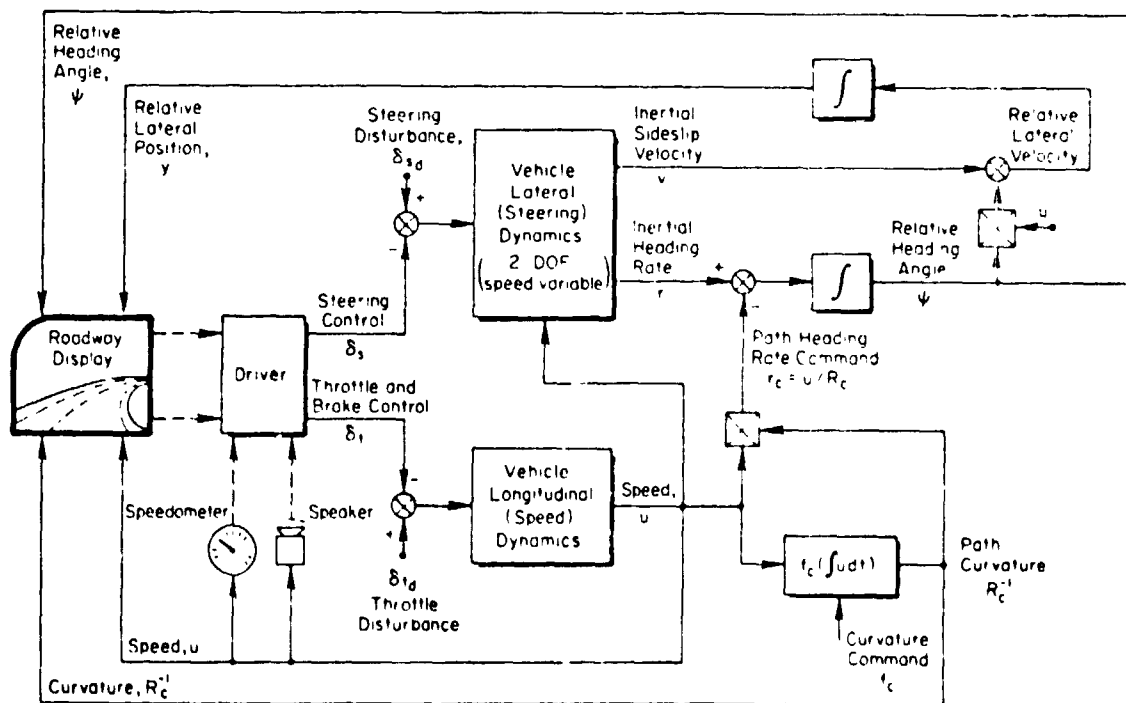


Figure 5. Simulator Steering and Speed Control Dynamics

the driver's throttle signal to measure his compensatory speed control response dynamics. Path commands can also be provided to the steering control task. However, here the driver receives some preview of the input from the displayed road curvature, so that measurements of driver response in this case relate to his pursuit and precognitive behavior (Ref. 10).

The lateral steering dynamics are basically linear two-degree-of-freedom equations (no roll axis), derived from tire and wind forces and moments acting on the car (Ref. 3). Small angle approximations are used (e.g., $\sin \psi \approx \psi$), and speed variations are assumed to be slow compared to relevant lateral car motions. The equations are speed variable in that the lateral response (e.g., steering gain and time constants) changes correctly with speed, and also a hold circuit is provided so that the car can be brought to a complete stop. The lateral equations do contain one nonlinearity which is a limit on the side force capability of the tires. As mentioned previously, this characteristic limits the speed at which curves can be negotiated as is the case in actual practice. Finally, various vehicle characteristics (weight, c.g. location, etc.) can be easily varied in order to study vehicle steering control handling qualities (Ref. 11).

The speed dynamics are given by a nonlinear first-order equation with a feedback term to account for wind resistance, tire friction, etc. The acceleration/deceleration capability for throttle inputs has finite limits to correspond to real car characteristics. In order to simplify the longitudinal kinematics, braking is set up to give a constant deceleration level corresponding to a maximum braking capability under ideal conditions (i.e., approximately 0.6 g). Subjects have reported the speed dynamics to be quite realistic and are typically not aware of the idealized braking characteristics.

The road curvature kinematics shown in Fig. 5 are an approximation which assumes that the rate of change of road curvature with respect to distance traveled is small. The path curvature develops as a function of distance down the road ($\kappa = \int u dt$), and the curvature command is used both as an input for the visually displayed curvature (which is unidirectional only) and the path heading rate command. The curvature command can be generated by an event programmer actuated circuit that generates a left-right or "S" curve command, or by a continuous command function. The circuitry is such that the driver can come to a complete stop on a curve with the display correctly showing no roadway motion.

APPLICATIONS

The simulation has been used for both control and decision-making studies. One of the original applications involved the effect of alcohol on steering control and has been reported in detail elsewhere (Ref. 7). More recently we have conducted exploratory studies on the effect of degraded preview (i.e., fog) on driver control. In Fig. 6 a driver's ability to regulate against a square pulse wind gust is illustrated. With a clear full view down the road the driver damps out the disturbance quite well, while with limited preview steering control is quite oscillatory.

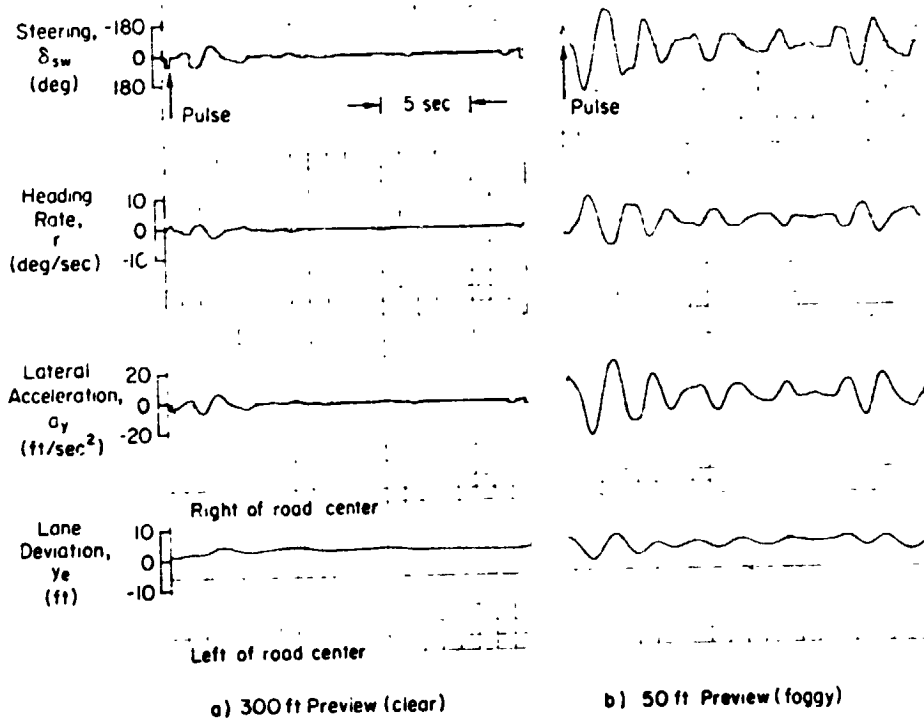


Figure 6. Preview Effect on Driver/Vehicle Response to a Pulse Wind Gust (run at a constant speed of 50 mph)

Using a random steering disturbance, the effect of preview on the driver's dynamic response and noise (remnant) output has also been measured as illustrated in Fig. 7. Measurements were obtained according to the technique given in Ref. 9. Then, parameters were fitted to the driver's describing function, and the root locus for the driver/vehicle heading mode was computed. This analysis (Fig. 7a) shows that the damping decreases under degraded preview, which is consistent with the transient response results of Fig. 6. The driver's remnant also increases significantly under degraded preview as shown in Fig. 7b.

Preliminary tests of the effect of alcohol on driver decision making have also been conducted using the driving scenario and decision tasks discussed previously. During the scenario the number of crashes and traffic tickets and the completion times were recorded. The subjects were offered a stake for completing a drive, and were rewarded for completion times less than 20 minutes to encourage timely progress past signaled intersections and obstacles. The subjects were also penalized for tickets (running red lights and exceeding the 40 mph speed limit) and "crashes" (running off the road and hitting adjacent cars and the obstacle). The results for three subjects are shown in Fig. 8. The results show the number of crashes to be quite sensitive to Blood Alcohol Concentration (BAC), and the large increase in crashes under alcohol was due primarily to excessive speed on curves and failure to look for adjacent cars before changing lanes.

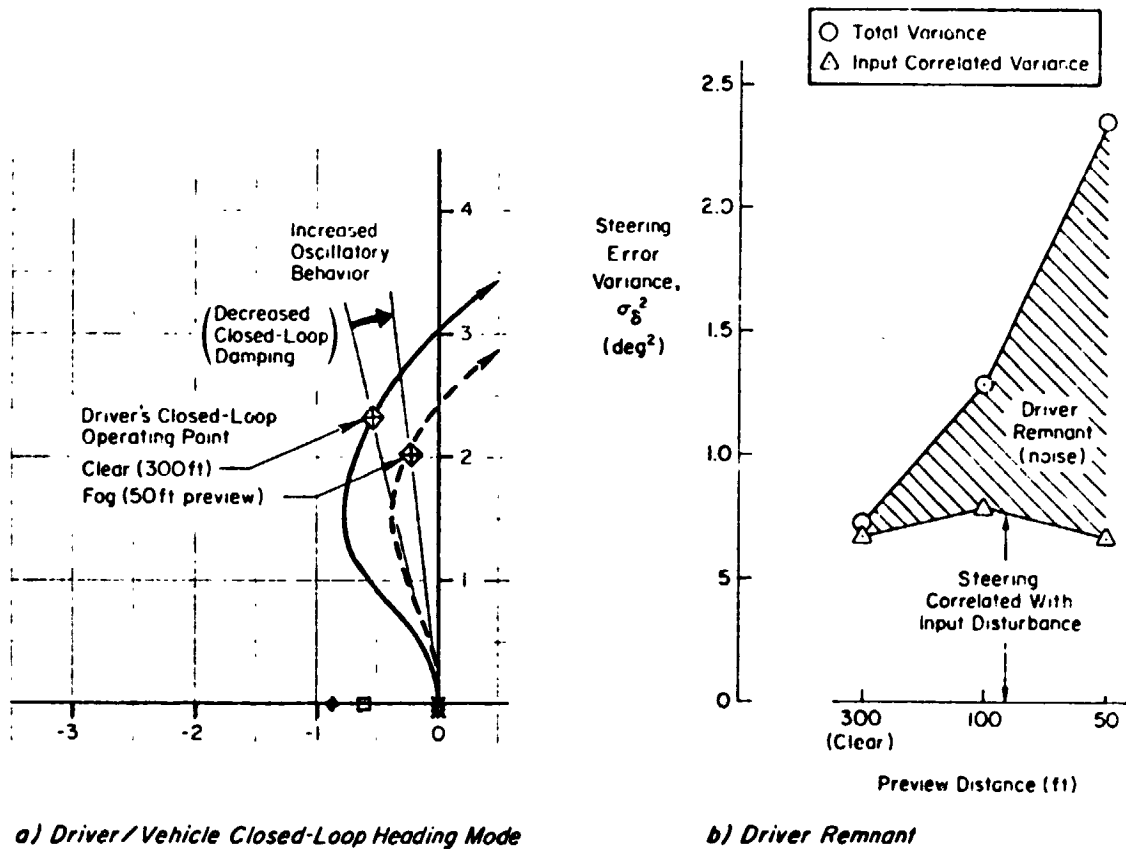


Figure 7. Preview Effect on Driver/Vehicle Dynamic Response and Remnant (run at a constant speed of 50 mph)

CONCLUDING REMARKS

In both the applications described above the subjects have adapted readily to the simulation with a minimum of training, thus allowing the studies to be conducted efficiently. The simulation is also easily reconfigured to allow a variety of research studies. The lateral equations of motion can be simply varied to give a wide range of steering characteristics. The speed equation can also be set up slightly unstable in order to require a given level of periodic monitoring by the driver to hold constant speed. In this way the driver's workload can be set to a given level in a plausible driving context in order to place controlled attentional demands on the driver (Ref. 12). Simple modification of the equations of motion will also allow the simulation of emergency conditions such as blowouts and wet or icy roads.

In addition to the research applications discussed here, this class of simulation should also be appropriate for driver training. The interactive display allows the subject to experience control and timing requirements in a variety of driving situations, and critical traffic situations can be simulated safely.

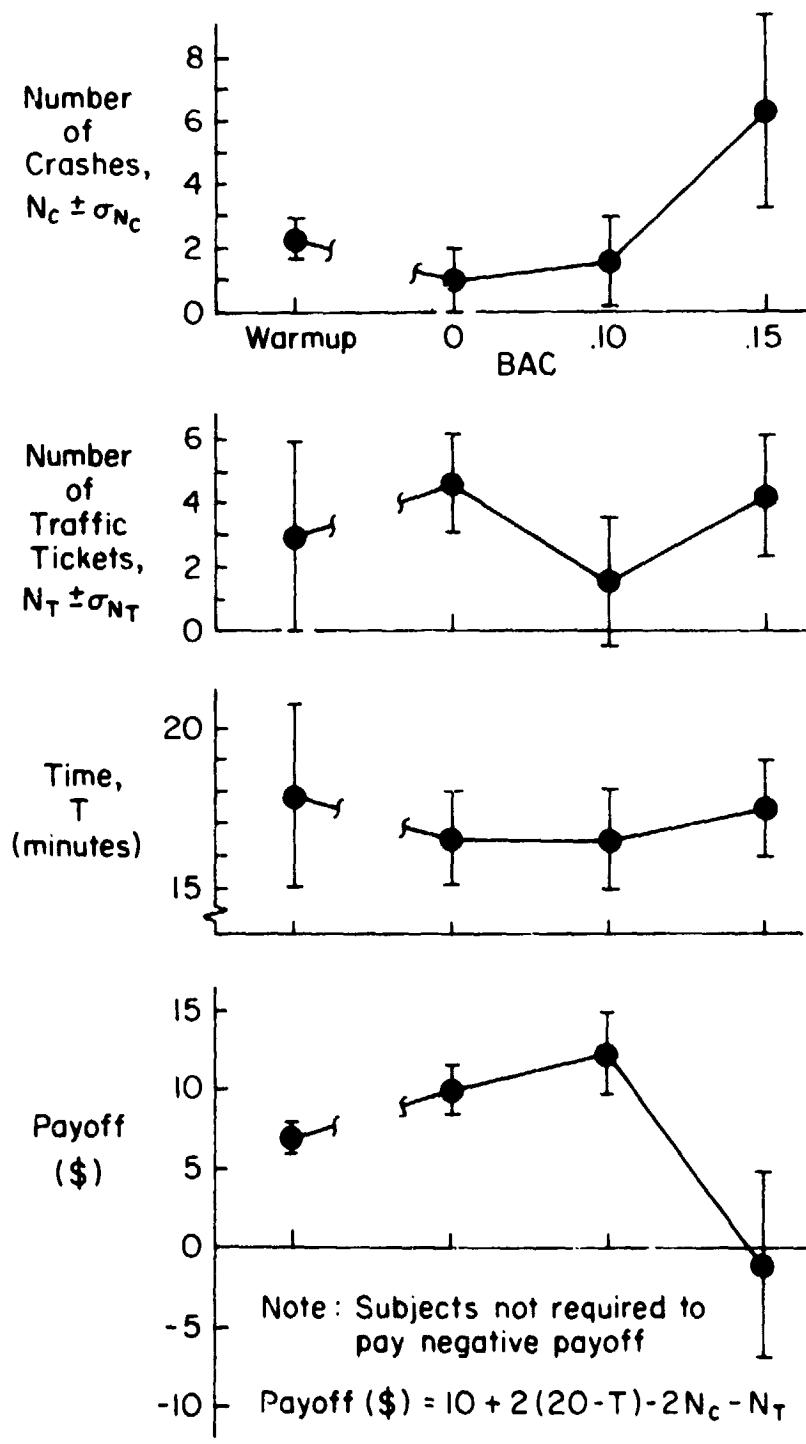


Figure 8. Alcohol Effects on Driving Simulator Performance for Three Subjects

REFERENCES

1. Simulation. AGARD Conference Proceedings No. 79, Jan. 1971.
2. Hulbert, S.; and Wojcik, C.: Driving Simulator Devices and Applications. SAE Paper 803A, Jan. 1964.
3. Weir, D. H.; Shortwell, C. P.; and Johnson, W. A.: Dynamics of the Automobile Related to Driver Control. Tech. Rept. 157-1, Systems Technology, Inc., July 1966.
4. McRuer, Duane; and Weir, David.: Theory of Manual Vehicular Control. Ergonomics, Vol. 12, No. 4, July 1969, pp. 599-633.
5. Weir, David H.; and McRuer, Duane T.: Measurement and Interpretation of Driver/Vehicle System Dynamic Response. Human Factors, Vol. 15, No. 4, Aug. 1973, pp. 367-378.
6. Weir, D. H.; and Wojcik, C. K.: Simulator Studies of the Driver's Dynamic Response in Steering Control Tasks. Driving Simulation, Highway Research Record No. 364, 1971, pp. 1-15.
7. Jex, H. R.; Allen, R. W.; DiMarco, R. J.; and McRuer, D. T.: Alcohol Impairment of Performance on Steering and Discrete Tasks in a Driving Simulator. DOT HS-801 302, Dec. 1974.
8. Gilliland, M. Gene; Kyropoulos, Peter; and Hirsch, T. J.: Simulation: Its Role in Driver Research and Highway Design. Vol. 8, North Carolina Symp. on Highway Safety, Spring 1973.
9. McRuer, Duane T.; Weir, David H.; Jex, Henry R.; Magdaleno, Raymond E.; and Allen, R. Wade: Measurement of Driver/Vehicle Multiloop Response Properties With a Single Disturbance Input. IEEE Trans., Vol. SMC-1, No. 4, Sept. 1971 (forthcoming).
10. McRuer, Duane T.; and Krendel, Ezra S.: Mathematical Models of Human Pilot Behavior. AGARD-AG-188, Jan. 1974.
11. McRuer, Duane T.; and Klein, Richard H.: Automobile Controllability — Driver/Vehicle Response for Steering Control. DOT-HS-801 401, Nov. 1974.
12. Jex, H. R.: Two Applications of the Critical Instability Task to Secondary Work Load Research. IEEE Trans., Vol. HFE-8, No. 4, Dec. 1971, pp. 270-282.

N75 33702

EFFECTS OF AUTOMOBILE STEERING CHARACTERISTICS ON
DRIVER VEHICLE SYSTEM DYNAMICS IN REGULATION TASKS

By Duane McRuer and Richard Klein

Systems Technology, Inc.
Hawthorne, California

SUMMARY

A regulation task which subjected the automobile to a random gust disturbance which is countered by driver control action is used to study the effects of various automobile steering characteristics on the driver vehicle system. The experiments used a variable stability automobile specially configured to permit insertion of the simulated gust disturbance and the measurement of the driver/vehicle system characteristics. The tests were conducted in two phases: a broad coverage of vehicle dynamics in which over 40 configurations of vehicle steering dynamics and steering gains were tested with an expert test driver; and a validation phase which covered 6 sets of vehicle dynamics with 16 subjects.

In both phases driver/vehicle system dynamics were measured and interpreted as an effective open-loop system describing function. Objective measures of system bandwidth, stability, and time delays were deduced and compared. These objective measures were supplemented by driver ratings.

A tentative optimum range of vehicle dynamics for the directional regulation task was established.

INTRODUCTION

The experiments described in this paper were accomplished as part of a major two-year research program (Ref. 1) conducted for the National Highway Traffic Safety Administration to explore, in part, the relationships between driver and vehicle dynamics in closed-loop control tasks. Reference 1 documents the entire program. Reference 2 is an introduction to the overall program, including the key maneuvers and performance measures developed. This paper presents experimental data relating to the effects of automobile steering dynamics on driver behavior in the continuous tracking or regulation tasks. The regulation task used was a maneuver that required a driver to maintain position within a lane on a straight stretch of highway in the presence of a simulated gusting crosswind. The simulation of the crosswind was accomplished as one function of the special steering apparatus described in Refs. 1 and 2. The crosswind simulated comprised five sinusoids at different amplitudes and frequencies so arranged and adjusted that the disturbance appeared random to the driver and a reasonable facsimile of a gusting crosswind condition.

Any analytical treatment or experimental measurements which intend to represent the facts of this type of task must recognize as fundamental the closed-loop feedback control character of driver/vehicle system operations. Feedback control is concerned with the maintenance of stability and the achievement of driver purposes in the face of varying time relationships. In the closed-loop context the vehicle-alone dynamics are subordinated to those of the driver vehicle system. Nonetheless, because the driver adapts his dynamic characteristics so as to achieve a more or less fixed set of closed-loop system properties, the vehicle-alone dynamics compel the driver to adopt responses peculiar to a specific vehicle. To the extent that these are easily accomplished by almost all drivers with large margins for intermittent, indifferent, and inattentive operation, the vehicle dynamics would be "good." On the other hand, vehicle-alone dynamics which require full-attention, highly precise driver responses to maintain system stability or which overextend the driver to the point that driver/vehicle system performance becomes inadequate will be "bad." In the feedback control system context, the objective measures which characterize these features of the driver and driver/vehicle system include such things as: system bandwidth and phase margin, driver effective time delays and lead equalization, etc. Subjective indicators in the same context are driver ratings of workload and controllability.

A complete quantitative description of the interactions between the driver and vehicle in the driver/vehicle system requires that these elements be replaced by mathematical attorneys. The vehicle dynamics are readily defined using nonlinear differential equations of motion which can be simplified and/or linearized for the constant speed directional regulation task of interest here. Fortunately, enough is also known about the physical "laws" of human operator dynamic behavior in control of vehicles to permit the construction of quantitative mathematical models for steering situations. A comprehensive up-to-date status of the empirical and analytical bases for mathematical models of human operators in an enormous variety of tasks is given in Ref. 37. Application of operator behavior laws derived from these empirical bases to the analysis of driver/vehicle problems has become very fruitful in the last decade (Refs. 3-26). Specific validation in both full-scale and driving simulation has given them further status as effective prediction tools (Refs. 22, 26, 27). These driver/vehicle model concepts permit the development of a cause-effect structure which allows a change in any of the elements of the system to be traced through to its logical effects on driver/vehicle system performance and objective measures.

The dynamics of the driver/vehicle system in the constant speed regulation task can be considered as a quasi-linear system which incorporates driver describing functions and driver-induced noise to characterize the driver and transfer functions to describe the vehicle. The interaction of these entities in the driver vehicle system is summarized briefly in the first section below. This provides a structure for the measurement of effective open-loop describing functions to quantify the dynamics of the driver/vehicle system. Special, but key, dynamic entities are the system crossover frequency, phase margin, and effective latency. These are used as the main summaries of objective experimental data given here. In the feedback control system context, these summary features characterize or imply the driver/vehicle system stability, response, and precision of control or accuracy.

Although the dynamic characteristics of contemporary production automobiles range over a broad spectrum, the highly adaptable characteristics of drivers permit millions of driver/vehicle systems to be operated with great precision. Yet this precision comes only at some cost in driver concentration and mental and physical workload. To provide an indication of these features, a driver rating scale for continuous control operations is introduced in the second section.

With these introductory and background aspects covered, we next turn to the full-scale experiments. These were divided into an initial or exploratory series in which many vehicle dynamic configurations were examined using an expert test driver, and a validation series which examined six sets of vehicle dynamics with 16 (eight male, eight female) subjects. The regulation test results from these two experimental series are treated in sequence in the third and fourth sections below.

DYNAMIC MODEL FOR MEASUREMENT OF LATERAL POSITION REGULATION

References 12 and 15, which will be followed here, use manual control system theory and data to structure models which describe driver steering control and the driver/vehicle closed-loop system. These models permit driver/vehicle performance to be predicted analytically for various conditions but, more important here, they provide a basis for measuring and assessing the effects on the system of changing the vehicle handling and response factors.

The model to be reviewed is for steering control of vehicle lateral position, with the driver actions regulating against disturbances while following a more or less straight or gently curving roadway. For this position regulation driver task, the theory (Refs. 12 and 15) and simulation experiments (Refs. 26-28) indicate that the driver's steering wheel output is predominantly a function of the lateral position error, y_e , and the vehicle heading, ψ . This is shown in the block diagram of Fig. 1 and is described in equation form by:

$$\delta_{sw} = Y_y Y_{\psi} y_e - Y_{\psi} \psi + Y_n n \quad (1)$$

The feedback to the steering wheel of position error via the driver, denoted by the quantity $Y_y Y_{\psi} y_e$, is needed to satisfy the basic guidance and control requirement for precision path following. That is, this component of steering wheel motion results in a front wheel steer angle which will tend to reduce any lateral position error the car may have. The inner loop feedback of vehicle heading, represented by $Y_{\psi} \psi$ in Eq. 1, provides the path damping needed for a stable, well-behaved, closed-loop system. Without a term to provide this function the driver/vehicle system would tend to oscillate. The final quantity, $Y_n n$, in Eq. 1 gives the effect of the driver-induced noise (or remnant) which always accompanies human operators.

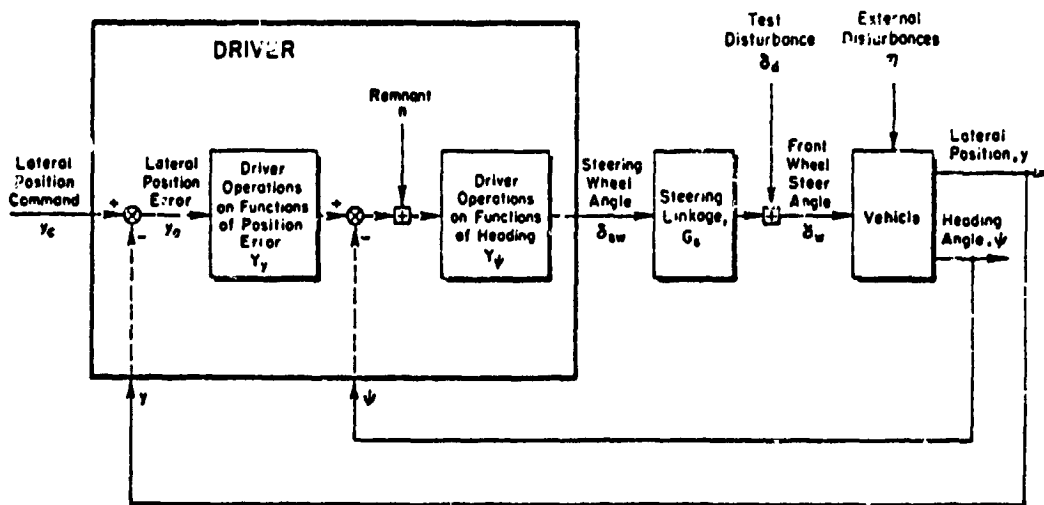


Figure 1. Block Diagram of Driver/Vehicle System for Lateral Steering Control with Simulated Gust Disturbances

To model the driver in Eq. 1 a nonlinear approach is taken in which the input-dependent describing functions, Y_ψ and Y_y , and a random noise (remnant) process, n , are used to characterize the driver's control and regulation actions. Because the describing functions are input-dependent elements within feedback loops, they are in principle functions of the forcing function and disturbances acting on the system and of the dynamics of the vehicle which the driver controls. Once the vehicle dynamics and system forcing functions are specified, the describing functions are as well, and the system can thenceforth be treated as a quasi-linear system contaminated with driver-induced noise.

The presumed driver response structure represented by Eq. 1 and the block diagram of Fig. 1 in no way implies that either lateral position or heading angle are directly perceived by the driver as such, but only that the driver responds in part to some function of these variables as picked up from the available visual display. Other possibilities which are entirely similar in their effect are described in Ref. 28, which is the basis for the developments immediately below.

The equations which describe the heading and lateral position outputs in terms of the driver describing functions, vehicle dynamics system inputs, and driver remnant can be derived from Eq. 1 and the block diagram of Fig. 1. The system inputs which require consideration include a lateral positional command, y_c , external disturbances, η , and the test disturbance, δ_d . As shown in Fig. 1, the position command is actually present in the driver component of the closed-loop system. In other words, the effective position command is to some extent driver induced. The general character of this command is, however, determined by the roadway, lane pattern, obstacles to be avoided, etc. The external disturbances, η , can arise from gusts, a side velocity from roadway-induced

disturbances, or from specially contrived force and/or moment generators attached to the vehicle. The test input, δ_d , is readily applied in actual or simulated cars by the addition of an extensible link or other differential device into the steering system. The system dynamic elements involved are the vehicle transfer functions $G_{\delta_w}^{\psi}$, $G_{\delta_w}^y$, and G_{η}^{ψ} , G_{η}^y which relate vehicle heading, ψ , and lateral position, y , to steer angle, δ_w , and external disturbances, respectively; the steering linkage transfer characteristic, G_s ; and the driver describing functions, Y_{ψ} and Y_y , already mentioned.

The equations of motion for lateral position and heading with these forcing functions, disturbances, and system dynamics are given by:

$$\begin{bmatrix} (1 + Y_y Y_{\psi} G_s G_{\delta_w}^y) & Y_{\psi} G_s G_{\delta_w}^y \\ Y_y Y_{\psi} G_s G_{\delta_w}^{\psi} & (1 + Y_{\psi} G_s G_{\delta_w}^{\psi}) \end{bmatrix} \begin{bmatrix} y \\ \psi \end{bmatrix} = \begin{bmatrix} G_{\delta_w} & Y_y Y_{\psi} G_s G_{\delta_w}^{\psi} & Y_{\psi} G_s G_{\delta_w}^y & G_{\eta}^y \\ G_{\delta_w}^{\psi} & Y_y Y_{\psi} G_s G_{\delta_w}^y & Y_{\psi} G_s G_{\delta_w}^{\psi} & G_{\eta}^{\psi} \end{bmatrix} \begin{bmatrix} \delta_d \\ y_c \\ n \\ \eta \end{bmatrix} \quad (2)$$

The front wheel steer angle is provided by the auxiliary equation:

$$\delta_w = \delta_d + Y_y Y_{\psi} G_s (y_c - y) + Y_{\psi} G_s (n - \psi) \quad (3)$$

The closed-loop system response functions for heading, lateral position, and front wheel steer angle are given as functions of the forcing function and disturbances in Table 1. The multiloop character of this system is indicated by the sum of $Y_{\psi} G_s G_{\delta_w}^{\psi}$ and $Y_y Y_{\psi} G_s G_{\delta_w}^y$ in the denominator and the presence of the coupling numerator terms, G_{η}^{ψ} and G_{η}^y , shown in the ψ and y numerator expressions (Ref. 29). The two primes on the denominator, D , indicate that two loops are closed.

In a single-loop system the denominator of the closed-loop system transfer functions will have a form in which the open-loop system transfer function is added to unity, i.e., $1 + G$. If we define an effective driver describing function, Y_p^* , in the fashion shown below this form can be achieved:

$$D'' = 1 + Y_{\psi} G_s (G_{\delta_w}^{\psi} + Y_y G_{\delta_w}^y) = 1 + Y_p^* G_s G_{\delta_w}^{\psi} \quad (4)$$

where

$$Y_p^* = Y_{\psi} \left(1 + Y_y \frac{G_{\delta_w}^y}{G_{\delta_w}^{\psi}} \right) = Y_{\psi} \left(1 + Y_y \frac{N_{\delta_w}^y}{N_{\delta_w}^{\psi}} \right) \quad (5)$$

TABLE 1

CLOSED-LOOP SYSTEM DYNAMICS

Denominator:

$$D'' = 1 + Y_{\psi} G_s (G_{\delta_w}^{\psi} + Y_y G_{\delta_w}^y) = 1 + Y_{\psi} G_s G_{\delta_w}^y \left[1 + \frac{U_o Y_y}{s} + \frac{Y_y}{s} G_{\delta_w}^v \right]$$

y Numerator:

$$D''_y = Y_y Y_{\psi} G_s G_{\delta_w}^y y_c + Y_{\psi} G_s G_{\delta_w}^y n + G_{\delta_w}^y \delta_d + (G_{\eta}^y + Y_{\psi} G_s G_{\eta}^y) \eta$$

ψ Numerator:

$$D''_{\psi} = Y_y Y_{\psi} G_s G_{\delta_w}^{\psi} y_c + Y_{\psi} G_s G_{\delta_w}^{\psi} n + G_{\delta_w}^{\psi} \delta_d + (G_{\eta}^{\psi} + Y_y Y_{\psi} G_s G_{\eta}^{\psi}) \eta$$

δ Numerator:

$$D''_{\delta} = Y_y Y_{\psi} G_s y_c + Y_{\psi} G_s n + \delta_d - Y_{\psi} G_s (Y_y G_{\eta}^y + G_{\eta}^{\psi}) \eta$$

In Eqs. 4 and 5 the effective single-loop, open-loop transfer characteristic is $Y_p^* G_s G_{\delta_w}^{\psi}$ or the equivalent, $Y_p^* G_{\delta_w}^{\psi}$. The effective driver describing function is seen to depend on the heading loop driver describing function, Y_{ψ} , and that for the lateral position loop, Y_y , as well as on the vehicle y and ψ transfer function numerators. This latter point is emphasized by the ratio $N_{\delta_w}^y / N_{\delta_w}^{\psi}$, a notation which represents the vehicle transfer function numerators specifically.

This effective single-loop, open-loop characteristic is especially simple to measure with the use of the test disturbance, δ_d . The front wheel steer response with δ_d and remnant as the system forcing characteristics is given by:

$$\delta = \frac{1}{1 + Y_p G_s G_{\delta_w}^{\psi} + Y_y G_{\delta_w}^y} [\delta_d + Y_{\psi} G_s n] = \frac{1}{1 + Y_p G_s G_{\delta_w}^{\psi}} [\delta_d + Y_{\psi} G_s n] \quad (6)$$

At frequencies where remnant effects can be considered negligible, an effective open-loop system can be formed by considering δ_d as the input and δ the error. Then the quantity $\delta_d/\delta - 1$ parallels the quantity [(input/error) - 1] in a single-loop system. Performing this operation gives:

$$\begin{aligned} \frac{\delta_d}{\delta} - 1 &= Y_\psi G_s (G_{\delta_w}^\psi + Y_y G_{\delta_w}^y) \\ &= Y_\psi \left[1 + Y_y \frac{G_{\delta_w}^y}{G_{\delta_w}^\psi} \right] G_s G_{\delta_w}^\psi \\ &= Y_p^* G_s G_{\delta_w}^\psi \end{aligned} \quad (7)$$

Here the quantity Y_p^* is seen to be obtained by taking the closed-loop response measurement, δ/δ_d , inverting it, subtracting 1, then dividing the known transfer function of the steering linkage and vehicle, $G_s G_{\delta_w}^\psi$. Y_p^* is particularly simple in form in that the driver's heading describing function, Y_ψ , is a multiplicative factor, while Y_y enters into the bracketed expression in a relatively simple way.

The driver/vehicle system dynamics measurements taken in the experiments reported here are based on Eq. 7. The data (Ref. 1) are presented in the effective open-loop system form $Y_p^* G_s G_{\delta_w}^\psi$ because this directly reveals bandwidth, crossover frequency, phase margin, and other key system dynamic data. The driver-alone characteristics can be deduced from the data, if desired, by the techniques described in Ref. 28.

INTRODUCTION TO DRIVER RATINGS AND THEIR CONNECTIONS WITH DRIVER DYNAMICS

Some facets of driver/vehicle control can be measured objectively. These include the vehicle's and the driver's dynamic characteristics and the associated driver/vehicle system dynamics and performance. Other features of the driver control task, such as mental workload, concentration, and attention demands on the driver, as well as the driver's subjective impression of the ease with which the car is controlled, can only be assessed by asking the driver. The factors listed above are like those which in the analogous case of aircraft handling are taken into account by a skilled test pilot in providing a pilot commentary and an associated pilot rating. For these, the Cooper-Harper Scale (Ref. 30) is used. From the part of this scale reproduced in Fig. 2 we see that pilot compensation (equalization) and effort (workload) are key factors in the ratings. It is, therefore, no surprise that the scale has proved to be especially useful as an index when comparing competing vehicles on a workload, pilot compensation, basis.

AIRCRAFT CHARACTERISTICS	DEMANDS ON THE PILOT IN SELECTED TASK OR REQUIRED OPERATION*	PILOT RATING
Excellent Highly desirable	Pilot compensation not a factor for desired performance	1
Good Negligible deficiencies	Pilot compensation not a factor for desired performance	2
Fair — Some mildly unpleasant deficiencies	Minimal pilot compensation required for desired performance	3
Minor but annoying deficiencies	Desired performance requires moderate pilot compensation	4
Moderately objectionable deficiencies	Adequate performance requires considerable pilot compensation	5
Very objectionable but tolerable deficiencies	Adequate performance requires extensive pilot compensation	6
Major deficiencies	Adequate performance not attainable with maximum tolerable pilot compensation. Controllability not in question	7
Major deficiencies	Considerable pilot compensation is required for control	8
Major deficiencies	Intense pilot compensation is required to retain control	9
Major deficiencies	Control will be lost during some portion of required operation	10

* Definition of required operation involves designation of flight phase and/or subphases with accompanying conditions.

Figure 2. Cooper-Harper Handling Qualities Rating Scale

Because closed-loop tasks are often critical from the standpoint of operator compensation or skill required, and because such tasks are often crucial in high workload phases of operations, one would expect some connections between subjective ratings (on a scale like the Cooper-Harper) and the operator and operator/vehicle system dynamics and performance. In fact, in control tasks involving the tracking of commands (e.g., curving roads) or regulation in the presence of disturbances (e.g., crosswinds), the operator adjusts his dynamic characteristics to the vehicle, forcing function, and disturbance characteristics in order to achieve some desired level (e.g., staying in a lane) of overall operator/vehicle system performance. To do this the operator's adapted dynamics must offset or make up for vehicle dynamic deficiencies. In other words, by virtue of the closed-loop feedback system nature of the operator/vehicle system and the adaptive characteristics of the operator, a duality exists between the vehicle dynamics and those the driver adapts in order to maintain overall system characteristics essentially constant. For this reason, the subjective ratings can be treated as being dependent on the vehicle dynamics directly. This permits an immense simplification in practice, because the operator dynamic characteristics do not always have to be

measured. Instead, the changes in vehicle dynamic properties can be used as independent variables which induce changes in the operator characteristics and, in turn, changes in the rating. But, let there be no mistake — the subjective ratings are indicative of operator behavior (in terms of workload, equalization, attention and concentration demands, etc.) as compelled by the vehicle dynamics in order to meet system necessities.

Essentially all that has been said above has been based on pilot aircraft systems rather than driver/vehicle systems, with the implication that a high degree of parallelism exists. Driver rating techniques have been employed with automobile scenarios (e.g., Refs. 31 and 32), although not to the degree that the techniques have been used in aircraft.

The scale we have adapted for regulation or compensatory tracking situations (shown in Fig. 3) is very similar to the Cooper-Harper Scale in that it emphasizes driver workload, compensation, and attentional demands. The scale is fundamentally open ended and intended to be interval. No numbers are shown. When using the scale the subject shows his assessment by simply marking a location along the lefthand side. These are later converted to numerical values by the analyst using a range from 0 to 10 corresponding to the ticks on the lefthand side. Because the scale is open ended, a rating greater than 10 is possible.

CONTROL DEMANDS ON DRIVER DURING REGULATION TASKS

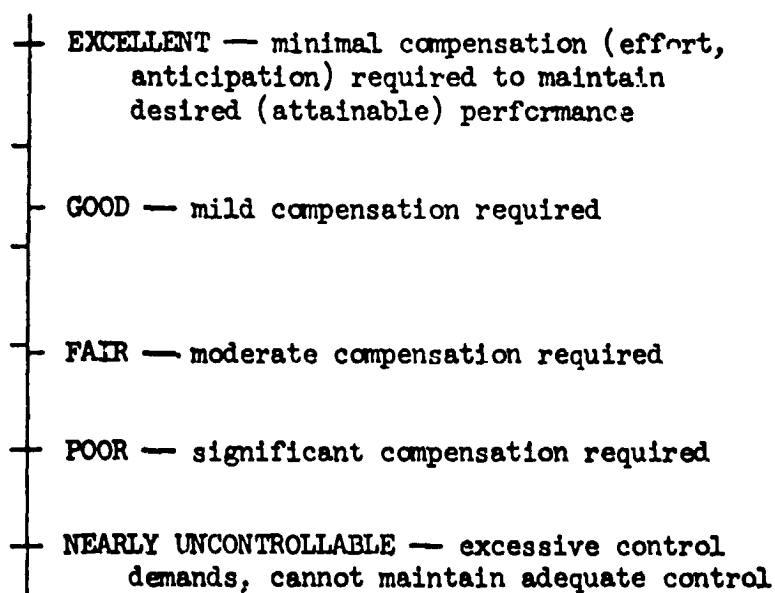


Figure 3. Driver Rating Scale for Regulation Tasks

Adjectives and descriptive phrases are located to the right of the scale. These are not at equal intervals. Instead, their location along the equally spaced scale is nonlinearly adjusted in accordance with the techniques outlined in Ref. 22. This is a relative location of these words and phrases on an underlying interval psychological continuum. To the extent that this procedure is successful, rating data based on the adjectives can then be treated as being on an interval scale, just as markings on the left are. Means and variances of the numerical ratings are then legitimate operations (Refs. 23 and 24).

TEST DRIVER VEHICLE REGULATION TASK RESULTS

In the regulation task the system block diagram is essentially that shown in Fig. 1. In the test series a random-appearing disturbance was applied to the variable stability and steering car by moving the front tires with the extensible link servomechanism. This serves to move the tires but not the steering wheel because the servo is installed in series with the driver and backed up by the power steering unit. To the driver the car's motions appear very similar to those present in a strongly gusting crosswind. The driver's regulation task is simply to keep the car centered in the lane by applying corrective steering inputs.

The regulation task at 50 mph was performed two or three times for each vehicle configuration (see Refs. 1 and 2) tested. The measurement interval was 1 sec. A representative sample of the primary driver vehicle system dynamic response data, given in terms of the effective single-loop, open-loop describing function, $Y_p G_{sw}^*$, is shown in Fig. 4. In this typical example the amplitude ratio is very close to the ideal crossover model form. Some of the describing function data (documented in Ref. 1, Vol. II) show amplitude ratio slopes somewhat more or less than -20 dB/decade, although they are still well approximated by a straight line.

To establish some elementary data trends consider the nearly neutral steer configuration. The crossover frequency, ω_c , and phase margin, ϕ_M , data for these three dynamic situations are shown in Fig. 5 as functions of the car's inverse yaw time constant, $1/T_r$. Note that crossover frequency is nearly constant and phase margin decreases slightly as $1/T_r$ decreases. The steering gain is indicated beside the range marks on the crossover frequency and phase margin data. These indicate that part of the differences in crossover frequency and phase margin may be associated with steering gain. However, such differences, if they do exist, are not ordered the same way for any given configuration (although $1/G_s = 2^\circ$ is generally the lowest ω_c).

The phase margin data can be converted to total system effective latency, τ_e , via:

$$\tau_e = \frac{\pi/2 - \phi_M}{\omega_c}$$

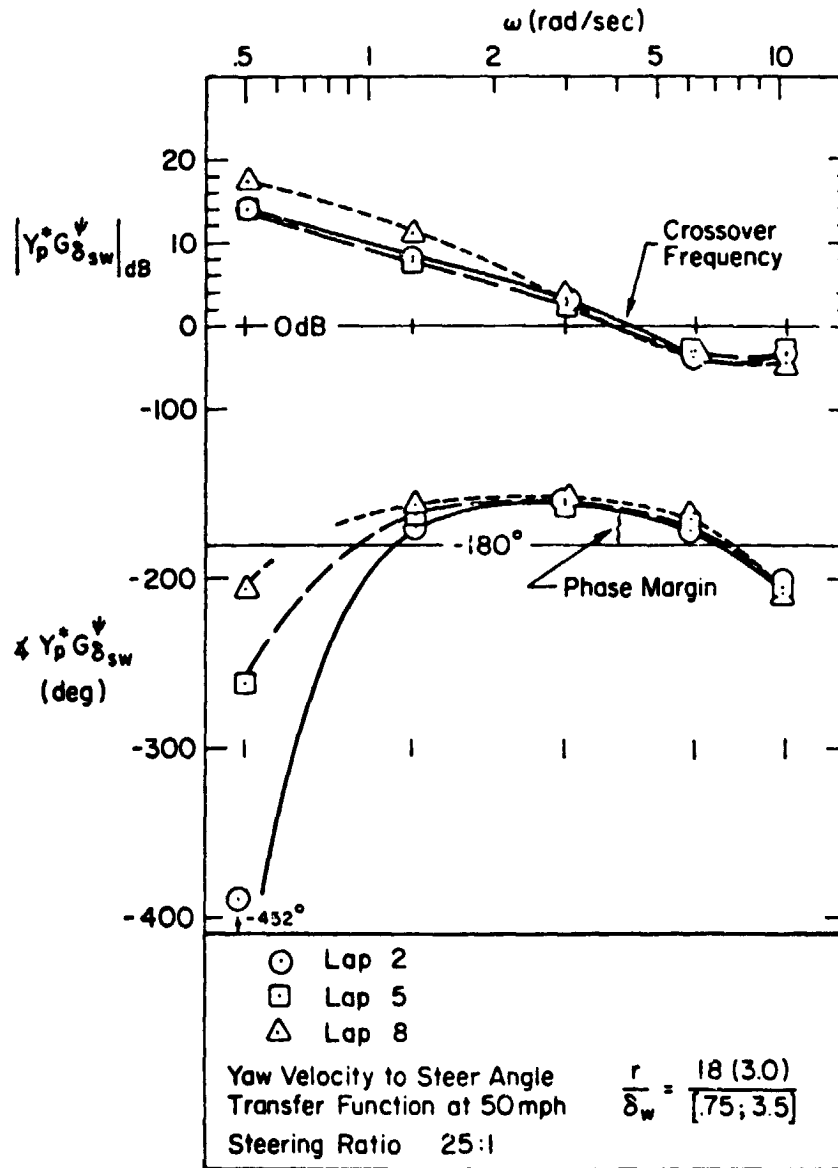
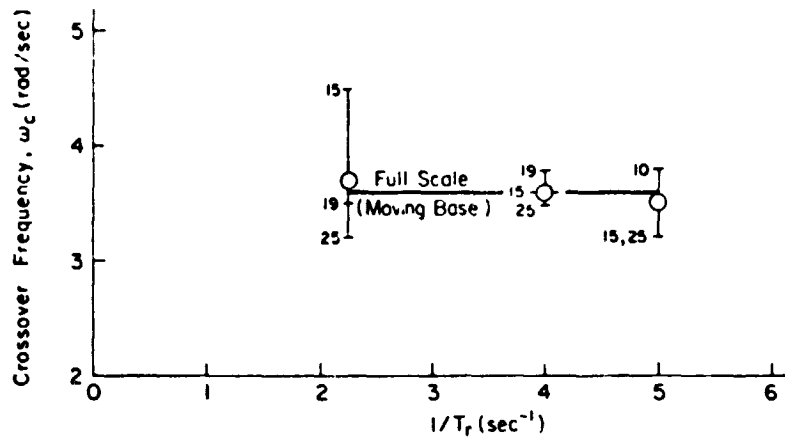
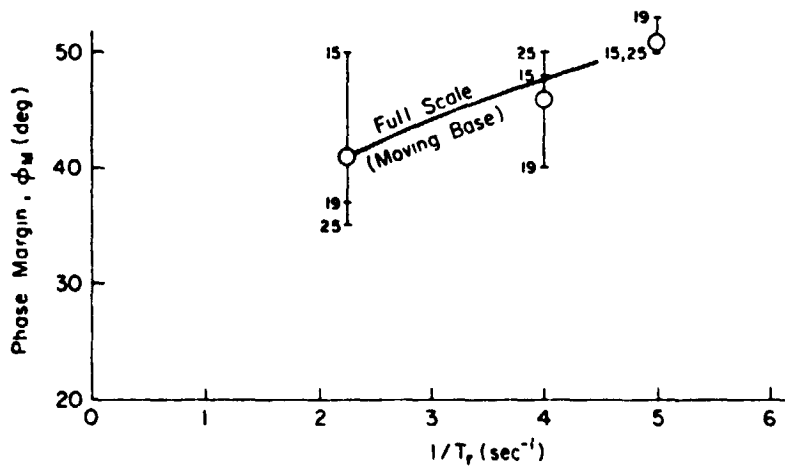


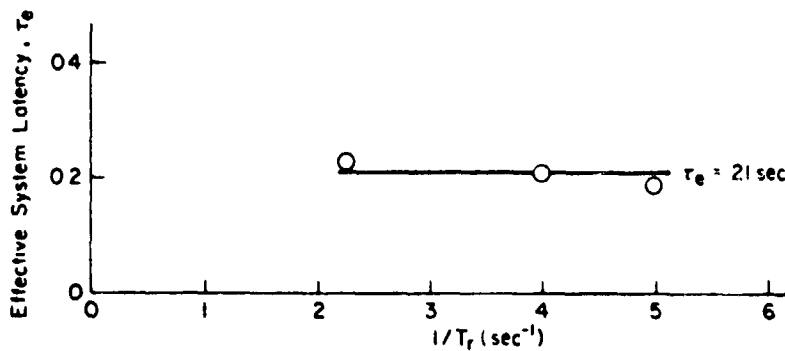
Figure 4. Typical Effective Open-Loop Describing Function for Test Driver Series



(a)



(b)



(c)

Figure 1. Closed-Loop System Characteristics for Test Drive Near-Neutral ($\epsilon_1 \approx 1$) Configurations

This fundamental measure is shown in Fig. 5c. It appears to be reasonably constant at $\tau_e = 0.21$ sec for the full-scale data over the range of $2.25 < 1/T_r < 4$.

When contrasted with fixed-base simulator data for the same driver and vehicle dynamic configurations (see Refs. 1 and 36) the data trends are generally similar over the $1/T_r$ range tested here, but there are major quantitative differences. The crossover frequency and phase margin for the full-scale tests are greater than those achieved in the fixed-base simulator, and the total system effective latency is less.

The regulation data for nine of the vehicle dynamic configurations driven by the test driver are summarized in Table 2 and shown in Figs. 6, 8, and 9. Table 2 data are averages for all steering gains, whereas the figures show the

TABLE 2
SUMMARY OF DESCRIBING FUNCTION PARAMETER FOR
TEST DRIVER REGULATION SERIES

YAW INVERSE TIME CONSTANT $1/T_r$ sec^{-1}	DIRECTIONAL MODE DAMPING RATIO ζ_1	DIRECTIONAL MODE UNDAMPED NATURAL FREQUENCY ω_1 rad/sec	CROSSOVER FREQUENCY ω_c rad/sec	PHASE MARGIN Φ_M deg	EFFECTIVE SYSTEM LATENCY τ_e sec
2.25	1.0	2.25	3.7	41	0.25
2.25	0.83	2.6	4.8	51	0.16
3	0.75	3.5	4.0	38	0.27
3	0.71	3.4	4.1	42	0.21
4	0.62	3.9	3.2	44	0.24
4.25	0.8	3.7	4.0	47	0.21
4	0.97	4.1	3.6	46	0.21
4	0.77	4.5	4.0	47	0.20
4	0.91	5.2	3.5	41	0.20
Mean			3.82	43.7	0.22
Standard Deviation			0.31	7.9	0.02

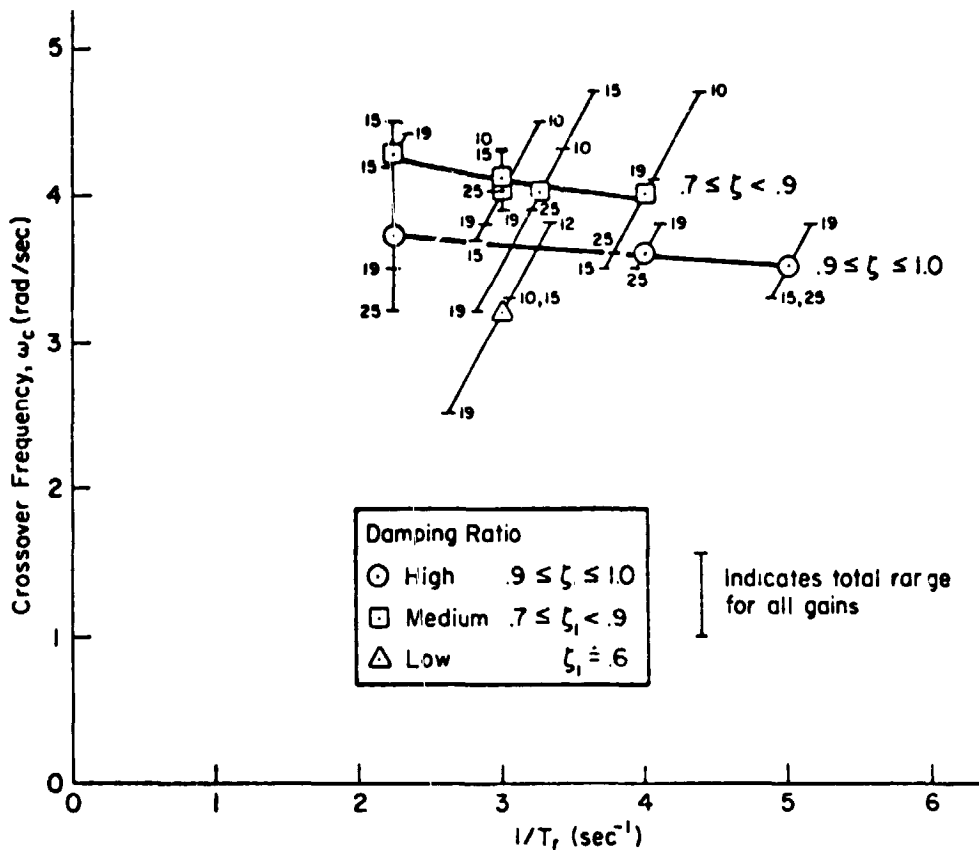


Figure 6. System Crossover Frequency as a Function of Inverse Yaw Time Constant for Test Driver Series

range. Consider first the crossover frequency data shown in Fig. 6. These indicate at least two basic trends which correspond to high and medium damping ratios, respectively. In general, the vehicle dynamics with $0.7 \leq \zeta_1 < 0.9$ permit a crossover frequency of about 4 rad/sec; whereas the dynamics with $\zeta_1 \approx 1$ have ω_c 's which are about 1/3 rad/sec less. This is an expected result since the effective phase lags due to the vehicle are less for the lower damping ratio cases than for the near neutral steer ($\zeta_1 \approx 1$) configurations. Accordingly, the driver can attain a higher system crossover frequency for these configurations for the same amount of driver lead generation. The big surprise is that this same characteristic is not present with the low damping ratio car ($\zeta_1 \approx 0.6$). The reasons for the low crossover frequency exhibited by the test driver here may be idiosyncratic; in any event, they are obscure.

The crossover frequency data shown in Fig. 6 show not only the average for all steering gains but also the range. The steering gains are indicated beside the range marks. Just as with the partial data set shown in Fig. 5, these show differences in crossover frequency associated with the various gains. Here again, the ω_c differences have no consistent order. That is, the crossover frequencies for ratios of 10, 15, 19, and 25 are not generally

ordered the same way when various (including repeat) configurations are considered. A weak case could be made for higher crossover frequencies with the "faster steering" ratios of 10 and 15 and lower crossover frequencies with the "slower" 25. The ω_c differences, in any event, are small.

The general consistency of the crossover frequency for the several steering gains and configurations again implies that the driver tends to compensate for changes in the steering ratio by adjusting his gain. This can be appreciated visually by comparing the steering wheel and steering wheel rate time histories at different steering ratios. Typical results for three regulation runs are shown in Fig. 7. All three parts of this figure show comparable yawing velocity and side acceleration traces. To achieve these nearly constant vehicle motions, the steering wheel and steering wheel rate activity have to increase markedly as the steering ratio is reduced from 10:1 to 25:1.

Unlike the crossover frequency data, the phase margin results given in Fig. 8 do not separate well as functions of the vehicle damping ratio. The mean phase margin would be 44 deg shown by the dashed line, with a standard deviation of 7 deg. Considering the overall accuracy of measurement, the variability of describing function data, and the fact that this includes the maverick datum at $1/T_r = 3$, this result is quite remarkable.

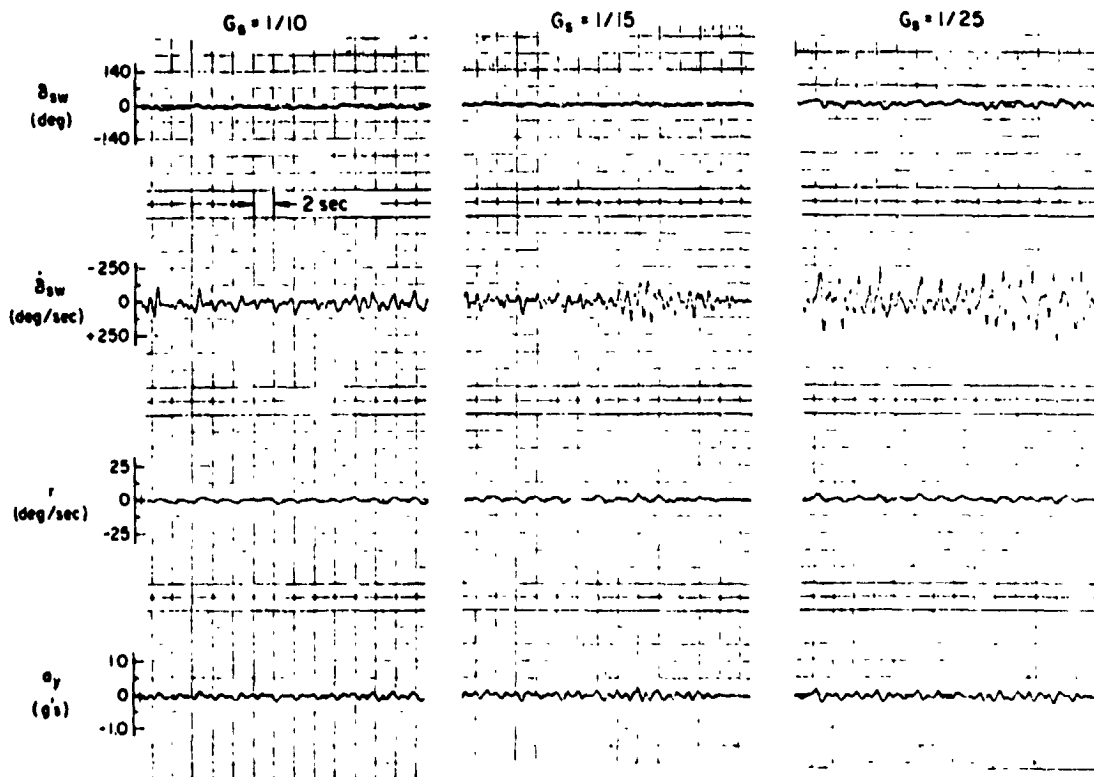


Figure 7. Comparison of Steering Wheel Activity and Vehicle Motions at Different Steering Ratios

The phase margin data are converted to total system effective latency and shown in Fig. 9. The points are closely clustered and support an average effective system latency of $\tau_e = 0.22$ sec with a standard deviation of about 0.03 sec. These data as a whole tie in very well with the $\zeta_1 \doteq 1$ subset previously described.

The driver ratings obtained for the regulation tasks were reasonably consistent and orderly. They clearly differentiated between configurations requiring low or moderate and high driver compensation/attention demands and other driver workload-related aspects. Iso-rating plots of vehicle gain vs. the yaw time constant are shown in Fig. 10. The lines are for medium and high damping ratios, i.e., $\zeta_1 > 0.7$. The general trends are similar to those obtained on the fixed-base simulator (Ref. 1), although the good region is narrower in the gain dimension and the right boundary is more definitively closed. The region within the "5" boundary represents an acceptable and satisfactory vehicle, whereas configurations outside the 6 boundary are both unacceptable from a workload and concentration standpoint and unsatisfactory in a closed-loop system performance context. The region between the 3 and 6 boundaries is for configurations which are marginal in some respect or other.

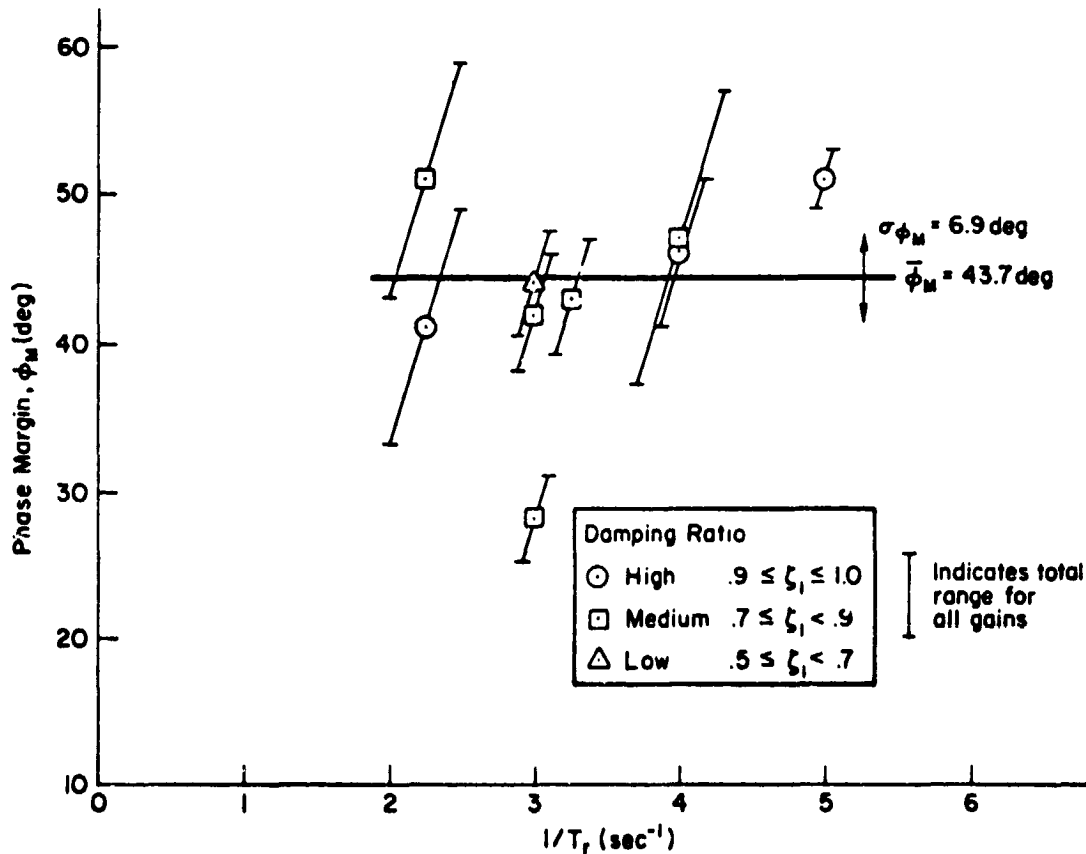


Figure 8. Phase Margin Data as a Function of Inverse Yaw Time Constant for Test Driver Series

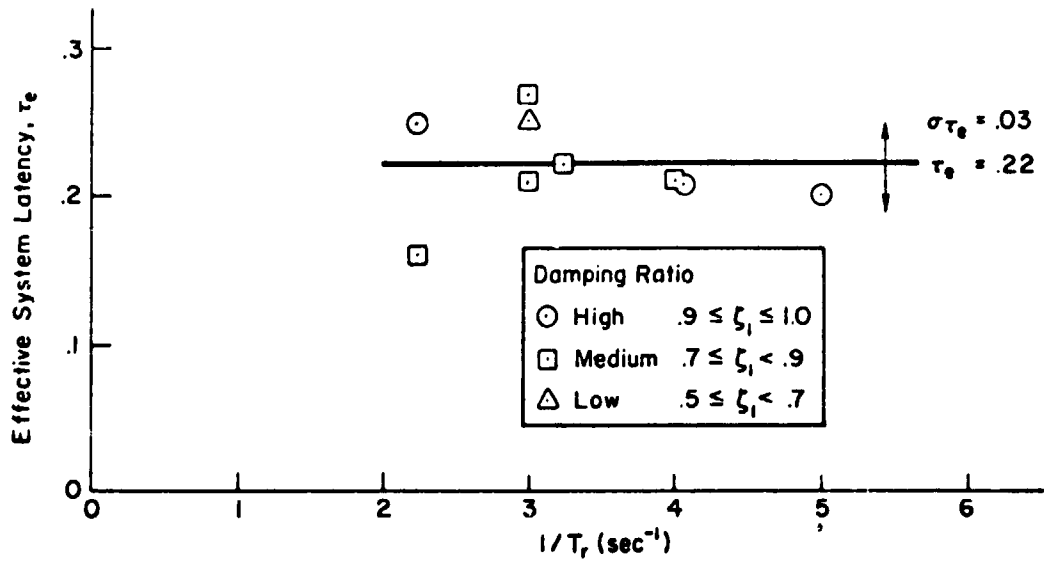


Figure 9. Effective System Response Latency as a Function of Yaw Time Constant for Test Driver Series

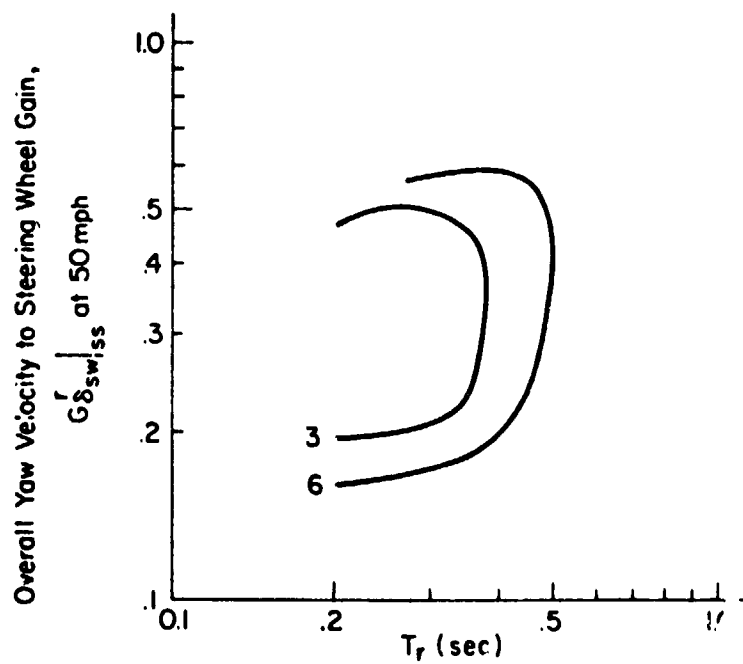


Figure 10. Test Driver Rating Boundaries for the Regulation Task at 50 mph

TYPICAL DRIVER/VEHICLE REGULATION TASK RESULTS

The initial full-scale testing series with an expert test driver provides a core of results which potentially could fully describe the compensatory system characteristics of the driver, the vehicle, and the driver/vehicle system and their interrelationships for a wide range of two-degree-of-freedom vehicle directional dynamics. A question that remains is how well will this structure generalize to typical drivers. To answer this question a series of validation experiments were run using six (including gain changes) vehicle dynamic configurations and sixteen subjects.

Vehicle Configurations and Subjects

The six laboratory vehicle configurations selected for validation testing are summarized in Table 3. Configuration A is typical of near-optimum vehicle dynamic characteristics found from the initial series with the test driver. The indicial response dynamics exhibit such "good" features as:

- Rapid initial rise time to the nominal steady-state level.
- Little overshoot following initial rise.
- No residual oscillation.

The superior features of this configuration from a driver/vehicle standpoint follow from these step response properties. Because the response is both rapid and lacks a significant overshoot, the driver has very little requirement to generate lead equalization in regulation tasks. When the vehicle's steering gain is in the best-rated region the driver's natural gain adjustment is also just right, i.e., the vehicle is neither too sluggish nor too sensitive in the amplitude of its response. The test driver ratings also indicated that attention demands, workload, and ease of imposing control (vehicle responsiveness) factors were all excellent.

To explore the sensitivity of the optimum dynamics to steering ratio variations, the A vehicle was used as the basis for three configurations, i.e., one in the previously determined optimum regions of steering gain and the other two near the upper and lower limits of acceptable steering ratios, respectively. Thus:

- A_1 — 19:1 (the optimum)
- A_2 — 25:1
- A_3 — 12:1

The other configurations were selected to similarly bound the "good" region of vehicle dynamics. Configuration B represents a lower frequency, medium

TABLE 3

SUMMARY OF VALIDATION SERIES VEHICLE CONFIGURATIONS

VEHICLE CONFIGURATION	STEERING RATIO	NATURAL FREQUENCY ω_1	DAMPING RATIO ζ_1	YAW VELOCITY TO STEER ANGLE TRANSFER FUNCTION $\frac{K_{\delta_w}^T(1/T_T)}{[\zeta_1; \omega_1]}$	STEADY-STATE STEERING GAIN $G_{\delta_w}^T _{50}$ (deg/sec), deg	REMARKS
A ₁	19:1	4.5	0.77		0.25	Near optimum, medium damping
A ₂	25:1	4.5	0.77	$\frac{24(4.0)}{[.77; 4.5]}$	0.19	Near optimum, but low gain
A ₃	12:1	4.5	0.77		0.39	Near optimum, but high gain
B	17:1	3.5	0.75	$\frac{18.4(3.0)}{[.75; 3.5]}$	0.27	Medium frequency, medium damping
C	9:1	3.0	0.62	$\frac{15.2(3.0)}{[.62; 3.0]}$	0.33	Medium frequency, low damping
D	11:1	5.8	0.57	$\frac{17.5(5.0)}{[.57; 5.8]}$	0.24	High frequency, low damping

damping configuration. Configuration C provides a low damping ratio case. Based on the initial tests, B and C should be near the boundary of allowable deviation from the optimum in terms of yaw time constant, undamped natural frequency, and damping ratio. Configuration D, which represents high frequency and low damping, was included because it exhibited excellent characteristics in discrete maneuvers. Its $1/T_T$ and gain characteristics are near optimum.

Eight male and eight female drivers were used for the validation testing. All subjects were in the 20-40 age group (average age 30), had average driving experience (15 years), good driving records, and averaged 70,000 driving miles per year. The subjects, their sex, age, occupation and personal car are listed in Table 4.

Effects of Vehicle Dynamics

Representative examples of the effective single-loop, open-loop describing function $Y_{DG_{sw}}^*$ are shown in Figs. 11 and 12. These serve several purposes. First, they indicate that the amplitude ratio is close to the ideal crossover model form. Second, they show that three typical subjects, one male and two

TABLE 4

SUBJECT CHARACTERISTICS — VALIDATION TESTING

SUBJECT INITIALS AND LETTER CODE	SEX	AGE	OCCUPATION	PERSONAL CAR
<u>Group I</u>				
DS — "C"	F	37	Housewife	'73 Chev. Impala
JR — "D"	F	37	Model	'71 Datsun 1600
RW — "E"	M	29	Production Supervisor	'66 Ford Truck. with Camper
<u>Group II</u>				
KD — "F"	M	26	Mechanic	'54 Chev. Pickup Truck
LT — "G"	F	40	Housewife	'73 Datsun 240Z
SG — "H"	M	25	Truck Driver	'72 Dodge Challenger
<u>Group III</u>				
RB — "I"	F	28	Artist, Counselor	'63 Buick
JC — "J"	M	34	Photographer	'69 Ford T-Bird
RC — "K"	F	37	Production Planner	'70 Gremlin
<u>Group IV</u>				
JZ — "M"	F	25	Housewife	'74 Fiat 124
HH — "N"	M	40	Instructor	'62 Chev. Wagon
JE — "O"	F	27	Housewife	'70 Datsun 510
<u>Group V</u>				
SH — "P"	M	29	Teacher	'72 Mazda Wagon
SS — "Q"	F	25	Teacher	'73 Chev. Vega
RB — "R"	M	29	Student	'72 Ford Pinto
<u>Group VI</u>				
GE — "L"	M	26	R and D Technician	'65 Ford Falcon

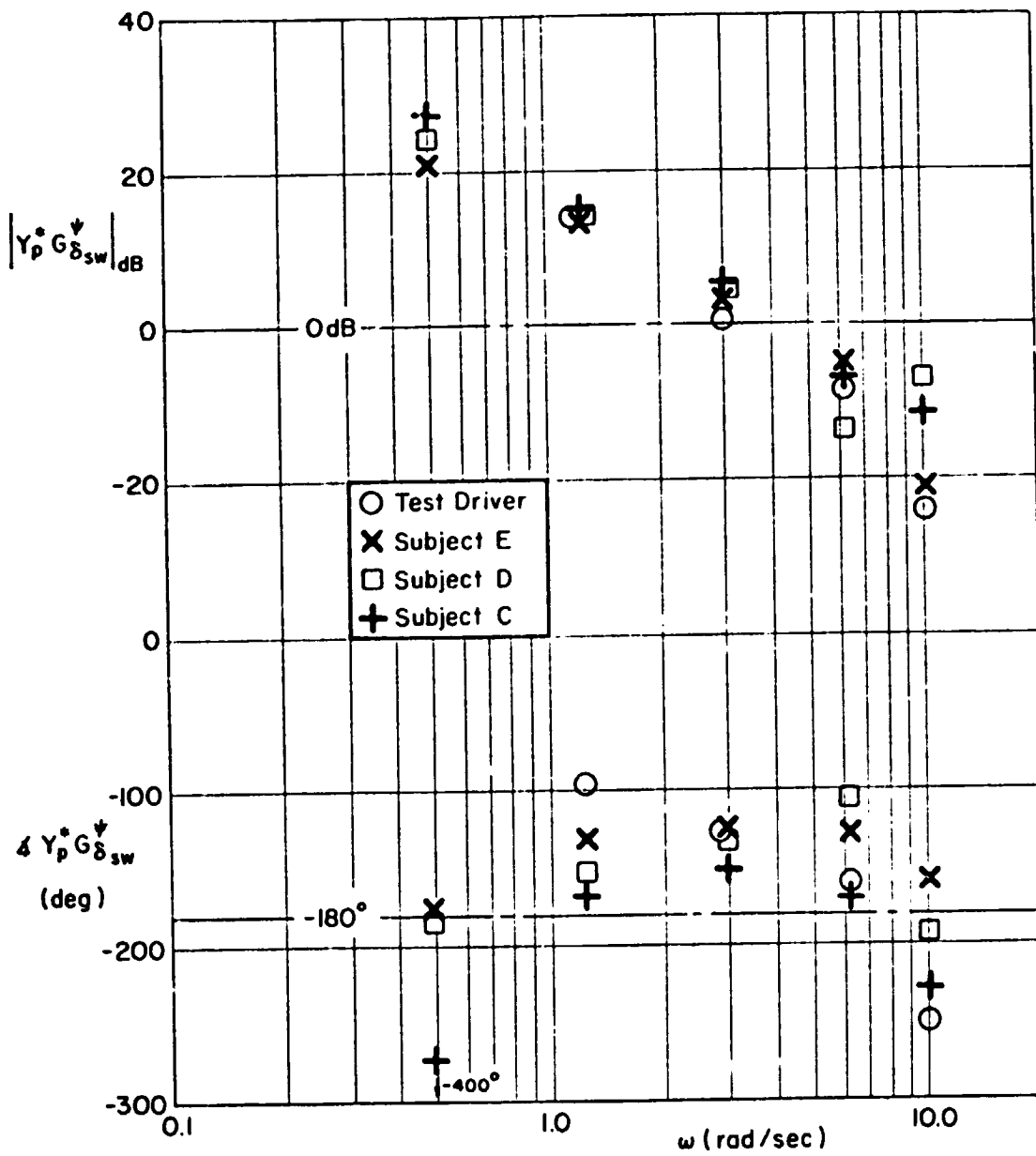


Figure 11. Comparison of Test Driver and Three Typical Subjects for Configuration A₁

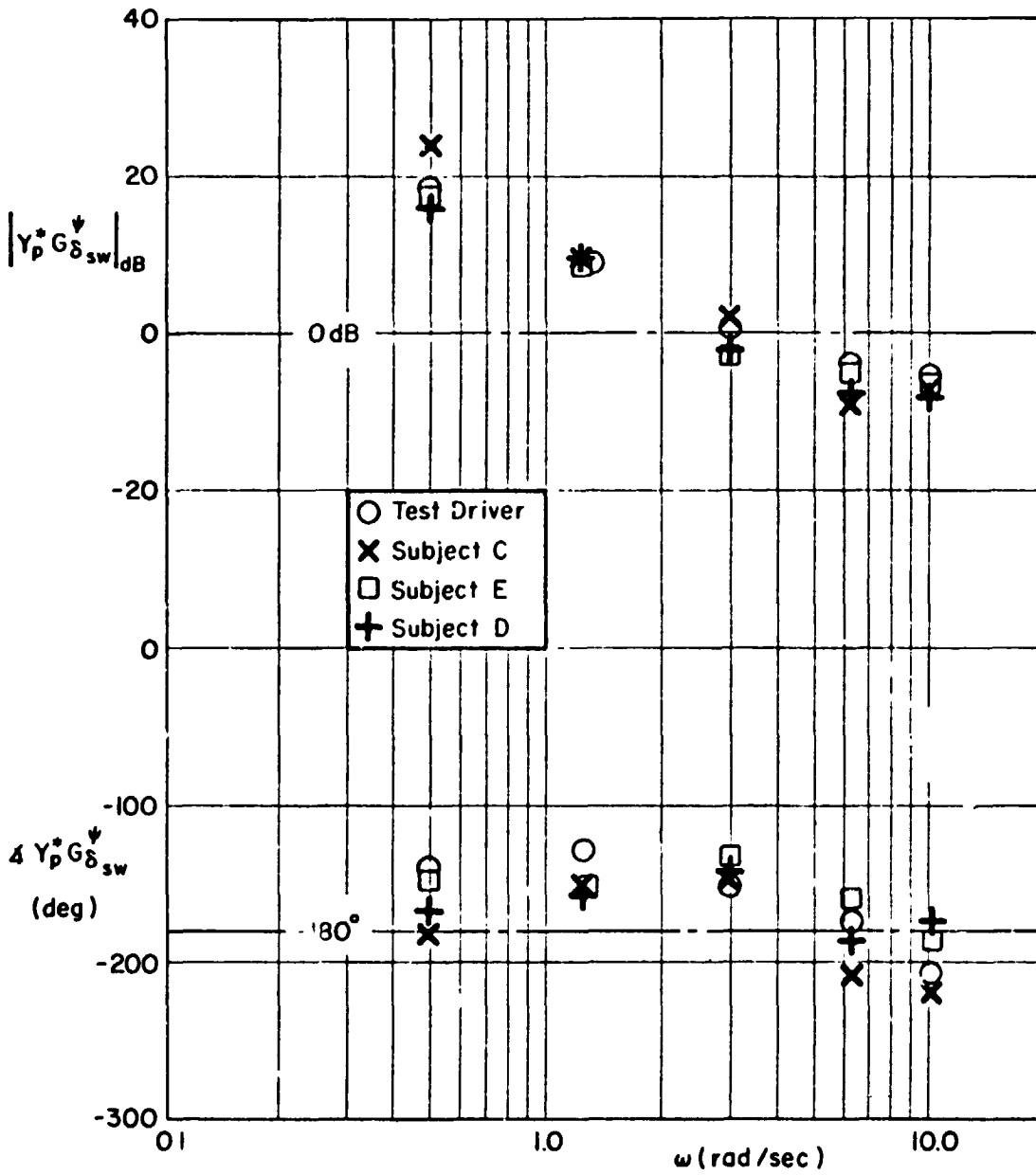


Figure 12. Comparison of Test Driver and Three Typical Subjects for Configuration B

females, and the expert test driver have very similar characteristics in this task. This is a general conclusion and not confined to the three drivers whose data are shown.

That these results are typical can be appreciated from Figs. 13 and 14 which show the crossover frequency and phase margin for the 16 subjects on Configurations A₁, B, C, and D. The test driver's data points for these same configurations are shown with ticks. In the crossover frequency plot the test driver and all 16 subjects' data are remarkably similar. Configuration D is not included in this consensus because the test driver data for this configuration were incomplete.

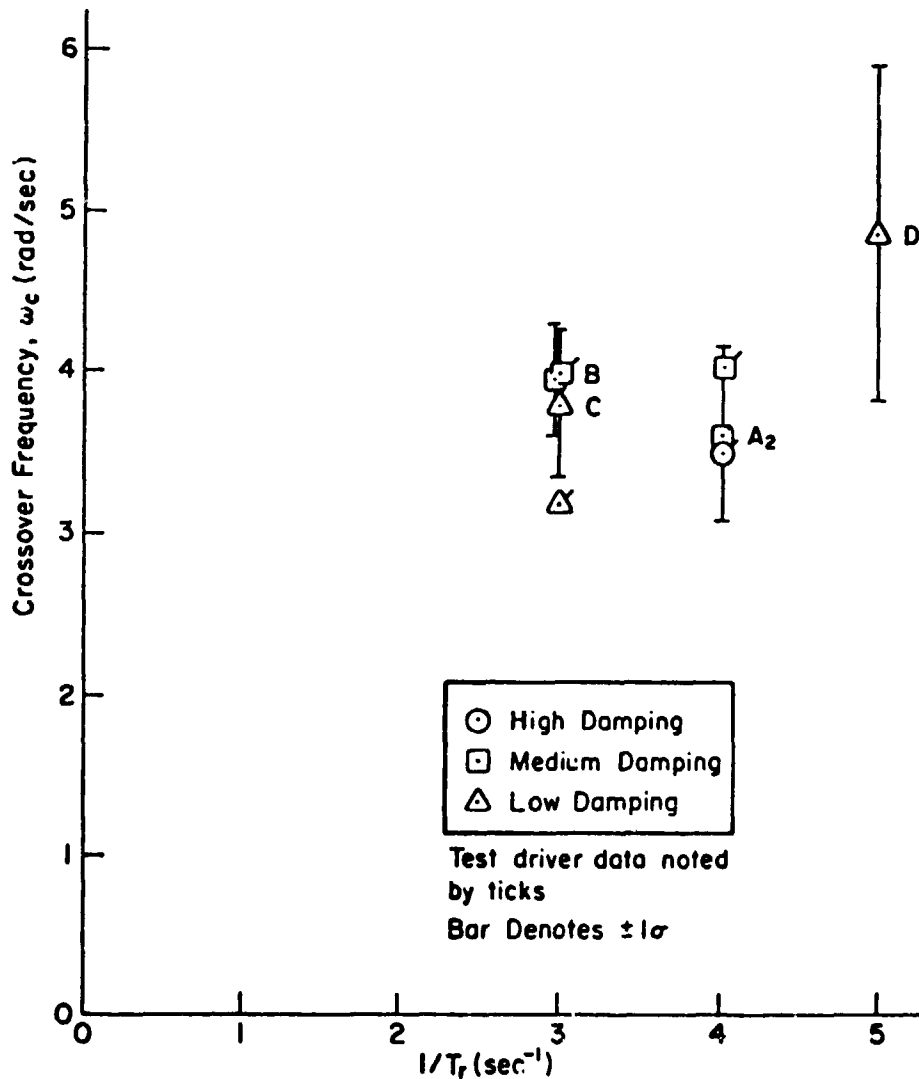


Figure 13. System Crossover Frequencies for All Subjects on Configurations A, B, C, D

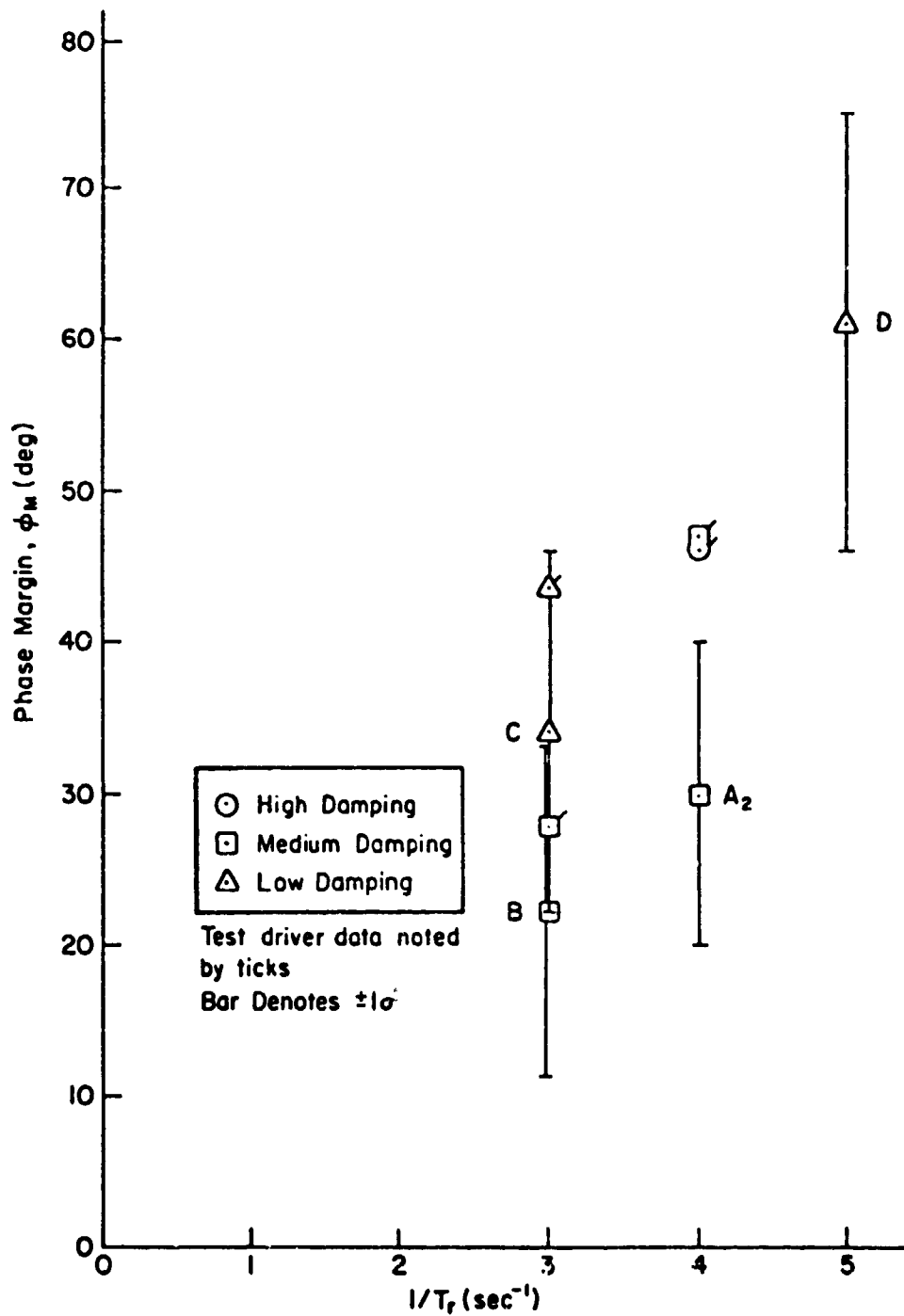


Figure 14. System Phase Margins for All Subjects on Configurations A₂, B, C, D

The phase margin data in Fig. 14 are considerably lower for the 16 subjects than for the test driver except for the test driver's one maverick point at $1/T_r = 3.0 \text{ sec}^{-1}$, which is in line with the phase margins for the 16 subjects.

These results are interpreted in terms of the effective system latency in Fig. 15. It appears that the total system latency for the test driver is about 0.1 sec less than the mean of all subjects. Consequently, we can conclude that the test driver was unusually skilled in the regulation maneuvers and that this skill is made manifest in his lower effective time delay.

A summary of driver/vehicle response data for male and female subjects is shown in Table 5. The phase margins are clearly sex-independent, while the males exhibit a slightly higher crossover frequency. The only statistically significant difference between male and female in the entire table is crossover frequency for the medium-frequency, low-damping Configuration C.

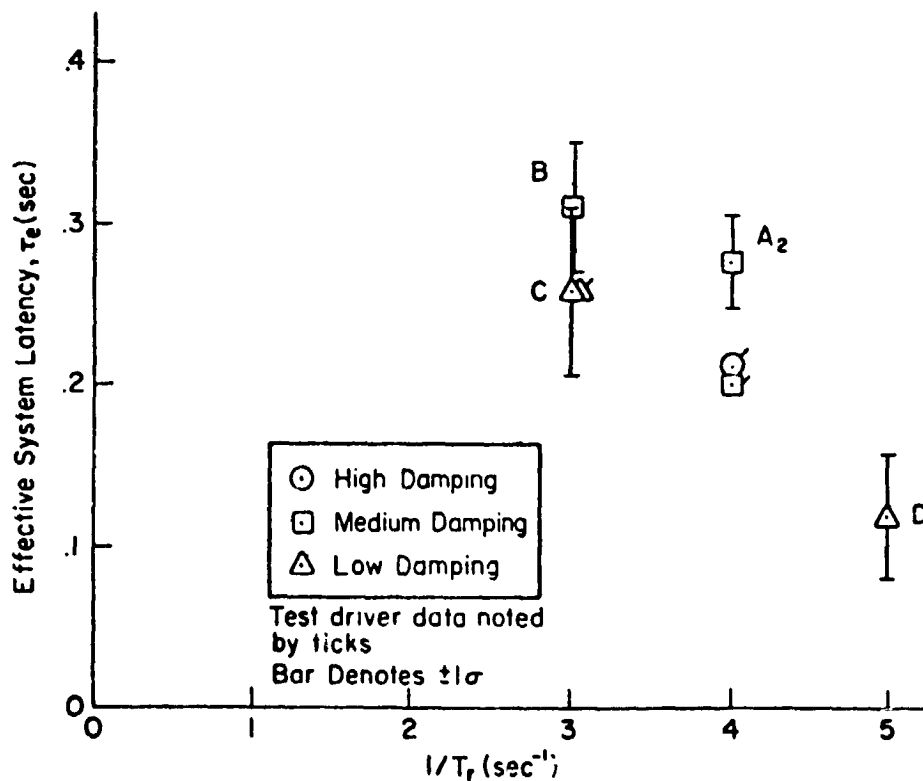


Figure 15. Effective System Latency for All Subjects on Configurations A₂, B, C, D

TABLE 5

SUMMARY OF DRIVER/VEHICLE RESPONSE DATA
FOR MALE AND FEMALE SUBJECTS

CONFIGURATION	CROSSOVER FREQUENCY ω_c (rad/sec)		PHASE MARGIN τ_M (deg)	
	MALE	FEMALE	MALE	FEMALE
A ₂ (Optimum)	3.86 ± 0.59	3.63 ± 0.55	28 ± 12	31 ± 8.7
B (Medium frequency and damping)	3.85 ± 0.55	3.65 ± 0.44	20 ± 12	19 ± 8.7
C (Medium frequency, low damping)	4.1 ± 0.2*	3.5 ± 0.23	32 ± 9.5	37 ± 14
D (High frequency, low damping)	5.2 ± 1.0	4.5 ± 1.2	62 ± 16	63 ± 16

*Significantly different from females at $\alpha < 0.01$.

Effects of Steering Gain Changes in Regulation Task

The effects of steering gain were evaluated between Configurations A₁, A₂, and A₃. For most of the subjects these configurations were set up in three separate test cars. Consequently, the regulation task (which used the variable stability and steering, VSS, car) was not able to be done at each steering ratio. For the three initial subjects, however, the VSS car was used as a test vehicle for all of the variable gain results. For these three we have, therefore, a relatively complete story.

The remaining subjects tested the normal steering ratio (19:1) using a standard 1974 Nova and the high steering ratio (12:1) on another 1974 Nova laboratory vehicle which had shortened steering knuckle lengths. For all subjects the effects of steering gain were evaluated through subjective ratings. Most subjects preferred the 19:1 steering ratio, although three males and three females showed a preference for other values. The test driver preferred a higher gain (12:1 steering ratio).

Differences were also obtained between the objective driver measures for the three "typical" drivers and the test driver. It will be recalled that the test driver readily modified his own gain to adapt to changes in steering gain, thereby keeping his crossover frequency and closed-loop characteristics relatively constant over the range of steering gains tested. This result was also anticipated because it constitutes a fundamental rule in man/machine system theory which, in turn, is based upon a large number of experiments with well-trained operators in a great variety of controlled elements. This background is recalled because the three typical drivers in this series did not behave in this fashion. Instead, as shown in Fig. 16, the subjects were not increasing their own internal gain to compensate for the reduction in that of the car. As a consequence of the reduced system crossover frequency, the system performance degraded. This is indicated by the increase in yawing velocity dispersion, σ_r , also shown in Fig. 16.

As a further comment on the Fig. 16 results it should be noted that two of the three subjects were female. In all of the previous man/machine system experiments in which controlled element gain variations have been made, conducted by many different investigators, the subjects have been exclusively male (Ref. 37). Because about a third of the driving population is female, this is an important consideration in driver/vehicle systems and this effect should be investigated further.

SUMMARY OF CONCLUSIONS

The results of these experiments provide a large number of fundamental conclusions. These are presented below under appropriate headings.

Driver and Driver Vehicle Dynamic Performance

1. In adjusting to different vehicle dynamics the typical and expert drivers adopted equalization which is well accounted for by the crossover model of manual control theory.
2. The typical driver adjustment to changes in steering gain did not always exhibit the expected vehicle gain offset by gain changes. This is at variance with test driver and general man/machine system results; however, it is based on results of only three of the 16 typical drivers.

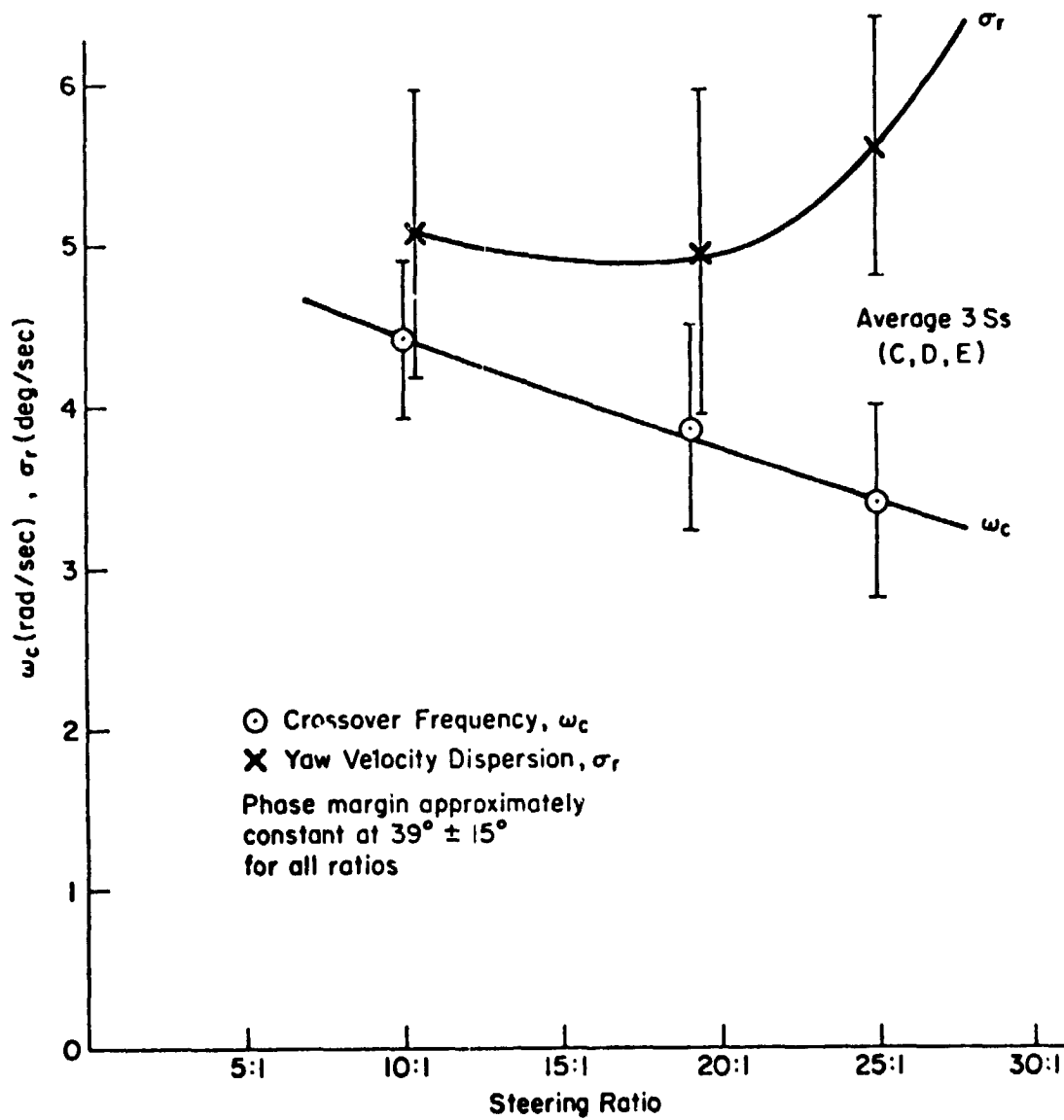


Figure 16. Driver/Vehicle System Crossover Frequency and Yaw Velocity Dispersion as a Function of Steering Ratio for Configuration A, Three Subjects (C, D, E)

3. System crossover frequency is:
 - The same as that of the test driver for three of the four vehicle dynamic configurations compared.
 - About constant at 3.7 rad/sec for three configurations, but higher for the medium frequency, low damping configurations.
 - Decreased as the steering sensitivity is decreased (based on three subjects).
4. System phase margin for the typical drivers:
 - Showed two distinct levels dependent on vehicle damping ratio; increasing with decreasing damping ratio.
 - Increased as $1/T_r$ increased.
 - Were about 15 deg lower than the test driver for the medium damping ratio configurations.
5. The effective system latency, τ_e , for the higher damping ratio configurations was about 0.3 sec. This is about 0.1 sec slower than that measured for the test driver.

Comparisons Between Subjects

1. Male drivers had slightly higher crossover frequencies than the females although this difference was statistically significant for only one configuration.
2. Phase margin data for male and female drivers are very close.

Driver Ratings

1. Driver opinion ratings appear highly consistent and clearly differentiate between regions of low, moderate, and high driver compensation and attention demands.
2. The rating space (of gain vs. yaw time constant) for $\zeta_1 \doteq 1$ is suitable for lower damping ratio data as well, i.e., $\zeta_1 \geq 0.7$.
3. The subjective evaluations appear to be more sensitive, in general, to vehicle configurations than the detailed objective factors. Consequently, it can be expected that more subtle differences in driver workload and attentional demands can be detected in this fashion than can be demonstrated objectively.

REFERENCES

1. McRuer, Duane T.; and Klein, Richard H.: Automobile Controllability — Driver/Vehicle Response for Steering Control. Vol. I: Summary Report, DOT HS-801 406. Vol. II: Supporting Experimental Results, DOT HS-801 407, Nov. 1974.
2. Klein, Richard; McRuer, Duane; and Weir, David: Test Procedures and Performance Measures Sensitive to Automobile Steering Dynamics. Eleventh Annual Conference on Manual Control (published in this volume).
3. Wohl, J. G.: Man-Machine Steering Dynamics. Human Factors, vol. 3, no. 3, 1961, pp. 222-228.
4. Crawford, A.; and Biggs, N. L.: A Theoretical Approach to the Study of Driving. Unpublished Lab. Note No. LN/192 AC.NLB, Dept. of Scientific and Industrial Research, Road Research Lab., 1962.
5. Todosiev, E. P.: The Action Point Model of the Driver-Vehicle System, Rept. No. 202-A-3, Ohio State University, Engineering Experimental Station, 1963.
6. Biggs, N. L.: Directional Guidance of Motor Vehicles — A Preliminary Survey and Analysis. Ergonomics, vol. 9, 1966, pp. 193-202.
7. Crossman, E. R. F. W.; Szostak, H.; and Cesa, T. L.: Steering Performance of Automobile Drivers in Real and Contact-Analog Simulated Tasks. Human Factors Society 10th Annual Meeting (Anaheim, California), 1966.
8. Weir, D. H.; and McRuer, D. T.: Driver Control During Overtaking and Passing. Tech. Rept. 157-2, Systems Technology, Inc., 1967.
9. Wierwille, W. W.; Gagne, G. A.; and Knight, J. R.: An Experimental Study of Human Operator Models and Closed-Loop Analysis Methods for High Speed Automobile Driving. IEEE Trans., vol. HFE-8, 1967, pp. 187-201.
10. Hoffmann, E. R.: A Study of Automobile Control. Ph.D. Thesis, Univ. of Melbourne, 1968.
11. Kondo, M.; and Ajimine, A.: Driver's Sight Point and Dynamics of the Driver Vehicle System Related to It. SAE Paper 680104, 1968.
12. Weir, D. H.; and McRuer, D. T.: A Theory for Driver Steering Control of Motor Vehicles. Highway Research Record, vol. 247, 1968, pp. 7-28.
13. Crossman, E. R. F. W.; and Szostak, H.: Man-Machine Models for Car Steering. Fourth NASA/University Conference on Manual Control, NASA SP-214, 1968.
14. Saran, D.; and Suggs, C. W.: Steering of Off-the-Road Vehicles — A Servo System Approach. J. of Agricultural Engrg., vol. 17, 1968, pp. 96-104.

15. Weir, D. H.; and McRuer, D. T.: Dynamics of Driver/Vehicle Steering Control. *Automatica*, vol. 6, no. 1, 1970, pp. 87-98.
16. Weir, D. H.; Alex, Fredric R.; and Ringland, Robert F.: Driver Control During Overtaking and Passing Under Adverse Conditions. Tech. Rept. 174-1, Systems Technology, Inc., 1969.
17. McRuer, D. T.; and Weir, D. H.: Theory of Manual Vehicular Control. *Ergonomics*, vol. 12, no. 4, 1969, pp. 599-633.
18. Yoshimoto, K.: Simulation of Man-Automobile Systems by the Driver's Steering Model with Predictability. *Bull. of Japanese Soc. of Mech. Engr.*, vol. 12, no. 51, 1969, pp. 495-500.
19. McLean, J. R.; and Hoffmann, E. R.: An Analysis of Driver's Control Movements. *Human Factors*, vol. 13, 1971, pp. 407-418.
20. McLean, J. R.: A Study of Driver Steering Control. Ph.D. Thesis, Univ. of Melbourne, 1972.
21. Delp, P.; Crossman, E. R. F. W.; and Szostak, H.: Estimation of Automobile Driver Describing Functions from Highway Tests Using the Double Steering Wheel. Seventh Annual Conf. on Manual Control, NASA SP-281, 1972, pp. 223-236.
22. Weir, D. H.; Hoh, R. G.; Heffley, R. K.; and Teper, G. L.: An Experimental and Analytical Investigation of the Effect of Bus-Induced Aerodynamic Disturbances on Adjacent Vehicle Control and Performance. Tech. Rept. 1016-1, Systems Technology, Inc., Nov. 1972.
23. Hoh, R. H.; and Weir, D. H.: Handling Properties of Diverse Automobiles and Correlation with Full Scale Response Data. Ninth Annual Conference on Manual Control (Cambridge, Mass.), May 1973.
24. McLean, J. R.; and Hoffmann, E. R.: The Effects of Restricted Preview on Driver Steering Control and Performance. *Human Factors*, vol. 15, no. 4, Aug. 1973, pp. 421-430.
25. Shaw, E. Y. N.: Mathematical Modelling of Driver Steering Control. Ph.D. Thesis, Univ. of Melbourne, 1973.
26. Weir, D. H., and McRuer, D. T.: Measurement and Interpretation of Driver, Steering Behavior and Performance. *Human Factors*, vol. 15, no. 4, Aug. 1973, pp. 367-378 (also SAE Paper 730098).
27. Allen, R. W.; Jex, H. R.; McRuer, D. T.; and DiMarco, R. J.: Alcohol Effects on Driving Behavior and Performance in a Car Simulator. Tenth Annual Conf. on Manual Control (Wright-Patterson AFB, Ohio), Apr. 1974.
28. McRuer, D. T.; Weir, D. H.; Jex, H. R.; Magdaleno, R. E.; and Allen, R. W.: Measurement of Driver/Vehicle Multiloop Response Properties with a Single

- Disturbance Input. IEEE Trans., vol. SMC-5, no. 5, Sept. 1975 (forthcoming). Also, Ninth Annual Conf. on Manual Control, May 1973.
29. McRuer Duane; Ashkenas, Irving; and Graham, Dunstan. Aircraft Dynamics and Automatic Control. Princeton Univ. Press (Princeton, N. J.), 1973.
 30. Cooper, G. E.; and Harper, R. P., Jr.: The Use of Pilot Ratings in the Evaluation of Aircraft Handling Qualities. NASA TN D-5153, Apr. 1969.
 31. Wojcik, C. K.; and Allen, R. W.: Studies of the Driver as a Control Element -- Phase No. 3. UCLA-ENG-7148, July 1971.
 32. Lincke, W.; Richter, B.; and Schmidt, R.: Simulation and Measurement of Driver Vehicle Handling Performance. SAE Paper 730489, May 1973.
 33. McDonnell, J. D.: Pilot Rating Techniques for the Estimation and Evaluation of Handling Qualities. AFFDL-TR-68-76, Dec. 1968.
 34. Guilford, J. P.: Psychometric Methods. McGraw-Hill (New York), 1954, pp. 263-270.
 35. Stevens, S. S.: The Psychophysics of Sensory Communications. Sensory Communication, W. A. Rosenblith, ed., MIT Press and Wiley (New York), 1961.
 36. McRuer, Duane; and Klein, Richard: Comparison of Human Driver Dynamics in Simulators with Complex and Simple Visual Displays and in an Automobile on the Road. Eleventh Annual Conf. on Manual Control (published in this volume).
 37. McRuer, Duane; and Krendel, Ezra: Mathematical Models of Human Pilot Behavior. AGARD-AG-188, Jan. 1974.

N75 33703

A KINESTHETIC-TACTUAL DISPLAY FOR STALL DETERRENCE*

Richard D. Gilson, Ronald W. Ventola,
and Robert E. Fenton

The Ohio State University
Columbus, Ohio

ABSTRACT

A kinesthetic-tactual display may be effectively used as a control aid per previous flight tests. Angle-of-attack (AOA) information would be continuously presented to a pilot, via this display, during those critical operational phases--approaches to landing, takeoff and departures, and accelerated maneuvers--where stalls are probable. He would then have a continuous indication of aerodynamic state, and thus perform the necessary control before a stall condition was reached.

A two-phase plan for evaluating this concept is presented. A first development phase would encompass:

- a) Display fabrication for a conventional control yoke;
- b) Its installation, together with other necessary instrumentation, in an experimental aircraft; and
- c) Preliminary flight testing by experienced pilots.

Upon completion of such a six-month effort, a 12-month evaluation phase, which would be designed to determine the efficacy of the display aid when a pilot is both distracted and under stress in critical flight situations, would be conducted.

INTRODUCTION

Aerodynamic stall/spin accidents are particularly lethal, accounting for 23.5% of the fatal general aviation accidents from 1967 through 1969 (1). Despite NTSB efforts in delineating the problem and suggesting various curatives, a substantial reduction in the number of such accidents remains an elusive goal. Thus, this problem, which is faced by an ever-increasing number of small aircraft users, remains among the most urgent in general aviation.

Stall-warning devices have generally involved the presentation of only "out-of-limit" information, and necessitate unexpected, yet immediate and

* The efforts reported here were sponsored by the Federal Aviation Administration (FAA), Contract No DOT-FA74WA-3515. The contents contained herein do not necessarily reflect FAA policy in all respects and it does not, in itself, constitute a standard specification or regulation.

appropriate action by the pilot. Inappropriate action can well result in times of heavy task loading and/or stress because of a missed, misinterpreted, or disregarded warning. The latter would be especially probable when the presentation were made via display lights and the pilot were looking elsewhere. If an auditory warning were employed, it may be in competition with other intermittently presented auditory signals; e.g., a landing-gear warning or voice transmissions (2).

Signals conveyed via the sense of touch, (i.e., with a tactual signal) such as with a "stick shaker", are more difficult to ignore and appear more effective (1). However, here again the signal is either "off" corresponding to a non-stall condition, or it is "on" (i.e., causing the control column to shake) when the aircraft is on the "ragged edge" of stalling. The warning is unexpectedly presented, and the pilot must respond immediately with the required corrective control action. There is at least the possibility that an incorrect and hazardous response could result.

If information pertaining to the aerodynamic state of an aircraft were continuously available in a form that was non-competitive with other vital visual and auditory information, this problem may be substantially reduced. In view of the viability of the tactual stick-shaker approach, continuous information transmission via the cutaneous modality would appear worthy of further exploration.

An effective kinesthetic-tactual display has been described (3), that involves the natural manipulation of a control handle with an embedded dynamic display to determine vehicular state information (e.g., angle of attack (AOA) of an aircraft). It consists of a rectangular metal slide mounted in the head of a control stick (see Figure 1), which is used to present continuous AOA (or more accurately, lift information. A forward protrusion of the servo-controlled slide corresponds to a larger-than-desired AOA, and the corrective response is movement of the yoke forward so as to decrease the error and return the slide to its neutral or flush position. The latter corresponds to achieving the desired AOA. Analogously, an aft protrusion such as is shown in Figure 1, (next page) corresponds to a less-than-desired AOA and necessitates an aft corrective control yoke motion. In essence, the pilot would receive information by feeling the displayed tactual signal and respond by "following" with the control so as to maintain the desired AOA.

During a preliminary inflight study, novice pilots, using either this tactual display or a visual display of AOA, were instructed to maintain both constant airspeed and altitude while flying tight turns about a point (4). Dramatic improvements in control of AOA, airspeed and altitude were obtained-- both in terms of variance and maximum deviation-- for the tactual versus the visual display condition.

This display appears to combine a number of advantages:

- (a) The AOA information is continuously available and the problems associated with a suddenly displayed warning



Figure 1. Prototype kinesthetic-tactile display installed in an experimental Cessna 172.

- (a) are essentially overcome.
- (b) Pilot reactions are less ambiguous because the display motion is both located at the point in space where the correcting action must be applied and it is consistent with the yoke motion;
- (c) The 'compelling' nature of the display makes it difficult to ignore--even in times of stress;
- (d) Timely and correct responses are promoted, almost without conscious thought; and
- (e) A pilot can exercise judgment with respect to its use.

For these reasons, this display would appear to be a prime candidate for providing pilots with sufficient, easy-to-interpret information for stall avoidance.

OPERATIONAL IMPLEMENTATION

The functional aspects pertaining to an operational implementation of this display are shown in the block diagram of Figure 2. There are three features of this implementation:

1. Control yoke and tactile display design;
2. Availability of AOA;
3. Operational envelope;

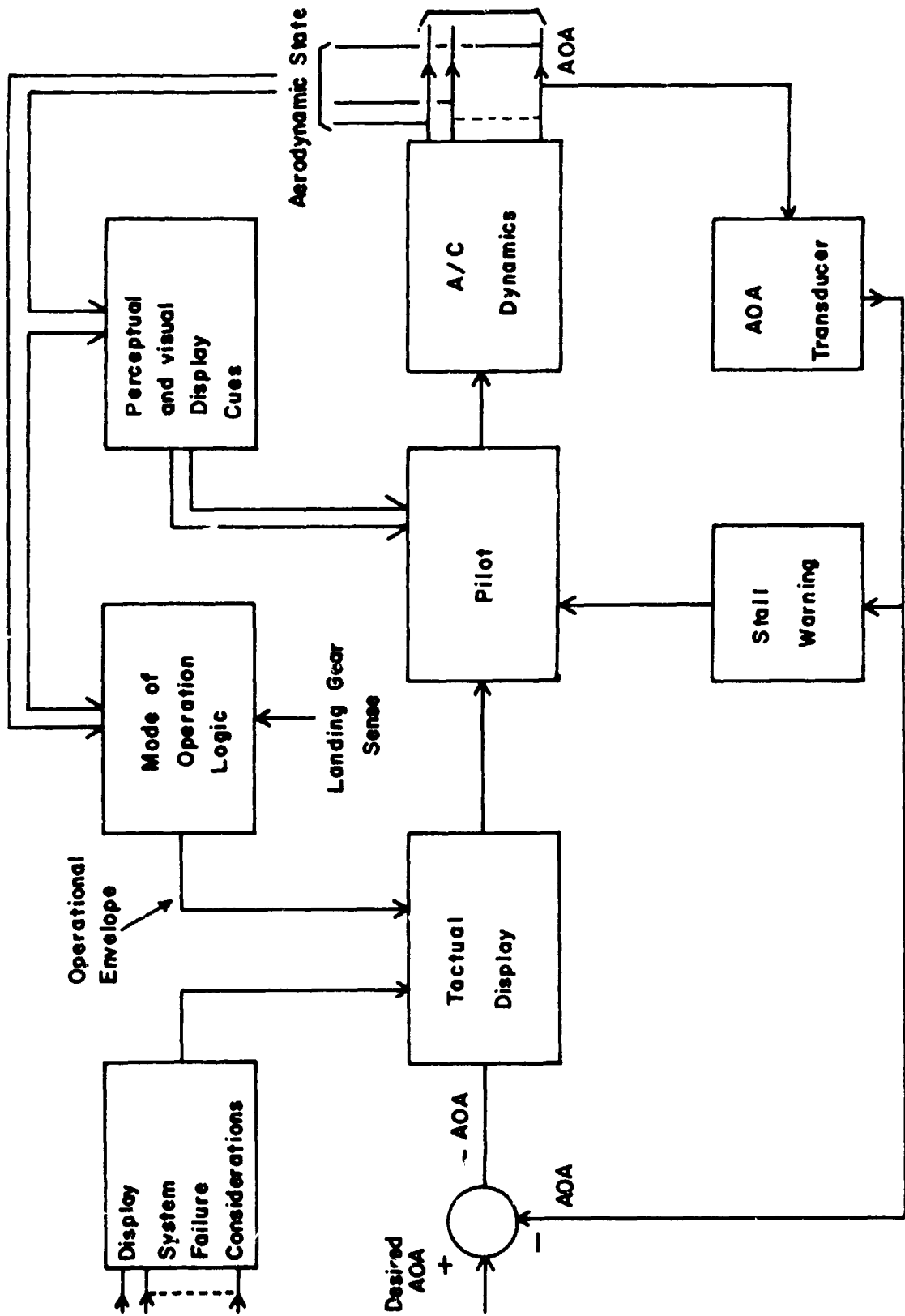


Figure 2. Functional Block Diagram

4. Stall warning; and
5. Display system failure considerations.

Control yoke and tactual display. Any practical embodiment must involve mounting the display into existing control yokes. A drawing of a modified control yoke is shown in Figure 3 along with all the display components which must be installed in the hand grip. Note that the size of the installation is such that it can be drilled and fitted into the "hand-sized" control yokes used by most of the major aircraft manufacturers.

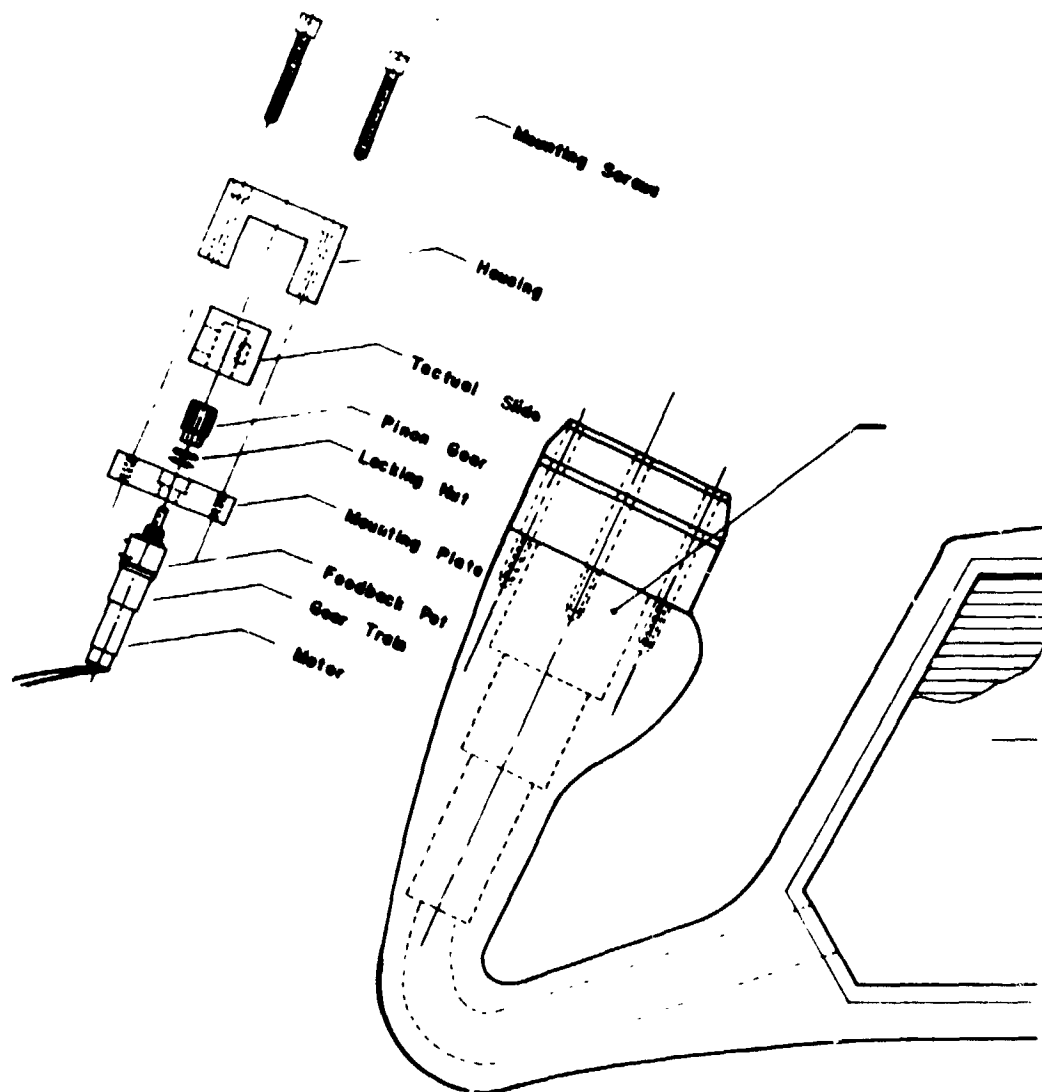


Figure 3. Modified yoke with component orientation.

The lefthand grip is the obvious choice for the display since "side-by-side" aircraft are designed to have virtually all aircraft control with the left hand and levers and switches controlled by a pilot's right hand.

Availability of AOA. The aerodynamic information to be displayed could be provided by various devices ranging from airspeed-pressure probes to angle-of-attack vanes. Airspeed-pressure probes, although currently installed in small airplanes, are not readily available for additional use because (a) such usage is precluded by Federal Air Regulations and, (b) the cost of the required differential pressure - to voltage transducer would exceed \$100 plus installation. Moreover, an airspeed measurement contains an inherent lag, and the desired airspeed depends upon both aircraft configuration (e.g., flap setting and landing-gear state) and aircraft gross weight.

Relative wind vane, AOA devices usually require special installation, have different desired values for various aircraft configurations and are often insufficiently rugged for common usage.

The design proposed here utilizes a "lift" transducer²--a component of the Safe Flight, Inc., SC150 visual speed-control display system--which can be approved (under a technical standard order) for use as a stall-warning device. It is rugged, characterized by a negligible dynamic lag, and a low cost. It can be installed in the same cutout in the wing as the stall reed, which it can replace. Finally, the desired value of its output, unlike that from an airspeed pressure probe or an AOA vane, is approximately constant with respect to both aircraft configuration and aircraft gross weight.

Operational envelope. There are two situations when a tactical display of AOA would be inappropriate--during ground operations and while in cruise flight. In the former, the display would be protruding fully forward corresponding to a stall condition, while in the latter it would be fully aft corresponding to cruise at high speed. To prevent false tracking and learning as well as hand irritation, the display should be deactivated and maintained in its "flush" or neutral position during such operations.

Consider the operational envelope presented in Table 1, which is based on flight data obtained from an OSU experimental Cessna 172, the display would be enabled up to 95 mph, and it would be disabled for speeds greater than 95 mph as these encompass the general cruise range for this aircraft. From data obtained during an approach, flare, touchdown and rollout the obvious choice would be to disable the display at the flare, at about 55 mph; however, the display would re-enable when the brakes were applied. This possibility can be eliminated by employing a landing-gear, weight sensor to provide a disabling signal. With this means for disabling the display, a pilot may touchdown or rotate the aircraft at whatever speed the environmental situation may warrant. (Table 1 next page)

In essence, the display would be enabled during the critical phases of takeoff, in the landing pattern and in the subsequent approach to landing. This should deter frequently encountered takeoff and departure stalls, as

² In this report, the measurement from such a transducer is referred to as AOA for convenience; however, it is not precisely the same as the measurement from a relative wind vane.

well as both accelerated and approach-to-landing stalls.

Stall warning. Per Federal Aviation Regulations, a clear and distinct stall-warning is required for small airplanes. This would be automatically incorporated in the concept advocated here, as the SC150 transducer includes a prestall switching circuit capable of energizing a stall-warning display.

This circuit could be used to actuate the currently employed audio and visual stall-warning displays without modification. Alternatively, other display concepts could be employed, including the most effective prestall warning yet employed--the stick shaker (1). This works well as it, by analogy 'previews' an aircraft's aerodynamic response--a shaking and buffeting motion--in a stall. However, the addition of a stick shaker is costly and could be an unnecessary expense when a tactual-stall deterrent was employed. The desired AOA, as well as the magnitude and direction of any error, are continuously presented via such a deterrent system. Thus, a pilot would be aware of any AOA deviations. In this context, it would seem sufficient to continue to employ an audio signal for stall warning. It should be clear, however, that a stick shaker could be provided on an optional basis.

OPERATIONAL ENVELOPE

Condition	Display Enabled	A/S range (mph)
Taxi- Roll	No	0 - 55
Rotation	Yes	55- 65
Climb	Yes	65-95
Cruise	No	95-
Approach	Yes	72
Flare	No	55

Table 1

Failure modes. Since an installed tactual display would not alter or affect an aircraft's manual controls or its control systems, a display failure would not affect the basic performance to be expected from the aircraft. Further, since the display would provide information in addition to that which is presently available (e.g., airspeed from a visual display and the required stall warning), its failure would simply leave a pilot with the

information presently available.³ Thus, a display failure should lead to no serious consequences.

If, after the evaluation testing, it were considered desirable to have an absolutely positive failure indication, one could employ a configuration such as that sketch in Figure 4. This configuration would be designed to meet two

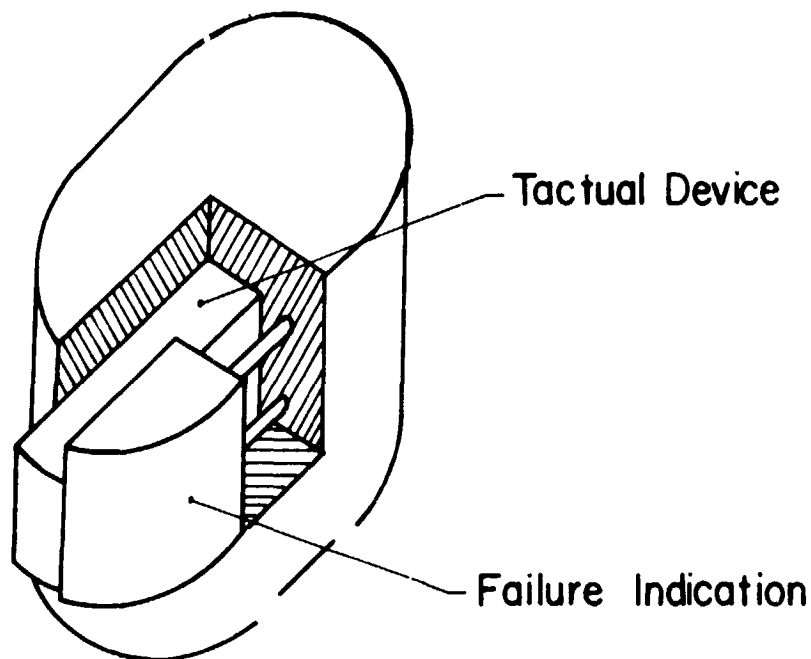


Figure 4. Failure indication concept.

criteria:

- (a) To indicate system failure positively; and
- (b) To prevent false control action arising from a potentially misinterpreted displayed signal.

In the event of a failure, a section of the grip would be moved out as shown so as to block a pilot's manipulation of the display slide, and prevent him from following any inappropriately displayed signal. Unfortunately, this or similar configurations would result in additional display/control yoke complexity and a substantially higher cost.

In any event, a display failure would not interfere with any of a pilot's normal control actions, and it would avoid the potential hazards associated with any system integrated into or overriding the aircraft's flight controls.

³ Note that neither the airspeed indicator nor the stall warning have built-in failure indications.

FLIGHT TESTING

A two-phase inflight study of the tactual stall-deterrent concept is planned. Hereafter, these phases will be referred to as the development phase and the evaluation phase.

Development phase. After, the mechanical and electronic portions of the display are fabricated, and installed in an experimental aircraft, preliminary flight testing will be conducted to:

- (1) Insure that the designed display is satisfactory under flight conditions;
- (2) Adjust the display parameters for both effective tracking and general pilot satisfaction; and
- (3) Adjust threshold circuits for stall warning and display enablement and disablement.

The flight tests will be conducted by certified flight instructors to evaluate display performance in both normal and abnormal flight situations; gust loading, accelerated and out-of-coordination maneuvers, and flight regimes wherein it will be necessary for a pilot to use both power and yoke control to correct AOA errors. Human factors considerations will also be assessed, such as minimum tactual display displacement thresholds required for detection and control, the effects of cold and perspiring hands, the effects of gloves worn while flying with the tactual display, and the effects of vibration and control pressures induced by the aircraft.

Evaluation phase--psychological aspects. The evaluation phase is designed to obtain answers to certain critical questions relating to the inflight effectiveness of the tactual stall deterrent. For example, it is generally believed that a stall/spin results from a pilot either being distracted from his primary task of flying or being under such stress that he doesn't notice a developing critical flight situation. In addition, the possibility of a display dependency must be considered; i.e., would a pilot become so dependent on this aid that effective flight control would be degraded if it failed.

Distractions. In order to determine the effects of distraction, the pilot subject will be "task-loaded" with additional duties. For the inflight situation, an auditory memory task would be both effective and valid for the following reasons: first, if memory performance were degraded while the pilot was flying with either display condition, then it is probable that one display condition was more demanding than the other; second, as increased loading on the pilot would be posed by the auditory task, one would expect that control would be more degraded with the more difficult of the two display conditions. Finally, an auditory task requiring memory is analogous to an inflight situation--operation in the traffic pattern. At tower-controlled airports, pilots are required to both listen, remember and do some simple problem solving while flying in the pattern. Many pilots refer to such flying with trepidation calling it highly taxing of their skills as well as introducing considerable stress.

Two important measures of pilot performance can be obtained. First, an objective measure of AOA variance--a clear indication of a pilot's control. Second, an objective measure of "residual" attention can be obtained via an analysis of the auditory task.

Stress. Elements of stress (strain) can be introduced in "low-time" pilots by their just being in a touch-and-go pattern. However, this level of stress would probably not be as great as that which is hypothetically present during some periods of excessive control errors. The "desired" level could be reached by unexpectedly instructing a pilot planning a touch-and-go to terminate the approach with a "go-around."

In practice, the latter results in a number of stall/spin accidents each year, and it is widely believed to be a high-stress event. Thus, its inclusion in the experimental protocol has the advantage of both inducing stress and face validity with actual events. Since performance of the auditory memory task would also be required, sufficient distractions and stress effects should be present.

Dependency. The final aspect of the evaluation would be concerned with the potential dependency of a pilot on the tactual display--especially if it were to result in superior control. Since the goal is to provide effective aid to a pilot, in a manner somewhat analogous to that of a flight director, it is highly undesirable that a pilot become exclusively dependent on the aid for control information.⁴

One potentially effective test for such dependency would be as follows:

A pilot would be instructed to execute a sequence of approaches to landing, first using only visual and then only tactual (or vice-versa) AOA information. He would be told a priori that a failure would be instigated at some unannounced time with each display condition. He would be required to respond by first requesting the use of indicated airspeed and, then with airspeed cues only, to continue the approach to landing.

There are two critical aspects to such a failure--these are detection by the pilot and his subsequent control. One measure of the former would be the delay time for detection. Additionally, if detection time were excessive, one would expect that substantial control errors would result and that a positive failure indicator, such as is shown in Figure 4 would be required.

If degraded performance were obtained after detection with the

⁴ This is, no doubt, a low probability circumstance in view of the varied visual, auditory and kinesthetic cues that a pilot also uses to sense speed and attitude information. Nevertheless, this possibility must be considered during the evaluation phase.

use of airspeed, as compared to that obtained in prior "normal" tests with airspeed alone, one would suspect that a dependency problem may exist. One solution would be improved performance from additional training in which failures were induced and subsequent aircraft control depended on airspeed indications only.

The major portion of the evaluation effort will be devoted to testing "low-time" pilots during takeoffs and departures, approaches to landings, and "go-arounds". A detailed protocol is included in Reference (5). Some test subjects, however, will also include flight instructors. The goal will be to obtain a measure of an experienced pilot's need for a stall deterrent. This would be especially helpful if it were related both to an aircraft with which a pilot was familiar and one with which he was unfamiliar.

CONCLUSIONS

Per previous efforts, (4) it appears that the effective use of a tactual display will result in more precise control of an aircraft--particularly when a pilot's visual attention is required outside the cockpit. When a kinesthetic-tactual display, such as that discussed here, is employed as a stall deterrent, it is anticipated that an increased level of safety would be achieved due to enhanced pilot awareness of his aircraft's state--especially the development of near-stall conditions. With the experimental protocol that has been developed (5), abundant evidence, either positive or negative should be obtained to test the validity of this conjecture.

REFERENCES

1. Special study, General Aviation Stall/Spin Accidents, 1967-1969. NTSB-AAS-72-8, September 18, 1972.
2. Munns, M. Ways to Alarm Pilot. Aerospace Medicine, 1971 42, 731-734.
3. Rule, R.G., and Fenton, R.E. On the Effects of State Information on Driver-Vehicle Performance in Car Following, IEEE Transactions SMC, No. 5, November 1972, pp. 630 637.
4. Gilson, R.D. and Fenton, R.F. Kinesthetic-tactual information presentations -- Inflight studies. IEEE Transactions SMC, No. 6, November 1974, pp. 531-535.
5. Gilson, R.D. and Fenton, R.F. Development of a Concept for a Stall-Deterrent Device for Small Airplanes, Federal Aviation Administration, Report No. FAA RD-75-53, in press.

SESSION IV
PERFORMANCE/WORKLOAD EVALUATION

Chairman: CHARLES E. BILLINGS

PRECEDING PAGE BLANK NOT FILMED

N75 33704

VERBAL WORKLOAD IN DISTRIBUTED AIR TRAFFIC MANAGEMENT

J. G. Kreifeldt¹: Tufts University, Medford, Ma. 02155
B. Pardo²: California State University, San Jose, Ca. 95192
T. Wempe³: NASA-Ames Research Center, Moffett Field, Ca. 94035
E. Huff⁴: NASA-Ames Research Center, Moffett Field, Ca. 94035

Presented at the 11th Annual Conference on Manual Control

ABSTRACT

Three different simulated ATC distributed-management systems were presented to three groups of three pilots and two controllers per group in order to investigate the effects of alternative traffic management possibilities on task performance and pilot-controller verbal workloads. The basic task required three piloted simulated STOL craft to merge between two computer-generated CTOL separated by approximately 5nm on a final runway approach.

Two new rule structures - sequencing and advisory - in addition to vectoring were studied in conjunction with CRT pilot displays incorporating Traffic Situation Displays with and without aircraft flight path predictors. The sequencing and advisory systems gave increasing control responsibility to the pilots.

Flight performance data, subjective evaluations and verbal data were analyzed in terms of four planned comparisons. In general, the nonvectoring alternatives were superior to vectoring, particularly in terms of reduced verbal workload. The verbal data were analyzed under several formats of successive detail ranging from raw word counts to message type categorizations. The influence of flight path predictors on verbal workload was also studied.

It was concluded that distributed-management systems could in practice significantly reduce controller verbal workload without reducing system performance. Implications of this conclusion suggest that distributed-management would allow controllers to handle a larger volume of traffic safely either as a normal operating procedure or as a failure mode alternative in a highly automated ground centered system.

INTRODUCTION

A series of experiments have been performed in the Man-Machine Integration Branch at NASA-Ames Research Center comparing distributed pilot-controller management systems to the more traditional ground-based vectoring philosophy of traffic management. These studies were made as part of a general program evaluating the possible impact and potentialities of various existing and state-of-the-art equipments and information available to controllers and pilots on air traffic management.

The experimental context was the degree of traffic management distribution between pilots and controllers made possible primarily by traffic situation displays in each aircraft. The experimental simulations incorporated as much realism as possible by using professional pilots and controllers, ground-based piloted simulators, air-air and air-ground information exchange. The experiments explored three different alternatives of traffic management distribution for simulated terminal approach control and the data were analyzed to determine the relative standing of each alternative on a number of measures such as safety, orderliness, efficiency, manual and verbal workloads, etc.

Analyses of flight performance measures, subjective evaluations and limited verbal data have been made and reported previously^{(1),(2)}. It is the purpose of this paper to report the results of the verbal communication data analyses in order to examine and compare the verbal workloads of pilots and controllers in the distributed management systems. It was a major hypothesis that distributed management could reduce the necessary verbal communication between pilots and controllers thereby reducing a major part of the controller workload⁽³⁾ without an equivalent increase in pilot verbal workload. A more extensive analysis of the verbal data can be found in Reference 4. The verbal data were also analyzed in a manner that could determine the impact of tactical flight path predictors on the verbal workload of pilots and controllers. Fine grained analyses were performed in an attempt to uncover traffic information verbally communicated in the experiments which could be instrumented and furnished to the pilots to reduce verbal workload.

The basic question of this paper is the extent to which alternative ATC traffic management configurations (sequencing and advisory) differ from the traditional vectoring one in terms of the verbal workload of pilots and controllers.

Previous analyses of flight performance measures and subjective evaluations indicated the nonvectoring conditions were generally at least as good as vectoring if not superior^{(1),(2)}.

METHOD

Both the three divisions of responsibility and the task used in the experiments were evolved from discussions with pilots and controllers in the San Francisco area in order to provide realistic simulations within the confines of the equipment and the experimental nature of the investigations.

1. Distributed Management Alternatives

Three divisions of responsibility - Vectoring (v), Sequencing (s) and Advisory (A) and four different pilot CRT traffic situation map displays were combined to produce the seven experimental conditions shown in Figure 1.

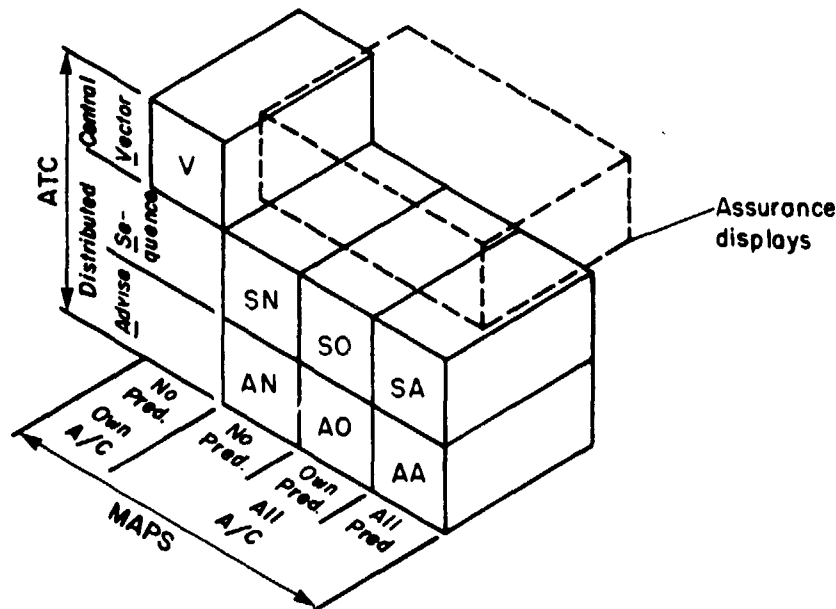


Figure 1. Divisions of Responsibility and Pilot Map Displays Used in The Traffic Management Simulations.

The three divisions of responsibility correspond to ground centralized (Vectoring), air centralized (Advisory) and a moderate division (Sequencing) in which controllers were responsible only for issuing sequencing (order of

landing) commands. Thus two extreme versions of management distribution and a more balanced version (sequencing) were studied. Pilot traffic situation displays (a map type) either showed only their own A/C (used only for vectoring) or all A/C in the problem. 30 second tactical path predictors of the A/C were displayed as ground track predictions on the pilots' traffic display in some conditions. The display effects of no predictors, predictor on own A/C only and predictors on all A/C were studied as part of the experimental paradigm. The Vectoring mode required controllers to vector each A/C as usual while in the Advisory mode, controllers were to refrain from anything interpretable as a command allowing the three pilots full control responsibility for solving the traffic problem.

2. Task

The basic task required that the three piloted A/C simulators considered to be of the STOL variety be inserted "between" two scheduled computer generated CTOL A/C which were on a final 3° approach. The STOLS started at 3000' with instructions to fly a 6° descent on the ILS with the task terminated for each A/C as it crossed the middle marker. Figure 2 shows a map like projection of the A/C at the problem start and a view of a pilot's CRT display during a test with an all A/C traffic situation display beneath the CRT vertical situation display. Each A/C has a predictor displayed although it is not apparent in this figure.

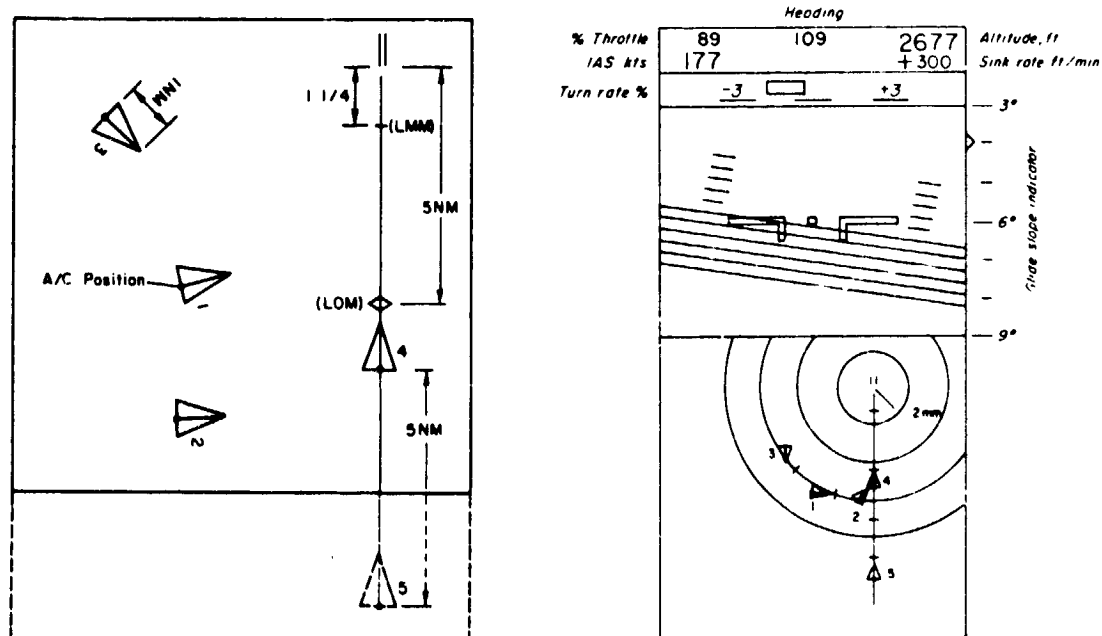


Figure 2. Ground Projection of the Task and a Pilot's CRT Display in a Non Vectoring Condition During a Trial.

A minimum of 30 sec. spacing crossing the middle marker (or 1 nm depending on the problem conditions) and a crossing speed of 120 KTS were specified as basic conditions in addition to other instructions. Initial heading, speeds and positions for the STOLS were randomized within constraints to allow a problem solution. A complete description of the task, instructions, displays etc. has been described previously^(1, 4).

3. Verbal Measures

The verbal intercommunications between pilots and between pilots and controllers were tape recorded for each experimental run. Each run lasted approximately 5 minutes. There were the seven conditions shown in Figure 1 with four trials per run (not including practice runs) and three independent groups of pilots and controllers. Thus, approximately seven hours of verbal data were recorded and analyzed.

The verbal data were first transcribed verbatim on to hard copy with the speaker(s) identified in every case and this copy was the basis for further reduction. Two basic types of analyses were made, a dynamic analysis of undifferentiated total word count per unit time which is useful in following the temporal pattern of verbal workload and a static analysis of the undifferentiated and categorized verbal data. Each analysis will be discussed in the appropriate section, Reference 4, can be consulted for a comprehensive discussion of the development and details of the verbal analysis methodology, comparisons with preexisting methods and the formulation of the basic task as a small group problem. This paper presents selected results from that reference.

RESULTS

The results of the verbal data analyses are presented in this section in two major categories displaying selected dynamic and static features.

1. Dynamic Analyses of the Verbal Data

Dynamic analyses of the verbal data are straightforward compilations of the number of words spoken per 30 second interval as determined by word counts made from the transcriptions which also had temporal markers where indicated from the original tape recordings. Data from all 3 groups are averaged and plotted against cumulative word count. The graphs permit the initial word rate and final word count to be seen directly. The ordering of each condition is indicated along the appropriate axes.

Consecutive points on a curve represent data from consecutive 30 second intervals.

Figure 3 shows the undifferentiated word rate for the pilots and controllers as well as the both combined ("system"). In comparing the graphs, the differences in abscissa scaling should be noted.

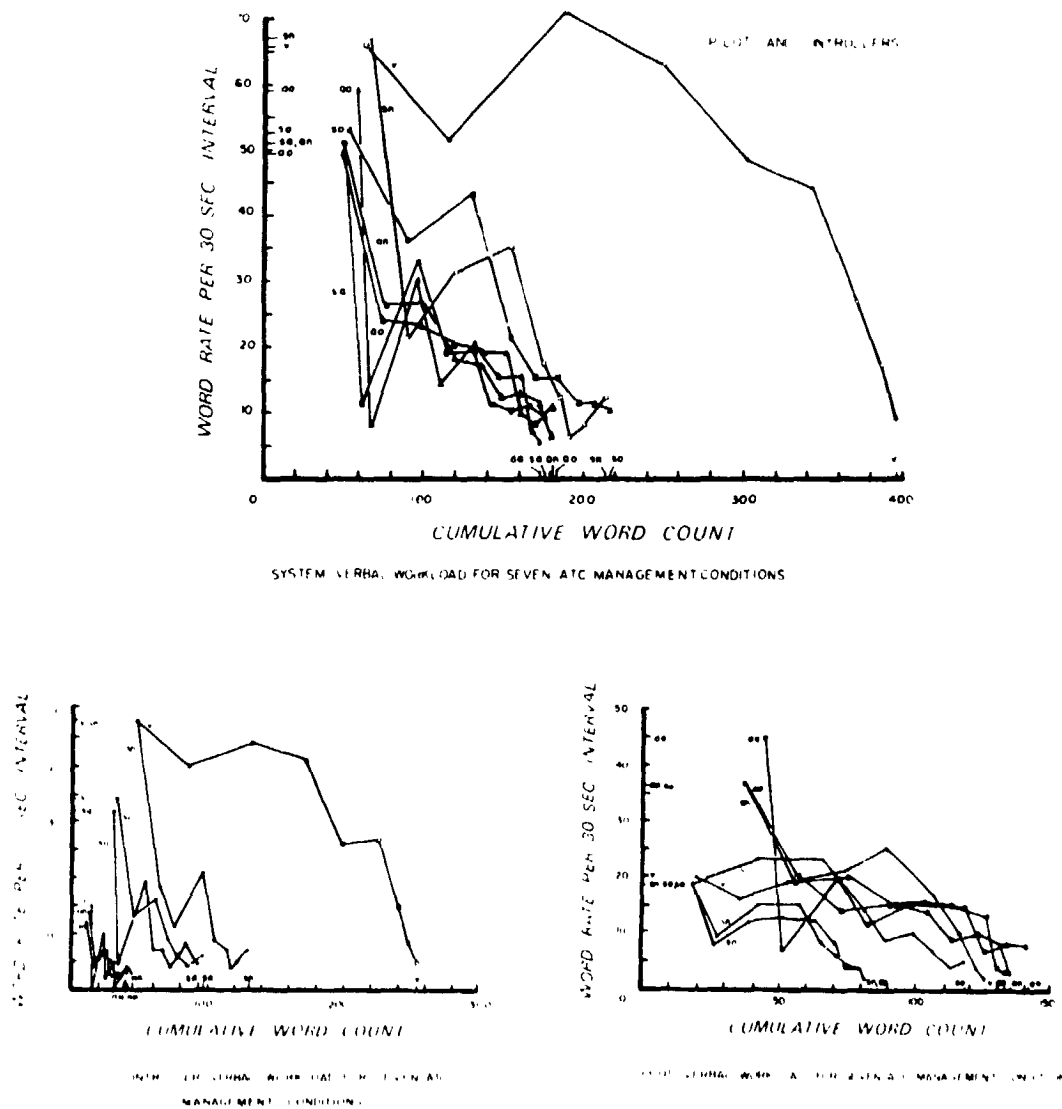


Figure 3. Word Rate - vs - Cumulative Word Count For the Seven Experimental Conditions. Pilots, Controllers and Total (system) Data are Shown Separately.

The most obvious feature of the graphs is the large difference in controller word rates for the vectoring condition as opposed to the sequencing and advisory conditions. For example, the single controller began the vectoring runs speaking at a rate of nearly one and one-half words per second for the first half minute to vector the three simulators and finished the run with a total of nearly 250 words. Both the initial word rate and cumulative word count decrease sharply for the controllers as their responsibility decreases in the system from vectoring to sequencing to advisory modes of distributed management. There is an indication that the sequencing condition in which no path predictors were displayed for the pilots had an initial controller verbal workload which was comparable to the vectoring condition.

The pilot data show that the initial word rates for the pilots as a group were essentially the same for vectoring and sequencing but slightly higher for the advisory conditions. The pilot cumulative word rate is highest for the advisory and vectoring condition and lowest for the sequencing condition. Thus, while the controller workload decreases as pilot responsibility increases, the pilots' workload increases as the responsibility moves away from a balanced distribution of management (sequencing). However, it should be remembered that the pilot verbal data shown is the sum total of each single pilot's data. The per pilot data could be considered as 1/3 of that shown. Thus, even in the highest verbal workload condition, any given pilot had approximately a 15 word per 30 sec. rate at the beginning of the advisory condition and would have spoken about 50 words over the total 5 minute period of the run. This should be compared to the single controller speaking at a rate of 50 words per 30 seconds at the beginning of the vectoring condition and speaking nearly 250 words over the period of the run.

The total system word rate shown in Figure 3 indicates the large difference between the vectoring and nonvectoring conditions, particularly in terms of the total words spoken. The similarity of the initial word rates indicates that a certain amount of initial information must be communicated while the spread in final word count between vectoring and nonvectoring conditions indicates that the vectoring condition is not conducive to the most efficient transfer of this information. Certainly it would seem that the initial word rate is limited in the vectoring condition since 45 words per 30 seconds is a very rapid speech rate. The tendency of the controller word rate to remain high whereas it falls rapidly for nonvectoring condition is a reflection of the fact that the ground centralized system can not take advantage of the strong self-organizing ability inherent in the pilot system with traffic situation displays and must, therefore, continue close communication for correction and direction of the individual A/C.

Several secondary features of the data can be noticed which may be task specific. The word rates invariably drop from their initial value prior

to rising again for all seven conditions except for an isolated case of sequencing-own predictor (S0) pilot communication. This initial decrease must reflect the ability of the system to proceed "open-loop" for a short time following initial communication of plans and intents. The final word rates are relatively constant regardless of condition which again suggests some necessary amount of final information or standard communication. The sequencing-no predictor (SN) condition produced the same average initial word rate from the controllers as did vectoring. In principle, the three sequencing conditions should have produced the same word rate from the controllers since no predictors were visible to them although they knew of their presence or absence from the pilots' displays. This higher than necessary word rate for SN might be attributable to lack of controller "assurance" that pilots had sufficient traffic information resulting in more volunteered controller information. It is likely that more extended operation in this condition would produce similar controller results for all the three sequencing conditions as it did for the three advisory conditions.

Although pilot initial word rates were the same for vectoring and sequencing conditions, the final word count for vectoring was higher than for sequencing which is clearly attributable to the fairly constant rate of pilot replies in vectoring during the course of the run.

Figure 4 shows the previous data averaged across conditions eliminating the predictor variable to compare the three ATC systems, and averaged across sequencing-advisory conditions to compare vectoring-nonvectoring conditions. This figure may be regarded as a summary of the preceding one with any possible predictor display effects suppressed.

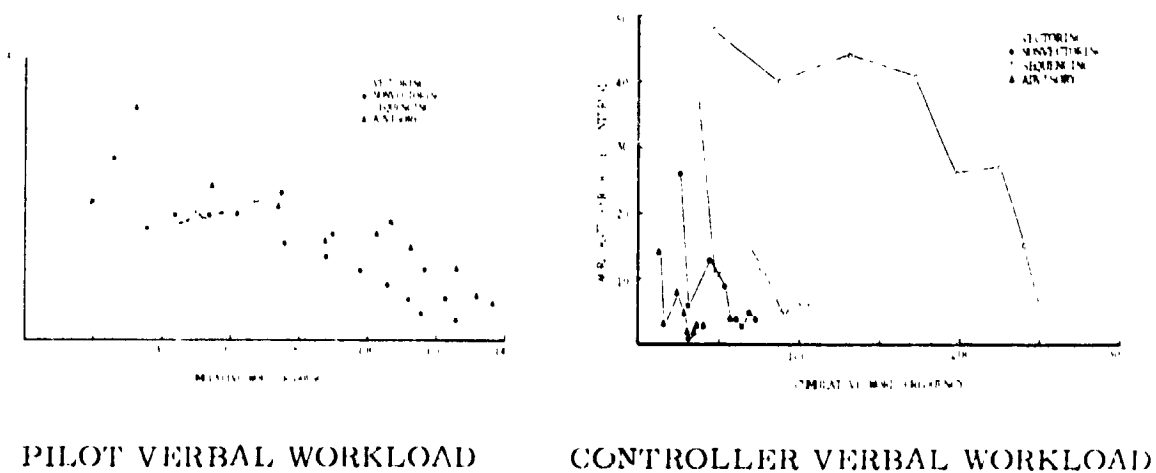


Figure 4. Word Rate - vs - Cumulative Word Count For the Basic ATC Systems. Pilot and Controller Data are shown separately.

The presence of path predictors on the pilots' displays did not appear to have any strong consistent effect. However, the data in Figure 3 suggests that the all predictor conditions (SA, AA) require less total pilot words and this was a consistent effect for all three groups except in one instance (Group I, Advisory). No such consistent effect was found for controllers group-by-group even though the effect averaged over groups in Figure 3 suggests that total controller word count decreases in the order of additional traffic information made available through path predictors on the pilot displays. This is a reasonable but not statistically defensible result at this point.

Since the task was successfully accomplished under all conditions, it appears that vectoring requires nearly twice as many words as necessary in the total system and from 3 to 5 times as many controller words based upon the minimum word counts among the seven conditions. Pilot total words are not increased significantly in nonvectoring conditions being slightly higher in the advisory conditions for which their higher initial group word rate could be an objection. However, on a per pilot basis, the individual word count and word rate is approximately 1/3 of that indicated.

Since total pilot word rate curves are about the same for the seven conditions, the composition (content) of the communication must be changing and this is detailed in the following sections.

2. Static Analyses of the Verbal Data

Analyses of the total word count and of the total message counts were also made. Although these suppress the dynamic features of communication they provide reasonable comparisons of the total verbal workloads.

The simplest analyses of the message types are based on the mutually exclusive identification of each message as a directed initiation (I), a directed response (R) in reply to a directed message and finally a nondirected general (G) announcement (e. g. "number 3 is reducing to 160"). Figure 5 shows the average number of messages in each category per 5 minute run to compare their absolute values and also shows the same data categories as a percentage of the total message to compare their volumetric size.

Clearly vectoring was nearly twice as message intensive as the nonvectoring conditions with a 50-50 split between pilot and controller message which is reasonable considering the pilot acknowledgment of controller commands in vectoring. It should be remembered that messages are the basic units of analyses here and not words as in the previous section.

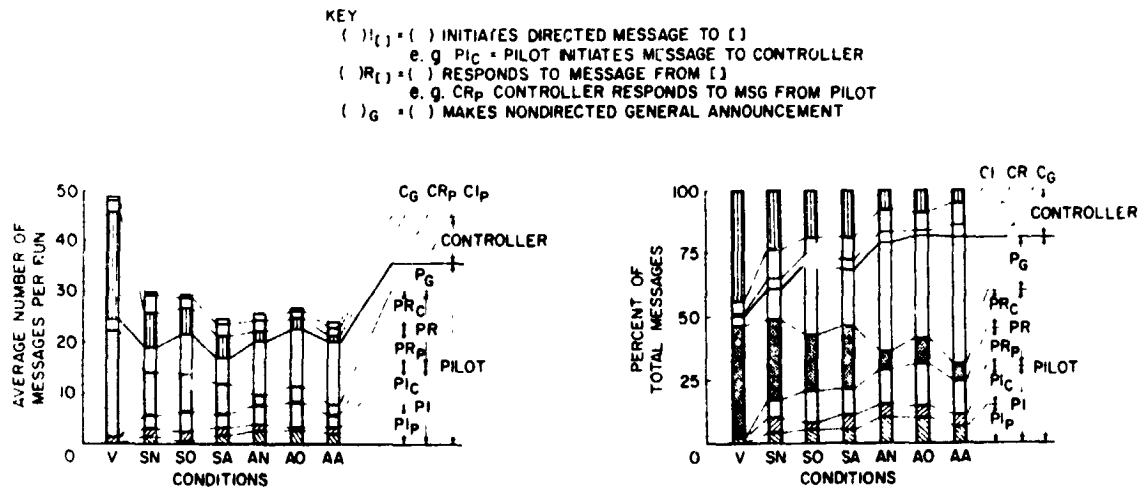


Figure 5. Average Number of Messages per Run and Their Percentage Distribution for Each of the Seven Experimental Conditions.

As the controller initiations decreased, their share in the total communication decreased along with the pilot's replies to controllers, which would be expected. On the other hand, the pilot-to-controller reply decrease was approximately balanced by an increase in the pilot-general announcement (usually an announcement of intent or action). Furthermore, the more air-centralized the distribution of management, the greater the percentage of pilot general messages. The analysis could not reveal for whom general announcements were indicated. However, the specific amount of pilot-to-pilot initiations (PI_p) is fairly small on both an absolute and relative basis although directed air-to-air initiations and replies together constitute approximately 25% of the pilots' total messages in the nonvectoring conditions.

Figure 6 presents the message data relative to total pilot messages and total controller messages to assess the changing nature of the total message workload content for air and ground separately as the distribution of management shifts.

Controller initiation content decreases as their responsibility decreases. This decrease in initiation content is opposed by an increase in the percentage of general announcements. The controllers' contribution to the total system messages is approximately 25% to 40% for advisory and sequencing conditions.

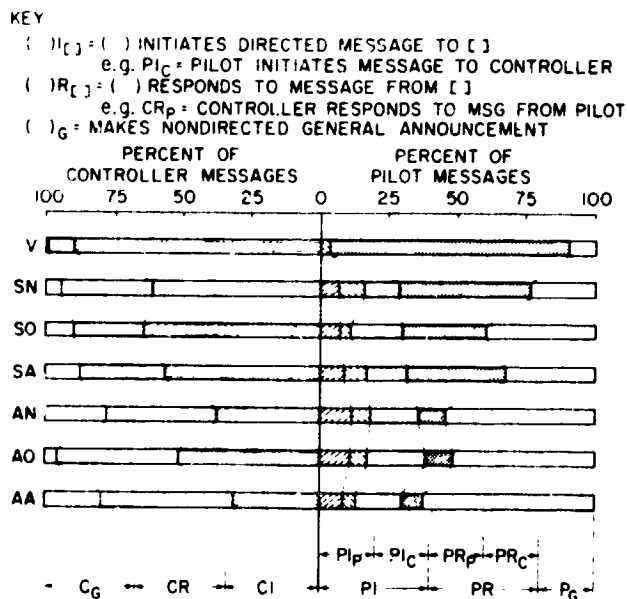


Figure 6. Average Number of Pilot and Controller Messages Per Run in Each of the Seven Experimental Conditions. Message Type Expressed as Percentage of All Messages.

Figure 5 suggests that although no clear distinction exists between predictor-no predictor conditions, the total number of pilot messages and total system messages was least in the all predictor conditions (SA, AA). This was a consistent effect for each group as well as for the average data shown. These differences appear to be attributable to the smaller controller-to-pilot initiations and pilot-to-controller replies in the all predictor cases. As mentioned previously, controllers were aware of the predictor element condition (none, own, all) of the pilots' displays during each run and therefore they may have felt more "assured" by the all predictors condition that the pilots had information of other A/C flight intentions.

Figure 7 is presented to compare the general structures of air-air and air-ground communication patterns in the vectoring and nonvectoring conditions. Data from all six nonvectoring conditions were averaged for the single nonvectoring structure. Comparisons are made on the basis of total word rate for air-ground, ground-air and air-air exchanges.

The individual A/C are arranged clockwise in the order of their actual final landing sequence without respect to their starting configurations.

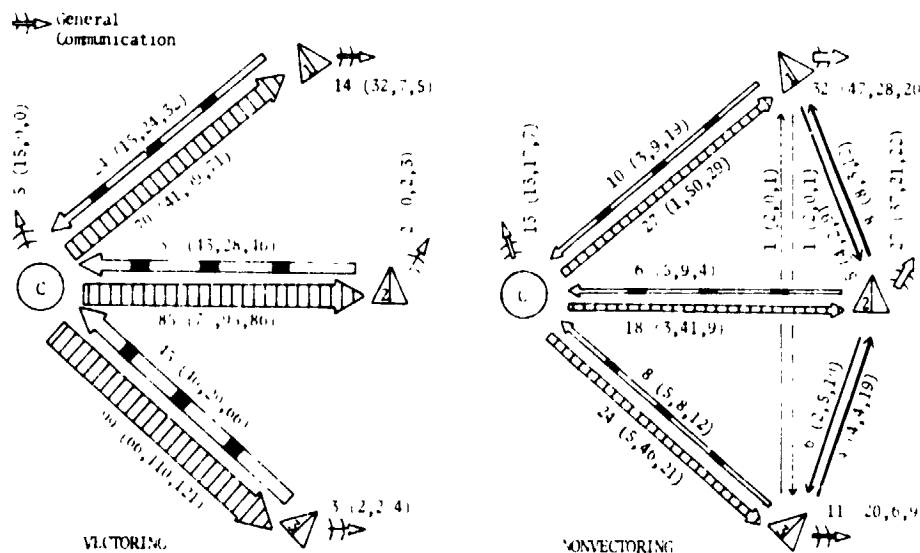


Figure 7. Schematic Representation of the Communication Patterns in the Vectoring and Six Averaged Non-vectoring Conditions. Numbers Indicate Total Word Count Per Run for Each of the 3 Groups and Their Grand Average.

Thus, each successive A/C in sequence could communicate longer than the preceding one. The numbers adjacent to the arrows represent average word counts for that link for the three groups. Values in parentheses indicate the individual group values. The width of the arrows is proportional to the associated mean word count. This figure reinforces previous statements that inter air-ground communication was less in the nonvectoring case but was somewhat compensated by the nonvectoring increase in air-air and pilot-general communication. The vectoring pattern shows quite clearly that the longer the A/C is in the problem the greater are the number of total air-ground words exchanged. On the other hand, this was not true for the nonvectoring case on the average even though, as in the vectoring case, the third A/C could communicate with controller an average of 71 seconds longer than the first A/C in final sequence. The pilot-general announcements decreased as their final sequence position decreased as well. This may be a type of "follow-the-leader" behavior in which successive A/C in the final sequence have respectively less "broadcast" announcements to make.

It was also observed that communication was greater between A/C in direct sequence than between A/C separated by a third A/C. A corollary of this observation for A/C in sequence is that the "center" A/C would tend to communicate more than those on the ends. Anecdotal observations during the course of experiments indicated that sequence order in the nonvec-

toring conditions was established early in the problem.

As a final observation it should be noted that there appear to be considerable difference between the individual group data in some instances indicating different styles of interactive problem solving. The analyses to follow which treat the data under 4 planned comparisons and categorize the verbal data at a finer level will also present individual group data.

3. Planned Comparisons of the Verbal Data

The verbal data flight measures and subjective evaluations were analyzed following the 4 planned comparisons of vectoring-nonvectoring (VE,NV), Sequencing-Advisory, (SE,AD), no predictors-predictors, (NP, PR), and own predictors-all predictors (OP,AP). Portions of the verbal data analyses only will be given here. More complete results for all the analyses can be found in references 2 and 4.

Figure 8 compares the mean word count for pilots and controllers separately and together under the planned comparisons. The mutually exclusive categories of statements, questions and replies are also given.

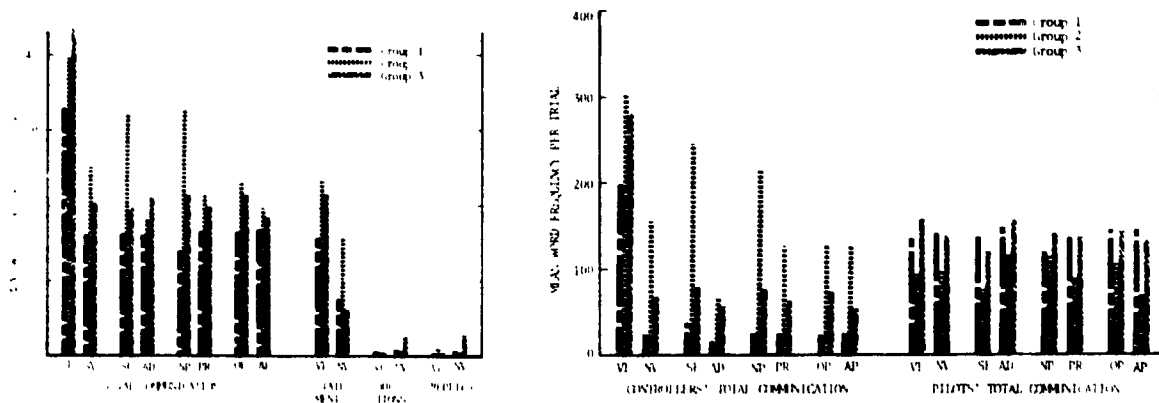


Figure 8. Mean Word Frequencies Associated with Four Planned Comparisons. Group Differences are Shown.

While the volume of total communication decreased in the nonvectoring conditions an average of 47% across the three groups ($p < .05$) the difference was mainly due to the 71% decrease in controller verbal workload ($p < .05$). Pilot verbal workload did not differ significantly between the two conditions. Previous analyses showed that although total pilot communication remained the same, the pattern shifted such that pilot-controller communication ave-

rated 77% less in the nonvectoring condition ($p < .05$) while interpilot and pilot-general communication increased.

The controller verbal workload decreased 57% in the advisory condition compared to the sequencing condition ($p < .02$) while pilot workload increased 33% ($p < .05$) in going from the sequencing to advisory mode of management. This increase in pilot communication in the advisory condition was due to an increase in inter-pilot communication ($p < .05$) and pilot-general announcements ($p < .10$).

The presence or absence of predictor elements on the pilots' displays did not appear to make any statistically significant difference in word count although in two of the groups both the pilot and the controller workloads decreased somewhat when predictors were used. Similarly, there was little difference between the own predictor-all predictor displays although the same two groups again showed a decrease when pilots saw predictors on all A/C rather than on their own A/C only.

Figure 9 presents the volume of communication according to selected message contents. The planned comparison format is used as before.

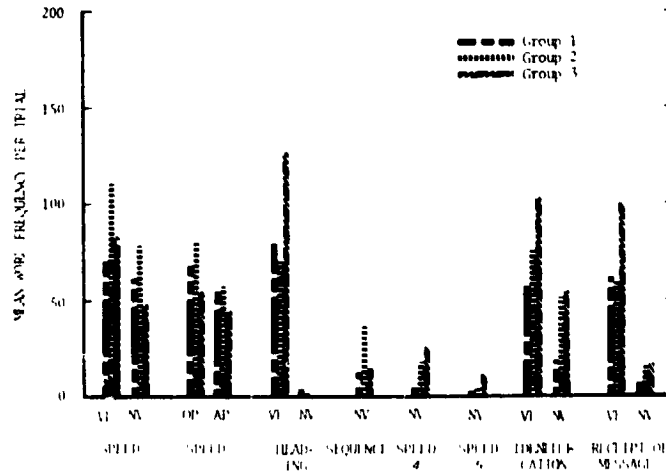


Figure 9. Planned Comparisons of Communication Associated With Several Information Content Categories.

There was less communication related to speed of the piloted A/C, identifications and message acknowledgments in the 6 nonvectoring cases on the average. Similarly, the presence of predictors on all the A/C (AP) rather than on own A/C only (OP) reduced the communications related to speed. The nonvectoring conditions produced communications directly related to sequence, and the speeds of the computer generated A/C (4 and 5).

Overall, more consistency among the three groups was observed for

pilots than for controllers.

DISCUSSION

The effect of decentralizing the controller component of ATC and providing pilots with more visual information on local traffic resulted in substantially reducing controller verbal workloads without increasing pilot verbal workload or decreasing task performance measures. The sequencing condition which was the most balanced air-ground distribution resulted in the lowest pilot workload and lowest total system workload. Allowing pilots full responsibility for the traffic management resulted in an increase in their verbal workload over the sequencing condition. Pilot display differences associated with the three predictor conditions had little overall influence on verbal communication although previous analyses indicated an overwhelming preference by pilots and controllers for predictor element display.

Although the pilots' verbal workload was similar in the vectoring and nonvectoring conditions, important differences in the pattern of communication were observed. For example, the information exchange between consecutive A/C in landing sequence was greater than that between two A/C not in direct sequence as would be expected. Such a result suggests the use of somewhat different pilot display information depending on the landing sequence configuration. Neither the sequencing-advisory conditions nor the various nonvectoring map displays notably affected the type of information communicated. Large differences were observed, however, between the vectoring and nonvectoring conditions where both the largest change in decentralization and map displayed information occurred. The low frequency of questions and replies in all conditions indicates that the information provided to the pilots and controllers in terms of statements, and on the displays was largely sufficient for the task. It was observed that much communication was devoted to identifications and acknowledgments of receipt of a message particularly in the vectoring condition. The reduction in communication concerning speed in the all-predictor condition compared to own-predictor suggests that incorporating predictors on other visible A/C is helpful. However, judging by the large amount of speed related communication, the use of predictor for speed determination was not very efficient by itself. Other methods for this purpose, such as direct numerical readings on the pilots' displays should be studied.

While the use of only three groups was not sufficient for a proper analysis of intergroup differences, it is suggested that group style may be an important factor in alternative ATC configurations. Intergroup pilot variations were comparable in the vectoring and no vectoring conditions suggest-

ing that they were similarly constrained by all conditions. Since controllers gave few commands in the nonvectoring conditions, their large intergroup variation mostly in terms of advisory messages suggests some ambiguity concerning their role in those conditions.

Overall, the sequencing condition appears to be most preferable in terms of verbal workload for the following reasons. The pilot initial word rate was no higher in sequencing than in vectoring but definitely higher in advisory. Controller initial word rate for sequencing was appreciably lower than for vectoring. Pilot and controller total word counts, separately and together, were also appreciably lower in sequencing than in vectoring. (Pilot total word count was slightly higher in advisory than vectoring. Although pilot initial word rate was twice as high in advisory than in vectoring the task was still accomplished with little apparent performance difference from vectoring^(1, 2, 4). The advisory condition naturally required the lowest initial word rate and final total word count of the controllers.)

From an operational viewpoint, sequencing would also seem preferable to advisory since the controllers issue and, therefore, know the order of landing. Their assurance that this order can be safely and expeditiously obtained without their direct intervention keeps their verbal workload low which could result in their handling a larger volume of traffic without overload. The dynamic analysis of word rate showed a sizable dip in word rate particularly for controllers in the nonvectoring conditions which suggests that the controllers need not keep a constant communication rate with a group of A/C once sequenced but could instead turn their attention to successive groups in order. This might have the effect of smoothing out their word rate.

Sequencing produced less directed pilot-pilot communications and pilot-general announcements than did advisory which again suggests that sequencing was a better balanced system.

Pilot traffic displays should incorporate own A/C path predictors only. There was some slight evidence that predictors on all A/C reduced verbal workload in some instances particularly in speed related communication. However, the effect though significant was slight. Overwhelming support for own predictor incorporation came from pilot evaluations based on their subjective estimates after each run of safety, orderliness, expeditiousness and workload⁽⁴⁾. Even controllers who were aware of the predictor display conditions without actually seeing them on their display were overwhelmingly in support of predictor elements for the pilot displays although the controllers supported the all predictor condition. The preference for own predictor rather than all predictor was reinforced by 13 out of 14 flight performance measures being favorable to the own predictor condition^(2, 4).

Therefore, in summary it is concluded that the sequencing mode of distributed management is a realistic alternative to vectoring (i. e. ground based centralized management). Sequencing with pilot CRT traffic displays incorporating a path predictor on their own A/C reduced controller and pilot verbal workloads, elicited positive support from pilots and controllers and did not compromise the performance of the basic task.

ACKNOWLEDGMENT

This research was performed at NASA-Ames Research Center in the Man-Machine Integration Branch under a 1973 NRC Research Associateship. The verbal data analyses were performed by the second author in partial fulfillment of the Master of Science degree at San Jose University while supported under grant 05 - 046 - 02 at NASA-Ames. Continued analyses of the experimental results are supported by a grant from the NASA-Ames University Consortium, NCAR-785-401.

1. Assistant Professor, Department of Engineering Design
2. M. S. Candidate, Department of Psychology
3. Research Scientist, Man-Machine Integration Branch
4. Branch Chief, Man-Machine Integration Branch

REFERENCES

1. Kreifeldt, J. G. , Wempe, T. E. , "Future Terminal Air Traffic Management Concepts", Proceedings of the 10th Annual Conference on Manual Control, April 9-11, 1974, WPAFB.
2. Kreifeldt, J. G. , Wempe, T. E. , "Human Decision Making in Future ATC Systems - Comparative Studies in Distributed Traffic Management", Proceedings of the 1974 International Conference on Systems, Man and Cybernetics, Oct. 2-4, 1974, IEEE 74 CHO 908-4 SMC.
3. Roberts, L. , Lundquist, G. , Findley, D. "Overview: The Role of Communication Systems in Air Traffic Management". IEEE Transactions on Communications, 1973, COM-21(5).
4. Pardo, B. , Effects of Verbal Communication and Task Variables of Different Air Traffic Control Configurations. Unpublished M. S. Thesis, Dept. of Psychology, San Jose Univ. San Jose, Cal. 8/75.

N75 33705

**EFFECTS OF AUTOMOBILE STEERING CHARACTERISTICS
ON DRIVER/VEHICLE SYSTEM PERFORMANCE
IN DISCRETE MANEUVERS**

By Richard H. Klein and Duane T. McRuer

Systems Technology, Inc.
Hawthorne, California

SUMMARY

A series of discrete maneuver tasks were used to evaluate the effects of steering gain and directional mode dynamic parameters on driver/vehicle responses. The importance and ranking of these parameters were evaluated through changes in subjective driver ratings and performance measures obtained from transient maneuvers such as a double lane change, an emergency lane change, and an unexpected obstacle. The unexpected obstacle maneuver proved more sensitive to individual driver differences than to vehicle differences. Results were based on full-scale tests with an experienced test driver evaluating many different dynamic configurations plus seventeen ordinary drivers evaluating six key configurations.

INTRODUCTION

The test program described in this paper is intended to quantify desirable vehicle dynamic characteristics from a closed-loop driver/vehicle response standpoint. In Ref. 1 the overall program was reviewed and the key maneuvers and performance measures described. This paper presents, in particular, the effects of automobile steering dynamics on the results of transient maneuvers, i.e., vehicle control tasks which could be termed discrete in time (as opposed to continuous tracking or regulation tasks). In the experimental series, these tasks were primarily a double lane change at 70 and 100 mph, where a driver can behave in a dual-mode fashion in his control actions; an emergency lane change at 30 mph, where the driver is faced with an unknown lane selection situation dictated by the switching of green-red traffic lights; and an unexpected obstacle avoidance maneuver evoked by an obstacle appearing from the side of the road forcing the driver to take evasive action. The double lane change was the maneuver most sensitive to vehicle dynamic differences since it was run at a higher speed where given differences in vehicle oversteer and understeer properties appear more distinctly. At lower speeds these vehicle characteristics are not as clearly differentiated.

The program variables were the vehicle directional dynamics, as defined by the yaw velocity to steer angle transfer function, and the steering wheel to front steer angle gain (commonly referred to as "steering ratio"). For the expert test driver, eight different vehicle directional dynamic configurations,

shown in Fig. 1, were tested extensively. A subset was used in the validation tests with 17 ordinary drivers. The configurations tested were chosen from a matrix of over 60 identified configurations, all using 1974 Chevrolet Nova hatchback sedans. The dynamic properties of the configurations shown in Fig. 1 were obtained by varying tire sizes, e.g., from a small B78-14 tire mounted on a 4 in. rim, to a large 11:30-15 tire mounted on an 8 in. rim; by adding lead weight to the rear bumper of the car such as in Configurations 58 and 60 shown on the righthand side; and by adding lateral acceleration feedback to the steering servo, such as shown on the six configurations on the left, where the level of lateral acceleration feedback ranged from 2.5 deg/g in an understeer direction to -2.5 deg/g in an oversteer direction. Steering ratio was varied for any one of these configurations by feeding forward an electrical signal proportional to steering wheel position. With this method it was possible to change from a very low ratio of approximately 25:1 to a very high ratio of 9:1. Several workers (Refs. 2-8) have previously shown that these directional-dynamic and vehicle-response scaling variables affect vehicle steering performance in various driving situations. The performance measures found most sensitive here to these changes in vehicle dynamics were the driver's steering activity, cone scores in specific maneuvers, and subjective driver ratings. With this introduction we can now turn to particular results.

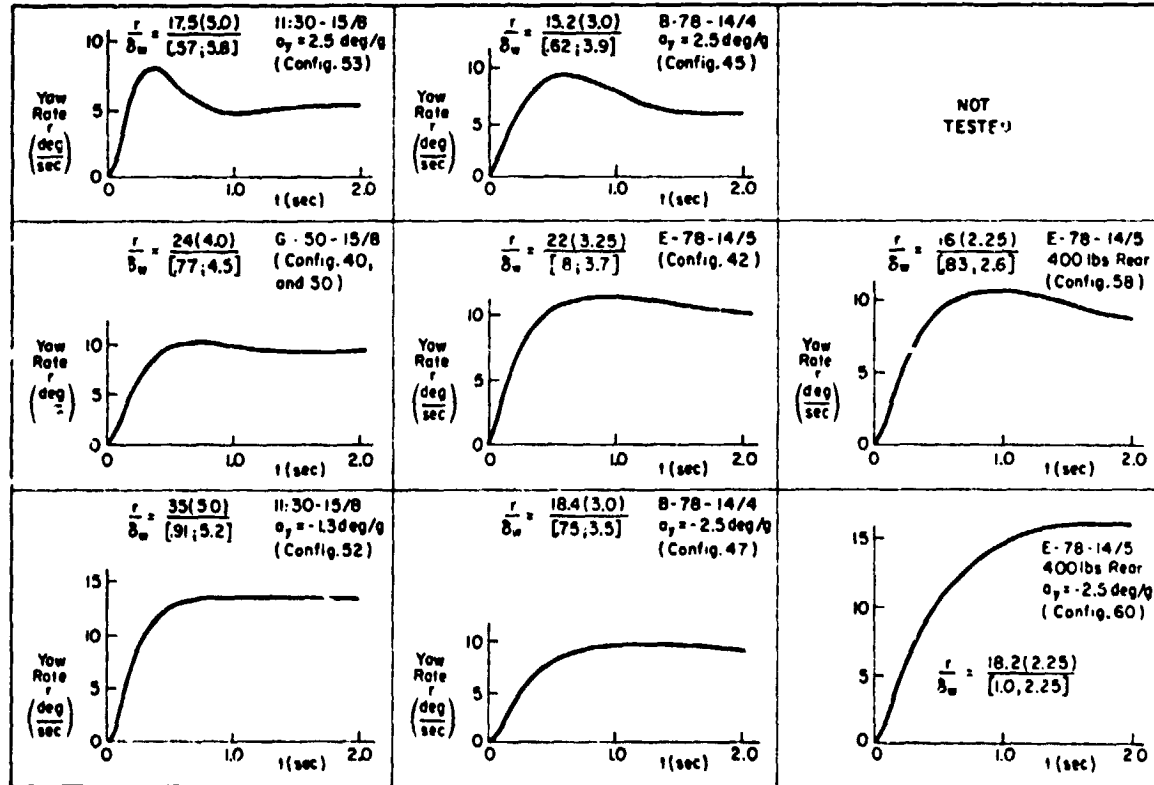


Figure 1. Yaw Velocity to Steer Angle Indicial Responses for Original Test Configurations

EXPERT DRIVER RESULTS

Figure 1 shows the average steering reversals used to accomplish the double lane change as a function of the yaw time constant, T_r , for the expert test driver. As the vehicle response slows down (T_r increases), more steering activity is required. For the lane change maneuvers the expert driver did not have any cone strikes. Performance for the unexpected obstacle was not obtained since he was aware of the unexpected obstacle and therefore could not be surprised by it. This test driver did, however, provide driver ratings which showed the effects of steering gain and vehicle responsiveness.

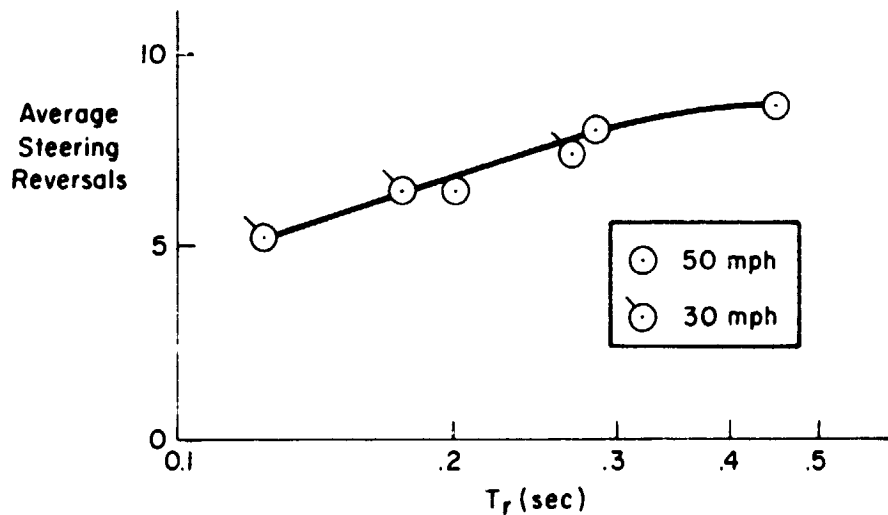


Figure 2. Steering Reversals to Accomplish Double Lane Change as Function of Yaw Time Constant

As described in Ref. 9 at least three different categories of driver rating scales are needed to properly differentiate the effects of vehicle parameter changes on driver behavior (response, workload, etc.) and on driver/vehicle system response and performance. That is, a separate scale is required for unattended operation, continuous tracking and/or regulation, and discrete command and vehicle response situations. The latter scale is the one used here. It is fundamentally non-adjectival and intended to be interval. It ranges between vehicle response characteristics which are excellent in that the transient maneuver is "very easy to accomplish," to characteristics which are "impossible to accomplish at task speed." When using the scale, the subject makes his assessment by simply marking a location along the lefthand side. Ten points are then allocated for the total interval, and numbers assigned by the analyst accordingly. The objective features included in the subjective assessment given by the driver rating include such factors as:

- Task performance
- Concentration and attentional demands
- Driver mental workload
- Effects of vehicle dynamics

These are the same kinds of factors which, in the analogous case of aircraft handling, are taken into account by a skilled test pilot in providing a pilot commentary and an associated pilot rating (Ref. 10). It has been demonstrated many times that the Cooper-Harper Scale subjective ratings are related to the pilot and pilot/vehicle system dynamics and performance (e.g., Ref. 11). Similar rating techniques have been employed with automobiles (e.g., Refs. 12 and 13) although not to the degree that the techniques have been used in aircraft. In fact, the large-scale study upon which this paper is based (Ref. 9) is one of the first comprehensive treatments in which automobile dynamics are related to driver ratings.

The test driver ratings for vehicle responsiveness and steering gain are shown in Fig. 3. The top portion of Fig. 3 shows the overall yaw velocity to steering wheel gain at 50 mph versus the yaw time constant, T_r . The driver ratings are reduced to iso-opinion lines corresponding to Levels 3 and 6. Ratings of 3 or better indicate the vehicle is very good; between 3 and 6, marginal; and above 6, poor. From the left figure we can see that a steady-state yaw response greater than 0.5 appears too responsive to the test driver

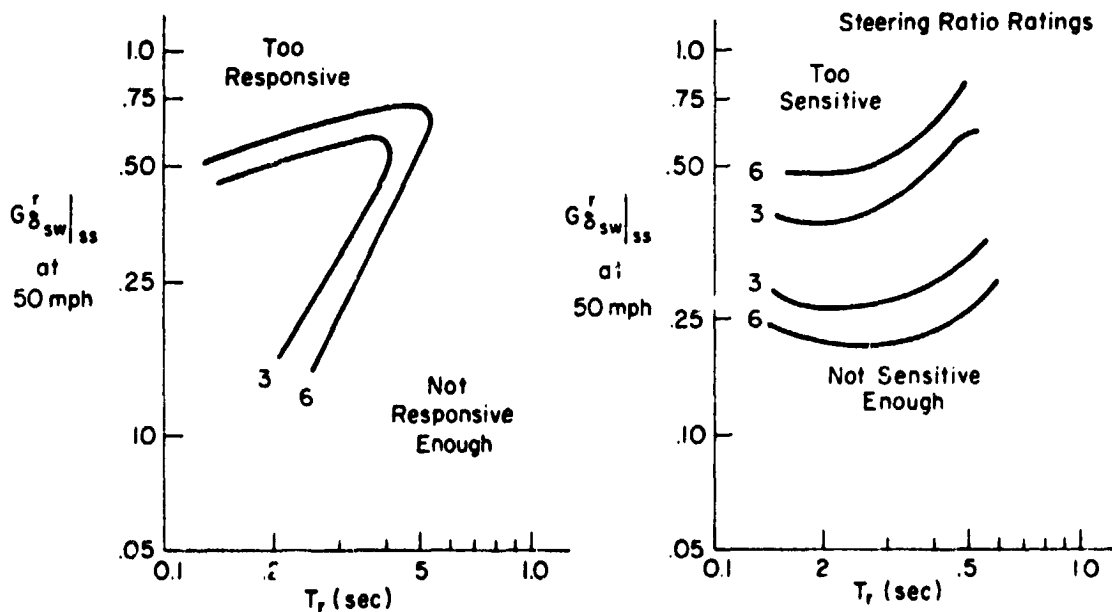


Figure 3. Driver Opinion Ratings of Vehicle Responsiveness and Steering Gain From the Expert Test Driver

and is relatively insensitive to the yaw time constant. However, on the lower righthand side, the driver ratings appear more sensitive to the change in yaw time constant than they do to the change in steering gain.

The right portion of Fig. 3 shows the driver ratings for steering ratio. In this figure it can be seen that there is very little sensitivity to the change in time constant and much more sensitivity to the change in overall steady-state yaw velocity gain. In particular, at 50 mph, steady-state yawing-velocity/steering-wheel-deflection values greater than 0.5 appear too sensitive, and yawing velocity gains below 0.2 appear not sensitive enough. By combining the results of the left and right portions of Fig. 3 a potential region of optimum vehicle characteristics, such as shown in Fig. 4, can be identified. This has boundaries on top and bottom dictated by the overall yaw velocity to steering wheel gain, and on the righthand side a sensitivity to yaw time constant based on the responsiveness ratings. This gives a tentative optimum vehicle region of vehicle dynamics.

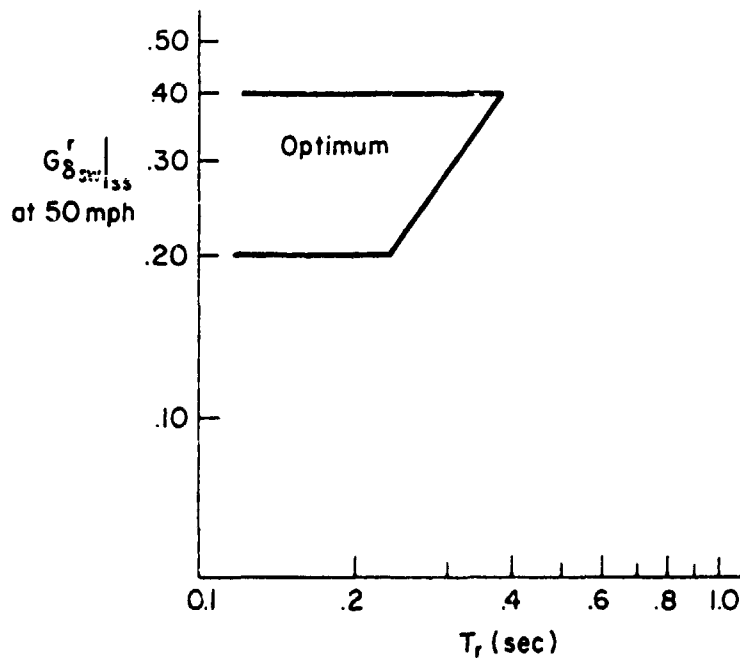


Figure 4. Tentative Boundaries of Optimum Vehicle Response at 50 mph as Determined from Subjective Ratings of Experienced Test Driver

REPRESENTATIVE DRIVER RESULTS

To validate the expert driver results we then proceeded to test 17 subjects, eight females and nine males, selected from the ordinary driver population. Four of the original eight vehicle dynamic configurations, one with three different steering gains, were used. These final test configurations are shown in Fig. 5.

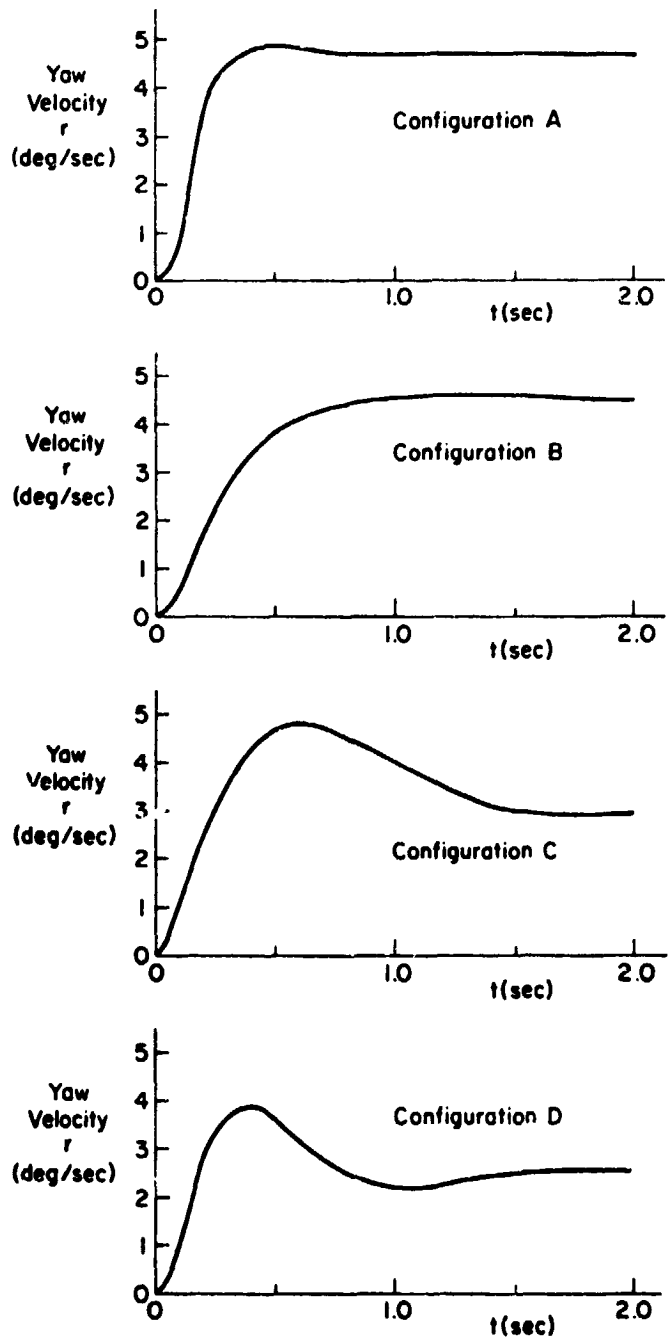


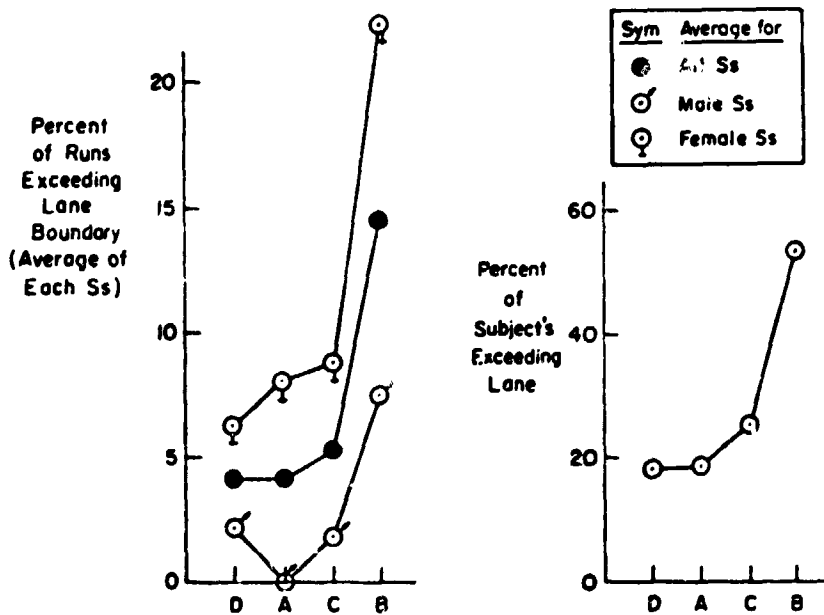
Figure 5. Yaw Velocity Response of Final Vehicle Test Configurations at 50 mph to 1 deg Step Steer Input

Configuration A at the top represents an ideal vehicle configuration, with characteristics within the tentative optimum region shown in Fig. 4. It has very good yaw damping, rapid response time, and very little overshoot to the step steer input. Configuration B is closer to a neutral steering configuration, with concomitant slower response times. Configurations C and D represent understeering configurations at low and high frequencies, respectively. Utilizing these four vehicle configurations for the 17 ordinary subjects, cone scores and steering activity were found to be sensitive measures. The latter also followed the test driver results.

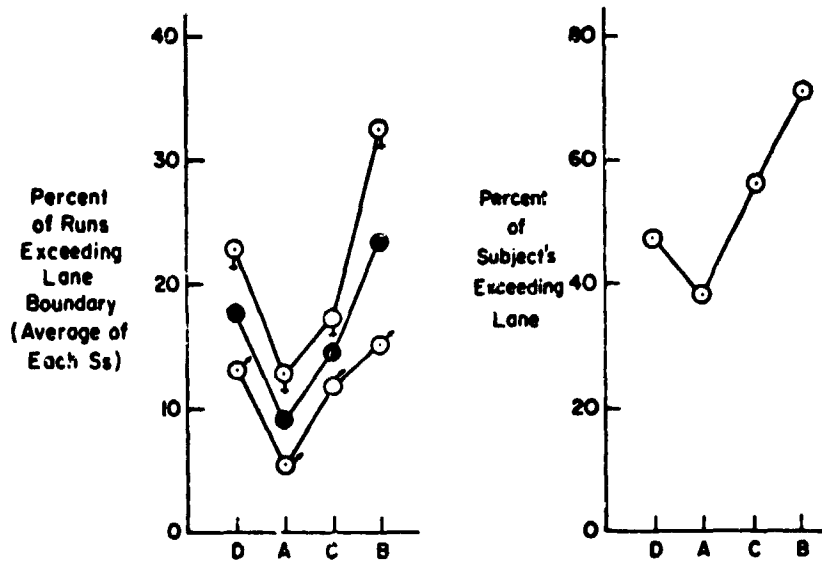
The sensitivity of cone scores to both the vehicle dynamics and steering gain are presented in Figs. 6 and 7, respectively. In Fig. 6 the effects of vehicle dynamics on lane exceedences in both the emergency lane change maneuver and the double lane change maneuver are given. At the left side are plotted the percentage of runs in which the driver exceeded the lane boundary, and the right side shows the percentage of subjects who actually exceeded the lane (in other words, those who produced the data in the lefthand plot). As an example, for the emergency lane change maneuver, 4-5 percent of the runs exceeded the lane boundaries for Configurations D, A, and C. However, the righthand side indicates that only 20-25 percent of the subjects tested actually exceeded the lane. From an overall standpoint the top portion of Fig. 6 shows that Configuration B resulted in a much higher percentage of lane exceedences than the other three configurations and also a much higher percentage of the subjects exceeding the lane. This implies Configuration B is less safe than the other three in such maneuvers. It might also be noted that female subjects on the average showed a much higher tendency to exceed the lane than males.

The same trends are exhibited for the double lane change maneuver shown on the bottom portion of Fig. 6. However, in this figure it can be seen that Configuration A, the more likely optimum dynamic configuration, produced the fewest number of lane exceedences and also had the lowest percent of subjects exceeding the lane. Configuration B again showed up its more undesirable characteristics.

The effects of steering gain on lane exceedences are shown in Fig. 7. The steering gains tested were all installed on the ideal vehicle configuration (A), and the three steering ratios are denoted by A_1 , A_2 , and A_3 where A_1 is the nominal 19:1 ratio, A_2 is a lower ratio of 15:1, and A_3 is a higher ratio of 23:1. The top portion of Fig. 7 gives the results for the emergency lane change maneuver. It shows that females exhibit a very large number of lane exceedences at the 23:1 ratio. On the average, only about 20-25 percent of the subjects exceeded the lane for all three steering ratios. For the double lane change maneuver shown in Fig. 7b the 15:1 steering ratio results in the fewest percentage of lane exceedences for both male and female subjects and also resulted in the fewest number of overall subjects exceeding the lane. Taking Fig. 7 in total it appears that one ratio is not optimum for all subjects for different maneuvers at different speeds and for different vehicle steer angle gains. However, if an average had to be chosen, the 19:1 steering ratio appears to be a good intermediate compromise. These results also show that the females may not be as adaptable to changes in steering gain as males. This is definitely a subject that should be looked into further.

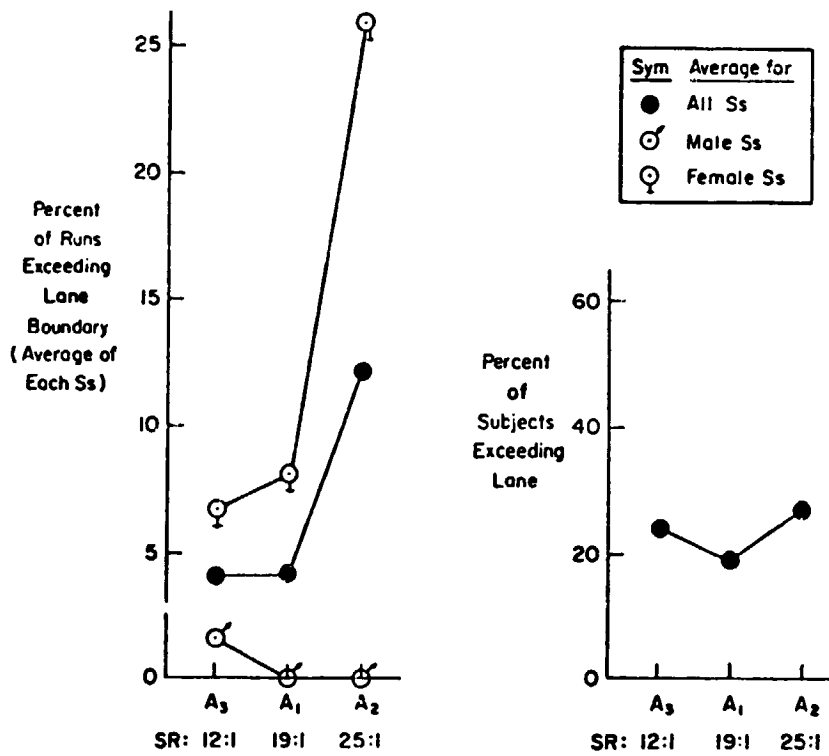


a) Emergency Lane Change Maneuver (30mph)

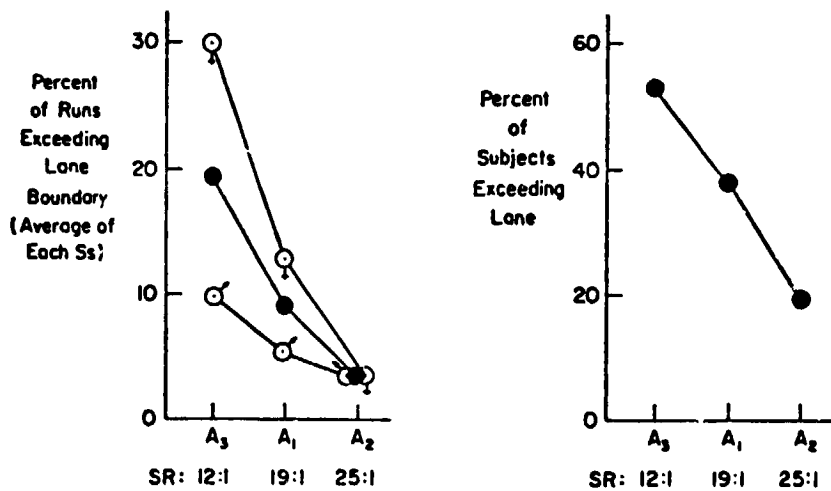


b) Double Lane Change Maneuver (50mph)

Figure 6. Effects of Vehicle Dynamics on Lane Exceedences



a) Emergency Lane Change (30 mph)



b) Double Lane Change (50 mph)

Figure 7. Effects of Steering Gain on Lane Exceedences

The average results of the driver ratings are shown in Fig. 8. These driver ratings are for the 50 mph double lane change and are plotted versus the change in inverse vehicle time constant, $1/T_r$. This figure shows that the most desirable vehicle configuration is the rapidly responding Configuration D with $1/T_r$ of 5. Next rated is Configuration A with a $1/T_r$ of 4 rad/sec. To show the consistency of the data, the average of three repeat runs is shown alongside Configuration A. Least desirable were Configurations C and B with ratings of 5 and 7, respectively. It is interesting to see that Configuration D, which had a low damping ratio (indicative of an understeering vehicle) combined with a rapid response, is classed better than one with higher damping and hence less yaw velocity overshoot. This indicates that drivers appear more sensitive to response time than to the overshoot, and therefore Configurations A and D were rated better than Configurations B and C.

Also shown on Fig. 8 as incidental information are the average ratings of the subjects for their own personal cars. These fell conveniently into two categories corresponding to "small" and "larger" personal cars. It is interesting to note that the small personal cars were rated as good as the ideal vehicle configuration, A₁. This may be due in part to the smaller overall size of these cars, which gave them more room to negotiate the 9 ft wide lane change corridor.

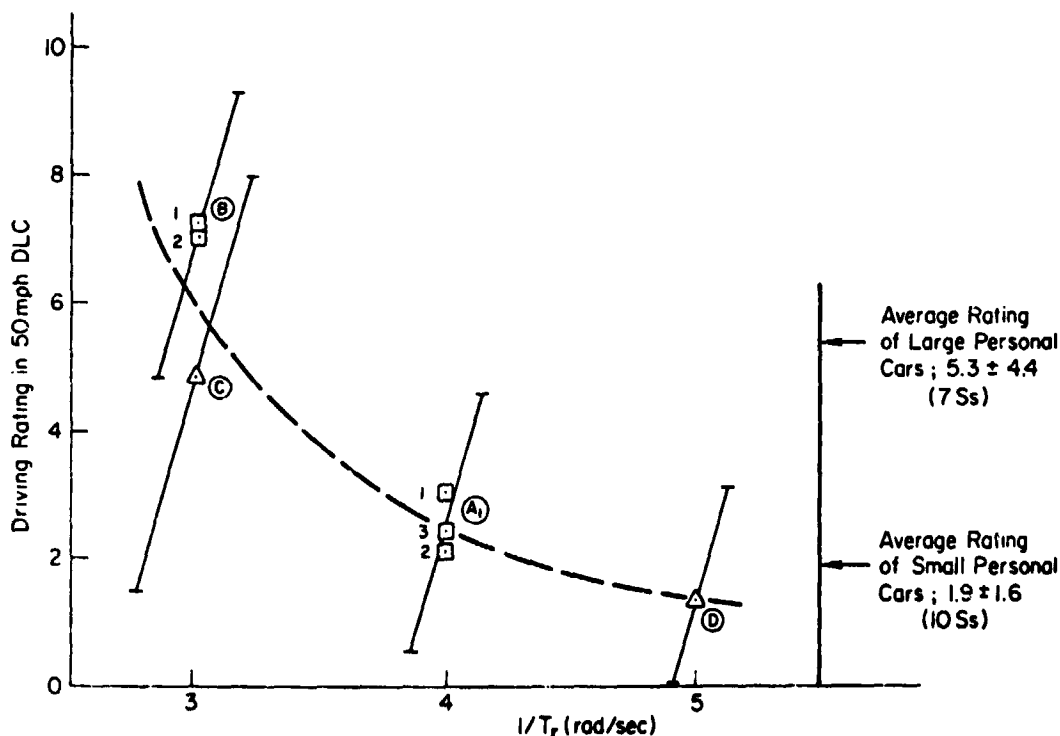


Figure 8. Average Driver Ratings of 17 Test Subjects for Double Lane Change Maneuver

In terms of subject preference for an ideal steering gain, the results support the tentative optimum boundaries of Fig. 4 and were more consistent for male than for female subjects. These results are shown in Fig. 9. For the male subjects shown on the lefthand side, six of nine preferred the 19:1 ratio [which produced an overall yaw velocity to steering wheel gain of 0.25 (deg/sec)/deg]; two preferred the 25:1 ratio; and only one preferred the 12:1 (since he equally liked 25:1 this subject's data appear inconsistent). The female subjects, shown on the righthand side, show five out of eight preferred the 19:1; two preferred 25:1 (one only barely); and again one preferred the 12:1 ratio. There is, however, a much wider spread in the females' ratings of the optimum vehicle gain (from 1 to 5.5) than the males, who rated the best in a range of 0.5 to 2.0.

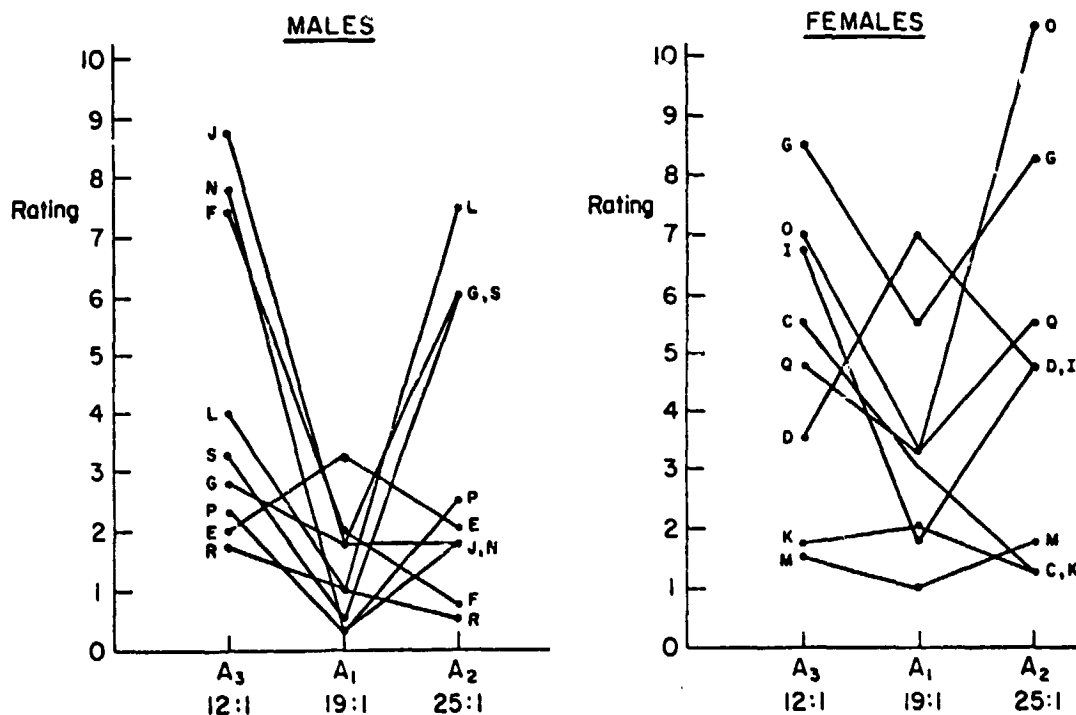


Figure 9. Ratings for Various Steering Gains on Configuration A in 50 mph Double Lane Change Maneuver

In regard to the unexpected obstacle results for the 17 drivers, the results were not conclusive with regard to vehicle dynamics. This occurred since all subjects were not able to drive each configuration and still encounter the obstacle with the same degree of unexpectedness. For example, on repeat runs with five subjects using a good vehicle, Configuration A, and a poorer vehicle, Configuration B:

- Two of the five missed the obstacle with the A car but hit it with the B car (a positive result).
- Two of the five missed it with both cars (a neutral result).
- One of the five hit it the first time with the good car and missed the obstacle the next three times with both the good and bad configurations (a neutral to negative result).

More interesting results were obtained from general driver response characteristics and when differences between drivers were compared. These are listed below.

- The reactions of the subject drivers to the unexpected obstacle demonstrated almost all possibilities. For example:
 - Seven steered around it
 - Eight hit it
 - Two stopped in front
- The peak steering wheel deflection was about 100 ± 40 deg. There was no significant difference between configurations in this connection; however, all drivers did not experience each configuration.
- In braking, the average effort was about 30 lb, creating about 0.5 g for stopping.
- Reaction times were quite slow. Approximately 1.2 ± 0.25 sec elapsed before any steering or braking action was taken. (The stopping distance at 0.5 g deceleration from 30 mph is 60 ft; 100 ft was available.)
- Heart rate was an excellent measure of unexpectedness. It typically went to greater than 160 beats/minute.

This brings us to the point of general summary and conclusions based on the results of the transient maneuver tasks. In general, the key vehicle parameters are (in order of importance): steering gain, yaw velocity numerator (which dictates the dominant path mode time constant, T_R), directional frequency, and, of least importance, the directional damping ratio. In more quantitative terms, it appears that:

- The range of desirable steady-state yaw velocity to steering wheel gains is between 0.2 and 0.4 (deg/sec)/deg at 50 mph for standard size vehicles and is dependent on the value of T_R for slower responding vehicles.

- The yaw velocity time constant, T_r , should be less than 0.3 sec for speeds up to 50 mph.
- There is a lower bound on acceptable directional response frequency and damping ratio. These are about 3 rad/sec and a ratio of 0.5, respectively, although not enough vehicles were tested with values less than these to be certain the results are definitive.

REFERENCES

1. Klein, Richard; McRuer, Duane; and Weir, David: Test Procedures and Performance Measures Sensitive to Automobile Steering Dynamics. Published in this volume.
2. Haynes, A. L.; Mika, H. S.; and Forbes, L. M.: Simulation Techniques in Automotive Human Factors Research. National Conference on Driving Simulation, 1961.
3. Forbes, L. M.: A Human Factors Evaluation of Steering Gear Ratios for the 196x Ford. Ford Motor Co. Rept. M-795-622.
4. Bundorf, R. T.: The Use of a Variable-Stability Vehicle in Handling Research. SAE Paper 650659, 1965.
5. Hoffmann, E. R.; and Joubert, F. N.: The Effect of Changes in Some Vehicle Handling Variables on Driver Steering Performance. Human Factors, vol. 8, no. 3, 1966, pp. 245-263.
6. Shoemaker, N.; and Dell'Amico, F.: A Pilot Experiment on Driver Task Performance with Fixed and Variable Steering Ratio. Cornell Aero. Lab. Rept. VK-2185-V1R, 1966.
7. Hildebrandt, T. J.; and Poskocil, A. R.: Objective Testing in Handling Research. SAE Paper 680015, 1968.
8. Sweatman, Peter: The Design of a Variable Characteristic Vehicle and Its Use in Driver Control Studies, Ph.D. Thesis, Univ. of Melbourne, Apr. 1973.
9. McRuer, Duane T.; and Klein, Richard H.: Automobile Controllability — Driver/Vehicle Response for Steering Control. Vol. I: Summary Report, DOT HS-801 406. Vol. II: Supporting Experimental Results, DOT HS-801 407. Nov., 1974.
10. Cooper, G. E.; and Harper, R. P., Jr.: The Use of Pilot Ratings in the Evaluation of Aircraft Handling Qualities. NASA TN D-5153, Apr. 1969.
11. McRuer, D. T.; and Krendel, E. S.: Mathematical Models of Human Pilot Behavior. AGARD-AG-188. Jan. 1974.

12. Wojcik, C. K.; and Allen, R. W.: Studies of the Driver as a Control Element -- Phase No. 3. UCLA-ENG-7148, July 1971.
13. Lincke, W.; Richter, B.; and Schmidt, R.: Simulation and Measurement of Driver Vehicle Handling Performance. SAE Paper 730489, May 1973.

ACKNOWLEDGMENT

This research was supported by the National Highway Traffic Safety Administration under Contract DOT-HS-359-3-762.

N75 33706

THE EFFECTS OF STABILITY AUGMENTATION ON
THE GUST RESPONSE OF A STOL AIRCRAFT
DURING A CURVED MANUAL APPROACH

By Milton B. Porter, Jr.
Air Force Flight Dynamics Laboratory

and

Robert L. Swaim
Purdue University

SUMMARY

The MLS approach path tracking of manually piloted STOL aircraft will be affected by severe atmospheric turbulence, and the system gust response can be significantly altered by Stability Augmentation Systems (SAS). In this study, the task of investigating the effect of SAS was formulated as two optimal control problems for stochastic systems: (1) to compute SAS gains with a rate-model-in-the-performance-index algorithm, and (2) to calculate the pilot gains and system gust response using an optimal pilot model.

Both problems were solved to yield reasonable low gains for the pilot and SAS, and the lateral-directional mode poles and the longitudinal short period poles could be placed accurately by the model matching algorithm. Of the longitudinal (SAS) poles achieved, the vertical rms path error was least for the unaugmented poles. The lateral rms path error was an order of magnitude larger than the vertical error and showed a plus or minus 50 percent variation with SAS. It increased with dutch roll frequency and damping, and it decreased most significantly with increased roll stability. The variation in lateral error with bank angle for curved flight was also a significant function of the augmented poles. There was a trade-off between minimum lateral and directional coupling and minimum lateral path error.

INTRODUCTION

Advanced air terminal navigation systems, such as MLS, provide the potential for increased landing rates by allowing multiple simultaneous curved approach paths. STOL aircraft are particularly suited for steep approaches and short radius turns feeding into the sides of the MLS sector. These curved trajectories have problems associated with manual path tracking, especially in severe turbulence. The pilot can be provided with an advanced display to reduce his workload, but feedback through the flight

director alone cannot adequately compensate for the gust response of the basic airframe. Stability Augmentation Systems (SAS) have the potential to improve path tracking in turbulence, but they are usually designed to compensate for other problems. It was desirable, then, to investigate the effect of SAS upon gust response in order to determine design tradeoffs and potential improvements. This paper is a summary of the author's doctoral thesis, reference 1. Three airspeed/flap configurations for the Breguet 941 STOL aircraft were investigated in reference 1, and the results for one of these are shown here.

Problem Definition

A parametric analysis of the effect of SAS upon gust response was accomplished. This analysis was separated into two tasks which were formulated as quadratic optimal control problems for stochastic systems: (1) to calculate the SAS gains for specified augmented poles using a rate-model-in-the-performance-index algorithm, and (2) to calculate the pilot model gains and system response for each set of SAS gains using a quadratic optimal pilot model.

SYMBOLS

$()_b$	banked flight variable
C_0, C_1	observation matrices
I	identity matrix
K_{d_z}	flight director gain on vertical flight path error
K_p	pilot gain
p	body axis perturbation roll rate
r	body axis perturbation yaw rate
s	Laplace domain variable
T_L	pilot Lead
y_2	observation vector for flight director design problem
α_g	equivalent gust angle of attack
β	sideslip angle
β_g	equivalent gust sideslip angle

δ_a, δ_r	aileron and rudder actuator states
$\delta_{a_s}, \delta_{r_s}$	SAS control variables
η_n	unit variance Gaussian white noise driving the remnant state equation
ϕ_0	trim bank attitude angle
ϕ	perturbation roll attitude angle

OPTIMAL CONTROL PROBLEM FORMULATION

The following formulation was used to describe both optimal control problems in this study. The problem is to calculate the optimal system feedbacks in the gains matrix H such that the control

$$u = -Hy \tag{1}$$

minimizes the performance index

$$J = \frac{1}{2} \lim_{t \rightarrow \infty} \int_{\Omega} z'(t, \omega) Q z(t, \omega) d\omega \tag{2}$$

where the system response vector is

$$z = Dx + Tu \tag{3}$$

the state stochastic differential equation is

$$\dot{x} = Ax + Bu + G\eta \tag{4}$$

the observation vector is

$$y = Cx \tag{5}$$

Ω is the domain of ω in the associated probability space, η is a vector of stochastic (Gaussian white noise) disturbances, A, B, C, D, G, and T are matrices of constant coefficients and Q is a symmetric positive semi-definite matrix of quadratic weights. This formulation provided for partial state feedback through the observation equation (5).

An algorithm for a gradient solution to this problem was derived in reference 2. The system matrices in that algorithm were partitioned to provide an efficient numerical solution. Computer programs implementing that algorithm were used for this study.

STABILITY AUGMENTATION DESIGN

Parametric variation of the augmented open loop system poles was accomplished by SAS designed for the wings level decoupled longitudinal and lateral-directional modes. The design technique used was a variation of the rate-model-in-the-performance index method described in reference 3. Complete, pure state feedback was provided to the elevator and throttle controls for the longitudinal mode and the aileron and rudder controls for the lateral-directional. The servo-actuator states were retained in this design method.

For the lateral-directional SAS design, the state and observation vectors of equations (4) and (5) were defined to be

$$x' = y' = [p, r, \beta, \phi, \delta_a, \delta_r, \delta_{a_c}, \delta_{r_c}] \quad (6)$$

where the first six states describe the aircraft and actuators and the last two were the random variables driving the aircraft and model. The stochastic actuator disturbances were first order filtered Gaussian white noise processes. The control vector was

$$u' = [\delta_{a_s}, \delta_{r_s}] \quad (7)$$

The rate-model stochastic differential equation was

$$\dot{x}_m = A_m x_m + G_m \eta \quad (8)$$

where the model had no actuators or controls.

The response vector was derived by subtracting the model and aircraft equations assuming approximate equality of the model and aircraft states and identical stochastic disturbance coefficients

$$z = \dot{x} - \dot{x}_m = (A - A_m)x + Bu \quad (9)$$

Then, the D and T matrices of equation (3) were obtained by eliminating zero rows from equation (9). The response vector for the lateral-directional mode became

$$z = [\Delta \dot{p}, \Delta \dot{r}, \Delta \dot{\beta}, \dot{\delta}_a, \dot{\delta}_r] \quad (11)$$

Selected elements of the upper left 4x4 partition of the model matrix, A_m , were calculated to vary the poles parametrically. This matrix partition was

$$A_{LD} = \begin{bmatrix} a_{11} & a_{12} & a_{13} & 0 \\ a_{21} & a_{22} & a_{23} & 0 \\ 0 & 1 & a_{33} & a_{34} \\ 1 & a_{42} & 0 & 0 \end{bmatrix} \quad (12)$$

Two alternate expressions for the model characteristic equation were as follows

$$\det(sI - A_{LD}) = (s^2 + 2 \zeta_d \omega_d s + \omega_d^2)(s + 1/T_R)(s + 1/T_S) = 0 \quad (13)$$

where the second expression contained the dutch roll frequency and damping and the roll and spiral poles. In order for both expressions to be identical, the coefficients of like powers of s had to be equal.

Subtracting these coefficients, we obtained a set of four equations

$$F'(x) = [f_1, f_2, f_3, f_4] = [0]' \quad (14)$$

where

$$x' = [a_{11}, a_{13}, a_{22}, a_{23}] \quad (15)$$

These elements of A_{LD} were chosen since the stability derivatives C_{1p} , C_{1r} , C_{nr} , $C_{n\beta}$ in these elements caused most significant variation in the lateral-directional poles. These poles were specified in equation (14), which was solved for the variable matrix elements by a Newton-Raphson iteration. These elements were then used in equation (9) to compute the SAS gains.

The longitudinal mode was handled in a similar manner. However, although the rate-model SAS design method placed all four lateral-directional

poles quite accurately, the longitudinal phugoid pole locations could not be controlled; only the longitudinal short period poles could be placed arbitrarily. This problem was most probably due to the special aerodynamic and thrust characteristics of the blown flap STOL and the increased coupling of the longitudinal short period and phugoid poles.

The augmented poles were varied over the acceptable flying quality region as determined from military and NASA specifications in references 4, 5, and 6. The pertinent region boundaries and augmented poles are shown in figures 1 and 2. The unaugmented short period poles were overdamped and are shown on the real axis in figure 1. Three other short period pole locations were investigated as shown.

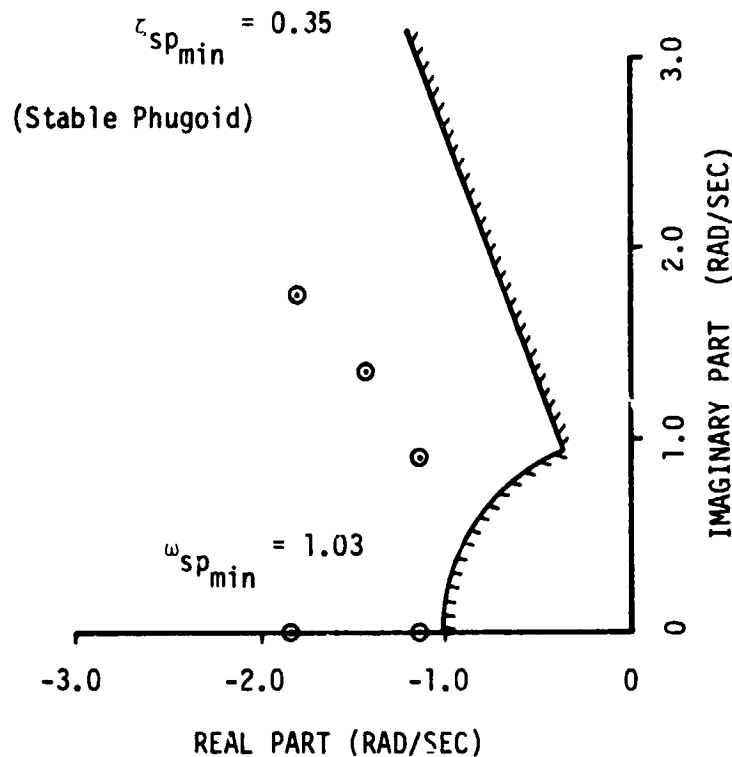


Figure 1
Longitudinal SAS Design

The specified model dutch roll poles are represented by the intersections of the lines in figure 2. The points are the SAS design poles, and they illustrate the accuracy of the pole placement algorithm. The roll and spiral poles were also varied parametrically. For reference, the unaugmented poles were as follows: dutch roll frequency and damping (1.33 rad/sec, .290), roll pole (-i.74 rad/sec), spiral pole (-.016 rad/sec), and both servo poles (-10 rad/sec).

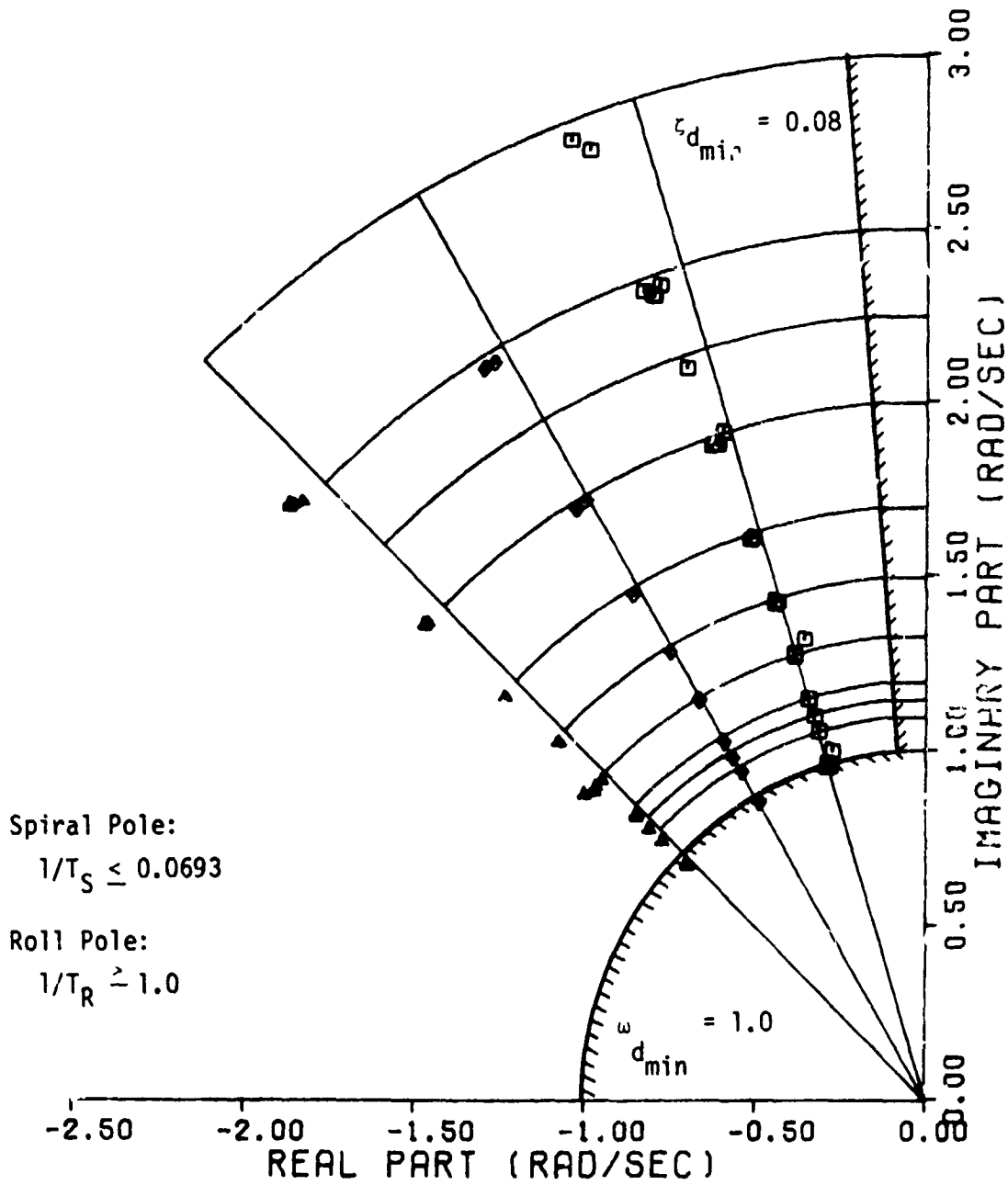


Figure 2
 Lateral-Directional SAS Design

PILOT GAINS AND SYSTEM RESPONSE

The complete piloted system diagram is shown in figure 3. The equations for this system for both wings level and horizontal banked flight were derived in reference 1. Results for one airspeed, 194 kilometers/hour (105 knots), and inboard flap setting, 45 degrees, are shown here. The elevator, aileron, and rudder actuators were represented by first order lags with 0.1 sec time constants and the engine throttle response by a first order lag with 1.0 sec time constant. The MLS signal and sensor errors were neglected. The flight director, pilot model, and gust model are discussed in the following sections.

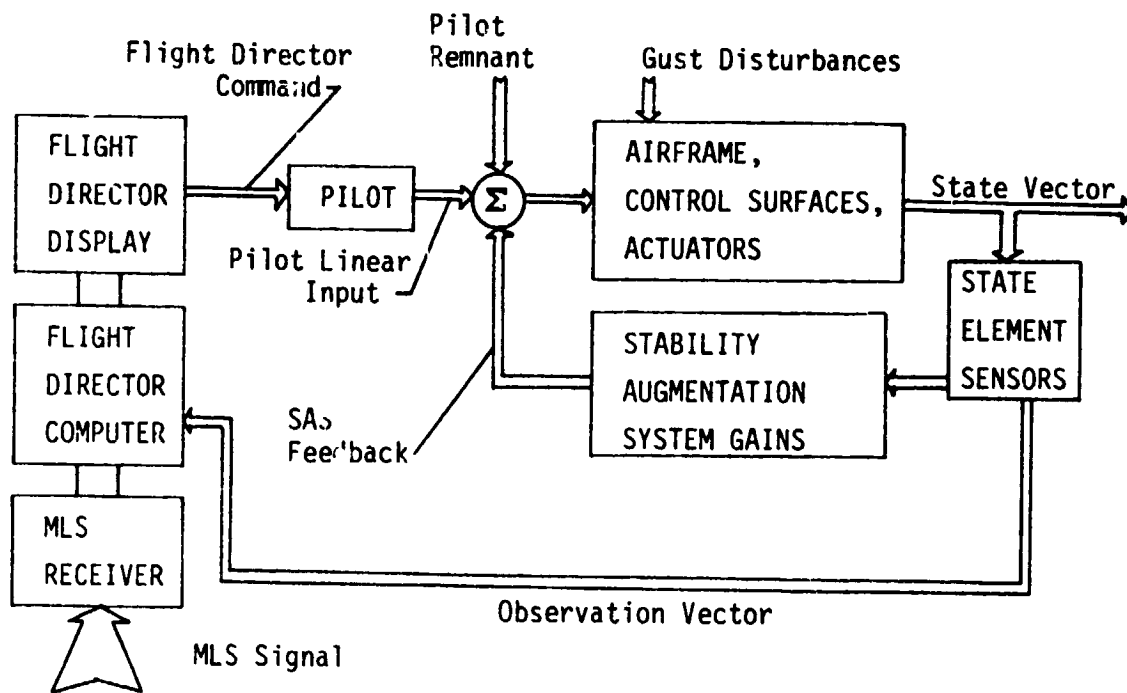


Figure 3

Piloted Aircraft System Diagram

Flight Director

The pilot was given a two-axis compensatory tracking task to control vertical and lateral path errors. The flight director commands were assumed to be presented on a cross-pointer display, and the pilot was assumed to be providing control inputs through the elevator and aileron. This control strategy was found to be inadequate for the longitudinal tracking task at the 111 kilometer/hour (60 knots) 98-degree flaps trim point even with stability augmentation feedbacks to both elevator and throttle. However, the strategy was adequate for the higher speed trim data used in this paper.

In the application of an overall optimal control system design concept, the flight director configuration and gains might be adjusted for each SAS gain set. However, for the purposes of this study, a simple configuration was chosen and the gains were fixed. The longitudinal mode command consisted of pitch attitude and vertical path tracking error feedbacks, and the lateral-directional command consisted of roll attitude, yaw attitude, and lateral tracking error feedbacks.

Since the pilot observed both tracking command pointer displacement and rate, the system observation vector contained both displacements and rates. This was represented by the system control equation for the longitudinal mode:

$$u = -Hy = -H \begin{bmatrix} y \\ \dot{y} \end{bmatrix} \quad (16)$$

To select the flight director gains, the problem was reformulated to introduce the gains into the control matrix as follows

$$u = -Hy = -HCx = -(HC_1) (C_0x) = -H_1y_2 \quad (17)$$

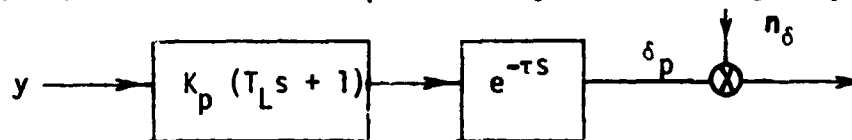
where the new control matrix is the product of the pilot gains matrix and the flight director gains

$$\begin{aligned} -H_1 = -HC_1 &= [K_p(K_p T_L)] \begin{bmatrix} 1 & K_{d_z} & 0 & 0 \\ 0 & 0 & 1 & K_{d_z} \end{bmatrix} \\ &= [K_p \quad (K_p K_{d_z}) \quad (K_p T_L) \quad (K_p T_L K_{d_z})] \end{aligned} \quad (18)$$

This optimal control problem was solved for the unaugmented system. As can be seen from equation (18), there are four expressions for the three unknown gains; so, the solution was only approximate, though satisfactory for this study.

Pilot Model

The mathematical pilot model was formulated in a manner similar to "paper pilot," reference 7. Two independent models consisting of gain, lead, delay, and remnant were introduced for the longitudinal and lateral-directional modes. Each model was represented by the following diagram,



The pure time delay was approximated by a first order Padé expression, and the equivalent pilot state vector equations for each mode became

$$\begin{aligned} \dot{x}_p &= - (2/ \tau) x_p + (4/ \tau) (K_p y + K_p T_L \dot{y}) \\ &= - (2/ \tau) x_p + (4/ \tau) u_p \end{aligned} \quad (19)$$

where the pilot control was

$$\begin{aligned} \delta_p &= x_p - (K_p y + K_p T_L \dot{y}) \\ &= x_p - u_p \end{aligned} \quad (20)$$

and the system control was

$$u = u_p = K_p y + K_p T_L \dot{y} \quad (21)$$

The time delay was selected to be $\tau = 0.3$ sec assuming a similarity of tracking tasks to that of reference 8. The remnant was represented as a first order filtered Gaussian white noise process with gain proportional to the variance of the system control

$$\dot{n}_\delta = -\omega_R n_\delta + \sigma_{u_p} \sqrt{\pi K_R} \eta_n \quad (22)$$

The remnant parameters were selected assuming scanning statistics similar to those of reference 8. Since the variance of the system control σ_{u_p} was present in equation (22), an iteration was required to achieve σ_{u_p} the final remnant level.

The final element of the pilot model was the quadratic performance index. A simple function, including the pilot state, the system control, and the flight director command was chosen

$$J = \frac{1}{2} \lim_{t \rightarrow \infty} \int_{\Omega} (q_x x_p^2 + q_y y^2 + q_u u_p^2) d\omega \quad (23)$$

This form assumed that the pilot was attempting to minimize the command tracking error while limiting his own control activity. The system control was required by the gradient algorithm.

The quadratic weights were chosen arbitrarily (in the absence of actual tracking data) to be $q_x = q_u = 1$, and $q_y = 100$.

The validity of this pilot model was partially verified by checking the pilot flight-director command open loop transfer function. The slope of the magnitude curve was found to be minus 20 dB/decade at a system cross over frequency between 3 and 4 radians/second. This agreed with the verbal rules for the model of reference 9. The phase margin was also ample.

Gust Model

The atmospheric turbulence model was taken from reference 4. The Dryden model for severe clear air turbulence was selected. The gust intensities were calculated at 30.48 meters (100 ft) altitude to be $\sigma_{u_i} = 1.98$ m/sec (6.5 fps), $\sigma_u = \sigma_v = 3.00$ m/sec (10 fps), and $\sigma_p = .074$ rad/sec. The horizontal intensity magnitudes were reduced from 4.88 m/sec (16 fps) as in reference 8. The statistically correlated equivalent pitch and yaw gust velocities were replaced as follows

$$q_g = -\dot{\alpha}_g, \quad r_g = \dot{\beta}_g \quad (24)$$

Since the model was anisotropic, it was necessary to transform the intensities for the banked flight cases by the following bank angle transformation

$$\sigma_{v_b}^2 = \sigma_w^2 \sin^2 \psi_0 + \sigma_v^2 \cos^2 \psi_0$$

$$\sigma_{w_b}^2 = \sigma_w^2 \cos^2 \psi_0 + \sigma_v^2 \sin^2 \psi_0$$
(25)

System Response

The results of the system response calculations are presented in this section. The rms vertical path tracking error is plotted versus longitudinal short period frequency in figure 4. The isolated point represents the unaugmented system where the short period frequency equivalent of the two real roots is plotted. The three augmented points have approximately the same damping (.7). There was little change in response due to damping, but there was a significant increase in vertical error due to increased short period frequency.

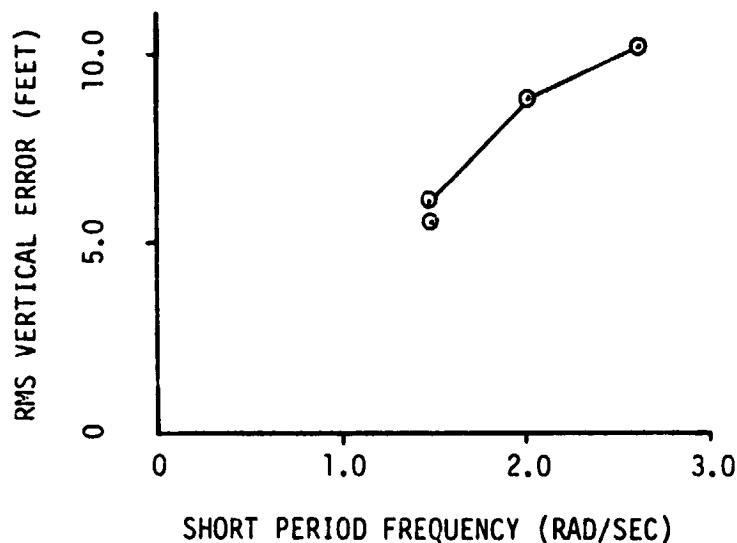


Figure 4

RMS Vertical Path Error

The rms lateral path tracking error is shown in figure 5. It can be observed immediately that the lateral error is an order of magnitude larger than the vertical error. For this reason, more attention was devoted to this mode. The circled point represents the unaugmented lateral-directional response. For the curves shown in figure 5, the roll and spiral poles were specified as -2.5 rad/sec, and -.07 rad/sec, respectively. Three damping ratios were specified (.290, .5, .707). For the family of three curves, the servo poles achieved were -43 rad/sec and -7 rad/sec. As more facility was gained in using the quadratic weights in the SAS design algorithm, the actuator state feedback gains were successfully reduced and the servo poles

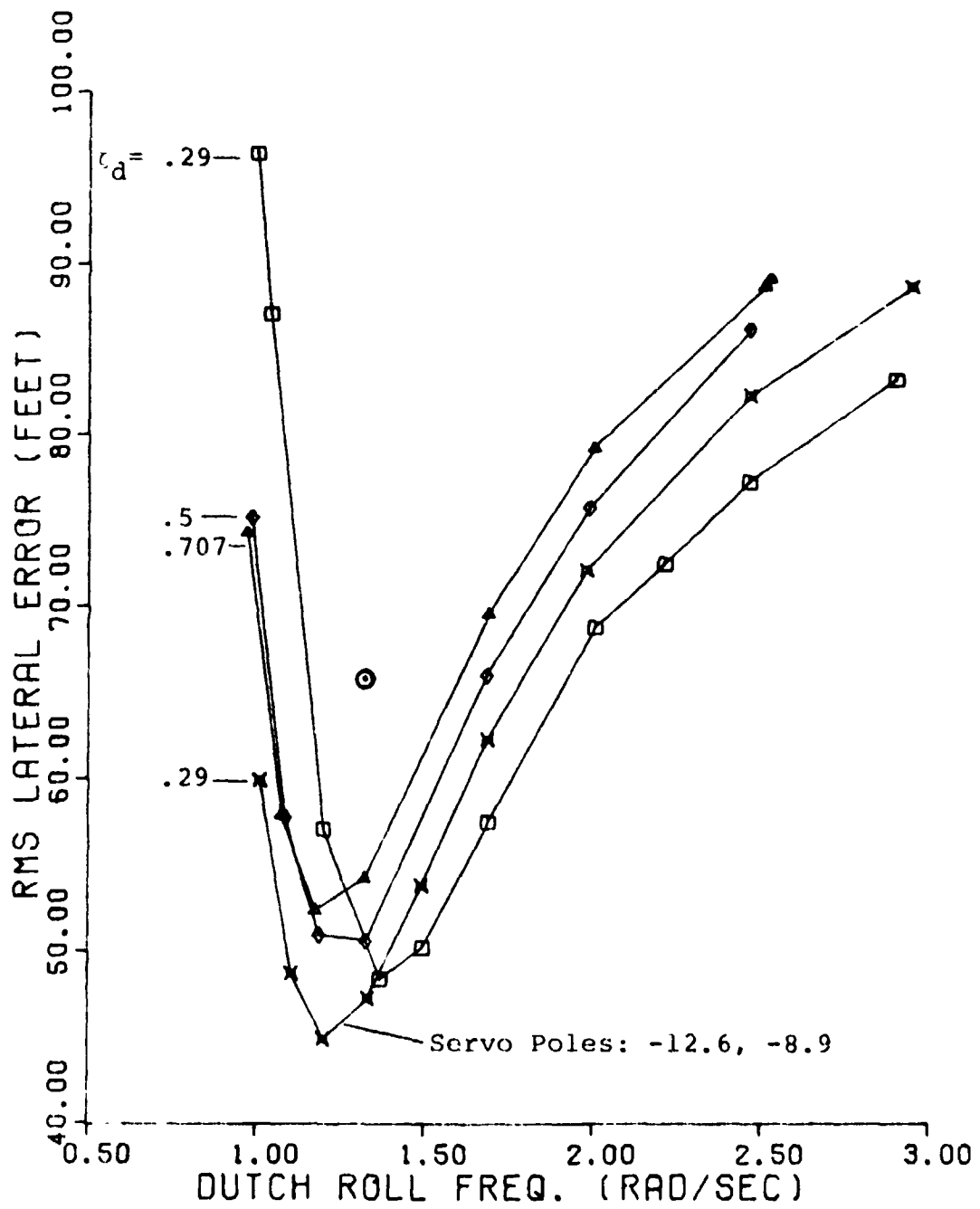


Figure 5

RMS Lateral Path Error versus Dutch Roll Frequency,
 105 Knots, $1/T_R = 2.5$, $1/T_S = .07$

restored nearer the unaugmented values. The fourth curve with crossed squares shows the response for poles of -12.6 rad/sec and -8.9 rad/sec. As shown in this figure, the rms lateral path tracking error increased slightly as damping was increased, but the increase was most significant as dutch roll frequency was increased above the unaugmented frequency. Below the unaugmented frequency there is a minimum point in each curve near a frequency of 1.2 rad/sec. There was also a small variation with servo poles. The most significant reduction in tracking error was achieved by increasing roll and spiral stability. The spiral stability was constrained for good turning performance, but the roll stability was increased until no further response improvement resulted, or until roll and servo pole coupling occurred. The lateral error response versus the roll pole is shown in figure 6.

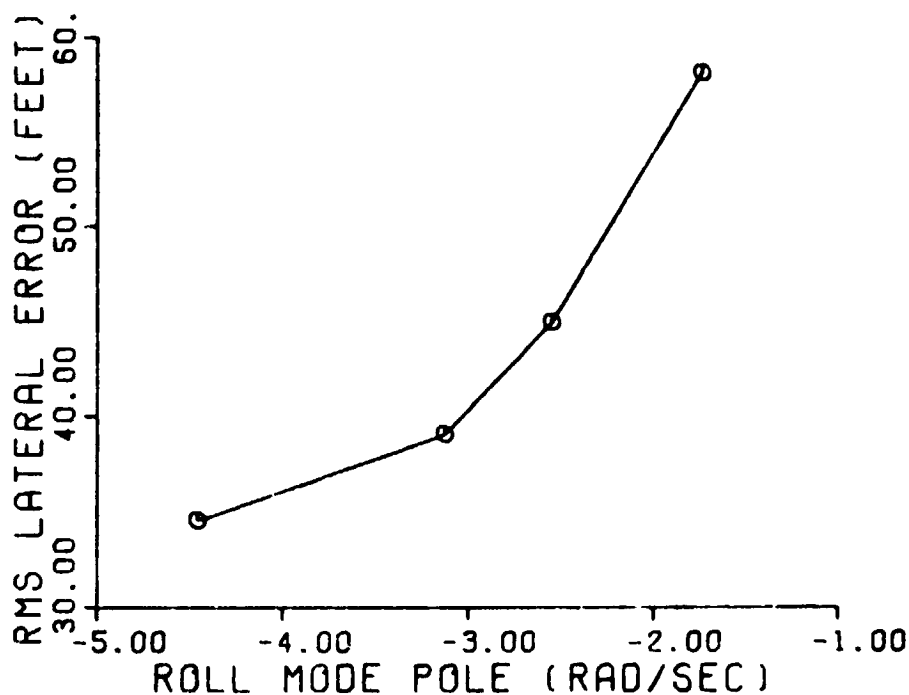


Figure 6

RMS Lateral Path Error versus Roll Mode Pole, 105 Knots,
 $\omega_d = 1.2$ rad/sec, $\zeta_d = .29$, $1/T_S = .07$

The Breguet 941 has a disturbing cross coupling between the lateral and directional modes. The amount of sideslip error due to aileron activity is a measure of this coupling. Figure 7 shows that the rms sideslip error decreased as the dutch roll frequency was increased. Unfortunately, this conflicts with the requirements for optimum lateral path tracking response which had the opposite trend with frequency.

Figure 8 shows the rms lateral path error versus bank angle for two dutch roll frequencies for the aircraft trimmed on a curved approach path.

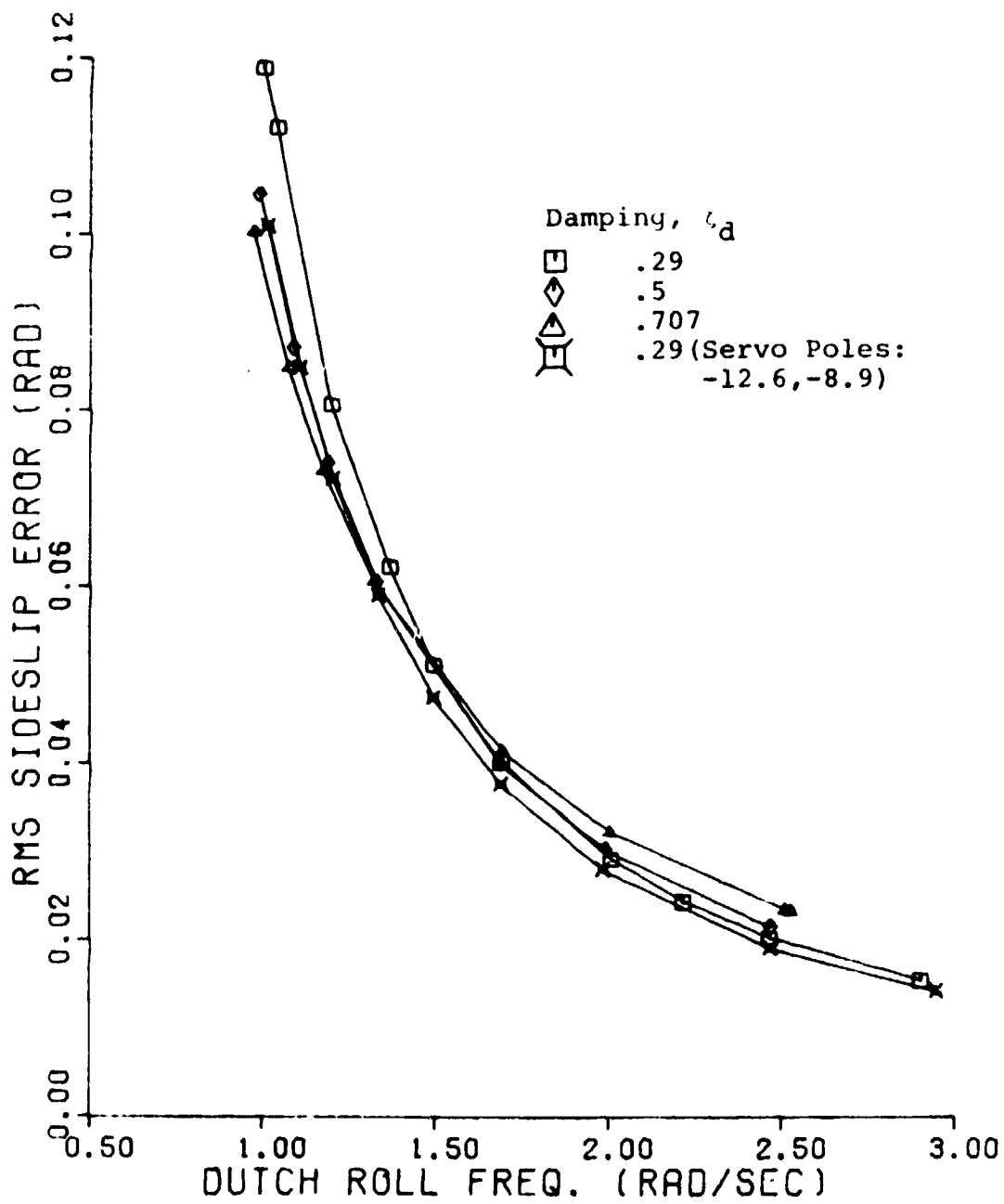


Figure 7

RMS Sideslip Error versus Dutch Roll Frequency, 105 Knots,
 $1/T_R = 2.5$, $1/T_S = .07$

For reference, for this trim airspeed of 194 kilometers/hour (105 knots) a horizontal turn with a radius of 762 meters (2500 feet) would correspond to a 21-degree bank angle. This figure shows that there is a smaller but significant variation in tracking error with bank angle, and this variation is also a function of the specific augmented poles.

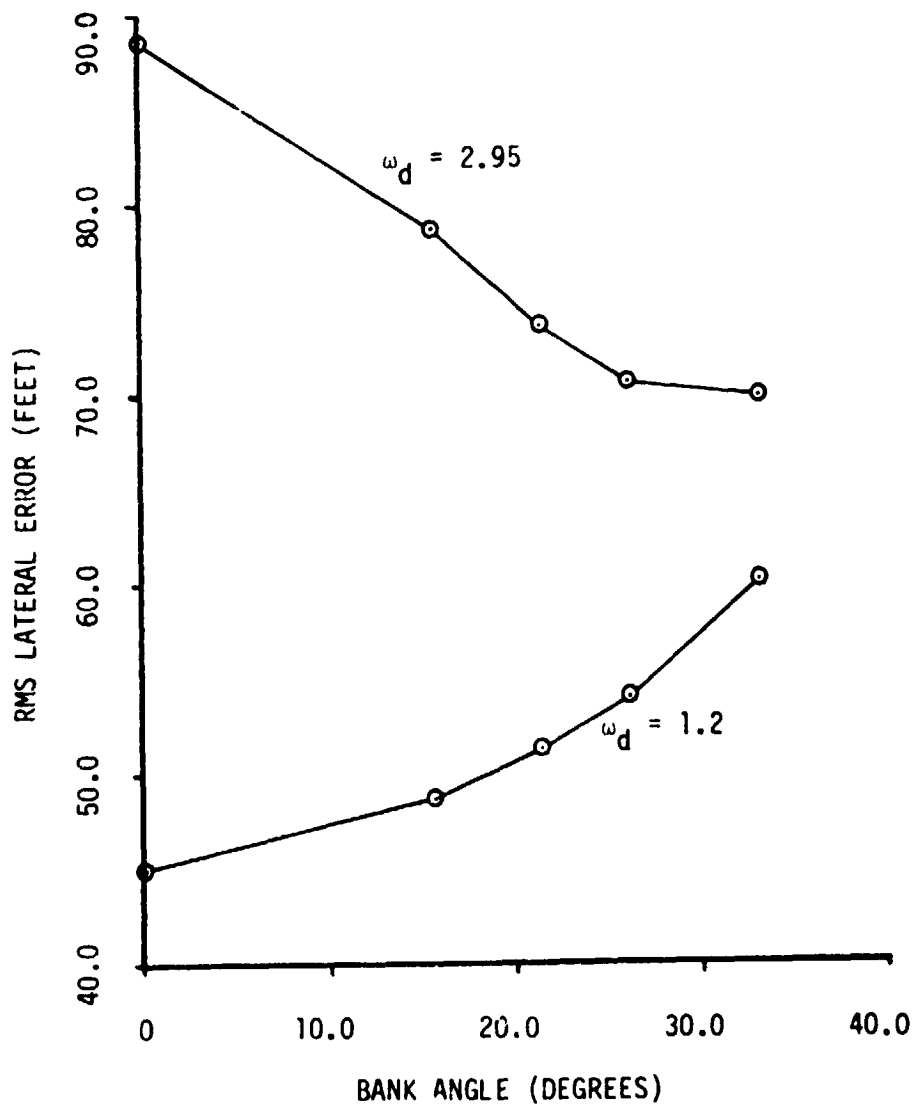


Figure 8
RMS Lateral Path Error versus Bank Angle

CONCLUSIONS

In conclusion, the SAS design algorithm worked efficiently to provide accurate pole placement, except for the phugoid poles, while yielding low feedback gains. The quadratic optimal pilot model compared well with previous frequency domain models and proved to be an efficient tool for calculating the system gust response. The gust response results showed that the lateral path tracking error was an order of magnitude greater than the vertical error. There was a plus and minus 50 percent variation in the lateral error for the augmented poles achieved in this study, and the lateral error was reduced most significantly by increasing roll stability. The conflict between optimum lateral path error and lateral and directional response decoupling implied a design trade-off. The lateral response error for banked flight was also dependent upon the specific augmented poles. Finally, one must bear in mind that the variation in gust response noted in this study was for augmented poles which all lay within the region of acceptable flying qualities as defined by existing specifications.

REFERENCES

1. Porter, Milton B.: The Effects of Stability Augmentation on the Gust Response of a STOL Aircraft During a Curved Manual Approach. PhD Thesis, Purdue University, 1975.
2. Heath, Robert E.: Optimal Incomplete Feedback Control of Linear Stochastic Systems. AFFDL-TR-73-36, 1973.
3. Van Dierendonck, A. J.: Design Method for Fully Augmented Systems for Variable Flight Conditions. AFFDL-TR-71-152, 1972.
4. Chalk, C. R., et al.: Background Information and User Guide for MIL-F-8785(ASG), "Military Specification - Flying Qualities of Piloted Airplanes." AFFDL-TR-69-72, 1969.
5. Anon.: Flying Qualities of Piloted V/STOL Aircraft. Military Specification, MIL-F-83300, 1970.
6. Innis, R. C., et al.: Airworthiness Considerations for STOL Aircraft. NASA TN D-5594, 1970.
7. Dillow, James D.: The "Paper Pilot" - A Digital Computer Program to Predict Pilot Rating for the Hover Task. AFFDL-TR-70-40, 1971.
8. Graham, D., et al.: Investigation of Measuring System Requirements for Instrument Low Visibility Approach. AFFDL-TR-70-102, 1971.

9. McRuer, D. T., et al.: Human Pilot Dynamics in Compensatory Systems: Theory, Model, and Experiments with Controlled Element and Forcing Function Variations. AFFDL-TR-65-15, 1965.

N75 33707

**SUBJECTIVE EVALUATION WITH FAA CRITERIA -
A MULTIDIMENSIONAL SCALING APPROACH**

by J. G. Kreifeldt, Ph. D.
L. Parkin, Ph. D. Candidate
Department of Engineering Design
Tufts University
Medford, Massachusetts 02155

T. E. Wempe, Research Scientist
E. F. Huff, Ph. D., Chief
Man/Machine Integration Branch
NASA-Ames Research Center
Moffett Field, California 94035

ABSTRACT

Decisions on modifications of the present ATC system are to be based at least partially on the FAA's global requirements for a safe, orderly and expeditious system. The difficulties in objectivizing measures for concepts such as orderliness in recent experimental simulations of distributed management alternatives to vectoring have led to studies of perceived orderliness in the ground tracks of five A/C during their simulated flights.

Dynamically developing ground tracks of the five A/C from 21 separate runs (7 conditions x 3 runs/condition) were reproduced from computer storage and displayed on CRTS to professional pilots and controllers for their evaluations and preferences under several criteria. The ground tracks were developed in 20 seconds as opposed to the 5 minutes of simulated flight using speed-up techniques for display.

Metric and nonmetric multidimensional scaling techniques are being used to analyze the subjective responses in an effort to (1) determine the meaningfulness of basing decisions on such complex subjective criteria, (2) compare pilot/controller perceptual spaces, (3) determine the dimensionality of the subjects' perceptual spaces and thereby (4) determine to the extent possible objective measures suitable for comparing alternative traffic management simulations based upon concepts such as "orderliness".

The work in progress will be discussed as to; the evidence for consistent ability to make these complex judgments; indications of differences

between pilots and controllers; and the dimensionality of perceived "orderliness" and other criteria.

INTRODUCTION

Three alternative ATC systems for managing terminal air traffic were simulated and studied during 1973 at NASA-Ames Research Center. The three alternatives could be characterized as ground-centered (vectoring), air-centered (advisory), and a more moderate division of control responsibility (sequencing). Of the three systems, sequencing proved superior on the basis of flight performance measures, verbal workload for pilots and controllers, and subjective evaluations.^{(1), (2), (3)} However, the FAA criteria for ATC systems are that they be safe, orderly, and expeditious and of these three criteria, orderliness is the most difficult to objectivize in a meaningful fashion. The relative safety and expeditiousness of the three simulated systems were determined from the flight performance measures in the context of the experiment with the result that sequencing was at least no less safe nor less expeditious than vectoring. Because it is apparently necessary to accept the criteria of "orderliness" as well in evaluating the three systems, and because, as mentioned above, no clear objective measures exist for this purpose, a multidimensional scaling approach using subjective evaluations of reconstructed ground projection movements of the 5 A/C in the problem was tried. This paper describes the initial work and results obtained to date.

Experimentally, it is necessary to demonstrate whether or not the alternative ATC systems differed in "orderliness" and if so, which system was most orderly. Since human observers serve as the evaluators, it is more to the point to determine if any of the systems is perceived as more orderly than the others. While it is not a priori clear that it is meaningful to ask humans to assess such vague qualities, the work of Pickett⁽⁴⁾ in particular suggests that in fact they can do so reliably and objectively in certain situations.

Actually, two features of the simulations were important in evaluating the results in addition to the previously reported comparisons--the relative orderliness of the systems just mentioned and any bias toward establishing starting configurations for the 5 A/C which were more favorable to accomplishing the problem under some conditions than others. For example, although starting positions for the A/C were randomized (from a finite set) among the conditions, it is possible that the generally inferior standing of vectoring could be due to less favorably situated starting positions. Favorableness of starting position, like orderliness, is difficult to objectivize in an a priori non-circular fashion and therefore estimates of "favorableness of starting position" were also obtained from human observers from reconstructed pictures of the starting positions.

Eleven professional pilots and eleven professional controllers served as expert witnesses in making the evaluations of favorableness of starting position and orderliness of the flights. As a precaution, none of the subjects took part in the original experiments which produced the data, although it is unlikely that the original subjects could recall which of the displayed ground projections and/or starting positions and ATC alternatives were associated.

Because pilots and controllers may be predisposed to "see things differently" because of their selective professions, this possibility was investigated as well.

In summary then, two major aspects were examined:

1. To what extent can human observers make reliable judgments of complex features? In particular, can "orderliness" of a system and any predisposition toward a favorable solution of the flight problem be subjectively evaluated?
2. Do the perceptions of the above features differ between pilots and controllers?

The purposes of these studies were:

1. To determine if any of the simulated ATC alternative systems was more orderly than the others following the FAA requirements for a safe, orderly, expeditious system.
2. To evaluate multidimensional scaling as a means for obtaining reliable estimates of similar subjective criteria in lieu of available objective measures.
3. To obtain if possible objective measures from the subjective scaling results to provide guidelines for directed design of other alternative ATC systems which when evaluated would possess a higher degree of orderliness.

METHODOLOGY

Although three different ATC systems (vectoring, sequencing, advisory) were evaluated in the original experiments, the sequencing and advisory conditions each had three levels of predictor information displayed on the pilots' traffic situation displays: no ground path flight predictors; a 30 sec. path predictor on own A/C only; 30 sec. path predictor on all 5 A/C. Thus, there were 7 different conditions. Sufficient data was stored from the original experiments to reconstruct the ground projected movements of all 5 A/C in dynamic fashion. Three runs of each of the 7 conditions (from one of the three original groups of pilots and controllers) were selected and presented to the human observers in paired comparison fashion on CRTS. The subject observers were not aware of the number of conditions nor the multiple runs precondition. The basic format for eliciting the subject responses was:

1. A pair of runs was presented simultaneously on a CRT. Each run showed 5 triangular A/C symbols. The original 5 minute run was speeded up to 20 sec. Each run was framed in a box so that the two boxes appeared side by side on the CRT.
2. The starting configurations remained stationary for 5 sec. during which the subject marked on a precoded sheet in effect:

- (1) "regarding the favorableness of the two starting configurations, if the two appear identically similar, write "9"; if they did not appear similar at all, write "0". Write any integer between (0,9) to express the degree of similarity of the favorableness of starting position."
- (2) "which one of the pair is more favorably situated (left or right)?"

3. After the 5 sec. allowed to record the above, the run commenced. The two runs were normalized to start and stop together in exactly 20 sec. Subjects saw the 5 A/C symbols move from their starting positions to their final positions for each run of the pair simultaneously. 10 seconds were allowed before the next run during which the subject marked on a precoded sheet in effect: (1) "regarding the orderliness of the two runs, if the two appeared identically similar write "9", if they did not appear similar at all, write "0". Write any integer between (0,9) to express the degree of similarity of the orderliness of the two runs.
(2) "which one of the pair was more orderly (left or right)?"

Presentation of all 210 pairs of the 21 runs required about 3 hours with rest periods every 70 presentations. Subjects were familiarized with the notion of judging similarity within each pair on a scale of 0 to 9 and received trial runs outside the selected set for practice. Subjects saw all 21 runs individually prior to making the 210 pair comparison runs in order to establish the range of the presentations.

The results of the scaling were analyzed by INDSCAL computer programs developed by Carroll and Chang⁽⁵⁾. The INDSCAL acronym stands for Individual Differences in Scaling and assumes basically that there is a common perceptual space which all the subjects share but that each subject differs by the amount of importance or weighting attached to each dimension of this common space.

This multidimensional scaling approach seeks to present a literal picture of the subjective space in which the (21) alternatives in question are arranged in a geometric configuration such that the metric distance between alternatives measures their perceived similarity. The closer together any two objects are, the more similar they are. INDSCAL also produces a literal picture of the subjects themselves arranged in the same dimensional space such that their relative position along each axis represents the relative weighting each attaches to that dimension. It is thus possible to make simultaneous comparisons among the alternatives as well as among the "perceivers" from a single program. Other programs are being used to determine the relative ordering by each subject of the 21 runs on "orderliness" and "favorableness of starting position."

It should be remarked here that it would have been impossible for a subject to rank order each run on a single scale of orderliness for example because the dynamic method of presenting the ground projections precluded

the usual "juggling" of the set of alternatives by the subject to an acceptable order. Also, although each single run could presumably be scaled from (0,9) and rank order then determined, little information is obtainable from this regarding the dimensions of orderliness. The paired comparison format is an easy and fairly natural method for evaluation and the analysis by INDSCAL can provide insightful information.

Because it is unwise to depend entirely on the results of any single scaling program, a nonmetric program⁽⁶⁾ was also used to analyze the data in a slightly different fashion for supporting purposes to establish whether or not the subjects were responding randomly or not.

DATA ANALYSIS

The similarities data were analyzed using both nonmetric and metric multidimensional scaling algorithms on the DEC SYSTEM 10 at Tufts University. These programs are described below.

Nonmetric Algorithm

The nonmetric algorithm used in our analysis was written by Prof. F. E. Curry of M.I.T. This program accepts a triangular input matrix containing the proximities data from one subject. The order of the input matrix is equal to the number of stimuli (n) and the rank order of a matrix element d_{jk} is assumed to be a measure of the amount of similarity between stimulus j and stimulus k . Thus, the algorithm requires only that the data be at least ordinal scaled.

The objective of the analysis is to represent the stimuli as points in an r dimensional euclidean space such that r is the minimum number of dimensions for which the rank order of the interstimulus distances d_{jk} can be made equal to, or closely match, the rank order of the corresponding data element d_{jk} . Bennet and Hays⁽⁷⁾ have shown that a configuration whose distances are monotone with even the most complex set of data on n stimuli exists in a space of no more than $n-1$ dimensions.

The process of nonmetric multidimensional scaling upgrades the data from an ordinal scale toward a ratio scale in the sense that it applies a set of $n(n-1)/2$ rank order constraints to the euclidean distances between n points represented as nr coordinates. As the number of constraints increases relative to the number of coordinates, the allowable values of the coordinates become increasingly restricted. By finding the lowest solution dimensionality r which permits a satisfactorily monotone fit to the data, one maximizes the ratio of constraints to coordinates and therefore maximally upgrades the data toward a ratio scale.

Since the existence of a satisfactory configuration for n stimuli is guaranteed in $n-1$ or fewer dimensions, the problem is to find the configuration. The nonmetric program first reads and stores the observed proximities data. The rank of each proximity datum pair is determined. If a group of elements have equal numerical value, each of the tied elements is assigned the same median rank. For example, if five elements have the value of zero and

no elements are in the set of lower value, then each of the five elements is assigned the median rank value of 3.

The program then obtains an r dimensional initial stimulus configuration of coordinates x_{jt} , where the first subscript denotes the stimulus and the second subscript denotes the dimension. This may be accomplished by one of three available techniques. The initial coordinates may be read in as data; they may be produced by a random number generator; or they may be generated from the proximities data by a procedure devised by Guttman and Lingoes⁽⁸⁾. The Guttman Lingoes procedure was used in our analysis.

The initial configuration serves as a starting point for an iterative process which hunts for the best fitting stimulus configuration. The first step translates the origin of the coordinate system to the centroid of the assumed stimulus configuration. The coordinates are then scaled by dividing each coordinate by the mean of the distances from the origin to the stimulus points. The distances d_{jk} between stimulus points are calculated and ranked. At this point, the option of reassigning ranks within groups of tied elements in the set of observed data δ_{jk} was used to produce maximum agreement between the rank values of the observed data and the corresponding calculated distances. If this option is not elected, each element within a tied group retains the group's median rank value, implying that the calculated distances corresponding to these elements ought to have equal values. The rank values of the elements in the observed data $R(\delta_{jk})$ are then compared with the rank values of the corresponding calculated interstimulus distances $R(d_{jk})$ to determine the rank discrepancy e_{jk} .

$$e_{jk} = R(\delta_{jk}) - R(d_{jk}) \quad (1)$$

The rank stress s_r for the stimulus configuration may now be calculated by the formula

$$s_r = \left(\sum_j \sum_k \frac{e_{jk}^2}{2} \right)^{1/2} \quad (2)$$

This is a measure of the goodness of fit between the observed data and the model. The rank stress is related to the Spearman rank correlation coefficient r_s by the formula

$$r_s = 1 - \left(\frac{12 s_r^2}{n(n^2-1)} \right) \quad (3)$$

The final step in an iterative cycle is to determine a better fitting stimulus configuration. An error gradient g_{jt} is calculated for each coordinate x_{jt}

$$g_{jt} = \sum_k \frac{e_{jk} (x_{jt} - x_{kt})}{\left(\sum_t (x_{jt} - x_{kt})^2 \right)^{1/2}} \quad (4)$$

The new coordinate X_{jt} is calculated from the old coordinate x_{jt} by the equation

$$X_{jt} = x_{jt} + c q_{jt} \quad (5)$$

The value of c , the step size at each iterative cycle, is a function of the rate of convergence of the solution as indicated by the history of the rank stress in previous iterative cycles.

The iterative process may be terminated upon completing a preselected number of iterations or upon reaching a preselected value of rank stress, whichever occurs first. The final configuration is then rotated to a principal components solution, with the dimensions ordered by the proportion of variance accounted for by the dimension.

Fifty-five sets of proximities data were analyzed in 10, 8, 6, 4 and 2 dimensions by the nonmetric program. Each solution was obtained by performing 30 iterations of the algorithm. There were eleven sets of observations for each of the following four categories: pilots' judgments on the degree of similarity of difficulty of the starting configuration of the landing simulation, controllers' judgments on the same; pilots' judgments on the similarity of orderliness of the dynamically displayed movements; and controllers' judgments on the same. In addition, eleven sets of data were produced by a random number generator such that the random sets contained the required number of elements, uniformly distributed in the same range as the data from the pilots and controllers. These eleven random sets were also processed by the algorithm for comparison with the real data.

The results of the nonmetric analysis are presented in Figure 1. The figure shows the means of the rank stress and corresponding Spearman rank correlation coefficients for the five classes of data as a function of the number of dimensions in the solution. The ordinates are measures of the degree to which the nonmetric models agree with the data.

The standard deviations about the plotted means are not shown. However, they were quite uniform at each solution dimensionality, varying from about 10, for the 10 dimensional solutions to about 40, for the 2-dimensional solutions.

The most striking feature of Figure 1 is that the stresses for solutions resulting from the four classes of data from real subjects group closely together, whereas the stress for the solutions resulting from data in which the ranks were randomly assigned are much higher. The difference between the random sets and each of the other sets was significant beyond the .1% level.

Although there was no statistical difference (at the .1% level) between pilots and controllers, at each dimension, the curves do suggest a slight difference such that controllers were uniformly slightly less consistent in making their judgments than were the pilots. (An Analysis of Variance would probably confirm this observation.)

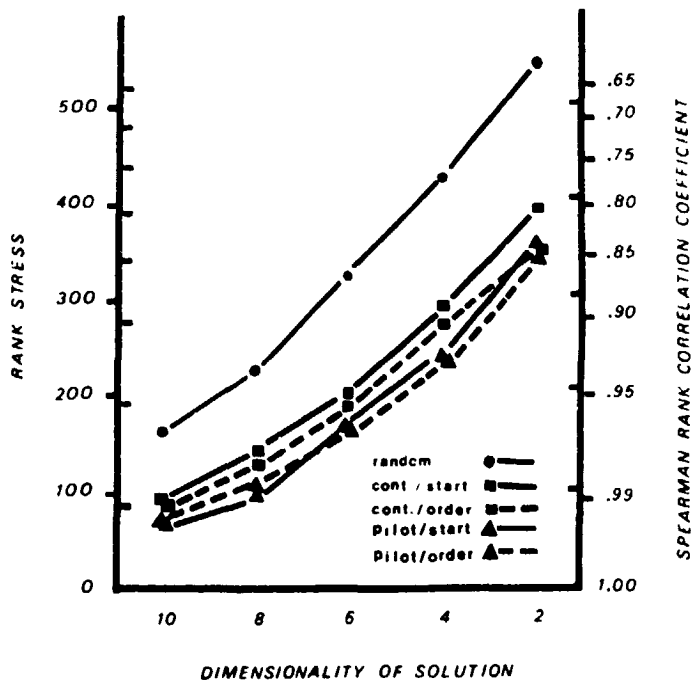


Figure 1 Rank Stress and Spearman Rank Correlation Coefficient Resulting from Nonmetric Scaling of Similarities Data.

These curves show the typical result that the "fit" becomes better as more dimensions are permitted even for the random data. However, it is possible to conclude from this limited nonmetric analysis that in fact the subjects were responding with a fair degree of consistency in making their paired comparison judgments of similarity. The minimum dimensionality of their perceptual spaces for a satisfactory fit (each was analyzed separately) appears to be on the order of 5-8 dimensions. (Actually the Guttman-Lingoes portion of the program indicated conservatively 10 dimensions as an adequate number.)

Metric Algorithm

The metric algorithm used for analysis is the INDSCAL program written by Carroll and Chang of Bell Laboratories. This algorithm is described in detail in references 5, 9 and 10. However, a brief description is given below.

INDSCAL is a metric algorithm since one of its underlying assumptions is that the data are interval scaled. Figure 2 is a representation of the input data.

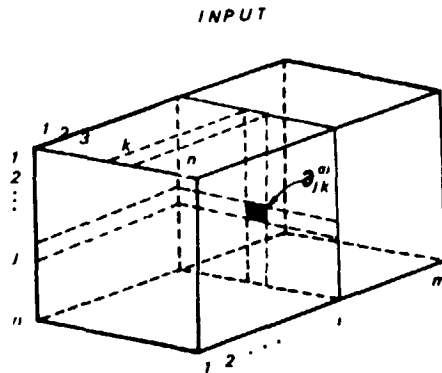


Figure 2 The Three-Way Input Data Matrix of Similarities for INDSCAL. Subjects are Numbered (1-m). Stimuli Numbered (1-n).

The input is in the form of a three-way matrix (n by n by m) of proximities data elements $d_{jk}^{(i)}$. The value of an element is assumed to be an estimate of the amount of similarity between stimulus j and stimulus k as judged by observer i.

The INDSCAL model is described by the following equations.

$$L_i [d_{jk}^{(i)}] \approx d_{jk}^{(i)} \quad (6)$$

where $L_i []$ is a linear operator and the distances $d_{jk}^{(i)}$ in the stimulus space are given by

$$d_{jk}^{(i)} = \left[\sum_t^r w_{it} (x_{jt} - x_{kt})^2 \right]^{1/2} \quad (7)$$

This model gives a representation of observed data as stimulus coordinates x_{jt} in a stimulus space which is common to all observers. In addition, a set of individual subject weights w_{it} are determined which scale dimension t in the stimulus space according to subject i's perception. The common stimulus space x_{jt} and the subject weights may be used to generate a stimulus space $y_{jt}^{(i)}$ which is appropriate to subject i.

$$y_{jt}^{(i)} = (w_{it})^{1/2} x_{jt} \quad (8)$$

The output from the INDSCAL program is, therefore, a rectangular array of stimulus coordinates x_{jt} and a second rectangular array of subject weights w_{it} as represented in Figure 3.

The analysis begins by adding a constant c_i to each element $d_{jk}^{(i)}$ of subject i's data to approximate a set of ratio-scaled observed distances $\hat{d}_{jk}^{(i)}$

$$\hat{d}_{jk}^{(i)} = d_{jk}^{(i)} + c_i \quad (9)$$

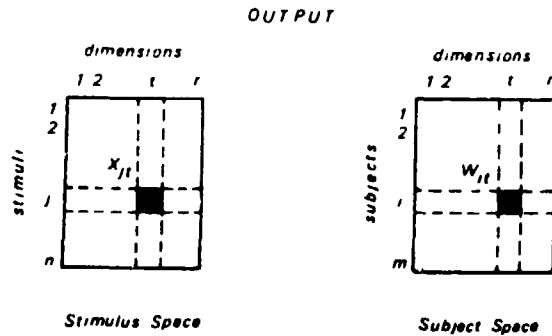


Figure 3 The Two Output Matrices from INDSCAL. A Group Stimulus Space Matrix and the Individual Subject Weights on each Dimension are Produced Simultaneously.

The constant c_i is given by

$$c_i = \max_{(j,k,l)} [\hat{\delta}_{jl}^{(i)} - \hat{\delta}_{jk}^{(i)} - \hat{\delta}_{kl}^{(i)}] \quad (10)$$

and has the effect of insuring that the triangular inequalities are satisfied.

A three-way scalar products matrix $b_{jk}^{(i)}$ is then constructed from the observed distances $\hat{\delta}_{jk}^{(i)}$ using Torgerson's equation (11).

$$b_{jk}^{(i)} = \frac{1}{2} \left[\hat{\delta}_{jk}^{(i)} - \frac{1}{n} \left(\sum_j (\hat{\delta}_{jk}^{(i)})^2 + \sum_k (\hat{\delta}_{jk}^{(i)})^2 - \sum_j \sum_k (\hat{\delta}_{jk}^{(i)})^2 \right) \right] \quad (11)$$

The scalar products matrix is now used to obtain the stimulus coordinates and subject weights by canonical decomposition. This process attempts to express the elements of the scalar products matrix as the sum (over dimensions) of a three factor product:

$$b_{jk}^{(i)} = \sum_t^r w_{it} X_{jt}^{(L)} X_{kt}^{(R)} \quad (12)$$

An initial stimulus configuration is either input by the analyst or generated by a random number generator. The decomposition is accomplished by repetition of a three step iteration cycle until a preselected number of cycles have been performed or until successive cycles fail to increase significantly the variance in the scalar products matrix which is accounted for by the model.

The first step in a cycle is described by rewriting equation (12) as:

$$b_s^{(i)} = \sum_t^r w_{it} y_{st} \quad (13)$$

where:

$$y_{st} = X_{jt}^{(L)} X_{kt}^{(R)} \quad \text{and: } s = n(j-1) + k$$

This may be written in matrix form as:

$$B = NG^T \quad (14)$$

The least squares solution W^* for the weight matrix W is:

$$W^* = BG(G^T G)^{-1} \quad (15)$$

In the second step, w_{it}^* and $x_{kt}^{(R)}$ are held constant and improved values for $x_{it}^{(L)}$ are sought. The scalar products matrix is expressed as:

$$b_{ju} = \sum_c \sum_t x_{jt}^{(L)} x_{ct}^{(R)} \quad (16)$$

where:

$$h_{ut} = w_{it}^* x_{kt}^{(R)} \quad \text{and: } u = m(i-1) + k$$

This may be expressed in matrix notation as:

$$B = X^{(L)} H^T \quad (17)$$

The least squares solution $X^{(L)*}$ for $X^{(L)}$ is given by:

$$X^{(L)*} = BH(H^T H)^{-1} \quad (18)$$

The estimate of $X^{(L)}$ is improved in the third step, which follows the arguments of the first two steps.

Although no explicit constraint is applied to insure that $X^{(L)}$ equal $X^{(R)}$ during the decomposition process, the symmetry of the scalar products matrix $b_{jk}^{(L)} = b_{kj}^{(L)}$ insures that the two matrices of stimulus coordinates will be equivalent in the sense that:

$$\begin{aligned} X^{(L)} &= C X^{(R)} \\ X^{(R)} &= C' X^{(L)} \end{aligned} \quad (19)$$

where C is an r by r matrix with nonzero diagonal elements.

INDSCAL runs were made on the observed proximities data to produce solutions in dimensionalities from 2 through 5. Both the observations on starting configurations and those on orderliness were studied by examining solutions resulting from three separate subject groupings: the eleven pilots as a group; the eleven controllers as a group; and all twenty-two subjects combined.

Table 1 summarizes the percentage of variance in the data accounted for by each dimension of the INDSCAL runs done by grouping both pilots and controllers together. Results from both "favorableness of starting position" and "orderliness of the flights" are presented. Similar data was obtained for pilots and controllers as two distinct groups and in general appears quite similar to that shown.

Table 1
 PER CENT OF TOTAL VARIANCE
 ACCOUNTED FOR BY INDSCAL SOLUTIONS

ORDER DATA

		dimensions					
		1	2	3	4	5	total
solution dimensionality	5	13.1	10.4	7.1	6.5	6.0	43.0
	4	14.0	10.9	8.6	5.9		39.4
	3	14.5	12.4	8.2			35.0
	2	17.5	13.0				30.5

START DATA

		dimensions					
		1	2	3	4	5	total
solution dimensionality	5	15.2	13.2	7.2	5.3	5.1	46.0
	4	13.5	13.4	9.1	8.0		44.0
	3	16.1	12.9	9.9			40.0
	2	17.4	15.1				32.5

The total percentage of variance accounted for by a solution is computed as the square of the correlation between the elements of the scalar products matrix b_{jk} (equation 11) and the corresponding element (right side of equation 12) resulting from the INDSCAL solution. The variance accounted for by each dimension t is computed by multiplying the total variance percentage by the fraction f_t of the total sum of squares of subject weights w_{it} which originates from dimension t .

$$f_t = \left(\sum_i^m w_{it}^2 \right) / \left(\sum_t^r \sum_i^m w_{it}^2 \right) \quad (20)$$

Increasing the number of dimensions increases the variance accounted for which is typical. The dimensions themselves are ordered in descending fashion on the amount of variance accounted for so that dimension 1 of the 4 and 5 dimensional solution, for example, is not necessarily the same. Further analyses are required in order to identify the meaning of each dimension.

A great virtue of INDSCAL is its ability to provide a subject configuration which is interpretable in several ways. Distance from the origin corresponds to the degree of fit between the subject's original data and that derived from applying his set of weights on each axis to the general solution. A subject at the (1,1) coordinate in a 2 dimensional space, for example, indicates perfect agreement between data and its reconstruction, while a subject at the origin indicates no agreement.

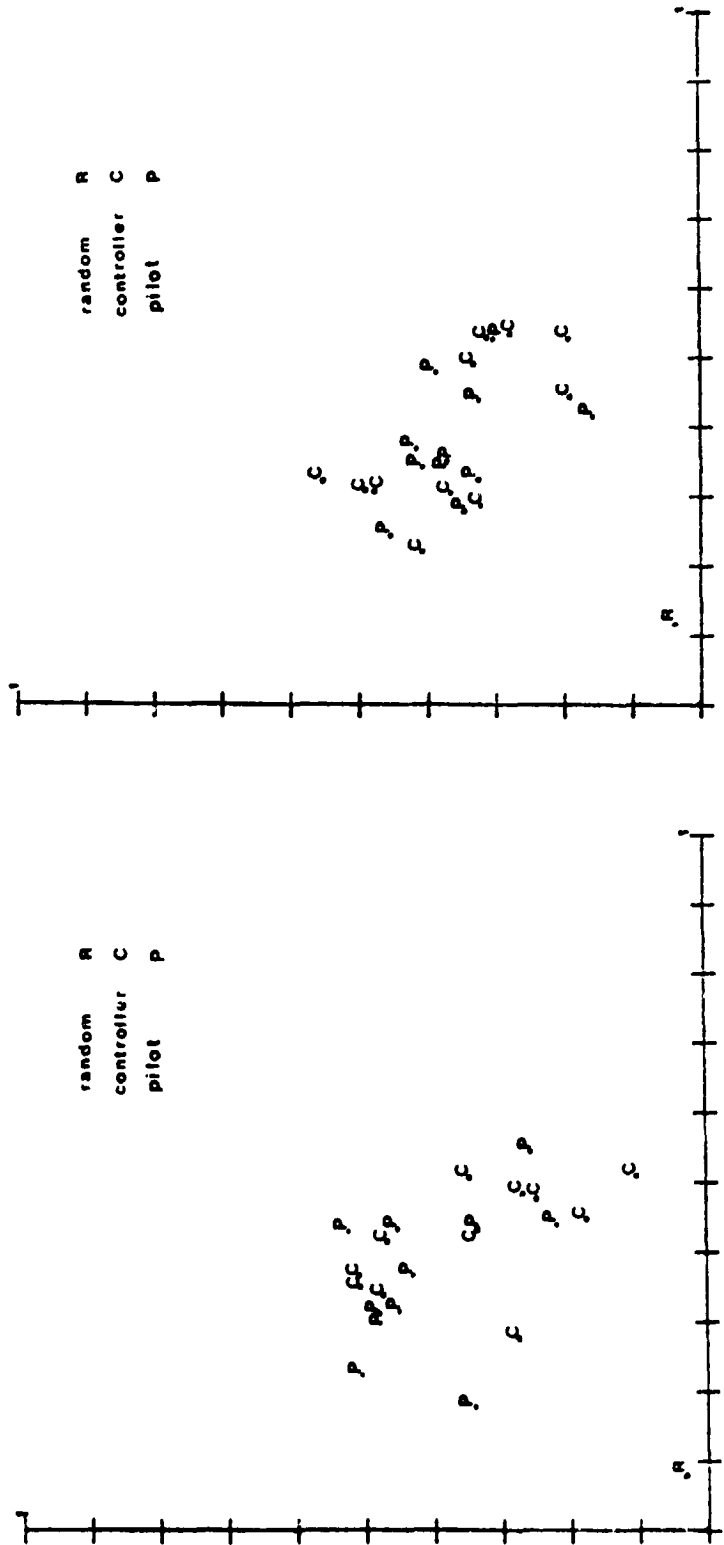
To test for the amount of "randomness" in the subject data a subject similarity matrix made of randomly assigned integers was included in the total group analysis as a check similar to the check procedure used in the nonmetric analysis.

Figure 4 shows the plots of the subject spaces w_{it} for two dimensional INDSCAL models of starting configuration data and orderliness data, respectively. Each of these runs included all twenty-two pilots and controllers as well as one random "subject."

It is clear that the subjects are in fact considerably removed from the random subject, indicating that they appear able to make internally consistent judgments to a significant extent on orderliness of the flights, for example. In this 2 dimensional solution, the correlation between data and the model was approximately 0.12 for the random subject, while the actual subjects had a median correlation of about .58.

There is a suggestion (not yet tested) that pilots attached more importance to the second dimension of the start data than did the controllers in this two dimensional analysis, indicating a possible difference in pilots' and controllers' perception of a favorable starting position. No clear distinction is present between the pilot and controller perceptions of orderliness.

Figure 5a shows the stimulus space x_{it} for a two dimensional model of starting configuration data taken from the eleven pilots. Figure 5b is the equivalent plot resulting from the controllers' data. Figure 6 is the two dimensional stimulus space resulting from combining the starting configuration data from all twenty-two subjects in one run.



SUBJECT SPACE: ORDER DATA

2 DIM SOLN

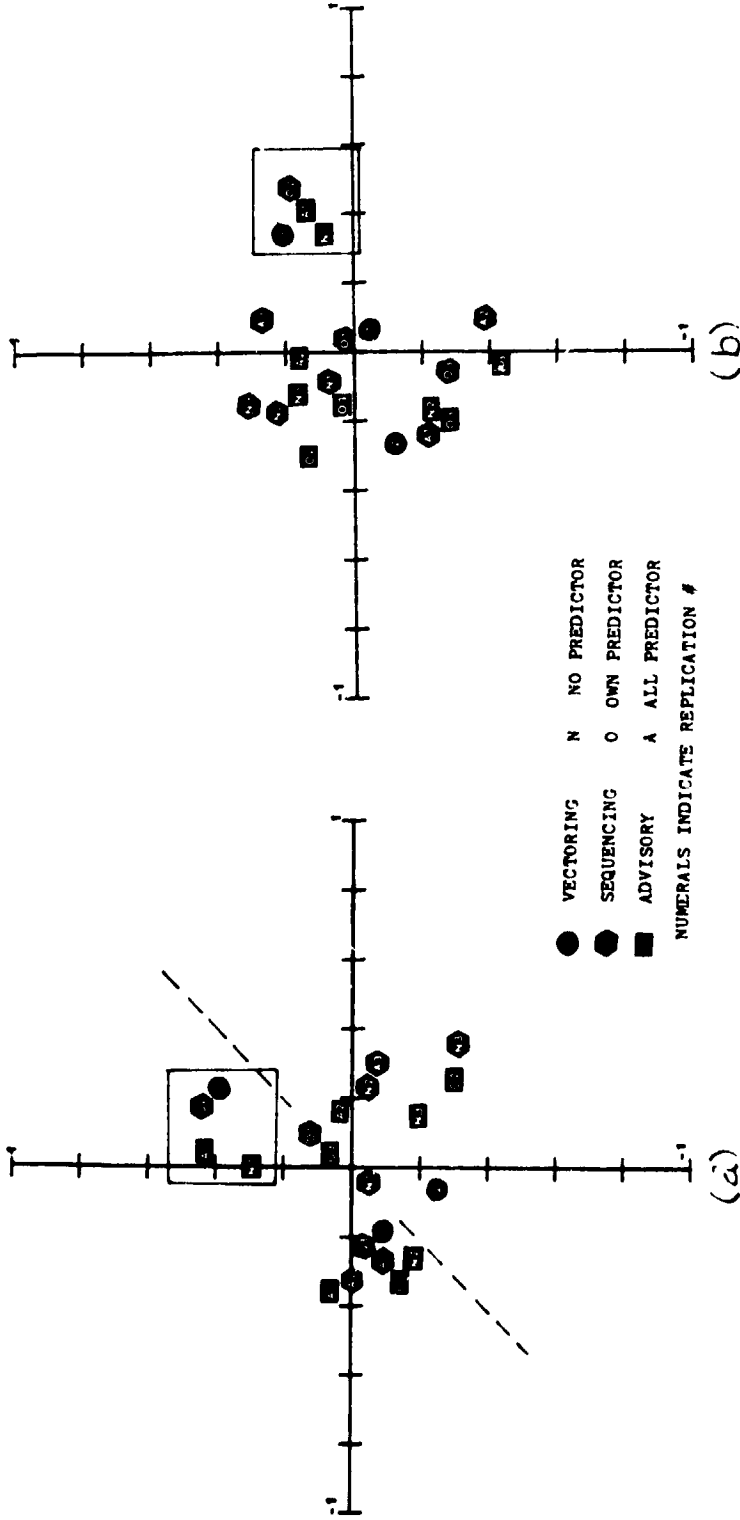
AXIS 1: HOR 2: VERT

SUBJECT SPACE: START DATA

2 DIM SOLN

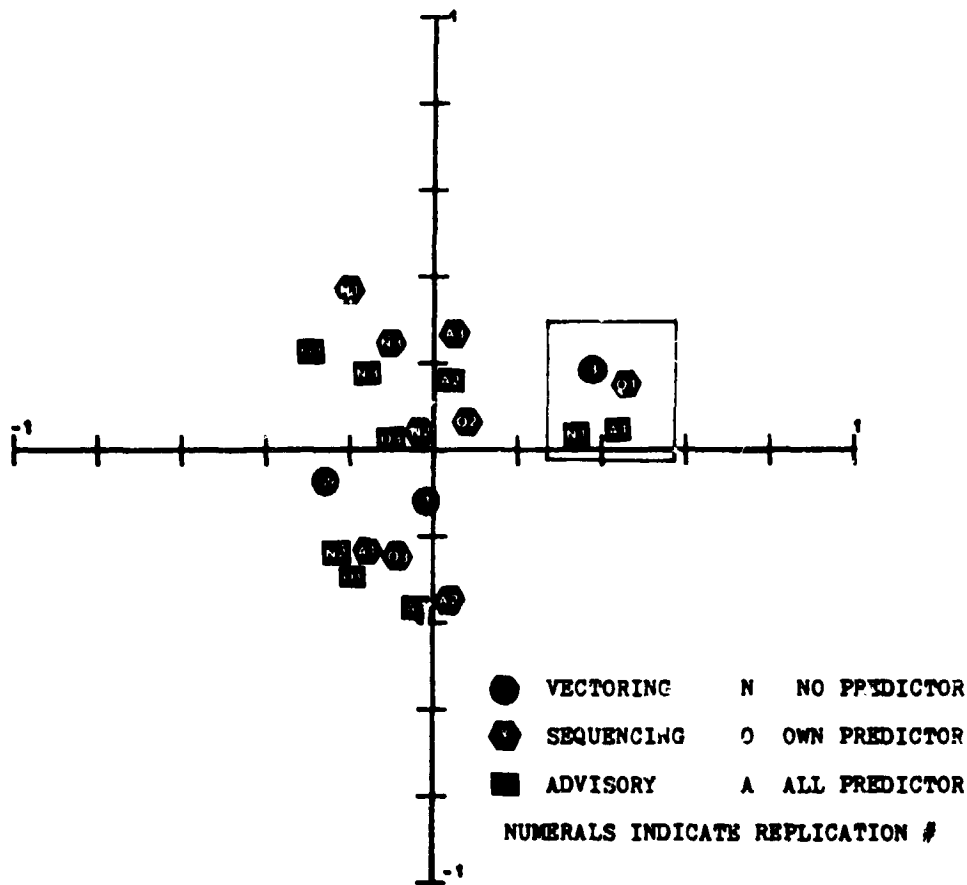
AXIS 1: HOR 2: VERT

Figure 4 Two Dimensional INDSCAL Subject Spaces from Judgments on Favorableness and Orderliness. Random Data Results are Included for Comparison.



(a) STIMULUS SPACE: START DATA 2 DIM SOLN PILOT ONLY AXIS 1: HOR AXIS 2: VERT
 (b) STIMULUS SPACE: START DATA 2 DIM SOLN CONTROLLER ONLY AXIS 1: HOR AXIS 2: VERT

Figure 5 Two Dimension INDSCAL Stimuli Spaces for the Favorableness Data. Pilot and Controller Groups Analyzed Separately. A High Degree of Organizational Correspondence is Indicated Particularly if Pilot Axes 1 and 2 are Interchanged.



STIMULUS SPACE: START DATA

2 DIM SOLN

AXIS 1: HOK

AXIS 2: VERT

Figure 6 Two Dimensional Group Stimulus Space for Pilots and Controllers Combined. The Boxed Stimuli may be Compared in Figures 5 and 6. No Cluster Patterns by Condition Should be Evident for Start Data.

The same four stimulus items appear in the box in the upper right quadrant of each group plot. Since each analysis was independently derived, this indicates that the data generated by each group results in very similar perceptual models demonstrating that the complex stimuli were very similarly perceived by the subjects. If the pilots' configuration were rotated about the dotted line, the pilot and controller plots would be almost identical. Figure 6 shows the analysis of the combined pilot-controller data and is quite similar to the individual group plots.

Two aspects of the plots are important. The first is that there does not seem to be any strong pattern of the stimuli within each plot. For example, the vectoring runs were not perceived as being similarly situated for favorableness of starting position as shown by their spread on each plot. The "scatter shot" pattern is in fact an indication that the favorableness of starting positions was more or less evenly distributed among the conditions as intended. This is important since there were no a priori measures available for evaluating this possibility. The second aspect is that there was in fact some sort of difference in perceived starting position favorableness as shown by the similarity of the two independent plots and by the individual subject correlation coefficients differing from that obtained from random subjects.

Figures 7a, 7b and 8 correspond to Figures 5a, 5b and 6 respectively except that the orderliness data plots are presented instead of starting configuration data.

As in the previous figures, these plots show considerable consistency among themselves. The manner in which some of the stimuli are grouped together constitutes another notable feature of these plots. The three advisory-own predictor runs (rectangles O1, O2, O3) group closely together in the lower right quadrant of these figures. Likewise the sequencing-own predictor runs (hexagons O1, O2, O3) and the sequencing-all predictors runs (hexagons A1, A2, A3) seem to be grouped together, suggesting some consistency in the degree of orderliness of these similar conditions. This might be further evidence that predictors tend to reduce variability, in this case, of orderliness. Again, the 3 vectoring runs (circles) are well separated evidencing their low inter-similarity of orderliness. It is not possible at this stage to say which conditions were perceived as more orderly, although this analysis is in progress.

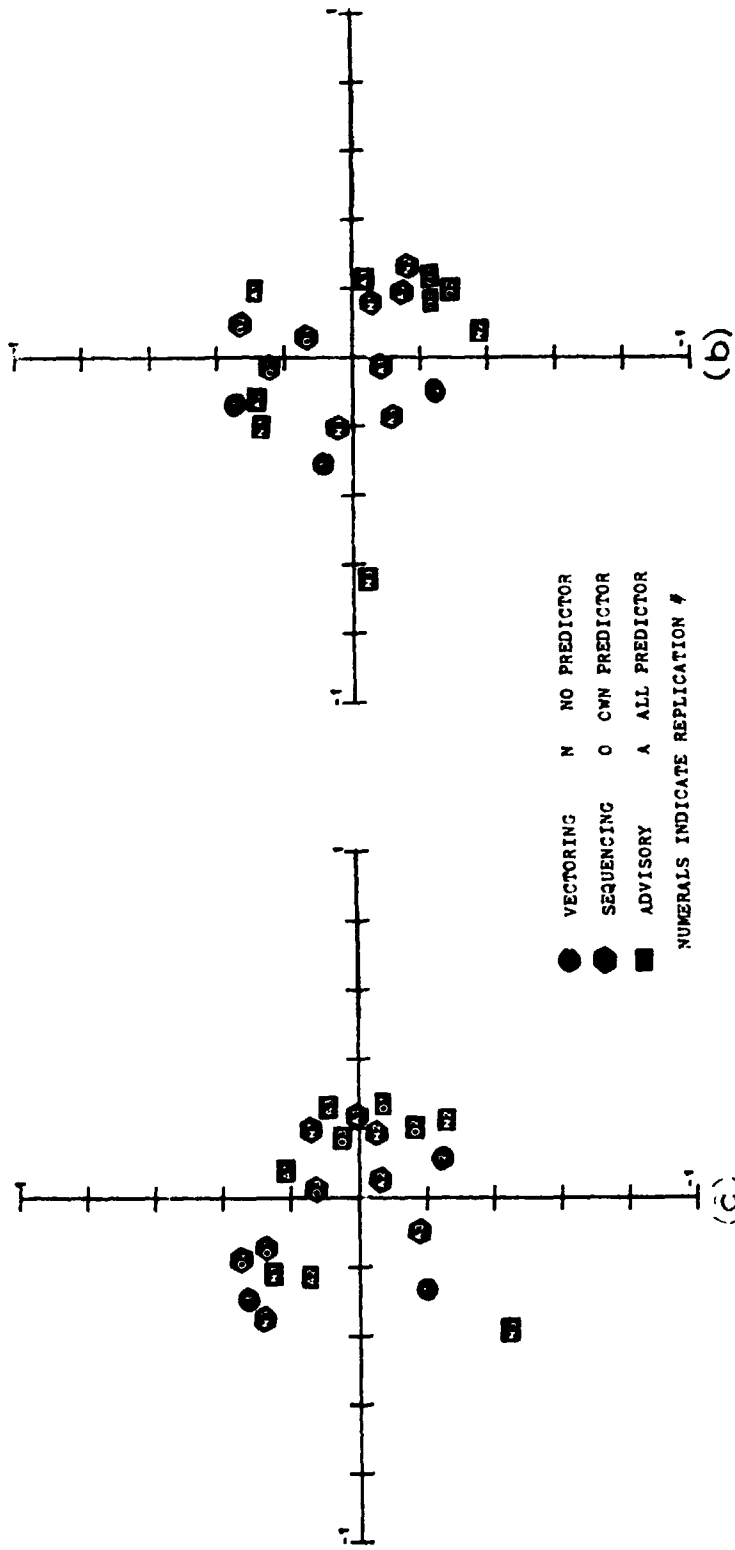
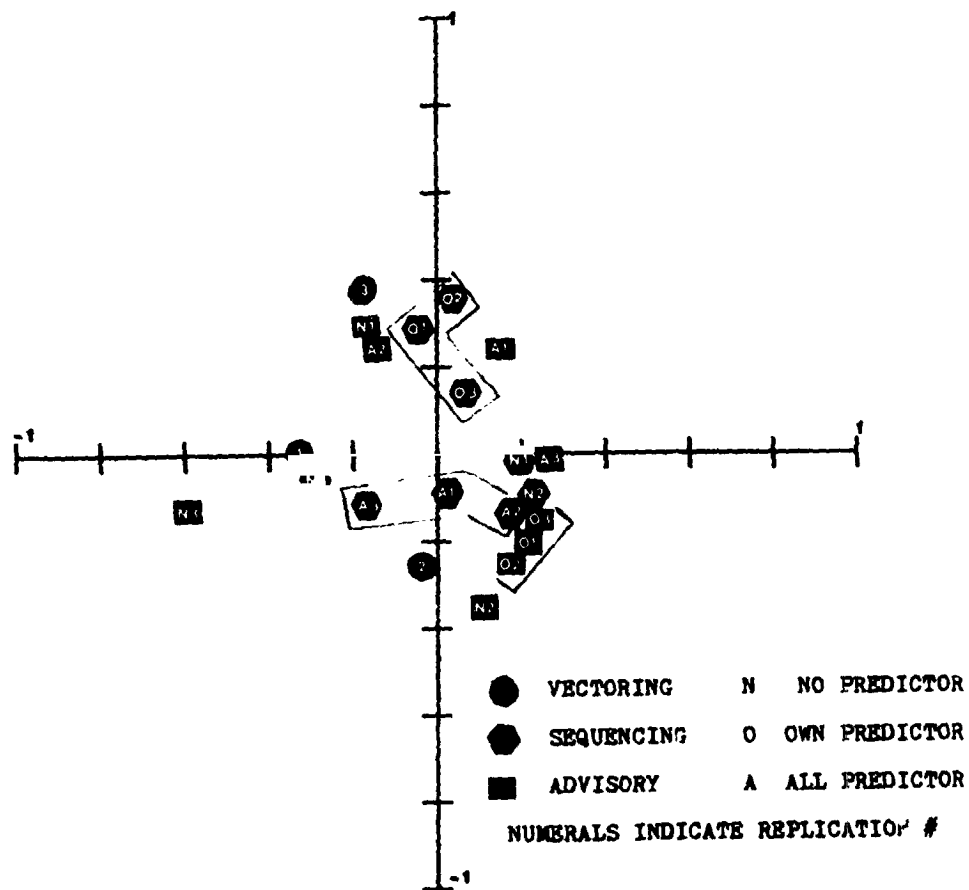


Figure 7 Two Dimensional INDSCAL Stimuli Spaces for the Orderliness Data. Pilot and Controller Groups Analyzed Separately. A High Degree Organization Correspondence is Indicated, Particularly after Rotation of about 45° of the Pilot Configuration.



STIMULUS SPACE: ORDER DATA

2 DIM SOLN

AXIS 1: HOR

AXIS 2: VERT

Figure 8 Two Dimensional Group Stimulus Space for Pilots and Controllers Combined. A High Degree of Similarity between Runs of the Same Predictor Conditions is Evident. Similarity of the Three Vectoring Runs is Low.

DISCUSSION

The most immediate conclusion to be drawn from these analyses is that subjects can perceive orderliness and favorableness of start positions consistently even though no objective measures or definitions were specified for these complex criteria. This strengthens the concept of including human observers as system measuring devices along with more traditional "objective" measures. Furthermore, there did not seem to be any great amount of difference between the perceptual spaces of pilots and controllers in either of the two types of judgments, suggesting that perception was not strongly colored by occupation.

It is probably safe to conclude that the lack of any strong patterns among the conditions in the start data implies a more or less equally distributed a priori difficulty of performing the task as intended. The opinion of the expert witnesses must be taken as "truth" in place of any noncircular objective measures. Thus more confidence can be placed in the comparisons based on objective measures reported in previous papers, e.g., the generally inferior performance of vectoring was not attributable to any predisposition toward a more difficult problem based upon the starting configurations.

On the other hand, the evidence of some clusters of the three runs from the same nonvectoring conditions in plots of perceived orderliness does seem to indicate that these conditions produced similarly "orderly" flights. (The subjects were not aware of the conditions generating the runs or that there were even multiple runs (3) under the same condition.) It is not expected that all runs from a given condition be perceived identically because of the natural variability in such realistic stimuli. However, again in spite of what might appear to be an impossible task, subjects did perceive differences in orderliness in a fairly consistent fashion among the 21 flights.

The size of the triangular clusters obtained by connecting the 3 runs from the same conditions is a rough measure of variability of the perceived stimuli. The triangular clusters are about the same size for the start data, indicating, as mentioned above, approximately equally distributed difficulty of start positions as desired. However, the size of the triangular clusters for orderliness are much smaller when predictors are used, indicating again the reduced variability typically associated with predictors. Further analysis will reveal the relative ordering of the conditions on the two judgments to determine which of the conditions is judged most orderly, for example.

The percentage of the total variance in the data accounted for by the nonmetric solution (Figure 1) is generally higher than in the metric solution ((INDSCAL). The 5 dimensional metric solution produced a correlation of about 0.68 between model and data, while the nonmetric solution of the same dimensionality produced a Spearman coefficient of 0.93. It should be remembered that the nonmetric solution operates on a single subject's data at one time and is thus able to "tailor" a fit better, whereas INDSCAL produces a simultaneous solution common to an entire group. The correlations between the orderliness data and model for the pilots (as derived from INDSCAL)

ranged from .447 to .634 for the two dimensional solution with similar results for controllers and similar results for the start data. (The random "subject" had a correlation of only 0.11 approximately by comparison.)

The dominance data, gathered concurrently with the proximity data, will be analyzed externally in the stimulus solution to determine each subject's preference order using a program such as PREFMAP by Carroll and Chang of Bell Laboratories. In addition, the original 15 objective measures are also being used with INDSCAL to produce an "objective" configuration of the 21 stimuli runs for comparison with the subjective perceptual spaces as well as produce indications of similarity among the measures themselves. An important goal of this project is to identify if possible the dimensions of the perceptual space as a means of objectivizing complex criteria such as orderliness for future use.

SUMMARY

Analyses of the similarities data on favorableness of starting position and orderliness of the flights (two complex criteria for which objective measures do not exist yet) indicate that this data gathered from subject observers was generated by an internally consistent, nonrandom process. Comparisons of the separately derived pilot and controller perceptual spaces indicate a high degree of perceptual similarity between the two groups in spite of their different professions.

The three runs of each of the seven conditions were judged about the same in terms of favorableness of starting configurations (as originally intended) so that differences in the objective analyses among the conditions do not depend upon any preferential bias toward easier solution because of starting configurations. On the other hand, marked differences appear in the judged orderliness of the flights in the seven conditions. The three runs of any of the four predictor conditions were judged more similar in orderliness than the runs from any non-predictor condition (vectoring, sequencing-no predictor, advisory-no predictor), which adds further evidence that predictors tend to reduce variability. The run similarity in orderliness between the own predictor and all predictor conditions was about the same.

It is concluded that human observers can be used for obtaining fairly consistent evaluations of complex stimuli using ill defined though commonly used important criteria. Analysis is therefore continuing to determine the relative ordering of the stimuli under the two criteria to supplement comparison results of the ATC systems using objective measures and to identify the dimensions of the perceptual spaces obtained.

REFERENCES

1. Kreifeldt, J.G., Wempe, T., "Future Terminal Air Traffic Management Concepts." Proceedings of the 10th Annual Conference on Manual Control WPAFB AFIT AFFDL. Dayton, Ohio, April 9-11, 1974.
2. Kreifeldt, J.G., Wempe, T.E., "Human Decision Making in Future ATC Systems. Comparative Studies in Distributed Management." Proceedings of the 1974 International Conference on Systems, Man and Cybernetics. Oct. 2-4, 1974, IEEE 74 CHO 908-4 SMC.
3. Kreifeldt, J., Pardo, B., Wempe, T., Huff, E., "Verbal Workload in Distributed Air Traffic Management." 11th Annual Conference on Manual Control. NASA-Ames Research Center, Moffett Field, Ca. May 20-23, 1975.
4. Pickett, R.M., "Applications of Texture Perception in the Analysis of Complex Optical Imagery." Aerospace Medical Research Laboratories Technical Report, AMRL-TR-71-81, AD 846658, May 1972.
5. Carroll, J.D., "Individual Differences in Multidimensional Scaling," in Multidimensional Scaling: Theory and Applications in The Behavioral Sciences, Vol. 1, Seminar Press, New York and London, 1972.
6. Kindly provided by Dr. Renwick Curry, Dept. of Aeronautics and Astronautics, M.I.T., Cambridge, Mass.
7. Bennett, J.F., Hays, W.L., "Multidimensional Unfolding: Determining the Dimensionality of Ranked Preference Data," Psychometrika, Vol. 25, 1960, pp. 27-43.
8. Lingo, J.C., Roskam, E.E., A Mathematical and Empirical Analysis of Two Multidimensional Scaling Algorithms, Psychometrika Supplement #19.
9. Carroll, J.D., Chang, J.J., "Analysis of Differences in Multidimensional Scaling via an N-Way Generalization of Eckart-Young Decomposition," Psychometrika, Vol. 35, No. 3, September, 1970.
10. Carroll, J.D., Wish, M., "Models and Methods for Three Way Multidimensional Scaling," article in Measurement, Psychophysics, and Neural Information Processing, Vol. 2, Freeman and Company, San Francisco, 1974.
11. Torgerson, W.S., Theory and Methods of Scaling, Wiley, New York, 1958.

ACKNOWLEDGEMENT

Funds for the support of this study have been allocated by Nasa-Ames Research Center, Moffett Field, California under Interchange NCAR-785-401.

N75 23708

SLUSHY WEIGHTINGS FOR THE OPTIMAL
PILOT MODEL

James D. Dillow, Douglas G. Picha, Ronald O. Anderson

ABSTRACT

A pilot model is described which accounts for the effect of motion cues in a well defined visual tracking task. The effect of visual and motion cues are accounted for in the model in two ways. First, the observation matrix in the pilot model is structured to account for the visual and motion inputs presented to the pilot. Secondly, the weightings in the quadratic cost function associated with the pilot model are modified to account for the pilot's perception of the variables he considers important in the task. Analytic results obtained using the pilot model are compared to experimental results and in general good agreement is demonstrated. The analytic model yields small improvements in tracking performance with the addition of motion cues for easily controlled task dynamics and large improvements in tracking performance with the addition of motion cues for difficult task dynamics.

INTRODUCTION

The fact that motion cues can have a significant effect on tracking performance has been demonstrated (Refs 1 and 2). In fact, in Ref 2 a set of plant dynamics is given for which it was found that tracking was only possible when motion was present. Thus it is clear that in certain cases, the effect of motion cues must be accounted for in a realistic pilot-vehicle analysis.

An approach is suggested in Ref 3. In Ref 3, experimental results are used to develop a relation between the lead time constant and the time delay in the pilot model for the case where no motion is present. A separate relation between the lead time constant and the time delay is developed for the case where the motion is present. The basic idea is that as the lead time constant decreases, the time delay decreases. With motion, a further decrease in the time delay results. The idea of a reduced time delay in the presence of correct motion cues is substantiated by the data of Ref 1. Reference 1 contains experimentally derived pilot transfer functions with and without motion cues. A comparison of the pilot transfer functions show that the high frequency phase droop is decreased with motion cues. Yet the shape of the amplitude curve is not much different with or without motion cues. This change in phase without a corresponding change in amplitude for the pilot transfer function suggests that the time delay is decreased when motion cues are present. This conclusion is consistent with the approach of Ref 3.

Unfortunately the approach of Ref 3 does not easily extend to those cases where the level of the motion cues are on the

order of the pilot's perceptual thresholds. Furthermore, the problem where the motion is not precisely correct can not be analyzed. This is the case in flight simulation where the motion often has to be "washed out" due to the physical constraints of the simulation facility. Nor does the approach of Ref 3 apply to the case where motion cues are contradictory to visual cues. An example of this possibility is flying a remotely piloted vehicle from a separate aircraft.

A model which accounts for the effects of motion cues in a direct and natural way is described in this paper. Furthermore it is relatively simple to extend the model to the case where "washed out" motion is present or to account for disorientation due to contradictory motion and visual cues. The model described here is based on the optimal pilot model described in Refs 4 through 9. The effects of different visual and motion cues (as well as peripheral cues and proprioceptive cues) are accounted for in the model in two ways. (1) First the observation matrix in the optimal pilot model is structured to account for the visual and motion inputs presented to the pilot. (2) Secondly, the weightings in the quadratic cost function associated with the optimal pilot model are modified to account for the pilot's perception of the variables he considers important in the task.

The procedure for modifying the quadratic cost function is described next. The approach is then demonstrated for a roll tracking task and results predicted by the model are compared to experimental results from Refs 1 and 2.

SLUSHY WEIGHTINGS

In the use of an optimal pilot model, a quadratic cost function of the form

$$J = \sum_{i=1}^m W_{y_i} \sigma_{y_i}^2 + R \sigma_{\delta}^2$$

is minimized using linear, quadratic, gaussian optimization theory. In J, σ denotes the rms value, y_i is the i th observed variable, δ is the control input, and W_{y_i} and R are weightings in the cost function. It is not clear how to physically interpret the term

$$R \sigma_{\delta}^2$$

in the cost function. The procedure that is followed is to pick R so that the neuromuscular lag in the pilot model is .1 sec. So, despite the lack of physical interpretation, the weighting R poses no difficulty in the determination of the optimal pilot model.

The term

$$\sum_{i=1}^m W_{y_i} \sigma_{y_i}^2$$

poses a different problem. The values of W_{y_i} may be difficult to pick a priori. This is one of the main arguments put forth against the optimal pilot model by its critics. Advocates of the optimal pilot model claim the values of the weightings, W_{y_i} , can be determined judiciously based on the pilot's interpretation of what he considers to be acceptable limits for the observed variables, y_i . Furthermore, it is claimed that the values of the weightings are constant for a given task, independent of plant dynamics, disturbances or commanded inputs. The idea of fixed or invariant weightings is consistent with the pilot modeling approach suggested by the paper pilot model (Refs 10 and 11). In the paper pilot model the cost function is the pilot's evaluation of the aircraft's handling qualities and by minimizing the cost function, the pilot has optimized the closed loop handling qualities.

The approach taken here is that the term

$$\sum_{i=1}^m W_{y_i} \sigma_{y_i}^2$$

does represent the pilot's concept of what is "good" for a given task, and the pilot will adapt his control strategy to minimize this quantity--with one exception. The pilot can not minimize what he doesn't perceive. For example, it is possible for instrument thresholds to effect the pilot's perception of the magnitude of a given variable. Thresholds have in the past been considered in computing performance; however, their effect on the cost function has not previously been considered. Furthermore, accelerations would not be perceived if there is no motion; however, in the presence of motion, acceleration may well be a factor in the pilot's assessment of "goodness". Thus it seems more reasonable in the optimal pilot model to minimize

$$J_p = \sum_{i=1}^m W_{y_i} \sigma_{y_{p_i}}^2 + R \sigma_{\delta_e}^2$$

where y_{p_i} is the perceived value of the i th observed variable and the values of W_{y_i} are fixed for a given task, independent of the observed variables, plant dynamics, disturbances and commanded inputs.

The cost function with perceived variables can be written as

$$\begin{aligned}
 J_p &= \sum_{i=1}^m W_{y_i} \frac{\sigma_{y_{p_i}}^2}{\sigma_{y_i}^2} \sigma_{y_i}^2 + R\sigma_{\delta_e}^2 \\
 &= \sum_{i=1}^m W_{y_i} K_{y_i}^2 \sigma_{y_i}^2 + R\sigma_{\delta_e}^2
 \end{aligned}$$

where K_{y_i} is the describing function gain corresponding to the i th observed variable, y_i , due to the threshold. In this form, the usual linear, quadratic, gaussian minimization theory can be used to compute the optimal pilot model gains. The weightings in the quadratic cost function are $W_{y_i} K_{y_i}^2$ and depend on thresholds and which variables are observed--hence the term slushy weightings. Since the describing function gains can not be computed a priori, the solution to the optimal pilot model is computed iteratively, where the values of $W_{y_i} K_{y_i}^2$ are computed each iteration until convergence is achieved.

A ROLL TRACKING TASK

The optimal pilot model with slushy weightings was tested against experimental results from Ref 1. In Ref 1 Shirley describes the results of a roll tracking task with and without motion cues for a large variety of controlled element dynamics, different input levels, and different input band widths. The task consisted of tracking a commanded roll input that was made up of a sum of sine waves. The tracking error was displayed on an oscilloscope in the cockpit. When the motion was included in the experiment, the error was also used to drive the roll motion of the cockpit. The dynamics of the motion system (a pure time delay) was accounted for in the visual system by passing the roll error through the simulated motion system dynamics. Thus the visual cues and motion cue were consistent. A block diagram of the experiment is shown in Fig. 1.

Input

The input, ϕ_i , was the sum of ten sine waves at fixed frequencies. The break frequency was defined as follows. At frequencies below the break frequency, the amplitudes of the sine waves were ± 1 . At frequencies above the break frequency, the amplitude of the sine waves were $\pm .1$.

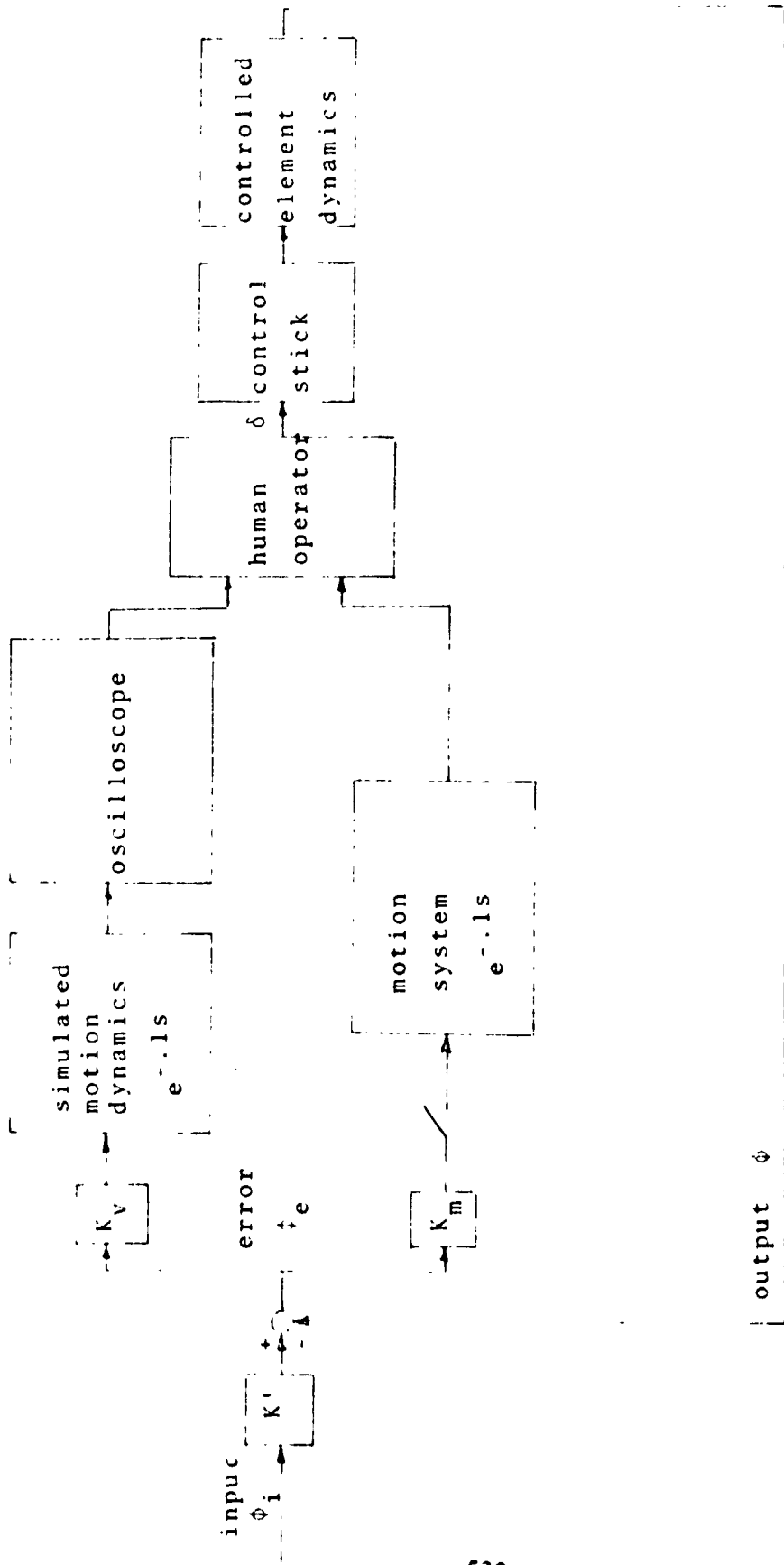


Figure 1. Compensatory Roll Tracking Task With and Without Motion Cues

For the analytic results using the pilot model, the input was modelled by four cascaded first order filters driven by gaussian white noise. The break frequency of the gaussian input was set so the integral of the power spectral density of the gaussian input matched as closely as possible the integral of the power spectral density of the sum of sine waves input. The break frequencies used are as follows:

ω_b , radians/sec	
sum of sine waves	gaussian (matched)
.7	1.1
2.5	2.0
5.0	4.0

The input could be scaled by a gain, K' , to vary the input power as shown in Fig. 1.

Dynamics

The dynamics of the roll motion system (no other axis was driven) was that of a pure time delay of .1 sec, good to 10 rad/sec. Thus in the analysis a .1 sec time delay was lumped into the .2 sec pure time delay for the pilot model, for a total of a .3 sec time delay.

The dynamics of the controlled element consisted of 3 types

$$(1) \frac{K}{s(\tau s + 1)}$$

$$(2) \frac{K}{s^2 + 2\zeta\omega_n s + \omega_n^2}$$

$$(3) \frac{K}{s(s^2 + 2\xi\omega_n s + \omega_n^2)}$$

Unfortunately, numerator terms usually associated with aircraft dynamics were not considered.

Control Stick Sensitivity

The control stick sensitivities were set for a given controlled element dynamics so that full stick motion was not used and so that the stick activity was not minute. The experimental results clearly indicate that the tracking performance is dependent on control stick sensitivity. For example, the tracking performance as a function of control sensitivity for a given set of controlled element dynamics are shown in Fig. 2. It is clear that there is an optimal stick sensitivity and an experiment run with non-optimal stick sensitivity will result in poorer tracking scores.

The optimal pilot model in its present form doesn't account for stick sensitivity. Thus it is assumed that the model results correspond to those obtained with optimal stick sensitivity. In those cases where a number of stick sensitivities were used experimentally, the case with the best tracking score was used to compare with the analytic results.

Motion Cues

The roll motion was driven by the roll error about an axis through the operator's belly button. Only roll motion was used and the motion was not washed out. The angle of rotation was proportional to the roll error delayed by .1 sec. This constant of proportionality, K_m , was chosen for each set of controlled element dynamics so that the roll motion was neither so small as to be useless or so large as to exceed $\pm 45^\circ$ during a run. Once the constant was chosen for one set of dynamics, it was maintained throughout the experiment.

Visual Cues

The visual display was a dot on an oscilloscope with lateral displacement proportional to the roll error. The cockpit was covered so that external visual cues could not be used when the motion was on. The oscilloscope gain, K_v , was chosen so that the dot did not reach the edge of the oscilloscope during the run, and yet, did not make just minor perturbations. The ratio K_v/K_m was constant throughout the entire experiment.

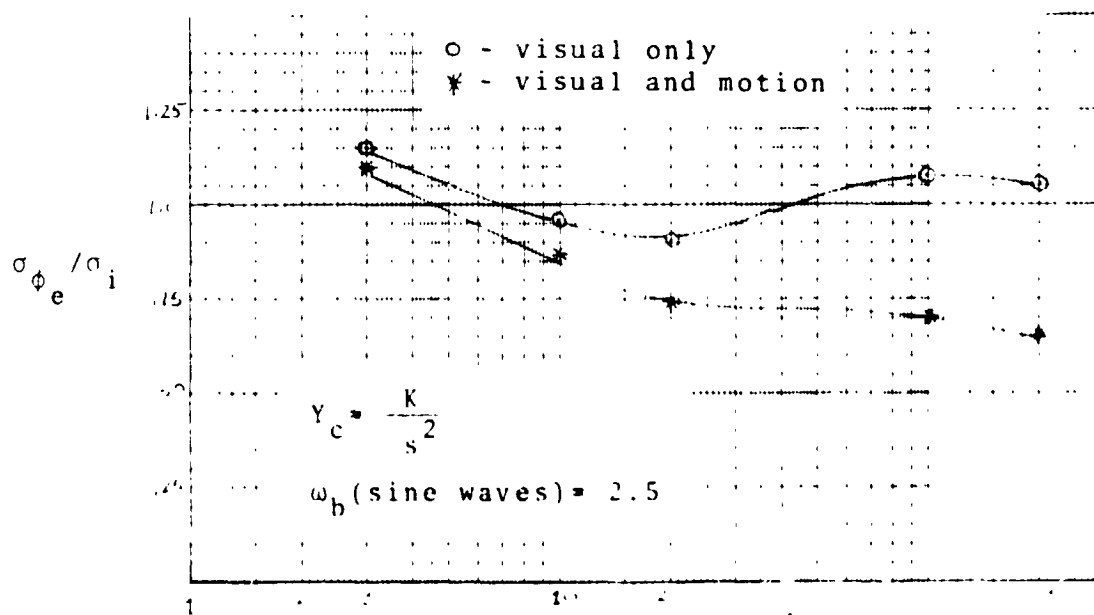


Figure 2. Tracking Performance as a function of Control Stick Sensitivity, F .

PILOT MODEL

In order to compute analytic results, certain parameters and structural properties of the optimal pilot model must be fixed. To the extent possible the parameters used were taken from previous applications of the optimal pilot model so that the analytic results could be considered as a prediction of experimental results.

Time Delay

A pure time delay of .2 sec was used in the pilot model. This value is consistent with Refs 4 through 9. The .1 sec pure time delay of the motion dynamics was added to the pilot time delay to give an effective time delay of .3 sec.

Neuromuscular Lag

A neuromuscular lag of .1 sec was used in the pilot model. This value is consistent with Refs 4 through 9.

Observation Noise

The noise to signal ratio for the observation noise was taken to be $.01\pi$, again consistent with Refs 4 through 9.

Neuromuscular Noise

The noise to signal ratio for the remnant or the neuromuscular noise was taken to be $.003\pi$ consistent with Refs 4 through 7 and 9. (1 & 8 blew it on this one.)

Observed Variables

The observed variables depend upon whether or not motion cues are used. Without motion cues, the roll error, ϕ_e , was observed. In applying the optimal pilot model, the first derivative any visual observation is assumed to be observed concurrently, hence the observation vector for visual cues is

$$\begin{bmatrix} \phi_e \\ \dot{\phi}_e \end{bmatrix}$$

With the addition of motion, rotational acceleration is also sensed via the vestibular system. It was assumed that the first derivative of the roll acceleration was also sensed. A more detailed model of the vestibular dynamics might be more appropriate for more involved motion. Roll error could also be sensed proprioceptively and in fact tracking scores were given in Ref 1 for tracking without visual cues.

Roll error sensed proprioceptively was not considered in the observation vector since it is redundant to that sensed visually, and the visual cues are supposed to be well above the visual thresholds. Thus with motion, the observation vector is

$$\begin{bmatrix} \phi_e \\ \dot{\phi}_e \\ \ddot{\phi}_e \\ \dot{\phi}_e \end{bmatrix}$$

Cost Function Weightings

The weightings used in the cost function were taken from Ref 9. In Ref 9, the weightings were picked so that pilot model results matched experimental results from Ref 12. The experimental roll task in Ref 12 was to maintain wings level in the presence of turbulence. The weightings are

$$W_{\phi_p} = 2.7$$

$$W_{\dot{\phi}_p} = 1.5$$

$$W_{\ddot{\phi}_p} = .02$$

where ϕ_p is the perceived roll error, $\dot{\phi}_p$ is perceived error rate, and $\ddot{\phi}_p$ is the perceived rotational acceleration (and error acceleration in this case).

It should be noted that for the case without motion, $\ddot{\phi}_p = 0$, which is equivalent to letting $W_{\ddot{\phi}_p} = 0$.

Thresholds

The thresholds could not be precisely determined from the experimental description in Ref 1. This is because the values of K_m and K_v are not given in Ref 1. Furthermore, K_m and K_v were different for different controlled element dynamics. The ratio K_m/K_v was held constant, however.

The approach taken was to fix the thresholds for all cases. The input was varied for different controlled element dynamics. This corresponds to varying K_m and K_v , but with a fixed ratio.

The thresholds used were as follows

<u>Observed Variable</u>	<u>Threshold</u>
ϕ_e	.89°
$\dot{\phi}_e$	3.38°/sec
$\ddot{\phi}_e$.5°/sec ²
$\dddot{\phi}_e$	10.°/sec ³

The thresholds for ϕ_e and $\dot{\phi}_e$ correspond to a linear display 1 meter from the operator's eyes scaled .1 cm/deg roll assuming .05° arc and .18° arc/sec visual thresholds. The threshold for

rotational acceleration was taken from Ref 13. The threshold on $\ddot{\phi}_e$ was a WAG (Wild Beast-of-Burden Guess).

The inputs used are as follows

Controlled Element Dynamics	rms Input, σ_i (degrees) ⁱ
$K/s(\tau s + 1)$	5.
$K/(s^2 + 2\xi\omega_n + \omega_n^2)$	3.
$K/s(s^2 + 2\xi\omega_n + \omega_n^2)$	2.

The exceptions to the above inputs are four cases for K/s^2 dynamics where the relative changes in the input are documented in Ref 1.

COMPARISON OF RESULTS

A tabulated comparison of the experimental results and the analytic results are given in Fig. 3. The cases are referred to by the "data" number of Ref 1. Experimental results and analytic results are compared by comparing normalized tracking scores, $\sigma_{\phi_e} / \sigma_i$. The results are also displayed in the scatter diagram of Fig. 4.

The agreement between the analytic scores and the experimental scores are generally good. The analytic results were particularly interesting in the case of data 17, 20, and 23. Note that in data 20 and 23 the only change from data 17 is the level of the input. As the input increased, the scores improved (decreased) and visa versa. The analytic scores not only followed the same trend, but accurately match the experimental results. The mechanism in the optimal pilot model that cause the scores to improve with increased input is the decreased effect of the visual threshold.

In three cases the analytic results did not compare well with the experimental results. For data 8 and 43, the optimal model predicts virtually no improvement in the tracking score due to motion, yet the experimental results show a significant improvement in tracking score. The analytic results agree with the conclusions of Refs 2 and 14; that is, for easily controlled dynamics, motion cues are not particularly helpful. It is possible that in these cases, the additional proprioceptive cue for roll error was of significant value since the motion was relatively small and the visual thresholds may have been of significance.

The analytic results for data 55 show a significant improvement with motion cues, yet experimentally, no improvement was measured. Again the analytic results agree with the conclusions of Refs 2 and 14. These references both concluded that for marginally unstable dynamics, the motion cues would

Data	Cues V=Visual M=Motion	Controlled Element	ω_b (sine)	σ_{in}	Scores $\sigma_{\phi_e} / \sigma_i$	
					Ref 1	Analytic
8	V	$\frac{K}{s}$	2.5	5	.45	.47
					.34	.45
17	V and M	$\frac{K}{s^2}$	2.5	3	.90	.84
					.74	.63
20	V and M	$\frac{K}{s^2}$	2.5	1.5	1.22	1.15
					.98	.80
23	V and M	$\frac{K}{s^2}$	2.5	6.0	.72	.72
					.55	.52
24	V and M	$\frac{K}{s^2}$.7	1.9	.87	.74
					.78	.50
27	V and M	$\frac{K}{s^2}$	5.0	3.74	1.04	1.23
					.82	1.12
29	V and M	$\frac{K}{s(s+1)}$	2.5	5	.63	.58
					.56	.45
32	V and M	$\frac{K}{s(s+2)}$	2.5	5	.57	.54
					.48	.44
33	V and M	$\frac{K}{s(s+4)}$	2.5	5	.58	.52
					.48	.43
40	V and M	$\frac{K}{s^2+5}$	2.5	3	.90	.70
					.72	.60
41	V and M	$\frac{K}{s^2+10}$	2.5	3	.74	.67
					.62	.54
43	V and M	$\frac{K}{s^2+5s+25}$	2.5	3	.60	.58
					.48	.58
55	V and M	$\frac{K}{s^2(s+2)}$	2.5	2	1.75	1.55
					1.75	.92

Fig. 3. Comparison of Experimental and Analytic Tracking Scores.

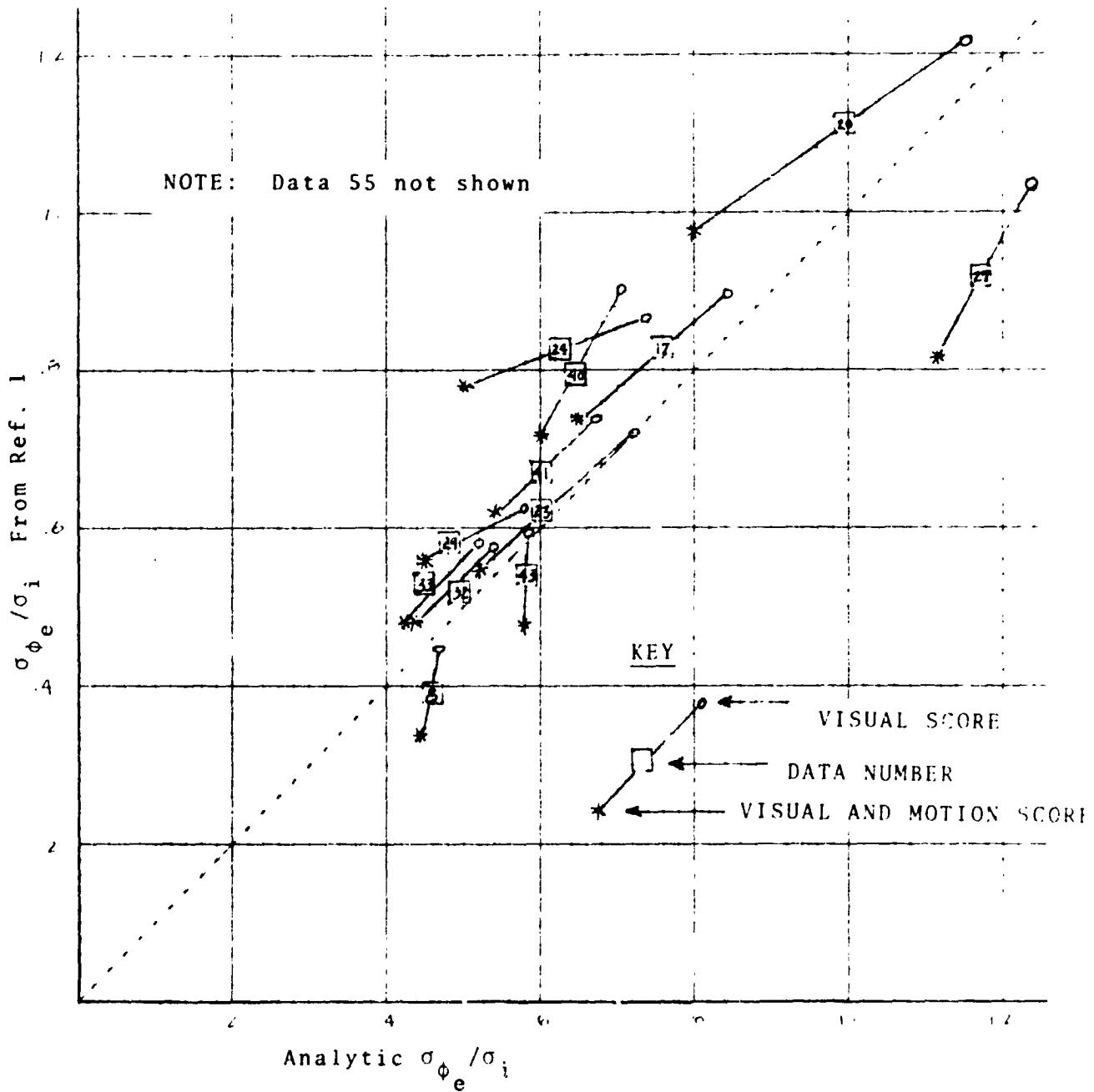


Figure 4. Scatter Diagram Comparison of Experimental and Analytic Results.

be helpful and should improve performance. It is possible that non-optimum stick sensitivity was a factor in the experimental results. It is also possible that there was sufficient high frequency oscillation to impair the reading of the oscilloscope and to cause undesirable vibration feedthrough to the stick. These effects can be accounted for in the optimal pilot model (Ref 15) but were not in this study.

CONCLUSIONS

The pilot model results generally agree well with the experimental results. Experimental improvements in tracking scores due to motion cues are matched by corresponding improvements in tracking scores by the optimal pilot model in all but three cases. Even in those cases it may be possible to account for the experimental results by including the proprioceptive cues and effects of vibration in the optimal pilot model.

The comparison of tracking scores is not a conclusive demonstration of the model. A comparison of experimentally derived and analytic pilot transfer functions is in order. It is possible that the apparent change in time delay seen in the phase data of the pilot transfer function (Ref 1) might be accounted for in the optimal model by the fact that the predictor in the optimal pilot model would be improved with the additional observations. The result would be that the effective time delay due to the combination of pure time delay and the predictor would be decreased with addition of motion inputs.

The experimental results show that control stick sensitivity will effect tracking scores and illustrates the need to extend the optimal pilot model so that the effect of stick sensitivity can be accounted for.

It would be possible to refine the model by including vestibular dynamics in the model based on existing models. Modelling peripheral cues or proprioceptive cues in the optimal model is conceptually no problem; however, threshold values and the structure of the observation matrix are now known.

The model described in this paper accounts for the motion cues in a straight forward way. The addition of the motion is accounted for by including sensed motion variables in the input to the pilot model. The weighting in the quadratic cost function are altered so that only the perceived state of the system to be controlled is used in the cost function.

The change in the weightings involves computing describing function gains; so once the thresholds are defined, the appropriate weightings are easily computed iteratively.

The model can be used to account for washed out motion in aircraft simulation. This would be done by including the simulator motion equations in the system equations used to structure the optimal pilot model. Performance with full motion could then be compared to that with washed out motion.

The effects of contradictory motion or confusing motion cues can also be modeled. The approach would be to structure

the pilot model based on correct motion cues and then use the contradictory motion as an input to the model. Obviously the optimal filter performance would degrade and the residuals would be a measure of the disorientation created by the incorrect motion cues.

REFERENCES

1. Shirley, R. S. Motion Cues in Man-Vehicle Control, MVT-68-1, Man Vehicle Laboratory, Cambridge, Mass., Jan 1968.
2. Junker, A. M. and C. R. Replogle. "Motion Effects on the Human Operator in a Roll Axis Tracking Task", Aviation Space and Environmental Medicine, to be published.
3. Ringland, R. F., et al. Motion Effects on an IFR Hovering Tasks, Analytic Predictions and Experimental Results, NASA CR 1933, Nov 1971.
4. Baron, S., et al. Application of Optimal Control Theory to the Prediction of Human Performance in a Complex Task, AFFDL-TR-69-81. Air Force Flight Dynamics Laboratory, Wright-Patterson Air Force Base, Ohio, March 1970.
5. Kleinman, D. L., et al. "An Optimal Control Model of Human Response, Parts 1 and 2", Automatica, vol. 6, May 1970.
6. Kleinman, D. L. and S. Baron. Manned Vehicle Systems Analysis by Means of Modern Control Theory, NASA CR-1753, National Aeronautics and Space Administration, Washington DC, Nov 1971.
7. Kleinman, D. L., et al. "A Control Theoretic Approach to Manned Vehicle System Analysis", IEEE Special Issue on the Linear-Quadratic-Gaussian Problem, December 1971.
8. Harvey, T. H. and J. D. Dillow. "Application of an Optimal Control Pilot Model to Air-to-Air Combat" AIAA Mechanics and Control of Flight Conference, AIAA Paper No. 74-917. August 1974.
9. Dillow, J. D. and D. G. Picha. Application of the Optimal Control Pilot Model to Analysis of Aircraft Handling Qualities, AFIT-TR-75-4, Air Force Institute of Technology, Wright-Patterson Air Force Base, to be published.
10. Dillow, J. D. The "Paper Pilot" - A Digital Computer Program to Predict Pilot Rating for the Hover Task. AFFDL-TR-70-40, Air Force Flight Dynamics Laboratory, Wright-Patterson Air Force Base, Ohio, March 1971.

11. Nolting, D. L., J. D. Dillow, and R. A. Hannen. "Paper Pilot Hovers Laterally", Proceedings of the Xth Annual Conference on Manual Control, April 1974.
12. Onstott, E. D., et al. Prediction and Evaluation of Flying Qualities in Turbulence, AFFDL-TR-71-162, Air Force Flight Dynamics Laboratory, Wright-Patterson Air Force Base, Ohio, February 1972.
13. Young, L. R. "Current State of Vestibular System Models", Automatica, Vol. 5, 1969, pp 369-383.
14. Young, L. R. "Some Effects of Motion Cues on Manual Tracking", J. Spacecraft and Rockets, October 1967, pp 1300-1303.
15. Levison, W. H. and P. D. Houck. "Guide for the Design of Control Sticks in Vibration Environments", AMRL-TR-74-127, Aerospace Medical Research Laboratory, Wright-Patterson Air Force Base, Ohio, February 1975.

N75 33709

A THEORETICAL STUDY OF THE PILOT AS A SYSTEM MONITOR

by P.H. Wewerinke
National Aerospace Laboratory NLR
the Netherlands

SUMMARY

The ever increasing complexity of aerospace vehicles, is associated with a greater emphasis on the monitor and decision making functions of the pilot. This paper deals with the perceptual load imposed on the pilot monitoring his system. A theoretical model of this load is tested against experimental data. This model is based on a system state estimation model to be associated with the internal representation of the task environment.

INTRODUCTION

It may be expected that the human's role in pilot/vehicle systems will be more and more characterized by monitoring and decision making. Therefore, these functions have to be incorporated when describing human operator's participation in manned vehicle systems.

As indicated in figure 1, a central aspect of the pilot's participation is the internal representation of the task environment. It enables the human operator to determine whether the present situation is incongruous with what should happen. In case of incongruity the required action pattern (to remove the incongruity) can be "known", implying that the corresponding response is merely "provoked" (control). Otherwise, the pros and cons of possible actions are weighed to solve the problem. According to a certain set of standards the "optimum" action is selected (decision making).

One common conceptual framework would be desirable to formulate the important pilot's functions and their mutual interference. It is believed that modern optimal control, estimation and decision theory provide this framework. In the next chapter, the human operator's monitor behavior is discussed, primarily in terms of the perceptual load involved. The model is based on the internal model of the task environment as incorporated in the optimal control model (Ref. 1).

INTERNAL REPRESENTATION

A submodel of the optimal control model consists of a Kalman filter-predictor. This state estimation submodel which is also involved in the human decision making models of Refs. 2 and 3, can be associated with an internal representation of the task environment.

The dynamic process describing the task environment is represented by the vehicle's equations of motion (Fig. 2)

$$\dot{x} = Ax + Bu + Ew \quad (1)$$

where x is the system state, u is the pilot's control input, and w represents the external disturbances and the displayed information

$$y = Cx + Du \quad (2)$$

It is assumed that this information is converted into an internal representation which is based on a noisy, delayed version of y

$$y_p(t) = y(t - \tau) + v_y(t - \tau) \quad (3)$$

where y_p represents the perceived information, τ is an equivalent time delay, and v_y represents an equivalent "observation" noise process.

This internal representation (\hat{x}) is expressed as

$$\dot{\hat{x}} = A_c \hat{x} + r \quad (4)$$

with $\hat{x}(\tau) = e^{A_c \tau} \hat{x}(0)$ given

where A_c is the closed loop control matrix (Ref. 4), and r is a zero-mean, Gaussian white noise process with covariance $R\delta(t-\tau)$.

In case the pilot only monitors the dynamic process given by eq (1) ($B=0$), A_c equals A in eq(4).

The foregoing model of the pilot's internal representation of the vehicle's state is used in the next chapter to operationalize pilot workload involved in his monitor task.

PERCEPTUAL LOAD

Theoretical analysis

Perceptual load is hypothetically constructed as the effect of the

perceived information on the human operator. It is hypothesized that the discrepancy between the internal representation (IR) of x , based on the displayed information, and the predicted (or expected) IR of x , is a measure for perceptual load imposed on the human operator. This difference, δ , is described by

$$\dot{\delta} = A_c \delta + r \quad (5)$$

with $\delta(\tau) = 0$

The covariance of δ, Δ , is given by

$$\dot{\Delta} = A_c \Delta + \Delta A_c' + R \quad (6)$$

with $\Delta(\tau) = 0$

Basically, R reflects the rate at which information enters the system. In the steady state situation ($\dot{\Delta}=0$), this is just balanced by the system damping (as expressed in A_c).

Experimental validation

In case of simple stimulus-response relationships, it is assumed that the total effect of the task situation on the human operator (workload) is predominantly reflected by his perceptual load, W_p , as defined in the previous paragraph. In terms of the optimal control model, this implies that motor noise is absent and response execution is represented by simple feedback gains (Ref. 4).

Essentially, the control model reduces to the "perceptual" model given by eq (3).

In reference 5 an exploratory experimental program is described to study pilot's control effort and its relationship with the optimal control model parameters. The dependent variables were subjective ratings (concerning task difficulty) and model parameters. The control task was varied by means of the controlled element dynamics.

For all the configurations for which motor noise was negligibly small, the perceptual load, W_p , was computed*. The result is compared with the subjective ratings for the controlled elements shown in figure 3. The computed (logarithm of the) perceptual load, W_p , is shown to be in excellent agreement with the subjective data.

*Although eq (6) can be related to multivariable situations only the displayed system output, m , was involved, so $W_p = \delta_m^2$

Extension to multi-input situations

In order to derive an absolute measure of perceptual load, it is proposed to weigh the foregoing perceptual load index with a quantity which reflects how alarming the perceived information is, or what its consequences are. This is mandatory when the effect of one source of information is compared or combined with another one (of different quality).

An absolute measure of perceptual load is hypothesized to be obtained when W_p is expressed in units of pertinent "target boundaries" (in case of monitoring), or in units of criterion levels (in case of continuous control with a zero reference). Furthermore, when n variables, representing non-redundant information, are perceived simultaneously, the total perceptual load is proposed to be given by

$$W_p = \prod_{j=1}^n \delta_{ii} \quad (7)$$

where δ_{ii} is the diagonal element of Δ

Experimentation will be necessary to validate this multi-variable model.

CONCLUDING REMARKS

The state estimation submodel of the optimal control model can be associated with an internal representation of the task environment. Based on this concept, a perceptual load index has been derived expressing the pilot's workload involved in his monitoring task.

The model is partly validated using experimental data (subjective ratings) of tracking tasks for which the effort involved in response selection and execution was assumed to be negligible compared with the perceptual load. An extension to multivariable task situations is suggested.

REFERENCES

1. Kleinman, D.L. and Baron, S.: Manned Vehicle Systems Analysis by Means of Modern Control Theory. NASA CR-1753, June 1971.
2. Levison, W.H. and Tunner, R.P.: A Control-Theory Model for Human Decision-Making. NASA CR-1955, December 1971.
3. Dattak, A.V. and Kleinman, D.L.: Current Status of Models for the Human Operator as a Controller and Decision Maker in Manned Aerospace Systems. ACARD CE 114 Symp. on Automation in Manned Aerospace Systems, 1972.

4. Kleinman, D.L. and Killingsworth, W.R.: A Predictive Pilot Model for STOL Aircraft Landing. NASA CR-2374, March 1974.
5. Wewerinke, P.H.: Effort involved in Single- and Two-Axis Manual Control Systems. NLR TR 75 (Forthcoming).

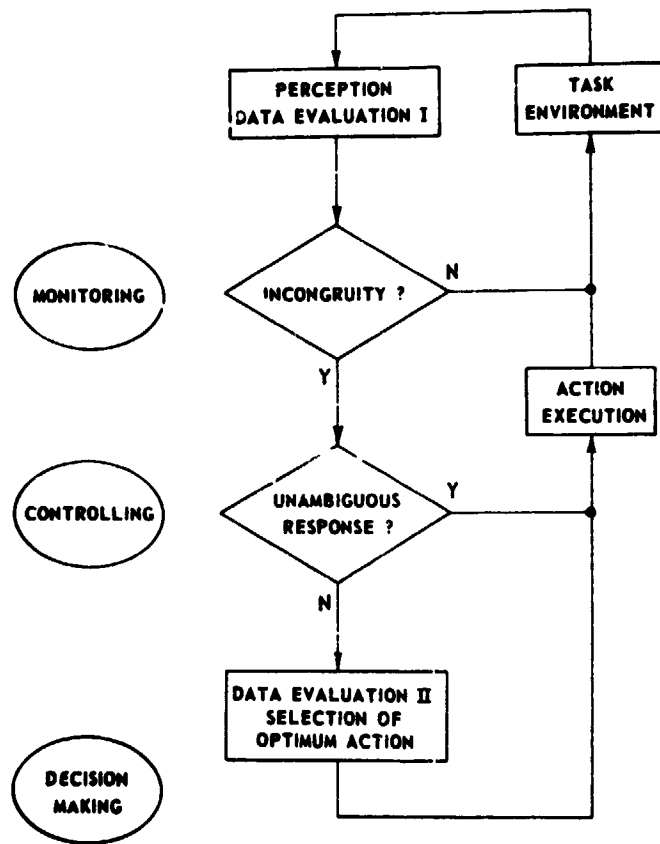


Fig. 1 Flow chart pilot's participation

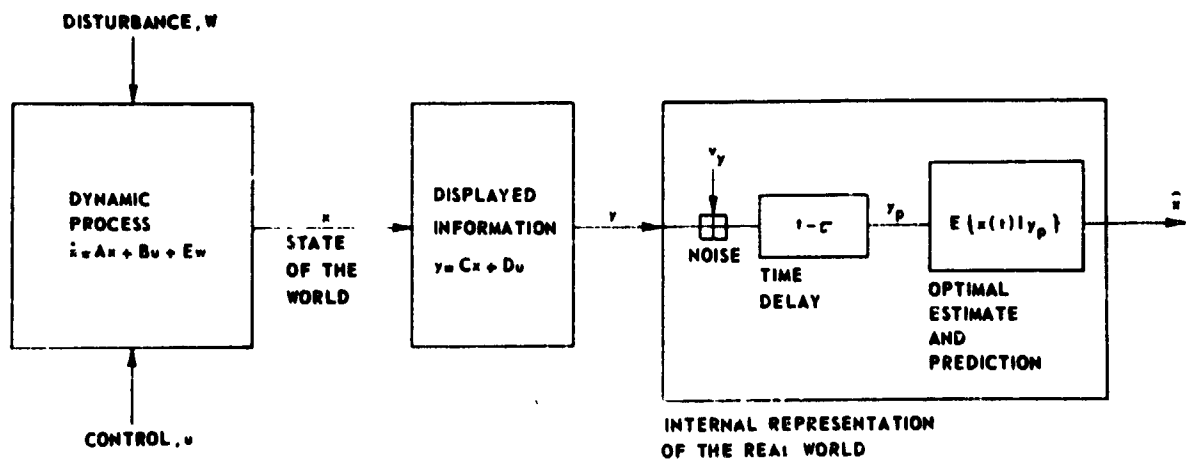


Fig. 2 Internal representation of task environment

C-7

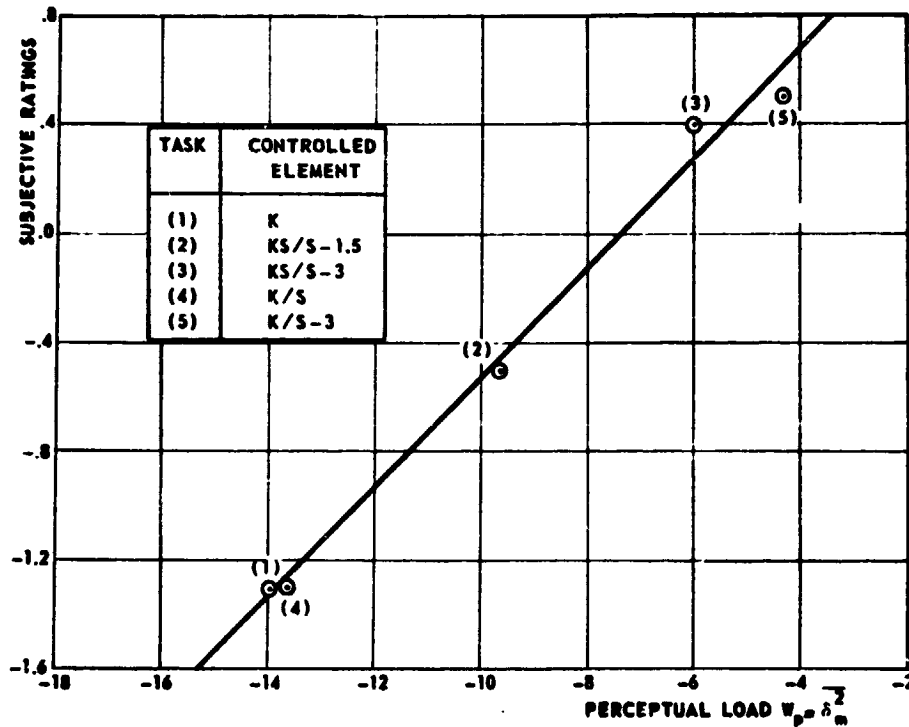


Fig. 3 Comparison of subjective ratings and computed perceptual load.
Averages of 4 subjects, 3 trials/subject.

N75 33710'

HUMAN PERFORMANCE EVALUATION IN DUAL-AXIS
CRITICAL TASK TRACKING

Dr. Malcolm L. Ritchie
Wright State University
Dayton, Ohio 45431

N. S. Nataraj
Sinclair Community College
Dayton, Ohio 45402

SUMMARY

A dual-axis tracking using Jex's critical task (Reference 1) was set up to evaluate human performance. The effects of control stick variation and display formats are evaluated. A secondary loading was used to measure the degradation in tracking performance.

INTRODUCTION

Jex, Allen and Jewell developed the multiloop critical tasks making some exploratory applications to control and display problems. The same autopacing principle and parameters as used for single axis critical instability tasks (Reference 2) were used. In this work, performance measures of critical divergence frequency (λ) i.e.: divergence frequency when the subject loses control, total run time (T) i.e.: the time from the on set of tracking until one of the errors exceeds the display and the switching time (t) i.e.: the time of rate shift on autopaced task, are evaluated for a number of controls and displays. The stress sensitivity of critical tracking tasks was investigated by using an auditory task.

METHOD

Apparatus

Using analog computer components, a dual-axis critical tracking task was instrumented. Figure 1 shows the block diagram and Figure 2 shows the analog mechanization of the task. Two EAI-TR-20 10 volt analog computers were used in a slaved configuration. The control sticks were identical U S A F type number C-1 Formation sticks with + 10.0 volts output.

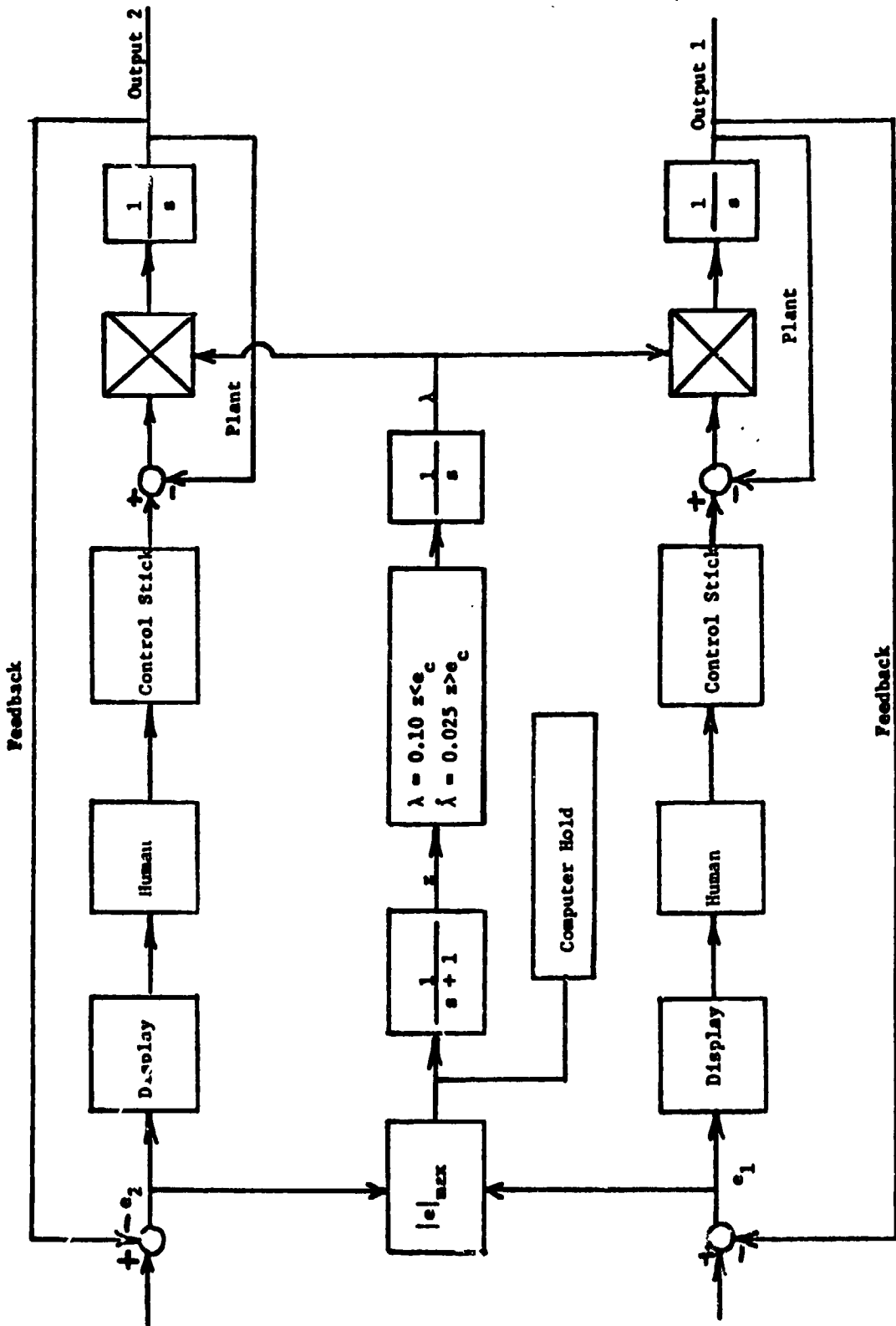


Figure 1. Block Diagram of Dual Axis Critical Task.

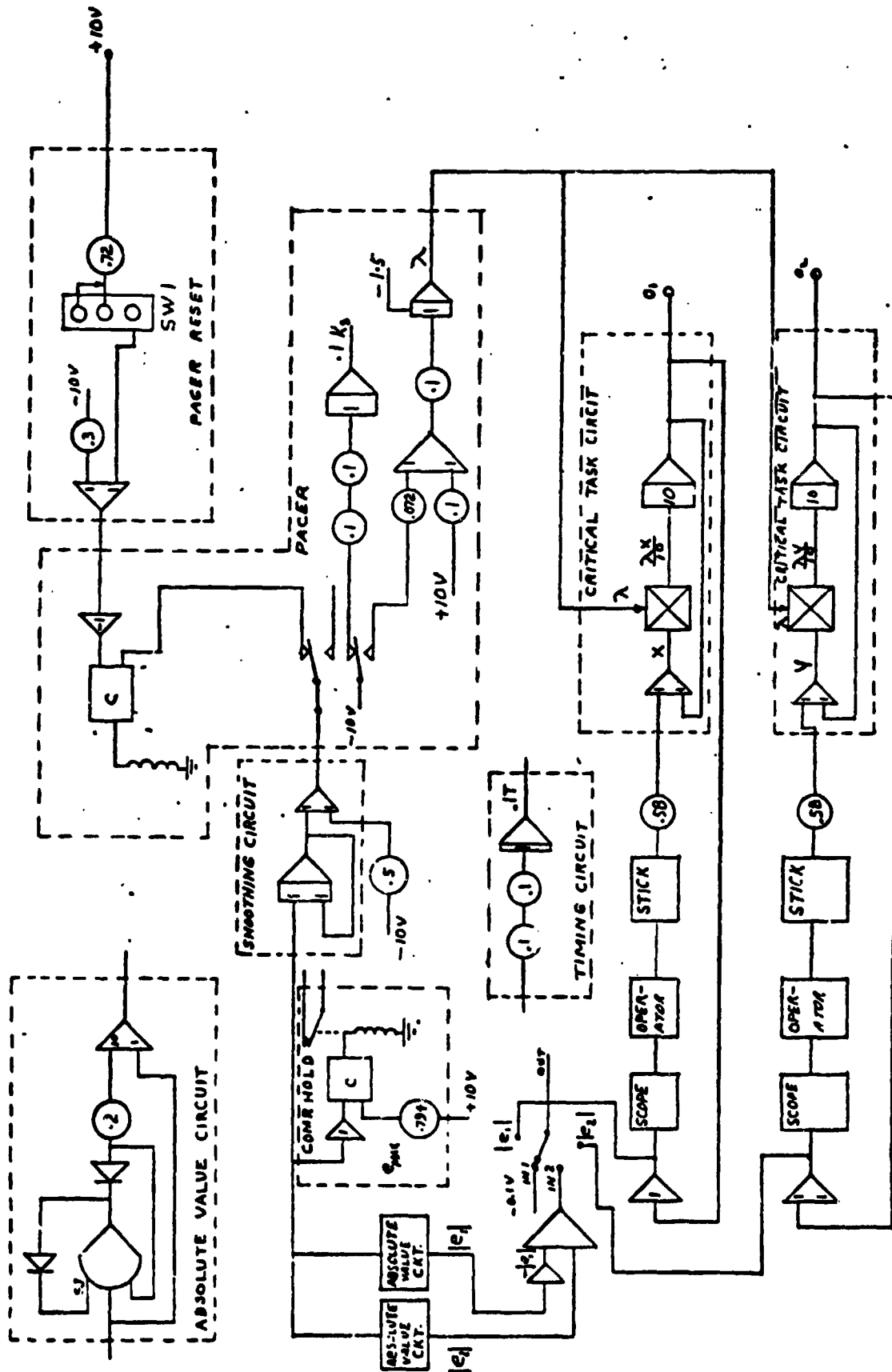


Figure 2. Analog Computer diagram of task.

Testing

Six male students were used as subjects. The subjects reported 20/20 vision and were free from any auditory and psychomotor deficiencies. The subjects were briefed concerning the experiment and the task prior to training. The task was to stabilize simultaneously two identical, increasingly instable, controlled elements (one in each axis). Both line displays and point displays with corresponding stick motion as shown in Table 1 were used. The secondary cognitive task used is a modification of Baddeley Telephone test reported by Guignard (Reference 3). The subordinate hypothesis is that the operator performance is not affected by the work load or by the interactions with any other stresses as different display formats or different stick motions.

Procedure

The subjects were given either a line or a point display on one or two oscilloscopes. They were also given one or two joy stick controls. The primary task was to keep the display on the oscilloscope centered for as long as possible by manipulating the joy stick motion forward and backward or sideward depending on the display motion. The trial was completed when the subject lost control of the display. The criterion was the duration for which the subject held the display within the range. A telephone test was given simultaneously with the tracking task for some trials. The subject's task was to listen carefully to each statement and decide promptly whether it is right (yes) or wrong (no), then call out the decision.

Secondary Task

The subject was given a series of purportedly logical statements, some of which were in fact logically absurd. The task was paced at one statement every five seconds and the number of errors committed were recorded. Omissions of answers were considered as errors.

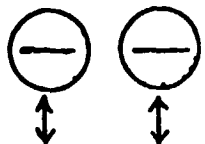
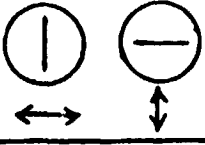
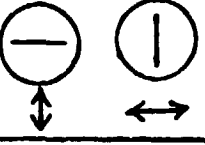
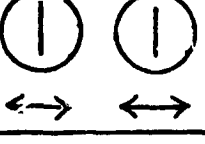
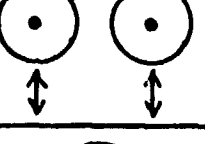
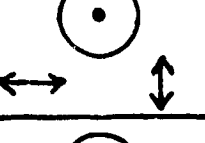
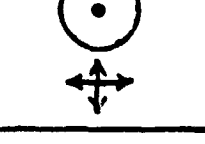
The tracking performance measures recorded for each tracking run were critical divergence frequency (λ), total run time (T) and switching time (t). These voltages were recorded on a Fluke 8000 A digital multimeter.

RESULTS

The detailed statistics are shown in an integrated tabular and graphic form (Tables 2a, 2b, 3 and 4 and Figures 3, 4 and 5).

The critical divergence frequency showed a small degradation due to loading conditions. Condition 6 showed the largest variability. The mean value did not vary much.

TABLE I
TRACKING DISPLAY CONDITIONS

CONDITION 1	
CONDITION 2	
CONDITION 3	
CONDITION 4	
CONDITION 5	
CONDITION 6	
CONDITION 7	
CONDITION 8	

DISPLAY 

STICK MOTION 

TABLE 2a - F VALUES: CELL TO CELL ANALYSIS BY ROWS
(without loading)

CELL POSITION	F VALUES		
	CRIT. DIV. FREQ.	TOTAL TIME	SWITCHING TIME
11-12	0.000	0.0732	0.1734
11-13	3.8787	4.0922	6.3822
11-14	4.4285	4.8378	12.1479
11-15	1.0624	1.4899	1.2860
11-16	7.4151	7.7492	3.5238
11-17	1.0481	0.7196	0.1344
11-18	1.8939	2.0711	0.5387
12-13	3.5496	4.1894	4.6193
12-14	3.9044	4.7966	8.7741
12-15	0.9918	1.6841	0.5545
12-16	7.1871	7.9091	2.5902
12-17	1.0233	0.9004	0.1576
12-18	1.5189	2.1542	0.0187
13-14	0.0069	0.0055	0.1491
13-15	0.8657	0.6594	1.9473
13-16	1.8724	1.9272	0.0212
13-17	0.2880	0.5039	3.2496
13-18	1.0756	0.9739	4.7906
14-15	0.8155	0.6447	3.9914
14-16	2.2003	2.2111	0.2382
14-17	0.2288	0.4705	5.4396
14-18	1.0742	1.0151	8.8348
15-16	4.2248	3.9734	1.0638
15-17	0.0638	0.0014	0.4274
15-18	0.0000	0.0081	0.6892
16-17	2.8889	3.3964	2.0881
16-18	4.6395	4.5833	2.7532
17-18	0.0698	0.0008	0.0009

TABLE 2b - F VALUES: CELL TO CELL ANALYSIS BY ROWS
(with loading)

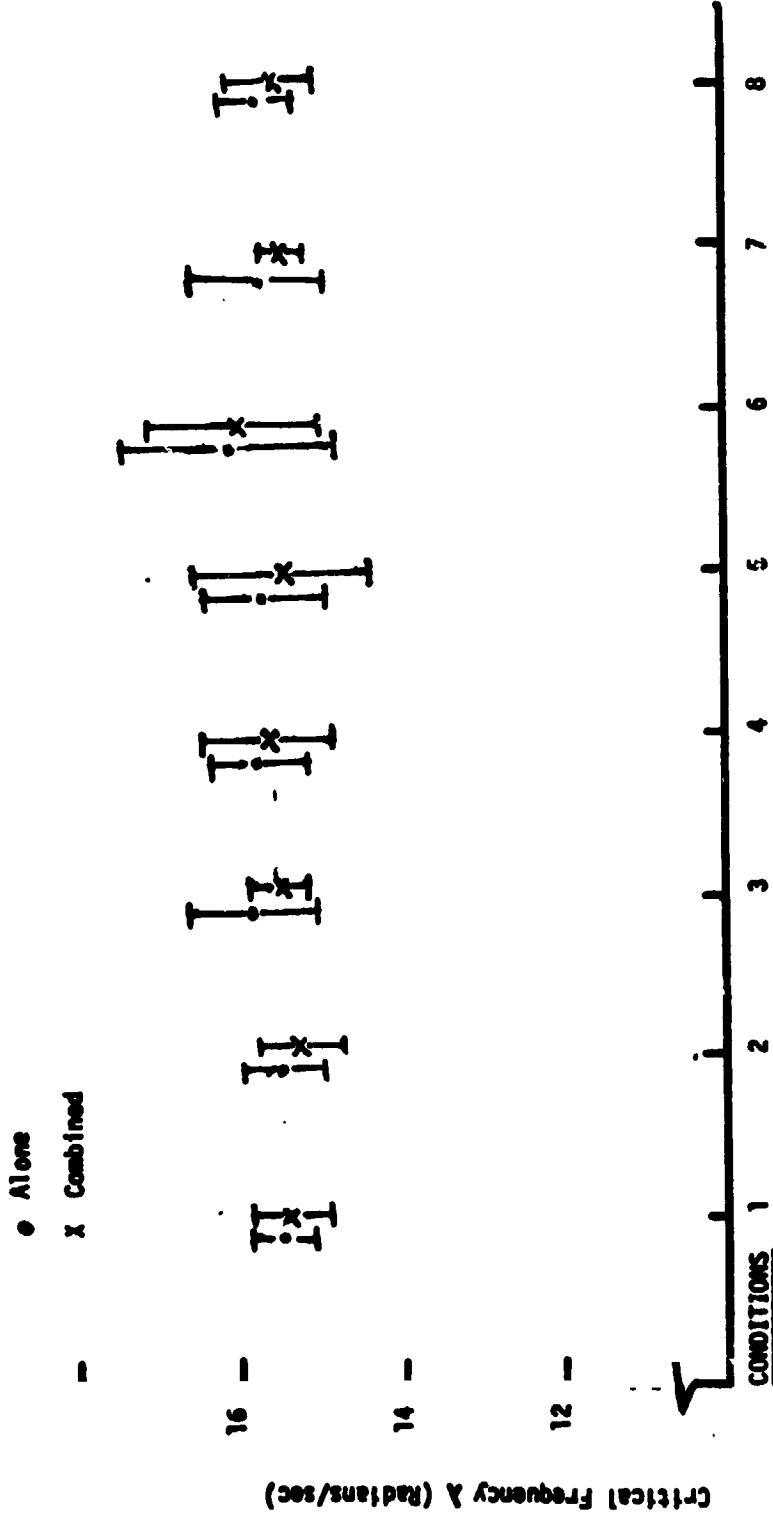
CELL POSITION	F VALUES		
	CRIT. DIV. FREQ.	TOTAL TIME	SWITCHING TIME
21-22	0.2214	0.0510	0.0145
21-23	0.0358	0.0551	0.0115
21-24	0.6922	0.7156	1.3000
21-25	0.1494	0.0055	2.0083
21-26	6.8257	7.1861	1.5481
21-27	5.3764	6.4881	17.6465
21-28	0.1008	6.0484	2.6958
22-23	0.4259	0.2110	0.0498
22-24	0.2479	0.4606	1.4299
22-25	0.4901	0.1438	1.6136
22-26	5.4596	6.4859	1.6724
22-27	7.8685	7.6340	13.6066
22-28	0.5673	0.0738	2.1070
23-24	0.9554	1.0317	1.1348
23-25	0.0672	0.0079	2.2807
23-26	7.4094	7.9181	1.4005
23-27	4.3134	5.2546	19.4613
23-28	0.0288	0.0150	3.0805
24-25	0.9527	0.7045	4.6541
24-26	3.0031	3.2244	0.0845
24-27	5.5733	6.4243	17.3016
24-28	1.0807	0.7032	5.6711
25-26	6.1912	5.7914	4.4860
25-27	0.7961	1.3108	1.7789
25-28	0.0020	0.0281	0.0002
26-27	14.5597	15.9681	12.5341
26-28	7.4264	6.7553	5.1329
27-28	2.5223	3.8301	2.8412

TABLE 3 - F VALUES: CELL TO CELL ANALYSIS BY COLUMN

CELL POSITION	F VALUES		
	CRIT. DIV. FREQ.	TOTAL TIME	SWITCHING TIME
11-12	0.0096	0.2099	0.0415
21-22	0.0067	0.0045	0.0757
31-32	4.7727	5.4985	4.5306
41-42	0.8963	1.1465	2.0678
51-52	2.2544	1.5110	3.9853
61-62	0.2488	0.2644	0.1202
71-72	6.1948	6.2675	6.8435
81-82	2.7331	2.1998	2.8019

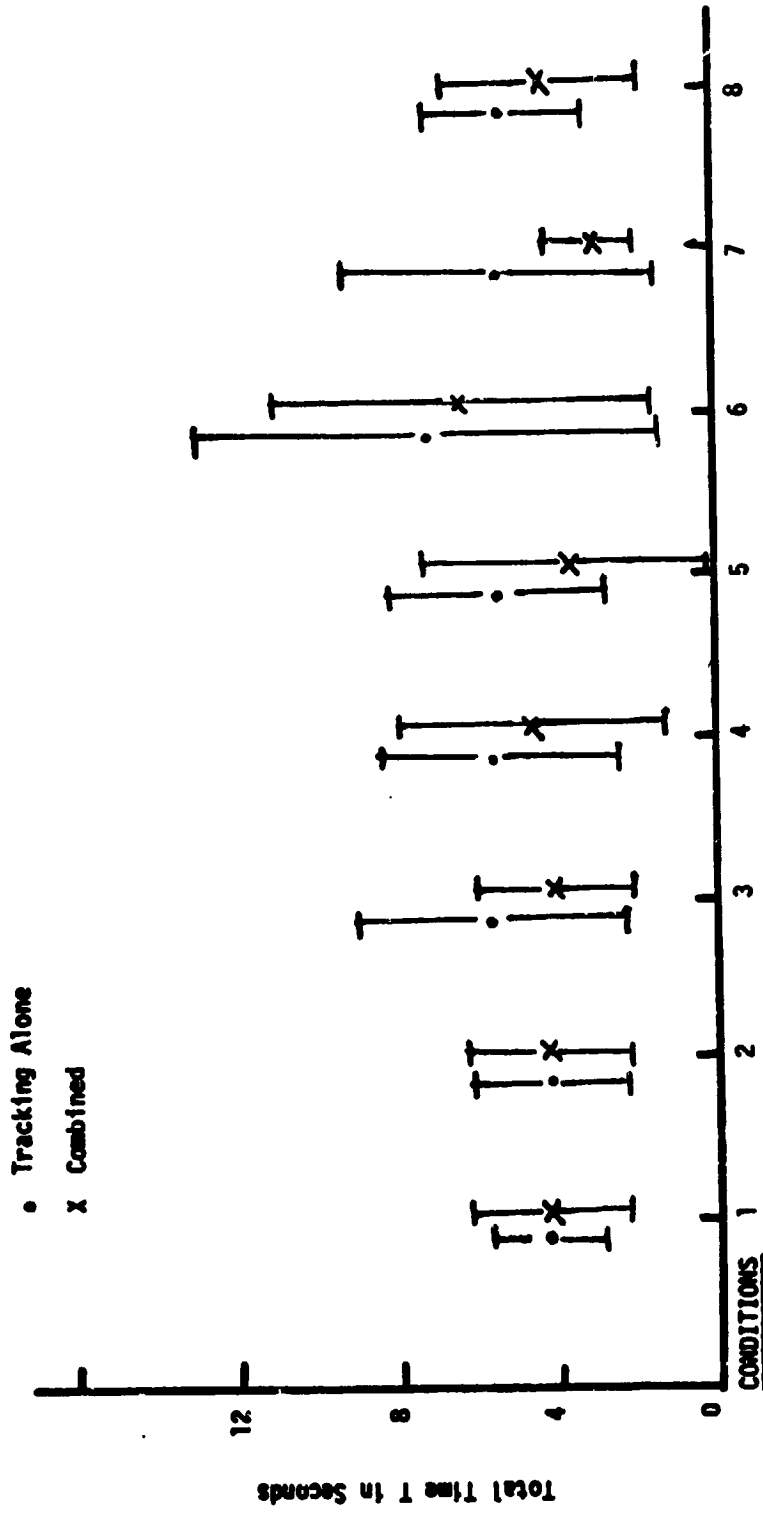
TABLE 4 - F VALUE: ROW TO ROW ANALYSIS

	F VALUES		
	CRIT. DIV. FREQ.	TOTAL TIME	SWITCHING TIME
Row 1 - Row 2	9.4554	9.6113	12.1304



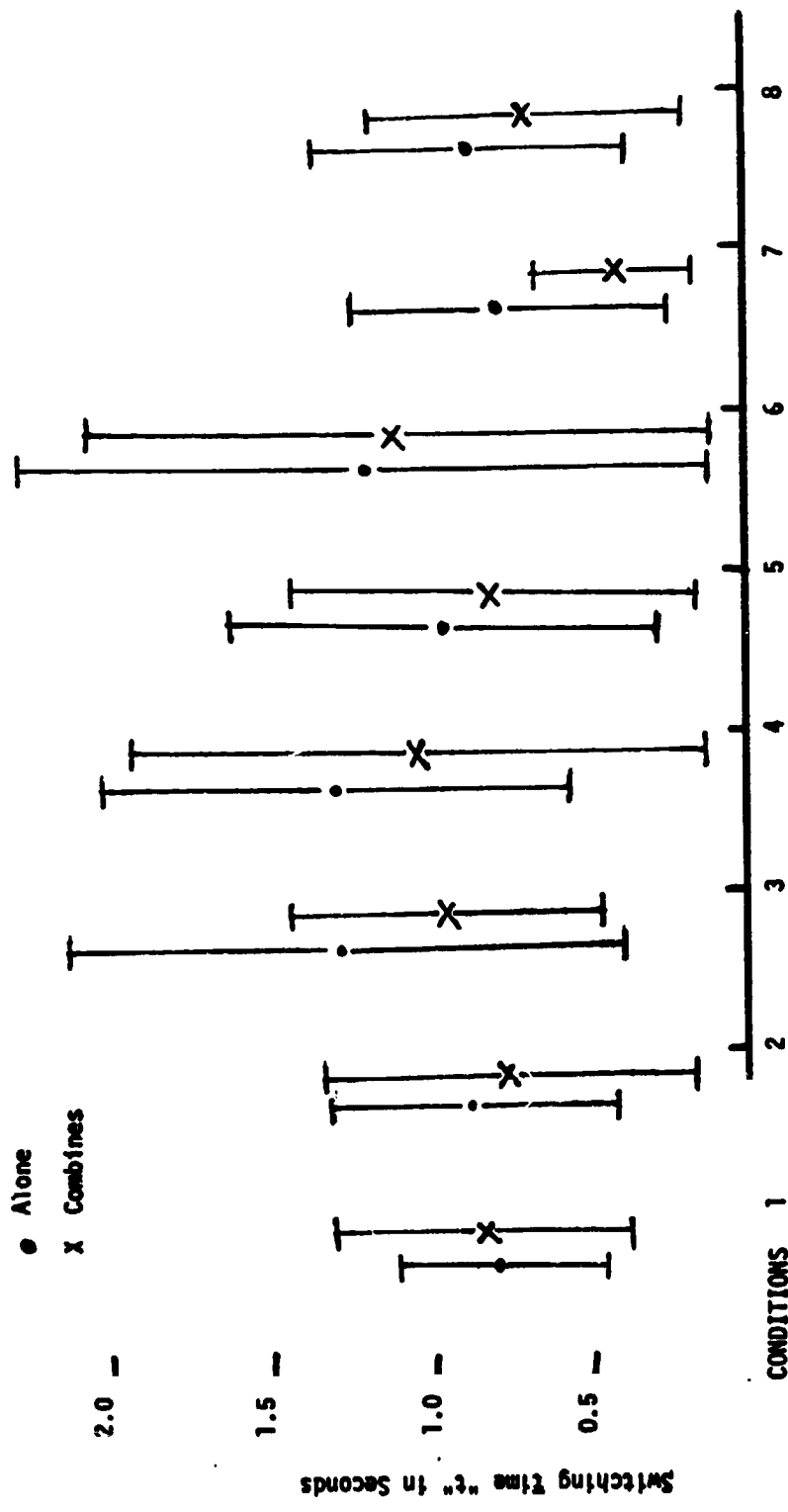
	Mean	Std. Dev.	N
Alone	15.503	.3217	36
Combined	15.471	.4605	36
Alone	15.495	.4655	36
Combined	15.242	.4835	36
Alone	15.789	.7955	36
Combined	15.449	.6090	36
Alone	15.771	.6813	36
Combined	15.602	.8090	36
Alone	15.628	0.6413	36
Combined	15.292	1.1564	36
Alone	16.159	1.391	36
Combined	16.009	1.1270	36
Alone	15.676	.9469	36
Combined	15.261	.2705	36
Alone	15.628	.4397	36
Combined	15.429	.5615	36

Figure 3 Critical frequency for tracking with and without secondary loading



<u>Mean</u>	
Alone	4.097
Combined	3.907
<u>Std. Dev.</u>	
Alone	1.399
Combined	2.014
N	36

Figure 4 Total time for tracking with and without secondary loading



<u>Mean</u>	
Alone	0.8083 0.8639 1.233 1.3028 0.9583 1.188 0.0277 0.833
Combined	0.8305 0.8138 0.8444 1.0254 0.7972 1.094 0.4170 0.6772
<u>Std.Dev.</u>	
Alone	0.3443 0.4564 0.9011 0.7644 0.6806 1.1208 0.5117 0.536
Combined	0.5333 0.6088 0.5341 0.3486 0.6722 1.0694 0.2555 0.4902

Figure 5 Rate switching time for tracking with and without secondary loading

The total time had the highest mean and the variability for condition 6. Except conditions 1 and 2, all the other conditions showed a general degradation under the effects of secondary loading.

Conditions 3, 4 and 6 yielded the highest mean for the switching time but condition 6 has the highest variability. All the conditions except 1 and 2 showed a deterioration in performance with loading.

Mean correct response showed the largest variability in conditions 1, 4 and 6 in which the motions of two displays were on the same axis.

Two way analysis of variance yielded these results. For a rejection at the 5% level, an F value of 3.92 is used. Based on this, there was a significant difference for all the three performance measures between the two line displays (condition 1) and the two dot displays (condition 6) with loading and without loading. The dot displays have a greater mean value. Among similar displays, the side motion of the sticks (condition 4) yielded greater mean compared to forward-backward motion (condition 1). Between conditions 1 and 4, it showed a significant difference without secondary loading. Under loading conditions there was a significant difference between two dot display and one dot display conditions comparing the loading and unloading conditions. A significant difference was observed in condition 7 only (Table 3).

CONCLUSIONS

The secondary loading did not affect the critical divergence frequency but deteriorated the performance measures of total tracking time and switching time (except in condition 2). The high correct response percentage under loading conditions indicated that the subjects were well motivated for the task. A large variability was exhibited in condition 6 and the subjects rated this condition to be the most comfortable one. The two dot displays and the sideward motion of the sticks showed higher mean values for the performance measures.

REFERENCES

1. Jex, H. R., Jewell, W. F. and Allen, R. W., "Development of the Dual Axis and Crosscoupled Critical Tasks," Proceedings of the 8th Annual Conference on Manual Control, 1972.
2. Jex, H. R., McDonnell, J. D. and Phatak, A. V., "A Critical Tracking Task for Man/Machine Research Related to the Operator's Effective Delay Time," Part I and II, NASA CR-116 and CR-674, November 1966/January 1967.

- | | | | | | | | | | |
|--|--|--|--|--|--|--|--|--|--|
| | | | | | | | | | |
|--|--|--|--|--|--|--|--|--|--|
3. Guignard, J. C., "A Telephone Test for Use in Combined Stress Experiments," Wright State University Environmental Stress Research Unit, Internal Memo 70-6, December 1970.

N75 33711

CONTINUOUS PERFORMANCE MEASUREMENT
IN FLIGHT SYSTEMS

By Edward M. Connelly, Nicholas A. Sloan,
and Robert M. Zeskind

Omnemii, Inc.

ABSTRACT

The desired response of many man-machine control systems can be formulated as a solution to an optimal control synthesis problem where the cost index is given and the resulting optimal trajectories correspond to the desired trajectories of the man-machine system. Optimal control synthesis provides the reference criteria and the significance-of-error information required for performance measurement. The synthesis procedure described in this paper provides a continuous performance measure (CPM) which is independent of the mechanism generating the control action. Therefore, the technique provides a meaningful method for on-line evaluation of man's control capability in terms of total man-machine performance.

The synthesis procedure converts a cost index such as

$$I = \int_0^{t'} F(X, t) dt$$

which is doubly dependent on system state (present state and initial state) into a function $\theta(X)$ of the state variable vector X . The $\theta(X)$ function is termed "cost-to-go" since its value is the cost to the objective if the desired (optimal) performance is utilized. The function is part of the CPM and has several interesting properties. First, its partial derivatives with respect to the state variables can be identified with the auxiliary variables generated by the Maximum Principle of Pontryagin. Second, the function is a Lyapunov function for the system if optimal performance is achieved. As a result, it acts as a convenient stability indicator for operation with man-in-the-loop.

The paper includes a description of the CPM, and a theoretical development of the synthesis procedure and its applications.

CONTINUOUS PERFORMANCE MEASUREMENT

Every performance measure consists of two parts:

1. The reference or criteria portion, and
2. The measurement of the significance (importance) of deviations from that criteria.

Continuous performance measurement (CPM) is a measurement technique whereby the desired reference control is known and the significance of any control errors is evaluated at each point in the problem space. Evaluation of control errors is based on the effect of those errors on total system summary performance. For example, if conservation of fuel is deemed most important in a particular control problem, the CPM continuously (instantaneously) evaluates the effect of any control errors on excessive use of fuel for the total task. Finally, the CPM is state determined so that, whatever path the controlled element takes, whether due to correct or incorrect controls, the CPM provides the reference and control error sensitivity information at the new state.

CLASSICAL PERFORMANCE MEASUREMENT

It should be recognized that this method of performance measurement differs significantly from classical methods which are generally summary, or at least averaged, measurements and do not include the desirable instantaneous reference and error sensitivity characteristics just described. Such summary measures provide a single numerical evaluation for the total run and thus, do not provide specific information about performance along the run. Summary measures do not reveal important information about how superior performance was achieved or what factors cause difficulties leading to poor performance. In training problems, the use of summary measure information results in non-specific feedback so that part of the trainee's learning task is to sort out what he did wrong from what he did right from the summary measure information. This, of course, requires additional runs just to accommodate the sorting process.

But, summary measures do provide useful information, particularly in providing the basis for computing the continuous performance measure (CPM). In order to understand this relationship, consider a problem where the controlled element, the vehicle, is supposed to move along an isolated reference path and the error (deviation) from

that path is presented to the operator in some way so that he can control the vehicle. Total system performance is scored in a standard way, such as, with the integral of the error squared. A summary measurement value is provided at the end of each run. As discussed previously, the summary performance measure has some serious limitations as follows:

1. The performance information is not specific as to what the operator is doing when he performs poorly or performs well,
2. There is no absolute reference,
3. The measure value is a function of initial problem conditions so that the operator does not know how to interpret the numerical summary score values, and
4. There is no direct measure of control error significance.

CONTINUOUS PERFORMANCE MEASUREMENT AND OPTIMAL CONTROL

Consider how a summary measure can be converted into an instantaneous measure. Suppose that the vehicle under control is at point A; it is displaced from the isolated reference path by amount A . Corresponding to each summary performance measure is a best incremental motion for the vehicle from point A. The best, as used here, means the incremental motion which is the portion of the total solution trajectory from point A to the terminal point that minimizes the summary measure selected. Since the vehicle will move from point A to another point B, and so forth, the use of the best control results in motion of the vehicle along the best solution path starting from A. The resulting summary measure value will be the lowest possible given the system started at point A. This solution path is a new reference path which may or may not intersect with the original isolated reference path. The new reference path is the optimal vehicle trajectory from point A and every point along that optimal path. If the optimal control rule and vehicle trajectory are determined everywhere in the problem space of interest, instead of just from point A, a reference control rule and corresponding vehicle trajectory are available at each point in the problem space.

The CPM is an instantaneous measure developed from the selected summary measure, which continuously determines the difference between best incremental control and the operator control. In addition, and very important, the CPM provides error sensitivity

weighting and with it, it is possible to evaluate the seriousness of any control operator error. Considering the CPM, it is easy to visualize that the reference system is no longer represented by an isolated reference trajectory, but that problem space is actually filled with reference trajectories. It may seem, at first, that a set of reference trajectories which fill the problem space may require a lot of storage, however, the reference functions and performance evaluation are used incrementally and, therefore, may be stored conveniently in their differential equation form.

CONSTRUCTION OF THE CPM

Reference Equations

Construction of the CPM begins with a mathematical model of the aircraft vehicle dynamics. The vehicle equations in this development are a set of differential equations which may or may not be linear. These equations are given by

$$\dot{x}_i = f_i(x, u), \quad i = 1, 2, \dots, n, \quad (1)$$

where x is the vehicle state vector

$$x = (x_1, x_2, \dots, x_n)$$

and u is the vehicle control vector (controller's inputs)

$$u = (u_1, u_2, \dots, u_m).$$

The control vector will probably be constrained in some way by the physical limitations of the equipment. For many problems, the constraints may take the form

$$|u_j| < k_j \quad (2)$$

where $j = 1, \dots, m$.

Cost Function

The cost function (CF) is of the form

$$I(u; t) = \int_0^t F(x, u) \, dt \quad (3)$$

If a fixed upper limit t_f is understood, then the CF is of the form $I(u; t_f) = I(u)$. It is required either that $F(x, u) > 0$ or that, in special cases $F(x, u) \geq 0$. Functions of this type are termed positive definite or positive semi-definite, respectively.

If the cost to be measured is "time to accomplish the task," then $F(x, u) \equiv 1$. Other quantities may be used to measure the operator's control cost, for instance "fuel used to accomplish the task" or "energy expended to accomplish the task."

Control Equation

In man-machine systems, the operator's control actions are the functional "analog" of the control equations. For this development, a fixed control policy is assumed for the purpose of computing the best policy. Once that is accomplished, the evaluation of any control including a human operator's control can be evaluated. The fixed policy is given in the form

$$u_k = g_k(x),$$

$$k = 1, \dots, m,$$

or in vector form by

$$u = g(x). \tag{4}$$

The Free System

Let $u = g(x)$ be a fixed control policy; then the free system is defined as the system with feedback control

$$\dot{x} = f(x, g(x)). \tag{5}$$

This system represents the behavior of the vehicle given a certain control policy.

The free system is said to be convergent if it satisfies the control task and the cost function takes on a finite value. This last condition means that for the fixed control policy $u = g(x)$ we have that $I(u) = I(u; t_f)$ has a finite value where t_f is the time required to achieve the control task.

Generating the Cost-to-Go (CTO) Functions

In this section the CTO function for the free system is constructed. For a particular control policy, $u = g(x)$, and a fixed time interval, $(0, t_f)$, the definition of the CF (3) yields

$$I(g(x)) = \int_0^{t_f} F(x, g(x)) \, d\tau \quad (6)$$

Let $x(t)$ be a solution of the free system and introduce a function $\theta(x)$ defined along $x(t)$ by

$$\theta(x(t)) = \int_t^{t_f} F(x(\tau); g(x(\tau))) \, d\tau \quad (7)$$

Thus, at the point $x(t)$ on the solution, $\theta(x(t))$ is the cost (resources) to be expended before $x(t)$ reaches its terminal value $x(t_f)$. This justifies the terminology "Cost-to-Objective." Notice that, as constructed, that $\theta(x)$ can be defined independently of solutions as a function of the state variable x so that along any solution $x(t)$

$$\left. \frac{d\theta}{dt} \right|_{x(t)} + F(x(t), g(x(t))) = 0 \quad (8)$$

For $\theta(x)$ defined along a particular solution by (7), equation (8) follows easily. The claim above means that, given a control policy $u = g(x)$, then there is a function $\theta(x)$ associated with it so that along any solution $x(t)$ of the free system equation (8) is true.

For a two-dimensional state variable $x = (x_1, x_2)$, Figure 1 indicates the behavior of convergent paths with respect to decreasing levels of $\theta(x)$. The following is a list of properties of the θ function:

- a. $\theta(x)$ decreases as $I(g(x); t)$ increases along a solution path.
- b. The CTO to the objective is zero, given that the present state is the objective, i.e., $\theta(0) = 0$.
- c. The CTO function $\theta(x)$ is positive for all points in the state space except the origin; i.e., $\theta(x)$ is positive definite. This is a result of the restriction $F(x, u) > 0$.

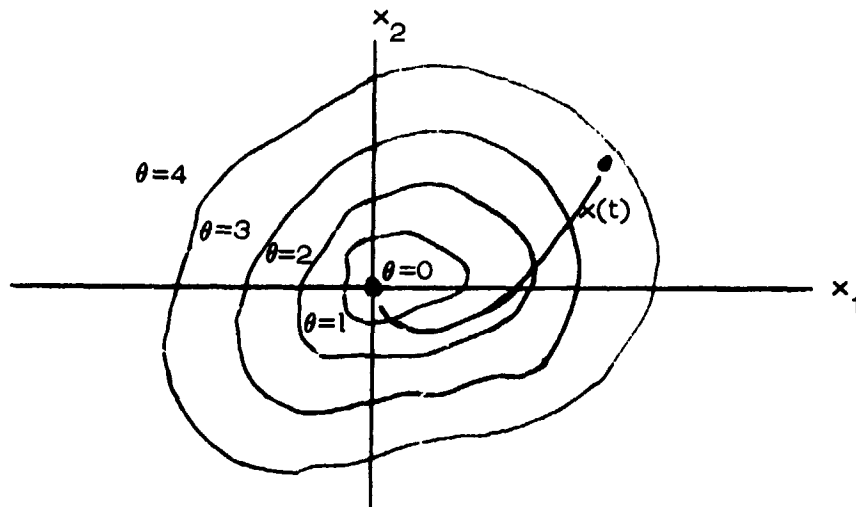


FIGURE 1 CTO FUNCTION $\theta(x)$

d. The function $\theta(x)$ is a convenient state space representation of the level of cost. The CTO function can be used as an indicator of system convergence in the special case where the origin is an equilibrium point of the system. $\theta(x)$ is a Lyapunov function for the free system with respect to the origin.

e. If the function F is $F(x,u) \equiv 1$ (i.e., the index I measures time), then $\theta(x)$ is the "time-to-objective."

f. For every free convergent system that yields a finite value of the cost function (i.e., a meaningful cost function), there exists a corresponding CTO function.

g. If t_f is the solution time, $\theta(x(t_f)) = 0$, since $x(t_f) = 0$. If $x(t_0)$ is the initial state, then $\theta(x(t_0)) = I(t_f)$.

h. The partial derivatives of $\theta(x)$ with respect to the state variables can be identified with the auxiliary variables generated by the Maximum Principle of Pontryagin.

Constructing the Performance Measure

The optimal control function $u^* = g^*(x)$ is defined as the control policy that minimizes the cost to reach the objective; i.e., if any other control policy is applied, the cost is either equal or greater than those needed by the optimal policy. Represent this by the relation

$$I(u^*) \leq I(u) \tag{9}$$

Figure 2 shows two paths from the initial state to the terminal state. Each path is associated with a different control policy. If u^* is the

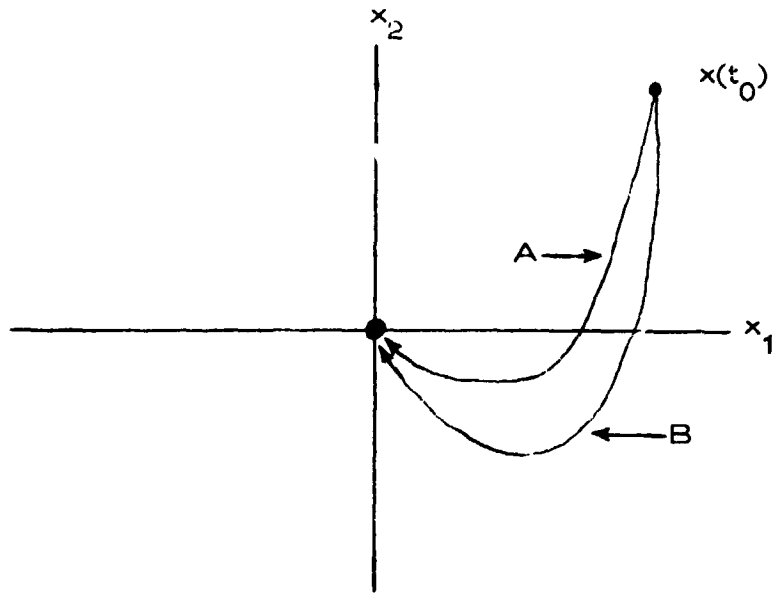


FIGURE 2 TWO POSSIBLE PATHS

optimal policy, then the cost incurred along its resulting path must be less than or equal to the resources depleted along any other path.

If the optimal control function u^* can be found, then the corresponding function θ^* can be computed. This function, $\theta^*(x)$, can be referred to as the "minimum CTO" or the "CTO" if the optimum control policy is used. Since $\theta^*(x)$ is a function of the state variables, its rate of change along paths produced by any control policy can be computed. That is, given any control policy $g(x)$, the free system can be solved with this control policy. Denoting this process by $\left. \frac{d\theta^*}{dt} \right|_g$, a new

function ϕ can be defined by

$$\phi(x, g(x)) = \left. \frac{d\theta^*}{dt} \right|_g + F(x, g(x)) \quad (10)$$

where $g(x)$ represents any control policy subject to the boundedness conditions of (2). If the optimal control policy is used, then, due to the construction of θ^* by (8)

$$\phi(x, g^*(x)) = \left. \frac{d\theta^*}{dt} \right|_{g^*} + F(x, g^*(x)) = 0 \quad (11)$$

Now it is asserted that a necessary and sufficient condition for $u^* = g^*(x)$ to be the optimum control policy is that

$$\phi(x, u^*) = \min_u \phi(x, u) = 0. \quad (12)$$

Condition (12) immediately implies that for any allowable control

$$\phi(x, u) \geq 0. \quad (13)$$

The function ϕ is the desired continuous performance measure which is the sum of the rate of reduction of least cost (θ^*) and the rate of cost incurred. Thus the instantaneous value of ϕ is the instantaneous effect of the control error on summary performance - thus allowing continuous evaluation of the operator control (u).

Constructing $\theta(x)$

$\theta(x)$ has been constructed along solutions of the plant by defining

$$\theta(x(t)) = \int_t^{t_f} F(x(\tau), g(x(\tau))) d\tau \quad (14)$$

From this equation one must have

$$\left. \frac{d\theta}{dt} \right|_{x(t)} + F(x(t), g(x(t))) = 0$$

and one derives

$$\frac{\partial \theta}{\partial x}(x(t)) \frac{dx}{dt} + F(x(t); g(x(t))) = 0 \quad (15)$$

along a solution

$$\frac{\partial \theta}{\partial x}(x(t)) f(x(t), g(x(t))) + F(x(t), g(x(t))) = 0 \quad (16)$$

Now let $\theta(x)$ be the solution of the first order partial differential equations

$$\frac{\partial \theta}{\partial x}(x) f(x, g(x)) + F(x, g(x)) = 0 \quad (17)$$

with the condition $\theta(0) = 0$, where $x = 0$ is the desired terminal state. Then θ is, only state-dependent and is free of any particular solutions.

A NECESSARY AND SUFFICIENT CONDITION FOR A POLICY TO BE OPTIMAL

In the previous section, it was stated that a necessary and sufficient condition for a policy u^* to be optimal is that

$$\phi(x, u^*) = \min_u \phi(x, u) = 0$$

The purpose of this section is to make this result more precise by indicating a proof. In order to establish the necessity, a proof by contradiction can be used. Let $u^* = g(x)$ be an optimal policy and suppose that there is another policy $u_0 = g_0(x)$ such that

$$\phi(x, g_0(x)) < \phi(x, g^*(x)) = 0 \quad (18)$$

Then

$$\left. \frac{d\theta^*}{dt} \right|_{g_0} + F(x, g_0(x)) < 0 \quad (19)$$

and thus

$$\frac{d\theta^*}{dt}(x_0(t)) < -F(x_0(t), g_0(x_0(t))) \quad (20)$$

where $x_0(t)$ is a trajectory of the vehicle under the control policy $u_0 = g_0(x)$. Integrating

$$\int_0^{t_f} F(x_0(\tau), g_0(x_0(\tau))) d\tau < - \int_0^{t_f} \frac{d\theta^*}{d\tau}(x_0(\tau)) d\tau \quad (21)$$

Therefore

$$I(u_0) < - [\theta^*(x_0(t_f)) - \theta^*(x_0(0))] = \theta^*(x_0(0)) = I(u^*) \quad (22)$$

since $x_0(t_f) = 0$, the terminal state. This contradicts the fact that u^* is optimal.

To show the sufficiency, assume that the solution time using the control policy u^* is t_1 . (23)

$$\int_{t_0}^{t_1} \phi(x, g^*(x)) d\tau = \int_{t_0}^{t_1} \frac{d\theta^*}{d\tau} d\tau + \int_{t_0}^{t_1} F(x, g^*(x)) d\tau = 0$$

but,

$$\int_{t_0}^{t_1} \left. \frac{d\theta^*}{d\tau} \right|_{g^*} d\tau = \theta^*(t_1) - \theta^*(t_0) \quad (24)$$

where

$$\theta^* (t_1) = 0 \quad (25)$$

Also

$$\int_{t_0}^{t_1} F(x, g^*(x)) \, d\tau = I(u^*; t_1) - I(u^*; t_0) \quad (26)$$

where

$$I(u^*; t_0) = 0 \quad (27)$$

Thus the cost of using the control policy u^* , represented by $I(u^*) = I(u^*; t_1)$, is

$$I(u^*) = \theta^* (t_0) \quad (28)$$

One can integrate (ϕ) in a similar manner assuming that the solution time for another control policy $u = g(x)$ is t_2 . Thus

$$\begin{aligned} \int_{t_0}^{t_2} \phi(x, g(x)) \, d\tau &= \int_{t_0}^{t_2} \frac{d\theta^*}{d\tau} \, d\tau + \int_{t_0}^{t_2} F(x, g(x)) \, d\tau \\ &= \theta^* (t_2) - \theta^* (t_0) + I(u; t_2) - I(u; t_0) \end{aligned} \quad (29)$$

but

$$I(u; t_0) = 0 \quad (30)$$

and $\theta^* (t_2) = 0$ since the desired state is the origin where θ^* is zero. Thus, the cost of using the control policy u represented by $I(u)$ is

$$I(u) = I(u; t_2) = \theta^* (t_0) + \int_{t_0}^{t_2} \phi(x, g(x)) \, d\tau \quad (31)$$

One has $\phi(x, g(x)) \geq 0$ and clearly the integral of this function must be greater than or equal to zero. Thus one concludes that

$$I(u^*) \leq I(u) \quad (32)$$

which is what was set out to be proven.

DEVELOPING THE PERFORMANCE MEASURE FOR A
LINEAR PLANT WITH QUADRATIC COST FUNCTION

Let x and u be vectors. x^T and u^T their respective vector transposes. Consider the plant

$$\dot{x} = Ax + Bu \quad (33)$$

with the cost index

$$I = \int_0^{\infty} \left[\frac{1}{2} x^T Qx + \frac{1}{2} u^T Ru \right] dt \quad (34)$$

Assume that u is not constrained and that Q and R are positive definite symmetric matrices. Then the optimal control for this system becomes

$$u^* = -R^{-1} B^T Kx \quad (35)$$

where K is the constant positive definite symmetric matrix solution of the nonlinear matrix algebraic equation

$$KA + A^T K - KBR^{-1} B^T K + Q = 0 \quad (36)$$

The continuous performance measure is given by:

$$\phi = \frac{\partial \theta}{\partial x} Ax + \frac{\partial \theta}{\partial x} Bu + \frac{1}{2} x^T Qx + \frac{1}{2} u^T Ru \quad (37)$$

Then, to minimize ϕ , one must have

$$\frac{\partial \phi}{\partial u} = \frac{\partial \theta}{\partial x} B + u^T R = 0 \quad (38)$$

This implies that the optimal controller is of the form

$$u^* = -R^{-1} B^T \left(\frac{\partial \theta}{\partial x} \right)^T \quad (39)$$

Equations (35) and (39) indicate that this is indeed true, i.e.,

$$\frac{\partial \theta}{\partial x} = x^T K \quad (40)$$

which means

$$\theta = \frac{1}{2} x^T Kx \quad (41)$$

Take

$$u = u^* + \Delta u = -R^{-1} B^T \left(\frac{\partial \theta}{\partial x} \right)^T + \Delta u.$$

Introduce this into (37) and, using (40), it can be shown that

$$\phi = \frac{1}{2} (\Delta u)^T R (\Delta u) \tag{42}$$

SESSION V
SYSTEM IDENTIFICATION

Chairman: RENWICK E. CURRY

PRECEDING PAGE BLANK NOT FILMED

N75 33712

PROBLEMS, QUESTIONS AND RESULTS IN THE USE OF THE BBN-MODEL

By Dieter Dey

VFW-Fokker, Bremen, Germany

SUMMARY

The work reported in this paper was done within the Human-Engineering Group of the Institute of Aeronautics and Astronautics of the Technical University of Berlin and is documented in detail in reference 1.

Starting with the human-engineering background a short but systematic review of the structure and the elements of the BBN-model is given to look at the inherent problems of the model. Numerical results of a simple example using the BBN-model are taken to demonstrate the influence of the variation of different parameters of the model on the covariance matrices of the state and observation vector.

It is shown that the parameters of the model could not be identified with measured mean squared values from a test.

SYMBOLS

<u>A</u>	system matrix
<u>B</u>	control matrix
<u>C</u>	observation matrix
<u>C</u> ^T	transposed observation matrix
E { }	estimate
e	control error
<u>G</u>	weighting matrix
G	weighting factor
<u>L</u>	optimal gain matrix
P _{y_i}	observation noise ratio of the state x _i
P _u	motor noise ratio of the control function u
<u>P</u>	covariance matrix of the estimation error

\underline{Q}	weighting matrix
\underline{R}	weighting matrix
t	time
T	observation time
T_N	neuromuscular lag time constant
$\underline{u}(t)$	optimal control vector at time t
$\underline{\dot{u}}$	derivative of the control vector
\underline{u}_c	commanded control vector
\underline{v}_u	motor noise vector with zero mean gaussian white noise elements
\underline{V}_u	power density matrix of the motor noise vector
\underline{v}_y	observation noise vector with zero mean gaussian white noise elements
\underline{V}_y	power density matrix of the observation noise vector
\underline{V}_y^{-1}	inverse power density matrix
\underline{w}	disturbance vector with zero mean gaussian white noise elements
\underline{W}	power density matrix of the disturbance vector
\underline{x}	state vector
$\underline{x}(t_0)$	initial value of the state vector
$\underline{\dot{x}}$	derivative of the state vector
\underline{x}_e	extended state vector
$\hat{\underline{x}}(t-\tau)$	estimate of the delayed state
\underline{X}	covariance matrix of the state vector
\underline{y}_p or \underline{y}	delayed and noisy observation vector
\underline{Y}	covariance matrix of the observation vector
\underline{y}_u	system output due to control input
$\delta(t-t')$	delta function at time $t-t'$
τ	delay time

INTRODUCTION

We studied the guidance and control of a VTOL-aircraft and looked at this task as a hierarchical structured control problem, reference 2. We could not find a tested model describing the human operator in such tasks and so we decided to take the BBN-model developed by Baron, Kleinman and Levison to describe the human operator dealing with a multi variable control problem, references 3 and 4.

The model is based on the assumption, that a well trained operator optimizes a quadratic optimization criterion. It could be used for stabilization tasks of linear, time-invariant systems. The model considers some special characteristics of the human operator as time delay, neuromuscular time lag, observation and motor noise and the ability to extract the first derivative of a displayed value.

Figure 1 shows the structure of the model. The human operator perceives y_p , the delayed and noisy information about the state of the system and its first derivatives. The optimal filter derives $\hat{x}(t-\tau)$, an estimate of the delayed state and the predictor gives $\hat{x}(t)$, the actual estimate of the state. The optimal controller generates $u(t)$, the optimal control vector. Without the introduction of motor noise and the neuromuscular lag time, we have a problem well known to control specialist.

In the state space the system to be controlled including the filter of the disturbance input is described by

$$\dot{\underline{x}}(t) = \underline{A} \underline{x}(t) + \underline{B} \underline{u}(t) + \underline{w}(t)$$

with the covariance matrix of the disturbance vector

$$E \left\{ \underline{w}(t) \underline{w}(t')^T \right\} = \underline{W} \delta(t-t')$$

The delayed and noisy observation vector is defined as

$$\underline{y}_p(t) = \underline{y}(t-\tau) + \underline{v}_y(t-\tau)$$

with the covariance matrix of the observation noise vector

$$E \left\{ \underline{v}_y(t) \underline{v}_y(t')^T \right\} = \underline{v}_y \delta(t-t')$$

Acquired is the controller which minimizes the optimization criterion

$$J(u) = E \left\{ \frac{1}{T} \int_0^T (\underline{x}^T \underline{Q} \underline{x} + \underline{u}^T \underline{R} \underline{u}) dt \right\}$$

At this point we believed, that the optimal control model was not documented for the use of human engineering specialists in a way, giving on one side enough insight in the problems and limitations of the model and on the other make it ready to use. So we decided to derive the equations for the optimal control model step by step, writing a guide book for its use.

CALCULATION OF THE COVARIANCE MATRIX OF THE STATE AND
OBSERVATION VECTOR

Figure 2 shows the optimal control of the described system with the cascade combination of an optimal filter, an optimal predictor and an optimal controller. Herein $\underline{M} = \underline{P} \underline{C}^T \underline{V}_y^{-1}$ is the steady state optimal observer gain matrix, weighting the difference between the estimated delayed state and the actual delayed state.

\underline{P} turns out to be the covariance matrix of the estimation error minimized by the Kalman filter.

$$\underline{P} = E \left\{ \left[\hat{x}(t) - x(t) \right] \left[\hat{x}(t') - x(t') \right]^T \right\}$$

With the analogy between optimal control and optimal filtering it can be shown, that \underline{P} is calculated with the Riccati differential equation.

$$\dot{\underline{P}} = \underline{A} \underline{P} + \underline{P} \underline{A}^T - \underline{P} \underline{C}^T \underline{V}_y^{-1} \underline{C} \underline{P} + \underline{W}$$

For the covariance matrix of the estimated state \underline{X} we get with the optimal feedback law

$$\underline{u}(t) = -\underline{L} \hat{x}(t)$$

and

$$\underline{L} = \underline{R}^{-1} \underline{B}^T \underline{K}$$

and \underline{K} being the stationary solution of the matrix Riccati equation

$$-\dot{\underline{K}} = \underline{A}^T \underline{K} + \underline{K} \underline{A} - \underline{K} \underline{B} \underline{R}^{-1} \underline{B}^T \underline{K} + \underline{Q}$$

$$\underline{X} = e^{\underline{A}t} \underline{P} e^{\underline{A}^T t} + \int_0^t e^{\underline{A}\delta} \underline{W} e^{\underline{A}^T \delta} d\delta + \int_t^\infty e^{\underline{A}(t-\delta)} e^{\underline{A}^T \tau} \underline{P} \underline{C}^T \underline{V}_y^{-1} \underline{C} e^{\underline{A}^T \tau} e^{\underline{A}(t-\delta)} d\delta$$

$$\underline{X} = \underline{XSK} + \underline{XP} + \underline{XD}$$

In this equation $e^{\underline{A}t} = \underline{\phi}(t)$ is the transition matrix of the system to be controlled and $e^{\underline{A}(t-\sigma)} = \underline{\phi}(t-\sigma)$ with $\underline{\bar{A}} = \underline{A} - \underline{B} \underline{L}$ is the transition matrix of the closed loop system. Instead of the integral equations it is possible to derive differential equations. So \underline{XP} is the solution of

$$\dot{\underline{X}} \underline{P} = \underline{A} \underline{X} \underline{P} + \underline{X} \underline{P} \underline{A}^T + \underline{W} \quad \text{at time } t$$

and \underline{XD} is the stationary solution of

$$\underline{\dot{X}}D = \underline{\bar{A}} \underline{XD} + \underline{XD} \underline{\bar{A}}^T + e^{\underline{A}\tau} \underline{P} \underline{C}^T \underline{V}_y^{-1} \underline{C} \underline{P} e^{\underline{A}^T \tau}$$

$e^{\underline{A}\tau}$ can be calculated from

$$\dot{\underline{\Phi}} = \underline{A} \underline{\Phi} \quad \text{at time } \tau$$

The covariance matrix of the observation vector \underline{y} is given by

$$E \left\{ \underline{y}(t) \underline{y}^T(t) \right\} = \underline{Y} = \underline{C} \underline{X} \underline{C}^T$$

INTRODUCTION OF A WEIGHTED CONTROL RATE

Now we have to introduce a weighting of the control rate, which results in the introduction of a first order lag element in the optimal controller. The performance criterion is now

$$J(\underline{u}) = E \left\{ \int_0^T \left(\underline{x}^T \underline{Q} \underline{x} + \underline{u}^T \underline{R} \underline{u} + \dot{\underline{u}}^T \underline{G} \dot{\underline{u}} \right) dt \right\}$$

There is to be defined an extended state vector

$$\underline{x}_e(t) = \left[\underline{x}(t), \underline{u}(t) \right]^T$$

so that we can use the former equations. For this extended state the differential equation we look at, has the form:

$$\dot{\underline{x}}_e(t) = \underline{A}_o \underline{x}_e(t) + \underline{B}_o \dot{\underline{u}}(t) + \underline{w}_o(t)$$

with the matrices

$$\underline{A}_o = \begin{bmatrix} \underline{A} & \underline{B} \\ \underline{0} & \underline{0} \end{bmatrix} \quad \underline{B}_o = \begin{bmatrix} \underline{0} \\ \underline{1} \end{bmatrix} \quad \underline{w}_o = \left[\underline{w}(t) \mid \underline{0} \right]^T$$

The optimal control law is now

$$\dot{\underline{u}}(t) = -\underline{L}_o \hat{\underline{x}}_e(t)$$

with the optimal gain matrix

$$\underline{L}_o = \underline{G}^{-1} \underline{B}_o^T \underline{K}_o$$

and \underline{K}_0 being the solution of the equation

$$\underline{K}_0 \underline{A}_0 + \underline{A}_0^T \underline{K}_0 - \underline{K}_0 \underline{B}_0 \underline{G}^{-1} \underline{B}_0^T \underline{K}_0 + \underline{Q}_0 = 0$$

with

$$\underline{Q}_0 = \begin{bmatrix} \underline{Q} & | & \underline{0} \\ \hline \underline{0} & | & \underline{R} \end{bmatrix}$$

The optimal control law can be written in the form

$$\dot{\underline{u}}(t) = -\underline{L}_1 \hat{\underline{x}}(t) - \underline{L}_2 \underline{u}(t)$$

in which \underline{L}_1 is the part of the optimal gain matrix weighting the old estimated state vector $\hat{\underline{x}}(t)$ and \underline{L}_2 is the part which weights the old control vector $\underline{u}(t)$. A comparison of this equation for $\underline{u}(t)$

$$\underline{T}_N \dot{\underline{u}}(t) + \underline{u}(t) = -\underline{L}_3 \hat{\underline{x}}(t) \triangleq \underline{u}_c$$

gives $\underline{L}_2 = \underline{T}_N^{-1}$ and $\underline{L}_3 = \underline{L}_2^{-1} \underline{L}_1 = \underline{T}_N \underline{L}_1$. So instead of the new control vector $\dot{\underline{u}}(t)$ an internal control vector (commanded control vector) $\underline{u}_c(t)$ is defined.

Figure 3 shows what has been done. In the model \underline{G} and \underline{T}_N are connected, the election of a special \underline{G} results after calculating \underline{L}_0 in some \underline{T}_N .

INTRODUCTION OF MOTOR NOISE

The motor noise is introduced by setting

$$\underline{T}_N \dot{\underline{u}}(t) + \underline{u}(t) = \underline{u}_c(t) + \underline{v}_u(t)$$

$$\underline{u}_c(t) = -\underline{L}_3 \hat{\underline{x}}(t) \quad \text{and} \quad E \left\{ \underline{v}_u \underline{v}_u^T \right\} = \underline{V}_u \delta(t-t')$$

At this point the model leaves the theoretical basis of optimal control theory, but it is said, that as long as

$$E \left\{ \underline{u}_c(t) \cdot \underline{u}_c^T(t) \right\} \gg E \left\{ \underline{v}_u(t) \cdot \underline{v}_u^T(t) \right\}$$

this could be tolerated and results in a suboptimal control. It is assumed, that the optimal control gain matrix \underline{L}_0 is unaffected by the introduction of the motor noise.

Putting the neuromuscular lag time elements to the system to be controlled, the motor noise can be handled together with the disturbance vector of the system. This results in the differential equation

$$\dot{\underline{x}}_e(t) = \underline{A}_1 \underline{x}_e(t) + \underline{B}_1 \underline{u}_c(t) + \underline{w}_1(t)$$

with

$$\underline{A}_1 = \begin{bmatrix} \underline{A} & | & \underline{B} \\ \hline \underline{0} & | & -\underline{I}_N^{-1} \end{bmatrix} \quad \underline{B}_1 = \begin{bmatrix} \underline{0} \\ \hline \underline{I}_N^{-1} \end{bmatrix} \quad \underline{w}_1 = \begin{bmatrix} \underline{w} \\ \hline \underline{I}_N^{-1} \underline{v}_u \end{bmatrix}$$

and

$$E \left\{ \underline{w}_1(t) \underline{w}_1^T(t') \right\} = \begin{bmatrix} \underline{W} & | & \underline{0} \\ \hline \underline{0} & | & \underline{I}_N^{-1} \underline{V}_u \underline{I}_N^{-1 T} \end{bmatrix} \delta(t-t') = \underline{W}_1 \delta(t-t')$$

To get the covariance matrix of the extended state vector we have to calculate

$$\begin{aligned} \underline{X}_e &= e^{\underline{A}_1 \tau} \underline{P}_1 e^{\underline{A}_1^T \tau} + \int_0^\tau e^{\underline{A}_1 \sigma} \underline{W}_1 e^{\underline{A}_1^T \sigma} d\sigma + \\ &+ \int_\tau^t e^{\underline{A}_1(t-\sigma)} e^{\underline{A}_1 \tau} \underline{P}_1 \underline{C}_1^T \underline{V}_y^{-1} \underline{C}_1 \underline{P}_1 e^{\underline{A}_1^T \tau} e^{\underline{A}_1^T(t-\sigma)} d\sigma \end{aligned}$$

with

$$\underline{A}_1 = \begin{bmatrix} \underline{A} & | & \underline{B} \\ \hline \underline{0} & | & -\underline{L}_o \end{bmatrix} \quad \underline{C}_1 = \begin{bmatrix} \underline{C} & | & \underline{0} \\ \hline \underline{0} & | & \underline{c} \end{bmatrix} \quad \underline{V}_y = \begin{bmatrix} \underline{V}_y & | & \underline{0} \\ \hline \underline{0} & | & \underline{v}_o \end{bmatrix}$$

The power density of the motor noise \underline{v}_u and the elements of the power density matrix $\underline{V}_y(i,i)$ are calculated with noise ratios from the associated measured mean squared values

$$V_y(i,i) = \pi p_{y_i} E \{ y_i^2 \}$$

and

$$V_u = \pi p_u E \{ u^2 \} = \frac{p_u \pi}{1 + p_u \pi} E \{ u^2 \}$$

CALCULATION OF AN EXAMPLE

To use the model you must have a computer program. We wrote a Fortran program, called KOVAR, which computes the covariance matrices \underline{X} and \underline{Y} and which allows a variation of the model parameters \underline{T}_N , p_{y_i} and p_u . The program together with flow charts is documented in detail in reference 1.

The program is built in three levels. The first level is the main program, the second level consists of a group of programs solving the five differential equations and a third level consists of a program solving differential equations with a method from Runge-Kutta (reference 5) and a matrix library. The library is introduced to run the program KOVAR on different computers. The Runge-Kutta method is more time taking than the iterative method proposed by Kleiman in reference 6, but has the advantage that it can be used for stationary and none stationary solutions and needs no proper chosen starting point. The Runge-Kutta method is steering its step width in accordance to a chosen accuracy limit. The computing time is very much depending on this accuracy value and the numerical range of the weighting factors of the \underline{Q}_0 matrix.

We now look at a very simple example given by the inventors of the model in references 3 and 4. Figure 4 shows the simulated system. The differential equations are

$$\begin{aligned}\dot{x}_1(t) &= -2x_1(t) + w(t) \\ \dot{x}_2(t) &= x_1(t) + u(t)\end{aligned}$$

They can be written in the form

$$\begin{bmatrix} \dot{x}_1 \\ \dot{x}_2 \end{bmatrix} = \begin{bmatrix} -2 & 0 \\ 1 & 0 \end{bmatrix} \begin{bmatrix} x_1 \\ x_2 \end{bmatrix} + \begin{bmatrix} 0 \\ 1 \end{bmatrix} \begin{bmatrix} u \\ 0 \end{bmatrix} + \begin{bmatrix} w \\ 0 \end{bmatrix}$$

with system matrix $\underline{A} = \begin{bmatrix} -2 & 0 \\ 1 & 0 \end{bmatrix}$ and control matrix $\underline{B} = \begin{bmatrix} 0 \\ 1 \end{bmatrix}$

The extended system to introduce the weighted control rate is

$$\begin{bmatrix} \dot{x}_1 \\ \dot{x}_2 \\ \dot{u} \end{bmatrix} = \begin{bmatrix} -2 & 0 & 0 \\ 1 & 0 & 1 \\ 0 & 0 & 0 \end{bmatrix} \begin{bmatrix} x_1 \\ x_2 \\ u \end{bmatrix} + \begin{bmatrix} 0 \\ 0 \\ 1 \end{bmatrix} \begin{bmatrix} \dot{u} \\ 0 \\ 0 \end{bmatrix} + \begin{bmatrix} w \\ 0 \\ 0 \end{bmatrix}$$

with $\underline{A}_0 = \begin{bmatrix} -2 & 0 & 0 \\ 1 & 0 & 1 \\ 0 & 0 & 0 \end{bmatrix}$ and $\underline{B}_0 = [0 \ 0 \ 1]^T$

The power density matrix is

$$W_0 = \begin{bmatrix} 8,8 & 0 & 0 \\ 0 & 0 & 0 \\ 0 & 0 & 0 \end{bmatrix}$$

For the observation vector we have

$$\begin{bmatrix} y_1 \\ y_2 \\ y_3 \end{bmatrix} = \begin{bmatrix} 0 & 1 & 0 \\ 1 & 0 & 1 \\ 0 & 0 & 0 \end{bmatrix} \begin{bmatrix} x_1 \\ x_2 \\ u \end{bmatrix} + \begin{bmatrix} v_{y_1} \\ v_{y_2} \\ 0 \end{bmatrix}$$

with

$$C_0 = \begin{bmatrix} 0 & 1 & 0 \\ 1 & 0 & 1 \\ 0 & 0 & 0 \end{bmatrix}$$

For the discussed example the optimization criterion is

$$J(u) = E \{ e^2 \} + G \cdot E \{ \dot{u}^2 \}$$

which gives with $e = -x_2$ a cost weightings matrix of

$$Q_0 = \begin{bmatrix} 0 & 0 & 0 \\ 0 & 1 & 0 \\ 0 & 0 & 0 \end{bmatrix}$$

The weighting of the control rate was chosen to $G=0.00017$, resulting in a neuromuscular lag time constant of $T_N=0.08$. In accordance to the references the noise ratios were $p_{y_1}=p_{y_2}=0.01$ and $p_u=0.003$. Subsequently the power density matrix of the observation noise has the form

$$Y_y = \begin{bmatrix} 0,00408 & 0 & 0 \\ 0 & 0,09739 & 0 \\ 0 & 0 & >0 \end{bmatrix}$$

The element 33 has to be greater than zero because the matrix has to be inverted. The element has no influence on the calculation due to the structure of the \underline{V}_y matrix and the observation matrix \underline{C} .

Now the gain matrix of the optimal controller \underline{L}_0 can be calculated giving the neuromuscular time constant \underline{T}_N . Having this we define the extended system of differential equations to calculate the covariance matrices \underline{X} and \underline{Y} . We get

$$\underline{A}_1 = \begin{bmatrix} -2 & 0 & 0 \\ 1 & 0 & 1 \\ 0 & 0 & -1/0,08 \end{bmatrix} \quad \underline{B}_1 = \begin{bmatrix} 0 \\ 0 \\ 1/0,08 \end{bmatrix}$$

$$\underline{W}_1 = \begin{bmatrix} 8,8 & 0 & 0 \\ 0 & 0 & 0 \\ 0 & 0 & 0,03921/(0,08)^2 \end{bmatrix}$$

The results of our program are shown in Table 1. They are in a good agreement with the reported data from references 3 and 4. The computing time for this example with an accuracy limit of the Runge-Kutta method of 10^{-5} was 11 minutes on a CDC 6600.

VARIATION OF THE PARAMETERS

We now started to variate the parameters \underline{T}_N , p_{y1} , p_{y2} , p_u and τ and looked at their influence on the covariances. It can be shown, that only the crosscovariances X_{12} and X_{23} give in addition to the diagonal elements $X_{22} = \hat{Y}_{11} = \bar{e}^2$, $X_{33} = \bar{u}^2$ and Y_{22} information about the systems performance. The complete nominal covariance matrices are:

$$\underline{X} = \begin{bmatrix} 2,19781 & 0,35498 & -1,48691 \\ 0,35498 & 0,11670 & -0,34920 \\ -1,48691 & -0,34920 & 3,74796 \end{bmatrix}$$

$$\underline{Y} = \begin{bmatrix} 0,11671 & 0,00578 & 0 \\ 0,00578 & 2,97195 & 0 \\ 0 & 0 & 0 \end{bmatrix}$$

Little numerical differences to the results in Table 1 came up with the use of a PDP 11/20 and mixed accuracy values for the Runge-Kutta method in this part of the work.

Figure 5 shows the influence of T_N or G on the elements of the covariance matrices. In addition to our calculations you see some values taken from reference 3.

Figure 6 shows the influence of the noise ratio p_{y1} on the covariances. The little influence of great noise ratios can be explained with the characteristics of the Kalman filter, which in these cases estimates the state vector on the basis of his internal model.

Figure 7 shows the effect of a variation of the noise ratio p_{y2} .

Figure 8 shows how a variation of the motor noise ratio p_u influences the covariances. We get a linear dependence and no effect on the crosscovariances.

Figure 9 shows the influence of τ on the covariances.

Table 2 shows the investigated range of parameters and the deviation of the covariances from their nominal values within that range expressed as percentage. Now we changed one parameter so far, that we could compensate its influence on the covariances with a variation of the other parameters. With this procedure we get the parameter range of Table 3.

Within this parameter range we can find an unlimited number of parameter combinations giving all the same covariance matrices. We can also come as close as we want to the measured data from reference 3. In the investigated range for p_{y2} we find no upper value which we could not compensate with other parameters.

CONCLUDING REMARKS

We can say, that the measured mean squared values are not enough to identify the parameters of the BBN-model. To do the identification one has additionally to adapt the describing function and the power density spectrum of the remnant. For this purpose the adapted state has to be defined more accurately.

We have to prove, that with the adaptation of the describing function and the power density spectrum reliable model parameters can be identified. If this is practicable the BBN-model has the performance of the well known quasi-linear model.

Only if we can prove, that also for complex multi-input and multi-output systems exact parameter values can be found, the model brings great advantages compared with the quasi-linear model.

The BBN-model presumes, that the human operator is capable of generating some exact inner models of the system to be controlled. The question is, how the model will work when the system and the control matrix of the filter and the predictor do not be the same as in the controlled system.

If these questions are answered, we can start to use the model to describe scanning behaviour, learning effects, workload and the effect of different information input and output systems on the performance of the human operator.

REFERENCES

1. Dey, D.; and Kirchhoff, U.: Beschreibungsmöglichkeiten für die Mehrgrößenregelungseigenschaften des Menschen bei der Fahrzeugführung. Institut für Luft- und Raumfahrt, technische Universität Berlin, März 1975.
2. Dey, D.; and Kirchhoff, U.: Das Problem des Zusammenwirkens von Flugzeugführer und Regler in der Flugführung. Institut für Luft- und Raumfahrt, Technische Universität Berlin, ILR 4, 1973.
3. Kleinman, D. L.; and Baron, S.: Manned Vehicle System Analysis by Means of Modern Control Theory. Bolt, Beranek and Newman Inc., NASA CR-1753, June 1971.
4. Kleinman, D. L.; Baron, S.; and Levison, W. H.: An Optimal Control Model of Human Response, Part I Automatica, Vol. 6, pp. 357-369, Pergamon Press, 1970.
5. Zurmühl, R.: Matrizen und ihre technische Anwendung. Springer Verlag, Berlin/Göttingen/Heidelberg, 1961.
6. Kleinman, D. L.: On an Iterative Technique for Riccati Equation Computation. IEEE Transaction on Automatic Control, Febr. 1968.
7. Pastoor, S.: Der Parameterraum des BBN-Modells. Diplomarbeit am Institut für Luft- und Raumfahrt, Technische Universität Berlin, Febr. 1975.

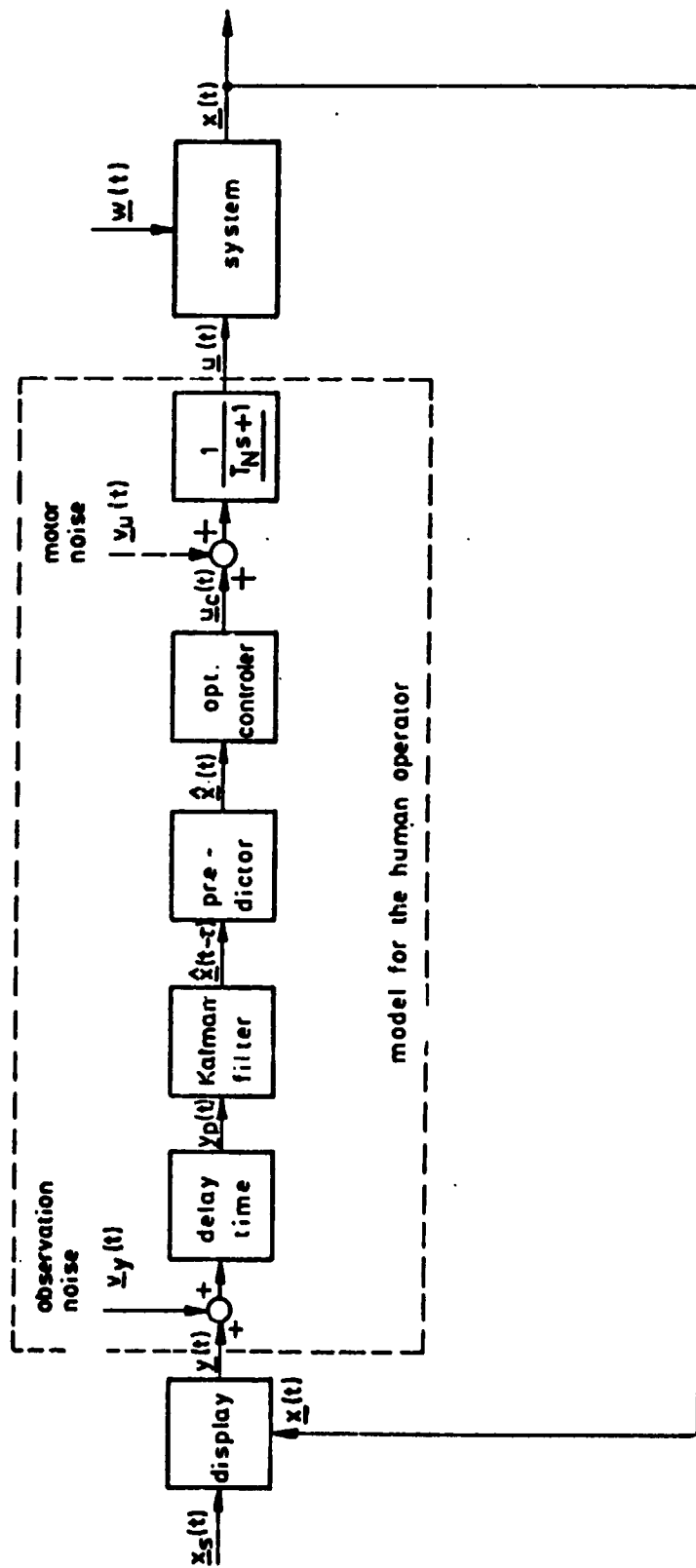


Fig. 1 : Structure of the BBN- model

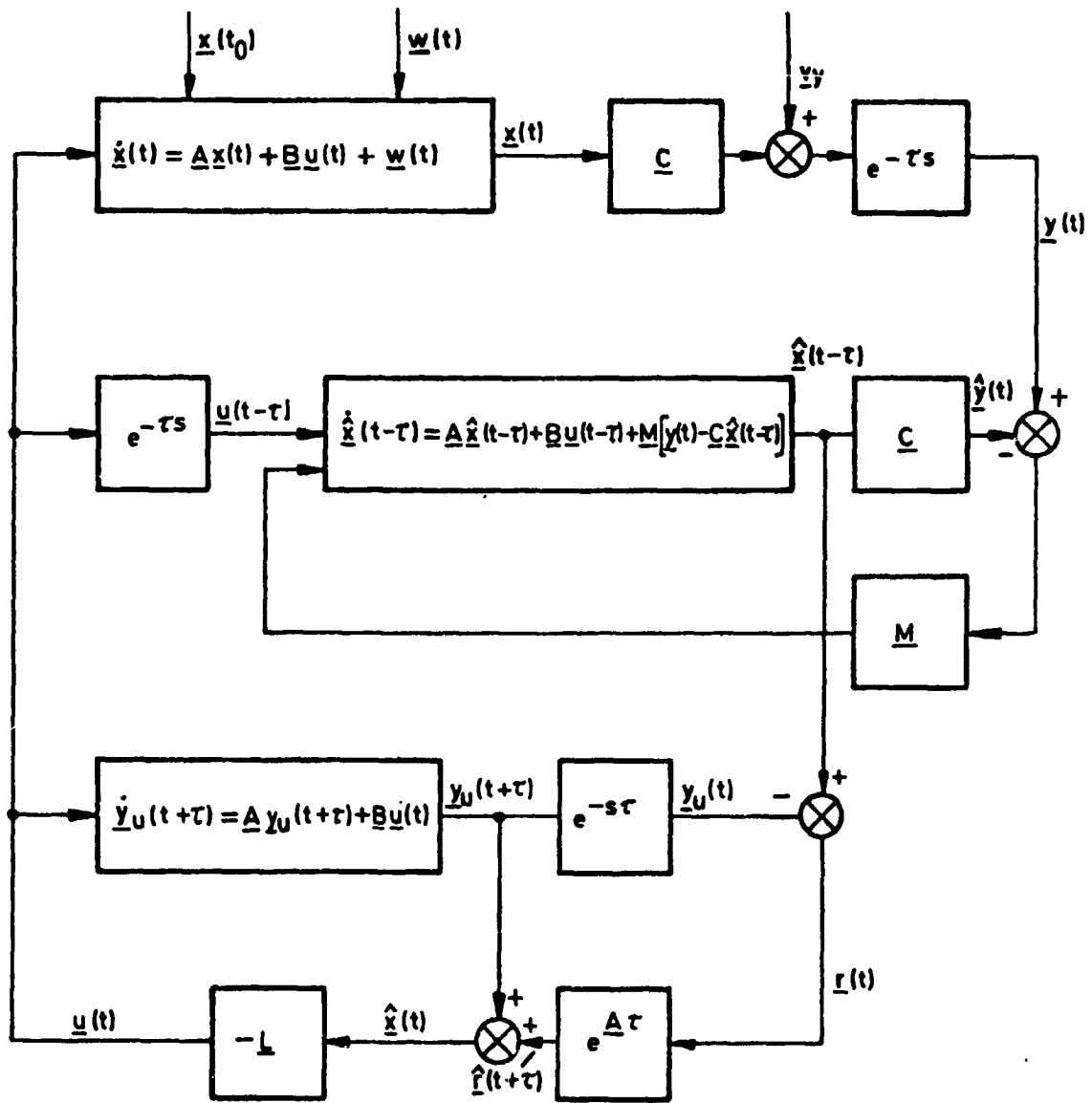


Fig. 2 : Optimal control of a linear system with a noisy and delayed observation vector

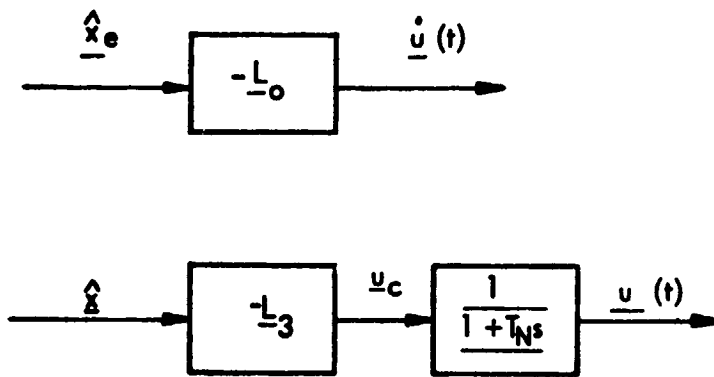


Fig. 3 : Separation of the neuromuscular lag element

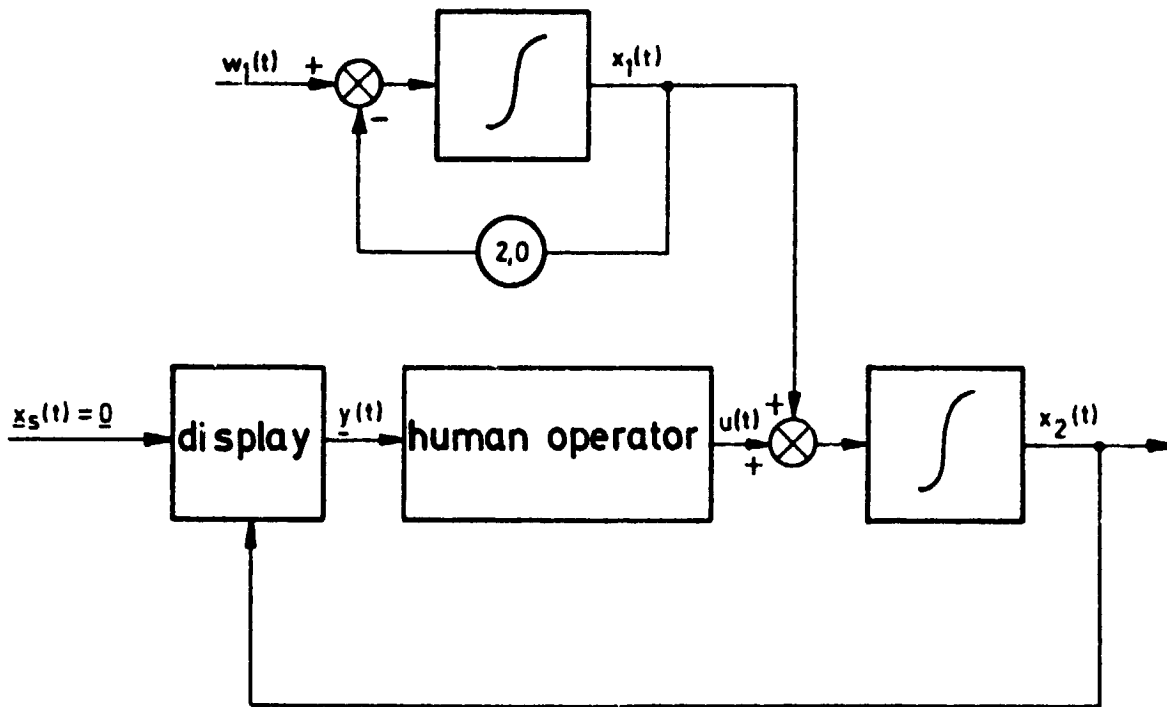


Fig. 4 : Control loop with a $1/s$ system

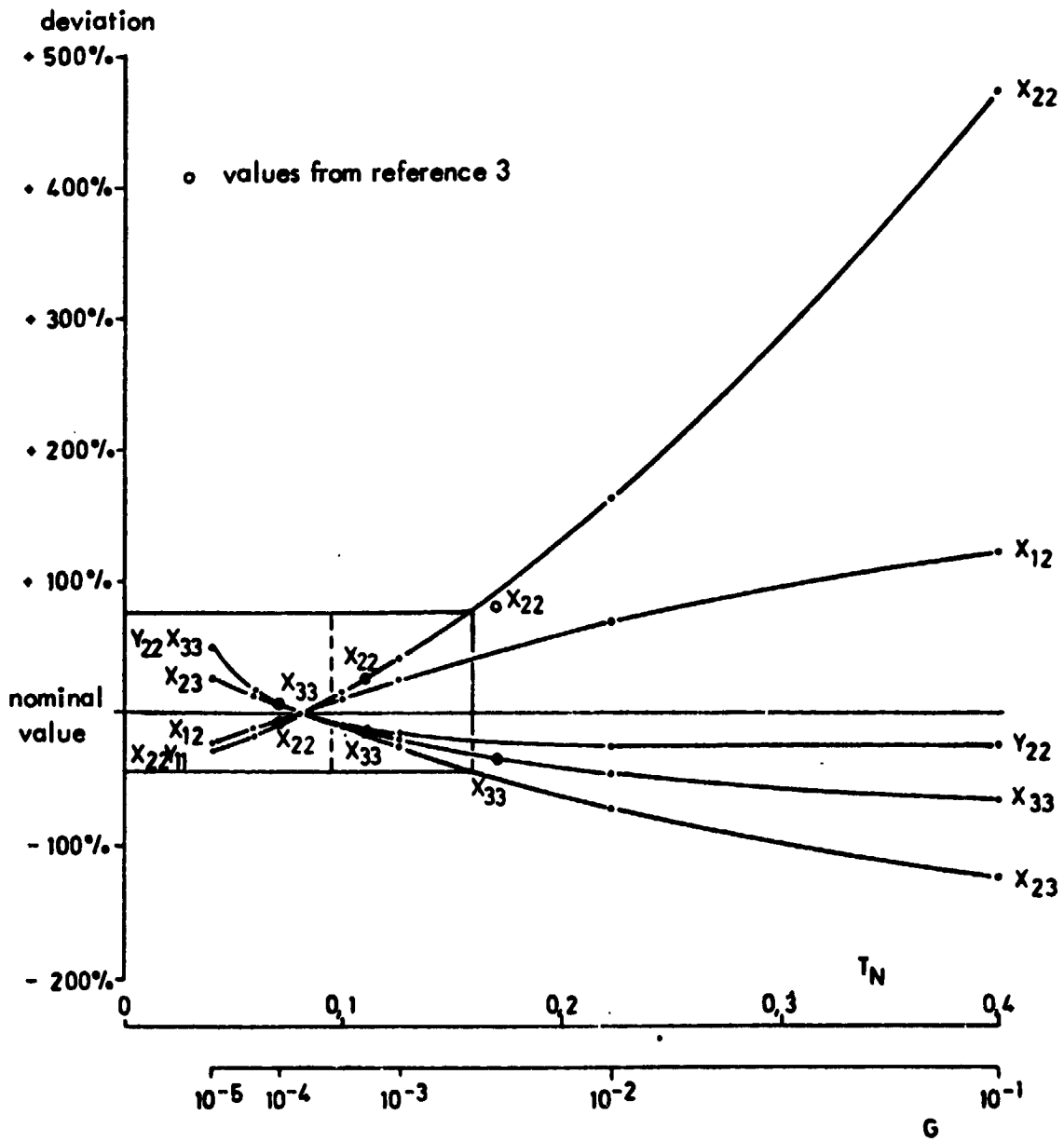


Fig. 5 : Deviation of the covariances from their nominal values in percent as a function of T_N or G

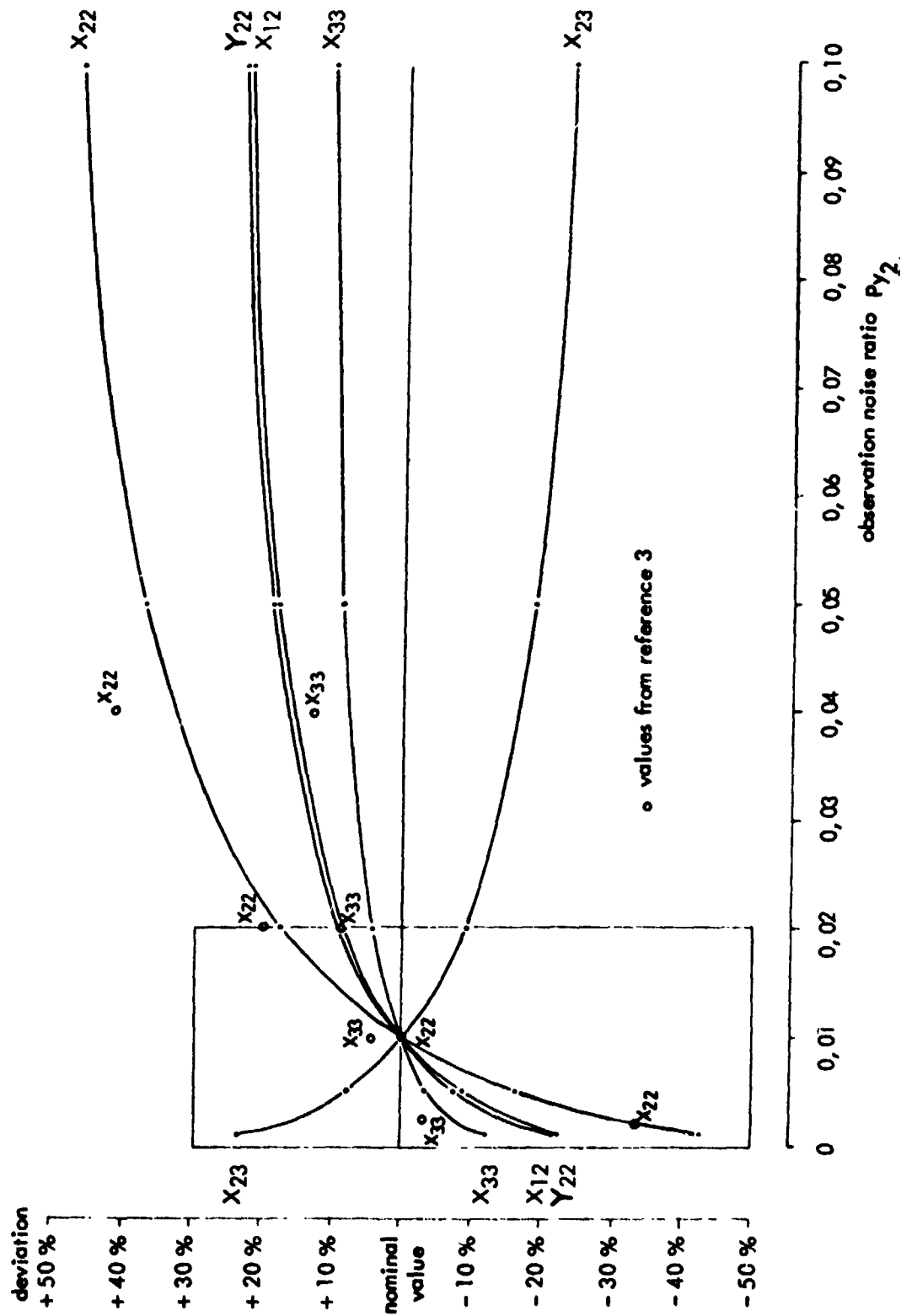


Fig. 7 : Deviation of the covariances from their nominal values as a function of P_{y2}

o values from reference 3

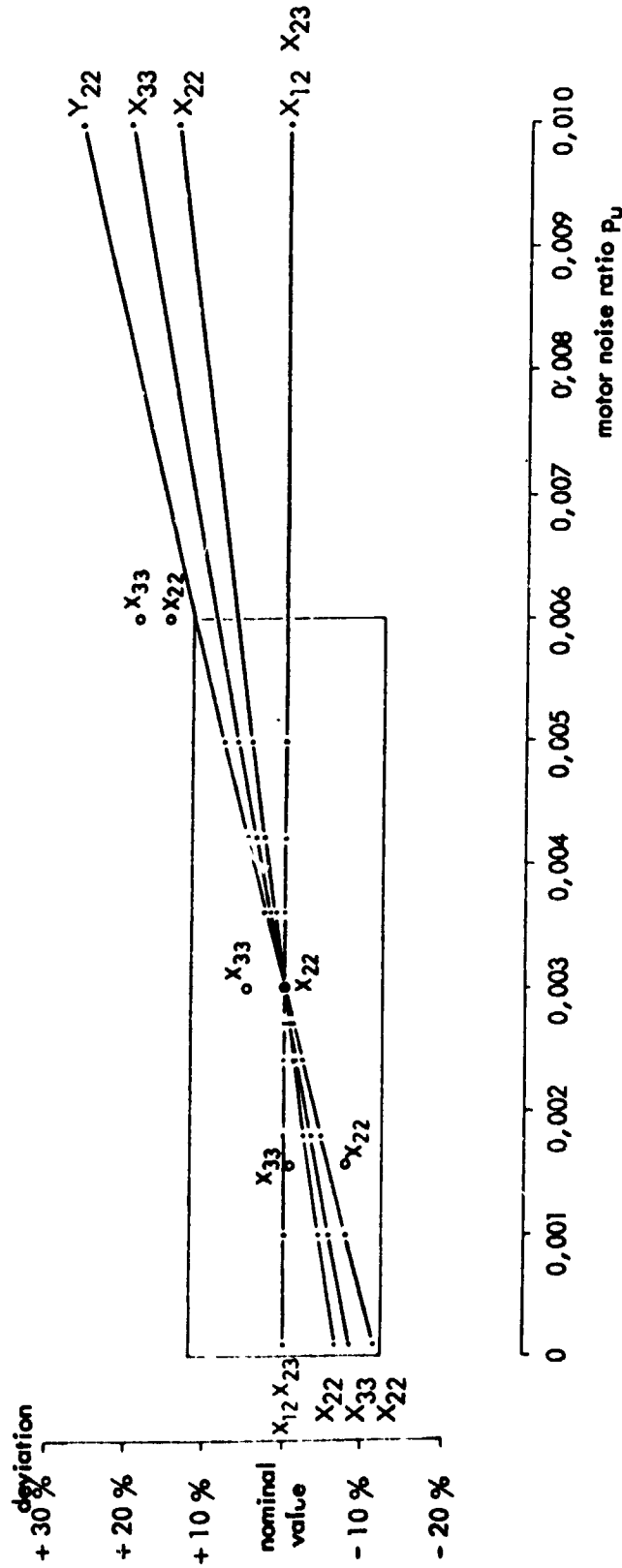


Fig. 8: Deviation of the covariances from their nominal values as a function of p_U

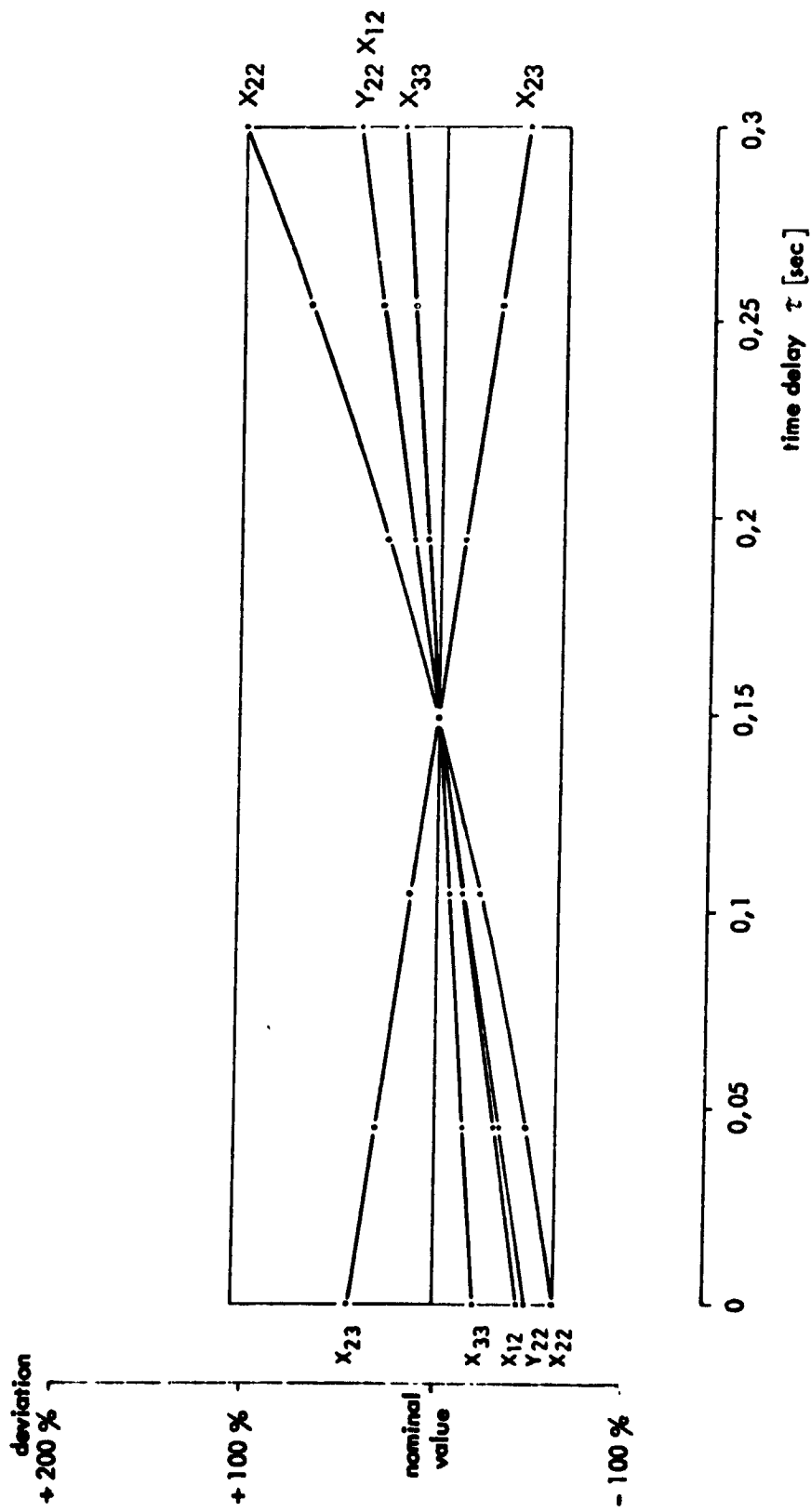


Fig. 9 : Deviation of the covariance from their nominal values as a function of τ

	values from reference 3		values from KOVAR
	measured	calculated	
$\overline{x_1^2}$	2,2	2,2	2,2
$\overline{x_2^2} = \overline{y_1^2} = \overline{e^2}$	0,13	0,12	0,118
$\overline{x_3^2} = \overline{u^2}$	4,2	3,83	3,787
$\overline{y_2^2}$	3,10	3,06	3,008

Tab.1 Measured and calculated mean squared values

	Invertigated range	Covariances				
		X ₂₂	X ₃₃	Y ₂₂	X ₁₂	X ₂₃
τ	0.0 - 0.3 sec	-60 %	-20 %	-45 %	-45 %	+45 %
		+100 %	+20 %	+45 %	+45 %	-40 %
P _{y1}	0.001 - 0.1	-20 %	-3 %	-6 %	-6 %	+6 %
		+40 %	+1.5 %	+3 %	+3 %	-3 %
P _{y2}	0.001 - 0.1	-42 %	-12 %	-22 %	-22 %	+23 %
		+47 %	+11 %	+22 %	+21 %	-24 %
P _u	0.0001 - 0.01	-7 %	-9 %	-12 %	0	0
		+14 %	+20 %	+26 %	0	0
G	10 ⁻⁵ - 10 ⁻¹	-30 %	+50 %	+50 %	-24 %	+24 %
T _N	0.04 - 0.4sec	+470 %	-65 %	-24 %	+120 %	-124 %

Tab.2 Deviations of the covariances from their nominal values expressed as percentage

Maximum range	Values of the other parameters	Deviation of covariances from their nominal values in percent				
		Δx_{22}	Δx_{33}	Δy_{22}	Δx_{12}	Δx_{23}
$\tau=0.05$	$P_{y2}=0.1$ $P_u=0.0045$	+5	0	-5	-10	+6
$\tau=0.25$	$P_{y2}=0.001$ $P_{y1}=0.001$	+1	0	+2	+2	+1
$P_{y1}=0.001$	$P_{y2}=0.001$ $\tau=0.25$	+1	0	+2	+2	+1
$P_{y1}=0.06$	$P_{y2}=0.004$	+8	-3	-8	-8	+8
$P_{y2}=0.001$	$P_{y1}=0.001$ $\tau=0.25$	+1	0	+2	+2	+1
$P_{y2}=0.1$	$P_u=0.0045$ $\tau=0.05$	+5	0	-5	-10	+6
$P_u=0.0001$	$\tau=0.17$	+5	-6	-6	+6	-6
$P_u=0.007$	$P_{y2}=0.005$	-8	+9	+6	-8	+8
$G=0.0001$	$P_u=0.0001$ $P_{y1}=0.03$	0	+2	0	-4	+4
$G=0.0004$	$P_{y2}=0.007$ $P_u=0.0043$	+9	-9	-9	+5	-5

Tab.3 Maximum range of parameters giving nearly the nominal covariances

N75 33713

PERFORMANCE EVALUATION OF TRACKING BASED
ON A LOW PASS FILTER MODEL

By Daniel W. Repperger
and Andrew M. Junker

Aerospace Medical Research Laboratory
Wright-Patterson Air Force Base, Ohio 45433

SUMMARY

The performance of a human in a closed loop tracking task can be determined by using a simple low pass filter model with a least squares identification algorithm. The crossover model and the extended crossover model can be shown to be special cases of the low pass filter model presented here. Performance in tracking can be easily determined by mean square tracking error (e_{RMS}) which can be written in terms of the parameters of the low pass filter model. A closed form expression for the effective time delay (τ_{eq}) is also obtained. The model presented here may have applicability in the analysis of non-linear or time varying closed loop systems. Experimental data from a roll axis tracking simulation is presented and simple prediction rules involving e_{RMS} and τ_{eq} are determined. A comparison is made between this model and the crossover model with respect to their differences and similarities.

INTRODUCTION

The study of methods to evaluate tracking performance in the classical closed loop tracking problem has been a subject of great interest. Probably the best known and most credible approach to determining tracking performance and pilot parameters is the crossover model [1]. A second approach to this problem is to relate the pilot parameters during the tracking task to qualitative ratings of pilots in the evaluation of flying capability. This is accomplished by the use of the paper pilot [2,3]. The paper pilot utilizes the Cooper Harper Ratings [4,5] to evaluate a pilot's opinion of the response characteristics of the aircraft. The optimal control model [6,7] has also been used to develop methods to predict pilot performance in the tracking task.

This paper is concerned with the relationship between performance in tracking and parameters of the man or man-machine in the closed loop. A performance model (termed the α model) is introduced here to more accurately illustrate a dependence between model parameters and tracking performance. The tracking problem of interest will first be defined.

THE TRACKING PROBLEM

Figure (1) illustrates the man in the loop problem considered here. The forcing function $f(t)$ consists of a low pass filtered white Gaussian noise source of a specified bandwidth. The human is presented the displayed signal $e(t)$ and his task is to align the system to be controlled with the forcing function input signal such that the error signal is as small (in magnitude) as possible. The only information given on the error signal was its display on a cathode ray oscilloscope. This type of tracking run is for the fixed base or static mode of operation (figure 2).

In the motion mode of operation (figure 2), the plant dynamics were identical as in the static case; however, stick control movements caused rotation of the simulator about the roll axis with the same knowledge of the visual display signal. Thus in the second mode of operation, the subject received information about the error through the visual display (as in the static mode) and, in addition, gained information about the plant's response from his motion sensors and vestibular system.

Three different plants were considered in this study of motion effects on performance:

$$\text{Plant 1: } G(s) = \frac{100.}{s(1 + s/5)(1 + s/6.0)} \quad (1a)$$

$$\text{Plant 2: } G(s) = \frac{100.}{s^2(1 + s/5)(1 + s/6.0)} \quad (1b)$$

$$\text{Plant 3: } G(s) = \frac{100.}{s^2(1 + s/2)(1 + s/5)(1 + s/6.0)} \quad (1c)$$

For the different plants considered here, the effect of motion information on performance was strongly dependent on which plant was being controlled. Using as a measure of performance Root Mean Square error (e_{RMS}) defined as:

$$e_{RMS}^2 = \frac{1}{T} \int_0^T e^2(t) dt$$

Where T was chosen to be 120 seconds, Table I illustrates the effect of motion information on performance in tracking (e_{RMS} values are in degrees):

TABLE I

Mode of Operation	Forcing Function = 0.25 radians	Forcing Function = 0.25 radians
Plant 1, Static Mode	$e_{RMS} = 5.70$	$e_{RMS} = 12.45$
Plant 1, Motion Mode	$e_{RMS} = 6.57$	$e_{RMS} = 13.73$
Plant 2, Static Mode	$e_{RMS} = 26.867$	$e_{RMS} = 46.99$
Plant 2, Motion Mode	$e_{RMS} = 10.87$	$e_{RMS} = 20.46$
Plant 3, Static Mode	$e_{RMS} = 79.43$	$e_{RMS} = 90.30$
Plant 3, Motion Mode	$e_{RMS} = 27.01$	$e_{RMS} = 38.25$

The above error scores represented mean eRMS scores averaged over 8 different subjects, who participated in 4 different (2 minute) tracking tasks held twice each day. The subjects were trained for 38 days prior to the data (six days of tracking) presented in Table I.

It is noted that for plant 1, the effect on performance of motion information was not significant; in fact in the motion case, performance was somewhat degraded. For plant 2, the presence of motion information aided in the tracking task. For the third plant, the presence of motion information resulted in a significant improvement in performance. An identification algorithm was used to determine the model parameters.

A LEAST SQUARES IDENTIFICATION ALGORITHM TO DETERMINE MODEL PARAMETERS

In the analysis of data from the roll axis tracking experiment, the method of obtaining model parameters was based on a least squares identification algorithm. Figure (3) illustrates this output error - least squares algorithm in which model parameters are identified using the displayed error as the input signal and the plant's position as the output signal.

In order for the identification problem to be well posed, the input-output parameters were assumed to be characterized by the following transfer function (second order structure):

$$G(s) = \frac{K(s + a)}{s^2 + bs + c} e^{-\tau_{eq} s} \quad (1)$$

The unknown parameters (K,a,b,c) are iterated upon until the following performance index is minimized:

$$J = \sum_{i=1}^N \bar{e}_i^2(t) \quad (2)$$

where $\bar{e}(t)$ is the output error

In order to identify the delay τ_{eq} , the input-output signals were shifted an integral multiple of the sampling rate until the performance index reached its lowest value. The value of time lag which gave J its lowest value was selected as the value of effective lag.

In using the identification algorithm with equation (1), state variables are chosen and the following canonical form results for the state equations and measurement equations:

$$\begin{bmatrix} \dot{x}_1 \\ \dot{x}_2 \end{bmatrix} = \begin{bmatrix} 0 & 1 \\ -a_1 & -a_2 \end{bmatrix} \begin{bmatrix} x_1 \\ x_2 \end{bmatrix} + \begin{bmatrix} b_1 \\ b_2 \end{bmatrix} u \quad (3a)$$

$$y = \begin{bmatrix} 1 & 0 \end{bmatrix} \begin{bmatrix} x_1 \\ x_2 \end{bmatrix} + \begin{bmatrix} 0 \end{bmatrix} \quad (3b)$$

The system equations (3a-b) represent a completely controllable and completely observable system. The identifiability conditions [11] are now satisfied and the modeling problem is well posed with a unique solution for the model parameters.

The best second order linear model obtained from the identification algorithm represents the best linear fit of the data despite its nonlinear or noisy nature. A credibility study on the identification algorithm was performed to compare answers obtained from this approach to other methods used to model man-machine systems.

A CREDIBILITY STUDY - IDENTIFY A KNOWN PLANT

In order to establish how answers obtained from the identification algorithm compare with other methods to model physical systems, various tests were made. To illustrate some of the results of these tests Plant II is used as an example.

The credibility of the algorithm was examined with respect to three variables of interest (sampling rate, real time duration of data, and ensemble averaging of data). Using as an input the stick voltage and as the output the position of the plant, the system being controlled was identified using input-output signals of different amplitudes and frequency content. The source of the different input-output signals was the response of the different subjects involved in the tracking experiment. Figure (4) illustrates the effect of ensemble averaging. For the 16 seconds of tracking data presented here the lower limit of credibility was .42 radians. It is noted that as the number of ensemble averages increase, the algorithm gives answers closer and closer to the lower limit. The upper limit of credibility was dependent on the sampling rate (50 Hz used here) and also on the signal to noise ratio in the data. For the plant identified here, the signal to noise ratio of about 10/1 restricted the upper frequency limit of credibility to about 10 radians (20 db below the highest identified signal strength).

A further study of credibility included an investigation of the system order assumption. The plant was first assumed to be second order and the identification was performed. The same data was then assumed to be from a third order plant and the identification was redone as a comparison. After ensemble averaging the answers for each assumed system order, the results are displayed in Figure (5). Between the upper and lower frequencies of credibility, the identified transfer functions appear approximately the same. Finally, the different methods of modeling were compared in Figure (6). The best second order model (12 ensemble averages) is compared to the best third order model (10 ensemble averages) displayed by the solid and dashed line, respectively. It is noted that the third order guess on the

system structure differed from the second order guess due to its flexibility in choosing the shape of the transfer function. Also, the data from this plant was corrupted with noise above 5 radians. Below 0.5 radians (where the other credibility limit occurs) it is noted that all the plots also become inconsistent. The thick solid line is the actual bode plot of the plant simulated and is drawn here as a comparison to the modeling approaches. It is noted that the upper credibility limit of only 5 radians occurred mainly because the plant's characteristics are down 40 db (and therefore are in the noise) from the peak signal strength at 5 radians. Most of the data to be presented here had an acceptable credibility range from 0.8 radians to over 10 radians.

ANALYSIS OF THE DATA FROM THE ROLL AXIS TRACKING SIMULATOR

It is of interest in the development of a model to predict performance to look at parameters for the man-machine. Figures (7), (8), and (9) illustrate the transfer function across the man-machine for plants I, II, and III respectively. It is observed that for plants where motion helps tracking, the man-machine parameters show more and more lead characteristics as the effect of motion improved performance. Figure (10) was obtained by using Fourier coefficients to demonstrate the increase in pilot lead due to motion information for the second plant.

Figure (9) illustrates an interesting effect due to the statistics of the answers obtained from the identification algorithm. In order to determine variance in the estimates of the parameters obtained here, it was decided to characterize the answers obtained here in terms of the natural frequencies (poles and zeros) and the d.c. gain. These parameters completely characterize the free and forced response solution of any differential equation and hence are an accurate representation of the time series. A mean and variance of these quantities was obtained and their values are displayed in Table II:

TABLE II

IDENTIFIED PARAMETERS-MEANS AND VARIANCES

Mode of Operation	K_{ave}	K_{var}	$Zero_{ave}$	$Zero_{var}$	$P1_{ave}$	$P1_{var}$	$P2_{ave}$	$P2_{var}$
Plant 1 Static	1.85	.46	4.24	.88	.25	.15	2.8	.32
Plant 1 Motion	2.93	1.33	4.1	1.3	.123	.049	12.9	7.3
Plant 2 Static	1.68	.53	1.16	.075	.35	0.2	2.9	0.4
Plant 2 Motion	3.32	1.13	1.72	.15	.141	.03	6.94	1.34
Plant 3 Static	3.12	1.2	1.27	0.5	.452	.19	3.7	0.8
Plant 3 Motion	3.38	1.6	.478	.29	.131	.08	4.66	0.96

It is noted that as the plant becomes more difficult to control (and motion aids in tracking), the variance in the identified parameters generally increased. This was due to an increase in remnant generated by the human. It was also noted that more remnant occurred for motion tracking compared to static tracking. When comparing plants in order of their difficulty to track, the more difficult the plant, the more remnant signal appeared. The method of estimating remnant was a ratio of linear power accounted for by the model to the total output power.

Figure (9) illustrates the Bode plot obtained by one standard deviation in parameters plotted in a worst case manner. The highest plot had the largest d.c. gain, closest zero and furthest poles. The lowest worst case plot is also illustrated. It is interesting that the minimum variation occurs near crossover.

Figures (7,8,9) show agreement with the results of Shirly and Young [8] in their extensive study of systems in which motion cues may help performance. It is now of interest to consider a simple model to relate parameters obtained from the identification algorithm to performance in tracking.

AN α MODEL TO RELATE PARAMETERS TO PERFORMANCE IN TRACKING

With reference to Figure (11), a possible model to relate performance to parameters is displayed. α is chosen as the frequency at which the man-machine gain characteristics are down by a factor of $1/\sqrt{2}$ from the (low frequencies) d.c. value. Although the characteristics of this model appear analogous to the crossover model, certain distinct differences of this performance model are apparent:

- (1) α is independent of system order, system stability, and may have some use for non-linear or nonstationary systems.
- (2) α is a value of frequency where the man-machine characteristics start to deteriorate (1/2 power point).
- (3) The slope of the man-machine system need not be 20 db/decade to analyze data and to compare performance.
- (4) The crossover model and extended crossover models can all be considered α models under the stationary, Gaussian, linearly assumptions.

It is of interest to now relate e_{RMS} and τ_{eq} to parameters obtained from the tracking problem.

A DEPENDENCE BETWEEN PERFORMANCE PARAMETERS AND IDENTIFIED PARAMETERS

With reference to Appendices (A,B) the following two approximations are derived:

$$e_{RMS} \approx K' \sigma / \alpha \quad (4a)$$

$$\tau_{eq} \approx K'' \sigma/\alpha \quad (4b)$$

Equation (4a) closely resembles the 1/3 power law of [1] which is derived under the crossover model considerations. Since sufficient data was available to evaluate this model in terms of e_{RMS} and the ratio σ/α , values of K' were computed for all 3 plants and forcing functions. Table III illustrates the ensembled averaged values of the e_{RMS} values over the different σ and α values (using $K' = e_{RMS}/(\sigma/\alpha)$).

TABLE III

Mode of Operation	Forcing Function = 0.25 radians	Forcing Function = 0.5 radians
Plant 1, Static Mode	$K' = 59.5$	$K' = 64.9$
Plant 1, Motion Mode	$K' = 65.7$	$K' = 68.65$
Plant 2, Static Mode	$K' = 137.0$	$K' = 121.0$
Plant 2, Motion Mode	$K' = 98.5$	$K' = 93.5$
Plant 3, Static Mode	$K' = 505.$	$K' = 290.$
Plant 3, Motion Mode	$K' = 715.$	$K' = 519.$

Figures (12,13) display plots of e_{RMS} versus σ/α for the three plants used in the analysis here. It is noted that as the remnant power increases (motion tracking versus static tracking and as the plants become more difficult), the linear prediction rules become less accurate. This result is due to the linear model not accurately representing the input-output characteristics under high noise levels. It is worthwhile to now compare the ability of this model to predict performance to the crossover model.

A COMPARISON OF THE α MODEL TO THE CROSSOVER MODEL IN TERMS OF PERFORMANCE PREDICTABILITY

In Appendix A it is shown that the relationship of e_{RMS} specified by equation (4a) depends on the approximation:

$$\alpha \tau_{eq} \ll 1 \quad (5)$$

For the corresponding derivation in the crossover model, the 1/3 power law utilizes the approximation:

$$\omega_c \tau_{eq} \ll 1 \quad (6)$$

where ω_c corresponds to the crossover frequency.

A comparison of the prediction law of equation (4a) with the 1/3 power law is mainly dependent on the constant linear relationship between e_{RMS} and the ratio σ/α . These linear relationships, however, are a consequence of the approximations equations (5) and (6). If we were to compare the approximations (5) and (6), the following result is of most interest:

$$\alpha < \omega_c \quad (7)$$

this follows since α is the frequency of the man-machine transfer function when its phase angle is -45° ; ω_c , however, is the frequency of the man-machine transfer function when its phase angle is -90° . Since the total transfer function is generally monotonic decreasing, it follows that:

$$\alpha \approx \omega_c \approx 1 \quad (8)$$

is always satisfied and thus the approximation of e_{RMS} specified by equation (4a) is at least as accurate as the crossover model.

One can observe that if α is defined as a smaller and smaller frequency, the prediction rule should be more accurate based on the approximation of equation (8). The difficulty in this case, however, is in the resolution problem or the ability to measure α accurately becomes more and more difficult. The definition of α chosen here (a half power point) is a compromise between the crossover frequency and a value which is too small to be measured accurately (due to a resolution problem).

CONCLUDING REMARKS

The use of modern identification methods can be combined with a simple low pass filter model to predict mean square tracking error. The performance model presented here has some application where direct use of the crossover model is not applicable.

ACKNOWLEDGEMENT

The authors would like to express their appreciation to Captain Jonathan P. Hull and his assistants at the Aerospace Medical Research Laboratory for their help in the ensemble averaging and plotting of the identified parameters.

REFERENCES

- [1] McRuer, D. and D. Graham, "Human Pilot Dynamics in Compensatory Systems-Theory, Models, and Experiments with Controlled Element Forcing Function Variations", Technical Report, AFFDL-TR-65-15, July 1965, Air Force Flight Dynamics Laboratory Research and Technology Division, Air Force Systems Command, Wright-Patterson Air Force Base, Ohio 45433.
- [2] Anderson, R. O., "A New Approach to the Specification and Evaluation of Flying Qualities", Air Force Flight Dynamics Laboratory, AFFDL-TR-69-120, November 1969.
- [3] Dillow, J. D., "The 'Paper Pilot' - A Digital Computer Program to Predict Ratings for the Hover Task", Air Force Flight Dynamics Laboratory, AFFDL-TR-70-40, January 1970.
- [4] Cooper, G. E., "Understanding and Interpreting Pilot Opinion", Aeronautical Engineering Review, March 1967.

- [5] Harper, R. P., Jr., "Pilot Evaluation of Handling Qualities", The Ninth Annual Meeting of the Human Factors Society, October 1965.
- [6] Kleinman, D. L., S. Baron, and W. H. Levison, "An Optimal Control Model of Human Response, Part I: Theory and Validation", Automatica, Vol. 6, pp. 357-369, 1970.
- [7] Kleinman, D. L., W. R. Killingsworth, "A Predictive Pilot Model for STOL Aircraft Landing", NASA CR-2374, March 1974.
- [8] Shirley, R. S. and L. R. Young, "Motion Cues in Man-Vehicle Control- Effects of Roll-Motion Cues on Human Operator's Behavior in Compensatory Systems with Disturbance Inputs", IEEE Transactions on Man-Machine Systems, Vol. MMS-9, No. 4, pp. 121-128, December 1968.
- [9] Papoulis, A., "Probability, Random Variables, and Stochastic Processes", McGraw-Hill, 1965.
- [10] McRuer, D. T. and E. S. Krendel, "The Man-Machine System Concept", Proc. IRE, Vol. 50, No. 5, May 1962, pp. 1117-1123.
- [11] Tse, E. and H. L. Weinert, "Structure Determination and Parameter Identification for Multivariable Stochastic Linear Systems", JAAC Preprints, 1973.

APPENDIX A

To derive an explicit dependence between σ_{RMS} (error scores) and the parameters describing the man-machine interaction, some approximations are made. First it is assumed that the Forcing Function is of a low pass nature with magnitude K_1 extending from 0.0 to a σ radians. If the man-machine transfer function is described by the low pass filter model, then the following first order approximation is valid (Figure 14):

$$\frac{X(s)}{E(s)} \approx \frac{K_2}{1 + s/\alpha} e^{-\tau_{eq} s} \quad (A.1)$$

where α is the same parameter as in the low pass filter model (corresponding to a -3 db reduction in magnitude of the transfer function $G(\mu)H(s)$ from the d.c. or low frequency values). It is noted that the delay term $e^{-\tau_{eq} s}$ is included in the analysis since the calculation of σ_{RMS} requires the exact time relationships of the variables $x(t)$ and $e(t)$. The magnitude plots were sufficient for the previous analysis but now the phase relationship between $x(t)$ and $e(t)$ must be known to accurately compute σ_{RMS} . Using the stationary, Gaussian assumptions, σ_{RMS} can be obtained from the autocorrelation function, defined as follows [9]:

$$R_{ee}(\tau) = E \{e(t)e(t + \tau)\} \quad (A.2)$$

where $E\{ \cdot \}$ denotes the expectation operation. Therefore, e^2_{RMS} can be obtained from $R_{ee}(0)$. To evaluate $R_{ee}(0)$, the Fourier transform of the energy spectrum is used. The transfer function between $e(t)$ and $f(t)$ is first derived.

$$\frac{E(s)}{F(s)} = \frac{1 + s/\alpha}{1 + s/\alpha + e^{-\tau/\alpha} s^2} \quad (A.3)$$

Therefore under the approximation of equation (A.1), the following integral expression for e^2_{RMS} follows from the Fourier transform:

$$e^2_{RMS} = \frac{\sigma K_1}{2\pi} \int_0^\sigma \left| \frac{j\omega + \alpha}{j\omega + \alpha + e^{-j\omega\tau_{eq}}} \right|^2 d\omega \quad (A.4)$$

The integral term of equation (A.4) can be written:

$$e^2_{RMS} = \frac{\sigma K_1}{2\pi} \int_0^\sigma \left| \frac{j\omega + \alpha}{\alpha + \alpha \cos(\tau\omega) + j(\omega - \alpha \sin(\tau\omega))} \right|^2 d\omega \quad (A.5)$$

It is desired to approximate the integral in the region $\sigma/\alpha < 1$ and $\omega\tau_{eq} \ll 1$. Taking into account the fact that ω is only evaluated in the region from 0 to σ radians, the integral of equation (A.5) is approximated by the following integral:

$$\frac{K_1 \sigma}{2\pi} \int_0^\sigma \frac{2\alpha^2}{\omega^2 - 2\omega\alpha \sin(\tau_{eq}\omega) + 4\alpha^2} d\omega \quad (A.6)$$

replacing $\sin(x)$ by x for $[\tau_{eq}\omega]$ small yields:

$$\frac{e^2_{RMS}}{\text{Power in Forcing Function}} \approx \frac{\alpha}{(1-2\alpha\tau_{eq})^{1/2}} \left[\tan^{-1} \left[\frac{\omega}{2\alpha} (1-2\alpha\tau_{eq})^{1/2} \right] \right]_0^\sigma \quad (A.7)$$

Evaluating the integration limits and expanding the inverse tangent function to two terms [1], [10] yields:

$$\frac{e_{RMS}^2}{\text{Power in Forcing Function}} \sim K'' \frac{\sigma^2}{\alpha^2} \quad (\text{A.8})$$

For constant power in the forcing function, e_{RMS} , can be approximated by:

$$e_{RMS} \sim K' \frac{\sigma}{\alpha} \quad (\text{A.9})$$

It is noted that the above derivation for e_{RMS} closely parallels the derivation of the 1/3 power law obtained in [1] and [10].

APPENDIX B

Derivation of an Effective Delay

With reference to Figure (14), it is desired to obtain an expression for effective time delay τ_{eq} as a function of the parameters identified in the closed loop. Since:

$$e(t) = f(t) - x(t) \quad (\text{B.1})$$

One possible definition of effective delay would be the effective time lag in the system's output $x(t)$ to a sudden change in the input $f(t)$. This type of definition would require (at least approximately) the following relationship to hold for incremental changes (or rapid input changes):

$$X(s) = F(s) e^{-s\tau_{eq}} \quad (\text{B.2})$$

If (B.2) is satisfied, then the error can be written as:

$$E(s) = F(s) [1 - e^{-\tau_{eq} s}] \quad (\text{B.3})$$

For small values of effective delay, the error signal is essentially zero; for large values of effective delay, the error signal becomes equal to the forcing function. This type of definition of effective delay has physical meaning in the description of man-machine performance. First, the real power in the error [e_{RMS}^2] will be evaluated using complex conjugate notation:

$$\text{Real power in error} = 1/2 E(j\omega) E^*(j\omega) \quad (\text{B.4})$$

$$= 1/2 F(j\omega) F(-j\omega) [2 - e^{-j\omega\tau_{eq}} - e^{j\omega\tau_{eq}}] \quad (\text{B.5})$$

Therefore (to first order):

$$e_{RMS}^2 \sim FF^2(j\omega) [1 - \cos \omega \tau_{eq}] \quad (\text{B.6})$$

Thus

$$1 - \cos \omega \tau_{eq} \sim \frac{e_{RMS}^2}{FF^2(j\omega)} \quad (\text{B.7})$$

But

$$\frac{e_{RMS}^2}{F^2(j\omega)} = K \sigma^2 / \alpha^2 \quad \text{From Appendix (A)}$$

It then follows that:

$$\cos \omega \tau_{eq} \approx 1 - K' \sigma^2 / \alpha^2 \quad (\text{B.8})$$

Expanding $\cos (X)$ to two terms yields:

$$\tau_{eq} \approx K'' \sigma / \alpha \quad (\text{B.9})$$

Where K'' accounts for a mean value of ω in the frequencies of interest in the analysis. The relationship equation (B.9) illustrates the dependence between τ_{eq} and the parameters of interest. The physical interpretation of equation (B.9) is that for man-machine systems with large α values, the effective delay is small. This is consistent with larger crossover frequencies and better performance. Also, if the forcing function bandwidth σ is increased, the effective delay will also increase. This result is consistent with a larger e_{RMS} score and poorer performance.

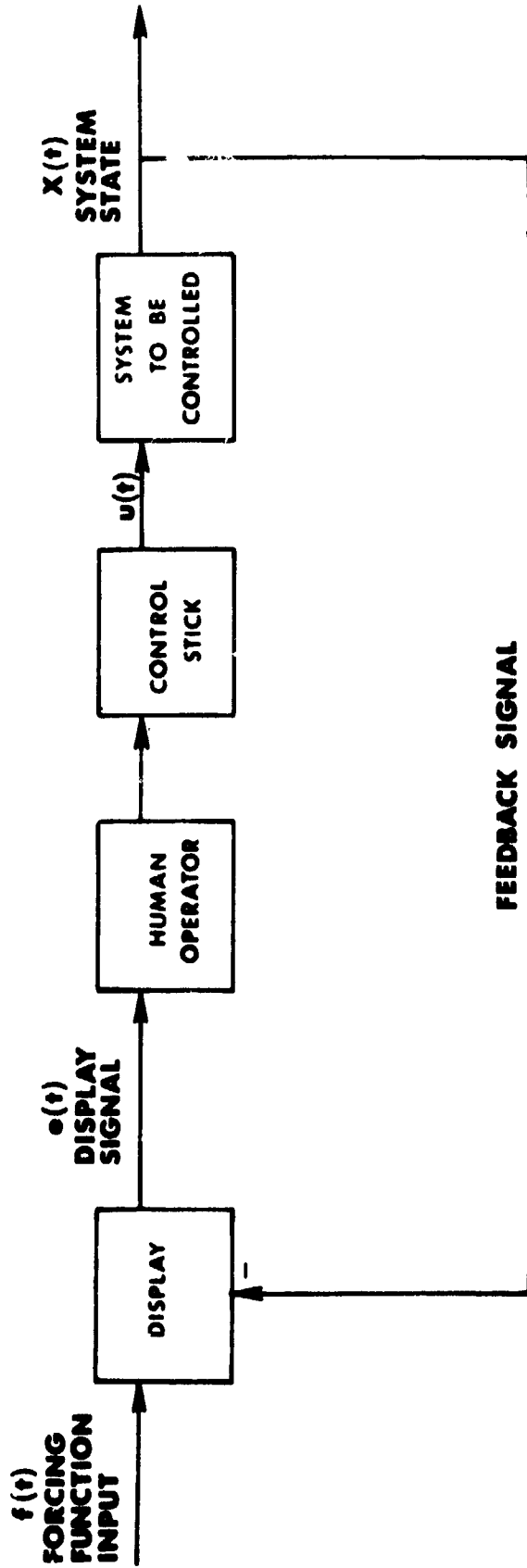


FIGURE 1

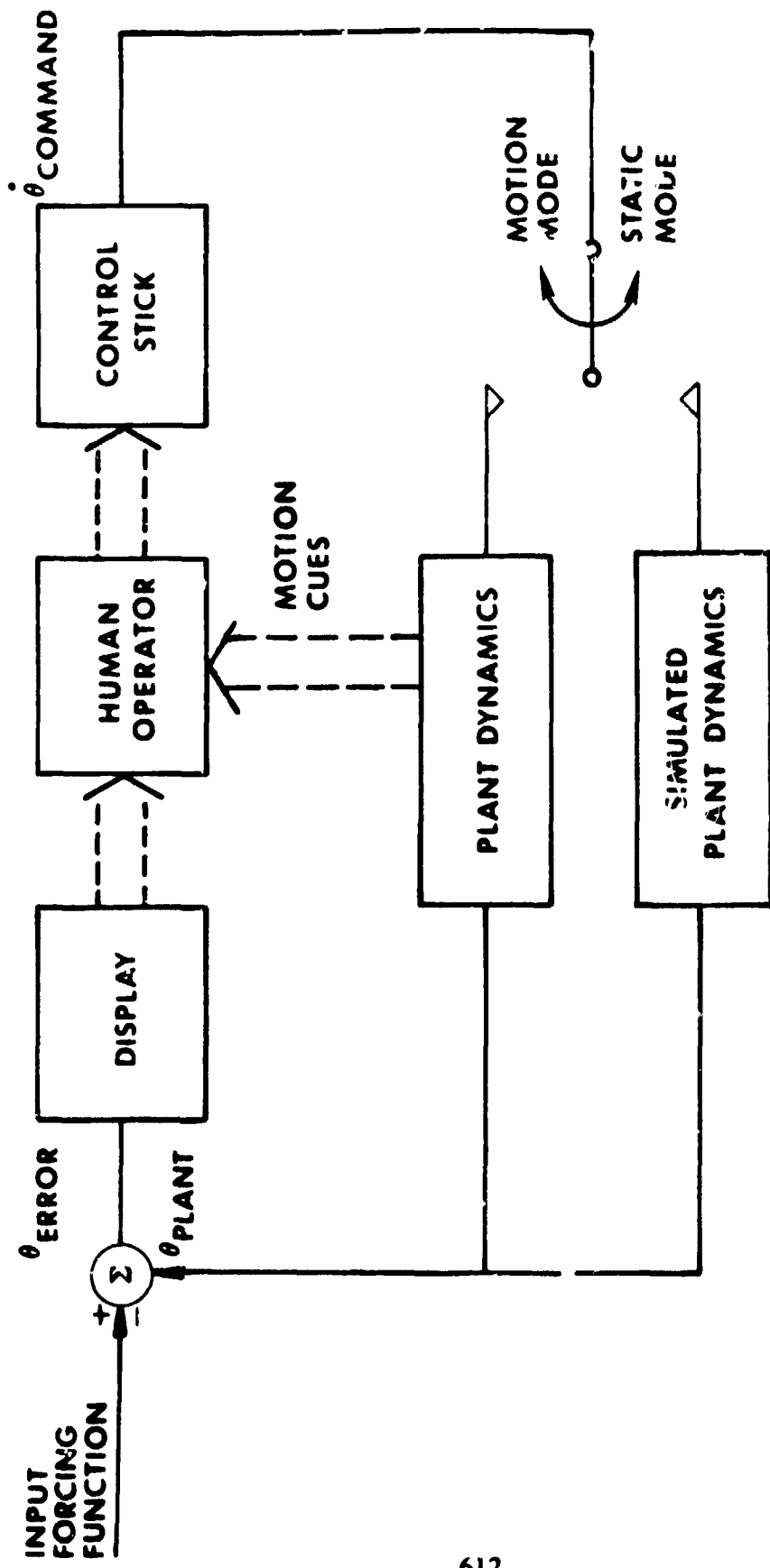
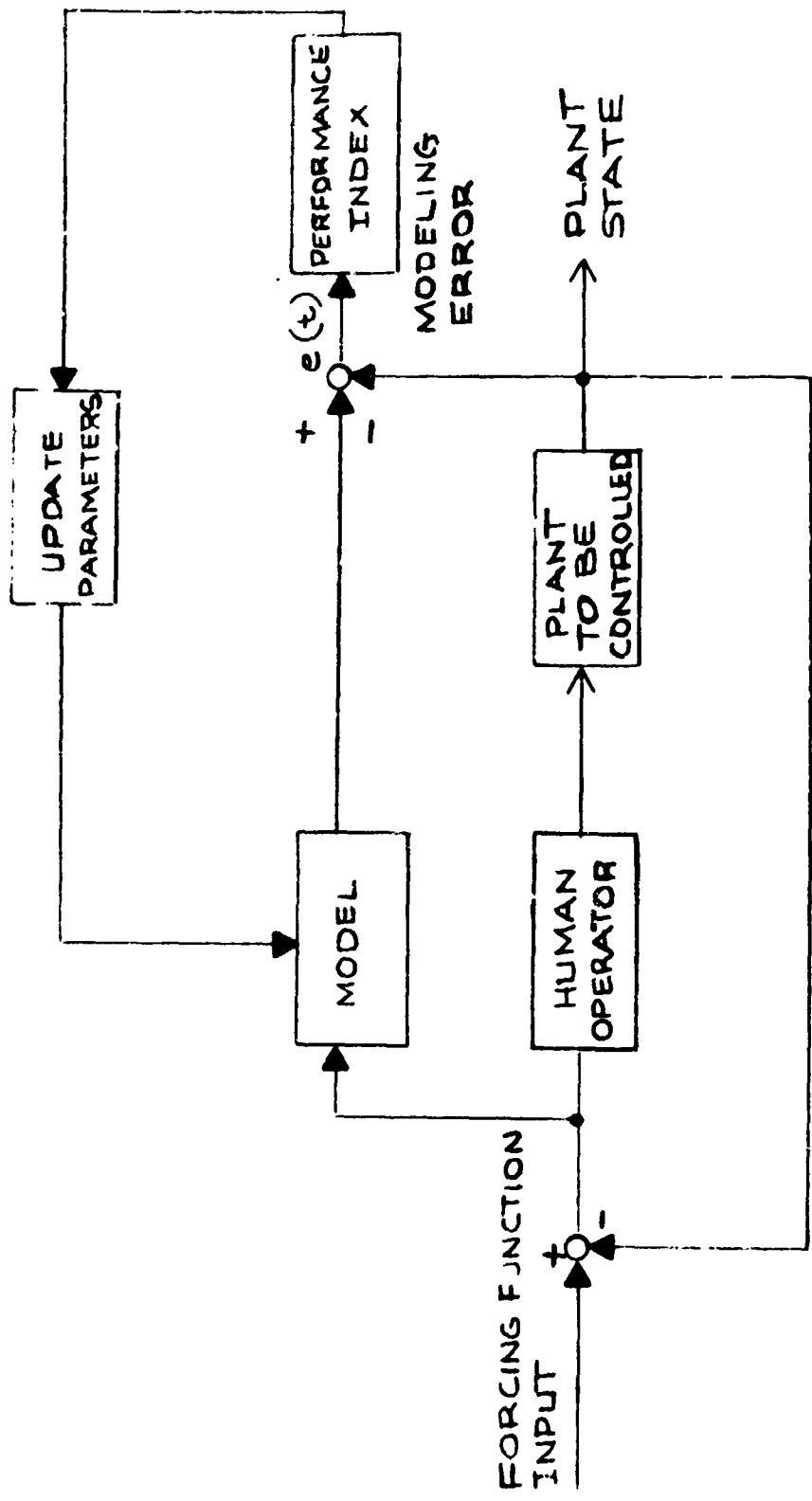


FIGURE (2)



MODELING TOOL TO EVALUATE MAN-MACHINE PARAMETERS

Figure 3

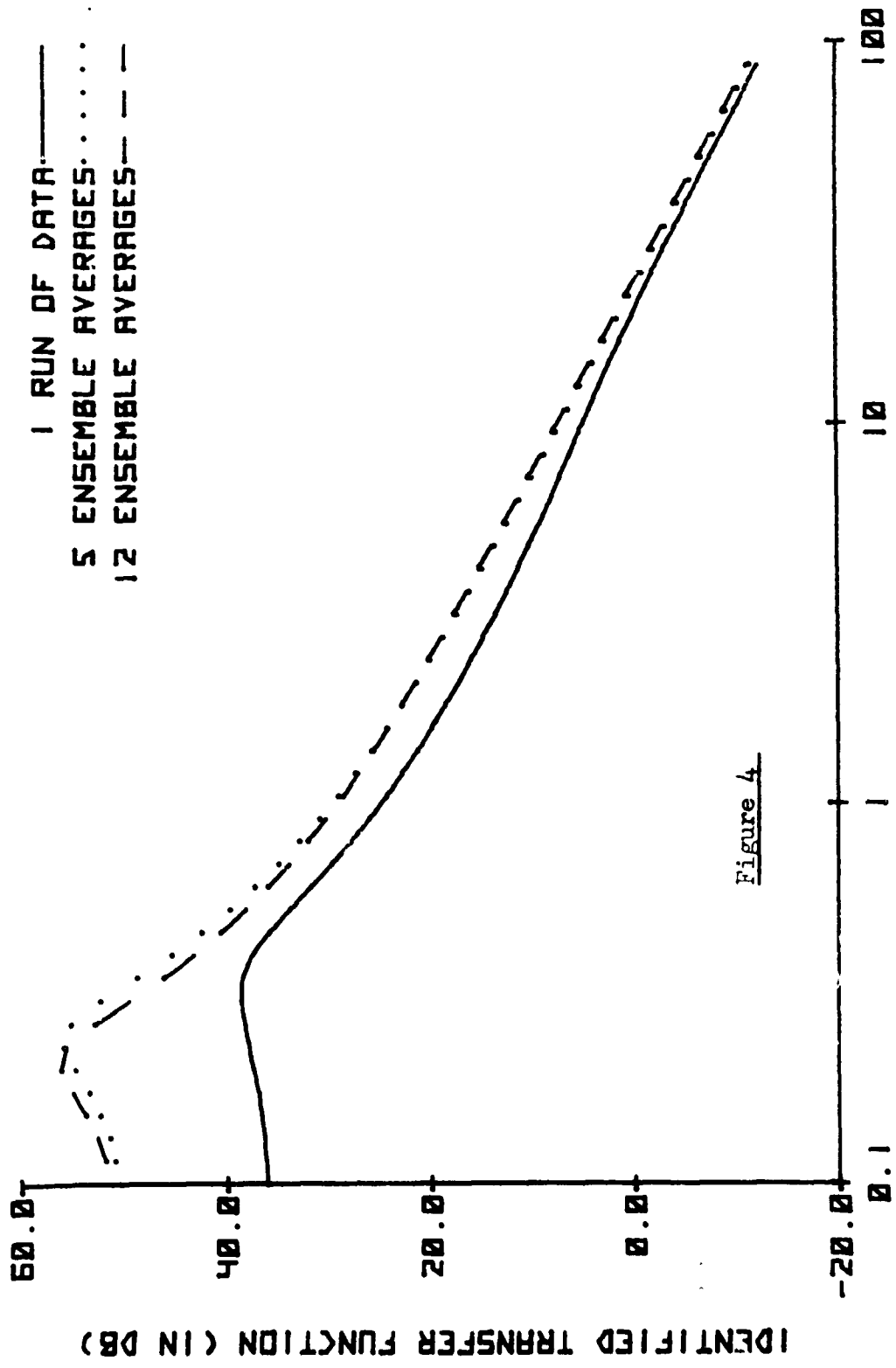


Figure 4

EFFECTS OF ENSEMBLE AVERAGES
 2ND ORDER GUESS OF THE PLANT

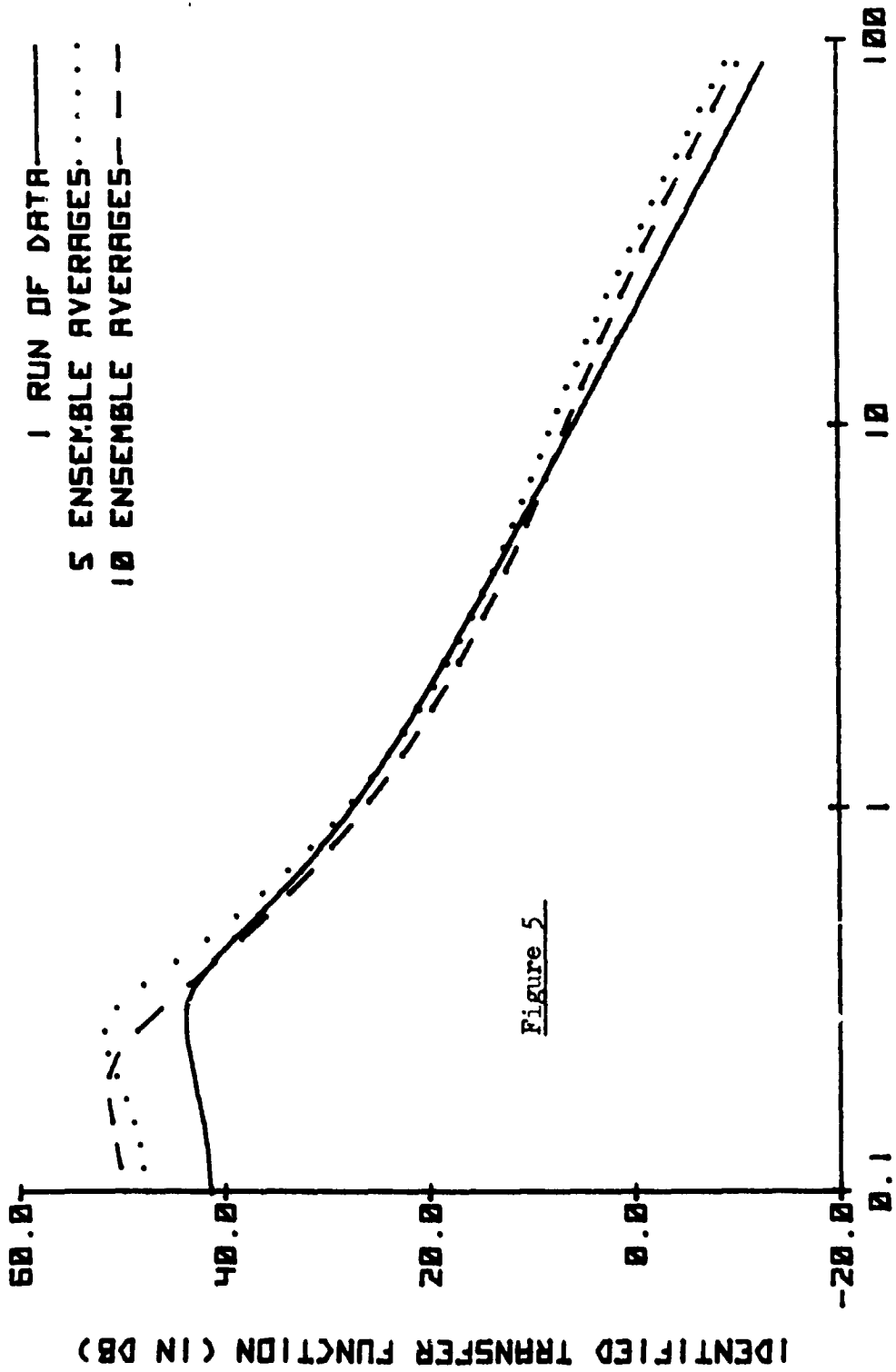


Figure 5

FREQUENCY (RAD IANS/SECOND)
 EFFECTS OF ENSEMBLE AVERAGES
 3RD ORDER GUESS OF THE PLANT

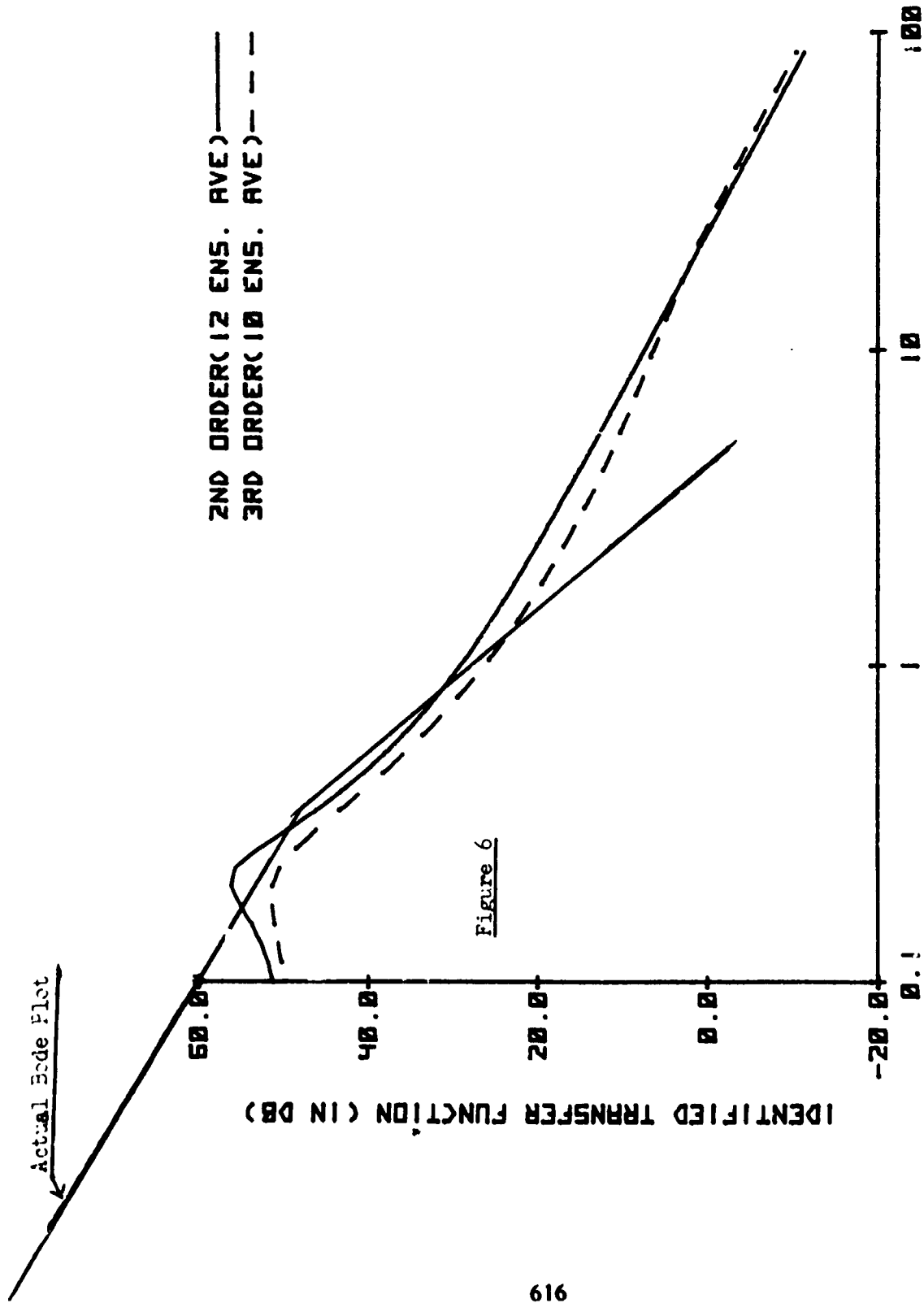


Figure 6

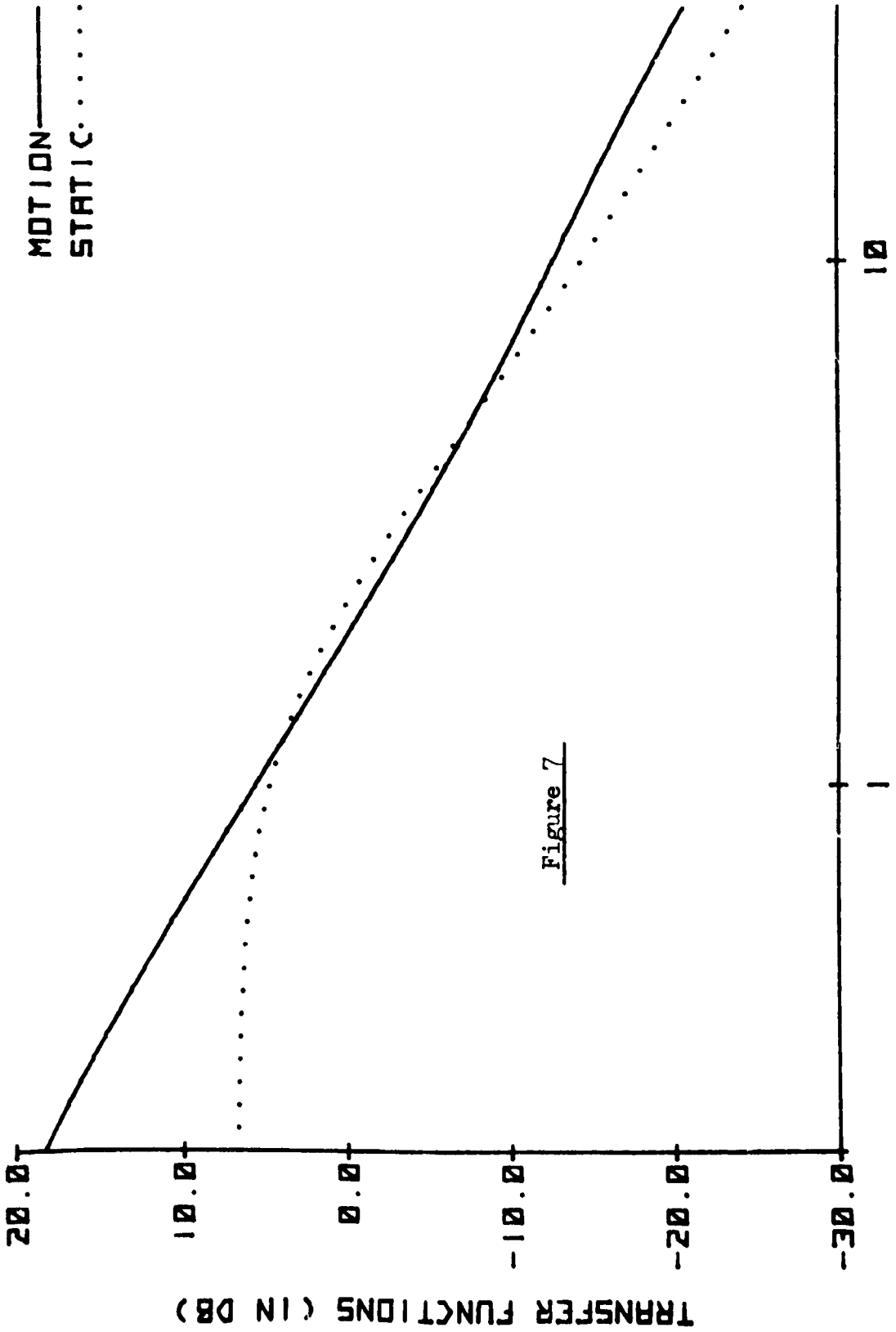


Figure 7

FREQUENCY (RADIAN/SECOND)
 MAN MACHINE PLANT NO 1
 FF2

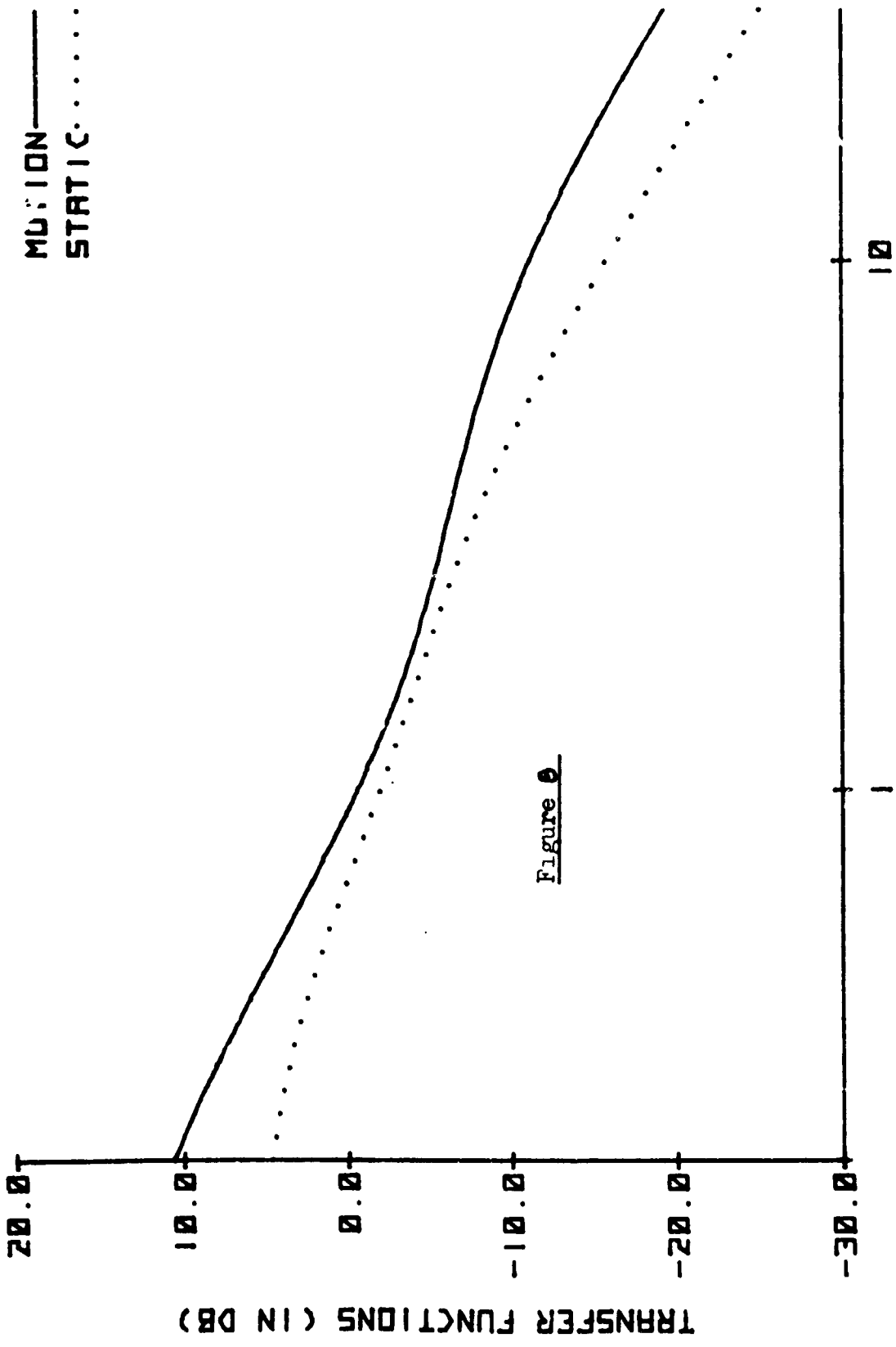


Figure 0

FREQUENCY (RADIAN/SECOND)
 MAN-MACHINE PLANT NO 2
 FF2

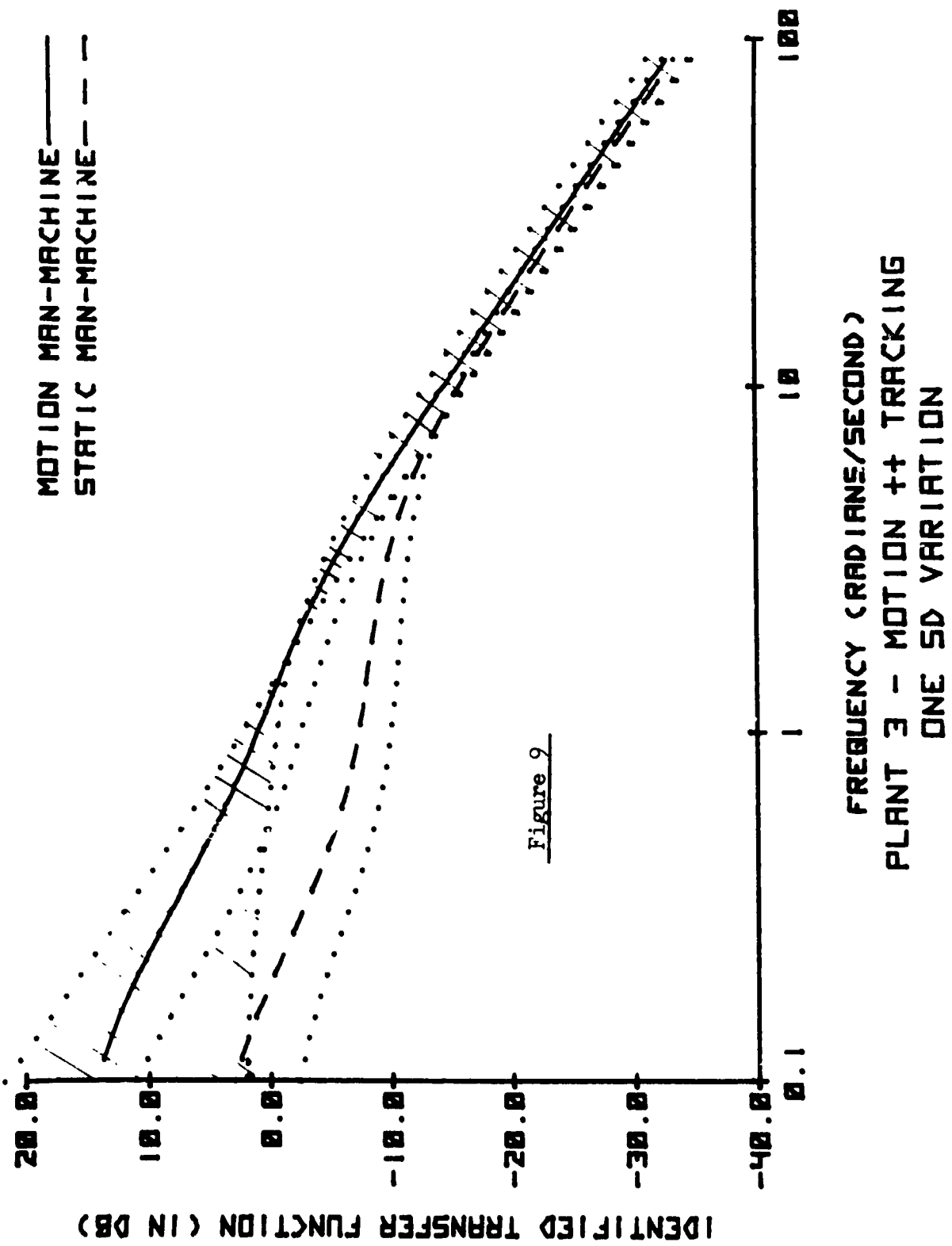
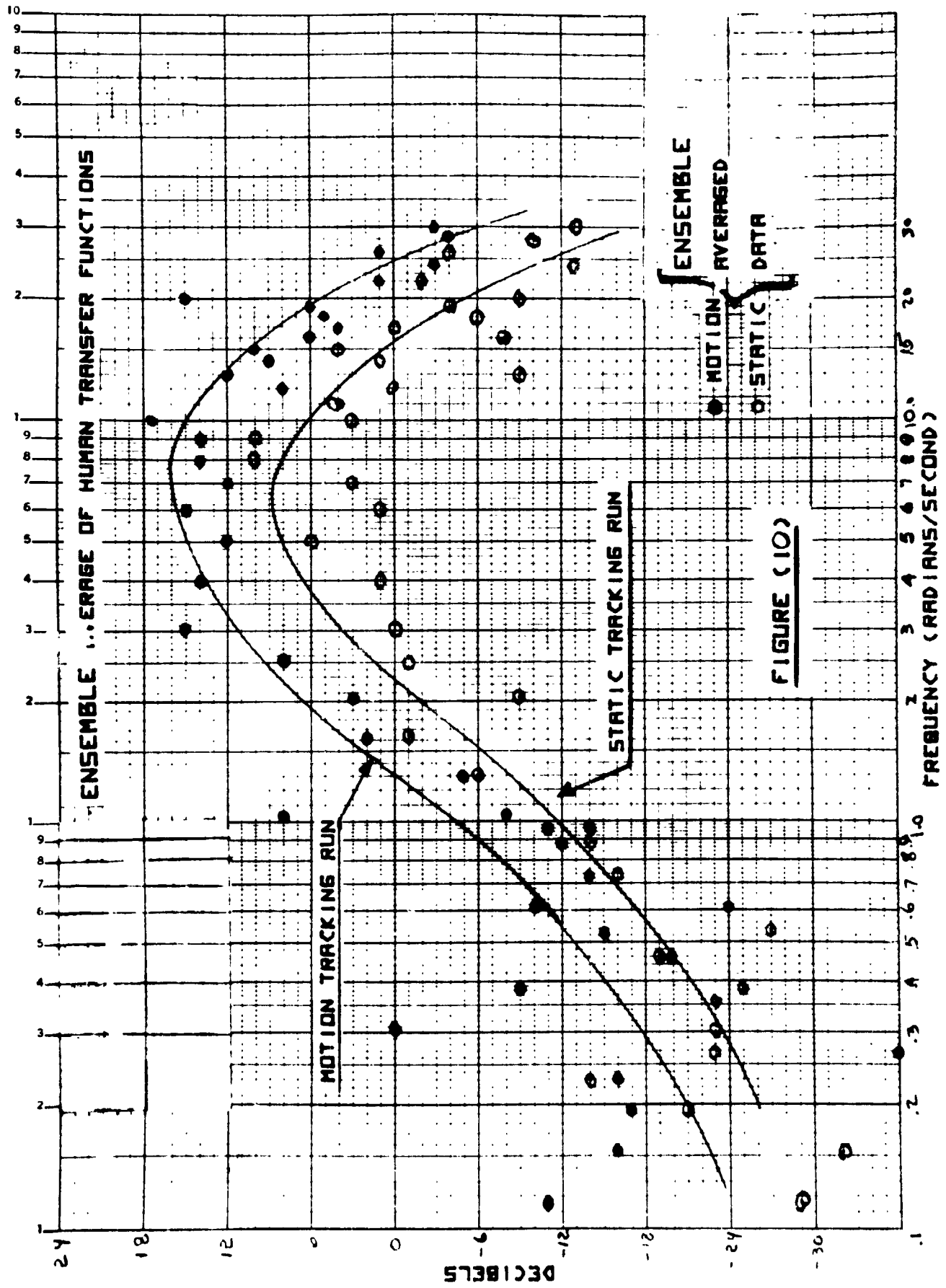
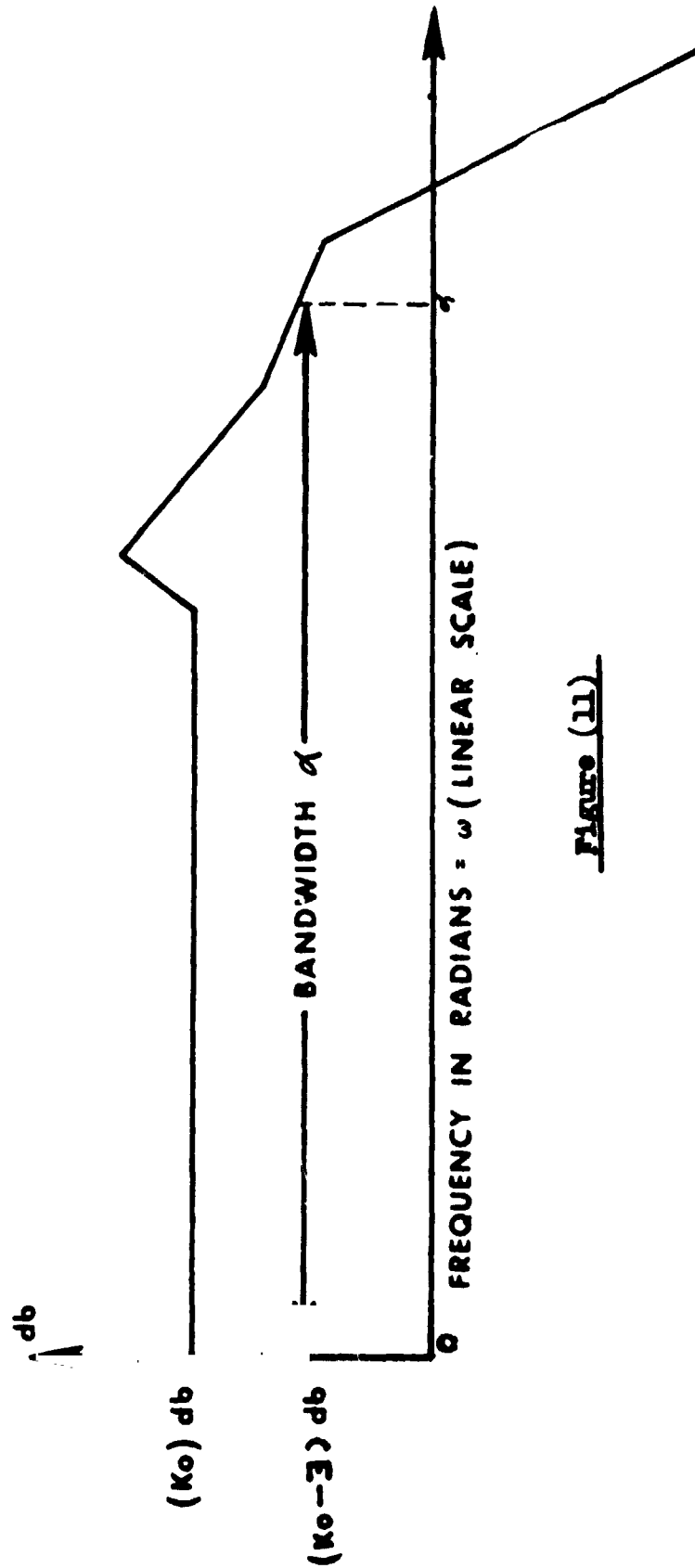


Figure 9



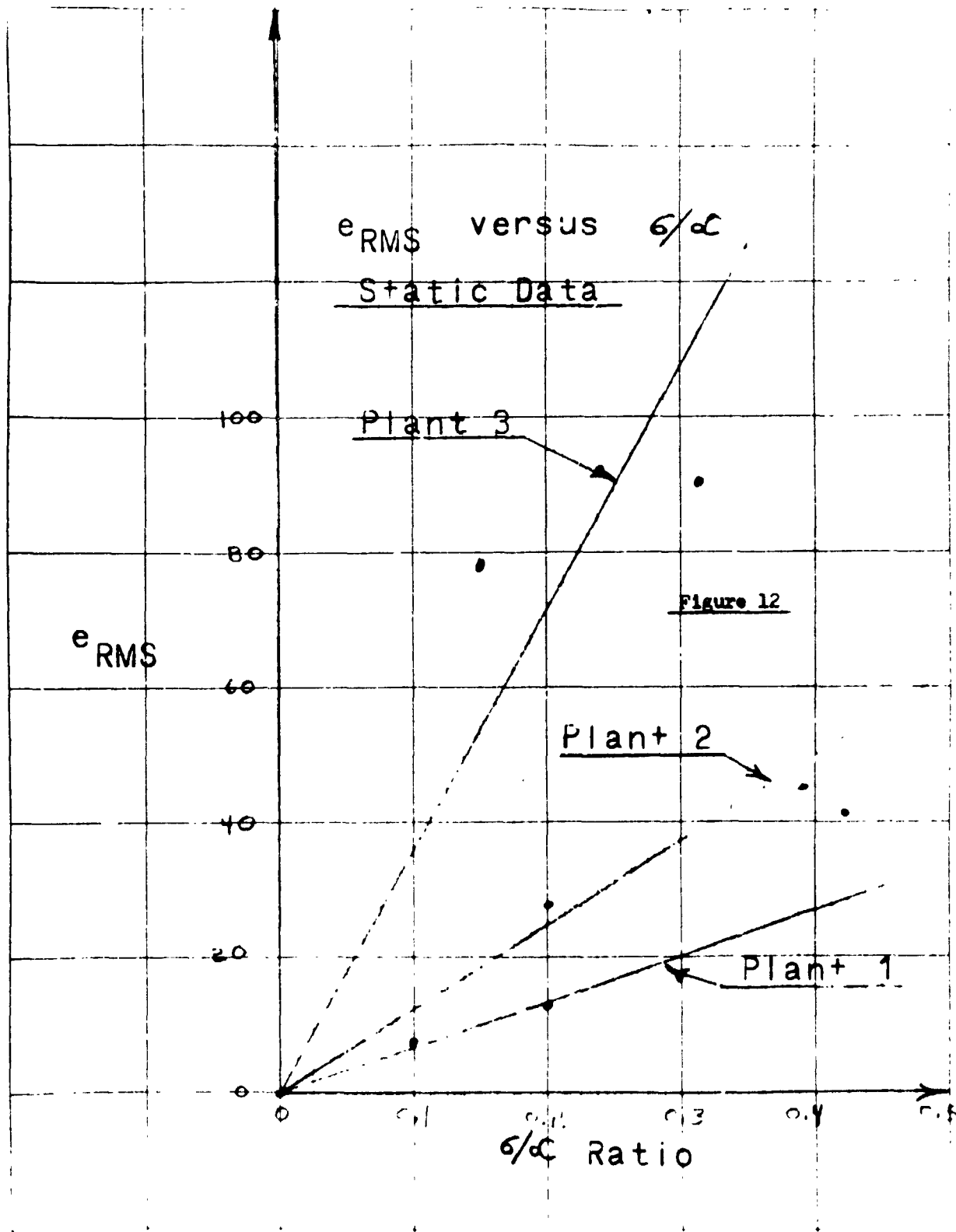
The α (performance) Model

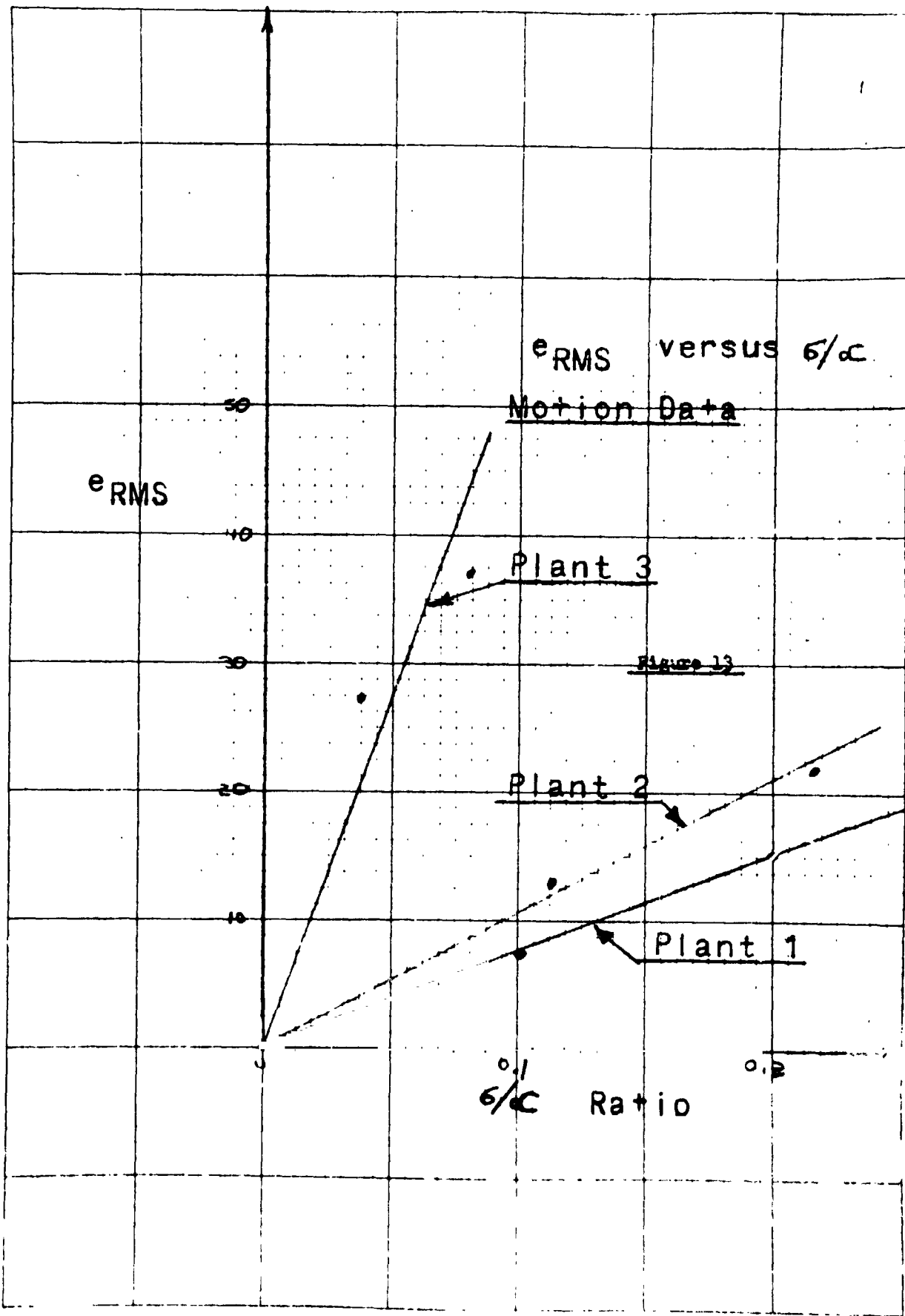
Man-Machine Transfer Function



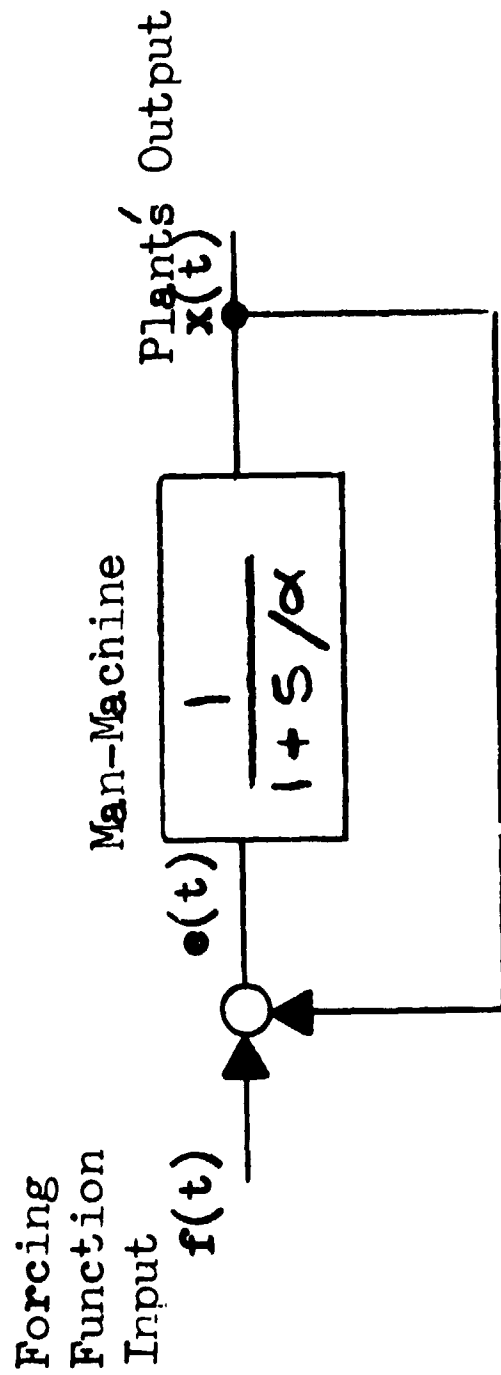
621

Figure (11)





PREDICTION RULES



$$e_{RMS} = K' \sigma / \alpha$$

$$\tau_{eq} = K'' \sigma / \alpha$$

Figure 14

N75 33714

A STUDY OF PILOT BEHAVIOR DURING CONTROLLING THE
LATERAL DIRECTIONAL MOTION OF AIRPLANES IN TURBULENT AIR

By Goro Beppu

National Aerospace Laboratory in Japan

SUMMARY

The pilot behaviors controlling the lateral directional motion of airplanes in turbulent air have been investigated by using the pilot transfer function which has been obtained by the analysis of flight test data. The pilot uses the gains for the aileron manipulation proportionally to bank angle so as to minimize r. m. s. of bank angle. The pilot rudder manipulations are done proportionally to rolling velocity, yawing velocity, and yaw angle. Namely, the pilot carries out the cross control for the rudder.

INTRODUCTION

Aircraft controllability studies are frequently based upon the opinion of the pilots of simulator tests or flight tests, and relating this opinion and the dynamic characteristics of the airplane. In addition to this method, we have an analysis in which the pilot behavior is expressed in the transfer function form. The pilot's transfer function is then used to determine the closed loop motions of the airplane with respect to stability and to gust response. It is considered that this analysis is of use in making a more thorough examination into the reasons for control problems. Thus far, this analysis has been used by several persons and its suitability has been proven. However, there is a problem in the use of this analysis for airplane design because it is necessary to accurately represent the complicated pilot behavior in the transfer function formula. After this problem is solved, the control problems in turbulent air are investigated for an airplane having large coupling between lateral and directional motions.

At first, the controllability limits of various roll-yaw couplings have been investigated in flight tests. Next, the pilot transfer functions, which describe the pilot behavior, have been found by analyzing the flight test data. Then, using this pilot transfer function, the gust responses of the airplane equation of motion, including pilot control, have been calculated

and r.m.s. of bank angle, yawing velocity, amount of aileron control and rudder control have been obtained. By calculating these r.m.s. for the case when the pilot gains are altered, it is examined why the pilot uses those gains that we have obtained by the analysis of the flight test data. Furthermore, the reasons for control problems are considered.

SYMBOLS

G_p	gain for the rudder manipulation proportional to p
G_r	gain for the aileron manipulation proportional to r
G_ϕ	gain for the rudder manipulation proportional to bank angle
G_ψ	gain for the aileron manipulation proportional to yaw angle
I_x	moment of inertia about X axis
I_z	moment of inertia about Z axis
K_p	gain for the aileron manipulation proportional to p
K_r	gain for the rudder manipulation proportional to r
K_ϕ	gain for the aileron manipulation proportional to bank angle
K_ψ	gain for the rudder manipulation proportional to yaw angle
L	rolling moment
L_G	(rolling moment due to gust)/ I
m	remnant of pilot control or mass of airplane
N	yawing moment
N_G	(yawing moment due to gust)/ I
n	noise
p	rolling velocity
r	yawing velocity

s	Laplace operator
Y	side force
τ_a	pilot reaction time delay of aileron control
τ_r	pilot reaction time delay of rudder control
β	sideslip
β_G	(side gust velocity)/(velocity of airplane)
δ_a	aileron deflection angle
δ_r	rudder deflection angle
ζ_ω	damping ratio of the quadratic of the numerator of p/δ_a
ζ_d	damping ratio of the Dutch roll mode of p/δ_a
ω	bank angle
ψ	yaw angle
ω	angular frequency
ω_ω	angular frequency of the quadratic of the numerator of p/δ_a
ω_d	angular frequency of the Dutch roll mode of p/δ_a

Stability Derivatives

$$Y_\beta = (\partial Y / \partial \beta) / m$$

$$Y_\omega = (\partial Y / \partial \omega) / m$$

$$N_p = (\partial N / \partial p) / I_z$$

$$N_r = (\partial N / \partial r) / I_z$$

$$N_\beta = (\partial N / \partial \beta) / I_z$$

$$N_{\delta_a} = (\partial N / \partial \delta_a) / I_z$$

$$N_{\delta_r} = (\partial N / \partial \delta_r) / I_z$$

$$N_{\delta a}^* = N_{\delta a} / L_{\delta a}$$

$$L_p = (\partial L / \partial p) / I_x$$

$$L_r = (\partial L / \partial r) / I_x$$

$$L_\beta = (\partial L / \partial \beta) / I_x$$

$$L_{\delta a} = (\partial L / \partial \delta_a) / I_x$$

Power Spectrum or Cross Spectrum

Φ_{np} cross spectrum between n and p

Φ_{nr} cross spectrum between n and r

$\Phi_{n\delta a}$ cross spectrum between n and δ_a

$\Phi_{n\delta r}$ cross spectrum between n and δ_r

Φ_{GG} power spectrum of gust

Root Mean Square (r. m. s.)

σ_r r. m. s. of r

σ_ψ r. m. s. of ψ

$\sigma_{\delta a}$ r. m. s. of δ_a

$\sigma_{\delta r}$ r. m. s. of δ_r

THE AIRPLANE CONFIGURATION INVESTIGATED

The small perturbation equations of lateral and directional motion are written as follows:

$$(s - Y_\beta)\beta + r - Y_\psi \psi = 0 \quad (1)$$

$$-N_\beta \beta + (s - N_r)r - N_p \psi = N_{\delta r} \delta_r + N_{\delta a} \delta_a \quad (2)$$

$$-L_\beta \beta - L_r r + s(s - L_p)\psi - L_{\delta a} \delta_a \quad (3)$$

The transfer function of rolling velocity response to an aileron input is:

$$\frac{p}{\delta_a} = \frac{L_{\xi a} s(s^2 + 2\zeta_{\omega} s + \omega^2)}{(s + \lambda_s)(s + \lambda_R)(s^2 + 2\zeta_d s + \omega_d^2)} \quad (4)$$

When the vector differences between the roots of the quadratic element in the numerator and those of the quadratic element in the denominator are large, the roll-yaw coupling becomes significant, and the aileron manipulation excites the Dutch roll mode to a large extent. Therefore, in order to realize a large roll-yaw coupling, the configuration of the airplane has been chosen in this work such that the roots of the numerator in equation (4) are greatly different from those of the Dutch roll mode. Namely, we chose a configuration whose $N_{\delta a}$ is large positively or negatively. For such a configuration, the relative positions of the roots of the numerator and those of the Dutch roll mode are shown in Figure 1. The response to an aileron step input is shown in Figure 2. In Figure 1, we can see that the roll response is oscillatory for the case of $N_{\delta a}^* = -0.2$, for which the distance between the numerator roots and those of the Dutch roll mode roots is large as shown in Figure 1.

EXPERIMENTS AND RESULTS

Flight tests were carried out in simulated turbulent air conditions, using a variable stability airplane (Beechcraft B65). The pilot was required to maintain the airplane in a steady level flight condition in simulated turbulent air. The tests were done at the altitude of 6000 ft and at the speed of 115 mph with the test run length of two minutes. During the tests, β , r , p , δ_a , δ_r , and the amount of turbulence were measured. An example of the measurements is shown in Figure 3.

The turbulent air conditions were simulated as follows: The airplane was disturbed by the movements of aileron and rudder actuated by servo motors proportionally to the noise signals recorded in a tape recorder. An example of the power spectral density of the noise is shown in Figure 4. R. m. s. of the noise was 0.9° when converted to the aileron deflection angle. The deflection of the rudder due to the noise signals was proportional to the aileron deflection because only the side gust was considered. The ratio of the rolling moment to the yawing moment due to the noise signal was as follows:

$$L_G : N_G = 1 : -0.16 \quad (5)$$

The sign of L_G is opposite to that of N_G because when the airplane is upset by the side gust producing a positive rolling moment, the airplane has negative yawing moment. The ratio in equation (5) is not equal to the ratio L_β to N_β . Because if equal, the pilot complains that the yawing motion is too large if compared with the rolling motion, and he will not feel such turbulence as a real gust. The reason for the value of N_G being small, is that we neglect the effect of the difference of gust velocity along the body. The ratio in equation (5) is determined by the pilot's opinion.

The results of the experiment are as follows: When N_{δ_a} was changed in sign to have positive value, $N_{\delta_a}^* = +0.2$ was the controllability limit, and the pilot commented that the yawing motion was large. When N_{δ_a} was negative, $N_{\delta_a}^* = -0.2$ was the controllability limit. According to the pilot's comments, his control response was as follows: When the airplane is upset by the side gust from the left, a positive rolling motion ensues. Then the pilot manipulates the aileron control wheel to alleviate this rolling motion and at the same time he deflects the right pedal, expecting the yawing motion due to the gust. But the aileron control generates positive yawing moment due to N_{δ_a} . Therefore, it follows that the first deflection of the pedal becomes too large and a positive yawing motion results. The pilot must add left pedal immediately after adding right pedal. So the pedal manipulation is troublesome in this case.

In Figure 1 the preceding controllability limits are described. In the same figure, the limit line which is defined in MIL F 8785B is also depicted. The differences between these experimental results and that of MIL F 8785B are noticeable. The reasons are now considered. MIL F 8785B is defined for the pilot who does not use the rudder to alleviate the yawing motion due to the gust. But our pilot used the rudder effectively to alleviate the yawing motion. As a result, the controllability limits of this experiment become wider than that of MIL F 8785B, except the case of positive N_{δ_a} . The positive N_{δ_a} case has a control difficulty which cannot be an attribute of the distance between the roots of the numerator quadratic term and those of the Dutch roll mode in equation (4).

PILOT DESCRIBING FUNCTIONS OBTAINED FROM FLIGHT TEST DATA

First of all, the pilot transfer function for the aileron control is considered. When the airplane is upset by some disturbance, the pilot who gets some motion and visual cues, manipulates the aileron to alleviate the airplane motion due to the disturbance. In the frequency range 0.05-1.0 Hz, the pilot attempts to make the bank angle displacement as small as possible. However, it is not clear how he uses motion and/or visual cues. So, the

following method is used in this work in order to determine the pilot transfer function. It is assumed that the pilot manipulates the aileron proportionally to the bank angle, the rolling velocity, the yaw angle, the yawing velocity with some reaction time delay τ_a . And the pilot also manipulates the aileron by the amount $m(t)$ which has no correlation with the external disturbance $n(t)$. The $\delta_a(t)$ is thus written as follows:

$$\delta_a(t) = -K_p \cdot p(t - \tau_a) - K_\omega \cdot \omega(t - \tau_a) - G_\psi \cdot \psi(t - \tau_a) - G_r \cdot r(t - \tau_a) + m(t) \quad (6)$$

where K_p , K_ω , G_ψ , and G_r are constants. Calculating the cross correlations of the disturbance $n(t)$ with $\delta_a(t)$, $\omega(t)$, $p(t)$, $\psi(t)$, $r(t)$, and $m(t)$, the cross spectrum can be obtained as follows:

$$\Phi_{n\delta_a}(j\omega) = \{ -(K_p + K_\omega / j\omega) \Phi_{np}(j\omega) - (G_r + G_\psi / j\omega) \Phi_{nr}(j\omega) \} e^{-j\tau_r \omega} \quad (7)$$

where $\Phi_{nm}(j\omega) = 0$, because $m(t)$ has no correlation with $n(t)$. Using the measured quantities n , δ_a , p , and r ; $\Phi_{n\delta_a}(j\omega)$, $\Phi_{np}(j\omega)$, and $\Phi_{nr}(j\omega)$ are calculated. Then the constants K_p , K_ω , G_ψ , G_r , and τ_a are determined by a matching technique such that equation (7) is satisfied for several ω values. The degree of accuracy of the final matching between $\Phi_{n\delta_a}(j\omega)$ and the right hand side of equation (7) is as shown in Figure 5. K_p , K_r , G_ψ , G_r , and τ_a , which are obtained by the above method, are shown in Table 1. In Table 1 it is seen that G_ψ and G_r are small. Thus it is concluded that $\delta_a(s)$ can be written as follows:

$$\delta_a(s) = -(K_p s + K_\omega) e^{-\tau_a s} \omega \quad (8)$$

For the rudder, the same method of calculation is used and the following equation is obtained.

$$\Phi_{n\delta_r}(j\omega) = \{ -(G_p + G_\omega / j\omega) \Phi_{nr}(j\omega) - (K_r + K_\psi / j\omega) \Phi_{nr}(j\omega) \} e^{-j\tau_r \omega} \quad (9)$$

Using the same matching technique as for the aileron control case, G_p , G_ω , K_r , K_ψ , and τ_r are determined. In this case, G_ψ is small. $\delta_r(s)$ can be written as follows:

$$\delta_r(s) = -G_p s e^{-\tau_r s} \omega - (K_r + K_\psi / s) e^{-\tau_r s} r \quad (10)$$

In this case, the term G_p has a peculiar feature. The reason for having the term G_p is as follows: When the airplane is upset by a side gust, the airplane begins a rolling motion at first and after some time delay the yawing motion develops, because of the larger moment of inertia about the yaw axis than that about the roll axis. Therefore, the pilot expects a yaw motion when the airplane begins a rolling motion due to the side gust, and he uses the rudder in order to suppress the yaw motion which follows the roll response. This behavior is represented by the term G_p . In this case, the degree of accuracy of the final matching is as shown in Figure 6. The constants G_p , G_φ , K_r , K_ψ , and τ_r are shown in Table 1.

EFFECTS OF THE PILOT GAIN ON THE WORKLOAD AND PERFORMANCE INDEX

Using the pilot transfer function (8) and (10), the equations of airplane lateral and directional motion in turbulent air, including the pilot control, are written as follows:

$$(s - Y_\beta)\beta + r - Y_\varphi \varphi = 0 \quad (11)$$

$$-N_\beta \beta + (s - N_r)r - N_p s \varphi = N_{\delta_r} \delta_r + N_{\delta_a} \delta_a - N_G \varphi \quad (12)$$

$$-L_\beta \beta - L_r r + s(s - L_p)\varphi = L_{\delta_a} \delta_a + L_G \varphi \quad (13)$$

$$\delta_a = -(K_p s + K_\varphi) e^{-\tau_a s} \varphi \quad (14)$$

$$\delta_r = -G_p s e^{-\tau_r s} \varphi - (K_r + K_\psi / s) e^{-\tau_r s} r \quad (15)$$

where N_G and L_G are the yawing and rolling moment due to the turbulent air.

Using the time series of noise (which were used in flight tests) as the input of the above equations, the above equations of motion have been solved by means of digital computer. The time series of the gust response r , φ , δ_a and δ_r are obtained. By integrating these time series and extracting the square root of the integrated values, r. m. s. σ_r , σ_φ , σ_{δ_a} , and σ_{δ_r} of r , φ , δ_a , and δ_r are obtained. Applying this method of calculation the following analysis has been carried out.

As K_φ changes, it is first examined how σ_φ and σ_{δ_a} change. As K_r changes, it is next examined how σ_r and σ_{δ_r} change.

(1) K_{ω} change: Curves of σ_r and σ_{δ_a} versus K_{ω} are shown in Figure 7. For all cases, as K_{ω} increases, σ_{δ_a} increases; however, σ_{ω} decreases for a small K_{ω} range to reach a minimum value but increases for a large K_{ω} range. When K_{ω} is small, the root of the spiral mode is small. Due to the smallness of the spiral mode root, the gain of the bank angle response to the gust is large in the low frequency range. As K_{ω} becomes larger, the gain of the bank angle becomes smaller. When K_{ω} is large, the stability of the system deteriorates due to pilot reaction time delay and the gain of the bank angle is large at large K_{ω} . These are seen in Figure 8, which is the linear scale Bode diagram. For all cases, we have the nearly smallest σ_{ω} at the gains which are obtained from the analysis of the flight test data. It is considered that the pilot controls the system, adjusting K_{ω} so as to minimize σ_{ω} . Namely, we have obtained large K_{ω} for $N_{\delta_a}^* = -0.2$ and small K_{ω} for $N_{\delta_a}^* = +0.2$.

(2) K_r change: Curves of σ_r and σ_{δ_r} versus K_r are shown in Figure 9. When K_r increases, σ_r continues to decrease until $K_r = +1.2$. So for the original case, the pilot chooses such gain K_r that σ_r becomes smaller than some value. For the cases $N_{\delta_a}^* = +0.2$ and $N_{\delta_a}^* = -0.2$, σ_r is larger than the original case, due to the fact that the aileron control causes the yawing moment for these cases. For the case $N_{\delta_a}^* = +0.2$, the pilot chooses a large gain K_r than the original case to make σ_r as small as σ_r of the original case, and this causes the control difficulties due to large rudder excursion. For the case $N_{\delta_a}^* = -0.2$, the pilot cannot make σ_r as small as σ_r of the original case due to the complicated rudder manipulation mentioned previously. Therefore, the control difficulties of this case are due to the complicated rudder manipulation.

CONCLUSIONS

The pilot behaviors during controlling the lateral directional airplane motion having large adverse or proverse yaw in turbulent air have been investigated by obtaining the pilot transfer function through the analysis of the flight test data and analyzing the airplane gust response including pilot controls. The conclusions of this investigation are as follows.

(1) The pilot aileron manipulations are performed proportionally to rolling velocity and bank angle with some reaction time delay. The gains for the aileron manipulation proportionally to bank angle are chosen by the pilot so as to minimize r. m. s. of bank angle.

(2) The pilot rudder manipulations are done proportionally to rolling velocity, yawing velocity, and yaw angle with some reaction time delay. Namely, as shown by the fact that the rudder is manipulated proportionally

to rolling velocity, the pilot carries out the cross control for the rudder. The pilot uses such gains for the rudder manipulation proportionally to yawing velocity that r. m. s. of yawing velocity becomes smaller than some value instead of getting the minimum value.

REFERENCES

1. McRuer, D. T. and Krendel, E. S.: The Human Operators as a Servo System Element. J. of Franklin Institute 267-5 (1959) 381 and 267-6 (1959) 511.
2. McRuer, D. T., Graham, D., and Krendel, E. S.: Human Pilot Dynamics in Compensatory Systems. J. of Franklin Institute 283-1 (1967) 1 and 283-2 (1967) 145.
3. Magdaleno, R. E., McRuer, D. T., and Moore, G. P.: Small Perturbation Dynamics of the Neuromuscular System in Tracking Tasks. NASA CR 1212 (1968).
4. Washizu, K. and Miyazima, K.: Some Consideration on the Controllability Limit of a Human Pilot. AIAA, Vol. 3, No. 5 (1965).
5. Washizu, K. and Goto, N.: On the Dynamics of Human Pilots in Marginally Controllable Systems. AIAA, Vol. 12, No. 3 (1974).
6. Ashkenas, I. L. and McRuer, D. T.: A Theory of Handling Qualities Derived from Pilot-Vehicle System Considerations. IAS Paper No. 62-39 (1962).
7. Ashkenas, I. L. and McRuer, D. T.: The Determination of Lateral Handling Quality Requirements from Airframe-Human Pilot System Studies. WADC TR 59-135 (1959).
8. Caporali, R. L., Lamers, J. P., and Toten, J. R.: A Study of Pilot-Induced Lateral-Directional Instability. Princeton University Aeronautical Engineering Report 604 (1962).
9. Seckel, E.: Stability and Control of Airplanes and Helicopters. p 287-290, Academic Press, New York, New York (1964).
10. Todosiev, E. P., Rose, R. E., Bekey, G. A., and Williams, H. L.: Human Tracking Performance in Uncoupled and Coupled Two-Axis Systems. NASA CR-532 (1966).

11. Franklin, J. A.: Turbulence and Lateral-Directional Flying Qualities. NASA CR 1718 (1971).
12. McRuer, D. T., Ashkenas, I., and Graham, D.: Aircraft Dynamics and Automatic Control. Systems Technology, Inc., (August 1968).
13. Chalk, C. R., Neal, T. P., Harris, T. M., Pritchard, F. E., and Woodcock, R. J.: Background Information and User Guide for MIL - F - 8785B (ASG), "Military Specification - Flying Qualities of Piloted Airplanes." AFFDL - TR - 69-72 (August 1969).
14. Adams, J. J.: A Simplified Method for Measuring Human Transfer Functions. NASA TN D-1783 (1963).
15. Adams, J. J. and Bergeron, H. P.: Measured Variation in the Transfer Function of a Human Pilot in Single-Axis Tasks. NASA TN D-1952 (1963).
16. Bergeron, H. P. and Adams, J. J.: Measured Transfer Functions of Pilots During Two-Axis Tasks With Motion. NASA TN D-2177 (1964).

Table I. Pilot Gain & Time Delay

(1) Aileron

	K_{ϕ}	K_{ρ}	G_{ψ}	G_{γ}	τ_a
Original Config.	0.85	0.25	0.07	0.03	0.3
$N_{\delta_a}^{\ddagger} = 0.2$	0.75	0.25	0.0	0.06	0.3
$N_{\delta_a}^* = -0.2$	1.05	0.25	0.08	0.0	0.3

(2) Rudder

	G_{ϕ}	G_{ρ}	K_{ψ}	K_{γ}	τ_r
Original Config.	- 0.0	- 0.15	0.0	0.7	0.2
$N_{\delta_a}^{\ddagger} = 0.2$	- 0.04	- 0.27	0.15	1.2	0.15
$N_{\delta_a}^* = -0.2$	- 0.02	- 0.19	0.45	0.6	0.15

Original configuration
 $N_{\dot{\alpha}}/L_{\dot{\alpha}} = +0.2$
 $N_{\dot{\alpha}} = -0.2$

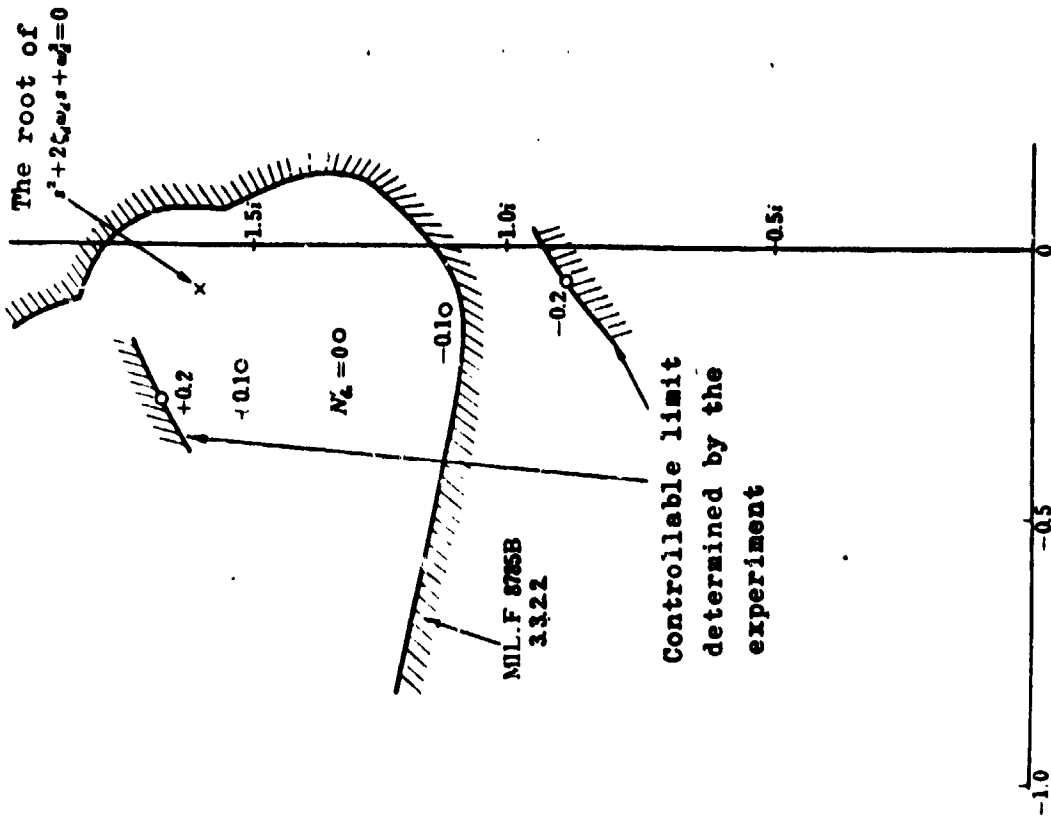
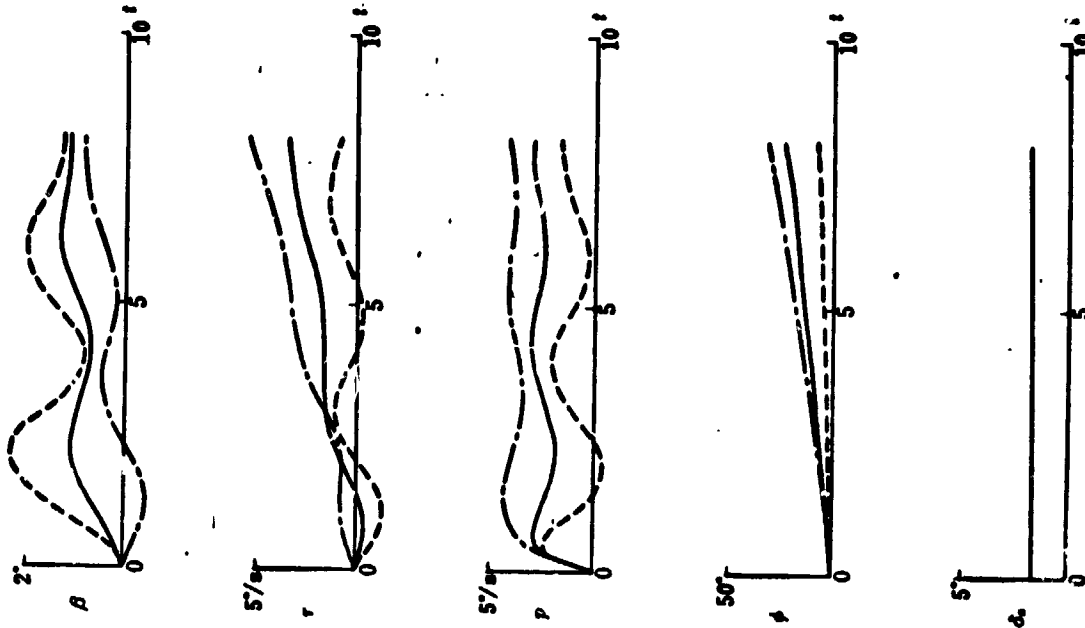


Fig 1 Quadratic roots of the denominator (X) and the - rator(O) of the transfer function

Fig 2 Airplane responses to the aileron input

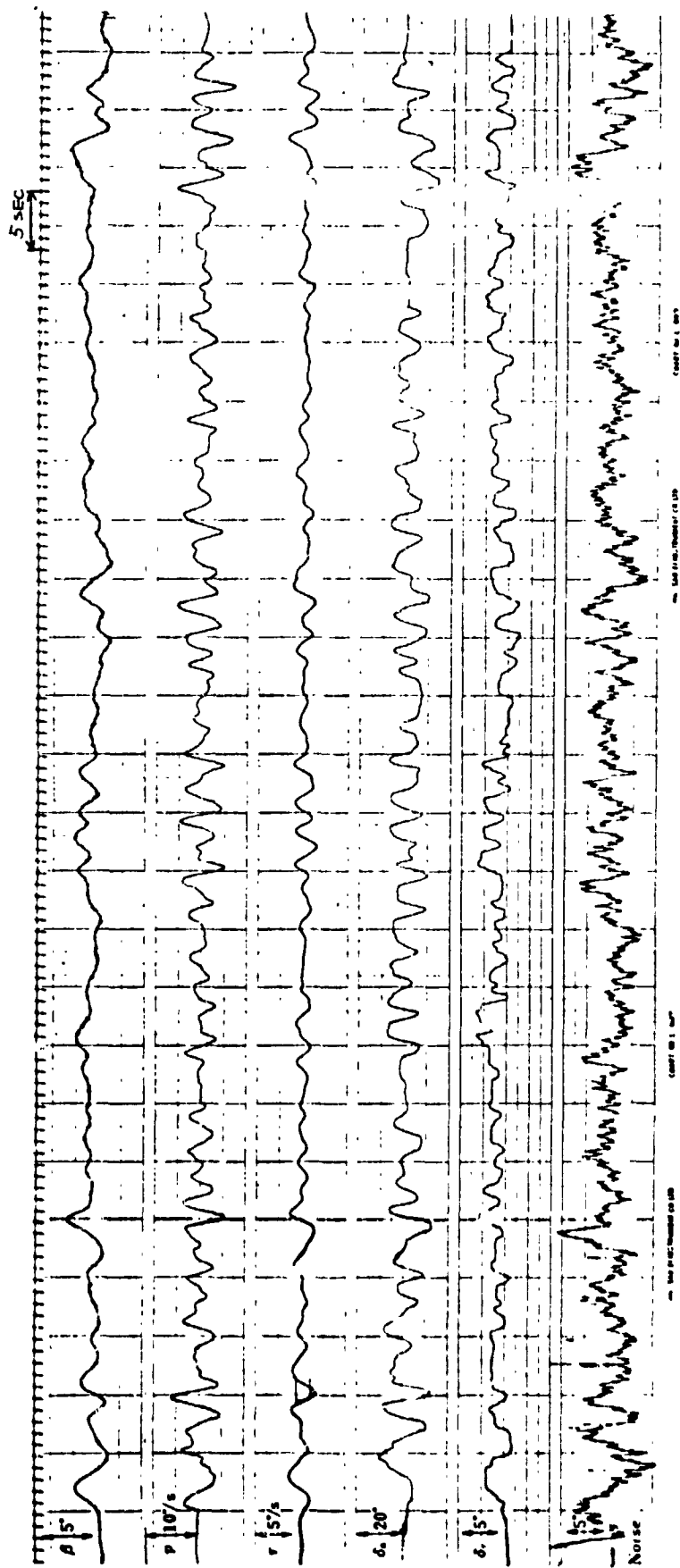


Fig 3 Measured data

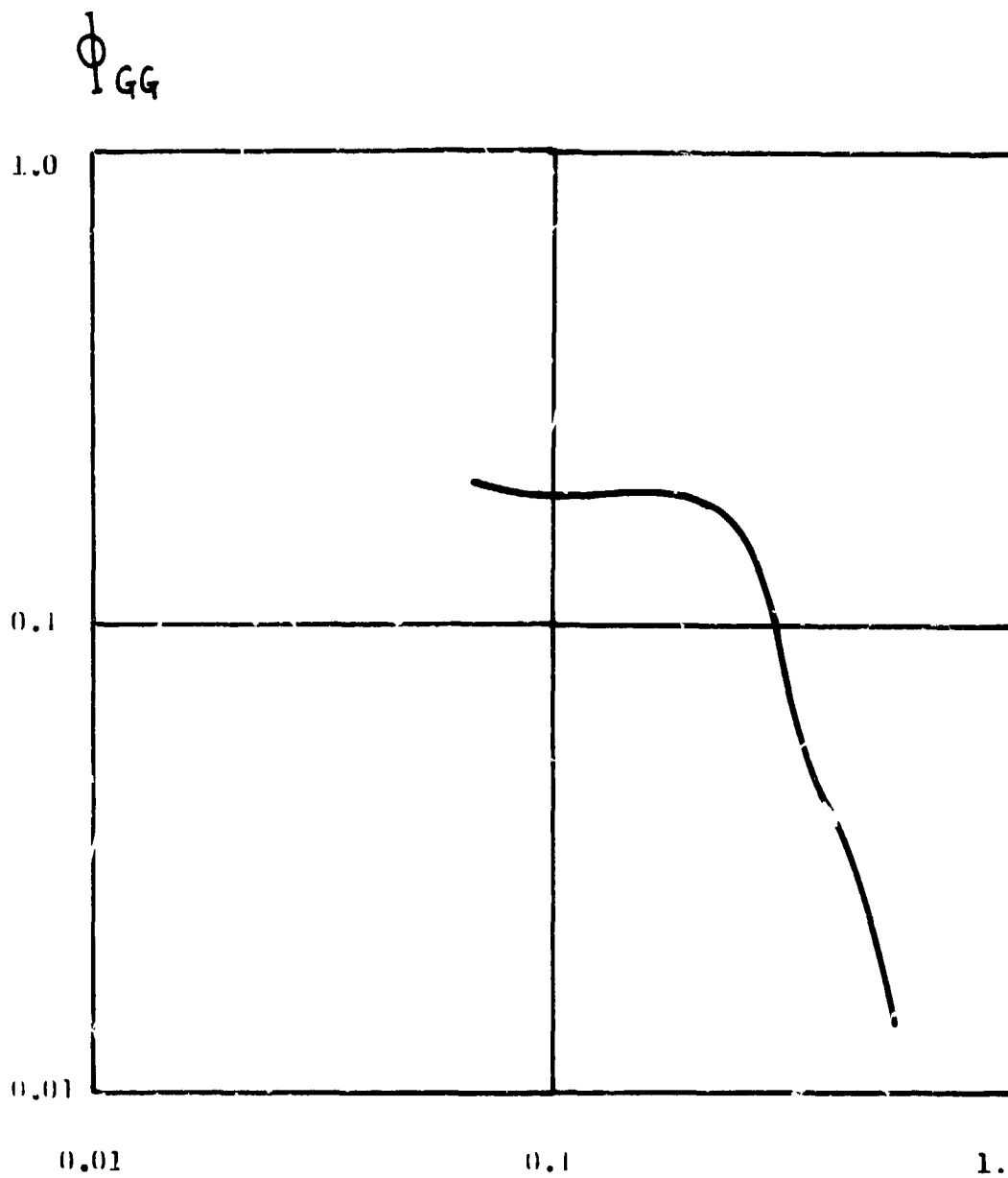


Fig. 4 Power Spectrum Density of Noise

5-2

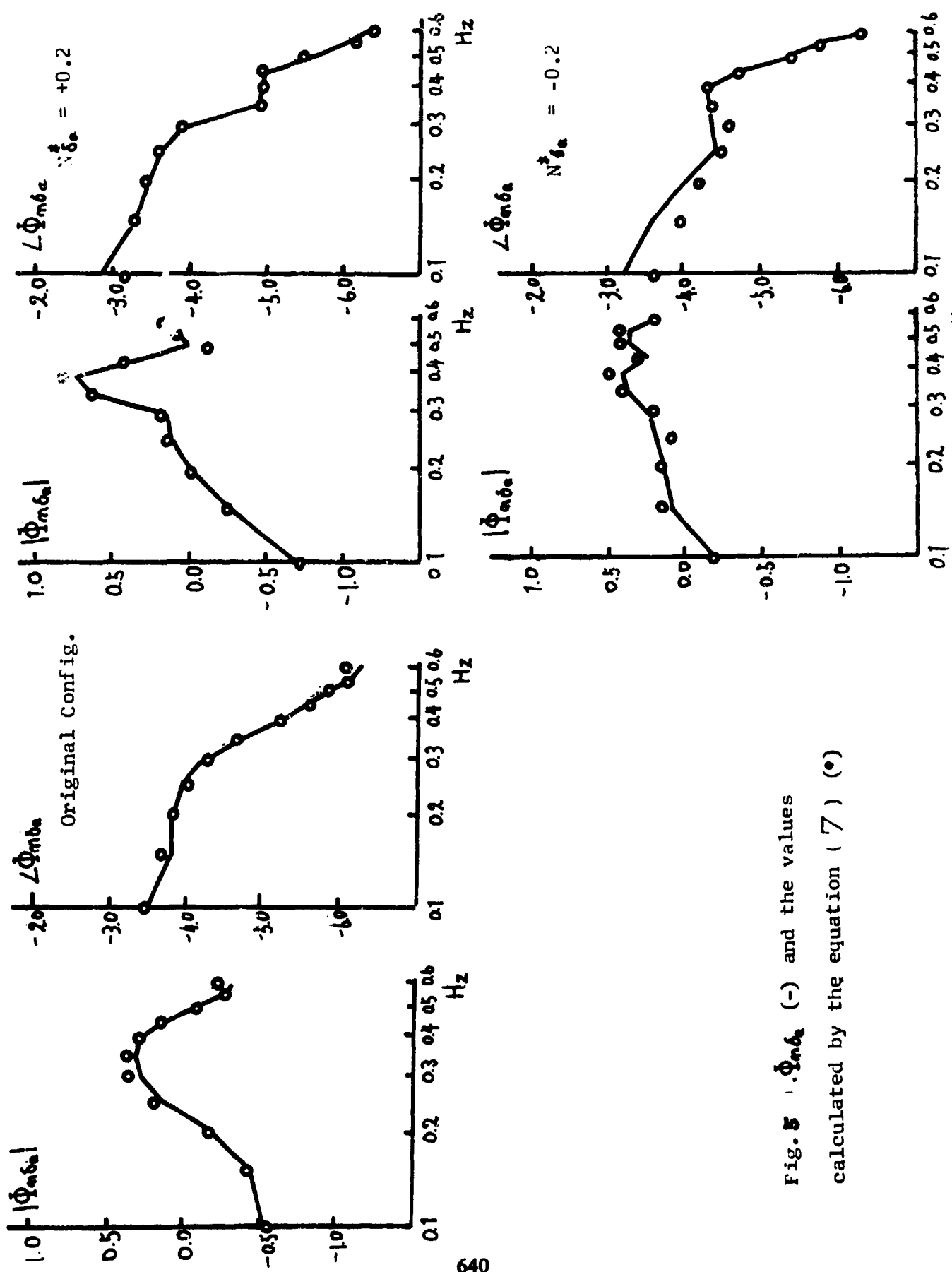


Fig. 5 $|\Phi_{mdb_a}|$ (-) and the values calculated by the equation (7) (o)

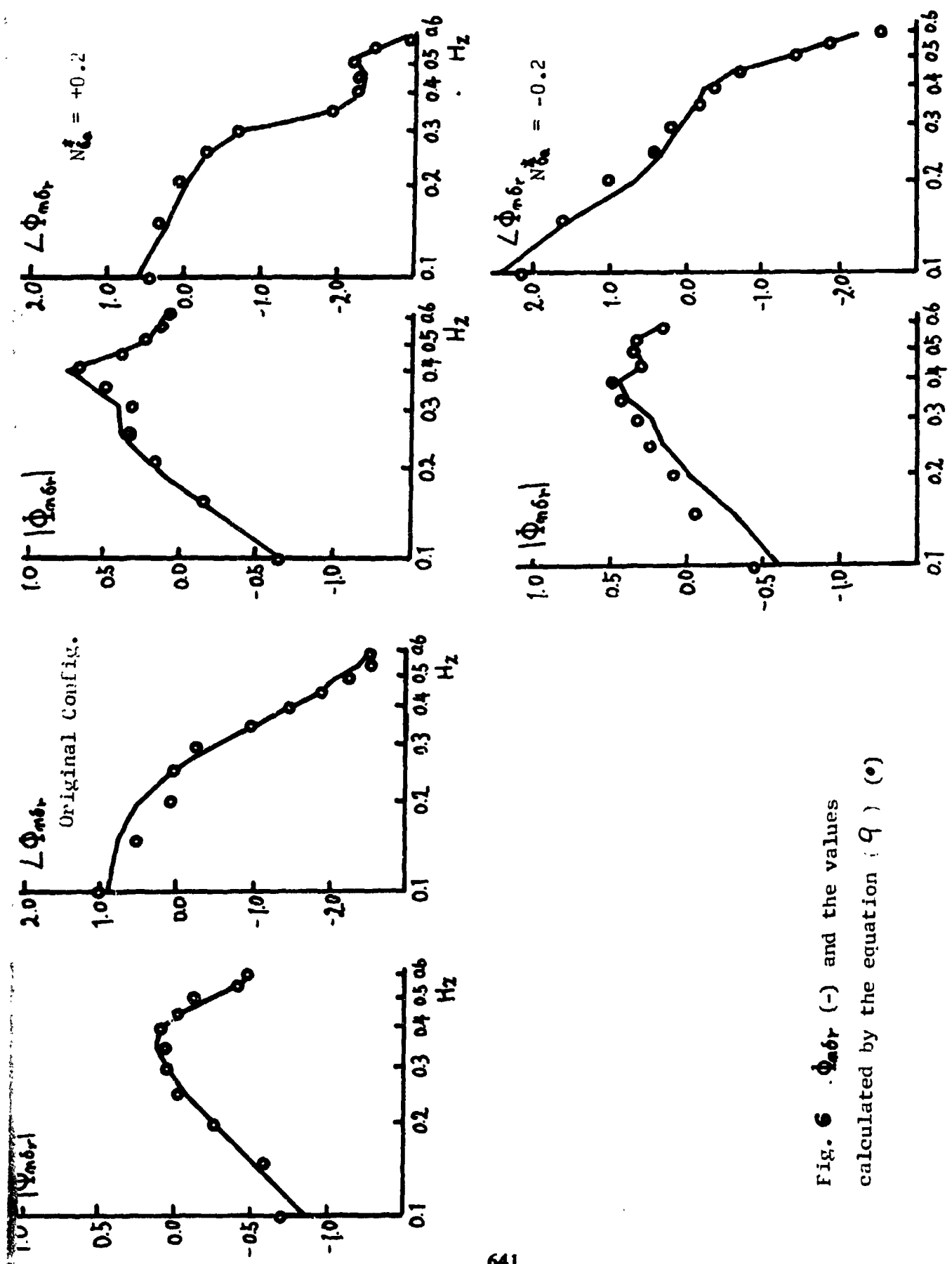


Fig. 6 $\Phi_{m\delta r}$ (-) and the values calculated by the equation (9) (o)

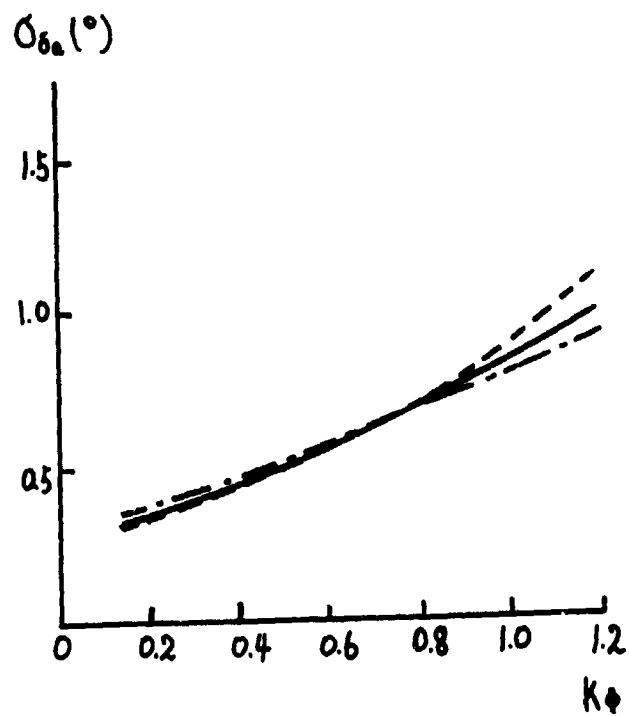
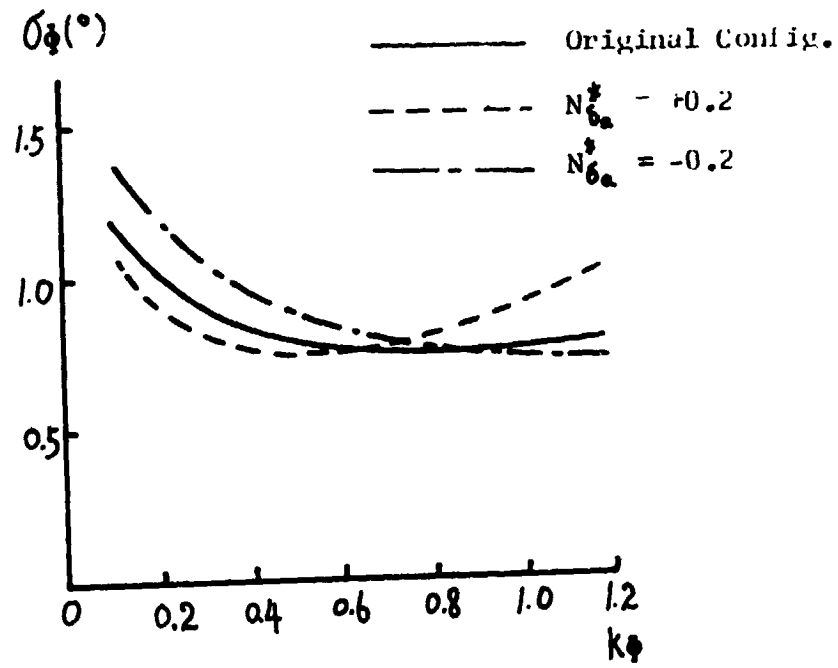


Fig. 7 Curves of σ_ϕ and σ_{δ_a} versus K_ϕ

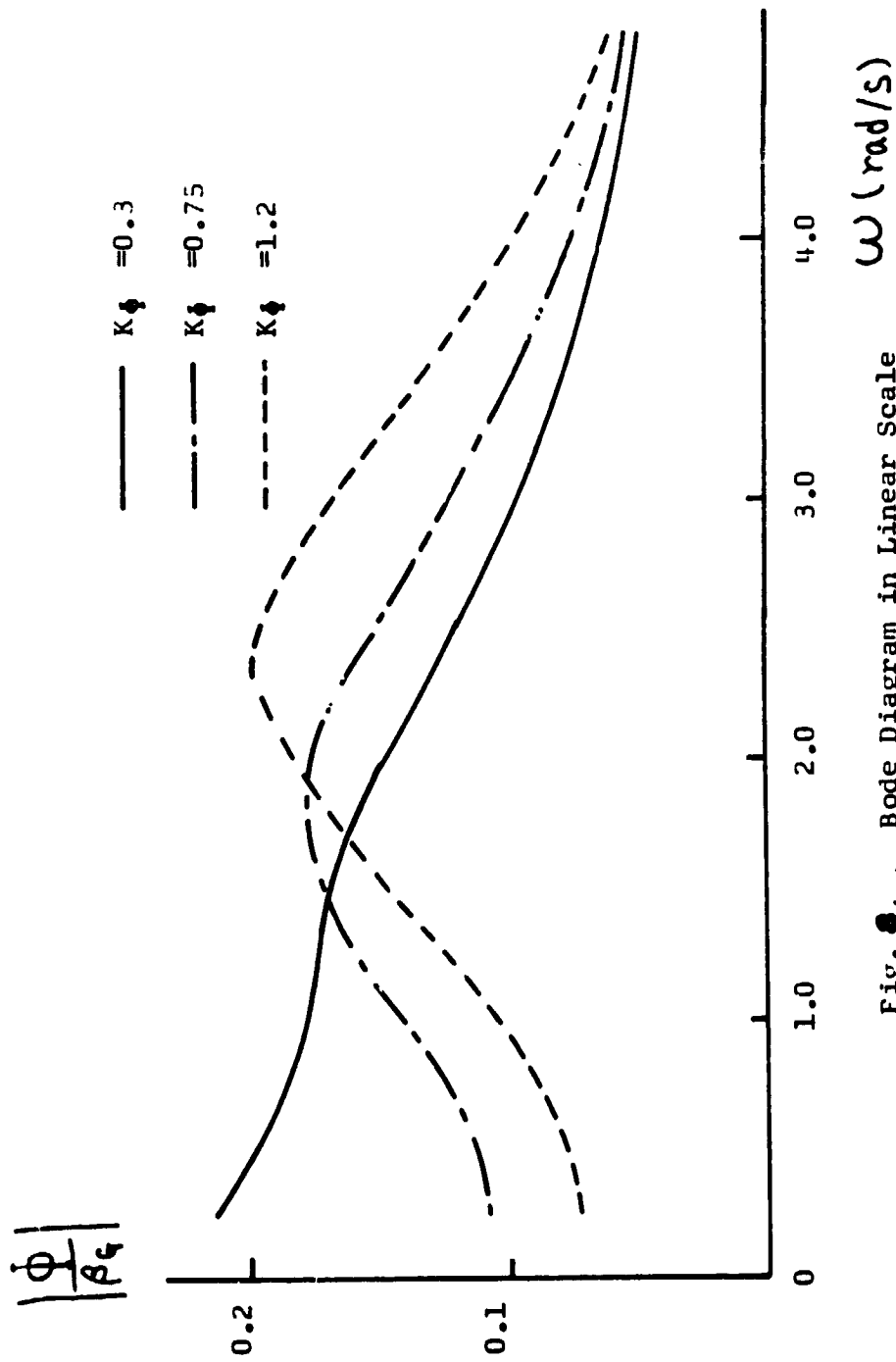


Fig. 3. . . Bode Diagram in Linear Scale

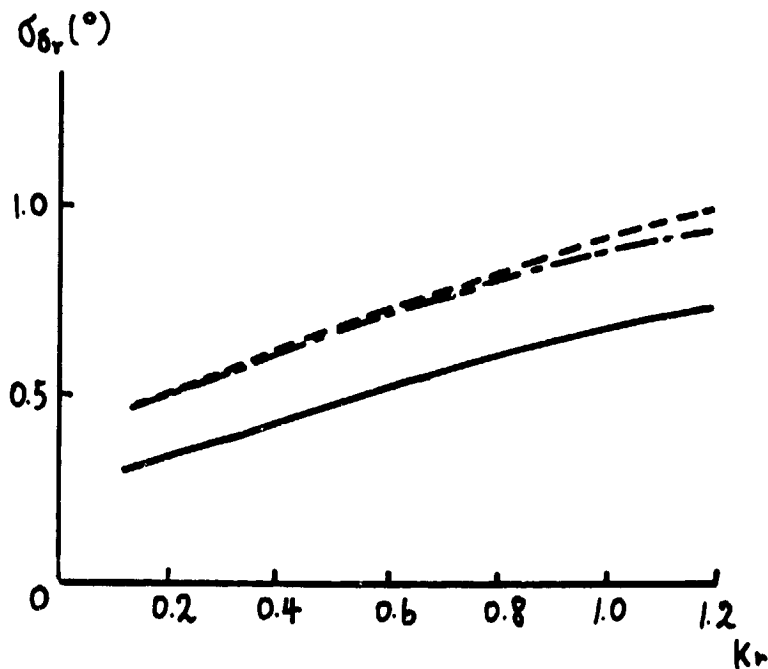
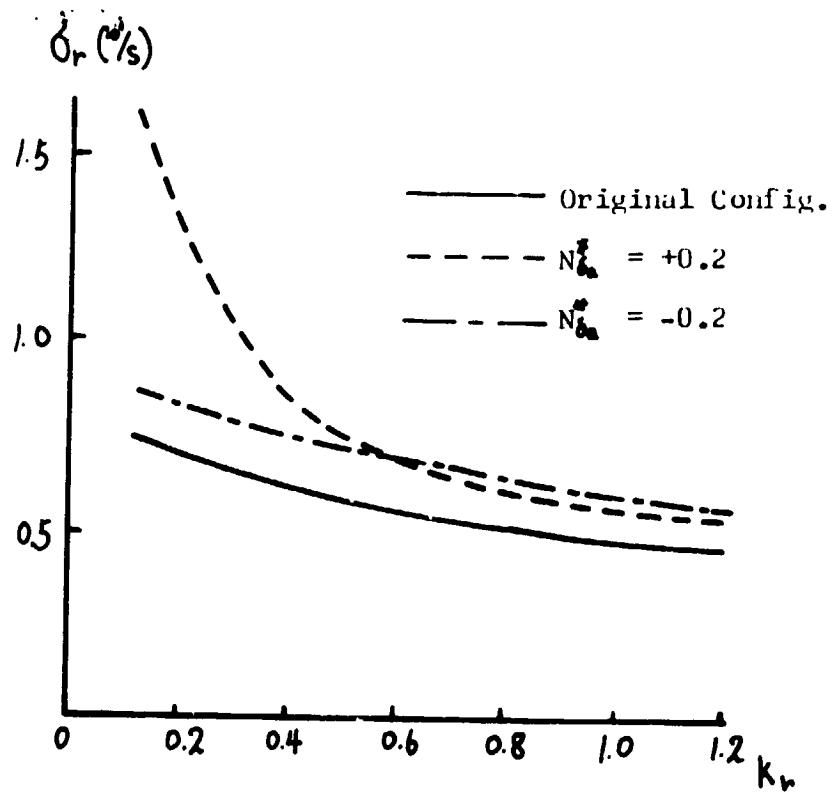


Fig. 9 Curves of σ_r and $\sigma_{\delta r}$ versus K_r

N75 33715

A MULTILoop APPROACH TO MODELING

MOTION SENSOR RESPONSES

By Andrew M. Junker,
Daniel W. Repperger and *John A. Neff

Aerospace Medical Research Laboratory
Wright-Patterson AFB, Ohio 45433

*Air Force Office of Scientific Research
Arlington, Virginia 22209

SUMMARY

By using a least squares identification algorithm, a multiloop approach was taken to effectively model the response characteristics of the motion sensors. The inputs to the model include the possible sources of information provided to the human via his motion sensing system. One input models the response of the angular acceleration sensors (second derivative of position) and the second input models the response of the linear sensors (sine of position). The third input is the visual display error provided to the human in the closed loop tracking experiment. Data from a roll axis tracking simulation was analyzed. The major source of pilot lead under the motion mode of operation is discussed for control of plants in which motion information improved performance and in which there was no improvement in performance.

INTRODUCTION

Roll axis compensatory tracking with and without the presence of motion was performed by three groups of four subjects each. Each group of subjects tracked with a different plant. The results were similar to those reported by other researchers [1,2,3], namely that as more lead was required by the human operator for successful control, tracking performance was improved with the presence of motion.

Because of the nature of the task, large amplitude roll motion was experienced by the human operator during tracking. Thus the motion that improved performance was due to linear and/or angular acceleration. In an effort to determine what effect each of these components of acceleration had on the human operator, a linear triple input single output model of the human operator was formulated. Then from the roll axis tracking data for three different plants, a least squares identification algorithm was used to find parameter values for the hypothesized model that would give the best linear fit to the input output data. It was hoped that the parameter values would give some insight into how man makes use of the motion information available

to him. The results of this work are presented in this paper.

METHOD

A. Experimental Setup

A closed loop roll axis motion simulator, capable of complete 360 degree roll, consisting of a drive system, seat, visual display and force stick control was used to generate human tracking data. The control task was to follow another aircraft in the roll axis. The aircraft to be followed was represented by a zero mean band limited Gaussian noise signal; one standard deviation was equivalent to a 120 degree roll angle. Two forcing function bandwidths were used, 0.25 and 0.5 radians per second. For the data used in this paper only the 0.5 radian/second input was considered.

The difference between the operator's position and the forcing function roll angle was presented to the human operator on an inside-out visual display. The human operator was told to minimize the error signal. With a zero error, the operator's position would exactly follow the input forcing function.

A side mounted force stick was used for the operator's output. A comfortable stick gain was selected and maintained throughout the entire experiment. The simulator could be operated in two modes; motion and static. In the motion mode the inputs to the human operator were simulator motion and visual display. For the static mode, the force stick output drove simulated plant dynamics. Thus, in the static mode, the human operator was deprived of motion information. In this way it was possible to isolate the effects of motion on tracking.

Three different plants were used for tracking. The plant transfer functions are listed in Table 1. The results in terms of root mean squared (RMS) error scores are presented in Table 2 and discussed in more detail in [4]. The resulting man-machine transfer functions are discussed in [5]. The important results are that for plant numbers 2 and 3 motion helped by giving the human operator the information needed to generate additional lead for improved system control.

For each of the three plants, three sets of four subjects each were used. They performed tracking runs until improvements in RMS error scores no longer occurred. At that point, time history data of upto ten tracking runs per subject was collected. Each tracking run for each subject lasted 120 seconds. The time history data was collected for subsequent system identification.

B. Hypothesized Model

For the tracking tasks considered, large amplitude motion made up of angular and linear acceleration components was experienced by the human operator. To account for these inputs, a linear triple input, single output model of the human operator was hypothesized. The form of this model

incorporated into the closed loop tracking task is shown in Figure 1. The three inputs are: displayed error (visual input), linear acceleration or lateral acceleration, and angular acceleration. The linear or lateral acceleration is defined as the force of gravity, which we normalized to one, times the sine of the simulator or plant angular position. The angular acceleration is simply the second derivative of the plant angular position. The output of the human operator model is the control stick voltage.

The linear model was defined as a second order system with different gains and zeros associated with each of the three inputs. This is expressed, in Laplace notation, in the following equation (1).

$$y(s) = \underbrace{\frac{c(s+d)}{(s+a)(s+b)}}_{H_1(s)} u(s) + \underbrace{\frac{e(s+f)}{(s+a)(s+b)}}_{H_2(s)} v(s) + \underbrace{\frac{g(s+h)}{(s+a)(s+b)}}_{H_3(s)} w(s) \quad (1)$$

Where: $y(t)$ = stick voltage
 $u(t)$ = displayed error
 $v(t)$ = linear acceleration $\sin \theta_p$
 $w(t)$ = angular acceleration $\ddot{\theta}_p$

and $H_1(s)$, $H_2(s)$ and $H_3(s)$ correspond to the transfer functions shown in Figure 1.

C. Parameter Identification

The three input single output system is rewritten in state variable notation in equations 2 and 3.

$$\begin{bmatrix} \dot{x}_1 \\ \dot{x}_2 \end{bmatrix} = \underbrace{\begin{bmatrix} 0 & 1 \\ -ab & -(a+b) \end{bmatrix}}_A \begin{bmatrix} x_1 \\ x_2 \end{bmatrix} + \underbrace{\begin{bmatrix} c & e & g \\ c(d-a-b) & e(f-a-b) & g(h-a-b) \end{bmatrix}}_B \begin{bmatrix} u \\ v \\ w \end{bmatrix} \quad (2)$$

$$y = x_1 \quad (3)$$

By using a least squares identification algorithm as discussed in [5], the values for the A and B matrices were found for all the three input single output time histories. From these values the transfer function values of equation (1) were computed. These values were computed for each subject, upto ten runs per subject for each of the three plants controlled.

RESULTS AND DISCUSSION

For each of the three plants we averaged parameter values across the four subjects. These values gave us average transfer functions H_1 , H_2 and H_3 for each plant. As we went from plant number 1 to numbers 2 and 3 we measured a marked improvement in tracking performance due to additional lead

information provided by the human operator. Because of this we anticipated some change in the transfer functions between the three plants to account for the additional lead.

The first transfer function considered is $H_1(s)$, associated with the displayed error input. The average values for the parameters for the three plants are presented in Table 3. Included with each mean value is the standard deviation for that value. For plant number 1, for which motion information did not improve performance, the human operator model is generating lead information from the display for control. But looking at the changes in gain and relative pole-zero placement for plants 2 and 3 as compared with plant 1, we see that the model is not generating any more lead information. This can also be seen in the magnitude Bode plot of the three transfer functions presented in Figure 2. From these results we conclude that our hypothesized model does not derive additional information from the displayed error for plants 2 and 3 in order to generate more lead.

Considering the linear or lateral acceleration next, the average values for the parameters for the three plants for transfer function $H_2(s)$ are presented along with standard deviations in Table 4. Keeping in mind that motion did not improve tracking for plant number 1, we would expect a change in the gain and/or pole zero placement that would indicate generation of lead information when going to plants 2 and 3. Looking at the parameter values across the three plants we see that the gain dropped and the zero moved further out relative to the movement of pole a . The net effect on the transfer function $H_2(s)$ can be seen in the magnitude Bode plot of Figure 3. Additional lead information is not being generated. The transfer function has a low pass filter structure which is cutting off sooner for plants 2 and 3. Thus we conclude that our hypothesized model does not generate additional lead for control from this input.

Finally listed in Table 5 are those values for transfer function $H_3(s)$ with angular acceleration as the input. Looking across plants we can see an increase in gain and a change in the pole zero placement such that for plant 1 the transfer function is low pass, for plant 2 flat and high pass for plant 3. This can be seen in the magnitude Bode plot of Figure 4. Therefore, comparing plant no. 1, where motion did not help tracking, to plants 2 and 3 where it did, the results suggest that the transfer function has been altered to make better use of the angular acceleration information for plants 2 and 3.

CONCLUSION

By comparing the three transfer functions for the model across the three plants we conclude that the least squares identification algorithm has selected parameter values in such a way as to make greater use of the angular acceleration input and not the linear acceleration input for control of the more difficult plants 2 and 3. Thus, for our hypothesized model we conclude that the improvement in tracking performance in the motion environment is due to the angular acceleration input. This suggests that man will use angular acceleration as the primary source of input when lead generation beyond that

which can be obtained from a display is required for system control in roll motion tracking.

REFERENCES

1. Shirley, R. S. and L. R. Young, "Motion cues in man-vehicle control", IEEE Transactions on Man Machine Systems, Vol MMS-9, No. 4, December 1968.
2. Stapelford, R. L., R. A. Peters and F. R. Alex, "Experiments and a model for pilot dynamics with visual and motion inputs", NASA CR-1325, May 1969.
3. Young, L. R., "Some effects of motion cues on manual tracking", J. Spacecraft and Rockets, pp. 1300-1303, October 1967.
4. Junker, A. M. and C. R. Replogle, "Motion effects on the human operator in a roll axis tracking task", submitted to Aviation Space and Environmental Medicine, will appear in June or July 1975 issue.
5. Repperger, D. W. and A. M. Junker, "Performance evaluation of tracking based on a low pass filter model", Paper Number 2 in section, System Identification of these proceedings, Eleventh Annual Manual, 1975.

TABLE 1 - Plant Dynamics Used

Plant No	Transfer Function Dynamics
1	$\frac{K}{s(2s+1)}$
2	$\frac{K}{s^2(2s+1)}$
3	$\frac{K}{s^2(4s+1)(2s+1)}$

TABLE 2 - RMS Error Scores

Mode of Operation	Forcing Function = 0.25 radians	Forcing Function = 0.5 radians
Plant 1 Static Mode	$e_{RMS} = 5.70$	$e_{RMS} = 12.45$
Plant 1 Motion Mode	$e_{RMS} = 6.57$	$e_{RMS} = 13.73$
Plant 2 Static Mode	$e_{RMS} = 26.967$	$e_{RMS} = 46.99$
Plant 2 Motion Mode	$e_{RMS} = 10.87$	$e_{RMS} = 20.46$
Plant 3 Static Mode	$e_{RMS} = 79.43$	$e_{RMS} = 90.30$
Plant 3 Motion Mode	$e_{RMS} = 27.01$	$e_{RMS} = 38.25$

TABLE 3 - Identified Parameter Values for H_1

PARAMETER	PLANT NO. 1	PLANT NO. 2	PLANT NO. 3
c (gain) mean	6.99	7.51	7.12
s.d.	.74	.91	.21
d (zero) mean	.70	.54	.89
s.d.	.52	.21	.83
a (pole 1) mean	10.22	12.42	15.38
s.d.	2.21	4.35	14.19
b (pole 2) mean	115.78	113.37	112.28
s.d.	6.29	5.22	17.76

TABLE 4 - Identified Parameter Values for H₂

PARAMETER		PLANT NO. 1	PLANT NO. 2	PLANT NO. 3
e(gain)	mean	6.08	4.86	5.61
	s.d.	2.97	1.93	1.56
f(zero)	mean	15.59	34.06	33.53
	s.d.	12.02	28.65	16.79
a(pole 1)	mean	10.22	12.42	15.38
	s.d.	2.21	4.35	14.19
b(pole 2)	mean	115.78	113.37	112.28
	s.d.	6.29	5.22	17.76

TABLE 5 - Identified Parameter Values for H₃

PARAMETER		PLANT NO. 1	PLANT NO. 2	PLANT NO. 3
g(gain)	mean	.745	1.209	1.568
	s.d.	.56	.83	.83
h(zero)	mean	18.22	12.24	6.52
	s.d.	8.40	5.28	3.60
a(pole 1)	mean	10.22	12.42	15.38
	s.d.	2.21	4.35	14.19
b(pole 2)	mean	115.78	113.37	112.28
	s.d.	6.29	5.22	17.76

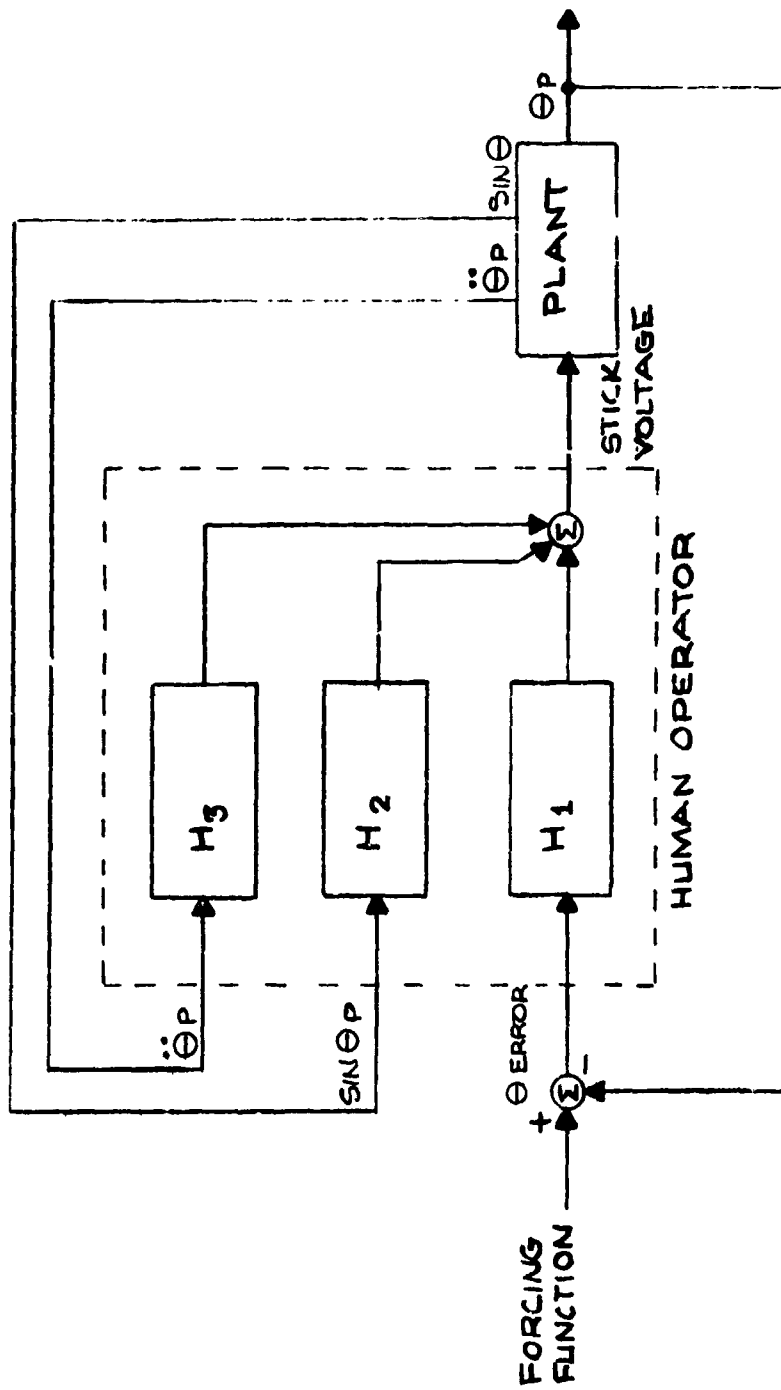


FIGURE 1
Hypothesized linear human operator model

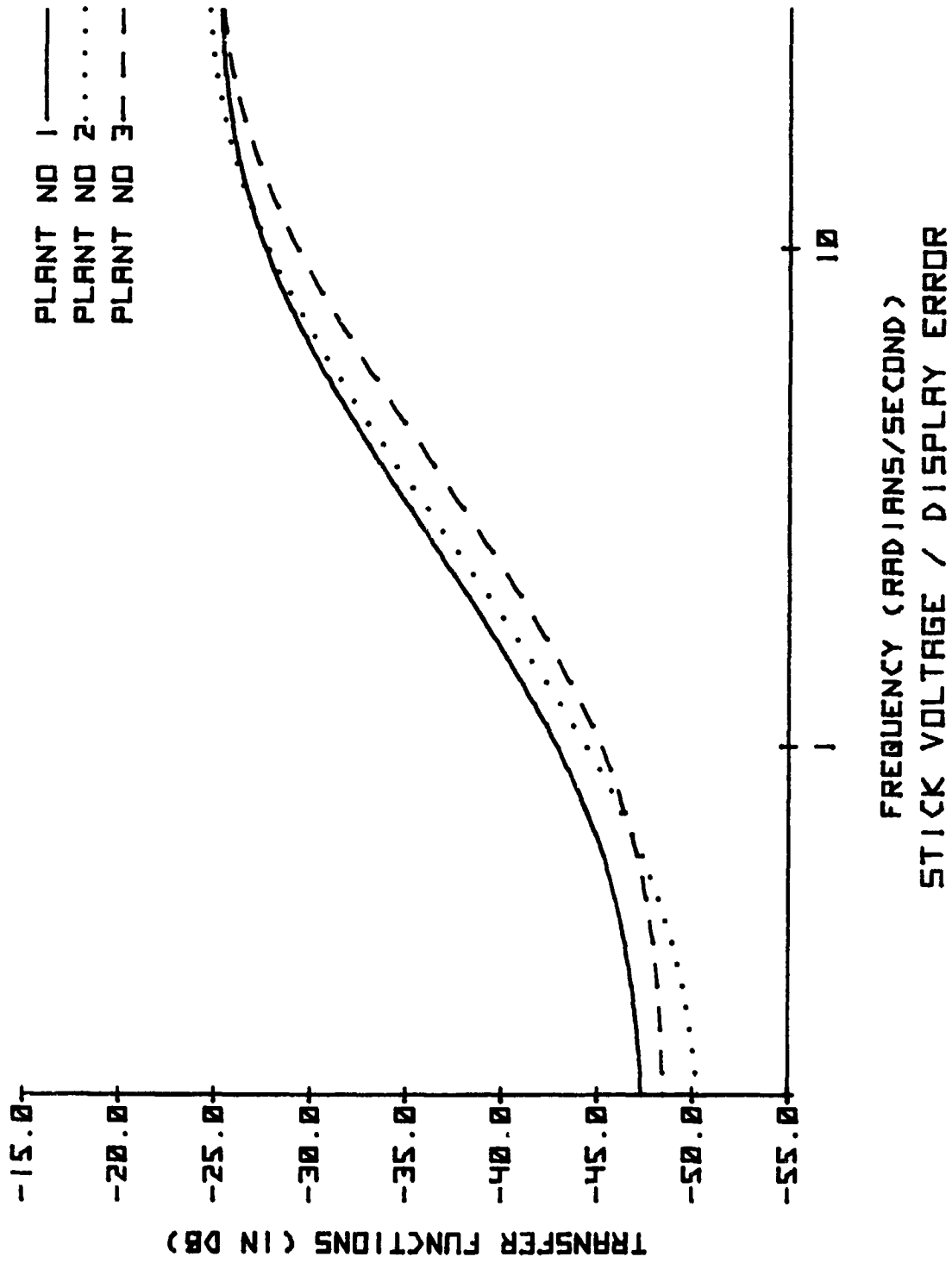


FIGURE 2

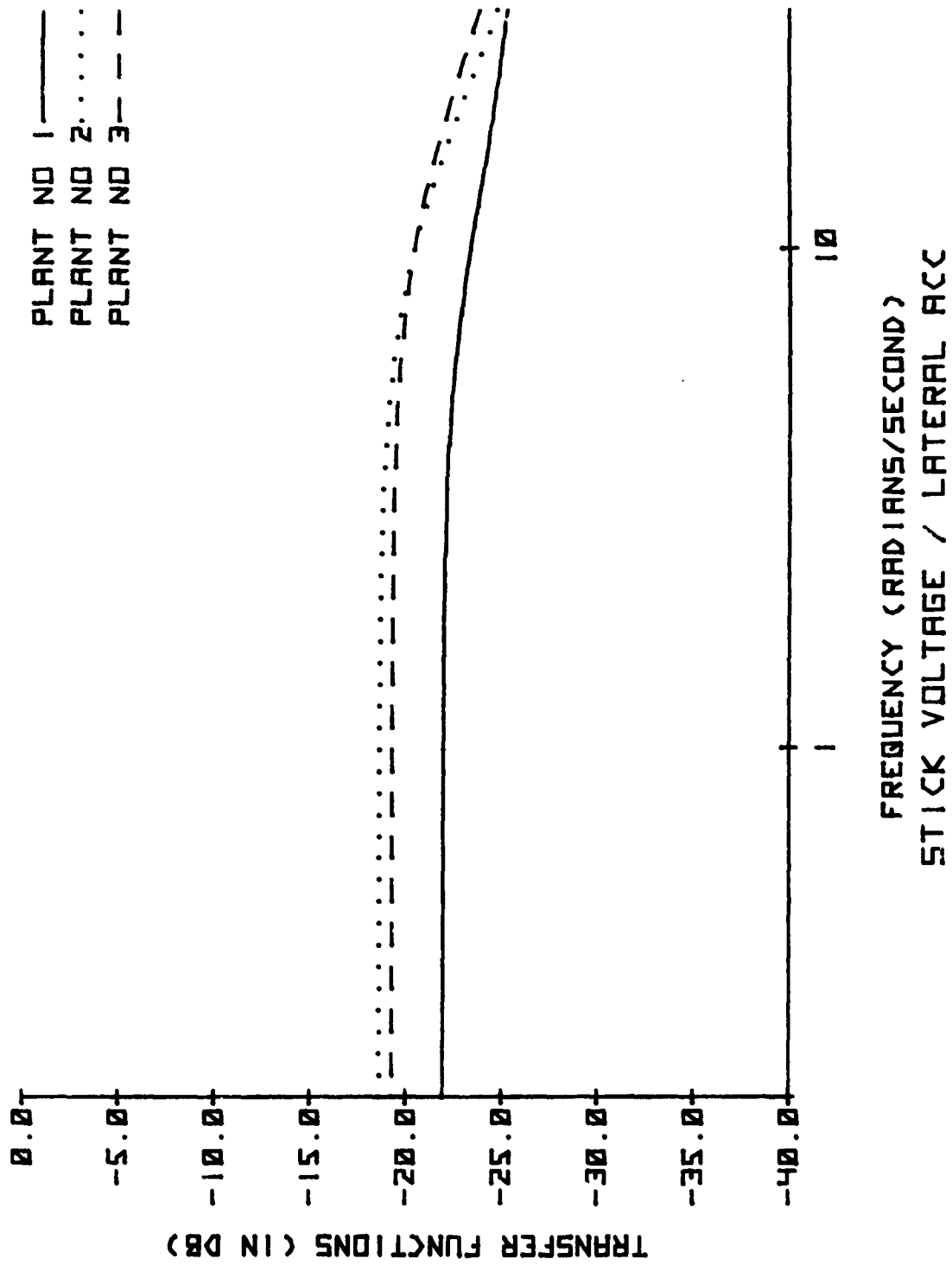


FIGURE 3

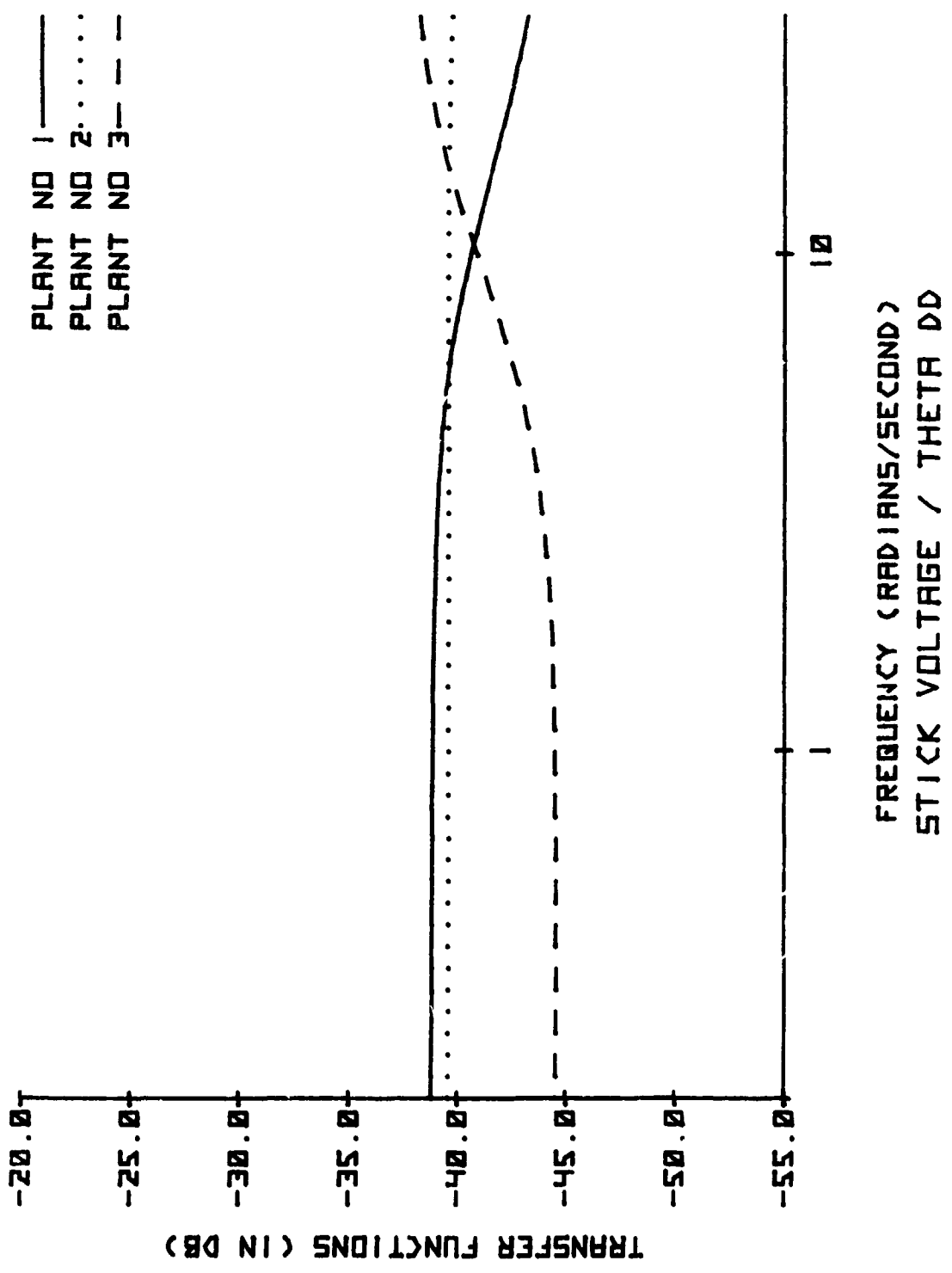


FIGURE 4

EFFECTS OF CONTROL-STICK PARAMETERS ON TRACKING

PERFORMANCE IN A VIBRATION ENVIRONMENT*

William H. Levison
Bolt Beranek and Newman Inc.
Cambridge, Massachusetts

175 03716

ABSTRACT

A set of manual control experiments was conducted to determine the effects of control-stick parameters on tracking performance in a vibration environment. Primary experimental variables were stick design parameters, stick location, and presence or absence of vibration. Stick parameters had little effect on rms tracking error under vibration conditions for the particular aircraft dynamics that were used in this study. Considerable effect on control activity was observed, however, which suggests that stick design parameters will significantly influence overall performance in systems that respond at vibration frequencies. Stick location had no significant effect on either tracking or biodynamic performance measures. The vibration-correlated component of tracking error was relatively small; vibration effects were accounted for largely by changes in pilot model parameters related to visual resolution, time delay, and motor-related remnant.

A model-based guide for the design of control sticks in a vibration environment is described. This model is based on the state-variable model for pilot/vehicle systems. Effects of vibration are represented as additional model elements and by changes in pilot-related parameters of the tracking model.

INTRODUCTION

In recent years aircraft have been constructed such that they can perform in environments that severely tax or exceed the limits of human tolerance. Severe vibration is one such environment.

Whole-body vibration acts in a number of ways to cause performance degradation of manned vehicle systems. Vibration is transmitted to the seat of the pilot by the aircraft and propagates through the pilot's torso and arm to the control stick to produce control inputs that are linearly

*This work was sponsored by the Aerospace Medical Research Laboratory, Wright-Patterson Air Force Base, under Contract No. F33615-74-C-4041. Lt. Philip D. Houck was the Technical Monitor for this contract and Project Engineer for the AMRL experimental program.

correlated with the vibration input. Vibration also increases the stochastic portion of the pilot's control activity (i.e., "remnant") due partly to visual interference effects (e.g., blurring due to relative eye-display motion) and, to a greater extent, to motor interference effects such as noise injected into proprioceptive feedback paths.

The effects of vibration on control performance are to some extent influenced by the design of the control stick. Accordingly, the Aerospace Medical Research Laboratory recently conducted a series of manual tracking experiments to determine mathematically the relation between control-stick design parameters and tracking performance in a vibration environment. Experimental data were provided to Bolt Beranek and Newman Inc., whose tasks were to (1) reduce the data to obtain engineering descriptions of tracking and biomechanical response behavior, (2) develop a mathematical model to account for the interaction between stick design parameters, vibration, and tracking performance, and (3) develop guidelines for the design of control sticks in a vibration environment.

The objective of this paper is to summarize briefly the results of this study. Extensive documentation of this effort is provided in [1].

EXPERIMENTAL PROCEDURE

A single-axis compensatory tracking task was performed using a simple integrator as the controlled element. The tracking input consisted of the sum of five sinusoids designed to approximate a first-order noise process with a break frequency of 2 rad/sec. The input was added to the subject's control response, the sum of these signals then being processed by the integrator to produce the tracking error displayed on a CRT. Fore-aft movement of the control stick produced vertical movement of the error indicator.

Half of the data trials were performed with the subject, control, and display subjected to vertical (i.e., z-axis) vibration. The spectrum of the platform vibration consisted of the sum of five sinusoids at frequencies of 2, 3.3, 5, 7, and 10 Hz. The sinusoids had random phase relationships and equal accelerations; the rms platform acceleration was approximately 0.3g.

Primary variables were (1) presence or absence of vibration, (2) stick location (center or side), and (3) control stick design. Six control sticks were used, with spring gradients ranging from 2 lb/in to 600 lb/in. For convenience, the three sticks with the weakest spring gradients are classified as "spring sticks"; the remaining three are classified as "stiff sticks".

A total of seven experimental subjects participated in all phases of this program; all results shown in this paper are the average response characteristics of these subjects. Accelerometers located on the shoulder, elbow, and on a bitebar held between the teeth allowed the computation of body, head, and limb response to vibration.

EXPERIMENTAL RESULTS

Biodynamic Response

Analysis of variance of rms accelerations of shoulder, body, and head indicated that neither stick location nor stick design had a significant effect on these variables. Consequently, describing functions relating body and head motion to platform vibration were computed from data averaged across the six sticks and averaged across side and center location. In addition, inter-subject variability was no greater than that observed for tracking performance (about 10% to 20% of the subject mean); hence, averaging biodynamic response measures across subjects was considered justified.

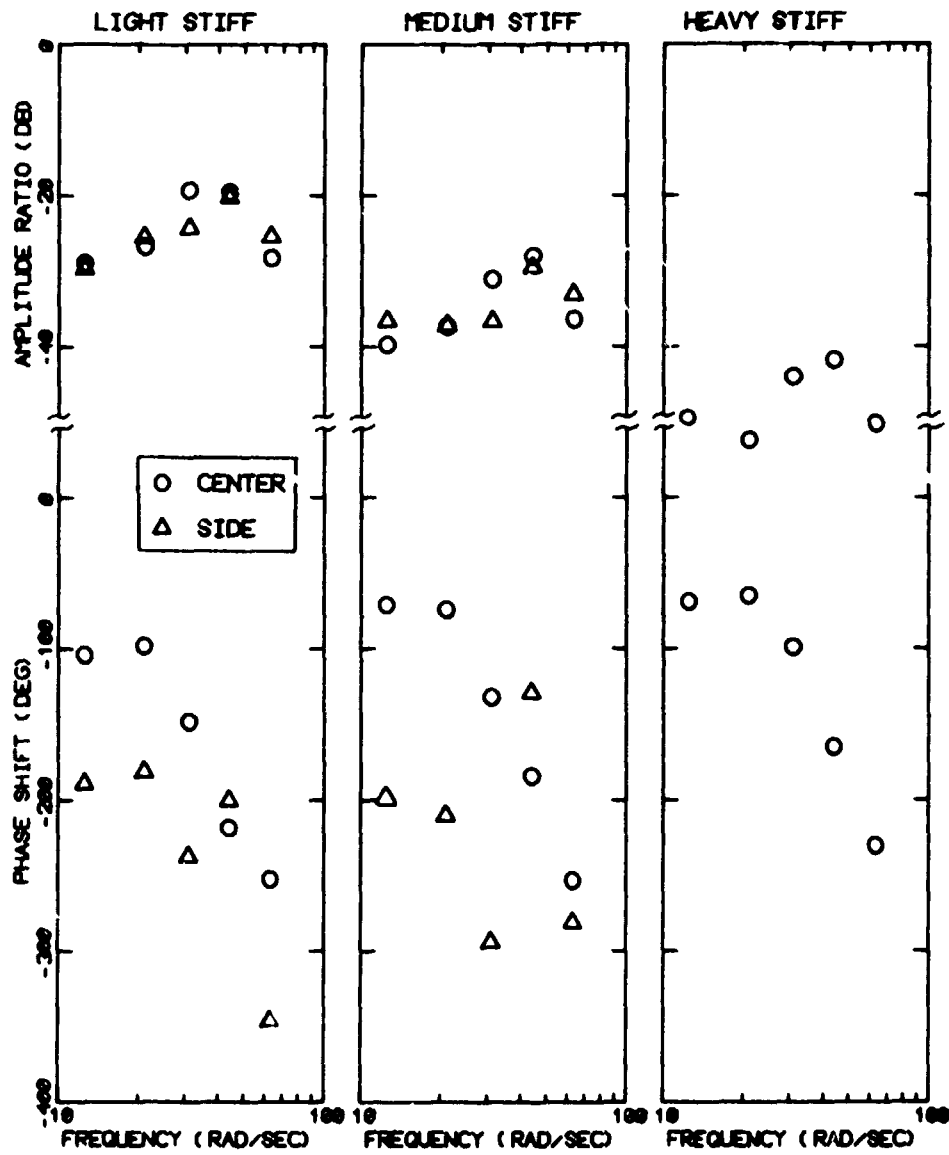
"Stick feedthrough" is defined as the portion of control motion that is linearly related to the platform vibration due to biomechanical coupling. Feedthrough describing functions were computed for all six control configurations. Average results for the three stiff sticks are shown in Figure 1; data for side and center locations (where available) are shown separately.

In order to be able to extrapolate these results to stick configurations not tested in these experiments, the impedance model of Figure 2 was postulated to isolate portions of the feedthrough mechanism that are related to the man and his coupling.

The impedance model of Figure 2 was postulated so that these results could be extrapolated to control configurations not explored in this experimental program. "Transfer impedance" Z_T and "output impedance" Z_O are assumed to reflect biodynamic properties of the pilot and of the biomechanical configuration and are assumed to be independent of control-stick characteristics. Z_S is the impedance of the stick. Theoretically, once Z_T and Z_O have been determined empirically in a given biodynamic environment, the feedthrough describing function can be determined for any set of stick characteristics by the equation:

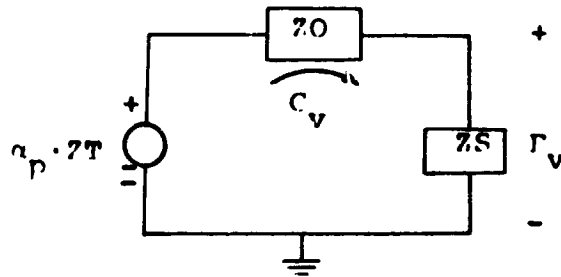
$$C_v = \frac{Z_T}{Z_O + Z_S} \cdot a_p \quad (1)$$

Regression analysis (described in [1]) was performed to yield the transfer and output impedances shown in Figure 3. To test the validity of this type of analysis, these impedance functions were then used, along with the stick impedances, to "predict" the variance of stick feedthrough



14L-244

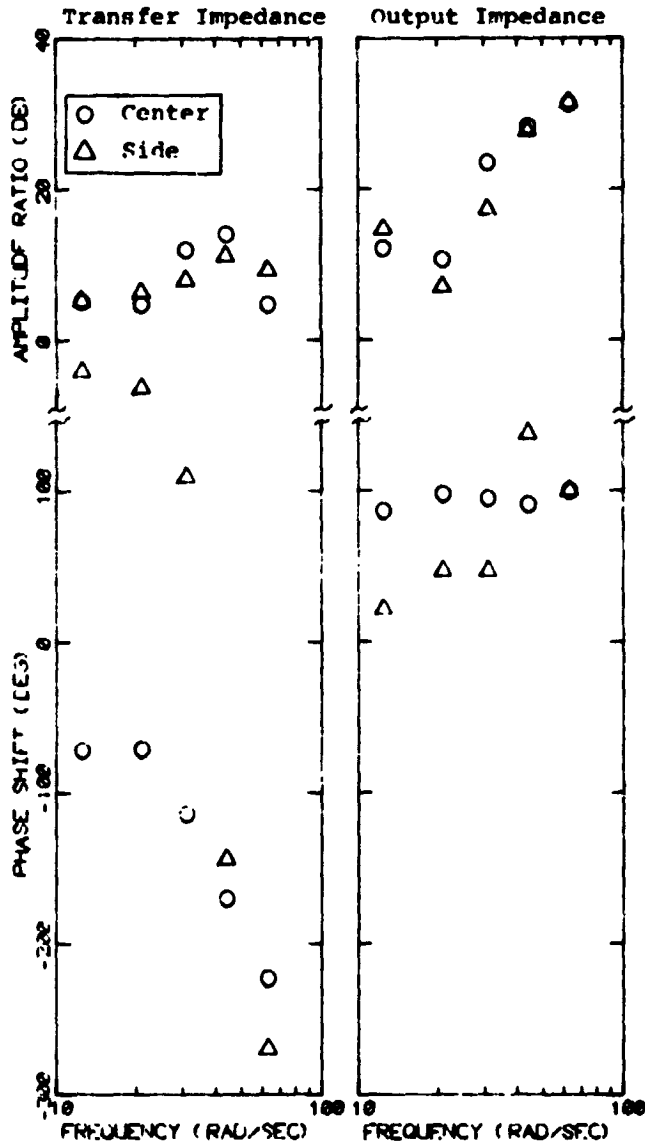
Figure 1. Average Control/Platform Describing Functions
 0 dB = 1 inch control deflection per g platform acceleration.



HL-236

- Z_T = Transfer Impedance
- Z_O = Output Impedance
- Z_S = Stick Impedance
- α_p = Platform Vibration
- C_v = Stick Displacement
- F_v = Stick Force

Figure 2. Impedance Model for Stick Feedthrough



41-237

Figure 3. Transfer and Output Impedances

0 dB = 1 lb force per g platform acceleration for transfer impedance, 1 lb force per inch deflection for output impedance.

for each control configurations. Comparisons of these predictions with corresponding experimental measures is shown in Figure 4. Except for one or two cases, predictions were reasonably accurate. Thus, we are justified in using the impedance model of Figure 2 to extrapolate experimental results to new stick configurations.

Average describing functions relating head translation α_h/α_p and head rotation α_θ/α_p to platform vibration are shown in Figure 5. By appropriate geometric analysis, one can compute the relative motion between head point-of-regard (HPR) and the display [1-2]; making assumptions concerning the ability of the oculomotor system to compensate for relative display movement, one can then estimate relative movement between the eye point-of-regard (EPR) and the display [1-3]. Average estimated relative displacement was approximately .083 inches; average relative velocity was about 2.9 inches/second [1].

Tracking Performance

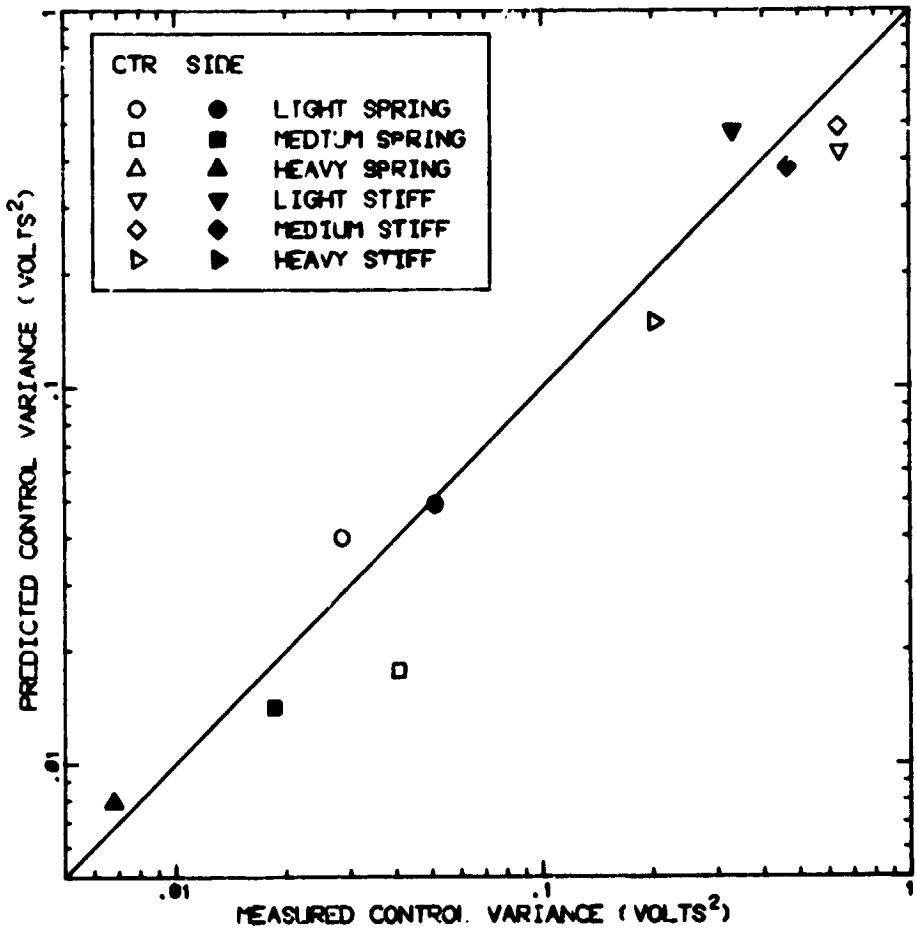
Analysis of variance revealed that stick location had no significant effect on either rms error or rms control scores. Consequently, further analysis of tracking results was performed on averages of data obtained from side and center locations.

A statistically significant interaction between stick design parameters and vibration was found. That is, the presence of vibration consistently increased both error and control scores, but the amount of these increases differed for the various stick configurations. This conclusion is demonstrated graphically by the performance scores shown in Figure 6.

Rms control scores are shown in terms of both volts and pounds of force in Figure 6. The change of control force with stick configuration (Figure 6c) resulted from the requirement of the pilot to adapt to varying control gains (measured as volts/pound). The increase in rms control activity with vibration was particularly great for the stiff sticks due to stick feedthrough.

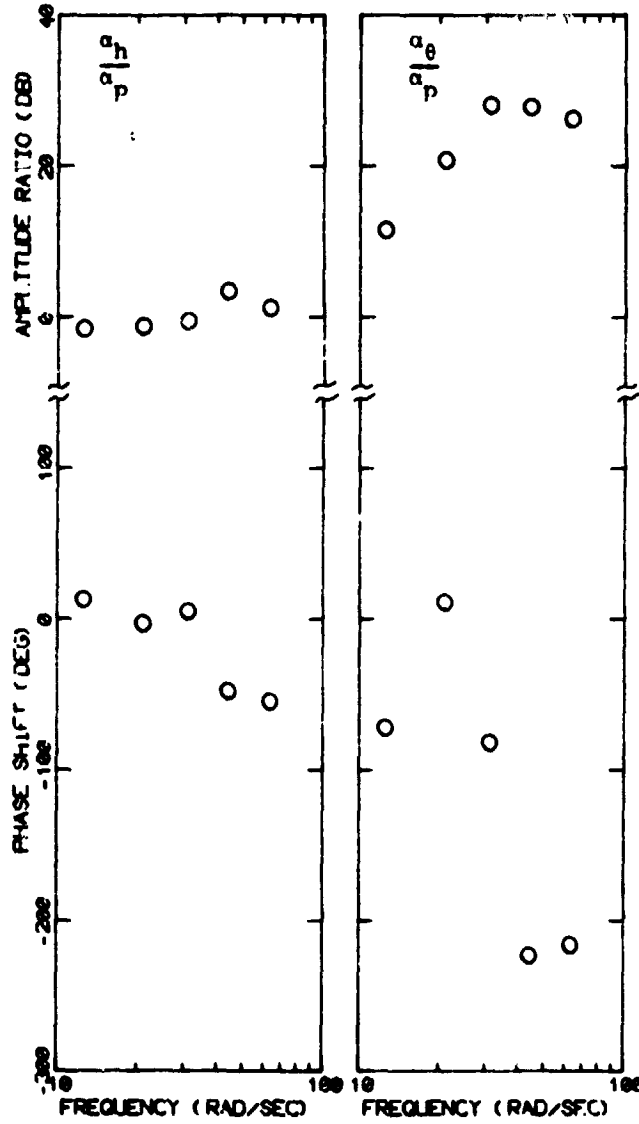
Although feedthrough components of the *control* inputs were sizeable for certain stick configurations, the vehicle dynamics filtered out much of this input so that feedthrough had a relatively small effect on system error. The increase in tracking error due to vibration was, instead, directly traced to an increase in pilot remnant, as was found to be the case in a previous study [2].

Frequency-domain measures are shown for the static and vibration environments for one of the stick configurations in Figure 7. Amplitude ratio and phase shift refer to the pilot describing function; "rem/cor" is the ratio of remnant-related stick power to input-correlated stick power at each input frequency. Remnant measures are "closed-loop"; i.e., remnant has not been reflected to an equivalent injected noise process.



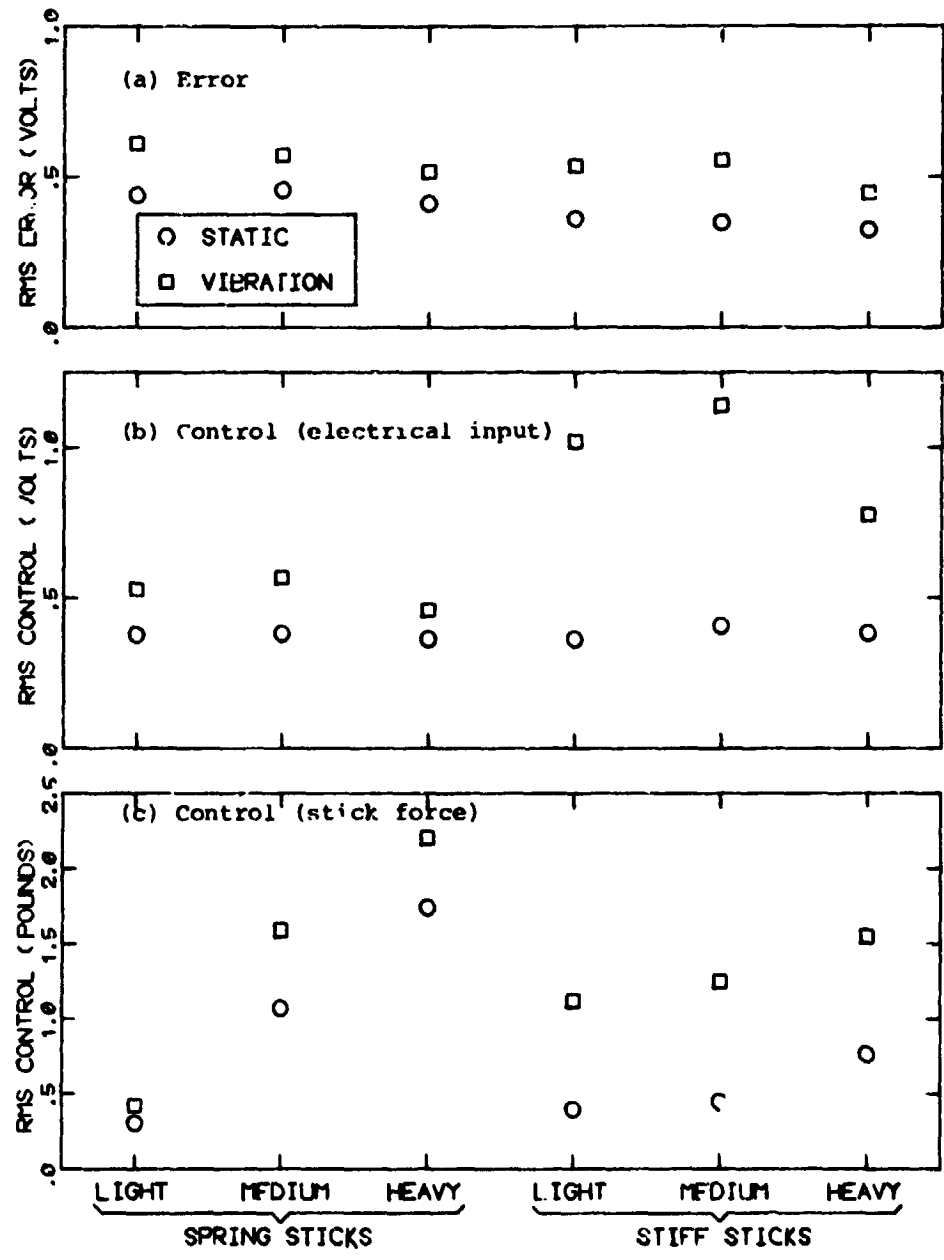
WPL-246

Figure 4. Comparison of Predicted and Measured Vibration-Correlated Control Variances



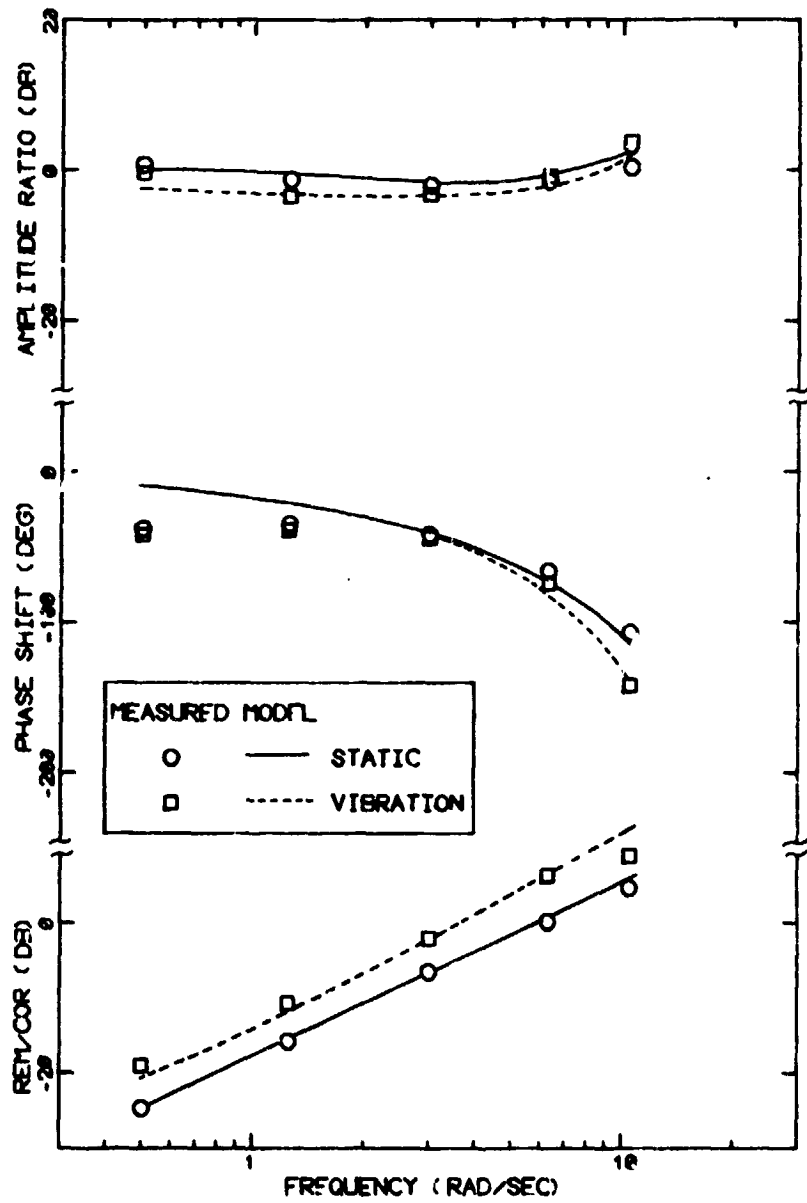
ML-208

Figure 5. Describing Functions for Head Motion
 0 dB = 1 g head translational and 1 deg/sec² head rotational acceleration p' g platform acceleration



44-253

Figure 6. Effects of Vibration on Rms Error and Control Scores



441-255

Figure 7. Frequency-Domain Measures for Light Spring Stick

All six stick configurations showed the trends revealed in Figure 7. The imposition of whole-body vibration caused the amplitude ratio to decrease at gain-crossover (about 3 rad/sec) and lower frequencies, but to increase at the highest measurement frequency of 10.5 rad/sec; high-frequency phase shift increased; and the ratio of remnant to correlated control power increased at all measurement frequencies.

Model analysis using the optimal-control pilot/vehicle model [4-5] was performed so that these performance changes could be interpreted in terms of changes in the pilot's basic information-processing capabilities. Details of the analysis procedure are given in [1]. The important results are reviewed here.

Analysis was first performed on the average static response measures with the aim of finding a single set of pilot-related parameter values to account for performance with all six stick configurations. (To account for differences due to stick design, a second-order representation of the pilot/stick interface was included in the representation of system dynamics.) Parameter values that reproduced the data satisfactorily were 0.15 seconds time delay, 0.1 seconds "motor lag" time constant, -21 dB observation noise/signal ratio, and 0.004 (about -30 dB) motor noise/signal ratio. These values are typical of those found in earlier studies of single-axis tracking [4-7].

Vibration data were then analyzed to find a single set of parameter values to account for performance with all six configurations. Furthermore, an attempt was made to find the least number of parameter changes that would provide a good match to experimental results. The following parameter changes were required to account for the effects of vibration: (1) time delay increased to 0.2 seconds, (2) motor noise/signal ratio increased tenfold to about 0.04, and (3) a "residual" observation noise variance equal to the estimated variance of relative motion between EPR and display was included. No changes were needed for motor lag or observation noise/signal ratio. Figure 6 shows that frequency-domain measures were matched well by the model (smooth curves).

DESIGN GUIDE

Having been "calibrated" for the effects of vibration, the pilot/vehicle model may be employed in the design of control-sticks in a vibration environment. Until further data have been obtained, however, application must be restricted to z-axis vibration and to the specific biomechanical configuration explored in this study.

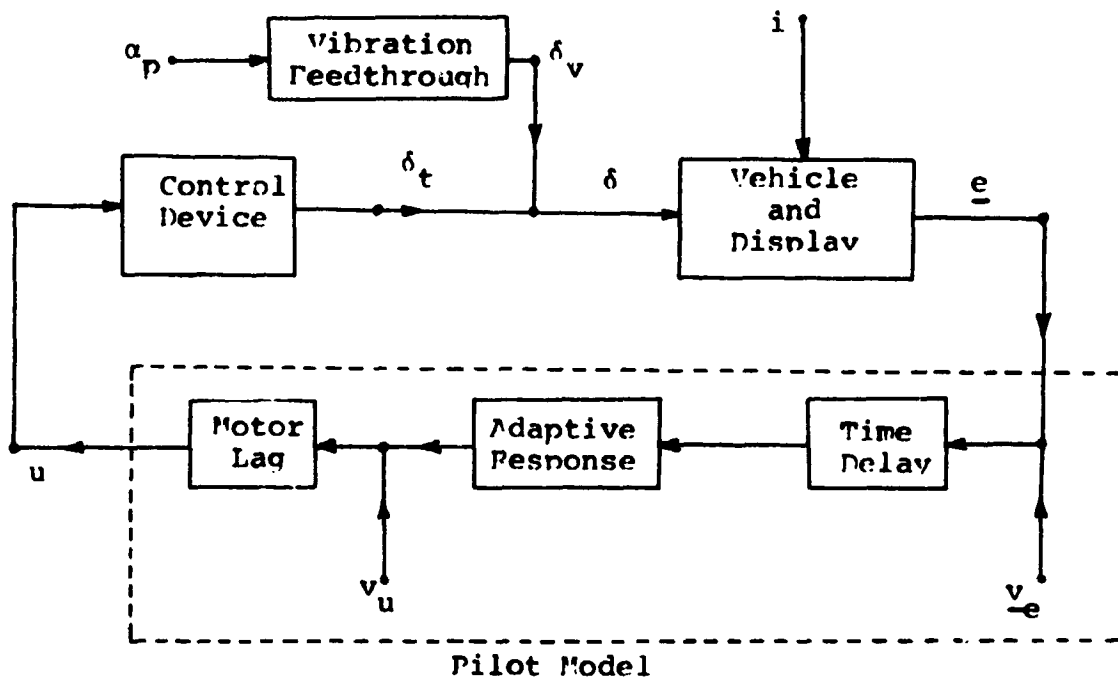
An outline of the model structure is diagrammed in Figure 8. This model consists of the optimal-control pilot/vehicle model referred to above, plus an element (labeled "vibration feedthrough") to account for control inputs linearly related to platform vibration. For simplicity of exposition we consider a single-variable tracking task; extension of the model to multi-input, multi-control systems is straightforward.

Input variables shown in Figure 8 are the tracking input, i , assumed to be a zero-mean Gaussian random process; the platform vibration, α_p ; the pilot's observation noise process, v_e ; and the pilot's motor noise process, v_u . Response variables include tracking error, e , the pilot's control force, u , the electrical control input provided by the control device, δ_t , the control input due to vibration feedthrough, δ_v , and the total control input, δ , given as the sum of the tracking and feedthrough control components. (We assume that platform vibration is at frequencies beyond the bandpass of the man/machine system so that the pilot cannot effectively track out the feedthrough-related inputs.) Error and observation noise are shown as vector quantities, since the pilot will generally obtain and use both displacement and velocity information from a single error indicator [7, 8].

The procedure for using this model to predict the effects of stick parameters on tracking performance is diagrammed in Figure 9 and is summarized below:

1. System dynamics are represented in state-variable format. Control-stick and display dynamics, as well as frequency-shaping of the tracking input, are included in this formulation.
2. Pilot-related model parameters not affected by vibration are assigned values from well-documented studies of pilot/vehicle performance in non-vibration environments. Parameters that appear to fall into this category are motor lag and observation noise/signal ratio.
3. Pilot parameters of time delay and motor noise/signal ratio are assigned values to reflect the effects of vibration.*

*Results of a current study [Air Force Contract No. F33615-75-C-5043] indicate that both time delay and motor noise/signal ratio increase linearly with rms shoulder acceleration. To predict these model parameters, we use existing empirical models of shoulder feedthrough to predict shoulder motion in a specific vibration environment.



WHL-236

Figure 8. Outline of the Model Structure

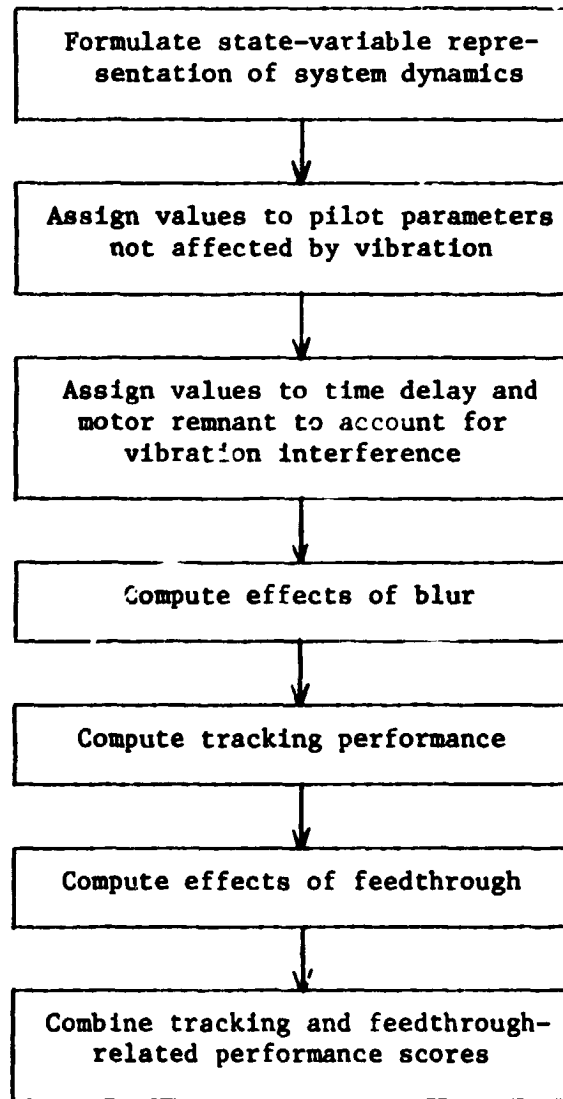


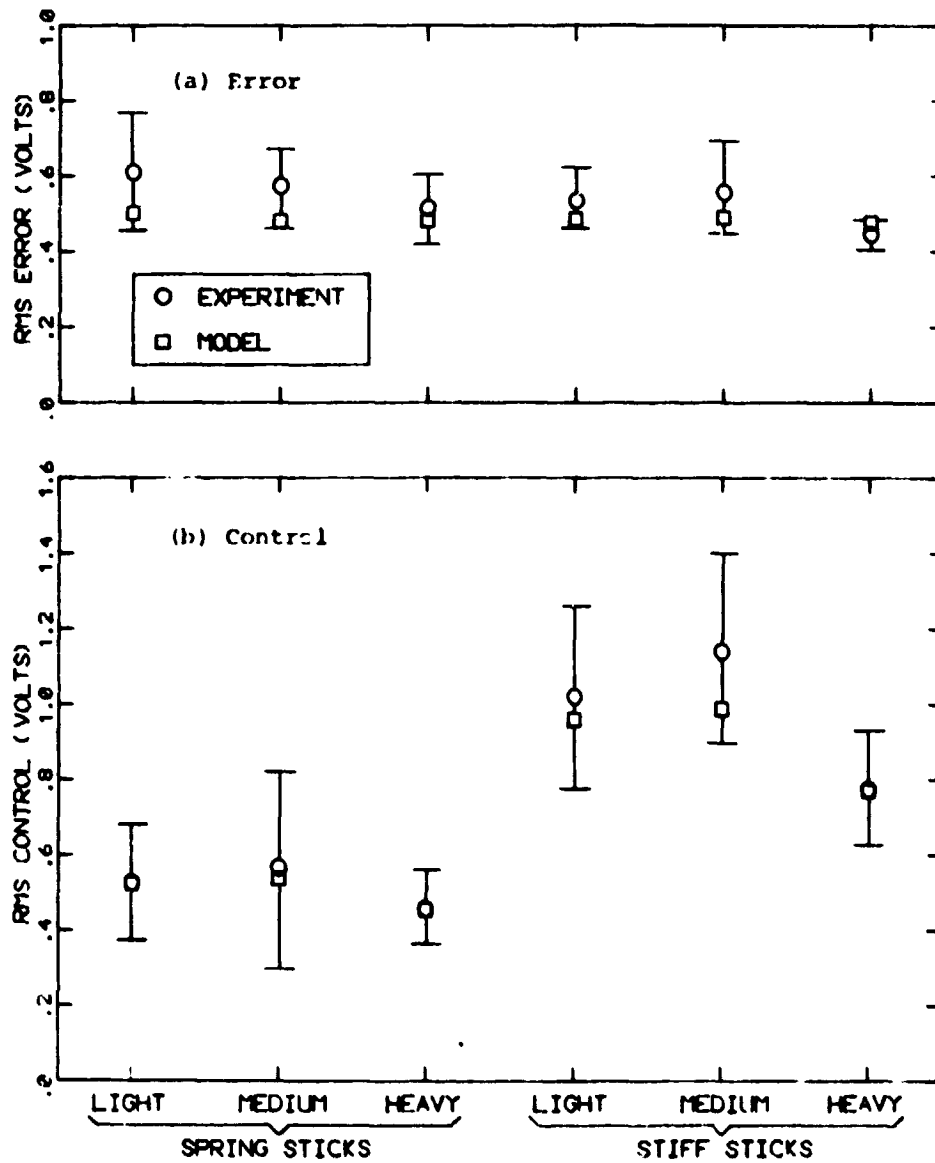
Figure 9. Procedure for Predicting Tracking Performance

4. Describing functions relating head motion to platform acceleration are used to estimate relative motion between the eye point-of-regard and the display. This motion variable determines the value of a model parameter related to visual resolution limitations.
5. All parameters of the pilot/vehicle model having now been defined, predictions of tracking performance (excluding stick feedthrough) are obtained.
6. The impedance model of Figure 2 is analyzed to predict the feedthrough describing function for the particular stick configuration of interest. Appropriate integrations are performed to obtain predicted error and control variances due to feedthrough.
7. Error variance related to feedthrough is added to the variance score predicted from the optimal-control model to yield total error variance.
8. Since a change in stick parameters will generally affect both tracking performance as well as feedthrough, the entire procedure is repeated to explore the effects of changing one or more parameters of the control stick.

This model was applied to the six control configurations explored in this study in order to determine whether or not the rules stated above would allow a consistently good match to the data obtained from all experimental conditions. The major experimental variable was spring gradient, although electrical gain had to be changed as well [1].

Model analysis was performed in the manner described in the preceding section. Figure 10 compares measured and model performance scores for the six configurations. (Scores include the effects of vibration feedthrough.) All scores are matched to within one standard deviation. Model results are not true "predictions", of course, since the data were used to determine the relation between pilot parameters and vibration. The ability to match all conditions with a single set of parameters, however, tends to validate the design procedure outlined above. Use of the model to predict the effects of control gain and stick damping is demonstrated in [1].

Although this paper has emphasized the relation between vibration effects and control stick design, the design guide suggested here can be used to explore a number of additional aspects of the manual control system. The pilot/vehicle model that forms the basis for this guide has been shown to account for the relation between pilot and system performance and such system parameters as vehicle dynamics [4, 5],



14L-240

Figure 10. Comparison of Measured and Predicted Rms Performance Scores (Vibration Present)

tracking input spectrum [4, 5], display gain [7], and attention sharing [6]. In addition, the model has been applied to multi-variable tasks in non-vibration environments [9, 10].

Results of a current study indicate that biodynamic response mechanisms are essentially linear for rms vibration inputs up to 0.3 g and that results can be extrapolated across single-sinusoid, sum-of-sinusoids, and random vibration spectra. Thus, it appears that the design guide can be applied to a variety of z-axis vibration environments.

Application of the design guide must be restricted, however, to z-axis vibration and to the specific biomechanical configuration explored in the AMRL experiments. This restriction is imposed because the biomechanical response patterns reported herein, as well as the relation between vibration and pilot parameter changes, are strictly empirical findings, not theoretical results. In order to apply the model to other axes of vibration and to other biodynamic environments, "calibration" experiments will be needed to determine the effects of vibration on pilot parameters and to quantify relevant biodynamic response mechanisms. Once reliable and useable theoretical models become available for predicting these relationships from a knowledge of the biomechanical configuration, these restrictions may be relaxed.

REFERENCES

1. Levison, William H. and Houck, Philip D.: Guide for the Design of Control Sticks in Vibration Environments. AMRL-TR-74-127, Aerospace Medical Research Laboratory, Wright-Patterson Air Force Base, Ohio, February 1975.
2. Allen, R. W., Jex, H. R. and Magdaleno, R. E.: Manual Control Performance and Dynamic Response During Sinusoidal Vibration. AMRL-TR-73-78, Aerospace Medical Research Laboratory, Wright-Patterson Air Force Base, Ohio, October 1973.
3. Meiry, Jacob L.: Vestibular and Proprioceptive Stabilization of Eye Movements. In Paul-Bach-Y-Rita, Carter C. Collins, and Jane E. Hyde (eds.), The Control of Eye Movements, Academic Press, N. Y., 1971, pp. 483-496.
4. Kleinman, David L., Baron, Sheldon and Levison, William H.: An Optimal-Control Model of Human Response, Part 1: Theory and Validation. Automatica, Vol. 6, 1970, pp. 357-369.
5. Kleinman, David L., Baron, Sheldon and Levison, William H.: A Control Theoretic Approach to Manned-Vehicle Systems Analysis. IEEE Trans. on Auto. Control, Vol. AC-16, No. 6, December 1971.

6. Levison, William H., Elkind, J. I. and Ward, J. L.: Studies of Multi-Variable Manual Control Systems: A Model for Task Interference. NASA CR-1746, May 1971.
7. Levison, William H.: The Effects of Display Gain and Signal Bandwidth on Human Controller Remnant. AMRL-TR-70-93, Aerospace Medical Research Laboratory, Wright-Patterson Air Force Base, Ohio, March 1971.
8. Levison, William H., Baron, S. and Kleinman, D. L.: A Model for Human Controller Remnant. IEEE Trans. Man-Machine Systems, Vol. MMS-10, No. 4, December 1969.
9. Kleinman, David L., and Baron, S.: Analytic Evaluation of Display Requirements for Approach to Landing. NASA CR-1952, November 1971.
10. Baron, Sheldon and Levison, W. H.: A Manned Control Theory Analysis of Vertical Situation Displays for STOL Aircraft. NASA CR-114620, April 1973.

N75 33717

EVALUATION OF OPTIMAL CONTROL TYPE MODELS FOR THE
HUMAN GUNNER IN AN ANTI-AIRCRAFT ARTILLERY (AAA) SYSTEM*

By Anil V. Phatak and Kenneth M. Kessler
Systems Control, Inc. (Vt)
1801 Page Mill Road
Palo Alto, California 94304

SUMMARY

The selection of the structure of optimal control type models for the human gunner in an anti-aircraft artillery (AAA) system is considered. Several structures within the LQG framework may be formulated. Two basic types are considered: (1) k th derivative controllers, and (2) proportional-integral-derivative (P-I-D) controllers. It is shown that a suitable criterion for model structure determination can be based on the ensemble statistics of the tracking error. In the case when the ensemble tracking steady state error is zero, it is suggested that a P-I-D controller formulation be used in preference to the k th derivative controller.

INTRODUCTION

The standard optimal control model (SOCM) for the human operator has been extensively used in the past [1-3] for modeling and predicting human performance in complex manned aircraft and weapon systems. The usual approach towards validating the standard optimal control model (SOCM) is well documented in the literature, and may be summarized in terms of the following two steps: (1) the model structure corresponding to the standard optimal control model is arbitrarily chosen. In particular, the human is assumed to behave as an optimal controller/estimator with a quadratic cost functional

$$J = E \int \{ (x, Qx) + q\dot{u}^2 \} dt$$

where (x, Qx) represents the quadratic cost due to the tracking error and $(\dot{u})^2$ reflects the penalty for the deviations in rate of change of control input from zero; and (2) the parameters of the standard optimal control model are chosen using empirical "rules of thumb" and iterated upon until a close fit (usually an "eye ball" fit) of the model predictions to actual data is obtained.

* This work was supported by Aerospace Medical Research Laboratory, Wright-Patterson AFB, Ohio, under Contract F 33615-75-C-0016.

that a more general k th derivative controller structure or possibly a proportional-integral-derivative (P-I-D) controller representation may be required for accurate modeling of the human gunner in an anti-aircraft artillery (AAA) tracking task. An overview of the analytical results follows.

THE ANTI-AIRCRAFT ARTILLERY TRACKING TASK

The general configuration of a manned anti-aircraft artillery task (AAA) is as shown in figure 1. The human gunner's task is to apply the proper azimuth and elevation control inputs via crank handles such that the gunsight tracks the target aircraft with minimum error. The objective of this paper is to evaluate the analytical and practical implications of optimal control type models for the human gunner in predicting overall weapon system effectiveness. The analysis of the tracking task assumes no coupling between azimuth and elevation axes, in order to illustrate the general methodology for selecting an optimal control model structure using available experimental or field test data. The analysis is further restricted to modeling the deterministic component of the gunner tracking response to quasi-deterministic target trajectories. Consequently, only the deterministic optimal controller model for the human gunner need be considered. The basic idea is to choose the optimal control

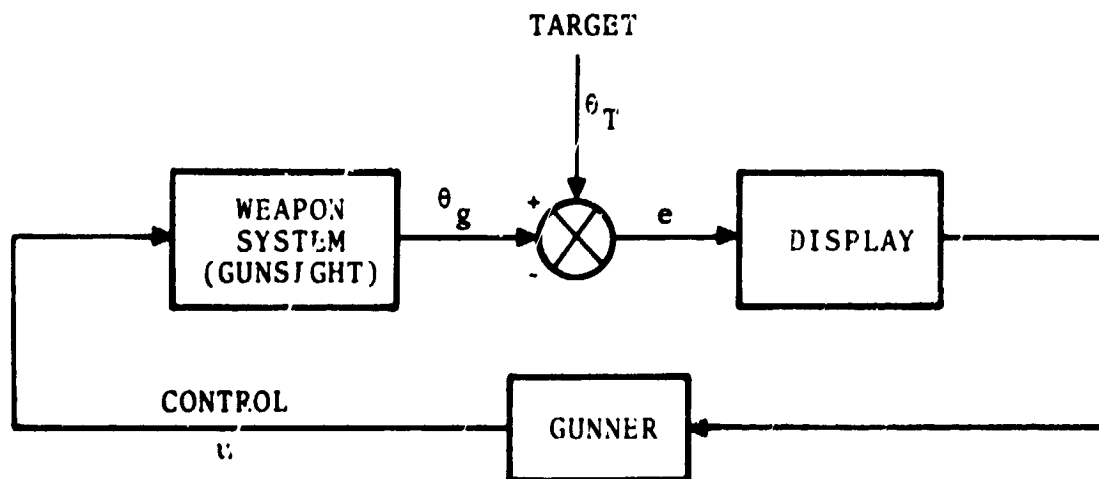


Figure 1: Configuration of a Manned AAA System

model structure that is most consistent with the characteristics of the steady state ensemble mean of the tracking error.

kTH DERIVATIVE CONTROLLER FORMULATION

As in the standard optimal control model formulation, the development of the kth derivative controller model requires state variable models for the target trajectory, the gunsight dynamics and perceived displays. The gunsight dynamics can be modeled by a single input/single output transfer function and can be put in the state variable form

$$\begin{aligned}\dot{x}_g &= A_g x_g + b_g u \\ \theta_g &= C_g x_g\end{aligned}\tag{1}$$

Similarly, it is reasonable to assume that the target motion in line-of-sight coordinates can be represented by an lth order polynomial in time with added colored noise describing the difference between the polynomial trajectory and the actual trajectory. Figure 2 shows the transfer function model for the target trajectory.

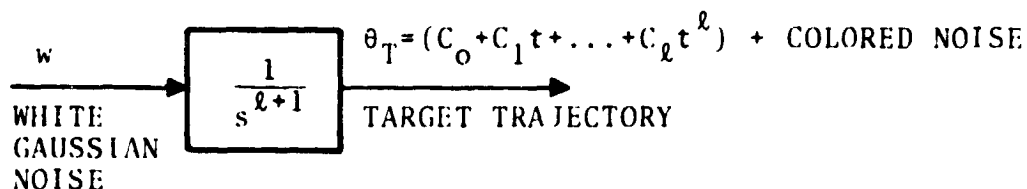


Figure 2: Target Trajectory Model

In state-variable form, the model is

$$\begin{aligned}\dot{x}_T &= A_T x_T + \Gamma w \\ \theta_T &= C_T x_T\end{aligned}\tag{2}$$

The gunner observes the tracking error

$$e = \theta_T - \theta_g\tag{3}$$

The kth derivative controller model assumes that the human minimizes a cost functional of the form

$$J = E \int_0^T \left\{ e^2 + (g u^{(k)})^2 \right\} dt, \quad k=0,1,2,\dots,\ell-1 \quad (4)$$

The solution to the above linear, quadratic cost, Gaussian (LQG) optimal control problem is of the form

$$u_{opt}^{(k)} = - [\lambda_T, \lambda_g, \lambda_u]^{-1} \begin{bmatrix} x_T \\ x_g \\ x_u \end{bmatrix} \quad (5)$$

where $x_u \triangleq [u, \dot{u}, \dots, u^{(k-1)}]^{-1}$ (6)

λ_T , λ_g and λ_u are the optimal feedback gain vectors on the target, gun sight and control state vectors, respectively. These can be computed explicitly by solving appropriate matrix Riccati equations.

Solving for the transfer function relating tracking error e to target motion, θ_T , gives

$$\frac{E(s)}{\theta_T(s)} = \frac{a_0 + a_1 s + \dots + a_{k-1} s^{k-1} + a_k s^k + \dots + a_{k+n} s^{k+n}}{D(s)} \quad (7)$$

where $\{a_i\}$ are functions of the optimal control gains $\lambda_T, \lambda_g, \lambda_u$ and the gun sight and target trajectory models, and $D(s)$ is some polynomial in s . An interesting result is that the $\{a_i, i=0,1, \dots, k-1\}$ can be shown to be identically zero. This result has a direct impact on the steady state properties of the tracking error response to the deterministic polynomial target trajectory input. Thus, if

$$\theta_T(t) = C_0 + C_1 t + \dots + C_\ell t^\ell$$

and

$$j = 1, 2, \dots, \ell+1, \quad \text{then}$$

$$e_{SS}^{(\ell-j+1)} = \lim_{t \rightarrow \infty} e^{(\ell-j+1)}(t) = \lim_{s \rightarrow 0} s \left[s^{(\ell-j+1)} E(s) \right] =$$

$$\begin{aligned}
&= \lim_{s \rightarrow 0} s^{\ell-j+2} \left[\frac{\cancel{a_0} + \cancel{a_1}s + \dots + \cancel{a_{k-1}}s^{k-1} + a_k s^k + \dots + a_{k+n} s^{k+n}}{D(s)} \right] \\
&\quad \cdot \left[\frac{C_0}{s} + \frac{C_1}{s^2} + \dots + \frac{C_\ell}{s^{\ell+1}} \right] \\
&= 0 \tag{8}
\end{aligned}$$

Table 1 shows the characteristics of the steady state tracking error for various values of k and ℓ .

Table 1: Implications of k Values on Steady State Tracking Error

CASE	STEADY STATE TRACKING ERROR
$k=1$	$e_{SS}^{(\ell)} = 0 \Rightarrow e_{SS} = \text{polynomial in } t \text{ of degree } (\ell-1)$
$k=2$	$e_{SS}^{(\ell-1)} = 0 \Rightarrow e_{SS} = \text{polynomial in } t \text{ of degree } (\ell-2)$
\vdots	
$k=j$	$e_{SS}^{(\ell-j+1)} = 0 \Rightarrow e_{SS} = \text{polynomial in } t \text{ of degree } (\ell-j)$
\vdots	
$k=\ell-1$	$\ddot{e}_{SS} = 0 \Rightarrow e_{SS} = \text{ramp}$
$k=\ell$	$\dot{e}_{SS} = 0 \Rightarrow e_{SS} = \text{constant}$
$k=\ell+1$	$e_{SS} = 0$

The above results in Table 1 can be used as the criterion in the selection of a specific integer value of k_1 as follows:

- (1) Compute the ensemble statistics of the tracking error using a sufficiently large number of experimental runs. That is, determine the ensemble mean steady state

error and its ensemble variance.

- (2) Fit the ensemble mean tracking error with a minimal degree polynomial in time. Determine the degree of the polynomial using stepwise regression and statistical hypothesis testing, taking into consideration the ensemble variance information in estimating the level of significance. Let m be the degree of this polynomial.
- (3) Then according to Table 1, $(\ell-j)$ must be equal to m . Therefore, a k^{th} derivative controller with $k=\ell-m$ must be selected to fit the tracking data under consideration.

However, it must be emphasized that the results given in Table 1 are met only as long as the modeling assumptions are accurate. In other words, the k^{th} derivative controller model is not robust. For the case when $e_{ss} = 0$, a value of $k=\ell+1$ is required in the formulation. For this case, a proportional-integral-derivative (P-I-D) controller model for the gunner is recommended over a k^{th} derivative controller representation in view of the robustness of the former and the lack of robustness in the latter model. Details of the P-I-D controller formulation are discussed next.

PROPORTIONAL-INTEGRAL-DERIVATIVE CONTROLLER (P-I-D) FORMULATION

A second type of human operator model that may be formulated within the LQG framework is the P-I-D controller [4]. In this case, the formulation requires the dynamic equations be written in terms of the tracking error.

For example, if

$$e(t) = \theta_T(t) - \theta_g(t)$$

and the gun model can be represented by

$$\frac{\theta_g(s)}{u(s)} = \frac{N(s)}{D(s)}$$

while the target model is

$$\frac{\theta_T(s)}{W(s)} = \frac{1}{s^{\ell+1}} ; \quad \ell=0,1,2,\dots$$

The P-I-D formulation requires the system equations be written in terms of the tracking error and its higher derivatives as follows:

$$\dot{\underline{e}} = A_e \underline{e} + B_e \tilde{u} + \Gamma_e \tilde{w}$$

where

$$\underline{e} = [e, \dot{e}, \dots, e^{\ell+n+1}]'$$

$$\tilde{u} = s^{\ell+1} N(s) u$$

$$\tilde{w} = D(s) w$$

This implies that the target trajectory can be modeled as shown in Figure 3. Note that for a P-I-D controller, the fit error between the actual target motion and the ℓ^{th} degree polynomial function is assumed to be colored noise that is obtained by passing white noise through $1/D(s) s^{\ell+1}$ where $D(s)$ represents the denominator of the gunsight transfer function.

If one computes the transfer function $E(s)/\theta_T(s)$ using the P-I-D controller structure, it can be shown that the steady-state tracking error $e_{ss} \equiv 0$. This is true even if the parameters of the assumed gunsight/target model are different from their true values. Thus, the P-I-D controller is insensitive to modeling assumptions and is, therefore, robust.

The transfer function for the human operator may be obtained by computing $\frac{u(s)}{E(s)}$. For the P-I-D controller, this is shown in figure 4.

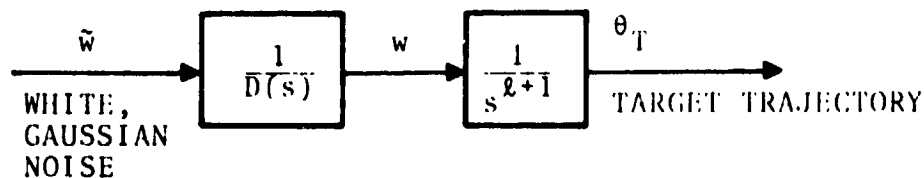


Figure 3: Block Diagram Showing θ_T (Target) Model

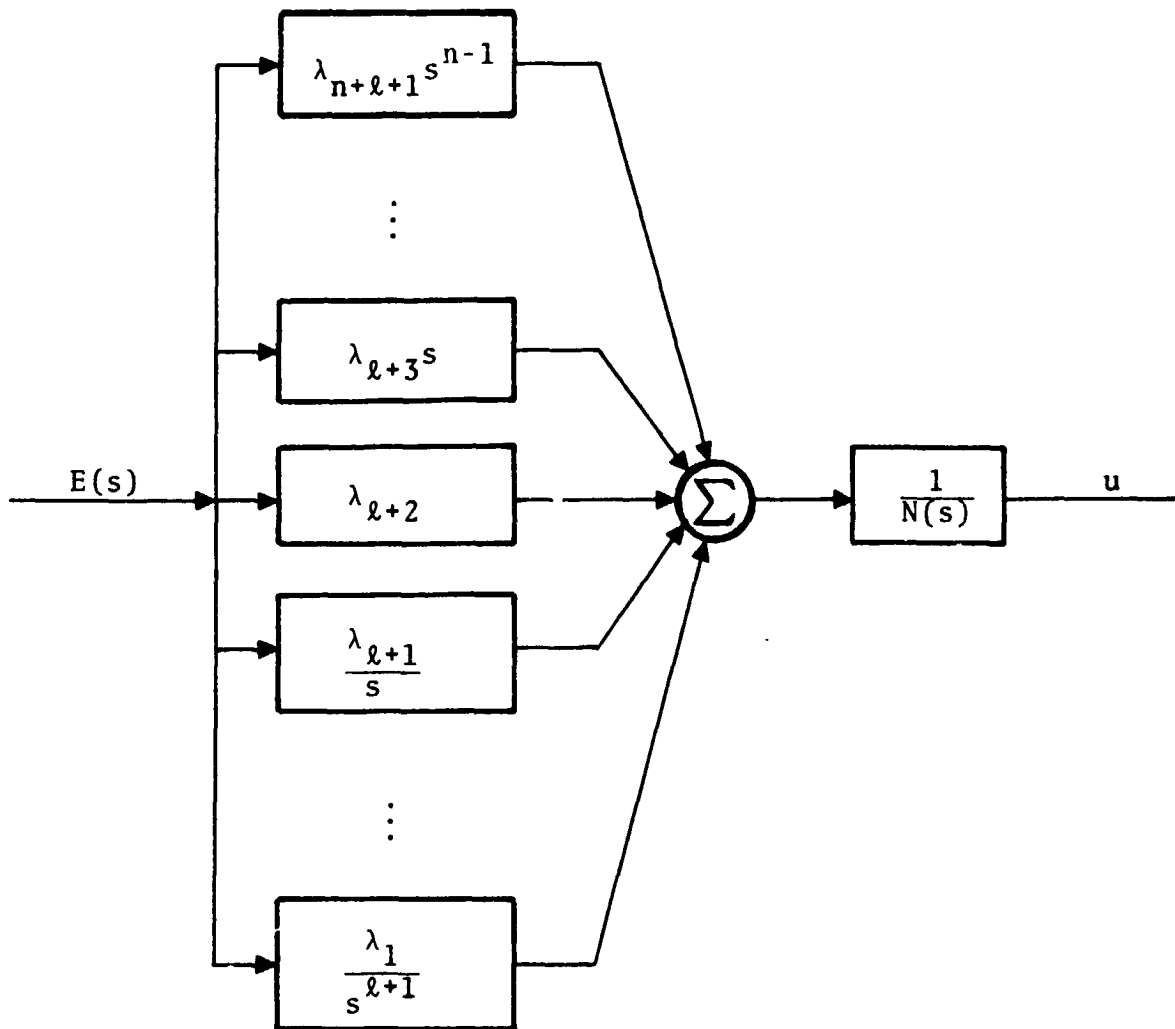


Figure 4: Block Diagram Showing P-I-D Controller as Pilot Model

CONCLUDING REMARKS

The ensemble mean of the tracking error provides a suitable criterion to select an appropriate structure of an optimal control pilot model, all within the framework of the LQG problem. The structure of the k^{th} derivative controllers allows the designer to appropriately match model predictions to the steady-state tracking error. For the case when the steady-state tracking error is zero, the selection of a P-I-D controller adds robustness to the design, and is recommended.

REFERENCES

1. Kleinman, D., et al., "A Control Theoretic Approach to Manned-Vehicle Systems Analysis," IEEE Trans. Auto. Cont., Vol. AC-16, pp. 824-832, 1971.
2. Phatak, A., et al., Identification of the Optimal Control Model for the Human Operator, Final Tech. Report, AMRL TR-74-49, Aerospace Medical Research Laboratory, September 1974.
3. Kleinman, D. and Perkins, T., "Modeling Human Performance in a Time-Varying Anti-Aircraft Tracking Loop," IEEE Trans. Auto. Cont., Vol. AC-19, pp. 297-306, 1974.
4. Athans, M., "On the Design of P-I-D Controllers Using Optimal Regulator Theory," Automatica, Vol. 7, pp. 643-647, 1971.

N75 33718

COMPARISON OF HUMAN DRIVER DYNAMICS IN SIMULATORS
WITH COMPLEX AND SIMPLE VISUAL DISPLAYS
AND IN AN AUTOMOBILE ON THE ROAD

By Duane T. McRuer and Richard H. Klein

Systems Technology, Inc.
Hawthorne, California

SUMMARY

As part of a comprehensive program exploring driver/vehicle system response in lateral steering tasks, driver/vehicle system describing functions and other dynamic data have been gathered in several milieu. These include a simple fixed-base simulator with an elementary roadway delineation-only display; a fixed-base statically operating automobile with a terrain-model-based, wide angle projection system display; and a full-scale moving-base automobile operating on the road.

Dynamic data with the two fixed-base simulators compared favorably, implying that the impoverished visual scene, lack of engine noise, and simplified steering wheel feel characteristics in the simple simulator did not induce significant driver dynamic behavior variations. The fixed-base vs. moving-base comparisons showed substantially greater crossover frequencies and phase margins on the road course, which can be ascribed primarily to a decrease in the driver's effective latency for the moving base. When considered with previous data, the moving-base full-scale vs. fixed-base simulator differences are ascribed primarily to the motion cues present on the road course rather than to any visual field differences.

INTRODUCTION

Over a period of several years, STI has conducted a variety of programs to explore driver/vehicle system behavior in directional control tasks. These programs have been conducted to satisfy different and, in general, unconnected purposes; yet similar techniques and procedures have been applied. As a consequence, and incidental to the individual program purposes, we have gathered driver/vehicle system describing function and other dynamic data in several different milieu. Comparison of data from three of these gives some interesting insights about visual cue needs in driving and about the effects of motion and visual cues when contrasted with visual cues alone. We, unfortunately, have to be satisfied with the "interesting insights" rather than more concrete significant differences because we have no common populations of subjects in the three situations.

The driver's visual field, in general, is extremely complicated and defies description. On the other hand, what is important in the visual field from the standpoint of guidance and control may be very simple to describe in principle and to determine in practice. To explore this with a "thought experiment," imagine an experimental series in which the visual field content is successively modified by removing texture and objects in the surround, adjusting delineation features, etc. Only the driver's visual field would be varied, and the factors to be held constant would include the vehicle dynamics, the driver subjects, and the excitation against which the car is to be regulated. For each treatment in this imaginary experimental series, a set of lane regulation tasks would be run and measurements made of the driver's dynamics and the driver/vehicle system performance. For those visual field variations in which there is no change indicated in the basic driver characteristics, the differences between the more complex and the simpler visual scenes would be redundant to the development of appropriate guidance and control feedback signals by the driver. On the other hand, if driver dynamic differences show up, the visual differences in the comparative scenes are important in terms of the particular driver functions modified. If this experiment were performed for a sufficient variety of visual scenes, we would have a complete story on the driver's guidance requirements in general.

This thought experiment can be expanded further to include the effects of motion cues by contrasting driver behavior measurements taken in a fixed-base situation with its full-scale automobile equivalent.

REVIEW OF EXPERIMENTS

We can now fill in the outline of this thought experiment with data taken from three experimental series. The first is the full-scale roadway experiments reported in Ref. 1. There the physical scene was that of a complete roadway, well marked, viewed through the windshield of a 1974 Chevrolet Nova. The automobile was fitted with a disturbance generator and Describing Function Analyzer, so that describing function and other driver/vehicle system measurements could be made. The general character and nature of the measurements in this and the other two experiments to be considered below were accomplished as described in Ref. 2. The driver's task was lane regulation in the presence of a simulated strongly gusting crosswind disturbance. The disturbance was applied by moving the front wheels with an extensible link servomechanism. This moves the tires but not the steering wheel, because the servo is installed in series with the driver, backed up by the power steering unit, which serves to isolate the servo motions from the steering wheel. The driver's regulation task is simply to keep the car centered in the lane by applying corrective steering inputs. In the Ref. 1 experiments this task was performed at 50 mph by all 18 subjects many times. The measurement interval was 2 seconds, and the primary driver/vehicle system dynamic response data are given in terms of the effective single-loop, open-loop describing function, $Y_{pG_{sw}}^*$. This measurement was taken with the STI/NASA Describing Function Analyzer (Ref. 3) per the measurement scheme outlined in Ref. 2. A representative sample is shown in Fig. 1. In this typical example the amplitude ratio is very close to an ideal crossover model form.

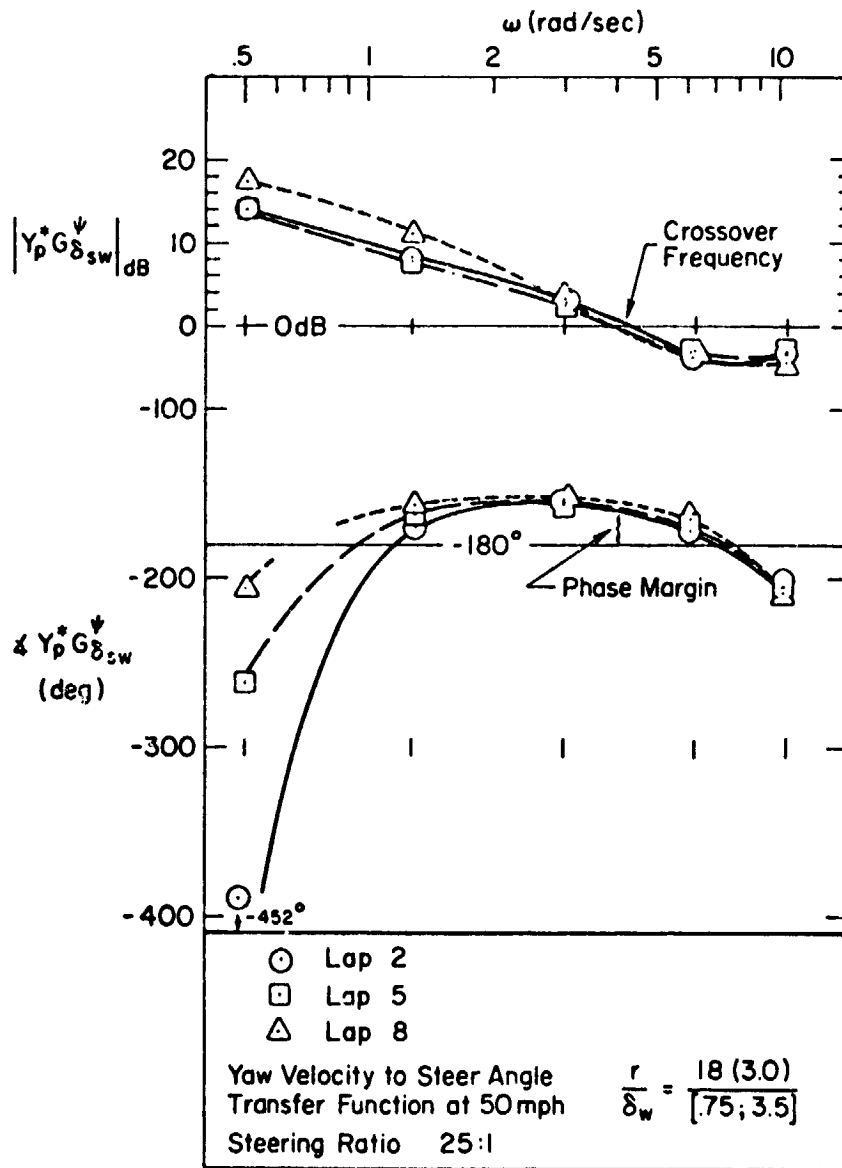


Figure 1. Typical Effective Open-Loop Describing Function for Initial Test Series

The second experimental series (Refs. 4 and 5) was conducted on a fixed-base simulation using the UCLA Driving Simulator. In this series the driver was seated in a 1965 Chevrolet sedan which was mounted on a chassis dynamometer. The dynamometer drum speed, controlled by the driver via the car's accelerator and brakes, determined the landscape velocity of a moving model landscape relative to a black and white TV camera. This was projected on a large screen to provide the driver's visual cues. The driver's steer angle output was fed to an analog computer containing the vehicle equations of motion, and thence to the TV camera servos which moved the "car" over the model terrain. The net motions of camera and model landscape provided the displayed motion presented to the driver. Because the included horizontal angle of the visual field was about 40 deg, the relative motion and geometric cues used for directional control were adequate for foveal and parafoveal vision. The visual field resolution was such that an object the size of an oncoming vehicle could be distinguished at an equivalent full-scale distance of about a quarter of a mile, which was the length of the moving belt landscape. The overall impression with the UCLA simulator is of a highly realistic driving situation in desert terrain under a dark overcast.

The third series was fixed-base operation in the STI simulator. Data from two experiments (Refs. 1, 6, and 7) in which this simulator was used are appropriate. In these experiments the visual scene was made as simple as possible, i.e., it consisted of two lane edges only, drawn in perspective on the CRT with decreasing intensity in the distance. Heading and lane deviations of the car resulted in motions of the road relative to a fixed mask of a car hood, left fender, and windshield outline. The simulator itself consisted of a modified 1968 Mustang cab with the steering wheel adjusted to approximate the force feel characteristics of a power steering unit.

DATA INTERPRETATION AND CONCLUSIONS

By comparing the driver/vehicle system performance data from these three experiments we can deduce the relative importance of features in the three visual scenes presented. The data most readily at hand are for the system crossover frequency and phase margin. These reflect primarily the driver lead equalization and heading gain properties.

The first and most direct comparison is between the STI simulator and the full-scale, moving-base results. Here the subject and the task are the same. The crossover frequency and phase margins for comparable vehicle dynamics are shown in Fig. 2 as a function of the vehicle yaw time constant, T_r . Note that the trends of full-scale and moving-base results are parallel but that the full-scale has a higher crossover frequency and a higher phase margin. Previous experiments (Refs. 8 and 9) in which separate describing function measurements were made for motion and visual cues indicate that this difference can be attributed to motion (vestibular) feedback effects (due primarily to the semicircular canals) which are active in the moving-base case and not in fixed base. When this effect is removed, the phase margin data essentially overlay one another and the crossover frequency curves are almost the same.

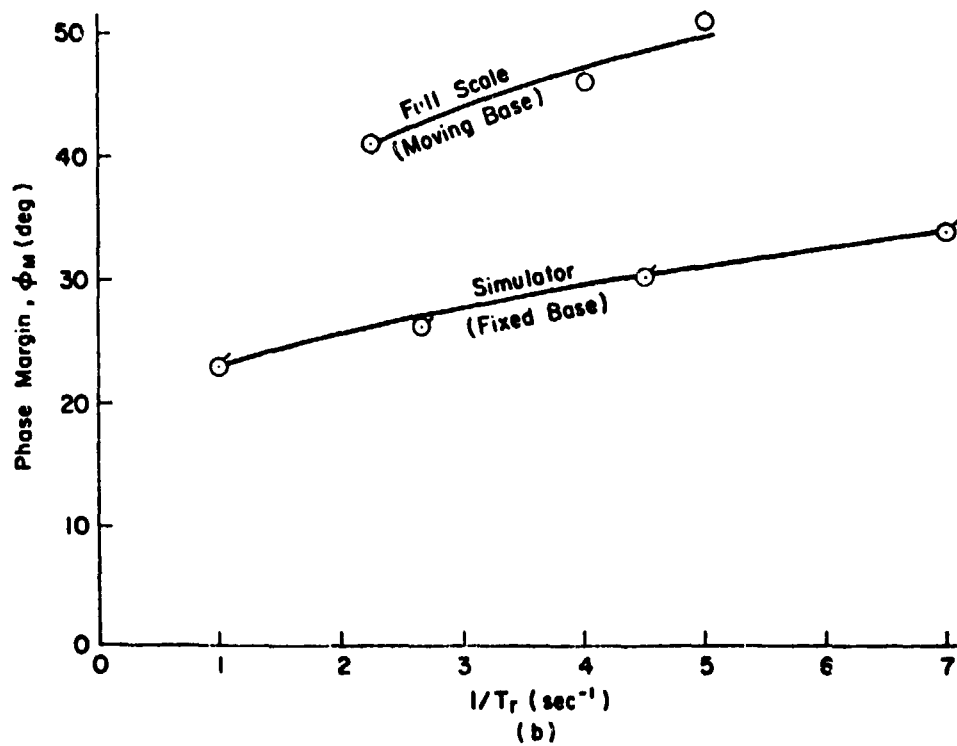
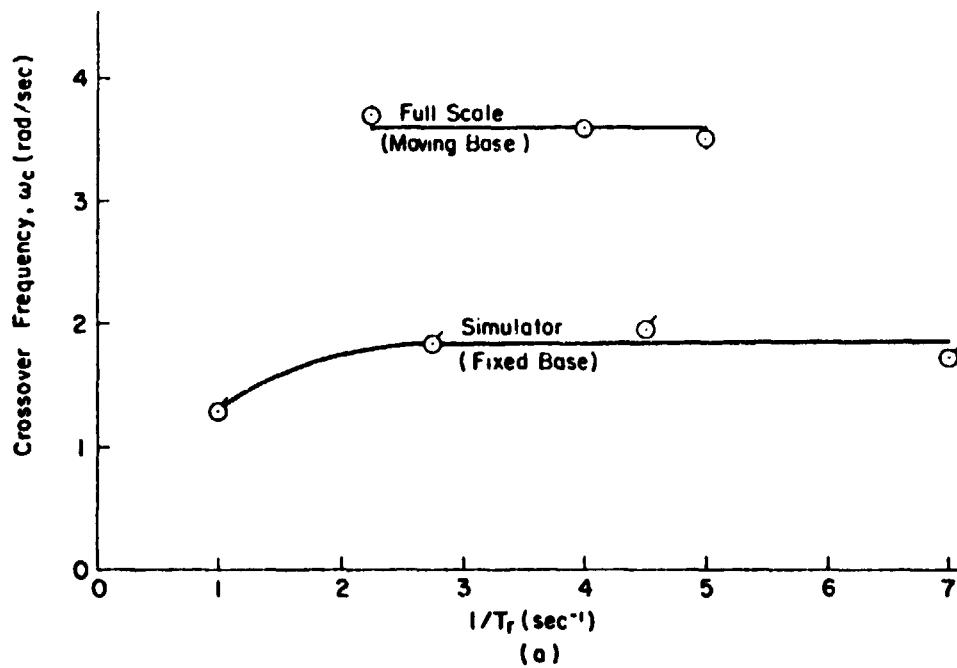


Figure 2. Comparison of Full-Scale Automobile and Fixed-Base Simulator Dynamics for Test Driver Subject

When the results from the UCLA simulation are compared with the STI fixed-base results, as shown in Fig. 3, it is seen that the crossover frequency and phase margin are very similar. The data points represent the mean and standard deviation for five drivers in the UCLA series, and the mean and standard deviation of repeat runs using one test driver in the STI series. Because the crossover frequency and phase margin data for the two simulation series compare favorably, the implication is that the impoverished visual scene, lack of engine noise, and simplified steering wheel feel characteristics present in the STI simulator did not induce significant driver dynamic behavior variations.

Shown in Fig. 4 is an associated comparison, this time in describing function form, contrasting the test driver and nine other subjects run in the STI simulator. These serve to indicate that the test driver used for both simulator and full-scale results is representative of a much larger randomly selected sample of the driving population.

In summary, the data for similar vehicle dynamics, moving base and fixed base, are compared, the differences between an impoverished visual field and the out-the-windshield actual field are seen to be unimportant to the development of the visual guidance cues. A key conclusion therefore is that a two-line roadway delineation only is sufficient to permit the development of appropriate driver feedback properties. These experiments therefore indicate very strongly that a visual field which has only two high-contrast lane markings presented to the driver with appropriate motion perspective is a sufficient visual scene from which to develop the requisite guidance and control information. Texture, other objects in the surround, etc., may provide useful but redundant information which is not essential to the driver's steering operations in the regulation task.

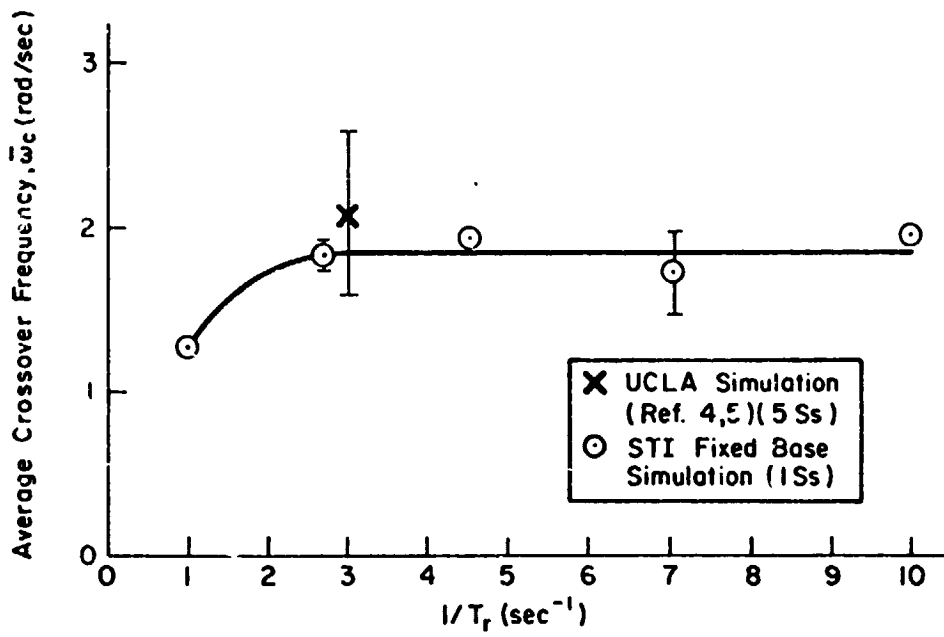
REFERENCES

1. McRuer, Duane T.; and Klein, Richard H.: Automobile Controllability — Driver/Vehicle Response for Steering Control. Vol. I: Summary Report, DOT HS-801 406. Vol. II: Supporting Experimental Results, DOT HS-801 407. Nov. 1974.
2. McRuer, Duane T.; Weir, David H.; Jex, Henry R.; Magdaleno, Raymond E.; and Allen, R. Wade: Measurements of Driver/Vehicle Multiloop Response Properties With a Single Disturbance Input. IEEE Trans., vol. SMC-5, no. 5, Sept. 1975 (forthcoming).
3. Allen, R. Wade; and Jex, Henry R.: A Simple Fourier Analysis Technique for Measuring the Dynamic Response of Manual Control Systems. IEEE Trans., vol. SMC-2, no. 5, Nov. 1972, pp. 638-643.
4. Weir, David H.; and McRuer, Duane T.: Measurement and Interpretation of Driver, Steering Behavior and Performance. Human Factors, vol. 15, no. 4, Aug. 1973, pp. 367-378. Also SAE Paper 730098.

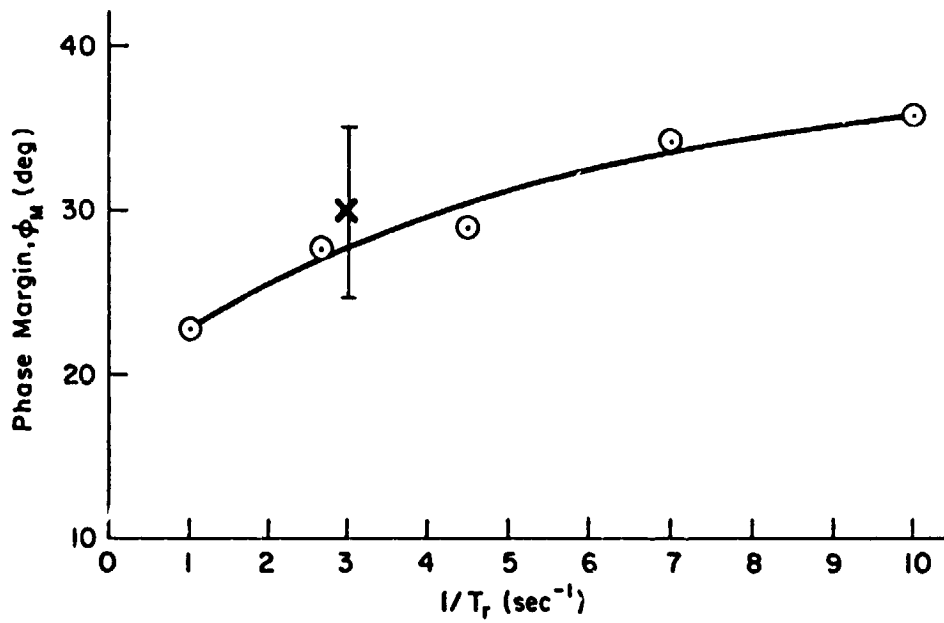
5. Weir, David K.; and Wojcik, Charles K.: Simulator Studies of the Driver's Dynamic Response in Steering Control Tasks. Driving Simulation, Highway Research Record No. 364, 1971, pp. 1-15.
6. Allen, R. Wade; Jex, Henry R.; McRuer, Duane T.; and DiMarco, Richard J.: Alcohol Effects on Driving Behavior and Performance in a Car Simulator. Proc. of the Tenth Annual Conference on Manual Control, Wright-Patterson AFB, Ohio, Apr. 1974.
7. Jex, Henry R.; Allen, R. Wade; DiMarco, Richard J.; and McRuer, Duane T.: Alcohol Impairment of Performance on Steering and Discrete Tasks in a Driving Simulator. DOT HS-801 302, Dec. 1974.
8. McRuer, Duane T.; and Krendel, Ezra S.: Mathematical Models of Human Pilot Behavior. AGARD-AG-188, Jan. 1974.
9. Stapleford, Robert L.; Peters, Richard A.; and Alex, Fredric R.: Experiments and a Model for Pilot Dynamics with Visual and Motion Input. NASA CR-1325, May 1969.

ACKNOWLEDGMENT

This research was supported by the National Highway Traffic Safety Administration under Contract DOT-HS-359-3-762.



a) Crossover Frequency, ω_c



b) Phase Margin, ϕ_M

Figure 3. Comparison of Data from Fixed-Base Simulator with Elaborate and Impoverished Visual Fields

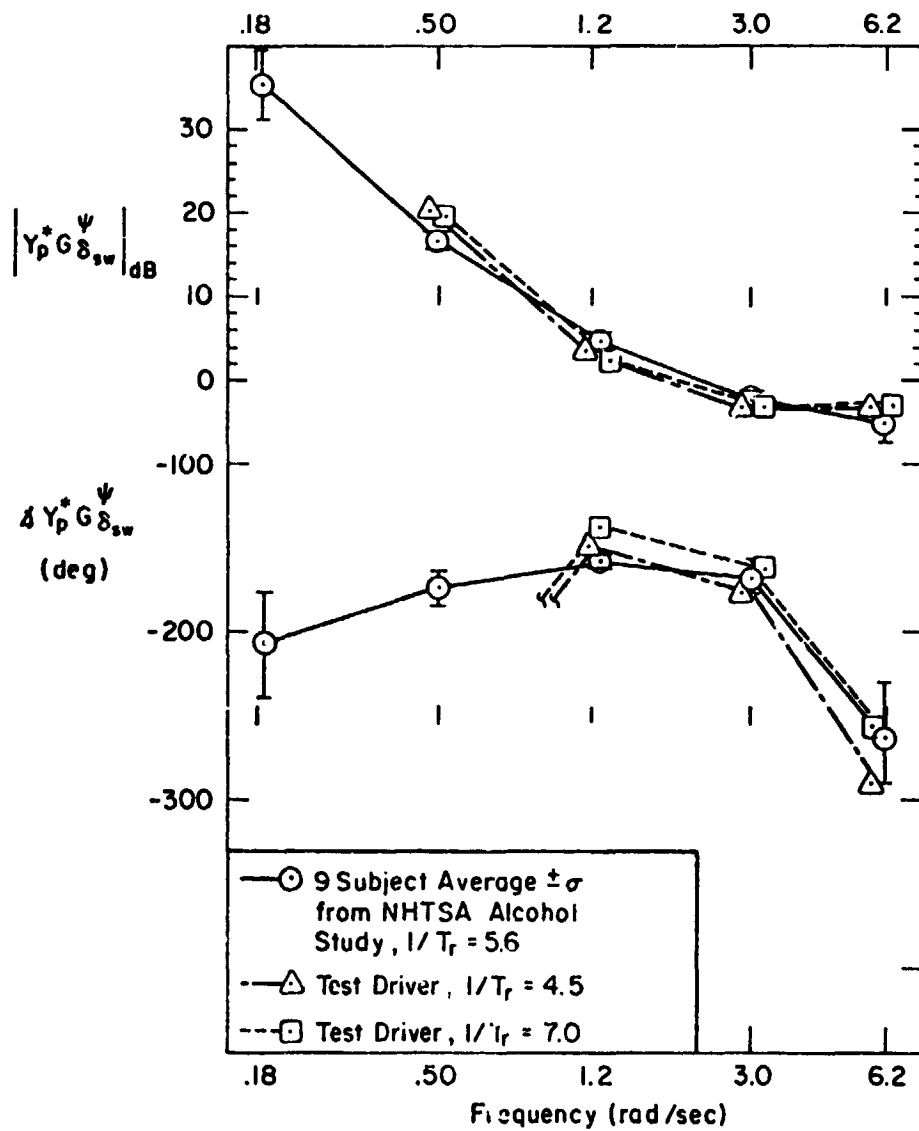


Figure 4. Comparison of Test Driver with Nine Subjects From a Previous NHTSA Study (Ref. 6)

N75 33719

MANUAL AND AUTOMATIC CONTROL OF SURFACE EFFECT SHIPS*

By Warren F. Clement, John J. Shanahan, and R. Wade Allen

Systems Technology, Inc., Hawthorne, California

SUMMARY

A recent investigation of crew performance in the motion environment of a large generic high speed surface effect ship by means of a motion base simulation addressed some of the helmsman's control tasks with an external forward visual field of the seascape and navigation and steering displays in the pilot house. In addition to the primary steering control task, a sub-critical speed tracking task provided a secondary surrogate for trimming the water speed of the craft. The results of helmsmen's steering describing function measurements are presented, and some suggestions for their interpretation are offered. The likely steering loop closures comprise heading and lateral displacement for the course-keeping task investigated. Also discussed is the manner in which these loop closures were implemented for automatic steering of the surface effect ship. Regardless of the influence of workload, steering technique, water speed and sea state, the helmsmen apparently adopted a disturbance regulation bandwidth of about 0.2 rad/sec for lateral displacement. Suggestions for reducing the variability in future helmsmen's measurements are offered.

INTRODUCTION

The Surface Effect Ship (SES) is an ocean-going vessel employing a self-generated aerostatic cushion in contact with the water surface for vertical support (Ref. 1). The SES has rigid shallow-draft side walls with flexible fore and aft skirts or seals to contain the pressurized air cushion while permitting the passage of surface waves through the cushion plenum. The side walls serve as keels to provide lateral stability in the manner of a catamaran. Because the SES rides on a cushion of air, it is less subject to the drag penalties which limit the speed of displacement-hull vessels. Consequently, the SES is capable of sustained higher speeds, and requires precision in course- and sea-keeping, especially in aggravated sea conditions.

The ability of crewmen to perform shipboard duties without undue fatigue or decreased proficiency has been the subject of recent investigations with

*This research was sponsored by the Surface Effect Ship Project Office of the Naval Ship Systems Command under Contract N00024-73-C-0914.

The authors also gratefully acknowledge significant contributions by their colleagues, Messrs. L. G. Hofmann, H. R. Jex, R. E. Magdaleno, and R. A. Peters of Systems Technology, Inc.

manned motion base simulation using motion predictions from a 2000-ton SES mathematical model (Ref. 2). A simulated mission profile with assigned crew tasks provided a disciplined scenario for measuring crew performance in the simulated ship motion environment. Various tasks involving facsimile ship-board operations at four duty stations were performed. One of the duty stations in the pilot house is that of helmsman. In the simulation the helmsman's assignment included a division of attention among steering, speed regulation, obstacle avoidance and communication tasks. Participating helmsmen were among SES crewmen with concurrent operational experience from the Surface Effect Ship Test Facility, Naval Air Test Center, Patuxent River, Maryland.

Our purpose here will be to report and interpret some measurements of helmsmen's describing functions during a precision straight-course-keeping task at high cruising speeds in a disturbed sea and involving the use of a compensatory electronic horizontal situation display of heading and lateral displacement errors not specific to any surface effect ship.

APPARATUS AND METHOD

A complement of 3 in. diameter rotary dial instruments provided the helmsman with compass heading, turn rate, rudder angle and water speed. A visual field simulator provided a collimated external view of the moving seascape and horizon properly correlated with the ship's motions experienced in the cab on the moving base. In addition, an optional automatic helm was provided for relief of manual steering duties while subjective rating analyses were being written and while the helmsman kept watch during four-hour missions.

The random-like steering disturbance was a sum of five non-harmonically related and randomly phased sinusoids whose relative amplitudes were approximately inversely proportional to frequency. This disturbance was generated within the NASA-STI Mark II Describing Function Analyzer (DFA) (Refs. 3 and 4) and applied to the mathematical model of the ship's rudder in linear combination with the helmsman's rudder command signal as shown in Fig. 1. The disturbance did not move the helmsman's wheel nor was it directly visible on the helmsman's rudder angle indicator, but its effects on turn rate, heading deviation and lateral displacement from the desired course were observable. The helmsman was instructed to minimize his lateral displacement error during each 100 sec interval when the DFA was used for cybernetic performance measurement.

The DFA computes on-line the finite Fourier transform, mean-square and mean of a signal in the control loop — in this case, the rudder error δ_e in Fig. 1 at each of the five input frequencies. The final describing function and error variance are computed off-line with a digital computer program based on some of the techniques in Ref. 4. The principles of the measurement of helmsman/SES multiloop response properties with a single disturbance input as used in these experiments are described in Refs. 5 and 6 where the principles are applied to pilot control of hovering vehicles and driver control of highway vehicles. The SES with its broad beam and side wall keels exhibits little rolling and side-slipping in common with catamarans and highway vehicles.

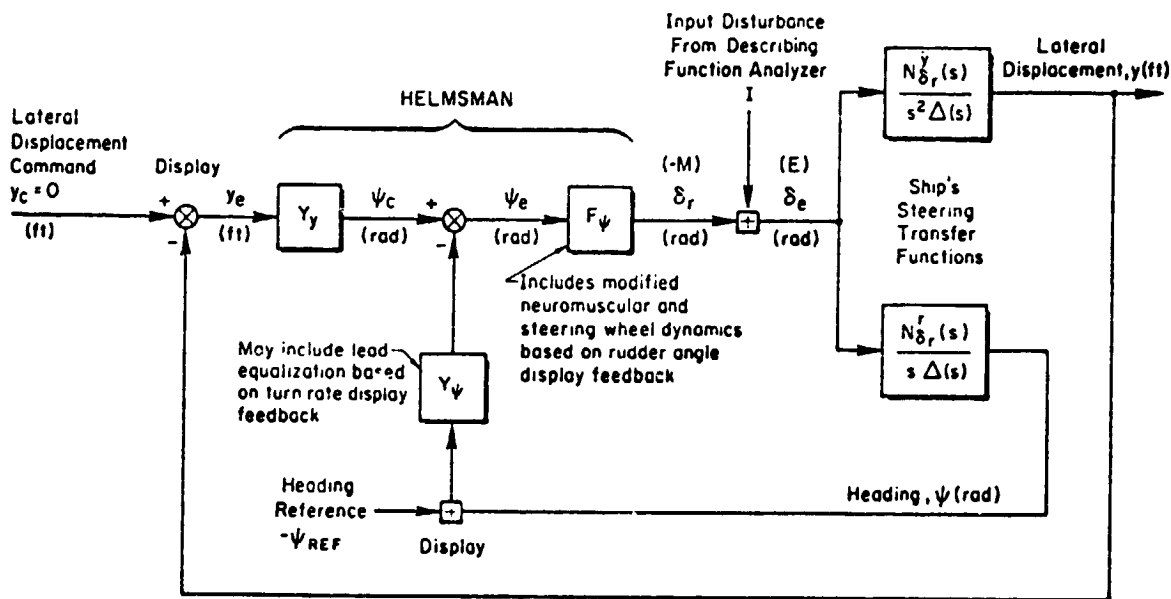


Figure 1. Block Diagram of Heading and Lateral Displacement Control Task as Configured for the Describing Function Analyzer

The helm itself was a 14 in. diameter marine steering wheel. An artificial feel spring was provided, and the wheel breakout torque and the kinetic Coulomb friction damping torque were adjusted to be less than those values currently used in order to examine more critically the possibilities for neuromuscular coupling, biodynamic amplification thereof and closed-loop steering stability limitations. The steering wheel rotation from stop to stop was 270 deg and the corresponding rudder travel, 30 deg, thereby giving a 9:1 steering ratio as in current practice.

The helmsman was asked to perform the steering-only task with both hands on the wheel to minimize the possibility of biodynamic coupling. In addition to the primary steering control task, a sub-critical* speed regulation task provided a secondary surrogate for trimming the water speed of the craft. Speed was regulated with the helmsman's left hand on a friction-restrained quadrant throttle lever with 60 deg of fore-aft travel, so that when the helmsman was instructed to perform both steering and speed control tasks, he maintained only his right hand on the steering wheel.

The ship's lateral-directional dynamic motions in response to the helm and disturbance were represented by linear constant coefficient differential

*"Sub-critical" is used in the manual control context here and must not be confused with the critical speed for the SES. A sub-critical task in the manual control context means that the rate of divergence of the open-loop controlled element as characterized by λ is below the critical level which is at the limit of human manual control capability.

perturbation equations in body axes with respect to a trimmed condition at constant speed. The ship's cab was assumed to be located at the center of gravity in developing the lateral-directional transfer functions given in Table 1 for a trimmed cruising condition.

The differential equation representing the divergent (unstable) controlled element for speed regulation, which was independent of the equations of lateral-directional craft motion, is given by Eq. 1:

$$\dot{u} = \lambda u + K_S \delta_t \quad (1)$$

The inverse time constant λ was chosen as 0.1 rad/sec for the simulation to approximate a slow sub-critical divergence which would require consistent but not overwhelming attention to the side task of speed regulation. Comments by

TABLE 1

TYPICAL LATERAL-DIRECTIONAL OPEN-LOOP CONTROL RESPONSE TRANSFER FUNCTIONS FOR A 2000T SES AT CRUISING SPEED

Denominator:

$$\begin{aligned} \Delta(s) &= [s^2 + 2(0.898)(0.469)s + (0.469)^2] \\ &\quad \times [s^2 + 2(0.198)(1.55)s + (1.55)^2] \\ \Delta(0) &= 0.528 \text{ sec}^{-4} \end{aligned}$$

Numerator for yaw rate response to rudder angle:

$$\begin{aligned} N_{\delta_r}^r(s) &= 0.999(s + 0.493)[s^2 + 2(0.191)(1.55)s + (1.55)^2] \\ N_{\delta_r}^r(0) &= 1.185 \text{ sec}^{-5} \end{aligned}$$

Numerator for lateral acceleration response to rudder angle:

$$\begin{aligned} N_{\delta_r}^{\ddot{y}}(s) &= -52.0(s + 0.983)(s - 1.03) \\ &\quad \times [s^2 + 2(0.191)(1.51)s + (1.51)^2] \\ N_{\delta_r}^{\ddot{y}}(0) &= 120 \text{ ft/sec}^6\text{-rad} \end{aligned}$$

the helmsman attested that the speed regulation task and the steering task together saturated the helmsman's workload. Yet there was only one out of four runs with both tasks where performance on the steering task appeared to degrade.

The helmsman's tasks are summarized in Fig. 2. Approximations to the lateral dynamics of Table 1 are shown to illustrate the low-frequency (i.e., long time constant) nature of the SES dynamics. Also, there is a non-minimum phase term in the lateral displacement dynamics such that the ship initially moves in a direction opposite to its final direction for a given rudder command. The lags and non-minimum phase characteristics combine to give apparent ship response delays in lateral displacement on the order of several seconds, which makes for a challenging dynamic control task. The various displays available to the helmsman help by allowing him to control intermediate states or derivatives of the final lateral displacement. In Fig. 1 the Y_y , $Y_{\dot{\psi}}$, and $F_{\dot{\psi}}$ terms account for the helmsman's operation on the variety of displayed information.

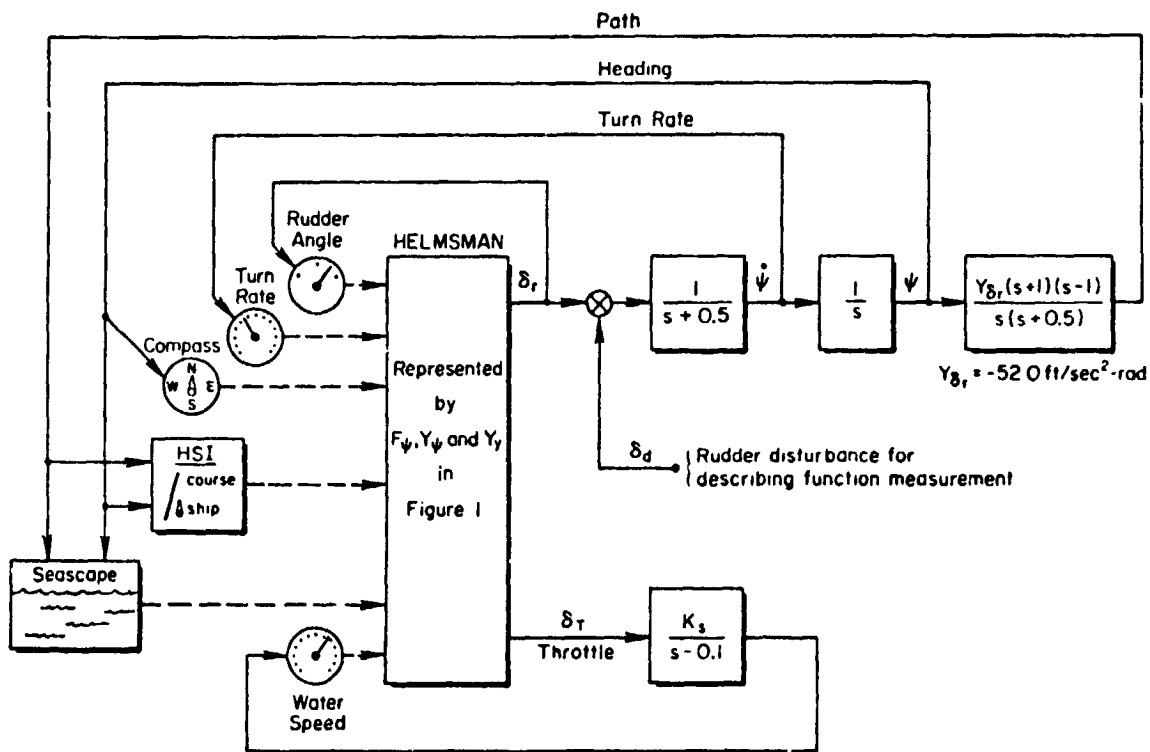


Figure 2. Helm Control Tasks

The automatic helm was provided for relief of manual steering duties at the option of the helmsman. The control law which provided for automatic steering of the simulated SES was:

$$\delta_r = -G_\psi(\psi - G_y y_e) \quad (2)$$

The steering loop closures consisted of an inner heading loop to provide necessary damping for the outer lateral displacement loop. The manner in which these closures were implemented for automatic steering can be represented by the block diagram form in Fig. 1, if we specialize $Y_y = G_y$, $Y_\psi = 1$, $F_\psi = G_\psi$, and neglect the effect of rudder actuator dynamics within G_ψ .

The open-loop transfer function for lateral displacement with the heading loop closed is provided in Eq. 3.

$$\frac{y}{y_e} = \frac{G_\psi G_y N_{\delta_r}^{\ddot{y}}}{s(s\Delta + G_\psi N_{\delta_r}^{\dot{y}})} \quad (3)$$

The closed-loop representation of the lateral displacement response to lateral displacement command is obtained directly from Eq. 3 and is given by Eq. 4.

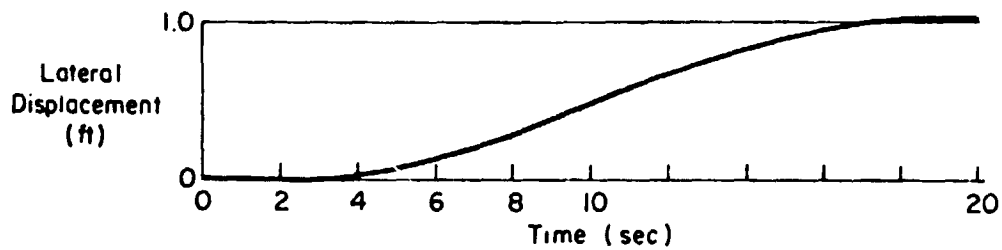
$$\frac{y}{y_c} = \frac{G_\psi G_y N_{\delta_r}^{\ddot{y}}}{s^2 \Delta + G_\psi N_{\delta_r}^{\dot{y}} s + G_\psi G_y N_{\delta_r}^{\ddot{y}}} \quad (4)$$

The heading and lateral displacement gains for the simulated SES automatic helm were designed so as to provide a 0.3 rad/sec bandwidth for the inner loop and a 0.1 rad/sec bandwidth for the outer loop. The open-loop frequency response is plotted in Fig. 3 for a typical cruising speed. The design values of gains G_ψ and G_y employed in the simulation are equal to 0.15 and 0.001 rad/ft, respectively. The unit step response of the closed-loop lateral displacement control system is shown in Fig. 3. Performance of the automatic helm was quite satisfactory for the intended purpose.

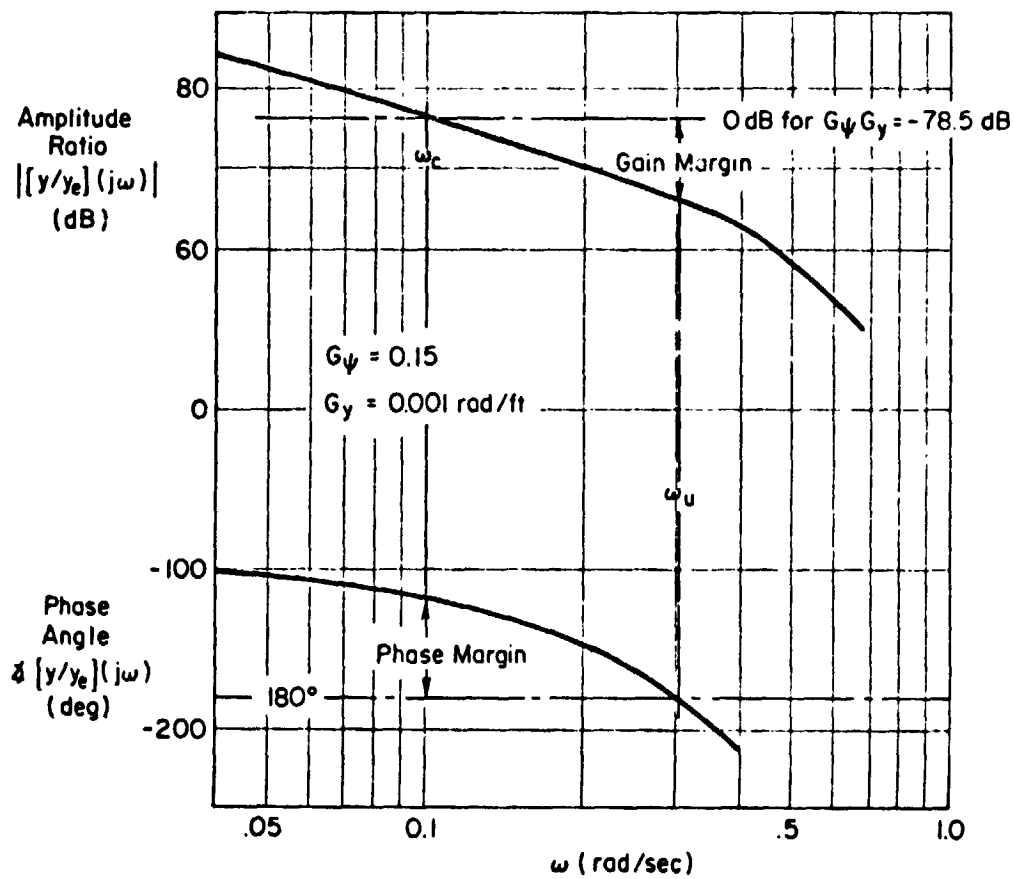
DESCRIBING FUNCTION MEASUREMENTS WITH MANUAL CONTROL

The forcing function provided by the DFA is labeled "I" in Fig. 1, where it is injected into the common path of the control loops as a disturbance by

END



a) Closed-Loop Unit Step Command Response of Lateral Displacement



b) Bode Diagram for Lateral Displacement Loop with Heading Loop Closed

Figure 3. Automatic Helm Used in 2000 Ton SES Simulation at Cruising Speed

summation with δ_r , the helm's steering signal to the rudder. If the disturbance I is viewed as a "command" input and the helmsman's rudder signal $\delta_r \equiv -M$, the negative motion feedback, the rudder error $e = E(-I - M)$ acts to disturb heading and to displace the ship laterally from the desired course. Thus, for our purpose, E represents an acceptable measure of closed-loop performance, the finite Fourier transform of which is computed by the DFA, and $[E/I](j\omega)$ represents the closed-loop error-to-input describing function.

The open-loop describing function of the helmsman's lateral displacement control technique in combination with the known mathematical model of the SES can be represented by $[M/E](j\omega)$, which may be obtained from the relationship:

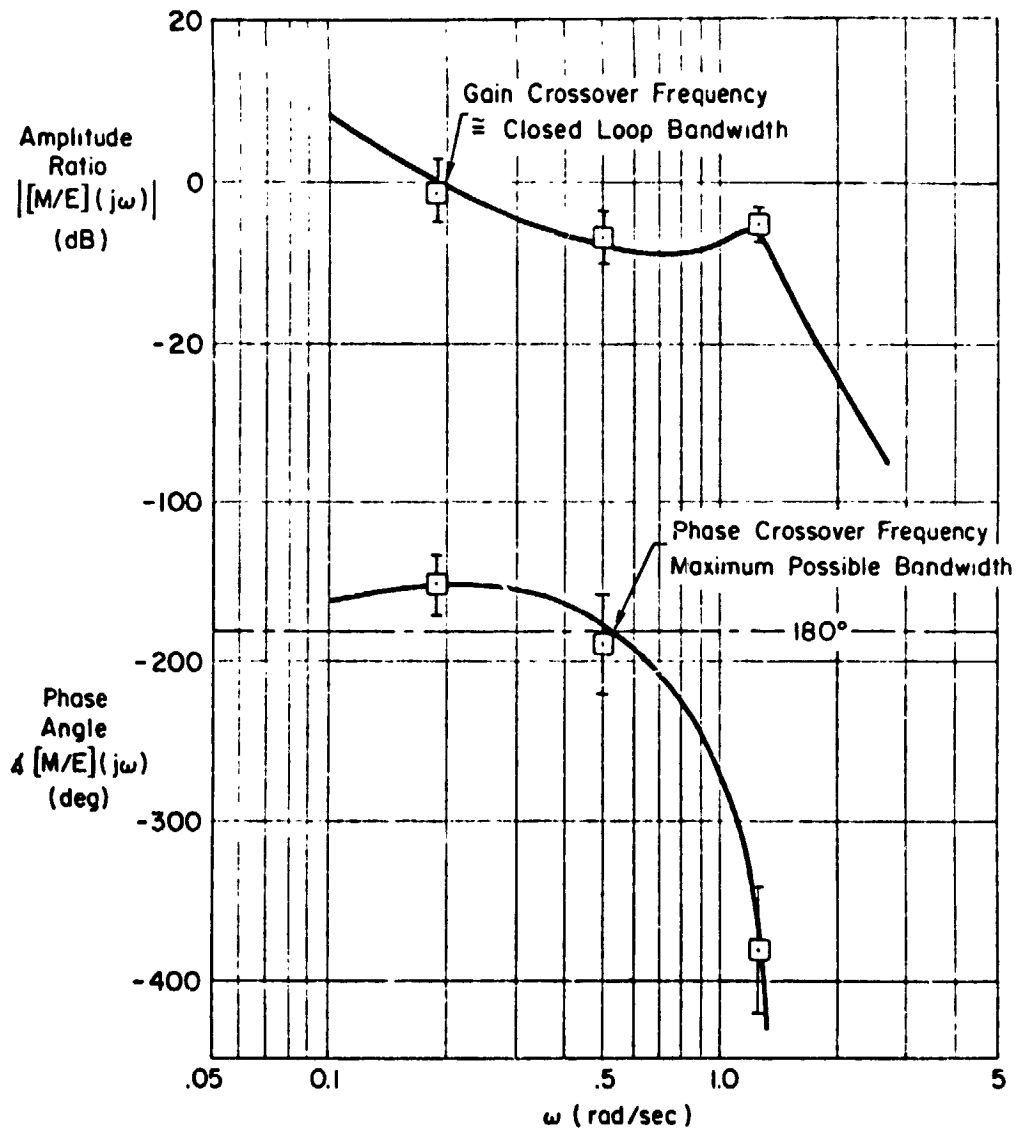
$$[M/E](j\omega) = \frac{1 - [E/I](j\omega)}{[E/I](j\omega)} \quad (1)$$

After identifying that portion of $[M/E](j\omega)$ which represents the known SES dynamics, the remaining portion will represent the combined equivalent of the loops, gains, frequency-dependent equalization and steering dynamics involved in the helmsman's control technique. A digital computer program based on Ref. 4 is used for identifying $[M/E](j\omega)$ and partitioning the result between the machine and the man.

Some of the results of applying that program to the SES simulation have been analyzed. We have found no significant differences in M/E which correlate with the different sea motion conditions tested. The only significant difference between helmsmen is in the average amplitude of M/E at the third measurement frequency, which is about 6 dB higher for the helmsman in Crew A than in Crew B.

An attempt was made to determine the influence, if any, of performing the subcritical speed control task on the measurements of M/E for the steering tasks. No influence is evident in the two runs for the helmsman in Crew B. However, for the helmsman in Crew A only one run with both tasks is available; its measurements appear more noisy with evidence of increased time delay in the steering task, and the phase crossover frequency apparently decreases from a value in excess of 0.5 rad/sec to about 0.2 rad/sec as a result of the division of attention. Yet, there is no evidence of a corresponding gain reduction by the helmsman in Crew A to provide more than 2.5 dB gain margin of stability when both tasks are being performed. There also was the possibility of biodynamic coupling from heaving motions to steering motions when the helmsman had only his right hand on the wheel while performing the speed control task with his left hand. Although we shall identify neuromuscular dynamic amplification in the results at the third measurement frequency, there is no evidence for biodynamic causation.

The mean values and standard deviation of M/E for six selected runs by the helmsman in Crew B are presented in Fig. 4. Four are runs for which the helmsman performed only the steering task, and two are runs for which he performed both the steering and speed control tasks simultaneously. The amplitudes and



Measurements represent the ensemble average and plus or minus one standard deviation of six runs by the helmsman in Crew B. The theoretical fitted describing function is based on Eq. 6 and represents the combination of the SES, the helmsman, displays and steering control.

Figure 4. Example of Open-Loop Describing Function Measurements at the Rudder Control Point for Manually Controlled Course-Keeping with a Simulated 2000 Ton SES

phase angles for M/E are presented only at the three lowest measurement frequencies corresponding to 0.1884, 0.5014, and 1.256 rad/sec, because M/E at the two higher measurement frequencies had very low signal-to-noise ratios and was dominated by noise. The average unit gain crossover frequency of the lateral displacement loop closure by each helmsman is slightly below 0.2 rad/sec, and the average phase crossover frequency is in the vicinity of 0.5 rad/sec.

The excessively variable and noisy measurements obtained here are, in part, the result of deliberately violating a caveat in using the DFA, viz., maintaining input magnitude sufficient to yield reasonable displayed error deviations (Ref. 7). This caveat was regrettably sacrificed in favor of crew motivation, because the helmsmen complained that higher input amplitudes produced abnormally great activity in turn rate and rudder displacement based on their experience, even though the input disturbance was applied to the innermost loop available at the rudder control point and not directly displayed on the rudder angle indicator. This resulted in a K/ω^2 power spectrum in displayed turn rate, whereas one should in future tests employ a sum of approximately equal amplitude sinusoids for the input at the rudder. This will allow the SES controlled element to shape the power spectra of the displayed signals and will yield better signal-to-noise ratios in the measurements. In retrospect we placed too much weight on crew experience, because at that point in time neither helmsman had had experience steering an SES in aggravated seas at cruising speeds by reference to instruments.

We shall now describe the rationale for partitioning M/E between the (known) controlled element and the helmsman in such a way as to infer forms for his describing functions. The results of applying these inferred forms within a theoretical model for M/E and fitting the same to the measurements are plotted in Fig. 4.

MANUAL CLOSURE OF HEADING AND LATERAL DISPLACEMENT LOOPS LEADING TO AN EXPLANATION OF THE MEASURED DESCRIBING FUNCTIONS

The topology of the helmsman's control technique represented in Fig. 1 is founded on foreknowledge of the K/s^2 form of the SES controlled element and includes the necessary heading and lateral displacement loops with provision for lead equalization in the heading loop. The helmsman is represented by partitioned describing functions F_ψ , Y_ψ and Y_y . The describing function, M/E, of the open-loop lateral displacement control technique from rudder error to helmsman's output is obtained from inspection of Fig. 1.

$$\frac{M}{E} = \frac{Y_\psi s N_r^r + Y_y N_r^{\ddot{y}}}{s^2 \Delta} F_\psi \quad (6)$$

Substitution in Eq. (6) of the typical numerical values for the ship's lateral-directional transfer functions in Table 1 will reveal the following key points:

- M/E is of the form K/s^2 at low frequency as we would expect.
- $|Y_\psi| \gg |Y_Y|$ in order that $sN_{\psi_r}^r$ may provide the requisite low-frequency lead equalization to convert M/E to the form K/s in the region of unit gain crossover.
- The characteristic directional oscillatory mode of the ship is quite low in frequency (approximately 0.5 rad/sec) but well damped.
- Y_ψ (or F_ψ) should adopt lead equalization in the vicinity of 0.5 rad/sec to maintain a well damped closed-loop directional mode.
- The characteristic rolling oscillatory mode is higher in frequency (approximately 1.5 rad/sec), lightly damped, but suppressed in amplitude by the zeros of the lateral and directional numerators.

We shall next discuss the procedure employed to establish F_ψ , Y_ψ and Y_Y which will provide plausible heading and lateral displacement control techniques to interpret the response measured by the DFA. We shall illustrate the procedure by adopting pure gain equalization within Y_ψ and deferring the mid-frequency lead equalization to F_ψ , although equivalent results can be obtained by adopting the converse equalization technique because $|Y_\psi| \gg |Y_Y|$. In either case pure gain equalization will suffice for Y_Y .

It was first necessary to determine the behavior of the numerator zeros of Eq. 6 as a function of Y_ψ/Y_Y and to select an appropriately large value for the gain ratio Y_ψ/Y_Y which would fix the location of the zeros for the overall lateral displacement control so as to provide the low-frequency lead equalization apparent in the measured response. The Bode root locus of the numerator zeros was therefore generated as depicted in Fig. 5. The gain ratio of 791 was selected for Y_ψ/Y_Y to provide M/E with a reasonable frequency interval having the form approaching K/s in the neighborhood of the unit gain crossover frequency, 0.19 rad/sec estimated from the DFA.

With the gain ratio of Y_ψ/Y_Y thus established, M/E is now represented partially in numerical form in Eq. 7, by allowing Y_ψ to covary with Y_Y in accord with the constant ratio selected above.

$$\frac{M}{E} = \frac{739 \cdot Y_Y (0.213)(0.315)[0.192, 1.526]}{s^2 \Delta} F_\psi \quad (7)$$

It now remains to determine the product $F_\psi Y_Y$ so that M/E in Eq. 7 will fit the set of three measurements in Fig. 3. Realizing that the helm itself was a relatively lightly damped spring-restrained steering wheel with a very low undamped natural frequency ω_N on the order of 1 rad/sec, we shall hypothesize that the important features of F_ψ can be represented by:

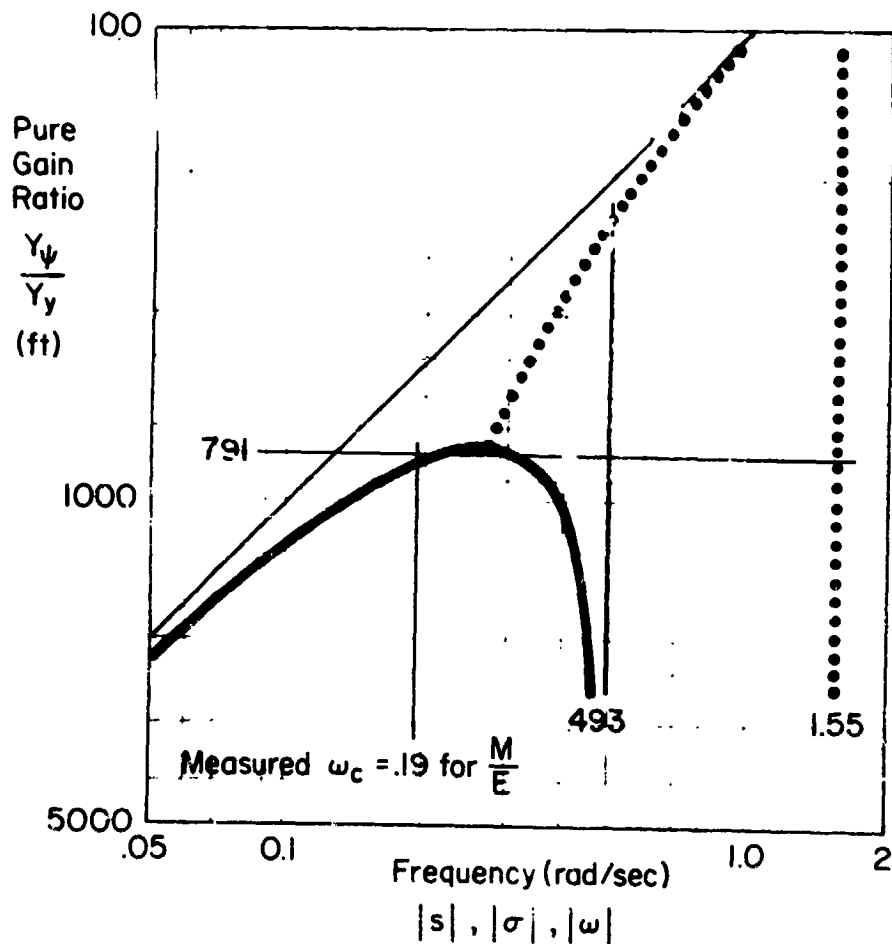


Figure 5. Bode Root Locus of the Zeros of $[Y_\psi s N_{\psi r}^F + Y_y N_{\psi r}^{\ddot{y}}]$ as a Function of the Pure Gain Ratio Y_ψ/Y_y for $|Y_\psi| \gg |Y_y|$ (Refer to the Numerator of Eq. 6)

$$F_\psi = \frac{K_\psi (1 + T_L s) e^{-\tau_d s}}{\left[1 + \frac{2\zeta_N s}{\omega_N} + \frac{s^2}{\omega_N^2} \right]} \quad (8)$$

Numerical estimates for the parameters in $F_\psi Y_y$ were based on the following observations and conditions:

- a) T_L is approximately 2 or 3 sec to provide a phase cross-over frequency in the neighborhood of the second DFA measurement frequency, 0.5 rad/sec, with the 5 or 6 dB

gain margin measured and to maintain a well-damped non-oscillatory characteristic directional mode of the ship emanating from Δ .

- b) ω_N is slightly in excess of 1 rad/sec and approximately equal to the third DFA measurement frequency, 1.25 rad/sec.
- c) ζ_N is either 0.08 (Crew A) or 0.15 (Crew B) to fit the describing function amplitude at the third DFA measurement frequency. These relatively low values of ζ_N are due in part to the lower-than-recommended values of Coulomb friction provided in the simulated artificial feel for the steering wheel. However, they also represent the fact that the helmsman will reduce the inherent steering wheel damping ratio anyway, because a portion of his time delay exists within his perceived rudder angle feedback loop or his proprioceptive steering angle feedback loop.
- d) τ_d is between 2 and 3 sec to fit the describing function phase angle at the third DFA measurement frequency.
- e) Y_y is a pure gain and the gain product $Y_y K_\psi$ is adjusted so that the amplitude of M/E matches that at the lowest DFA measurement frequency.

The quite satisfactory results of the fitting procedure for the helmsman in Crew B are displayed in Fig. 3 and tabulated in Table 2 for both helmsmen, and a summary block diagram equivalent is shown in Fig. 6.

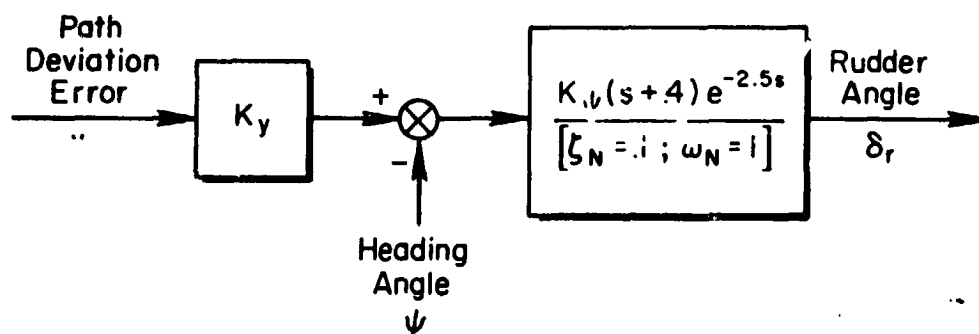


Figure 6. Summary Block Diagram of Helmsman's Control Response

TABLE 2

NUMERICAL VALUES REPRESENTING THE HELMSMEN

	<u>Crew A</u>	<u>Crew B</u>
Y_{ψ}/Y_Y (ft)	791.	791.
$Y_Y K_{\psi}$ (rad/ft)	0.0000927	0.0000981
$Y_{\psi} K_{\psi}$	0.0733	0.0776
ω_N (rad/sec)	1.25	1.25
T_L (sec)	3.	2.5
ζ_N	0.08	0.15
τ_d (sec)	2.9	2.4
ω_c (rad/sec)	0.18	0.19
Phase margin (deg)	29.	28.
ω_u (rad/sec)	0.5	0.525
Gain margin (dB)	7.	8.

CONCLUSIONS

An examination of the open-loop steering describing function measurements in the SES simulation has shown that, regardless of sea motion condition, both helmsmen adopted average heading and displacement gains so as to maintain the closed-loop displacement bandwidth in the neighborhood of 0.2 rad/sec with acceptable margins of stability in phase and gain. This is an adequate bandwidth for course-keeping at SES cruising speeds. Additional adopted first-order lead equalization appears within the heading loop between 0.3 and 0.5 rad/sec to maintain a well-damped characteristic directional mode of the ship. This lead equalization may be generated by perceiving the turn rate indicator. Additional adopted first-order lead equalization appears within the heading loop between 0.3 and 0.5 rad/sec to maintain a well-damped characteristic directional mode of the ship. This lead equalization may be generated by perceiving the turn rate indicator.

Although no evidence for biodynamic amplification appears in these results, relatively lightly damped and amplified steering wheel dynamics appear at about 1.25 rad/sec as an intended artifact of the simulation. The relatively low damping is due in part to the lower-than-recommended values of Coulomb friction provided in the simulated artificial feel for the steering wheel to reduce

breakout torque. However, the spring gradient in the steering wheel was also too low. Consequently, the natural frequency of neuromuscular actuation was too low, and the helmsman reduced the inherent steering wheel damping ratio even more, because a portion of his time delay exists within his perceived rudder angle feedback loop.

That the helmsmen were scanning the rudder angle indicator is corroborated by their commentary. This is presumably a part of the transfer of training for steering low speed displacement-hull ships. However, with a stiffer and more linearly damped artificial feel system with a lower breakout force, the proprioceptive feedback available from the steering wheel will provide a superior equivalent to visual rudder angle feedback from the panel instrument. As a result, the neuromuscular dynamics will be desirably higher in frequency and suppressed in amplitude. This will yield a better margin of stability and improved course-following performance in aggravated seas.

The overall effective time delay of the helmsmen estimated from the open-loop describing function measurements is between 2 and 3 sec. This is about 2 sec larger than would be expected to accompany the adopted equalization when using the electronic horizontal situation display. Such a relatively large time delay may be caused by scanning delays among the helmsman's instruments and visual field and by a division of attention among his other tasks during the measurement interval. We therefore recommend training in the more effective use of integrated horizontal situation displays for steering.

REFERENCES

1. a) Aronson, R.: Birth of the 100-Knot Navy. Machine Design, Vol. 45, No. 13, May 31, 1973, pp. 20-25.
b) Hudlock, R.: Toward the 100-Knot Navy. Astronautics and Aeronautics, Vol. 11, No. 9, Sept. 1973, pp. 6-10.
2. Skolnick, A.: Crew Performance Requirements in the Vibratory Environments of Surface Effect Ships. Presented at the Session "B" of the AND Aerospace Medical Panel Specialists Meeting, Oslo, Norway, 22-25 / 1974.
3. Jex, H. R.; and Allen, R. W.: Research on a New Human Dynamic Response Test Battery; Part I, Test Development and Validation; Part II, Psychophysiological Correlates. Proceedings of the Sixth Annual Conference on Manual Control, Air Force Institute of Technology, 7-9 Apr. 1970.
4. Allen, R. W.; and Jex, H. R.: A Simple Fourier Analysis Technique for Measuring the Dynamic Responses of Manual Control Systems. Proceedings of the Sixth Annual Conference on Manual Control, Air Force Institute of Technology, 7-9 Apr. 1970, pp. 785-801.
5. Teper, G. L.: An Effective Technique for Extracting Pilot Model Parameter Values from Multi-Feedback, Single-Input Tracking Tasks. Proceedings of the Eighth Annual Conference on Manual Control, University of Michigan, 17-19 May 1972, pp. 23-33.

6. McRuer, D. T.; Weir, D. H.; Jex, H. R.; Magdaleno, R. E.; and Allen, R. W.: Measurement of Driver/Vehicle Multiloop Response Properties with a Single Disturbance Input. Proceedings of the Ninth Annual Conference on Manual Control, Massachusetts Institute of Technology, 23-25 May 1973, pp. 217-232.
7. Peters, R. W.; and Allen, R. W.: Operation Manual for Describing Function Analyzer, Model 1003, Serial 1001. Working Paper 406-2, Systems Technology, Inc., Oct. 1970.

SYMBOLS

e	Naperian Base, 2.71828...
E	Error signal output to DFA (I - M)
E/I	DFA error-to-input describing function
F_{ψ}	Helmsman's heading feedforward describing function including neuromuscular steering actuation dynamics (dimensionless)
G_y	Lateral displacement gain of automatic helm (rad/ft)
G_{ψ}	Heading gain of automatic helm (dimensionless)
I	DFA disturbance input to rudder steering axis
j	$\sqrt{-1}$
K_s	Throttle control-to-speed response gain (ft/sec-rad)
K_{ψ}	Gain equalization in F_{ψ} (dimensionless)
M	Closed-loop motion output with respect to DFA input
M/E	Open-loop output to error describing function as measured by DFA
$N_{\psi r}^r$	Controlled element transfer function numerator polynomial representing yaw rate response to rudder displacement (1/sec)
$N_{\psi r}^{\ddot{y}}$	Controlled element transfer function numerator polynomial representing lateral acceleration response to rudder displacement (ft/sec ² -rad)
s	Laplace operator, $\sigma \pm j\omega$
T_L	Time constant of lead equalization in Y_{ψ} or F_{ψ} (sec)
u	Perturbed longitudinal water speed of craft with respect to trimmed speed (ft/sec)

y	Lateral displacement of craft (ft)
y_c	Lateral displacement command (ft)
y_e	Lateral displacement error ($y_c - y$)
Y_y	Helmsman's lateral displacement describing function (rad/ft)
Y_ψ	Helmsman's heading feedback describing function (dimensionless)
δ_e	Rudder angle error (rad)
δ_r	Perturbed rudder deflection angle with respect to trimmed angle (rad)
δ_t	Throttle displacement (rad)
Δ	Characteristic determinant, transfer function denominator
ζ_N	Damping ratio of second-order lag in F_ψ representing effective neuromuscular actuation dynamics modified by proprioceptive or visual feedback (dimensionless)
λ	Inverse time constant of the first-order sub-critical tracking task (rad/sec)
σ	Real part of the complex variable s (rad/sec)
τ_d	Effective helmsman's time delay, including transport, equalization and scanning contributions (sec)
ψ	Heading of craft (rad)
ψ_c	Heading command ($Y_y y_e$) (rad)
ψ_e	Heading error ($\psi_c - \psi$) (rad)
ω	Circular frequency; imaginary part of the complex variable s (rad/sec)
ω_c	Unit gain crossover frequency (rad/sec)
ω_N	Undamped natural frequency of second-order lag in F_ψ representing effective neuromuscular actuation dynamics modified by proprioceptive or visual feedback (rad/sec)
ω_u	Unstable phase crossover frequency (rad/sec)

Abbreviations

dB	Decibel
deg	Degree
DFA	Describing Function Analyzer
ft	Foot
in.	Inch
rad	Radian
sec	Second
SES	Surface effect ship
(\cdot)	(raised period) Time Derivative Operator d/dt (1/sec)

**THE EFFECTS OF BEDREST ON CREW PERFORMANCE
DURING SIMULATED SHUTTLE REENTRY**

By Henry R. Jex, Richard A. Peters,
Richard J. DiMarco, and R. Wade Allen

Systems Technology, Inc.
Hawthorne, California

SUMMARY

This paper describes a simplified space shuttle reentry simulation performed on the NASA Ames Research Center Centrifuge. Anticipating potentially deleterious effects of physiological deconditioning from orbital living (simulated here by 10 days of enforced bedrest) upon a shuttle pilot's ability to manually control his aircraft (should that be necessary in an emergency) a comprehensive battery of measurements was made roughly every 1/2 minute on eight military pilot subjects, over two 20-minute reentry G_z vs. time profiles, one peaking at 2 G_z and the other at 3 G_z . Alternate runs were made without and with g-suits to test the help or interference offered by such protective devices to manual control performance. A very demanding two-axis control task was employed, with a "subcritical instability" in the pitch axis to force a high attentional demand and a severe loss-of-control penalty. The results show that pilots experienced in high G_z flying can easily handle the shuttle manual control task during 2 G_z or 3 G_z reentry profiles, provided the degree of physiological deconditioning is no more than induced by these 10 days of enforced bedrest.

(Details are published in — Jex, Henry R; Peters, Richard A; DiMarco, Richard J.; and Allen, R. Wade: The Effects of Bedrest on Crew Performance During Simulated Shuttle Reentry. Volume II: Control Task Performance. NASA CR-2367, October 1974.)